EPIGENETICS IN CANCER: MECHANISMS AND DRUG DEVELOPMENT

EDITED BY: Xiao Zhu, Biaoru Li and Zhenhua Xu
PUBLISHED IN: Frontiers in Cell and Developmental Biology and Frontiers in Genetics

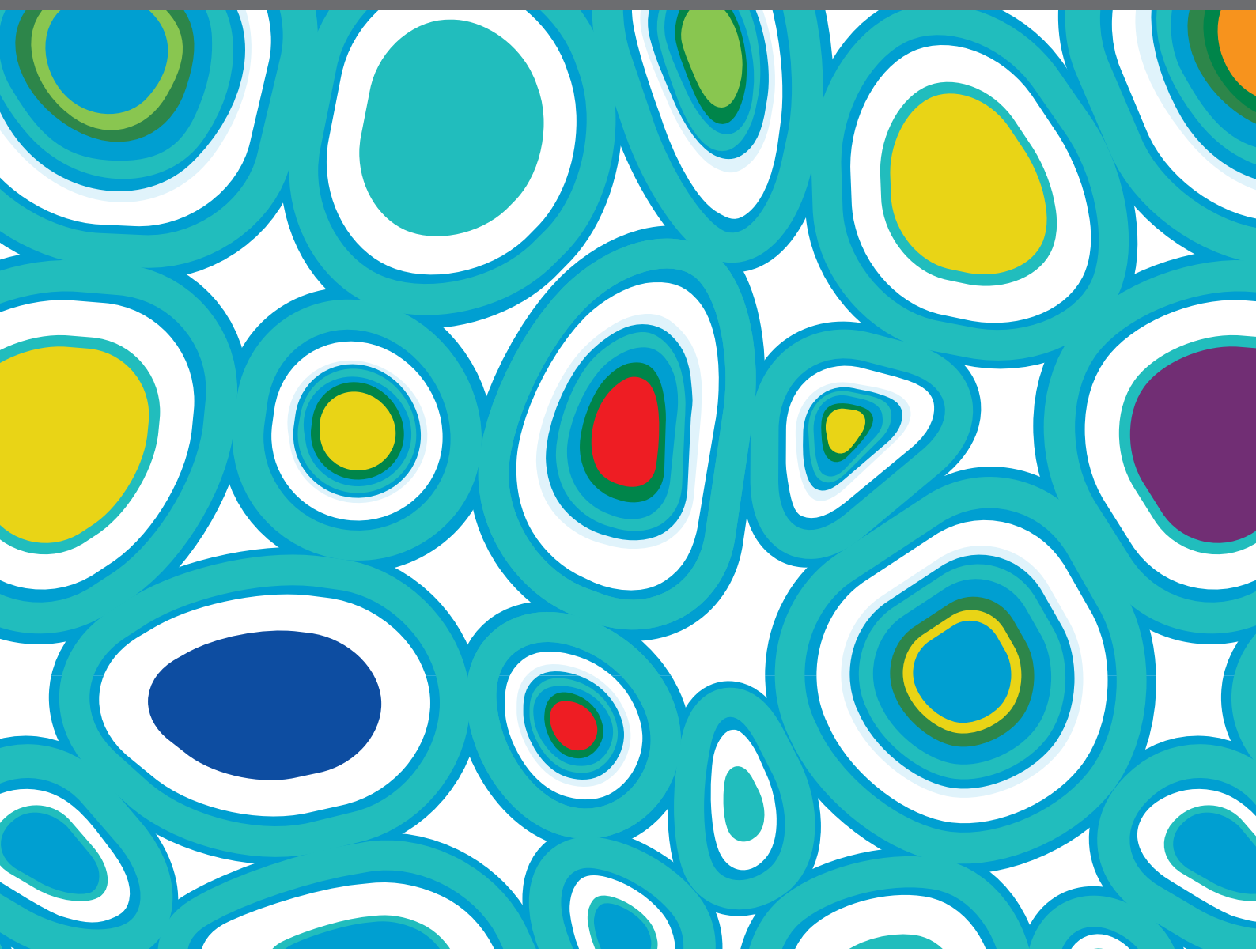

frontiers Research Topics

ISSN 1664-8714
ISBN 978-2-88974-376-6
DOI 10.3389/978-2-88974-376-6

About Frontiers

Frontiers is more than just an open-access publisher of scholarly articles: it is a pioneering approach to the world of academia, radically improving the way scholarly research is managed. The grand vision of Frontiers is a world where all people have an equal opportunity to seek, share and generate knowledge. Frontiers provides immediate and permanent online open access to all its publications, but this alone is not enough to realize our grand goals.

Frontiers Journal Series

The Frontiers Journal Series is a multi-tier and interdisciplinary set of open-access, online journals, promising a paradigm shift from the current review, selection and dissemination processes in academic publishing. All Frontiers journals are driven by researchers for researchers; therefore, they constitute a service to the scholarly community. At the same time, the Frontiers Journal Series operates on a revolutionary invention, the tiered publishing system, initially addressing specific communities of scholars, and gradually climbing up to broader public understanding, thus serving the interests of the lay society, too.

Dedication to Quality

Each Frontiers article is a landmark of the highest quality, thanks to genuinely collaborative interactions between authors and review editors, who include some of the world's best academicians. Research must be certified by peers before entering a stream of knowledge that may eventually reach the public - and shape society; therefore, Frontiers only applies the most rigorous and unbiased reviews.
Frontiers revolutionizes research publishing by freely delivering the most outstanding research, evaluated with no bias from both the academic and social point of view. By applying the most advanced information technologies, Frontiers is catapulting scholarly publishing into a new generation.

What are Frontiers Research Topics?

Frontiers Research Topics are very popular trademarks of the Frontiers Journals Series: they are collections of at least ten articles, all centered on a particular subject. With their unique mix of varied contributions from Original Research to Review Articles, Frontiers Research Topics unify the most influential researchers, the latest key findings and historical advances in a hot research area! Find out more on how to host your own Frontiers Research Topic or contribute to one as an author by contacting the Frontiers Editorial Office: frontiersin.org/about/contact

EPIGENETICS IN CANCER: MECHANISMS AND DRUG DEVELOPMENT

Topic Editors:
Xiao Zhu, Guangdong Medical University, China
Biaoru Li, Augusta University, United States
Zhenhua Xu, Children's National Hospital, United States

Citation: Zhu, X., Li, B., Xu, Z., eds. (2022). Epigenetics in Cancer: Mechanisms and Drug Development. Lausanne: Frontiers Media SA. doi: 10.3389/978-2-88974-376-6

Table of Contents

frontiers | Frontiers in Genetics

EDITORIAL
published: 28 June 2022
doi: 10.3389/fgene.2022.831704

Editorial: Epigenetics in Cancer: Mechanisms and Drug Development

Huiqing Yuan[1,2,3†], *Yongmei Huang*[2,3,4†], *Susu Tao*[2,3,4†], *Biaoru Li*[5†], *Zhenhua Xu*[6†], *Yi Qi*[2,3,4*], *Binhua Wu*[2,3,4*], *Hui Luo*[2,3,4*] *and Xiao Zhu*[1,2*]

[1]School of Laboratory Medicine and Biomedical Engineering, Hangzhou Medical College, Hangzhou, China, [2]The Marine Biomedical Research Institute, Guangdong Medical University, Zhanjiang, China, [3]Southern Marine Science and Engineering Guangdong Laboratory (Zhanjiang), Zhanjiang, China, [4]The Key Lab of Zhanjiang for R&D Marine Microbial Resources in the Beibu Gulf Rim, Guangdong Medical University, Zhanjiang, China, [5]Cancer Center, Medical College of Georgia, Augusta University, Augusta, GA, United States, [6]Center for Cancer and Immunology, Children's National Health System, Washington, DC, DC, United States

Keywords: cancer therapy, epigenetic drugs, DNA methylation, histone deacetylation, tumor inhibitors

Editorial on the Research Topic

Epigenetics in Cancer: Mechanisms and Drug Development

OPEN ACCESS

Edited and reviewed by:
Michael E. Symonds, University of Nottingham, United Kingdom

***Correspondence:**
Yi Qi
qiyi7272@gdmu.edu.cn
Binhua Wu
wubinhua@gdmu.edu.cn
Hui Luo
luohui@gdmu.edu.cn
Xiao Zhu
bioxzhu@yahoo.com

†*These authors have contributed equally to this work*

Specialty section:
This article was submitted to Epigenomics and Epigenetics, a section of the journal Frontiers in Genetics

Received: *08 December 2021*
Accepted: *04 May 2022*
Published: *28 June 2022*

Citation:
Yuan H, Huang Y, Tao S, Li B, Xu Z, Qi Y, Wu B, Luo H and Zhu X (2022) Editorial: Epigenetics in Cancer: Mechanisms and Drug Development. Front. Genet. 13:831704. doi: 10.3389/fgene.2022.831704

This research topic "*Epigenetics in Cancer: Mechanisms and Drug Development*" consists of 14 articles contributed by more than 120 authors in the fields of cancer epigenetics and therapeutics. The topic enumerates collecting different research directions including transcription and chromatin roles in gene regulation, DNA modifications, RNA epigenetics, non-coding RNA, and epigenomic methods. In addition to bringing the newest findings on epigenetic mechanisms, a special focus will be given to novel and promising therapeutic drugs aimed at reversing specific epigenetic alterations.

In recent years, new targets of tumor immunotherapy have been found. For example, a checkpoint with forkhead associated and ring finger domain (*CHFR*) is one of the keys to immune checkpoints, and its activity is lost through promoter hypermethylation or mutation in many tumor and cancer cell lines. Chen et al. demonstrated that the epigenetic characteristics of the *CHFR* gene were a new prognostic feature. Dong et al. discussed the latest findings of the potential application of PIWIL1 in chemotherapy resistance of tumors through multiple signaling pathways.

The occurrence of cancer is related to the abnormal expression of many genes. Opioid binding protein/cell adhesion molecule-like (*OPCML*) is a protein-coding gene that has been associated with a variety of cancers, including ovarian cancer. Shao et al. observed that the DNA methylation level of the *OPCML* promoter region CG25853078 was positively correlated with its expression.

C-terminal Src kinase (Csk) and Csk homologous kinase (Chk) are the main endogenous inhibitors of Src family kinases (SFK) (Chueh et al., 2021). Zhu et al. found that increased DNA methylation levels may be caused by increased DNMT levels, leading to decreased expression of CHK mRNA and CHK protein and promoting the increase of carcinogenic characteristics of colon cancer cells. Epigenetic regulation of the CHK expression in colon cancer cells has significant biological effects, including cell proliferation, wound healing, and cell invasion.

In epigenetic modification, mRNA modification plays the same role as DNA methylation. Scientists have identified more than 100 chemical modification methods of RNA, among which N6-methyl adenine (m6A) accounts for 80% of RNA methylation modification (Zhou et al., 2020). M6A methylation modification has been proven to be reversible, which is controlled by methyltransferases (writers), methylated readers, and demethylases (Tan et al., 2021). The fat and obesity-related protein (FTO) has been identified as the first m6A methylase inhibitor and has been one of the most attractive target proteins for the development of m6A methylase inhibitors to treat cancer (Lu et al.).

More than ten kinds of posttranslational modifications (PTM) can occur on histones entangled with DNA, including methylation, acetylation, propionylation, phosphorylation, and ubiquitination. The most common ones are methylation and acetylation. Histone methylation is regulated by histone methyltransferases (HMTs) and histone demethylases (HDMs) (He and Lomberk). HMTs and HDMs balance each other to maintain histone methylation levels, and their imbalance may promote cancer. Acetylation is regulated by HATs and histone deacetylases (HDACs) (Zhang et al.; Li et al., 2022).

Abnormal DNA methylation has become a recurrent carcinogenic event (Liang et al., 2021). Zhu et al. emphasized that genetic aberrations rather than phenotypes (DNA methylation) can be targeted by identifying the molecular basis of carcinogenesis. In addition, although the restoration of the epigenome to normal is seen as a therapeutic strategy, it has not yet been proven to be the primary mechanism of treatment. It is necessary to create drugs that interfere with adaptive mechanisms, and this method is increasingly being proven.

In conclusion, the "*Epigenetics in Cancer: Mechanisms and Drug Development*" research topic highlights the importance of developing novel epigenetic targets for cancer therapy.

AUTHOR CONTRIBUTIONS

XZ, HL, BW, and YQ conceived the work. HY, YH, and ST wrote and drafted the manuscript. BL, ZX, and XZ discussed and edited the manuscript. All authors read and approved the final version of the manuscript.

FUNDING

This work was supported partly by Guangdong University Youth Innovation Talent Project (2020KQNCX023), the Scientific Research Fund of Guangdong Medical University (GDMUM202002), the non-funded science and technology project of Zhanjiang City (2020B01007), the 2020 Undergraduate Innovation Experiment project of Guangdong Medical University (ZZZF006), the Southern Marine Science and Engineering Guangdong Laboratory Zhanjiang (ZJW-2019-007), and the Public Service Platform of South China Sea for R&D Marine Biomedicine Resources (GDMUK201808).

REFERENCES

Chueh, A. C., Advani, G., Foroutan, M., Smith, J., Ng, N., Nandurkar, H., et al. (2021). CSK-homologous Kinase (CHK/MATK) is a Potential Colorectal Cancer Tumour Suppressor Gene Epigenetically Silenced by Promoter Methylation. *Oncogene* 40, 3015–3029. doi:10.1038/s41388-021-01755-z

Li, M., Lan, F., Li, C., Li, N., Chen, X., Zhong, Y., et al. (2022). Expression and Regulation Network of HDAC3 in Acute Myeloid Leukemia and the Implication for Targeted Therapy Based on Multidataset Data Mining. *Comput. Math. Methods Med.* 2022, 1–14. doi:10.1155/2022/4703524

Liang, R., Li, X., Li, W., Zhu, X., and Li, C. (2021). DNA Methylation in Lung Cancer Patients: Opening a "window of Life" under Precision Medicine. *Biomed. Pharmacother.* 144, 112202. doi:10.1016/j.biopha.2021.112202

Tan, S., Li, Z., Li, K., Li, Y., Liang, G., Tang, Z., et al. (2021). The Regulators Associated with N6-Methyladenosine in Lung Adenocarcinoma and Lung Squamous Cell Carcinoma Reveal New Clinical and Prognostic Markers. *Front. Cell Dev. Biol.* 9, 741521. doi:10.3389/fcell.2021.741521

Zhou, Y., Kong, Y., Fan, W., Tao, T., Xiao, Q., Li, N., et al. (2020). Principles of RNA Methylation and Their Implications for Biology and Medicine. *Biomed. Pharmacother.* 131, 110731. doi:10.1016/j.biopha.2020.110731

Conflict of Interest: The authors declare that the research was conducted in the absence of any commercial or financial relationships that could be construed as a potential conflict of interest.

Publisher's Note: All claims expressed in this article are solely those of the authors and do not necessarily represent those of their affiliated organizations or those of the publisher, the editors, and the reviewers. Any product that may be evaluated in this article, or claim that may be made by its manufacturer, is not guaranteed or endorsed by the publisher.

frontiers in Cell and Developmental Biology

ORIGINAL RESEARCH
published: 09 December 2020
doi: 10.3389/fcell.2020.598205

PD-L1 Is a Tumor Suppressor in Aggressive Endometrial Cancer Cells and Its Expression Is Regulated by miR-216a and lncRNA MEG3

Daozhi Xu[1†], Peixin Dong[1†], Ying Xiong[2†], Rui Chen[2], Yosuke Konno[1*], Kei Ihira[1], Junming Yue[3,4] and Hidemichi Watari[1]*

[1] Department of Obstetrics and Gynecology, Hokkaido University School of Medicine, Hokkaido University, Sapporo, Japan, [2] Department of Gynecology, State Key Laboratory of Oncology in South China, Sun Yat-sen University Cancer Center, Guangzhou, China, [3] Department of Pathology and Laboratory Medicine, University of Tennessee Health Science Center, Memphis, TN, United States, [4] Center for Cancer Research, University of Tennessee Health Science Center, Memphis, TN, United States

OPEN ACCESS

Edited by:
Xiao Zhu,
Guangdong Medical University, China

Reviewed by:
Xingyun Qi,
Rutgers, The State University of New Jersey, United States
Zhimin Wei,
Affiliated Hospital of Qingdao University, China

***Correspondence:**
Peixin Dong
dpx1cn@gmail.com
Yosuke Konno
konsuke013@gmail.com

[†] These authors have contributed equally to this work

Specialty section:
This article was submitted to Epigenomics and Epigenetics, a section of the journal Frontiers in Cell and Developmental Biology

Received: 24 August 2020
Accepted: 12 November 2020
Published: 09 December 2020

Citation:
Xu D, Dong P, Xiong Y, Chen R, Konno Y, Ihira K, Yue J and Watari H (2020) PD-L1 Is a Tumor Suppressor in Aggressive Endometrial Cancer Cells and Its Expression Is Regulated by miR-216a and lncRNA MEG3. Front. Cell Dev. Biol. 8:598205. doi: 10.3389/fcell.2020.598205

Background: Poorly differentiated endometrioid adenocarcinoma and serous adenocarcinoma represent an aggressive subtype of endometrial cancer (EC). Programmed death-ligand-1 (PD-L1) was known to exhibit a tumor cell-intrinsic function in mediating immune-independent tumor progression. However, the functional relevance of tumor cell-intrinsic PD-L1 expression in aggressive EC cells and the mechanisms regulating its expression remain unknown.

Methods: PD-L1 expression in 65 EC tissues and 18 normal endometrium samples was analyzed using immunohistochemical staining. The effects of PD-L1 on aggressive EC cell growth, migration and invasion were investigated by cell functional assays. Luciferase reporter assays were used to reveal the microRNA-216a (miR-216a)-dependent mechanism modulating the expression of PD-L1.

Results: Positive PD-L1 expression was identified in 84% of benign cases but only in 12% of the EC samples, and the staining levels of PD-L1 in EC tissues were significantly lower than those in the normal tissues. Higher PD-L1 expression predicts favorable survival in EC. Ectopic expression of PD-L1 in aggressive EC cells results in decreased cell proliferation and the loss of mesenchymal phenotypes. Mechanistically, PD-L1 exerts the anti-tumor effects by downregulating MCL-1 expression. We found that PD-L1 levels in aggressive EC cells are regulated by miR-216a, which directly targets *PD-L1*. We further identified a mechanism whereby the long non-coding RNA MEG3 represses the expression of miR-216a, thereby leading to increased PD-L1 expression and significant inhibition of cell migration and invasion.

Conclusion: These results reveal an unappreciated tumor cell-intrinsic role for PD-L1 as a tumor suppressor in aggressive EC cells, and identify MEG3 and miR-216a as upstream regulators of PD-L1.

Keywords: PD-L1, MEG3, miR-216a, long non-coding RNA, EMT, endometrial cancer

INTRODUCTION

Endometrial cancer (EC) is the most common gynecologic malignancy in developed countries, with approximately 89,929 deaths worldwide in 2018 (Bray et al., 2018). ECs are classified into various histological subtypes: including endometrioid EC, serous EC, clear-cell EC, and mixed (usually endometrioid and serous components) EC (Gaber et al., 2016). Unlike the majority of ECs, which are usually associated with well-differentiated endometrioid histology, early stage disease, and a more favorable prognosis, poorly differentiated endometrioid ECs and serous ECs are generally seen in older patients, are more aggressive, and are characterized by a high rate of recurrence and metastasis (Gaber et al., 2016).

In the early stage of tumor metastasis, an epithelial-mesenchymal transition (EMT) program occurs and contributes to the acquisition of invasive properties, enabling epithelial cells to lose polarity and adhesion capacity, but acquire the features of mesenchymal cells (Valastyan and Weinberg, 2011). A small cohort of transcription factors (such as TWIST1, ZEB1, Snail, and Slug) is recognized to affect EMT induction by controlling the expression of epithelial genes (for example, ZO-1 and E-cadherin) and mesenchymal genes (including Vimentin and HSP47) (Valastyan and Weinberg, 2011). MCL-1, a member of the Bcl-2 family of proteins, plays an essential role in promoting cell survival and metastasis in many cancers (De Blasio et al., 2018) and was discovered to be the key EMT inducer in EC (Konno et al., 2014). The EMT process is also regulated by complex epigenetic regulatory mechanisms, such as DNA methylation and histone modifications, as well as non-coding RNAs, including microRNAs (miRNAs) and long non-coding RNAs (lncRNAs) (Kiesslich et al., 2013; Xu et al., 2020). However, the molecular mechanisms governing EMT in aggressive EC remain poorly understood.

Evasion of the immune system is classified as a hallmark of cancer, which allows cancer cells to escape the attack from immune cells (Hanahan and Weinberg, 2011). Tumor cells can exploit the programmed death-1 (PD-1) immune checkpoint pathway to evade immune cells (Okazaki and Honjo, 2007). Programmed death-ligand-1 (PD-L1) is a critical immune checkpoint ligand expressed on the surface of tumor cells, and binding of PD-L1 to its receptor PD-1 on activated T cells inhibits anti-tumor immunity by reducing the proliferation, cytokine secretion, and cytotoxic ability of T cells (Okazaki and Honjo, 2007). Despite this well-characterized function of PD-L1 in cancer, emerging studies demonstrate a tumor cell-intrinsic function of PD-L1 in mediating EMT and immune-independent tumor progression (Dong et al., 2018c). Elevated expression levels of PD-L1 were detected in diverse tumors, and PD-L1 upregulation was significantly correlated with poor survival (Dong et al., 2018c). For example, PD-L1 was highly expressed in cervical cancer tissues, and overexpression of PD-L1 significantly increased cancer cell proliferation and invasion (Dong et al., 2018a). However, the silencing of PD-L1 expression in cholangiocarcinoma cells and lung cancer cells promoted tumor growth (Tamai et al., 2014; Wang X. et al., 2020). In patients with melanoma (Taube et al., 2012), colorectal cancer (Droeser et al., 2013), or Merkel-cell carcinoma (Lipson et al., 2013), higher PD-L1 expression was significantly correlated with improved survival, indicating that tumor cell-intrinsic PD-L1 may exert either pro- or anti-tumor functions, and that its roles might be tissue- or tumor-type dependent.

Previous studies have shown conflicting results regarding the expression patterns of PD-L1 and its prognostic value in EC (Marinelli et al., 2019). The fraction of ECs that are positive for PD-L1 expression varied from 14 to 59% (Mo et al., 2016; Li et al., 2018; Engerud et al., 2020). Although it was reported that PD-L1 expression has no significant impact on patient survival (Engerud et al., 2020), recent studies presented contrary results showing that higher PD-L1 expression in EC samples was associated with improved survival (Yamashita et al., 2017; Liu et al., 2019; Zhang et al., 2020). Also, increased PD-L1 expression in EC cells was significantly correlated with well-differentiated histology and a lower risk of myometrial invasion and lymphatic spread (Zhang et al., 2020).

Until now, the biological function of PD-L1 and the mechanisms associated with PD-L1 expression in aggressive EC cells have not yet been explored. In this study, we found that PD-L1 protein expression was frequently downregulated in EC tissues and that increased PD-L1 expression level was associated with prolonged survival rates of EC patients. Our data identified PD-L1 as a novel tumor suppressor in aggressive EC cells and showed that loss of PD-L1 expression enhances the invasive abilities of EC cells by inducing EMT through the upregulation of MCL-1 expression. We further define a molecular mechanism whereby the long non-coding RNA MEG3/microRNA-216a (miR-216a) axis mediates the repression of PD-L1 in aggressive EC cells. Thus, this work uncovered a unique, tumor-suppressor function of PD-L1 in an aggressive subtype of EC, where options for effective treatment are limited.

MATERIALS AND METHODS

Patients and Tissue Specimens

Acquisition and use of human tissue samples was approved by the Research Medical Ethics Committee of Sun Yat-sen University Cancer Center. Written consent was obtained from each patient before sample collection. A total of 65 human primary EC tissues and 18 normal endometrium samples were obtained from the patients who underwent surgical resection without preoperative treatment, at the Sun Yat-sen University Cancer Center. The diagnosis of EC or normal endometrium was confirmed by histological examination. All clinical and pathological features, including tumor grade, tumor stage, tumor size, and myometrial invasion, were obtained from hospital records.

Immunohistochemistry of Human Tissues

Immunohistochemical (IHC) staining was performed as we previously described (Konno et al., 2014). In brief, formalin-fixed, paraffin-embedded tissues of 65 primary EC tissues and 18

normal endometrium tissues were analyzed for the expression of PD-L1. Sections from these tissues were deparaffinized in xylene, rehydrated in grades of alcohol, rinsed in tap water, and blocked with 3% hydrogen peroxide. After antigen retrieval by citrate buffer using a microwave oven, the sections were incubated with the primary antibody against PD-L1 (dilution 1:200, clone E1L3N, Cell Signaling, Danvers, MA, United States) at 4°C overnight. For positive control, this study used human cervical cancer tissues with previously characterized levels of PD-L1 expression (Dong et al., 2018a). Negative control slides without primary antibodies were also included. The IHC staining score was assessed by two experienced pathologists who were blinded to the patients' clinicopathological data. For the purpose of this study, the stromal tissue was excluded from scoring. Scoring was based on intensity and extensity. The percentage of stained cells was determined as: 0 (no positive cell), 1 (<10%), 2 (10–50%), and 3 (>50%). The intensity of IHC staining was determined as: 0 (no staining), 1 (weak staining), 2 (moderate staining), and 3 (strong staining). The overall IHC score of each section was calculated by adding the proportion score to the intensity score of each case (range, 0–6), as previously reported (Konno et al., 2014). Any sample was defined as having positive PD-L1 staining if the overall IHC score was ≥1, and any sample was defined as having negative PD-L1 staining if the overall IHC score was 0. Overall IHC scores of ≥2 were defined as a high expression of PD-L1 staining, and overall IHC scores of <2 were defined as a low expression of PD-L1 staining, based on receiver operating characteristic (ROC) analysis.

Human Cell Lines and Cell Culture

Human EC cell lines, including HEC-50 (JCRB Cell Bank, Osaka, Japan) and HOUA-I (RIKEN Cell Bank, Tsukuba, Japan), were derived from poorly differentiated endometrioid EC. The human EC cell line HEC-1 (JCRB Cell Bank, Osaka, Japan) was derived from a moderately differentiated endometrioid EC and has invasive properties. The highly invasive sub-population of HEC-50 cells (referred to as HEC-50-HI cells) was generated using Matrigel invasion chambers, as we previously described (Dong et al., 2011). The immortalized human endometrial epithelial cell line (EM) was a kind gift from Dr. Satoru Kyo (Shimane University, Japan) (Kyo et al., 2003). The human cervical cancer cell line HeLa was obtained from the American Type Culture Collection (ATCC). These cells were cultured in DMEM/F12 medium (Sigma-Aldrich, St. Louis, MO, United States) supplemented with 10% fetal bovine serum (FBS) (Invitrogen, Carlsbad, CA, United States). The human serous EC cell line SPAC-1-L was kindly provided by Dr. Fumihiko Suzuki (Tohoku University, Sendai, Japan) and maintained in RPMI-1640 medium (Sigma-Aldrich, St. Louis, MO, United States) supplemented with 10% FBS (Invitrogen).

Transient Transfection

The *PD-L1* cDNA expresion vector pCMV6-PD-L1 (PD-L1-vec, RC213071), the *MCL-1* cDNA expression vector pCMV6-MCL-1 (MCL-1-vec, RC200521), the MEG3 expression vector pCMV6-MEG3 (MEG3-vec, SC105816) and the pCMV6 control vector (Ctr-vec, PS100001) were purchased from OriGene (Rockville, MD, United States). The *PD-L1*-specific siRNA (PD-L1-siRNA, s26547), the *MCL-1*-specific siRNA (MCL-1-siRNA, AM51331), the MEG3-specific siRNA (MEG3-siRNA, n272552), the negative control siRNA (Ctr-siRNA, AM4611), miR-216a mimic (PM10545), control mimic (AM17110), miR-216a inhibitor (AM10545) and control inhibitor (AM17010) were purchased from Invitrogen (Carlsbad). The cells were seeded in growth medium at a density of 40–50% 1 day before transfection. Transfection of vector, siRNA, miRNA mimics or miRNA inhibitor into EC cells was carried out using the Lipofectamine 2000 reagent (Invitrogen) following the manufacturer's instructions. After 48 h, the cells were harvested for the following tests.

Western Blotting

Protein extracts for western blotting were prepared in M-Per Mammalian Protein Extraction Reagent (Pierce, Rockford, IL, United States), separated by SDS-polyacrylamide gels, and then transferred to PVDF membrane (GE Healthcare Life Sciences, Piscataway, NJ, United States). Membranes were incubated with primary antibodies including: PD-L1 (1:1000, clone E1L3N, Cell Signaling), MCL-1 (1:1000, #4572, Cell Signaling), ZO-1 (1:1000, #5406, Cell Signaling), Vimentin (1:1000, A01189, GenScript, Edison, NJ, United States), and GAPDH (1:3000, sc-47724, Santa Cruz Biotechnologies, Santa Cruz, CA, United States), and then with HRP-conjugated secondary antibody. Finally, blots were developed with the ECL detection kit (Amersham Pharmacia Biotech, United Kingdom). GAPDH served as the loading control. Immunoblot images were quantified using the NIH Image software.

PD-L1 Knockdown and Overexpression in EC Cells

To silence *PD-L1* gene expression, lentiviral particles encoding two short hairpin RNA RNAs (shRNAs: HSH064502 and HSH099746) targeting *PD-L1* and a control shRNA (CSHCTR001) were purchased from Genecopoeia (Guangzhou, China). Stably transfected HEC-50 cells were selected using 1 μg/mL puromycin (Sigma-Aldrich, St. Louis, MO, United States). For overexpressing PD-L1 in SPAC-1-L cells, PD-L1-vec and Ctr-vec were used to transfect SPAC-1-L cells using the Lipofectamine 2000 reagent (Invitrogen). Stable PD-L1-overexpressing SPAC-1-L cells and control cells were selected using 0.5 mg/mL neomycin (Sigma-Aldrich, St. Louis, MO, United States) and confirmed by western blotting for PD-L1.

Cell Proliferation Assay

Cell proliferation was investigated using the Cell Counting Kit-8 (CCK-8) assay (Dojindo, Japan) according to the manufacturer's instructions. Five thousand cells were seeded per well in a 96-well plate and cultured for the indicated times. 10 μl of CCK-8 reagent was added into each well and incubated for 1 h. The absorbance was assessed at 450 nm by a microplate reader

(Bio-Rad, Hercules, CA, United States). Each experiment was performed in triplicate.

Wound-Healing Assay

Wound-healing assay was performed as previously described (Konno et al., 2014). In brief, confluent cells were scraped by a 200 μl pipette tip to create a wound, and debris was removed by PBS washing. Growth media were replaced with fresh media containing Mitomycin C (5 μg/ml, Sigma-Aldrich, St. Louis, MO, United States) and incubated for 12 h. Cells were imaged after creation of the wound and 12 h later. Distance migrated was quantitated by taking pictures at 0 and 12 h.

Transwell Invasion Assay and Transwell Migration Assay

For invasion assays, 5×10^4 cells suspended in medium without FBS were plated on the upper wells of Matrigel-coated Transwell plates (8 μm pore size, Corning Costar Co., Lowell, CA, United States). The insert was incubated in 750 μl medium with 10% FBS. After culturing for 24 h, the membranes were treated with 10% formaldehyde for 3 min, and then stained with 2% crystal violet for 15 min at room temperature. The non-invasive cells were removed by swiping the top of membrane with cotton swabs. Cells that invaded across the transwell membrane were counted using a light microscope in 10 randomly selected high-power fields. Transwell migration assays were performed in the same manner as the transwell invasion assays, except that the membrane was not coated with Matrigel, and the incubation time was 12 h.

Caspase-Glo 3/7 Assay

The enzymatic activity of caspase-3/7 was determined using the Caspase-Glo 3/7 assay kit following the manufacturer's instructions (Promega, Madison, WI, United States), as previously reported (Konno et al., 2014). Briefly, 3×10^3 cells were plated in triplicates in 96-well plates and transfected as indicated. An equal amount of Caspase-Glo 3/7 substrate was added to the culture and subsequently incubated for 3 h. Following incubation, caspase-3/7 activities were evaluated as an indicator of cell apoptosis using a GloMax-96 Microplate luminometer (Promega). The results were shown as the fold change relative to the control cells.

Gain-of-Function Screening for PD-L1 Based on Cell Functional Assays

The indicated EC cell lines or human cervical cancer cell line HeLa were transiently transfected with PD-L1-vec or Ctr-vec using the Lipofectamine 2000 reagent (Invitrogen). After incubation for 48 h, cell proliferation, apoptosis, migration, and invasion were determined using CCK-8 assay, Caspase-Glo 3/7 assay, transwell migration assay, and transwell invasion assay, respectively. The results were given as the fold changes in cell proliferation, apoptosis, migration and invasion of the PD-L1-vec-transfected cells as compared to the Ctr-vec-transfected cells.

Quantitative Reverse Transcription-PCR (qRT-PCR)

Total RNA was isolated with the TRIzol reagent (Invitrogen). Total mRNA was reversely transcribed into cDNA using an M-MLV Reverse Transcriptase Kit (Invitrogen). Quantitative RT-PCR was performed using SYBR Premix Ex Taq II (Takara, Shiga, Japan) in an ABI-7300 Real-Time PCR system (Applied Biosystems, Foster City, CA, United States). The primers used were as follows: human *PD-L1*, sense: GTGGC ATCCAAGATACAAACTCAA, anti-sense: TCCTTCCTCTTG TCACGCTCA; human *ZO-1*, sense: GGAGAGGTGTTCCG TGTTGT, anti-sense: GAGCGGACAAATCCTCTCTG; human *Vimentin*, sense: TGAGTACCGGAGACAGGTGCAG, anti-sense: TAGCAGCTTCAACGGCAAAGTTC; human *Snail*, sense: GACCACTATGCCGCGCTCTT, anti-sense: TCGCTy GTAGTTAGGCTTCCGATT; human *MCL-1*, sense: CCAAGG CATGCTTCGGAAA, anti-sense: TCACAATCCTGCCCCAG TTT; human MEG3, sense: TCCATGCTGAGCTGCTGCCAAG, anti-sense: AGTCGACAAAGACTGACACCC; and human *GAPDH*, sense: GAAGGTGAAGGTCGGAGTC, anti-sense: GAAGATGGTGATGGGATTTC. *GAPDH* was used as an internal control. The levels of miR-138/193a/216a/217 were measured using the NCode SYBR GreenER miRNA qRT-PCR analysis kit (Invitrogen) according to the manufacturer's protocol. The forward primers for miRNA analysis had the same sequences as the mature miRNAs. The relative expression of these miRNAs was normalized against that of the U6 endogenous control.

Luciferase Reporter Assay

Human *PD-L1* 3′-untranslated region (3′-UTR) luciferase reporter vector and the Luc-Pair™ Duo-Luciferase Assay Kit were purchased from GeneCopoeia (Rockville, MD, United States). Mutations (MUT) of the miR-216a binding site in the *PD-L1* 3′-UTR were generated using a QuickChange site-directed mutagenesis kit (Stratagene, La Jolla, CA, United States). EC cells with 60–70% confluency were co-transfected with the wild-type (WT) or mutant *PD-L1* 3′-UTR luciferase reporter vector, together with miR-216a mimic, miR-216a inhibitor, or the respective control, using the Lipofectamine 2000 reagent (Invitrogen). 48 h later, cell lysates were collected and the Firefly and Renilla luciferase activities of each group were tested following the protocol of the Luc-Pair™ Duo-Luciferase Assay Kit (GeneCopoeia). The Firefly luciferase activities were normalized by Renilla luciferase activities.

Statistical Analysis

All experiments were carried out with at least three replicates. Data are presented as the mean ± standard error of the mean. Statistical analysis was performed using SPSS 18.0 statistical software (SPSS, Chicago). Comparisons between two groups were made using the two-tailed Student's *t*-tests and Mann–Whitney *U* tests. The χ^2-tests and Fisher's exact tests were applied to analyze the relationship between PD-L1 expression and clinicopathological status. Differences were considered statistically significant when $P < 0.05$.

RESULTS

Downregulation of PD-L1 Correlates With Poor Survival in EC

First, the mRNA expression of *PD-L1* in different cancer types was assessed by comparing normal vs. tumor tissues using the UALCAN portal, which contains the Cancer Genome Atlas (TCGA) gene expression data from 31 cancer types for further analysis (Chandrashekar et al., 2017). Consistent with our previous study (Dong et al., 2018a), we observed relatively higher levels of PD-L1 in human cervical cancer tissues as compared to normal tissues (**Figure 1A**). Interestingly, the mRNA expression of *PD-L1* in primary EC tissues was lower than that in the normal samples (**Figure 1A**). To verify these results, we examined the expression of *PD-L1* in the TCGA datasets at the Firebrowse website (Deng et al., 2017). The results revealed that *PD-L1* expression was clearly elevated in cervical cancer tissues compared with normal tissues (**Figure 1B**). However, EC tissues showed a decrease in PD-L1 levels as compared to normal tissues (**Figure 1B**). Similarly, the comparison of PD-L1 expression in EC tissues vs. normal tissues though the Wanderer and ENCORI databases (Li et al., 2014; Díez-Villanueva et al., 2015) demonstrated significantly lower expression of PD-L1 in EC tissues (**Figures 1C,D**).

To determine whether PD-L1 protein expression was also differentially regulated in EC tissues, we extracted the IHC images from the Human Protein Atlas (HPA) database (Uhlén et al., 2015). As expected, PD-L1 was expressed at high levels in human cervical cancer tissues but not in the adjacent normal tissues (**Figure 1E**). In contrast, IHC staining of EC tissues and adjacent normal tissues with the same antibody showed that PD-L1 levels are very low or completely absent in most EC cells (**Figure 1E**).

To establish the prognostic importance of PD-L1 expression in EC, we visited the KM plotter (Nagy et al., 2018) and HPA databases to analyze the effects of PD-L1 expression in patients with EC. Higher expression of PD-L1 was associated with increased overall survival in EC patients (**Figure 1F**). When individual tumor grades (1, 2, and 3) were considered, higher PD-L1 represented a favorable factor for the prognosis of EC patients at histological grade 3 ($P = 0.014$) (**Supplementary Figure 1**). There was a marginally significant relationship between increased PD-L1 expression and improved overall survival in patients at histological grade 2 ($P = 0.073$) (**Supplementary Figure 1**). There was no association of PD-L1 expression with survival in EC patients at histological grade 1 (data not shown). These results suggested that increased PD-L1 expression predicts favorable survival in EC (practically those patients with high-grade disease).

The Protein Expression of PD-L1 Is Downregulated in Human EC Tissues, and PD-L1 Acts as a Tumor Suppressor in Aggressive EC Cells

To further explore the expression of PD-L1 in EC, we examined PD-L1 protein expression in 65 primary EC tissues and 18 normal endometrium tissues using IHC analysis. For our study, we used a rabbit monoclonal antibody (clone E1L3N, Cell Signaling), which is highly sensitive and specific for the detection of PD-L1 protein (Kluger et al., 2017; Keller et al., 2018), and which was validated in our previous IHC study (Dong et al., 2018a).

The positive PD-L1 staining in EC cells was localized mainly in the cytoplasm, although some membranous localization was seen (**Figure 2A**). As illustrated in **Figure 2B**, PD-L1 was broadly expressed in normal tissues; however, PD-L1 expression was absent or low in EC tissues. The positive staining rate of PD-L1 was 84% in benign samples, but only 12% in EC samples ($P < 0.00001$) (**Figure 2B**). Moreover, the mean PD-L1 staining score in EC tissues was significantly lower than that in normal tissues ($P = 0.00001$) (**Figure 2C**). A trend of higher PD-L1 expression was noted in patients younger than 50 years, and in patients with low-grade tumors (grade 1/2), early stage tumors (stage I), smaller tumor size (tumor diameter $\leq$3 cm), or superficial myometrial invasion ($\leq$1/2), although this did not reach statistical significance ($P > 0.05$) (**Supplementary Figure 2**).

Consistent with the immunocytochemistry results, our western blotting analysis confirmed that PD-L1 protein was expressed at lower levels in all aggressive EC cell lines compared to a normal endometrial cell line (EM) (**Figure 2D**). In particular, PD-L1 expression in the serous EC cell line SPAC-1-L was much weaker than that in other EC cells (**Figure 2D** and **Supplementary Figure 3A**). HEC-50-HI cells, the sub-population of HEC-50 cells, are more invasive than the parental HEC-50 cells and exhibit mesenchymal phenotypes (Dong et al., 2011). Interestingly, HEC-50-HI cells showed lower levels of PD-L1 expression than the parental cells (**Figure 2D**), indicating that PD-L1 may modulate the invasive properties of aggressive EC cells.

To examine this possibility, we transfected the human *PD-L1* cDNA expression vector or the control vector into five aggressive EC cell lines and cervical cancer cell line HeLa for 48 h, and performed a gain-of-function screening using cell functional assays. Consistent with our previous observations (Dong et al., 2018a), we found that the overexpression of PD-L1 could significantly enhance the proliferation, migration, and invasion, but reduce apoptosis of HeLa cells (**Figure 2E**). Our functional screening revealed that overexpressing PD-L1 expression in all aggressive EC cells significantly attenuated cell proliferation, migration, and invasion, while inducing cell apoptosis (**Figure 2E**). Taken together, these results indicated that loss of PD-L1 protein expression is a frequent event in EC, and that PD-L1 plays tumor-suppressive roles in aggressive EC cells.

Loss of PD-L1 Induces Cell Proliferation and Triggers EMT in Aggressive EC Cells

Next, we investigated whether decreased PD-L1 expression is required for enhanced aggressive EC cell proliferation and invasiveness. We established SPAC-1-L cells stably overexpressing PD-L1 and control cells (**Figure 3A** and **Supplementary Figure 3B**), as well as HEC-50 cells stably expressing control shRNA, or two PD-L1 shRNAs (PD-L1-sh-1

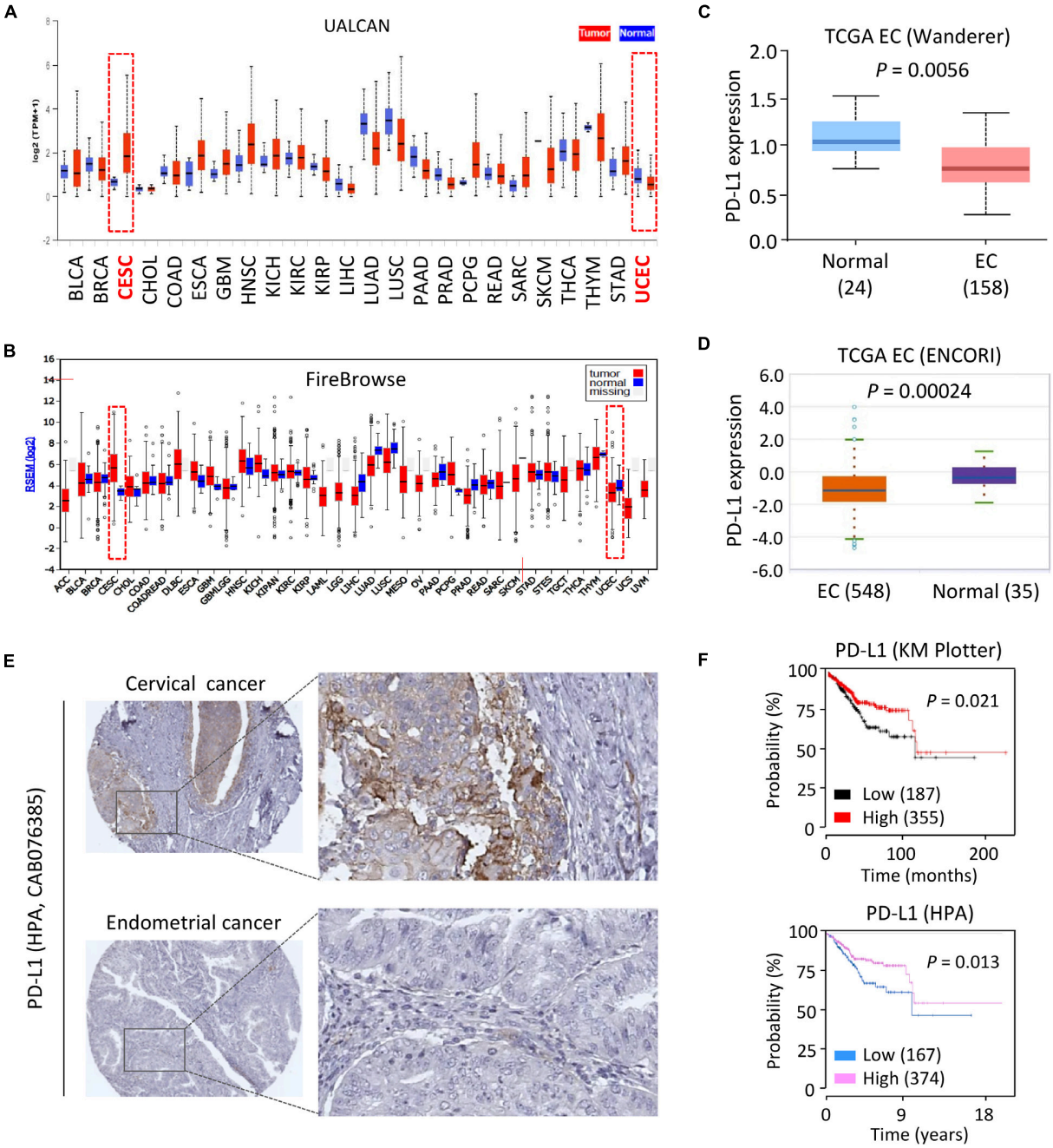

FIGURE 1 | Downregulation of PD-L1 Correlates with Poor Survival in EC. **(A,B)** Analysis of PD-L1 expression in human cancer tissues and normal tissues using the TCGA data retrieved from the UALCAN database **(A)**, and FireBrowse database **(B)**. CESC: human cervical cancer; UCEC: human endometrial cancer. **(C,D)** PD-L1 mRNA expression in EC samples and normal samples was analyzed using the Wanderer database **(C)** and ENCORI database **(D)**. **(E)** IHC staining for PD-L1 in human cervical cancer tissues and EC tissues with the same antibody (CAB076385, the HPA website) showed that high levels of PD-L1 were present in primary cervical cancer tissues. In contrast, PD-L1 was negatively or weakly stained in most EC tissues. **(F)** The probability of overall survival in EC patients expressing high or low PD-L1 levels was assessed using the KM plotter database (upper) and the HPA database (bottom). Red indicates CESC (human cervical cancer) or UCEC (human endometrial cancer).

or PD-L1-sh-2) that silenced PD-L1 expression (**Figure 3A** and **Supplementary Figure 3B**). Because PD-L1-sh-2 showed better performance than PD-L1-sh-1, we used PD-L1-sh-2 for all the downstream experiments.

Although SPAC-1-L cells are invasive, this cell displays an epithelial-like morphology. Overexpression of PD-L1 did not influence the appearance of SPAC-1-L cells (data not shown). However, PD-L1 knockdown in HEC-50 cells

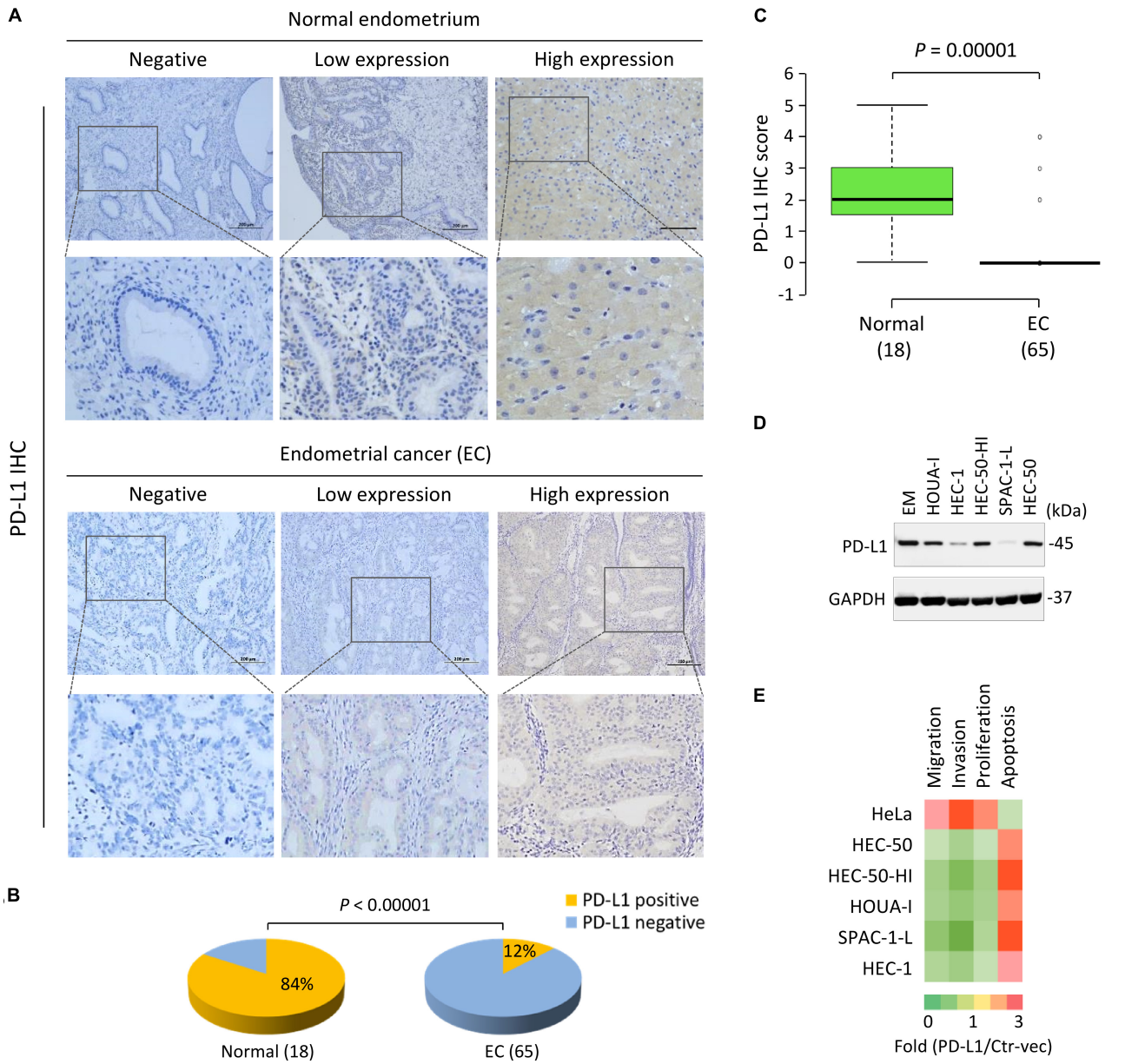

FIGURE 2 | PD-L1 is Frequently Downregulated in EC Tissues and Acts as a Tumor Suppressor in Aggressive EC Cells. **(A)** Representative immunohistochemical staining (IHC) images of PD-L1 in EC tissues and normal endometrium tissues. Scale bar, 200 μm. PD-L1 staining was mostly detected in cell cytoplasm and membrane. **(B)** The pie chart showing the percentages of the population with PD-L1-negative or PD-L1-positive expression in EC tissues and normal endometrium tissues, determined by IHC analysis. **(C)** The mean PD-L1 staining score in EC tissues and normal tissues. The mean PD-L1 staining score in EC tissues was significantly lower than that in the normal tissues. **(D)** PD-L1 protein levels in a normal endometrial cell line (EM) and human aggressive EC cell lines were determined by western blot analysis. **(E)** A gain-of-function screening for PD-L1 that affects the proliferation, apoptosis, migration and invasion of aggressive EC cells. The indicated EC cell lines or human cervical cancer cell line HeLa were transiently transfected with PD-L1 expression vector (PD-L1-vec) or the control vector (Ctr-vec), and subjected to cell functional assays. Heatmap depicting the fold changes in cell proliferation, apoptosis, migration and invasion of the PD-L1-vec-transfected cells when compared with the Ctr-vec-transfected cells.

induced cell scattering (**Figure 3B**). Compared to control cells, overexpression of PD-L1 significantly decreased the proliferative and invasive capabilities of SPAC-1-L and HEC-50 cells, while silencing of PD-L1 in HEC-50 and SPAC-1-L cells significantly enhanced these abilities (**Figures 3C–E** and **Supplementary Figures 4A–C**). These results indicated that EMT may be involved in the PD-L1-suppressed migratory and invasive abilities of aggressive EC cells.

Using the Expression Atlas database (Papatheodorou et al., 2020), which includes RNA sequencing datasets from human cancer cell lines, we generated a heatmap showing the expression levels of *PD-L1*, EMT regulators (*MCL-1* and *Snail*), epithelial

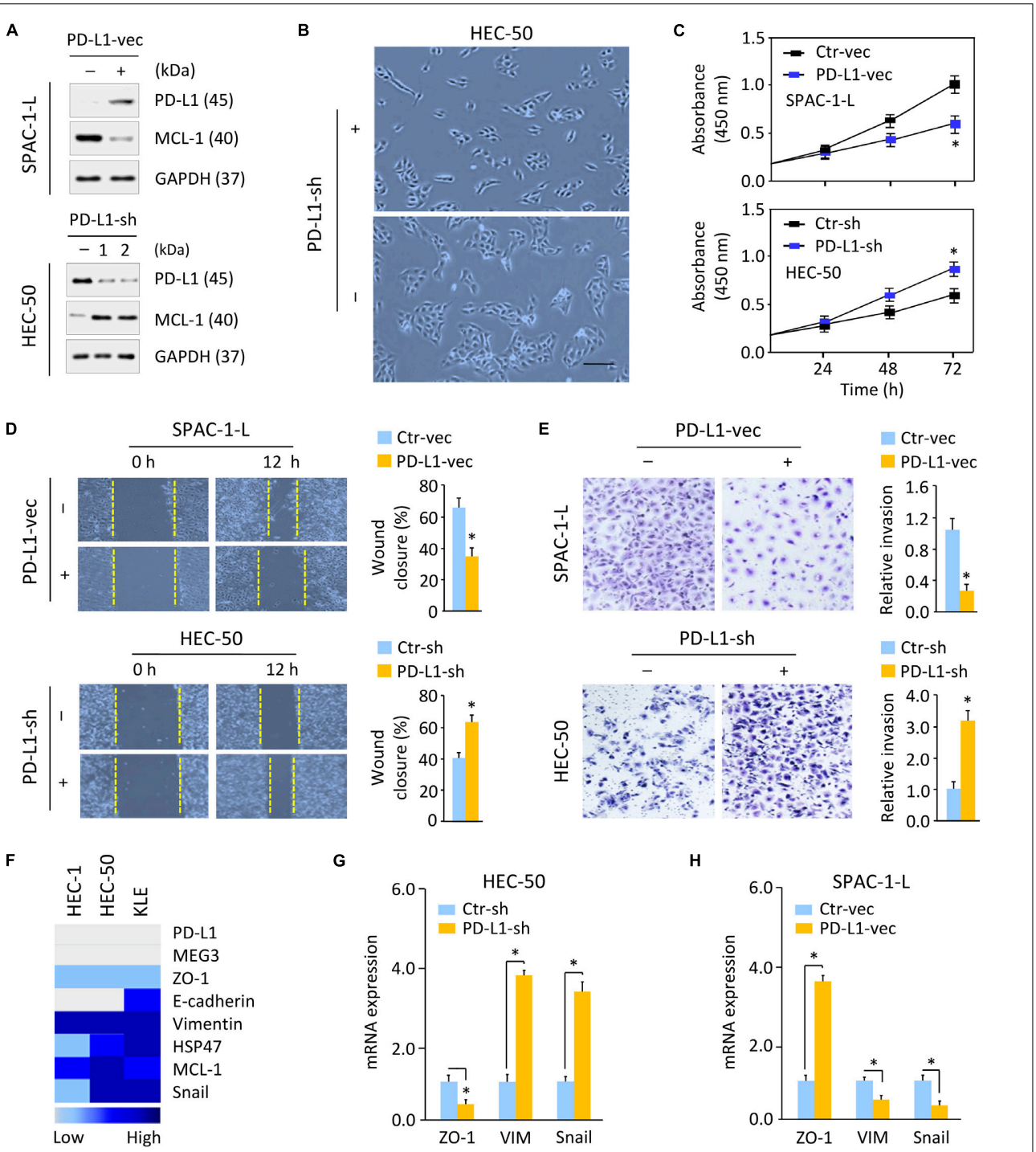

FIGURE 3 | Loss of PD-L1 Induces Cell proliferation and Triggers EMT in Aggressive EC Cells. **(A)** Western blotting analysis of PD-L1 and MCL-1 expression in SPAC-1-L cells overexpressing PD-L1, and in PD-L1-silenced HEC-50 cells. **(B)** Cellular morphology of HEC-50 cells after knockdown of PD-L1. Scale bar, 100 μm. **(C–E)** Proliferation **(C)**, wound-healing **(D)**, and invasion **(E)** assays in EC cells after overexpression or knockdown of PD-L1. **(F)** A heatmap showing gene expression levels in human aggressive EC cell lines (Expression Atlas database). **(G,H)** Examination of gene expression in HEC-50 cells after knockdown of PD-L1 **(G)** and in SPAC-1-L cells after overexpression of PD-L1 **(H)** was performed using qRT-PCR assays. VIM, Vimentin. *$P < 0.05$.

markers (*E-cadherin* and *ZO-1*) and mesenchymal markers (*Vimentin* and *HSP47*) in three aggressive EC cell lines (HEC-1, HEC-50, and KLE). These cells expressed low levels of *PD-L1*, *E-cadherin*, and *ZO-1*, but high levels of *MCL-1*, *Snail*, *Vimentin*, and *HSP47* (**Figure 3F**). Western blotting and qRT-PCR analysis confirmed that, knocking down PD-L1 in HEC-50 cells enhanced

the expression of MCL-1, *Vimentin*, and *Snail*, and reduced the levels of *ZO-1* (**Figures 3A,G**). We also observed that overexpression of PD-L1 in SPAC-1-L cells led to the inhibition of EMT, featured with upregulation of *ZO-1*, and downregulation of MCL-1, *Vimentin*, and *Snail* (**Figures 3A,H**). Together, these data suggested that PD-L1 antagonizes EMT signaling-regulated migration and invasion in aggressive EC cells.

PD-L1 Represses EMT by Decreasing MCL-1 Expression

As our previous findings pointed out the involvement of MCL-1 in EMT and the invasion of aggressive EC cells (Konno et al., 2014), we addressed whether PD-L1 regulates the EMT process and the invasion of HEC-50 cells by modulating MCL-1. We found that the silencing of MCL-1 expression with MCL-1-specific siRNA largely reversed PD-L1-sh-induced mesenchymal cellular morphology, and significantly inhibited the migratory and invasive ability that was enhanced by knockdown of PD-L1 (**Figures 4A–C**). Our western blotting assays further demonstrated that siRNA-induced downregulation of MCL-1 could abrogate the repression of ZO-1, and the induction of Vimentin expression by PD-L1 inhibition (**Figure 4D** and **Supplementary Figure 3C**). We then asked whether PD-L1 reduced cell growth and invasiveness through repressing MCL-1 expression in SPAC-1-L cells. Overexpression of PD-L1 in SPAC-1-L cells caused an upregulation of ZO-1 and a downregulation of Vimentin, and significantly reduced cell growth and invasion. However, restoration of MCL-1 partially abolished these effects of PD-L1 (**Supplementary Figures 5A,B**).

The IHC staining images for MCL-1, ZO-1, and HSP47 were obtained from the HPA database. The IHC staining of EC tissues from the same patient showed a high MCL-1 and HSP47 expression and a low ZO-1 expression in EC tissues as compared to adjacent normal tissues (**Figure 4E**). The correlation between *MCL-1*, *ZO-1*, and *HSP47* expression and overall survival was analyzed using the KM plotter database. Kaplan–Meier survival analysis showed that those EC patients with high levels of *MCL-1* and *HSP47* and low levels of *ZO-1* had a significantly worse overall survival rate (**Figure 4F**). Taken together, these data demonstrated that PD-L1 represses the EMT features of aggressive EC cells by reducing MCL-1 protein expression.

PD-L1 Is a Direct Target of Oncogenic MiR-216a

We sought to identify the potential miRNAs that directly target *PD-L1* in aggressive EC cells. A flowchart describing our screening process of miRNAs was shown in **Figure 5A**. We first performed a miRNA prediction analysis using the TargetScan[1] and miRcode databases[2]. As a result, 31 miRNAs appeared simultaneously in these two databases. Next, screening of the KM plotter database enabled us to find 12 miRNAs, whose expression is associated with a worse prognosis in EC (**Supplementary Figure 6**). Analysis of the TCGA EC datasets through the miR-TV database (Pan and Lin, 2020) showed that, nine miRNAs exhibited a significantly higher expression in EC tissues compared with normal tissues (**Supplementary Figure 7A**). The expression of these nine miRNAs in TCGA EC tissues was examined using the cBioPortal database (Gao et al., 2013). Four miRNAs, including miR-138, miR-193a, miR-216a, and miR-217, were amplified in patients with EC (**Supplementary Figure 7B**).

Using qRT-PCR assays, we validated that, of the four miRNAs, only miR-216a and miR-217 were consistently upregulated in aggressive EC cells as compared to EM cells (**Figure 5B** and **Supplementary Figure 7C**). Thus, we determined that miR-216a and miR-217 were likely candidates for further investigation. Compared to the respective controls, the mRNA expression of *PD-L1* decreased markedly when miR-216a (but not miR-217) was overexpressed in HEC-50 cells (**Figure 5C**). Conversely, the expression of PD-L1 increased significantly after miR-216a (but not miR-217) was inhibited in SPAC-1-L cells (**Figure 5C**).

Luciferase reporter assays were further conducted by employing a luciferase reporter vector containing the *PD-L1* 3′-UTR sequence flanking the putative binding site of miR-216a. Mutations in the putative binding sites were created as controls. The overexpression of miR-216a significantly reduced the luciferase activities of WT *PD-L1* 3′-UTR in HEC-50 cells, and the inhibition of miR-216a increased the luciferase activities of WT *PD-L1* 3′-UTR in SPAC-1-L cells (**Figure 5D**). The transfection with miR-216a mimic or miR-216a inhibitor into EC cells showed no significant effects on the luciferase activities of MUT *PD-L1* 3′-UTR (**Figure 5D**). These results were validated by western blotting assays showing that overexpression of miR-216a suppressed the protein expression of PD-L1, whereas inhibition of miR-216a increased the levels of PD-L1 in EC cells (**Figure 5E** and **Supplementary Figure 3D**). These data suggested that PD-L1 is a direct target of miR-216a in aggressive EC cells.

To determine the role of miR-216a in aggressive EC cells, we overexpressed miR-216a in HEC-50 cells that have a low endogenous expression of miR-216a, and also transfected miR-216a inhibitor into SPAC-1-L cells expressing high levels of miR-216a. Overexpression of miR-216a significantly induced the migration and invasion of HEC-50 cells (**Figure 5F**). Cell migration and invasion were significantly reduced in SPAC-1-L cells following knockdown of miR-216a (**Figure 5G**). Consistently, the mRNA expression of *MCL-1* and *Vimentin* was upregulated, whereas the levels of *ZO-1* were decreased, when miR-216a was overexpressed (**Figure 5H**). In contrast, miR-216a-silenced SPAC-1-L cells showed decreased *MCL-1* and Vimentin, and increased *ZO-1* expression (**Figure 5H**). These results demonstrated that PD-L1 is a direct target of oncogenic miR-216a in aggressive EC cells.

MEG3 Acts as an Upstream Regulator of MiR-216a and PD-L1

Long non-coding RNAs play key roles in human cancers, including aggressive EC (Dong et al., 2019b). Several lncRNAs, such as NEAT1 and MEG3, were reported to regulate cancer tumorigenesis and metastasis through their interactions

[1]http://www.targetscan.org/vert_72/

[2]http://www.mircode.org/

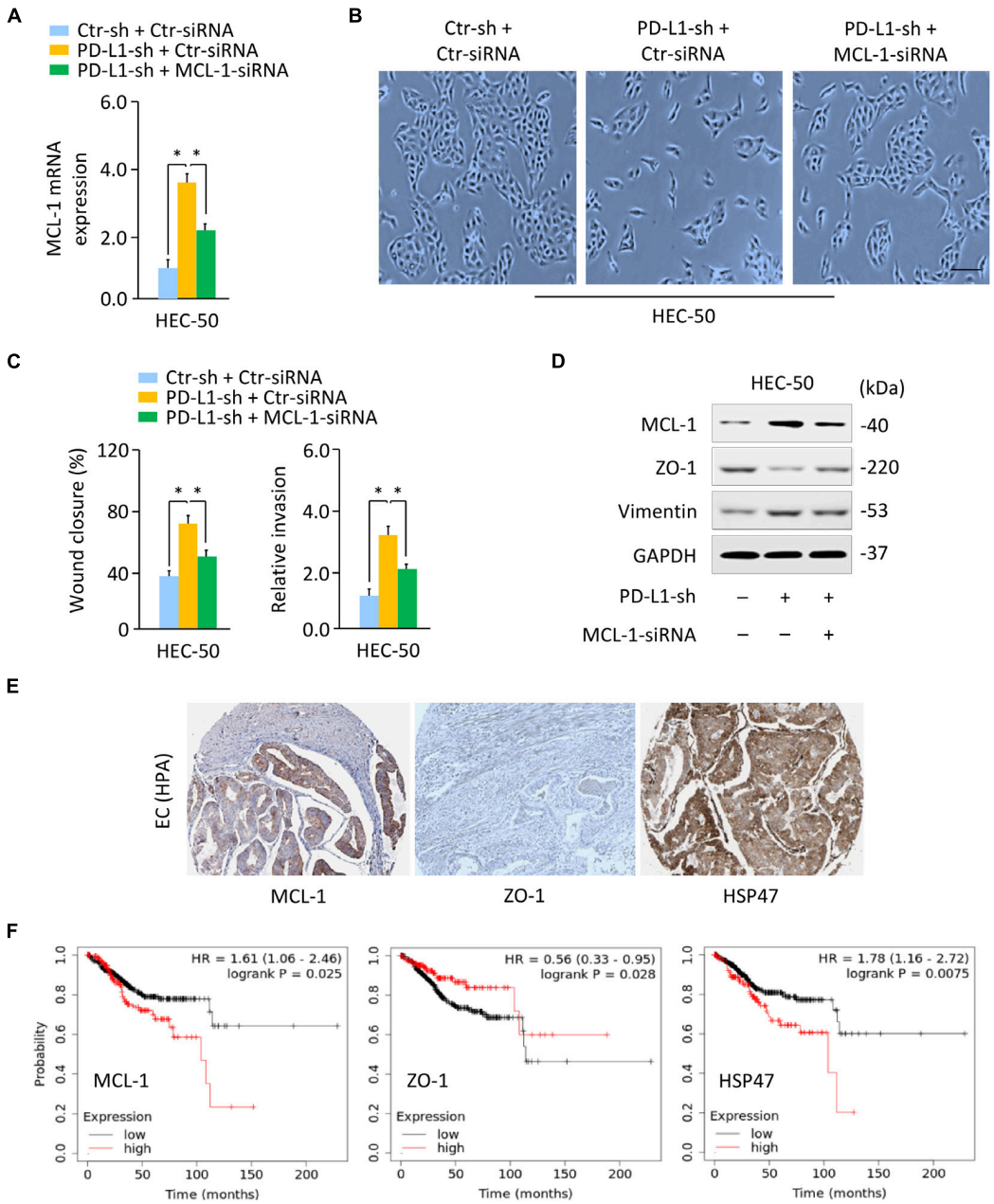

FIGURE 4 | PD-L1 Represses EMT by Decreasing MCL-1 Expression. **(A)** PD-L1-silenced HEC-50 cells or control cells were transfected with (or without) MCL-1 siRNA, and *MCL-1* mRNA expression was verified using qRT-PCR analysis. **(B)** Cellular morphology of HEC-50 cells shown in panel **(A)**. Scale bar, 100 μm. **(C)** Wound-healing and invasion assays in HEC-50 cells transfected as indicated. **(D)** Western blotting analysis of the indicated proteins in HEC-50 cells transfected as indicated. **(E)** The IHC staining results were obtained from the HPA database. Immunohistochemical staining of EC tissues from the same patient showed a high MCL-1 and HSP47 expression and a low ZO-1 expression in EC tissues. **(F)** The correlation between the indicated genes and overall survival in patients with EC (KM plotter database). $^*P < 0.05$.

with DNA, RNA, and proteins (Dong et al., 2018b, Dong et al., 2019a,b). To elucidate the mechanisms governing PD-L1 expression, we predicted the lncRNAs that may interact with miR-216a, by performing a sequence alignment analysis through the ENCORI and LncBase Predicted v.2 databases (Paraskevopoulou et al., 2016). To increase the prediction accuracy, we extracted the overlapping part of the prediction results across these two databases, and identified 26 candidate lncRNAs (data not shown). Analysis of the TCGA EC database in the GEPIA database (Tang et al., 2017) further showed that, high expression of three candidate lncRNAs (including MEG3, RPARP-AS1, and SNHG5) was a favorable prognostic marker for EC (**Supplementary Figure 8A**). According to the results from the ENCORI database, only MEG3 (but not RPARP-AS1

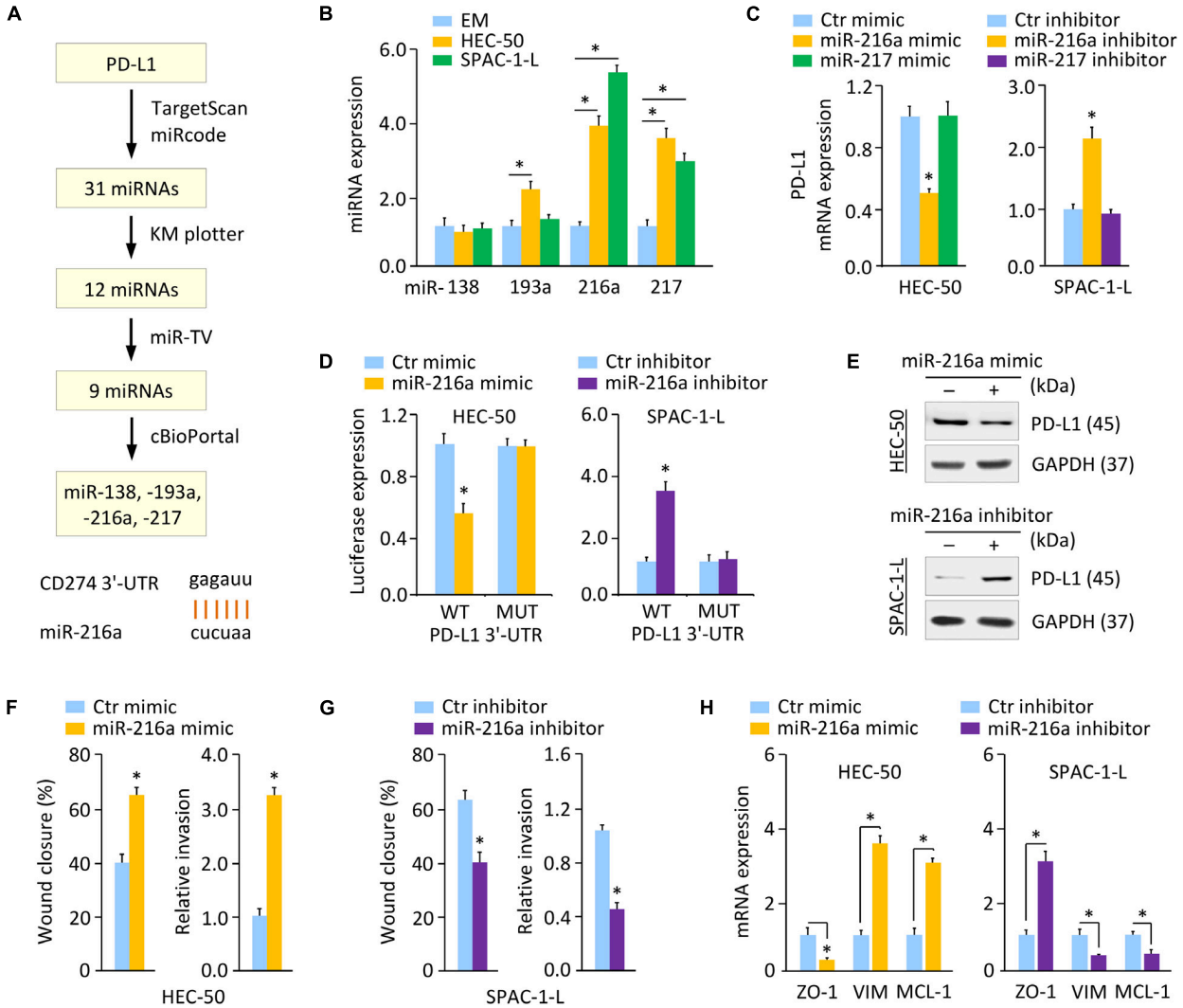

FIGURE 5 | PD-L1 is a Direct Target of Oncogenic MiR-216a. **(A)** Workflow for identifying potential miRNAs that regulate the expression of PD-L1 (upper). Computational prediction of duplex formation between miR-216a with the *PD-L1* 3′-UTR sequence (bottom). **(B)** qRT-PCR analysis of the indicated miRNAs in HEC-50, SPAC-1-L, and EM cells. **(C)** *PD-L1* mRNA expression was examined using qRT-PCR assays in EC cells transfected as indicated. **(D)** Luciferase reporter assays in EC cells transfected with the wild-type (WT) or mutant (MUT) *PD-L1* 3′-UTR, along with miR-216a mimic or miR-216a inhibitor, respectively. **(E)** Western blotting analysis of PD-L1 expression in HEC-50 cells transfected with miR-216a mimic (or control mimic), and in SPAC-1-L cells transfected with miR-216a inhibitor (or control inhibitor). **(F,G)** Wound-healing and invasion assays in HEC-50 cells after overexpression of miR-216a **(F)**, or in SPAC-1-L cells after knockdown of miR-216a **(G)**. **(H)** The mRNA expression of the indicated genes was examined in HEC-50 cells after overexpression of miR-216a, and in SPAC-1-L cells after knockdown of miR-216a. VIM: Vimentin. $^*P < 0.05$.

and SNHG5) exhibited significantly lower expression in TCGA EC tissues as compared to the normal tissues (**Figure 6A**). Comparison of the expression of MEG3 in three aggressive EC cell lines (HEC-1, HEC-50, and KLE) via the Expression Atlas database revealed that, similar to *PD-L1* and *ZO-1*, the expression level of MEG3 was also low in these cells (**Figure 3F**). Using qRT-PCR analysis, we discovered that the levels of MEG3 were significantly downregulated in HEC-50 and SPAC-1-L cells compared with EM cells (**Figure 6B**), suggesting a potential tumor-suppressor role for MEG3 in aggressive EC cells.

Long non-coding RNAs were considered to act as sponges for miRNAs and inhibit their expression (Dong et al., 2018b, Dong et al., 2019a). Given that MEG3 acts as a tumor suppressor to regulate EC progression by functioning as a competing endogenous RNA (Dong et al., 2019b), and that MEG3 contains the predicted miR-216a-binding site (**Supplementary Figure 8B**), we speculated that MEG3 might positively regulate the levels of PD-L1 by decreasing miR-216a expression in aggressive EC cells. In line with this notion, knocking down MEG3 promoted but the ectopic expression of MEG3 inhibited miR-216a expression in aggressive EC cells (**Figures 6C,D**). The role of MEG3 in suppressing cell migration was confirmed by wound-healing assays in HEC-50 and SPAC-1-L cells (**Figure 6E,F**). Consistent with these results, we found that

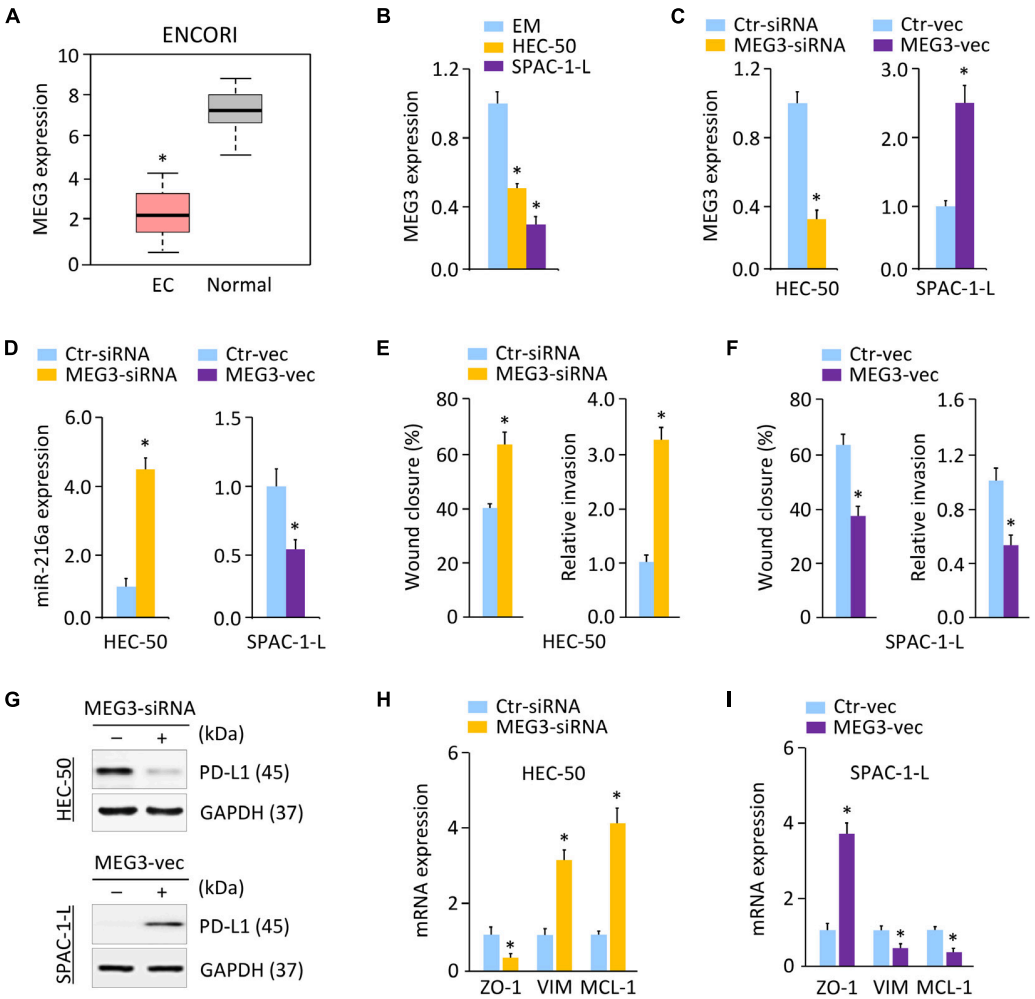

FIGURE 6 | MEG3 Acts as an Upstream Regulator of MiR-216a and PD-L1. **(A)** MEG3 expression in TCGA EC tissues and normal tissues (ENCORI database). **(B)** qRT-PCR analysis of MEG3 expression in HEC-50, SPAC-1-L and EM cells. **(C)** MEG3 levels in HEC-50 cells transfected with MEG3 siRNA (or control siRNA), and in SPAC-1-L cells transfected with MEG3 expression vector (or control vector). **(D)** miR-216a expression was measured in HEC-50 cells transfected with MEG3 siRNA (or control siRNA), and in SPAC-1-L cells transfected with MEG3 expression vector (or control vector). **(E)** Wound-healing and invasion assays in HEC-50 cells transfected as indicated. **(F)** Wound-healing and invasion assays in SPAC-1-L cells transfected as indicated. **(G)** Examination of PD-L1 expression in HEC-50 cells following knockdown of MEG3, and in SPAC-1-L cells following overexpression of MEG3, using western blotting assays. **(H,I)** The mRNA expression of the indicated genes in HEC-50 cells following knockdown of MEG3, and in SPAC-1-L cells following overexpression of MEG3. VIM: Vimentin. $^*P < 0.05$.

knockdown of MEG3 inhibited the protein expression of PD-L1 compared to control cells, while overexpression of MEG3 increased the expression of PD-L1 in EC cells (**Figure 6G** and **Supplementary Figure 3E**). Our qRT-PCR experiments showed that transfection with MEG3-specific siRNA downregulated *ZO-1*, and upregulated *Vimentin* and *MCL-1* in HEC-50 cells (**Figure 6H**). However, overexpression of MEG3 had the opposite effects in SPAC-1-L cells (**Figure 6I**). As expected, the inhibition of MEG3 in SPAC-1-L cells significantly induced cell proliferation and invasion, whereas overexpression of MEG3 could significantly reduce the proliferation and invasion of HEC-50 cells (**Supplementary Figures 9A–C**). Taken together, these data supported the possibility that MEG3 negatively regulates the expression of miR-216a, thus abolishing the miR-216a-induced repressive effects on the *PD-L1* 3′-UTR.

DISCUSSION

The incidence rate of aggressive EC has been rapidly increasing in the United States and Japan (Yamagami et al., 2017; Clarke et al., 2019). The highly metastatic and often treatment-refractory nature of aggressive EC correlates with poor patient survival (Gaber et al., 2016). A better understanding of the mechanisms behind the tumorigenesis and metastasis of aggressive EC is urgently needed to improve the early diagnosis and effective treatment of this cancer. EMT induction and immune evasion have been demonstrated to promote cancer development (Valastyan and Weinberg, 2011; Gonzalez et al., 2018). Although recent studies have linked EMT processes to immune escape (Terry et al., 2017; Dong et al., 2018c), little is known about the functional significance of PD-L1 in

aggressive EC cells. Our study demonstrates a new tumor-suppressor role of PD-L1 in repressing the proliferation and EMT-associated migration and invasion in aggressive EC cells, and reveals that the downregulation of MEG3 and induction of its downstream effector miR-216a is likely a novel mechanism underlying the downregulation of PD-L1 observed in EC tissues (**Figure 7**).

The expression pattern of PD-L1 and its prognostic value in EC is seemingly controversial in the literature (Mo et al., 2016; Li et al., 2018; Marinelli et al., 2019; Engerud et al., 2020). These conflicting results may be attributed to either technical reasons or different clinical features of the analyzed samples (Marinelli et al., 2019). By employing a validated antibody that exhibited high sensitivity and high specificity (Dong et al., 2018b; Nagy et al., 2018), we found that, compared with normal endometrium samples, the protein expression of PD-L1 was frequently lost in EC tissues. In line with previous reports describing an inverse correlation between the levels of PD-L1 and the degree of tumor malignancy in human EC (Engerud et al., 2020; Zhang et al., 2020), we found that higher protein expression of PD-L1 seems to correlate with younger patient age, low-grade disease, early stage tumors, smaller tumor size, or superficial myometrial invasion. Future studies with a larger sample size are necessary to validate our current data.

Moreover, previous research has shown that, in patients with metastatic melanoma (Taube et al., 2012), colorectal cancer (Droeser et al., 2013), Merkel-cell carcinoma (Lipson et al., 2013), and EC (Liu et al., 2015), higher PD-L1 expression was correlated with improved overall survival rates, suggesting that high PD-L1 expression may be a favorable prognostic marker in several types of cancer. Consistent with these reports, our data suggest that PD-L1 loss can identify EC patients with a worse probability of survival, and that lower expression of PD-L1 was particularly associated with shorter overall survival in high-grade ECs, indicating that a PD-L1-negative expression signature might be an indicator of poor prognosis in ECs with aggressive behaviors.

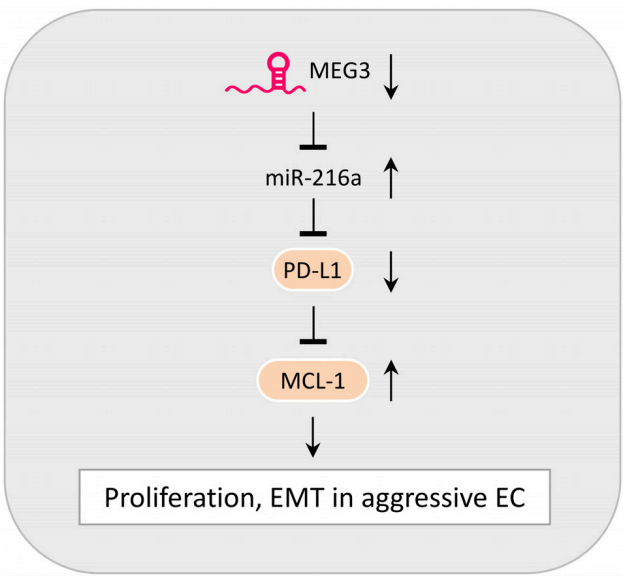

FIGURE 7 | Model Summarizing the Role of MEG3, MiR-216a, PD-L1, and MCL-1 in Controlling the Proliferative and Invasive Potential of aggressive EC cells. The downregulation of MEG3 causes an elevation of miR-216a expression. By targeting the 3′-UTR of *PD-L1* mRNA, miR-216a suppresses PD-L1 expression. PD-L1 serves as a tumor-suppressor to inhibit the proliferation, EMT and invasive potential of aggressive EC cells via repressing MCL-1 expression.

Programmed death-ligand-1 exhibits pro-tumor effects via various mechanisms (Clark et al., 2016; Gupta et al., 2016; Gato-Cañas et al., 2017). Tumor cell-intrinsic PD-L1 promotes melanoma tumorigenesis *in vivo* through activating the mTOR signaling (Clark et al., 2016). In murine melanoma cells, PD-L1 confers resistance to interferon cytotoxicity and accelerates tumor progression via a STAT3/caspase-7-dependent pathway (Gato-Cañas et al., 2017). PD-L1 was also shown to enhance tumor sphere formation of ovarian cancer cells possibly by increasing SOX2 expression (Gupta et al., 2016). The molecular link between high PD-L1 expression and EMT in cancer cells has been noticed (Chen et al., 2017; Qiu et al., 2018). In glioblastoma multiforme cells, PD-L1 activates the EMT process by upregulating Slug, β-catenin and Vimentin and by downregulating E-cadherin, via activation of the RAS/MEK/ERK signaling (Qiu et al., 2018). Overexpression of PD-L1 enhances the levels of mesenchymal genes (ZEB1, N-cadherin, and Vimentin), and contributes to the EMT phenotypes of esophageal cancer cells (Chen et al., 2017). However, silencing PD-L1 in cholangiocarcinoma cells by shRNA can increase tumorigenic potential and ALDH activity (Tamai et al., 2014). Furthermore, overexpression of PD-L1 significantly decreases the activities of PI3K/AKT and RAS/MEK/ERK pathways, leading to the suppression of lung cancer cell growth *in vitro* and in xenografts (Wang X. et al., 2020), providing evidence for the tumor suppressive role of PD-L1 in specific tumor type. Our study revealed that, via repression of MCL-1, PD-L1 could induce the expression of ZO-1, while suppressing the expression of Vimentin. These results showed that tumor cell-intrinsic PD-L1 has tumor-suppressive functions in aggressive EC cells, at least through its negative modulation of EMT. Thus, the silencing of PD-L1 may underline the molecular mechanisms for inducing and maintaining the mesenchymal state of aggressive EC cells.

Activation of the PI3K/AKT axis is known to be a central feature of EMT in numerous cancers (Dong et al., 2014). In addition, aberrant activation of the RAS/MEK/ERK pathway in human cancer cells allows them to undergo EMT via the upregulation of Snail (Tripathi and Garg, 2018). MCL-1 is an important downstream effector of PI3K/AKT and RAS/MEK/ERK signaling (Xiang et al., 2018). In this study, we demonstrated that the upregulation of MCL-1 caused by PD-L1 silencing contributes to EMT in aggressive EC cells. Further investigation will be required to determine whether PD-L1 represses the expression of MCL-1 to attenuate EMT in aggressive EC cells, through the PI3K/AKT and RAS/MEK/ERK signaling pathways.

Since PD-L1 has a critical role in suppressing anti-tumor immunity, cancer immunotherapy (in particular antibodies that block the PD-1/PD-L1 interaction) was considered to be a revolution in cancer treatment (Postow et al., 2015), and has generated clinical benefit in a subset of patients with EC (Green et al., 2020). Recently, alternative strategies (such as combination therapies with chemotherapy and siRNA against PD-L1 (Yoo et al., 2019)), have been proposed. A nanocarrier-aided delivery of PD-L1 siRNA, together with gemcitabine, resulted in a significant reduction in pancreatic cancer growth (Yoo et al., 2019). However, our cell functional study revealed that tumor cell-intrinsic PD-L1 plays an anti-tumor role in multiple aggressive EC cell lines, and downregulation of PD-L1 is sufficient to stimulate the EMT features and cell invasion in an MCL-1-dependent manner. Thus, designing therapeutic strategies aimed at knocking down PD-L1 expression in aggressive EC may lead to unexpected outcomes, possibly by accelerating EMT and metastasis. Future research is needed to explore this possibility.

Although a tumor-suppressive role for miR-216a has been reported (Zhang et al., 2017), this miRNA was identified as an oncogenic miRNA in many cancers, including EC (Wang Q.A. et al., 2020), ovarian cancer (Liu et al., 2017), hepatocellular carcinoma (Xia et al., 2013), and renal cell carcinoma (Chen et al., 2018). The direct target genes of miR-216a include *PTEN* in EC (Wang Q.A. et al., 2020), and *PTEN* and *SMAD7* in hepatocellular carcinoma (Xia et al., 2013). We have validated that, by directly targeting *PD-L1* 3′-UTR, miR-216a decreases PD-L1 levels to promote EMT and cell invasion in aggressive EC cells. It would be interesting to further determine the downstream targets of miR-216a and the clinical significance of miR-216a-regulated pathways in this clinically important subtype of EC.

Prior studies demonstrated that MEG3 is located at human chromosome 14q32.3 and is a novel tumor-suppressor lncRNA in many tumors, including EC (He et al., 2017; Dong et al., 2019b). Restoring the expression of MEG3 could suppress cancer initiation, progression, metastasis and chemoresistance (He et al., 2017). MEG3 levels were downregulated in EC tissues compared with that in adjacent non-tumor tissues, and EC patients with low MEG3 expression exhibited shorter overall survival compared with patients with high expression levels (Dong et al., 2019b). Here, we defined an anti-cancer function of MEG3 through the regulation of EMT in aggressive EC cells. Multiple molecular mechanisms, including gene deletion and promoter hypermethylation, contribute to the loss of MEG3 expression in tumor cells (He et al., 2017). Further studies are necessary to unravel the regulatory mechanisms of MEG3 expression in EC development.

CONCLUSION

In summary, our findings reveal that PD-L1 has a tumor cell-intrinsic role in suppressing the proliferation and EMT features of aggressive EC cells. This study identifies MEG3 and miR-216a as critical upstream regulators of PD-L1, thus providing a previously unreported mechanism responsible for PD-L1 dysregulation in aggressive EC cells.

DATA AVAILABILITY STATEMENT

The original contributions presented in the study are included in the article/**Supplementary Material**, further inquiries can be directed to the corresponding author/s.

ETHICS STATEMENT

The studies involving human participants were reviewed and approved by The Research Medical Ethics Committee of Sun Yat-sen University Cancer Center. The patients/participants provided their written informed consent to participate in this study.

AUTHOR CONTRIBUTIONS

DX, PD, and YK designed the experiments. DX, PD, YX, and RC performed the experiments. JY, YK, KI, and HW analyzed the data. DX and PD wrote the manuscript. All authors read and approved the final manuscript.

FUNDING

This work was supported by a grant from JSPS Grant-in-Aid for Scientific Research (C) (18K09278 and 19K09769) and an NIH/NCI grant 1R21CA216585-01A1 to JY.

ACKNOWLEDGMENTS

We thank Dr. Zhujie Xu for excellent technical assistance.

SUPPLEMENTARY MATERIAL

The Supplementary Material for this article can be found online at: https://www.frontiersin.org/articles/10.3389/fcell.2020.598205/full#supplementary-material

REFERENCES

Bray, F., Ferlay, J., Soerjomataram, I., Siegel, R. L., Torre, L. A., and Jemal, A. (2018). Global cancer statistics 2018: GLOBOCAN estimates of incidence and mortality worldwide for 36 cancers in 185 countries. *CA Cancer J. Clin.* 68, 394–424. doi: 10.3322/caac.21492

Chandrashekar, D. S., Bashel, B., Balasubramanya, S. A. H., Creighton, C. J., Ponce-Rodriguez, I., Chakravarthi, B. V. S. K., et al. (2017). UALCAN: a portal for facilitating tumor subgroup gene expression and survival analyses. *Neoplasia* 19, 649–658. doi: 10.1016/j.neo.2017.05.002

Chen, L., Xiong, Y., Li, J., Zheng, X., Zhou, Q., Turner, A., et al. (2017). PD-L1 expression promotes epithelial to mesenchymal transition in human

esophageal cancer. *Cell Physiol. Biochem.* 42, 2267–2280. doi: 10.1159/000480000

Chen, P., Quan, J., Jin, L., Lin, C., Xu, W., Xu, J., et al. (2018). miR-216a-5p acts as an oncogene in renal cell carcinoma. *Exp. Ther. Med.* 15, 4039–4046. doi: 10.3892/etm.2018.5881

Clark, C. A., Gupta, H. B., Sareddy, G., Pandeswara, S., Lao, S., Yuan, B., et al. (2016). Tumor-intrinsic PD-L1 signals regulate cell growth, pathogenesis, and autophagy in ovarian cancer and melanoma. *Cancer Res.* 76, 6964–6974. doi: 10.1158/0008-5472.CAN-16-0258

Clarke, M. A., Devesa, S. S., Harvey, S. V., and Wentzensen, N. (2019). Hysterectomy-corrected uterine corpus cancer incidence trends and differences in relative survival reveal racial disparities and rising rates of nonendometrioid cancers. *J. Clin. Oncol.* 37, 1895–1908. doi: 10.1200/JCO.19.00151

De Blasio, A., Vento, R., and Di Fiore, R. (2018). Mcl-1 targeting could be an intriguing perspective to cure cancer. *J. Cell Physiol.* 233, 8482–8498. doi: 10.1002/jcp.26786

Deng, M., Brägelmann, J., Kryukov, I., Saraiva-Agostinho, N., and Perner, S. (2017). FirebrowseR: an R client to the broad institute's firehose pipeline. *Database (Oxford).* 2017:baw160. doi: 10.1093/database/baw160

Díez-Villanueva, A., Mallona, I., and Peinado, M. A. (2015). Wanderer, an interactive viewer to explore DNA methylation and gene expression data in human cancer. *Epigenet. Chrom.* 8:22. doi: 10.1186/s13072-015-0014-8

Dong, P., Kaneuchi, M., Watari, H., Hamada, J., Sudo, S., Ju, J., et al. (2011). MicroRNA-194 inhibits epithelial to mesenchymal transition of endometrial cancer cells by targeting oncogene BMI-1. *Mol. Cancer* 10:99. doi: 10.1186/1476-4598-10-99

Dong, P., Konno, Y., Watari, H., Hosaka, M., Noguchi, M., and Sakuragi, N. (2014). The impact of microRNA-mediated PI3K/AKT signaling on epithelial-mesenchymal transition and cancer stemness in endometrial cancer. *J. Transl. Med.* 12:231. doi: 10.1186/s12967-014-0231-0

Dong, P., Xiong, Y., Yu, J., Chen, L., Tao, T., Yi, S., et al. (2018a). Control of PD-L1 expression by miR-140/142/340/383 and oncogenic activation of the OCT4-miR-18a pathway in cervical cancer. *Oncogene* 37, 5257–5268. doi: 10.1038/s41388-018-0347-4

Dong, P., Xiong, Y., Yue, J., Hanley, S. J. B., Kobayashi, N., Todo, Y., et al. (2018b). Long non-coding RNA NEAT1: a novel target for diagnosis and therapy in human tumors. *Front. Genet.* 9:471. doi: 10.3389/fgene.2018.00471

Dong, P., Xiong, Y., Yue, J., Hanley, S. J. B., and Watari, H. (2018c). Tumor-intrinsic PD-L1 signaling in cancer initiation, development and treatment: beyond immune evasion. *Front. Oncol.* 8:386. doi: 10.3389/fonc.2018.00386

Dong, P., Xiong, Y., Yue, J., Xu, D., Ihira, K., Konno, Y., et al. (2019a). Long noncoding RNA NEAT1 drives aggressive endometrial cancer progression via miR-361-regulated networks involving STAT3 and tumor microenvironment-related genes. *J. Exp. Clin. Cancer Res.* 38:295. doi: 10.1186/s13046-019-1306-9

Dong, P., Xiong, Y., Yue, J. J. B., Hanley, S., Kobayashi, N., Todo, Y., et al. (2019b). Exploring lncRNA-mediated regulatory networks in endometrial cancer cells and the tumor microenvironment: advances and challenges. *Cancers (Basel)* 11:234. doi: 10.3390/cancers11020234

Droeser, R. A., Hirt, C., Viehl, C. T., Frey, D. M., Nebiker, C., Huber, X., et al. (2013). Clinical impact of programmed cell death ligand 1 expression in colorectal cancer. *Eur. J. Cancer* 49, 2233–2242. doi: 10.1016/j.ejca.2013.02.015

Engerud, H., Berg, H. F., Myrvold, M., Halle, M. K., Bjorge, L., Haldorsen, I. S., et al. (2020). High degree of heterogeneity of PD-L1 and PD-1 from primary to metastatic endometrial cancer. *Gynecol. Oncol.* 157, 260–267. doi: 10.1016/j.ygyno.2020.01.020

Gaber, C., Meza, R., Ruterbusch, J. J., and Cote, M. L. (2016). Endometrial cancer trends by race and histology in the USA: projecting the number of new cases from 2015 to 2040. *J. Racial Ethn. Health Disparities* doi: 10.1007/s40615-016-0292-2 [Epub ahead of print].

Gao, J., Aksoy, B. A., Dogrusoz, U., Dresdner, G., Gross, B., Sumer, S. O., et al. (2013). Integrative analysis of complex cancer genomics and clinical profiles using the cBioPortal. *Sci. Signal.* 6:l1. doi: 10.1126/scisignal.2004088

Gato-Cañas, M., Zuazo, M., Arasanz, H., Ibañez-Vea, M., Lorenzo, L., Fernandez-Hinojal, G., et al. (2017). PDL1 signals through conserved sequence motifs to overcome interferon-mediated cytotoxicity. *Cell Rep.* 20, 1818–1829. doi: 10.1016/j.celrep.2017.07.075

Gonzalez, H., Hagerling, C., and Werb, Z. (2018). Roles of the immune system in cancer: from tumor initiation to metastatic progression. *Genes Dev.* 32, 1267–1284. doi: 10.1101/gad.314617.118

Green, A. K., Feinberg, J., and Makker, V. A. (2020). Review of immune checkpoint blockade therapy in endometrial cancer. *Am. Soc. Clin. Oncol. Educ. Book* 40, 1–7. doi: 10.1200/EDBK_280503

Gupta, H. B., Clark, C. A., Yuan, B., Sareddy, G., Pandeswara, S., Padron, A. S., et al. (2016). Tumor cell-intrinsic PD-L1 promotes tumor-initiating cell generation and functions in melanoma and ovarian cancer. *Signal. Transduct Target Ther.* 1, 16030–16039. doi: 10.1038/sigtrans.2016.30

Hanahan, D., and Weinberg, R. A. (2011). Hallmarks of cancer: the next generation. *Cell* 144, 646–674. doi: 10.1016/j.cell.2011.02.013

He, Y., Luo, Y., Liang, B., Ye, L., Lu, G., and He, W. (2017). Potential applications of MEG3 in cancer diagnosis and prognosis. *Oncotarget* 8, 73282–73295. doi: 10.18632/oncotarget.19931

Keller, M. D., Neppl, C., Irmak, Y., Hall, S. R., Schmid, R. A., Langer, R., et al. (2018). Adverse prognostic value of PD-L1 expression in primary resected pulmonary squamous cell carcinomas and paired mediastinal lymph node metastases. *Mod. Pathol.* 31, 101–110. doi: 10.1038/modpathol.2017.111

Kiesslich, T., Pichler, M., and Neureiter, D. (2013). Epigenetic control of epithelial-mesenchymal-transition in human cancer. *Mol. Clin. Oncol.* 1, 3–11. doi: 10.3892/mco.2012.28

Kluger, H. M., Zito, C. R., Turcu, G., Baine, M. K., Zhang, H., Adeniran, A., et al. (2017). PD-L1 studies across tumor types, its differential expression and predictive value in patients treated with immune checkpoint inhibitors. *Clin. Cancer Res.* 23, 4270–4279. doi: 10.1158/1078-0432.CCR-16-3146

Konno, Y., Dong, P., Xiong, Y., Suzuki, F., Lu, J., Cai, M., et al. (2014). MicroRNA-101 targets EZH2, MCL-1 and FOS to suppress proliferation, invasion and stem cell-like phenotype of aggressive endometrial cancer cells. *Oncotarget* 5, 6049–6062. doi: 10.18632/oncotarget.2157

Kyo, S., Nakamura, M., Kiyono, T., Maida, Y., Kanaya, T., Tanaka, M., et al. (2003). Successful immortalization of endometrial glandular cells with normal structural and functional characteristics. *Am. J. Pathol.* 163, 2259–2269. doi: 10.1016/S0002-9440(10)63583-3

Li, J. H., Liu, S., Zhou, H., Qu, L. H., and Yang, J. H. (2014). starBase v2.0: decoding miRNA-ceRNA, miRNA-ncRNA and protein-RNA interaction networks from large-scale CLIP-Seq data. *Nucleic Acids Res.* 42, D92–D97. doi: 10.1093/nar/gkt1248

Li, Z., Joehlin-Price, A. S., Rhoades, J., Ayoola-Adeola, M., Miller, K., Parwani, A. V., et al. (2018). Programmed death ligand 1 expression among 700 consecutive endometrial cancers: strong association with mismatch repair protein deficiency. *Int. J. Gynecol. Cancer* 28, 59–68. doi: 10.1097/IGC.0000000000001120

Lipson, E. J., Vincent, J. G., Loyo, M., Kagohara, L. T., Luber, B. S., Wang, H., et al. (2013). PD-L1 expression in the Merkel cell carcinoma microenvironment: association with inflammation, Merkel cell polyomavirus and overall survival. *Cancer Immunol. Res.* 1, 54–63. doi: 10.1158/2326-6066.CIR-13-0034

Liu, H., Pan, Y., Han, X., Liu, J., and Li, R. (2017). MicroRNA-216a promotes the metastasis and epithelial-mesenchymal transition of ovarian cancer by suppressing the PTEN/AKT pathway. *Onco Targets Ther.* 10, 2701–2709. doi: 10.2147/OTT.S114318

Liu, J., Liu, Y., Wang, W., Wang, C., and Che, Y. (2015). Expression of immune checkpoint molecules in endometrial carcinoma. *Exp. Ther. Med.* 10, 1947–1952. doi: 10.3892/etm.2015.2714

Liu, S., Qin, T., Jia, Y., and Li, K. P. D. - (2019). L1 expression is associated with VEGFA and LADC patients' survival. *Front. Oncol.* 9:189. doi: 10.3389/fonc.2019.00189

Marinelli, O., Annibali, D., Aguzzi, C., Tuyaerts, S., Amant, F., Morelli, M. B., et al. (2019). The controversial role of PD-1 and its ligands in gynecological malignancies. *Front Oncol.* 9:1073. doi: 10.3389/fonc.2019.01073

Mo, Z., Liu, J., Zhang, Q., Chen, Z., Mei, J., Liu, L., et al. (2016). Expression of PD-1, PD-L1 and PD-L2 is associated with differentiation status and histological type of endometrial cancer. *Oncol. Lett.* 12, 944–950. doi: 10.3892/ol.2016.4744

Nagy, Á, Lánczky, A., Menyhárt, O., and Győrffy, B. (2018). Validation of miRNA prognostic power in hepatocellular carcinoma using expression data of independent datasets. *Sci. Rep.* 8:9227. doi: 10.1038/s41598-018-27521-y

Okazaki, T., and Honjo, T. (2007). PD-1 and PD-1 ligands: from discovery to clinical application. *Int. Immunol.* 19, 813–824. doi: 10.1093/intimm/dxm057

Pan, C. Y., and Lin, W. C. (2020). miR-TV: an interactive microRNA Target Viewer for microRNA and target gene expression interrogation for human cancer studies. *Database (Oxford)*. 2020:baz148. doi: 10.1093/database/baz148

Papatheodorou, I., Moreno, P., Manning, J., Fuentes, A. M., George, N., Fexova, S., et al. (2020). Expression Atlas update: from tissues to single cells. *Nucleic Acids Res.* 48, D77–D83. doi: 10.1093/nar/gkz947

Paraskevopoulou, M. D., Vlachos, I. S., Karagkouni, D., Georgakilas, G., Kanellos, I., Vergoulis, T., et al. (2016). DIANA-LncBase v2: indexing microRNA targets on non-coding transcripts. *Nucleic Acids Res.* 44, D231–D238. doi: 10.1093/nar/gkv1270

Postow, M. A., Callahan, M. K., and Wolchok, J. D. (2015). Immune checkpoint blockade in cancer therapy. *J. Clin. Oncol.* 33, 1974–1982. doi: 10.1200/JCO.2014.59.4358

Qiu, X. Y., Hu, D. X., Chen, W. Q., Chen, R. Q., Qian, S. R., Li, C. Y., et al. (2018). PD-L1 confers glioblastoma multiforme malignancy via Ras binding and Ras/Erk/EMT activation. *Biochim. Biophys. Acta Mol. Basis Dis.* 1864, 1754–1769. doi: 10.1016/j.bbadis.2018.03.002

Tamai, K., Nakamura, M., Mizuma, M., Mochizuki, M., Yokoyama, M., Endo, H., et al. (2014). Suppressive expression of CD274 increases tumorigenesis and cancer stem cell phenotypes in cholangiocarcinoma. *Cancer Sci.* 105, 667–674. doi: 10.1111/cas.12406

Tang, Z., Li, C., Kang, B., Gao, G., Li, C., and Zhang, Z. (2017). GEPIA: a web server for cancer and normal gene expression profiling and interactive analyses. *Nucleic Acids Res.* 45, W98–W102. doi: 10.1093/nar/gkx247

Taube, J. M., Anders, R. A., Young, G. D., Xu, H., Sharma, R., McMiller, T. L., et al. (2012). Colocalization of inflammatory response with B7-h1 expression in human melanocytic lesions supports an adaptive resistance mechanism of immune escape. *Sci. Transl. Med.* 4:127ra37. doi: 10.1126/scitranslmed.3003689

Terry, S., Savagner, P., Ortiz-Cuaran, S., Mahjoubi, L., Saintigny, P., Thiery, J. P., et al. (2017). New insights into the role of EMT in tumor immune escape. Version 2. *Mol. Oncol.* 11, 824–846. doi: 10.1002/1878-0261.12093

Tripathi, K., and Garg, M. (2018). Mechanistic regulation of epithelial-to-mesenchymal transition through RAS signaling pathway and therapeutic implications in human cancer. *J. Cell Commun. Signal.* 12, 513–527. doi: 10.1007/s12079-017-0441-3

Uhlén, M., Fagerberg, L., Hallström, B. M., Lindskog, C., Oksvold, P., Mardinoglu, A., et al. (2015). Proteomics. Tissue-based map of the human proteome. *Science* 347:1260419. doi: 10.1126/science.1260419

Valastyan, S., and Weinberg, R. A. (2011). Tumor metastasis: molecular insights and evolving paradigms. *Cell* 147, 275–292. doi: 10.1016/j.cell.2011.09.024

Wang, Q. A., Yang, Y., and Liang, X. (2020). LncRNA CTBP1-AS2 sponges miR-216a to upregulate PTEN and suppress endometrial cancer cell invasion and migration. *J. Ovarian Res.* 13:37. doi: 10.1186/s13048-020-00639-2

Wang, X., Yang, X., Zhang, C., Wang, Y., Cheng, T., Duan, L., et al. (2020). Tumor cell-intrinsic PD-1 receptor is a tumor suppressor and mediates resistance to PD-1 blockade therapy. *Proc. Natl. Acad. Sci. U.S.A.* 117, 6640–6650. doi: 10.1073/pnas.1921445117

Xia, H., Ooi, L. L., and Hui, K. M. (2013). MicroRNA-216a/217-induced epithelial-mesenchymal transition targets PTEN and SMAD7 to promote drug resistance and recurrence of liver cancer. *Hepatology* 58, 629–641. doi: 10.1002/hep.26369

Xiang, W., Yang, C. Y., and Bai, L. (2018). MCL-1 inhibition in cancer treatment. *Onco Targets Ther.* 11, 7301–7314. doi: 10.2147/OTT.S146228

Xu, D., Dong, P., Xiong, Y., Yue, J., Konno, Y., Ihira, K., et al. (2020). MicroRNA-361-mediated inhibition of HSP90 expression and EMT in cervical cancer is counteracted by oncogenic lncRNA NEAT1. *Cells* 9:632. doi: 10.3390/cells9030632

Yamagami, W., Nagase, S., Takahashi, F., Ino, K., Hachisuga, T., Aoki, D., et al. (2017). Clinical statistics of gynecologic cancers in Japan. *J. Gynecol. Oncol.* 28:e32. doi: 10.3802/jgo.2017.28.e32

Yamashita, H., Nakayama, K., Ishikawa, M., Nakamura, K., Ishibashi, T., Sanuki, K., et al. (2017). Microsatellite instability is a biomarker for immune checkpoint inhibitors in endometrial cancer. *Oncotarget* 9, 5652–5664. doi: 10.18632/oncotarget.23790

Yoo, B., Jordan, V. C., Sheedy, P., Billig, A. M., Ross, A., Pantazopoulos, P., et al. (2019). RNAi-mediated PD-L1 inhibition for pancreatic cancer immunotherapy. *Sci. Rep.* 9:4712. doi: 10.1038/s41598-019-41251-9

Zhang, D., Zhao, L., Shen, Q., Lv, Q., Jin, M., Ma, H., et al. (2017). Down-regulation of KIAA1199/CEMIP by miR-216a suppresses tumor invasion and metastasis in colorectal cancer. *Int. J. Cancer* 140, 2298–2309. doi: 10.1002/ijc.30656

Zhang, S., Minaguchi, T., Xu, C., Qi, N., Itagaki, H., Shikama, A., et al. (2020). PD-L1 and CD4 are independent prognostic factors for overall survival in endometrial carcinomas. *BMC Cancer* 20:127. doi: 10.1186/s12885-020-6545-9

Conflict of Interest: The authors declare that the research was conducted in the absence of any commercial or financial relationships that could be construed as a potential conflict of interest.

frontiers in Genetics

ORIGINAL RESEARCH
published: 15 December 2020
doi: 10.3389/fgene.2020.592436

HOXA5 Expression Is Elevated in Breast Cancer and Is Transcriptionally Regulated by Estradiol

*Imran Hussain[1], Paromita Deb[1], Avisankar Chini[1], Monira Obaid[1], Arunoday Bhan[1], Khairul I. Ansari[1], Bibhu P. Mishra[1], Samara A. Bobzean[2], S. M. Nashir Udden[3], Prasanna G. Alluri[3], Hriday K. Das[4], Robert Matthew Brothers[5], Linda I. Perrotti[2] and Subhrangsu S. Mandal[1]**

[1] Department of Chemistry and Biochemistry, The University of Texas at Arlington, Arlington, TX, United States, [2] Department of Psychology, The University of Texas at Arlington, Arlington, TX, United States, [3] Department of Radiation Oncology, The University of Texas Southwestern Medical Center, Dallas, TX, United States, [4] Department of Pharmacology and Neuroscience, University of North Texas Health Science Center, Institute for Healthy Aging, Fort Worth, TX, United States, [5] Department of Kinesiology, The University of Texas at Arlington, Arlington, TX, United States

OPEN ACCESS

Edited by:
Xiao Zhu,
Guangdong Medical University, China

Reviewed by:
Lin An,
Sanofi, United States
Guangyu Wang,
Houston Methodist Research Institute, United States

***Correspondence:**
Subhrangsu S. Mandal
smandal@uta.edu

Specialty section:
This article was submitted to Epigenomics and Epigenetics, a section of the journal Frontiers in Genetics

Received: *07 August 2020*
Accepted: *26 October 2020*
Published: *15 December 2020*

Citation:
Hussain I, Deb P, Chini A, Obaid M, Bhan A, Ansari KI, Mishra BP, Bobzean SA, Udden SMN, Alluri PG, Das HK, Brothers RM, Perrotti LI and Mandal SS (2020) HOXA5 Expression Is Elevated in Breast Cancer and Is Transcriptionally Regulated by Estradiol. Front. Genet. 11:592436. doi: 10.3389/fgene.2020.592436

HOXA5 is a homeobox-containing gene associated with the development of the lung, gastrointestinal tract, and vertebrae. Here, we investigate potential roles and the gene regulatory mechanism in HOXA5 in breast cancer cells. Our studies demonstrate that HOXA5 expression is elevated in breast cancer tissues and in estrogen receptor (ER)-positive breast cancer cells. HOXA5 expression is critical for breast cancer cell viability. Biochemical studies show that estradiol (E2) regulates HOXA5 gene expression in cultured breast cancer cells *in vitro*. HOXA5 expression is also upregulated *in vivo* in the mammary tissues of ovariectomized female rats. E2-induced HOXA5 expression is coordinated by ERs. Knockdown of either ERα or ERβ downregulated E2-induced HOXA5 expression. Additionally, ER co-regulators, including CBP/p300 (histone acetylases) and MLL-histone methylases (MLL2, MLL3), histone acetylation-, and H3K4 trimethylation levels are enriched at the HOXA5 promoter in present E2. In summary, our studies demonstrate that HOXA5 is overexpressed in breast cancer and is transcriptionally regulated via estradiol in breast cancer cells.

Keywords: HOXA5, breast cancer, estradiol, gene expression, estrogen receptors, chromatin

INTRODUCTION

HOX genes are a highly conserved family of homeobox-containing genes that play pivotal roles in cell differentiation, development, and embryogenesis (Krumlauf, 1994; Zakany and Duboule, 2007). The collinear expression of HOX genes are critical in anterior–posterior patterning during embryogenesis (Akam, 1987; Mlodzik et al., 1988; Duboule and Dolle, 1989; McGinnis and Krumlauf, 1992; Mallo et al., 2010). In humans, there are 39 HOX genes that are classified as HOXA-D clusters (Acampora et al., 1989; Garcia-Fernandez, 2005; Holland et al., 2007; Mallo and Alonso, 2013), and they primarily function as transcription factors (Svingen and Tonissen, 2006; Plowright et al., 2009; Ladam and Sagerstrom, 2014; Zheng et al., 2015; Morgan et al., 2016). They bind to their target gene promoters via their homeodomain and control gene expression

(Hanson et al., 1999; Shah and Sukumar, 2010; Boube et al., 2014; Taniguchi, 2014). Though HOX genes were originally described to exhibit collinear expression, especially during embryogenesis, recent studies demonstrate that each HOX gene may be independently regulated and expressed in various adult tissues (Taylor et al., 1998; Neville et al., 2002; Takahashi et al., 2004; Dunwell and Holland, 2016; Rux and Wellik, 2017). Additionally, HOX gene expressions are misregulated in a variety of cancers (Grier et al., 2005; Shah and Sukumar, 2010; Gray et al., 2011; Bhatlekar et al., 2014). HOX genes are associated with cancer cell proliferation, angiogenesis, and tumor growth (Hayashida et al., 2010; Ansari et al., 2011a,b; Shrestha et al., 2012; Hussain et al., 2015; Deb et al., 2016). HOX gene expression is increasingly recognized as a potential biomarker and target of therapeutic intervention. For example, HOXB9, a key player in mammary gland development, is upregulated in breast cancer, regulates growth and angiogenic factors, and is a potential biomarker (Ansari et al., 2011b; Shrestha et al., 2012). Similarly, another HOX gene, such as HOXC6, implicated in mammary gland development and breast cancer, regulates tumor growth factors and induces 3-D-colony formation (Ansari et al., 2011a; Hussain et al., 2015). HOXB7 overexpression is linked with cell proliferation, neoplastic transformation, and tumorigenesis (Wu et al., 2006; Nguyen Kovochich et al., 2013). Spinal cord associated HOXA10 expression is upregulated in breast cancer and is regulated by estradiol (Chu et al., 2004). Thus, HOX genes are emerging as major players in gene regulation and cancer; however, their detailed functions and gene regulatory mechanism remains elusive.

Homeobox-containing gene HOXA5 is a critical player in the development of lung, gastrointestinal tract, spleen, kidney, and vertebrae (Larochelle et al., 1999; Jeannotte et al., 2016). It regulates the expression of various proteins in conjunction with other paralogs during the ontogeny of normal development (Larochelle et al., 1999; Jeannotte et al., 2016). Studies also demonstrate that HOXA5 expression plays a critical role in development of the murine central nervous system (Joksimovic et al., 2005). In addition to its critical role in development, HOXA5 expression is dysregulated in breast epithelium and is linked to breast cancer biogenesis (Raman et al., 2000a,b). Here, we investigate if HOXA5 expression is associated with breast cancer and study its transcriptional regulatory mechanism in breast cancer cells. We demonstrate that HOXA5 expression is elevated in breast cancer, and its expression is regulated by estradiol (E2).

EXPERIMENTAL SECTION

Cell Culture, Antisense Oligonucleotide (ASO)-Transfection, and E2 Treatments

CCL228 (colon cancer), H358 (lung cancer), HeLa (cervical cancer), JAR (choriocarcinoma placenta), MCF10 (normal breast epithelial), MCF7 (ER-positive breast cancer), T47D (ER-positive breast cancer), and MDA-MB-231 (ER-negative breast cancer) cells (from ATCC) were cultured in DMEM that was supplemented with 10% fetal bovine serum (FBS), 2 mM L-glutamine, and 1% penicillin/streptomycin (100 units and 0.1 mg/mL, respectively) (Wang et al., 2010; Ansari et al., 2011a, 2012a; Shrestha et al., 2012; Kasiri et al., 2013; Bhan et al., 2014a; Hussain et al., 2015; Deb et al., 2016).

For the estrogen treatment, MCF7 cells were cultured in phenol red–free DMEM-F-12 supplemented with 10% charcoal-stripped FBS for at least 3 generations. Cell were then treated with 17β-E2 for 6 h and then subjected to RNA and protein extraction.

All the ASOs were synthesized commercially from IDT-DNA. MCF7 cells (grown in phenol red–free DMEM-F-12 supplemented with 10% charcoal-stripped FBS) were transfected with ASOs using iFECT transfection reagent (KD Medicals, Inc.) with antisense oligonucleotides for 48 h (Ansari et al., 2011a; Kasiri et al., 2013). ASO-transfected cells were then treated with 1 nM E2 for 4 h followed by RNA and protein extraction for further analysis.

Immunohistological Analysis of Breast Cancer Tissue Microarray

Breast cancer tissue microarrays (US Biomax Inc) were immunostained with DAB staining using HOXA5 antibody as described by us previously (REF). Microarray slides was initially deparaffinized by immersing in xylene (twice, 10 min each), then sequentially in 100, 95, and 70% ethanol (5 min each) and then incubated in 0.1 M sodium citrate buffer (at 95°C, 15 min) for antigen retrieval. For the immunostaining, the slide was immerged in 3% H_2O_2 (15 min), washed with PBS (x2), blocked with buffer containing donkey serum, and then incubated with HOXA5 antibody (overnight). Slides were washed thrice (PBS) and then incubated (1.5 h) with donkey secondary antibody (biotinylated). Slides were then washed and incubated with avidin–biotin complexes (1.5 h), again washed with PBS, followed by washes with 0.1 M Tris-HCl (pH 7.4, twice). The slide was subjected to peroxidase labeling (incubated with a DAB substrate, Vector Laboratories), dehydrated (immersed sequentially in 70, 95, and 100% ethanol), cleaned (incubated in citrisolv agent), and mounted using DPX mounting solution. Slides were analyzed under a microscope (Nikon Eclipse TE2000-U, Japan).

RNA and Protein Extraction, RT-PCR, and Western Blots

RNA extraction: cells were resuspended in DEPC-treated buffer A (20 mM Tris-HCl, pH 7.9; 1.5 mM $MgCl_2$; 10 mM KCl and 0.5 mM DTT; 0.5 mM EDTA), incubated on ice (10 min), and then centrifuged. The supernatant was subjected to phenol-chloroform extraction. RNA was precipitated using ethanol. The precipitated RNA was dissolved in DEPC-treated water, quantified, and then reverse-transcribed into cDNA as described by us previously (500 ng RNA, 2.4 μM of oligo-dT, 100 units MMLV reverse transcriptase, 1X first strand buffer, 100 μM dNTPs each, 1 mM DTT, and 20 units of RNaseOut in 25 μL total reaction volume). The cDNA was diluted to 100 μL and then analyzed using regular PCR and qPCR (PCR primer in **Table 1**). For the qPCR, 5 μL cDNA was mixed with 5 μL of SsoFast EvaGreen supermix (Biorad) and PCR primers (100 μM

TABLE 1 | Primers used for cloning, RT-PCR, ChIP, and antisense experiments.

Primers	Forward primers (5′-3′)	Reverse primers (5′-3′)
PCR PRIMERS		
GAPDH	CAATGACCCCTTCATTGACC	GACAAGCTTCCCGTTCTCAG
HOXA5	ACTCATTTTGCGGTCGCTAT	TTGTAGCCGTAGCCGTACCT
HOXA5-ERE1	CGAGTCCGGCTGAACGGCGG	TAGGCACCCAAATATGGGGTA
HOXA5-ERE2	TTATTTCTCCAATTGGCTAAA	CCGGCGAGGATGCAGAGGAT
ERα	AGCACCCTGAAGTCTCTGGA	GATGTGGGAGAGGATGAGGA
ERβ	AAGAAGATTCCCGGCTTTGT	TCTACGCATTTCCCCTCATC
ANTISENSES		
HOXA5	GTCCCTGAATTGCTCGCTCA**	
ERα antisense	TCCCACCTTTCATCATTCCC**	
ERβ antisense	GCCACACTTCACCATTCCCA**	
Scramble antisense	CGTTTGTCCCTCCAGCATCT**	

**Phosphorothioate antisense oligonucleotides.*

each), and then PCR-amplified in a CFX96 qPCR system. Protein extracts: Whole cell protein extracts were made by suspending the cells in whole cell extraction buffer (50 mm Tris–HCl, pH 8.0; 150 mM NaCl; 1 mM EDTA; 0.05% NP-40; 0.2 mM PMSF; 0.5 mM DTT; and 1× protease inhibitor cocktail). Proteins were quantified and analyzed by Western blotting (alkaline phosphatase method).

Chromatin Immunoprecipitation (ChIP) Assay

ChIP analyses were performed using similar procedures described by us previously (Wang et al., 2010; Ansari et al., 2011a, 2012a; Shrestha et al., 2012; Kasiri et al., 2013; Bhan et al., 2014a; Hussain et al., 2015; Deb et al., 2016). Briefly, MCF7 (treated with different conditions) cells were fixed in 4% formaldehyde (15 min), followed by quenching with 125 mM glycine and washed with PBS (twice). They were lyzed (SDS lysis buffer), and the chromatin was sheared by sonication (∼150–450 bp in length, checked by agarose gel). The sonicated chromatins (precleaned using protein-G agarose beads) were immunoprecipitated with antibodies against ERα, ERβ, H3K4-trimethyl, RNAPII, MLL1, MLL2, MLL2, MLL3, CBP, p300, H4 acetylation, and β-actin, independently. The immunoprecipitated DNA fragments were purified and analyzed by PCR using promoter-specific primers shown in **Table 1**.

Flow Cytometry Analysis

MCF7 cells transfected with HOXA5 and scramble ASOs (48 h) were harvested and centrifuged (1,000 × g for 5 min at 4°C). Cells were washed with PBS (cold, twice), fixed (70% ethanol/PBS, 1 h, 4°C), and stored overnight at −20°C. Cells were stained with propidium iodide (PI) by resuspending in PI solution (0.5 μg/mL, 2 h) and then analyzed by FACS (Beckman Coulter, Fullerton, CA, USA) (31).

Animal Studies

Adult, 90-days-old, experimentally naïve, female Sprague–Dawley rats ($n = 12$) (purchased commercially) and maintained in accordance with the National Institutes of Health Guidelines for the Care and Use of Laboratory Animals as described by us previously (Betancourt et al., 2010; Bhan et al., 2014a,b; Hussain et al., 2015). Rats were anesthetized (2%−3% isoflurane-oxygen vapor mixture), ovariectomized (OVX), and allowed to recover (for 4–5 days post-surgery) as described previously (Betancourt et al., 2010; Bhan et al., 2014a,b; Hussain et al., 2015). Vaginal lavage testing was performed daily for 8 consecutive days to confirm cessation of estrous cycling (Inagaki et al., 2012). Rats were given subcutaneous injections of E2 (5 μg/kg, dissolved in peanut oil, 5 μg/mL stock) ($n = 4$) 24 and 4 h prior to sacrifice (via rapid decapitation). Mammary gland tissue was collected, flash frozen on dry ice, and stored at −80°C. RNA and proteins were extracted from mammary tissues and analyzed by RT-PCR and Western blotting (Betancourt et al., 2010; Bhan et al., 2014a,b; Hussain et al., 2015).

Statistical Analyses

Experiments were repeated at least thrice ($n = 3$). The RT-qPCR experiments were performed in three parallel replicates and repeated at least thrice. The data presented in the figures is expressed as averages ± standard error. Statistical significance between various groups (control vs. treated) were determined using one- or two-way analysis of variance (ANOVA) followed by multiple comparisons with Dunnett correction (GraphPad Prism). Other statistical evaluations were performed using the Student *t*-test. Data was considered statistically significant when the *p*-value was <0.05.

RESULTS

HOXA5 Is Elevated in Breast Cancer

In an effort to understand the potential role of HOXA5 in breast cancer, initially we examined HOXA5 expression in various cancer cells and breast cancer tissues. Briefly, RNA from different cell lines was analyzed by RT-qPCR. These analyses demonstrated that HOXA5 expression is elevated in MCF7 and T47D (ER-positive breast cancer cells) in comparison to MDA-MB-231 (ER-negative breast cancer cells) (**Figure 1A**). For the tissue expression analysis, a breast cancer tissue microarray (commercial) was analyzed for HOXA5 expression level. Briefly, the tissue microarray containing the breast cancer tissue and surrounding normal tissue was immunostained using a HOXA5 antibody and analyzed under a microscope. Interestingly, these analyses show that HOXA5 expression is elevated in most breast cancer tissues relative to their normal counterparts (**Figures 1B–D**).

To investigate further, we also examined HOXA5 expression in different types of breast cancer patients using a preexisting cancer gene expression database using cBioPortal online data analysis tool (https://www.cbioportal.org) (**Figure 2**). The data provided by cBioPortal includes mutations, deletions, and copy-number amplifications (Cerami et al., 2012; Gao et al., 2013). These analyses demonstrate that HOXA5 expression is

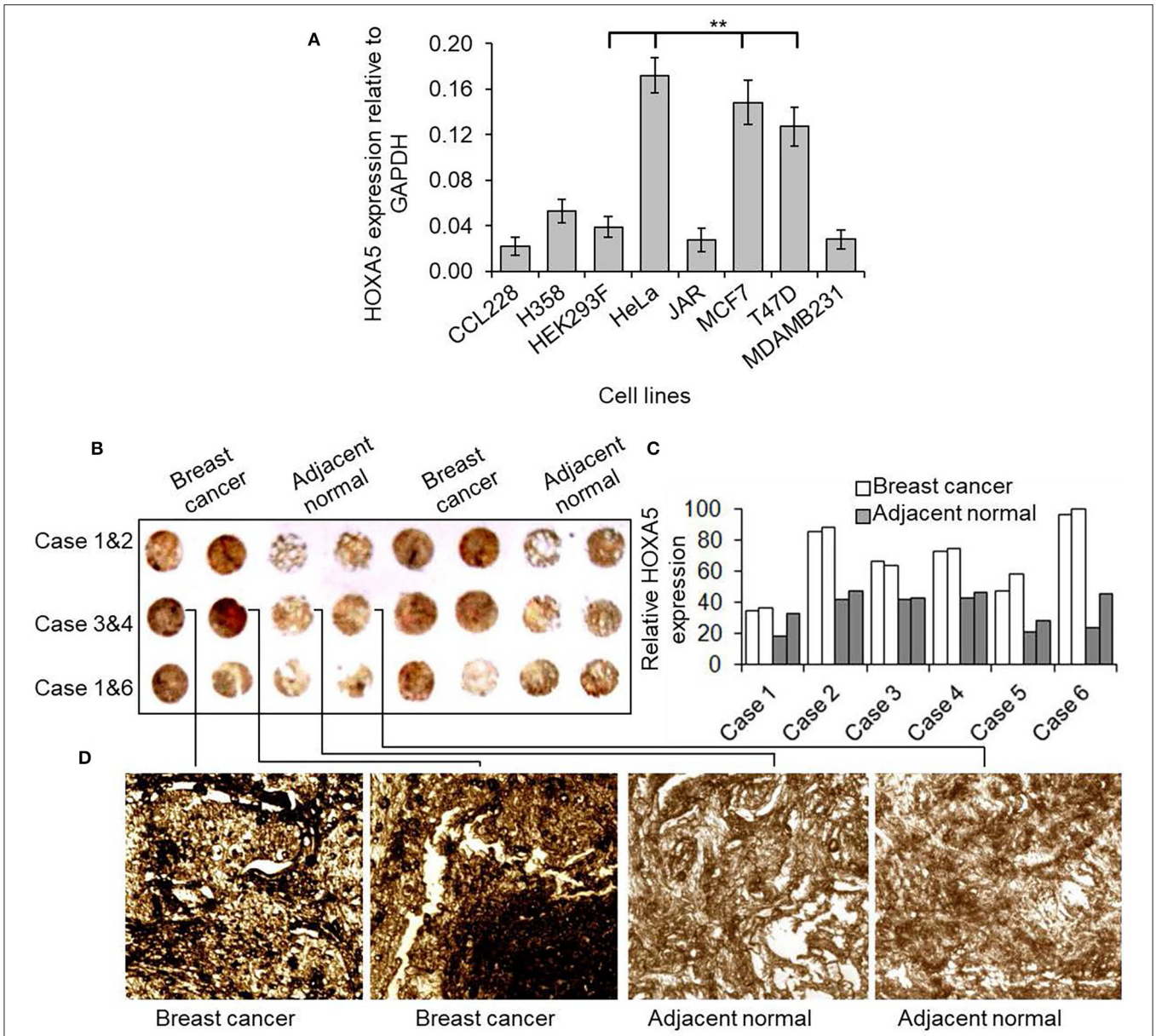

FIGURE 1 | HOXA5 expression in breast cancer cells and tissues. **(A)** Comparison of HOXA5 expression in different cell lines. The total RNA was isolated from CCL228 (colon cancer), H358 (lung cancer) HeLa (cervical cancer), JAR (placental cancer), MDAMB231 (ER-negative breast cancer), T47D (ER-positive breast cancer), MCF7 (ER-positive breast cancer) cell lines and analyzed by RT-qPCR using primers specific to HOXA5 and GAPDH (loading control). HOXA5 expression relative to GAPDH is plotted. Bars indicate averages ± standard errors ($n = 3$). **denotes $p < 0.0001$ compared to HEK293F control cells **(B–D)** HOXA5 expression in breast cancer tissue. Tissue microarray slide (containing six cases of human breast cancer cases and respective adjacent normal breast tissue) was subjected to DAB staining with HOXA5 antibody. The HOXA5 expression level was quantified **(C)**. A magnified view of case 3 is in **(D)**.

significantly amplified in various breast cancer tissues, such as in MBC project, BRCA (INSERM 2016), breast (METABRIC), and invasive breast carcinoma (TCGA PanCan), further suggesting potential association of HOXA5 in breast cancer. Taken together, these observations demonstrate that HOXA5 is overexpressed at least in some subset of breast cancer and may contribute to breast cancer growth. The overexpression of HOXA5 in the ER-positive breast cancer cells suggests its potential regulation by E2.

HOXA5 Knockdown Suppressed the Breast Cancer Cell Viability

As HOXA5 expression is upregulated in breast cancer, we knocked it down in MCF7 cells and analyzed its impacts on viability. HOXA5 antisense or scramble-ASO were transfected into MCF7 cells separately (48 h) followed by analysis of HOXA5 expression levels using the RNA (RT-qPCR) and protein levels (Western blots). Cells were also visualized under a fluorescence

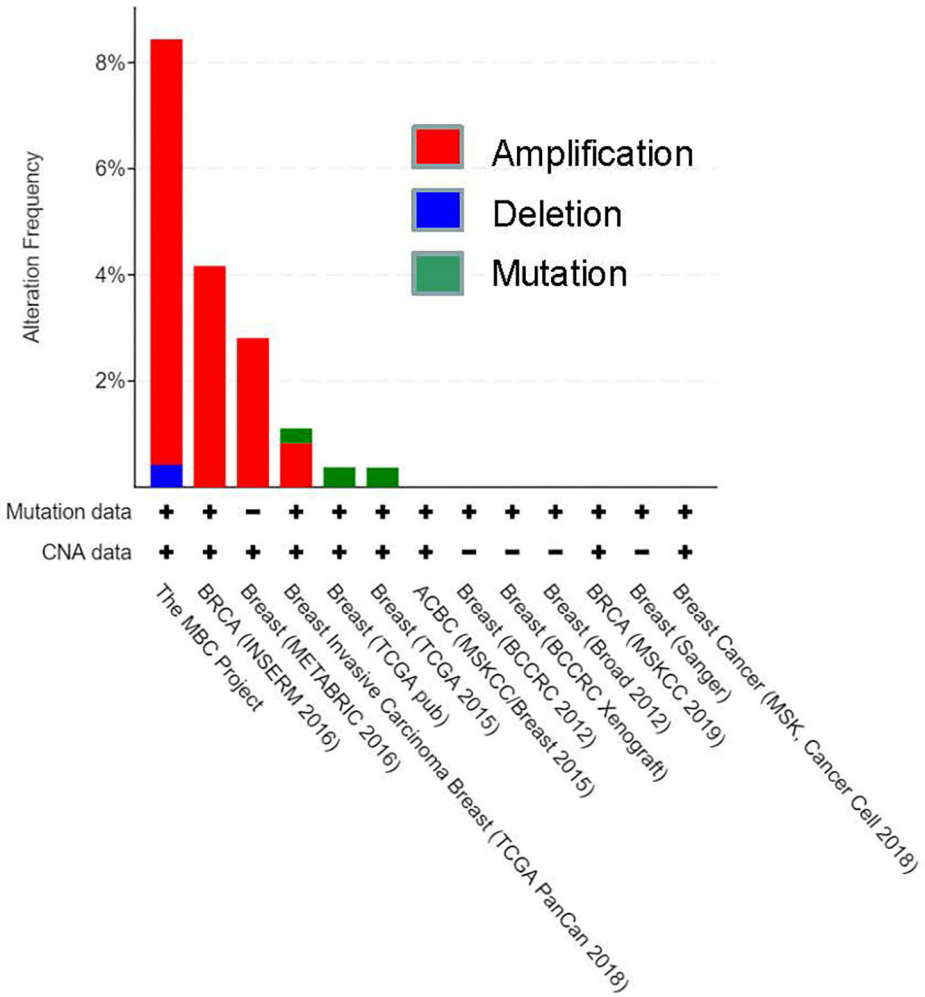

FIGURE 2 | CBioportal analysis of breast cancer database for HOXA5 expression. HOXA5 expression in different types of breast cancer patients using a preexisting cancer gene expression database using a cBioPortal online data analysis tool (https://www.cbioportal.org). The data provided by cBioPortal includes mutations, deletions, and copy-number amplifications for HOXA5; CAN, copy number alteration.

microscope or analyzed by flow cytometry. Our analyses show that HOXA5 expression is decreased upon transfection with HOXA5 ASO (**Figures 3A–C**), and this results in decrease in growth of MCF7 cells compared to controls (**Figure 3D**). Microscopic analysis shows that, upon HOXA5 knockdown, cells appear unhealthy, rounded up, and dead (**Figure 3E**).

To examine if HOXA5 may regulate cell-cycle progression, we knocked it down in MCF7 cells using HOXA5 ASO and analyzed it by flow cytometry. Interestingly, upon HOXA5-ASO transfection, G0/G1 and S phase cell populations were decreased with an increase in apoptotic cells compared to controls (**Figure 3F**). At 4 μg of HOXA5 ASO treatment, the cell population at the S (decreased from 12.9 to 11.1%) and G2/M phases (reduced from 26 to 21.8%) were reduced although about 28% of cells were apoptotic, and these affected were further pronounced at higher HOXA5 ASO concentrations (**Figure 3F**), suggesting the critical role of HOXA5 in regulation of cell-cycle progression.

E@ Regulates HOXA5 Gene Expression *in vitro* and *in vivo*

As HOXA5 expression is elevated in breast cancer cells and tissues, we investigated its potential regulatory mechanism by E2 in MCF7 cells. Briefly, MCF7 cells were treated with 17β-E2. RNA was isolated and analyzed by RT-PCR for the expression of HOXA5. An antiestrogen, tamoxifen, was also used in conjunction with E2 to explore the specificity and to understand the E2-mediated regulatory mechanism of HOXA5. Interestingly, E2 treatment induced HOXA5 expression in a concentration-dependent manner (**Figures 4A,B**). HOXA5 expression was increased by 4.5-fold upon exposure to 1 nM of E2. Notably, treatment with the antiestrogen tamoxifen suppressed E2-induced HOXA5 expression (**Figures 4A,B**). These observations suggest potential regulation of HOXA5 via E2 and ERs.

To further examine the physiological significance of HOXA5 and its endocrine regulation *in vivo*, we analyzed its expression in

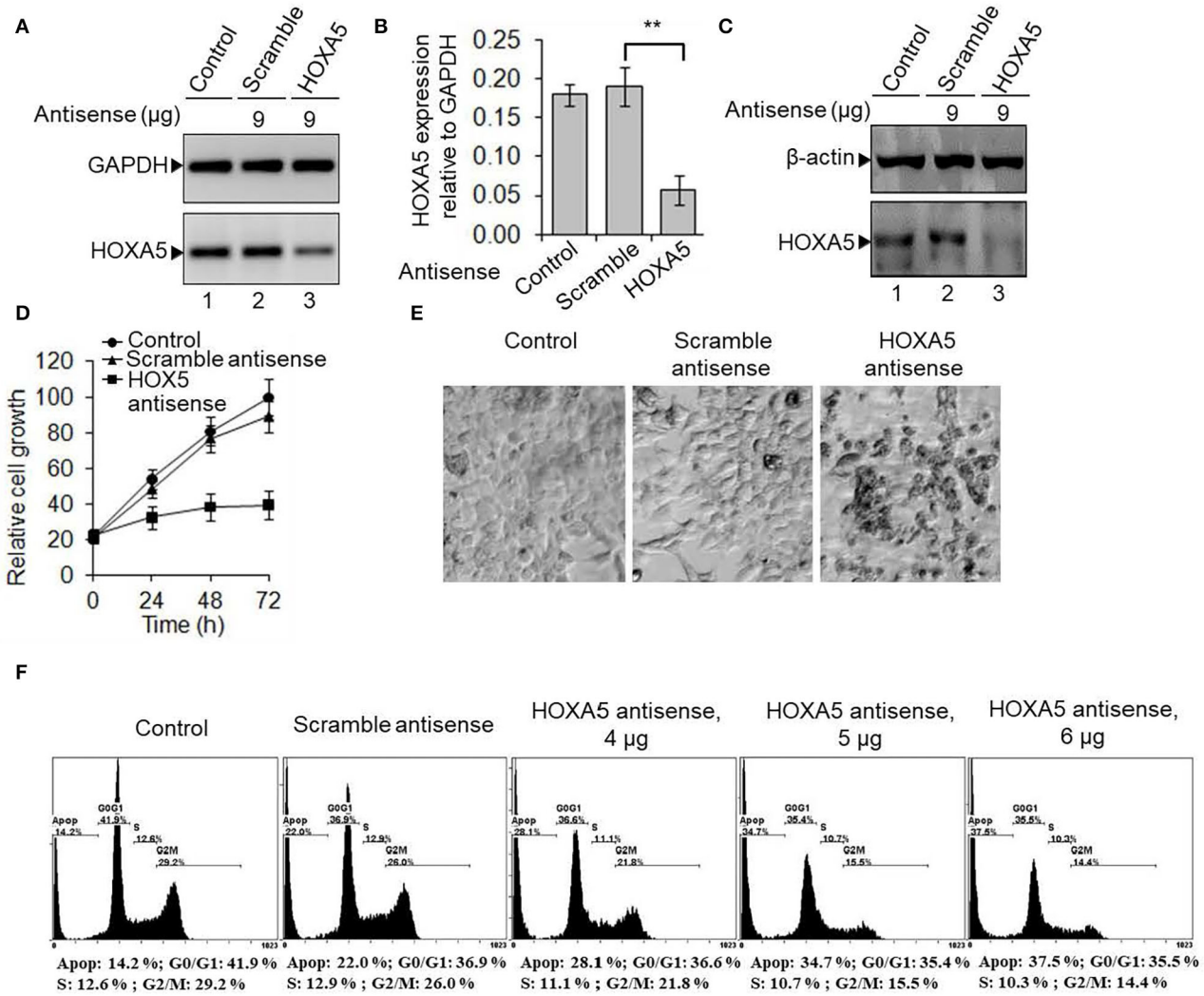

FIGURE 3 | HOXA5 knockdown affects cell viability and cell-cycle progression. **(A–C)** MCF7 cells were transfected with HOXA5-specific and scramble antisense for 48 h, RNA was analyzed by RT-PCR with primers specific to HOXA5 (**A**, quantification in **B**). GAPDH was used as normalization control. Bars indicate averages ± standard errors ($n = 3$). **denotes $p < 0.0001$ compared to scramble control. Proteins were analyzed by Western blot using HOXA5 and β-actin (loading control) antibodies **(C)**. **(D,E)** Impact of HOXA5 knockdown on cell growth and viability. MCF7 cells were transfected with HOXA5-specific and scramble-antisense oligonucleotides. Live cell numbers were counted under HOXA5 knockdown conditions for varying periods of time and plotted in **(D)**. Data points indicate averages ± standard errors ($n = 3$). **denotes $p < 0.0001$ compared to scramble control. Morphologies of cells were visualized under a microscope (Nikon Eclipse TE2000-U) **(E)**. Bars indicate standard errors ($n = 3$). **(F)** Flow cytometry analysis. MCF7 cells were treated with HOXA5 and scramble antisense separately for 48 h and subjected to flow cytometry analysis. Panel 1: Control cells treated with no antisense, panel 2: cells treated with scramble-antisense, panels 3–5: cells treated with increasing concentration of HOXA5-specific antisense. The cell populations at different stages of the cell cycle are shown inside the respective panels.

the mammary tissue of OVX female rats treated with E2 (5 µg/kg) (Betancourt et al., 2010; Bhan et al., 2014a,b; Hussain et al., 2015). The OVX procedure was performed to minimize the effects of endogenous estrogens. Interestingly, RT-qPCR and Western blot analysis demonstrate that HOXA5 expression is elevated in the rat mammary tissues upon treatment with E2 (**Figures 4C–E**), indicating potential E2-mediated regulation of HOXA5 *in vivo*.

ER Coordinates E2-Induced HOXA5 Expression

ERs are crucial players in estrogen signaling (Nilsson and Gustafsson, 2000, 2002). In general, ERs are activated upon binding to E2. The activated ERs dimerize and bind to their target gene promoters. Along with ERs, various ER co-regulators and chromatin-modifying enzymes are also recruited and modify the chromatin and induce ER target gene expression (Nilsson et al., 2001; Nilsson and Gustafsson, 2002; Barkhem et al., 2004; Dreijerink et al., 2006; Lee et al., 2006; Mo et al., 2006). To understand the importance of ERs in HOXA5 gene regulation, we analyzed the HOXA5 expression in ER knocked down (using ERα or ERβ-specific ASO) and E2-treated MCF7 cells. As seen in **Figure 5**, ERα or ERβ levels were knocked down upon treatment with respective ASO (lanes 5–7, **Figure 5A**, qPCR data in **Figure 5B**). Interestingly, the level of E2-induced expression of

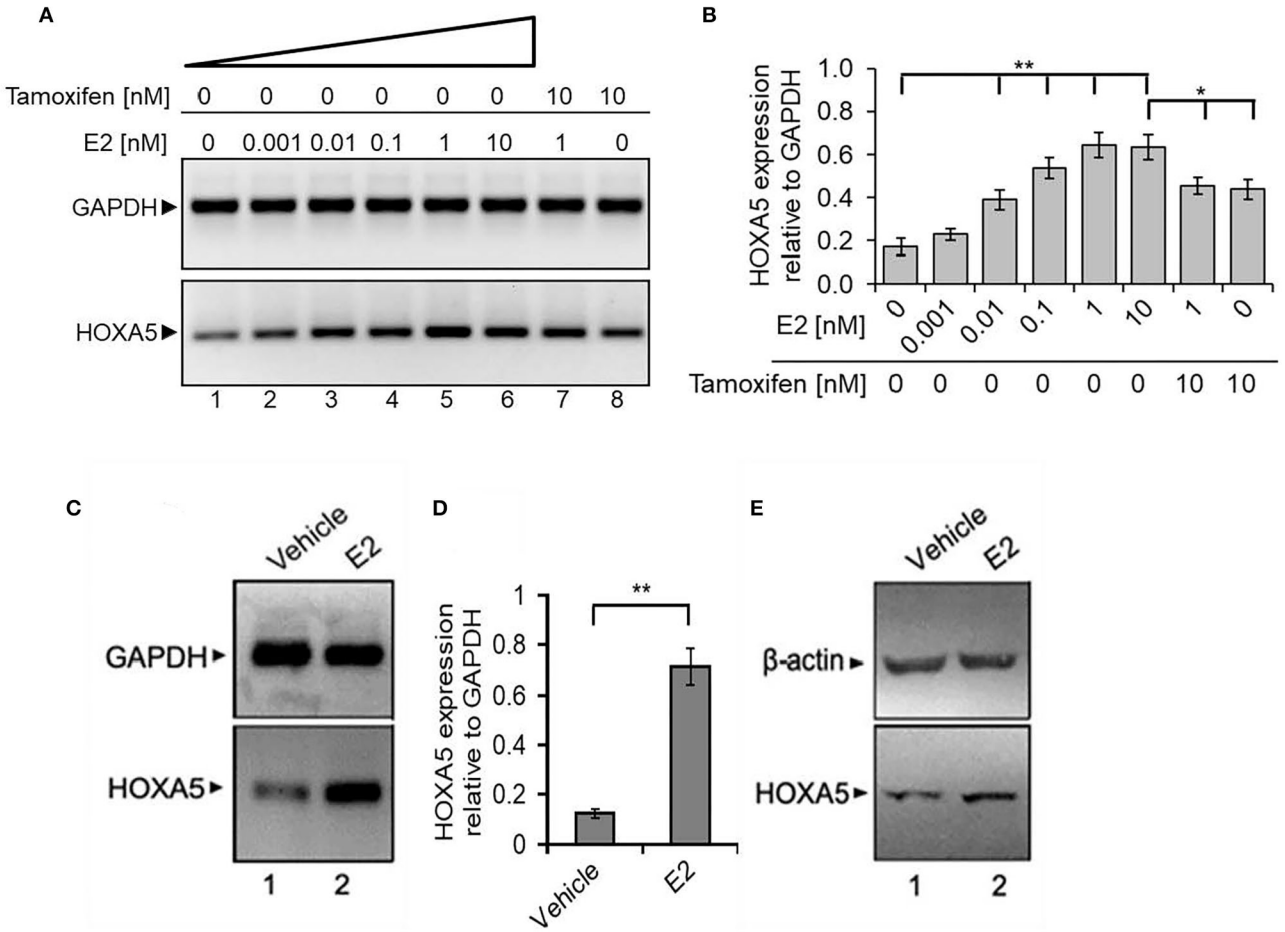

FIGURE 4 | E2-induced expression of HOXA5. **(A,B)** E2-induced expression of HOXA5 in MCF7 cells. MCF7 cells (grown in phenol red–free media and charcoal-stripped FBS) were treated with varying concentrations (0–10 nM) of E2 for 6 h in the presence and absence of 10 nM tamoxifen. RNA analyzed by RT-PCR using primers specific to HOXA5 and GAPDH (control). An agarose gel analysis picture of the PCR products is shown in **(A)**, and qPCR analysis (expression of HOXA5 relative to GAPDH) is in **(B)**. Bars indicate averages ± standard errors ($n = 3$). **denotes $p < 0.0001$ compared to untreated controls; *denotes $p < 0.001$ compared to 10 nM E2. **(C–E)** Effects of E2 on HOXA5 expression in OVX rats *in vivo*. OVX female rats were treated with E2 (5 μg for 24 h) or vehicle (peanut oil/saline). RNA and protein were isolated from the mammary glands of the control and E2-treated animals. RNA was analyzed by RT-PCR using rat-specific primers for HOXA5 (quantification in **D**); GAPDH was used as a loading control. Each experiment was repeated thrice with three parallel replicates. Bars indicate averages ± standard errors, **denotes $p < 0.0001$ compared to vehicle control. Western blot analysis of the HOXA5 protein levels from the protein samples obtained from control, E2-treated mammary gland tissues of animals are shown in **(E)**. β-actin was used as the loading control. Each experiment was repeated at least thrice ($n = 3$).

HOXA5 was suppressed significantly upon knockdown of ERα or ERβ (lanes 5–7, **Figures 5A,B**). Scramble-ASO does not have any major impact on the E2-dependent HOXA5 expression (lanes 2–4, **Figures 5A,B**). The level of E2-induced HOXA5 expression is further suppressed by the combined knockdown of ERα and ERβ (lane 7, **Figures 5A,B**).

As ERα and ERβ are associated with HOXA5 expression, we examined their binding to the HOXA5 promoter (Ansari et al., 2011b). We performed the ChIP assay using antibodies against ERα, ERβ, and β-actin (control), and the immunoprecipitated DNA were analyzed by PCR using primers spanning the estrogen-response element (ERE) regions of the HOXA5 promoter. Notably, promoter sequence analysis shows the presence of two potential EREs at the HOXA5 promoter upstream of the transcription start site (**Figure 6A**). ChIP analysis shows that levels of ERα and ERβ (but not β-actin) were enriched in the ERE1 and ERE2 regions of the HOXA5 promoter in the presence of E2 (**Figure 6B**, qPCR data in **Figure 6C**). Taken together, the antisense-mediated knockdown and ChIP analysis demonstrate the involvement of both ERα and ERβ HOXA5 gene expression in the presence of E2.

Along with ERs, ER co-activators are crucial players in ER target gene expression. Therefore, in addition to ERs, we analyzed the enrichment level of several well-known ER co-regulators: CBP/p300 (histone acetylase) and mixed lineage leukemias (MLL, histone methyltransferases) (Ansari et al., 2011b). Additionally, we also analyzed the level of

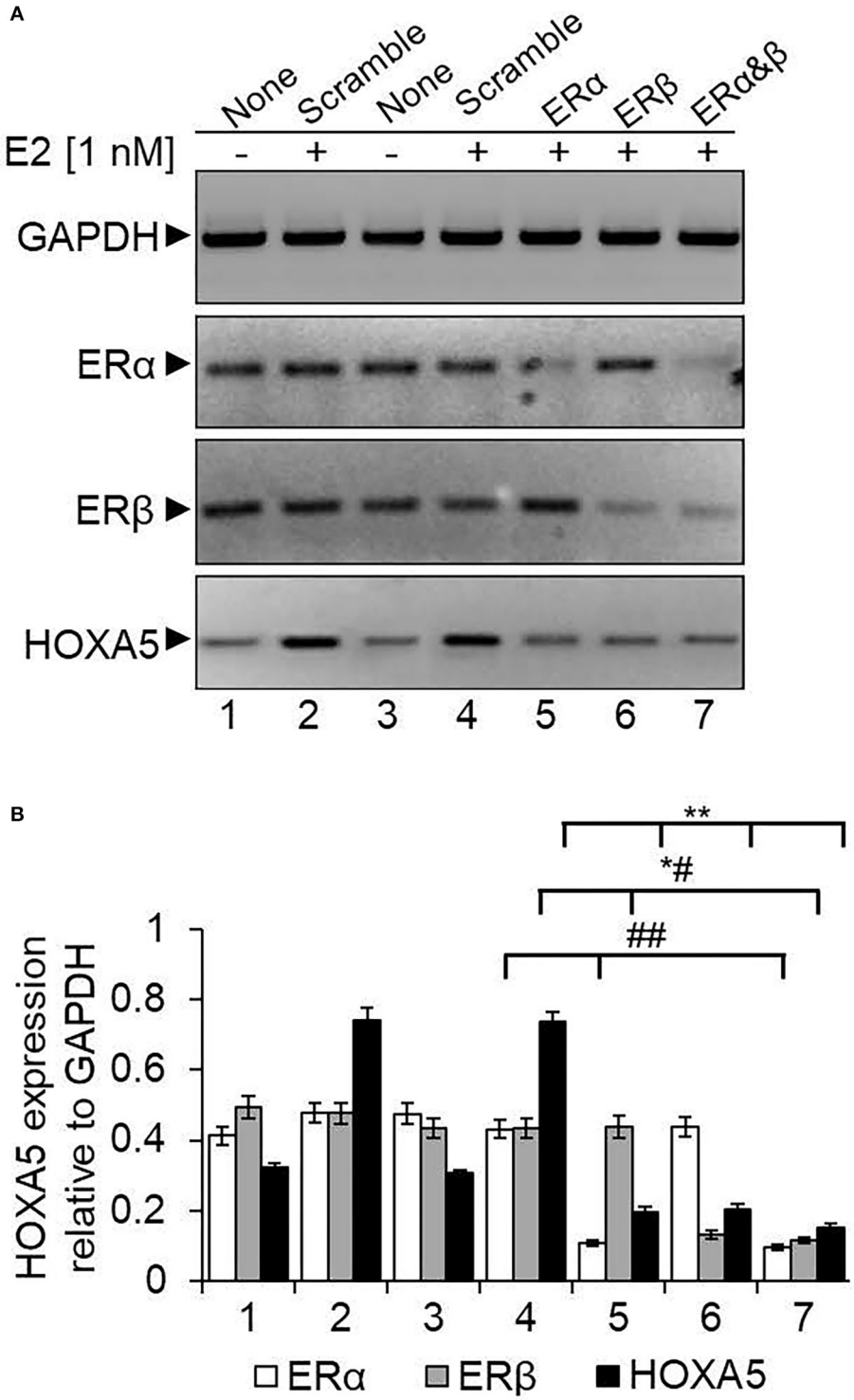

FIGURE 5 | Knockdown of ERs and its impact on E2-induced HOXA5 expression. MCF7 cells were transfected with ERα or ERβ-specific ASOs or a scramble antisense for 48 h, followed by treatment with E2 (1 nM, 6 h). RNA was analyzed by RT-qPCR by using primers specific to HOXA5, ERs, and GAPDH (control) separately **(A)**. Lane 1: control cells (no E2); lane 2: cells treated with E2; lanes 3 and 4: cells treated with scramble antisense in the absence and presence E2; lanes 5 and 6: cells treated with ERα and ERβ antisense, respectively, followed by exposure to E2; lane 7: cells transfected with 1:1 mixture of ERα and ERβ antisenses in the presence of E2. The qPCR analysis data is in **(B)**. qPCR reactions were carried out in three parallel replicates, and each experiment was repeated at least thrice ($n = 3$). Bars indicate averages ± standard errors. **indicates $p < 0.0001$ compared to E2-treated scramble control (for HOXA5 target); *# indicates $p < 0.0001$ compared to E2-treated scramble control (for ERβ target); ## indicates $p < 0.0001$ compared to E2-treated scramble control (for ERα target).

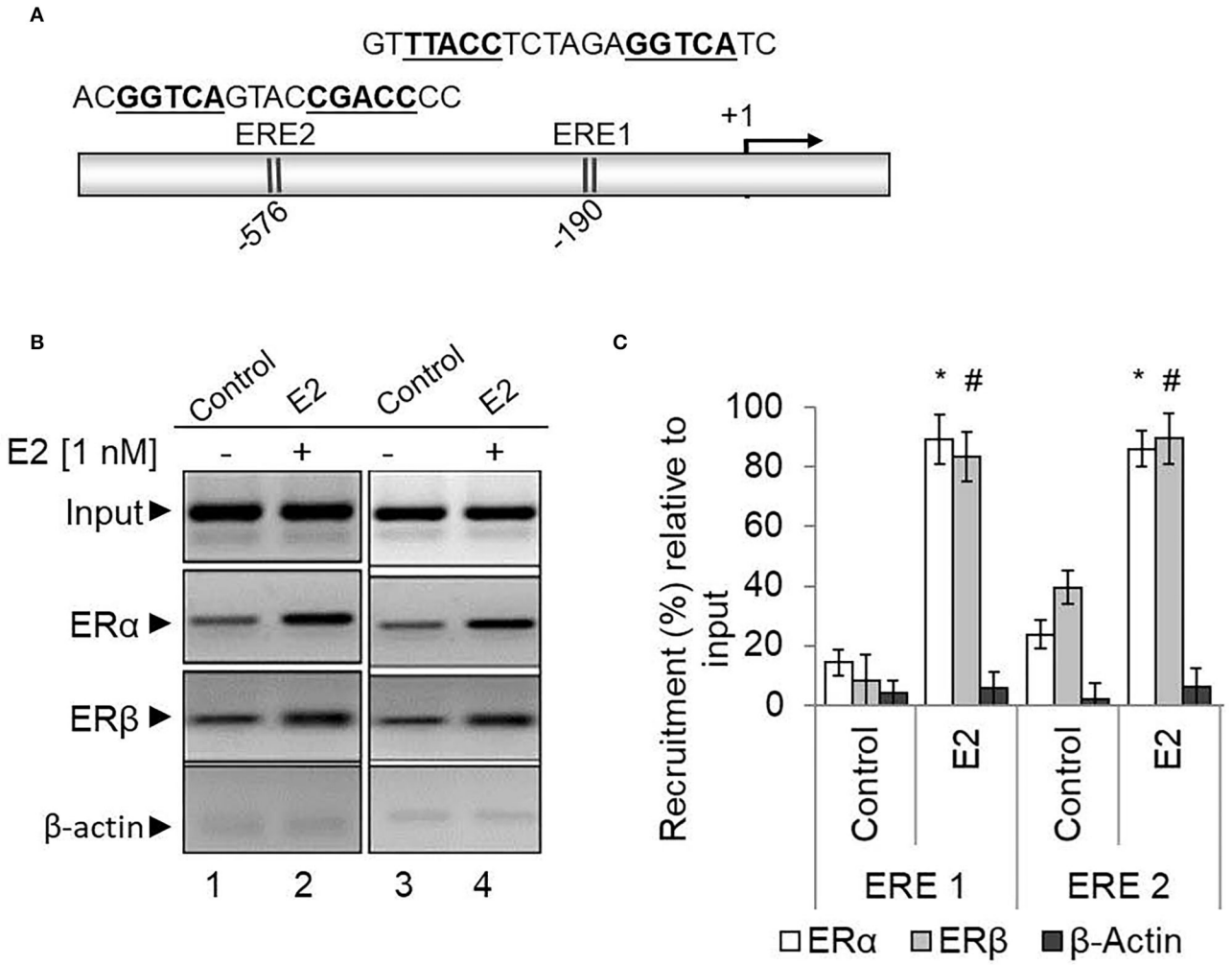

FIGURE 6 | ERα and ERβ enrichment on the HOXA5 promoter ERE in the presence of E2. The HOXA5 promoter contains two putative ERE regions (ERE1 and ERE2) near the transcription start site **(A)**. E2-treated (nM E2 for 6 h) and control (untreated) MCF7 cells were analyzed by ChIP assay using antibodies against ERα, ERβ, and β-actin (control). The ChIP DNA was analyzed by regular PCR (agarose gel analysis, **B**) and qPCR **(C)** using HOXA5 promoter primers (ERE1 and ER2 regions). Bars indicate averages ± standard errors ($n = 3$). *denotes $p < 0.0001$ compared to ERα ChIP control; $^{\#}$denotes $p < 0.0001$ compared to ERβ ChIP control for both the EREs.

histone acetylation and H3K4 trimethylation at the HOXA5 promoter using ChIP in the absence and presence of E2. Notably, promoter histone acetylation and H3K4 trimethylation are post-translational histone modifications associated with gene activation. Interestingly, our ChIP analysis shows that E2 treatment resulted in enrichment of CBP, p300, histone methylases MLL2 and MLL3 (**Figures 7A–C**). Histone acetylation, H3K4 trimethylation, and RNA polymerase II (RNAPII) levels were also elevated at the HOXA5 promoter with E2 treatments (**Figures 7A,B**). The E2-dependent enrichment in CBP/p300 acetyltransferase and MLL-histone methylases MLL2 and MLL3 and the histone acetylation and methylation levels, suggest that, along with ERs, these ER co-regulators are associated with E2-dependent HOXA5 gene expression.

DISCUSSION

HOX gene expression is well-known to guide cellular differentiation, organogenesis, and development (Krumlauf, 1994; Zakany and Duboule, 2007). Increasing studies demonstrate that hormones, such as estrogen, retinoic acid, etc., influence the expression of developmental genes, including HOX genes. Posterior HOX genes appear to be regulated by estrogens and progesterones, and anterior HOX genes are regulated by retinoids. HOXA5, which acts a transcription factor, plays a critical role in embryonic development. Beyond this, an emerging group of studies shows the dysregulation of HOXA5 in various solid/adult/pediatric/cancers or hematological malignancies and linked with higher pathological grade and poorer disease outcome (Chen et al., 2004; Wang et al.,

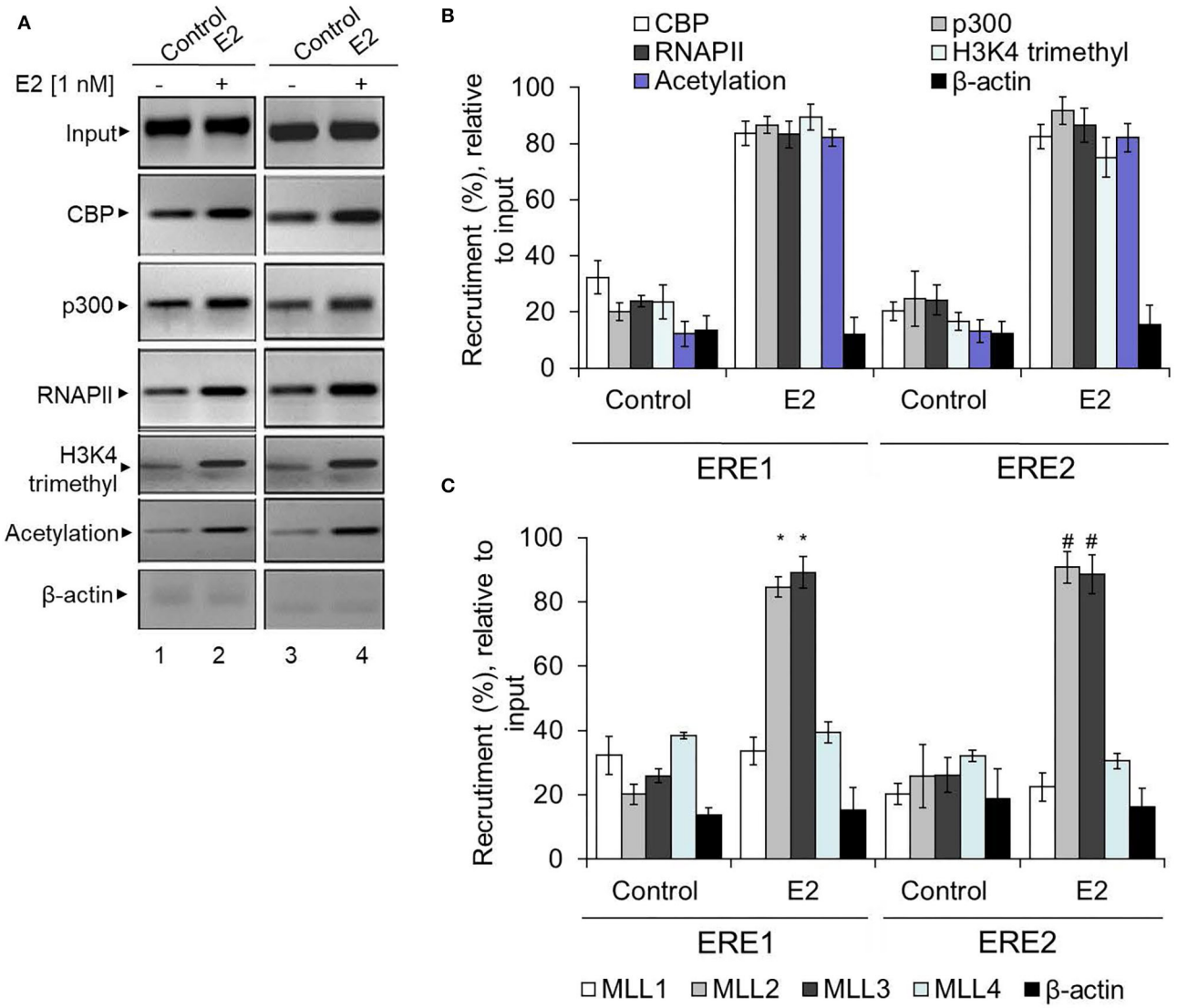

FIGURE 7 | Enrichment of ER co-regulators at the HOXA5 promoter EREs. E2-treated (1 nM, 6 h) MCF7 cells were analyzed by ChIP assay using different antibodies. The ChIP DNA was analyzed by PCR using HOXA5 promoter primers (ERE1 and ERE2 regions). An agarose gel analysis showing the recruitment of selected factors on the ERE1 and ERE2 regions of the HOXA5 promoter is shown in **(A)**. qPCR analysis of the ChIP DNA samples showing the enrichment (relative to input) of CBP, p300, MLL1, MLL2, MLL3, MLL4, H3K4-trimethyl, histone acetylation, RNAP II, and β-actin into the ERE1 and ERE2 regions of the HOXA5 promoter region in the presence of E2 is shown in **(B,C)**. For **(B,C)**, bars indicate averages ± standard errors ($n = 3$). *denotes $p < 0.0001$ compared to respective ChIP control for ERE1; #denotes $p < 0.0001$ compared to respective ChIP control for ERE2.

2019). However, the detailed mechanism by which HOX genes influence differentiation and development and how it is regulated or misregulated in diseases/various carcinomas is still emerging and less understood. Here, we explore any association and function of HOXA5 in breast cancer and investigate its potential mechanism of transcription.

Our studies demonstrate that HOXA5 expression is also augmented in breast cancer tissues in comparison to the corresponding adjacent normal breast tissues. Additionally, c-bioportal-based meta-analysis of preexisting gene expression databases in breast cancer patients also show that HOXA5 expression is elevated in breast cancer patients. HOXA5 expression is also found to be elevated in ER-positive breast cancer cells. Additionally, our studies also demonstrate that HOXA5 expression is important for cell-cycle progression as well as cell viability of breast cancer cells. HOXA5 downregulation results in cell-cycle arrest and apoptosis in breast cancer cells. These observations suggest that HOXA5 expression is elevated in breast cancer at least in some subset of breast cancer and may be critical for breast cancer cell proliferation. As HOXA5 is elevated in ER-positive breast cancer cells and breast cancer tissues, we investigated its gene regulation potential via E2. These studies demonstrate that E2 indeed regulates the transcription of HOXA5 *in vitro*, in ER-positive breast cancer cells (MCF7), and this expression is suppressed upon treatment with an antiestrogen, tamoxifen, suggesting the potential regulation of

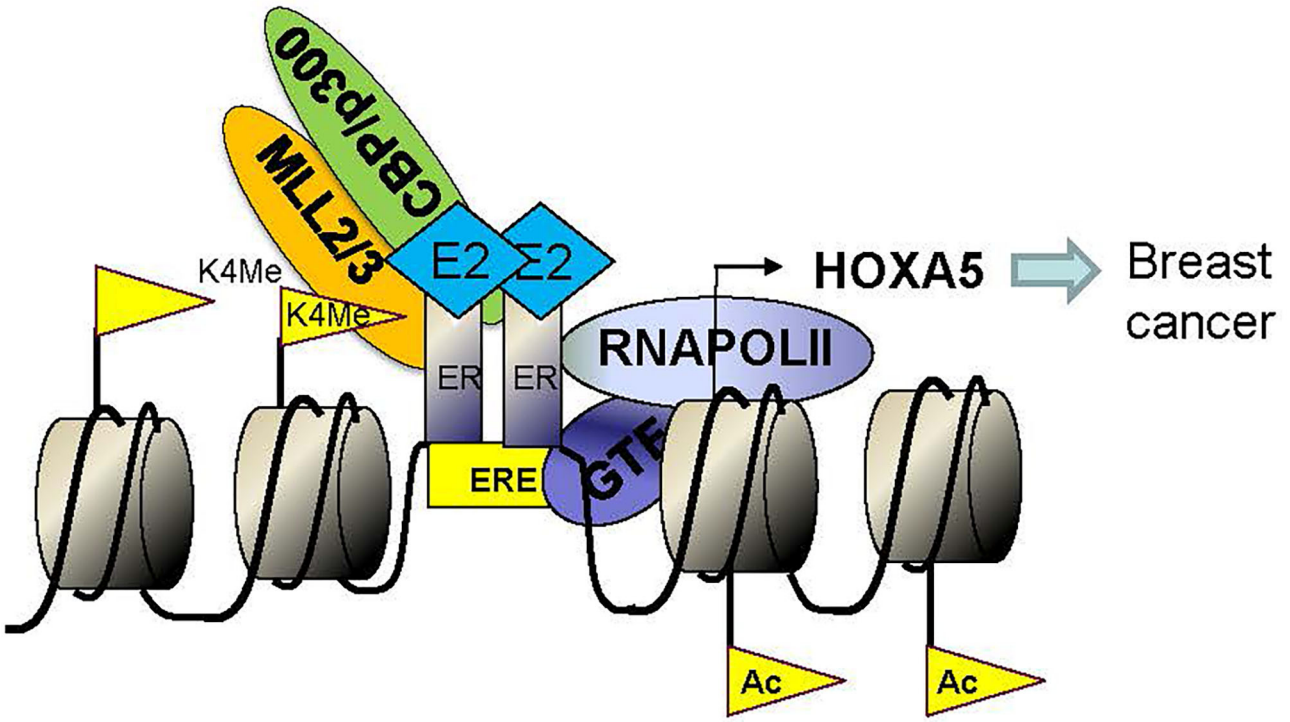

FIGURE 8 | Model showing the mechanism of E2-mediated activation of HOXA5. Binding of E2 induces conformational change in ERs and induces dimerization and activation of ERs. Activated ER dimers enter the nucleus, bind to the HOXA5 promoter (EREs). ER co-regulators (CBP, p300, MLL2, MLL3, and others) also bind to the HOXA5 promoter, modify chromatins (H3K4-trimethylation via MLL2 and MLL3 and histone acetylation via CBP/p300), aid in recruitment of RNA polymerase II (RNAP II) and general transcription factors (GTFs) to the promoter and ultimately lead to transcription activation of HOXA5.

HOXA5 via E2 and ERs. Additionally, we also observed that HOXA5 expression is elevated in the mammary tissues of OVX Sprague–Dawley rats, further supporting our observation that HOXA5 expression is regulated by estrogen *in vivo*.

Mechanistic studies demonstrate that E2-dependent HOXA5 expression is coordinated via involvement of ERs and ER co-activators. Knockdown of either ERα or ERβ suppressed E2-dependent HOXA5 expression in MCF7 cells. ChIP analysis demonstrates that ERs and ER co-activators, CBP/p300 (acetyl-transferases), and MLL2 and MLL3 (histone H3K4-methylases) are enriched at the HOXA5 promoter (ERE regions) in the presence of E2. Along with histone acetyl-transferases and histone methylases, the level of histone H3K4 trimethylation and histone acetylation level was elevated at the HOXA5 promoter. Notably, histone acetylation and H3K4 trimethylation are linked to gene activation. The enrichment of histone acetyl-transferases (CBP/p300) and histone H3K4 trimethylases (MLL2 and MLL3) and the histone acetylation and H3K4 trimethylations at the HOXA5 promoter in the presence of E2 suggest their important roles in E2-mediated regulation of HOXA5 expression in breast cancer.

Overall, our studies demonstrate that HOXA5 gene expression is regulated by E2, and its expression is upregulated in breast cancers. The E2-mediated regulation of HOXA5 is coordinated via involvement of estrogen receptors, CBP/p300 histone acetyl-transferases, and the MLL family of histone methyl-transferases. CBP/p300 and MLL-histone methylases act as ER co-regulators in regulation of HOXA5 expression in breast cancer. A model showing the mechanism of E2-mediated HOXA5 gene activation is shown in **Figure 8**. Notably, multiples lines of evidence support our observations that increased H3K4-trimethylation and histone acetylation contribute to E2-induced HOXA5 expression. For example, Yan et al. demonstrate that inhibition of histone deacetylase HDAC8 (by HDAC inhibitor) increases histone acetylation and HOXA5 expression, which, in turn, induces tumor-suppressor p53 induction (Yan et al., 2013). Another study shows that oxidative stress–mediated repression of HDAC8 induces histone H3 acetylation and HOXA5 expression that controls plasticity of lung cancer stem-like cells (Saijo et al., 2016). Similar to histone acetylation, histone H3K4 trimethylation is well-known to activate HOX gene expression, including HOXA5 expression (Okada et al., 2006; Mishra et al., 2009; Ansari et al., 2012b; Burillo-Sanz et al., 2018). Enhancer elements present around the HOXA cluster regulates HOXA cluster gene spatiotemporal expression, and deletion impairs HOX5 gene activation in embryonic stem cells (Cao et al., 2017). Thus, our results showing the roles of H3K4 trimethylation and histone acetylation are in agreement with previous studies. Although histone acetylation and H3K4-trimethylation result in gene activation, H3K27 trimethylation by polycomb repressive complex (PRC) results in HOXA5 gene silencing and contributes to cell differentiation and development

(Xi et al., 2007). Transcription factor CTCF facilitates the stabilization of PRC2 and H3K27 trimethylation at the HOXA locus and represses HOXA gene (including HOXA5) expression (Xu et al., 2014). Mutation in CTCF results in increased HOXA cluster gene expression. Similarly, ASXL1 mutation facilitates myeloid transformation through inhibition of PRC2-mediated HOXA5 repression (Abdel-Wahab et al., 2012). An independent study reports that HOXA5 expression is repressed in a subset of human breast cancer tissues, and this loss occurs via promoter hypermethylation (Teo et al., 2016). The study shows that HOXA5 loss in tumor cells causes reduced downstream target expression involved in maintaining epithelial integrity, which leads to a subsequent increase in invasion and migration. This suggests the potential presence of multiple modes of action of HOXA5 in different breast cancer subsets. Nevertheless, our studies demonstrate that HOXA5 expression is upregulated, at least in a subset of breast cancer, and is regulated by estrogen *in vitro* and *in vivo*, and therefore, may play critical roles in in breast cancer.

DATA AVAILABILITY STATEMENT

The raw data supporting the conclusions of this article will be made available by the authors, without undue reservation.

ETHICS STATEMENT

The animal study was reviewed and approved by IACUC, University of Texas at Arlington.

AUTHOR CONTRIBUTIONS

IH did most of the experiments, performed the data analysis, and contributed to the manuscript writing. PD, AC, MO, KA, and AB assisted the different biochemical experiments. SB and LP coordinated the animal experiments. SU, PA, RB, and HD helped with the cancer-related studies. SM designed the experiments, supervised the study, and written the manuscript. All authors contributed to the article and approved the submitted version.

FUNDING

Research in Mandal laboratory was supported by grant from National Institute of Health 1R15HL142032.

ACKNOWLEDGMENTS

We thank all the Mandal lab members for helpful discussions.

REFERENCES

Abdel-Wahab, O., Adli, M., LaFave, L. M., Gao, J., Hricik, T., Shih, A. H., et al. (2012). ASXL1 mutations promote myeloid transformation through loss of PRC2-mediated gene repression. *Cancer Cell* 22, 180–193. doi: 10.1016/j.ccr.2012.06.032

Acampora, D., D'Esposito, M., Faiella, A., Pannese, M., Migliaccio, E., Morelli, F., et al. (1989). The human HOX gene family. *Nucleic Acids Res.* 17, 10385–10402. doi: 10.1093/nar/17.24.10385

Akam, M. (1987). The molecular basis for metameric pattern in the Drosophila embryo. *Development* 101, 1–22.

Ansari, K. I., Hussain, I., Kasiri, S., and Mandal, S. S. (2012a). HOXC10 is overexpressed in breast cancer and transcriptionally regulated by estrogen via involvement of histone methylases MLL3 and MLL4. *J. Mol. Endocrinol.* 48, 61–75. doi: 10.1530/JME-11-0078

Ansari, K. I., Hussain, I., Shrestha, B., Kasiri, S., and Mandal, S. S. (2011a). HOXC6 Is transcriptionally regulated via coordination of MLL histone methylase and estrogen receptor in an estrogen environment. *J. Mol. Biol.* 411, 334–349. doi: 10.1016/j.jmb.2011.05.050

Ansari, K. I., Kasiri, S., Mishra, B. P., and Mandal, S. S. (2012b). Mixed lineage leukaemia-4 regulates cell-cycle progression and cell viability and its depletion suppresses growth of xenografted tumour *in vivo*. *Br. J. Cancer* 107, 315–324. doi: 10.1038/bjc.2012.263

Ansari, K. I., Shrestha, B., Hussain, I., Kasiri, S., and Mandal, S. S. (2011b). Histone methylases MLL1 and MLL3 coordinate with estrogen receptors in estrogen-mediated HOXB9 expression. *Biochemistry* 50, 3517–3527. doi: 10.1021/bi102037t

Barkhem, T., Nilsson, S., and Gustafsson, J. A. (2004). Molecular mechanisms, physiological consequences and pharmacological implications of estrogen receptor action. *Am. J. Pharmacogenom.* 4, 19–28. doi: 10.2165/00129785-200404010-00003

Betancourt, A. M., Eltoum, I. A., Desmond, R. A., Russo, J., and Lamartiniere, C. A. (2010). *In utero* exposure to bisphenol A shifts the window of susceptibility for mammary carcinogenesis in the rat. *Environ. Health Perspect.* 118, 1614–1619. doi: 10.1289/ehp.1002148

Bhan, A., Hussain, I., Ansari, K. I., Bobzean, S. A., Perrotti, L. I., and Mandal, S. S. (2014a). Histone methyltransferase EZH2 is transcriptionally induced by estradiol as well as estrogenic endocrine disruptors bisphenol-A and diethylstilbestrol. *J. Mol. Biol.* 426, 3426–3441. doi: 10.1016/j.jmb.2014.07.025

Bhan, A., Hussain, I., Ansari, K. I., Bobzean, S. A., Perrotti, L. I., and Mandal, S. S. (2014b). Bisphenol-A and diethylstilbestrol exposure induces the expression of breast cancer associated long noncoding RNA HOTAIR *in vitro* and *in vivo*. *J. Steroid Biochem. Mol. Biol.* 141, 160–170. doi: 10.1016/j.jsbmb.2014.02.002

Bhatlekar, S., Fields, J. Z., and Boman, B. M. (2014). HOX genes and their role in the development of human cancers. *J. Mol. Med.* 92, 811–823. doi: 10.1007/s00109-014-1181-y

Boube, M., Hudry, B., Immarigeon, C., Carrier, Y., Bernat-Fabre, S., Merabet, S., et al. (2014). Drosophila melanogaster Hox transcription factors access the RNA polymerase II machinery through direct homeodomain binding to a conserved motif of mediator subunit Med19. *PLoS Genet.* 10:e1004303. doi: 10.1371/journal.pgen.1004303

Burillo-Sanz, S., Morales-Camacho, R. M., Caballero-Velazquez, T., Carrillo, E., Sanchez, J., Perez-Lopez, O., et al. (2018). MLL-rearranged acute myeloid leukemia: Influence of the genetic partner in allo-HSCT response and prognostic factor of MLL 3′ region mRNA expression. *Eur. J. Haematol.* 100, 436–443. doi: 10.1111/ejh.13037

Cao, K., Collings, C. K., Marshall, S. A., Morgan, M. A., Rendleman, E. J., Wang, L., et al. (2017). SET1A/COMPASS and shadow enhancers in the regulation of homeotic gene expression. *Genes Dev.* 31, 787–801. doi: 10.1101/gad.294744.116

Cerami, E., Gao, J., Dogrusoz, U., Gross, B. E., Sumer, S. O., Aksoy, B. A., et al. (2012). The cBio cancer genomics portal: an open platform for exploring multidimensional cancer genomics data. *Cancer Discov.* 2, 401–404. doi: 10.1158/2159-8290.CD-12-0095

Chen, H., Chung, S., and Sukumar, S. (2004). HOXA5-induced apoptosis in breast cancer cells is mediated by caspases 2 and 8. *Mol. Cell Biol.* 24, 924–935. doi: 10.1128/MCB.24.2.924-935.2004

Chu, M. C., Selam, F. B., and Taylor, H. S. (2004). HOXA10 regulates p53 expression and matrigel invasion in human breast cancer cells. *Cancer Biol. Ther.* 3, 568–572. doi: 10.4161/cbt.3.6.848

Deb, P., Bhan, A., Hussain, I., Ansari, K. I., Bobzean, S. A., Pandita, T. K., et al. (2016). Endocrine disrupting chemical, bisphenol-A, induces breast cancer associated gene HOXB9 expression *in vitro* and *in vivo*. *Gene* 590, 234–243. doi: 10.1016/j.gene.2016.05.009

Dreijerink, K. M., Mulder, K. W., Winkler, G. S., Hoppener, J. W., Lips, C. J., and Timmers, H. T. (2006). Menin links estrogen receptor activation to histone H3K4 trimethylation. *Cancer Res.* 66, 4929–4935. doi: 10.1158/0008-5472.CAN-05-4461

Duboule, D., and Dolle, P. (1989). The structural and functional organization of the murine HOX gene family resembles that of Drosophila homeotic genes. *EMBO J.* 8, 1497–1505. doi: 10.1002/j.1460-2075.1989.tb03534.x

Dunwell, T. L., and Holland, P. W. (2016). Diversity of human and mouse homeobox gene expression in development and adult tissues. *BMC Dev. Biol.* 16:40. doi: 10.1186/s12861-016-0140-y

Gao, J. J., Aksoy, B. A., Dogrusoz, U., Dresdner, G., Gross, B., Sumer, S. O., et al. (2013). Integrative analysis of complex cancer genomics and clinical profiles using the cBioPortal. *Sci. Signal.* 6:pl1. doi: 10.1126/scisignal.2004088

Garcia-Fernandez, J. (2005). The genesis and evolution of homeobox gene clusters. *Nat. Rev. Genet.* 6, 881–892. doi: 10.1038/nrg1723

Gray, S., Pandha, H. S., Michael, A., Middleton, G., and Morgan, R. (2011). HOX genes in pancreatic development and cancer. *J. Pancreas* 12, 216–219.

Grier, D. G., Thompson, A., Kwasniewska, A., McGonigle, G. J., Halliday, H. L., and Lappin, T. R. (2005). The pathophysiology of HOX genes and their role in cancer. *J. Pathol.* 205, 154–171. doi: 10.1002/path.1710

Hanson, R. D., Hess, J. L., Yu, B. D., Ernst, P., van Lohuizen, M., Berns, A., et al. (1999). Mammalian Trithorax and polycomb-group homologues are antagonistic regulators of homeotic development. *Proc. Natl. Acad. Sci. U.S.A.* 96, 14372–14377. doi: 10.1073/pnas.96.25.14372

Hayashida, T., Takahashi, F., Chiba, N., Brachtel, E., Takahashi, M., Godin-Heymann, N., et al. (2010). HOXB9, a gene overexpressed in breast cancer, promotes tumorigenicity and lung metastasis. *Proc. Natl. Acad. Sci. U.S.A.* 107, 1100–1105. doi: 10.1073/pnas.0912710107

Holland, P. W. H., Booth, H. A. F., and Bruford, E. A. (2007). Classification and nomenclature of all human homeobox genes. *BMC Biol.* 5:47. doi: 10.1186/1741-7007-5-47

Hussain, I., Bhan, A., Ansari, K. I., Deb, P., Bobzean, S. A., Perrotti, L. I., et al. (2015). Bisphenol-A induces expression of HOXC6, an estrogen-regulated homeobox-containing gene associated with breast cancer. *Biochim. Biophys. Acta* 1849, 697–708. doi: 10.1016/j.bbagrm.2015.02.003

Inagaki, T., Frankfurt, M., and Luine, V. (2012). Estrogen-induced memory enhancements are blocked by acute bisphenol A in adult female rats: role of dendritic spines. *Endocrinology* 153, 3357–3367. doi: 10.1210/en.2012-1121

Jeannotte, L., Gotti, F., and Landry-Truchon, K. (2016). Hoxa5: a key player in development and disease. *J. Dev. Biol.* 4:13. doi: 10.3390/jdb4020013

Joksimovic, M., Jeannotte, L., and Tuggle, C. K. (2005). Dynamic expression of murine HOXA5 protein in the central nervous system. *Gene Exp. Patterns* 5, 792–800. doi: 10.1016/j.modgep.2005.03.008

Kasiri, S., Ansari, K. I., Hussain, I., Bhan, A., and Mandal, S. S. (2013). Antisense oligonucleotide mediated knockdown of HOXC13 affects cell growth and induces apoptosis in tumor cells and over expression of HOXC13 induces 3D-colony formation. *RSC Adv.* 3, 3260–3269. doi: 10.1039/c2ra22006g

Krumlauf, R. (1994). Hox genes in vertebrate development. *Cell* 78, 191–201. doi: 10.1016/0092-8674(94)90290-9

Ladam, F., and Sagerstrom, C. G. (2014). Hox regulation of transcription: more complex(es). *Dev. Dyn.* 243, 4–15. doi: 10.1002/dvdy.23997

Larochelle, C., Tremblay, M., Bernier, D., Aubin, J., and Jeannotte, L. (1999). Multiple cis-acting regulatory regions are required for restricted spatio-temporal Hoxa5 gene expression. *Dev. Dyn.* 214, 127–140. doi: 10.1002/(SICI)1097-0177(199902)214:2<127::AID-AJA3>3.0.CO;2-F

Lee, S., Lee, D. K., Dou, Y. L., Lee, J., Lee, B., Kwak, E., et al. (2006). Coactivator as a target gene specificity determinant for histone H3 lysine 4 methyltransferases, *Proc. Natl. Acad. Sci. U.S.A.* 103, 15392–15397. doi: 10.1073/pnas.0607313103

Mallo, M., and Alonso, C. R. (2013). The regulation of Hox gene expression during animal development. *Development* 140, 3951–3963. doi: 10.1242/dev.068346

Mallo, M., Wellik, D. M., and Deschamps, J. (2010). Hox genes and regional patterning of the vertebrate body plan. *Dev. Biol.* 344, 7–15. doi: 10.1016/j.ydbio.2010.04.024

McGinnis, W., and Krumlauf, R. (1992). Homeobox genes and axial patterning. *Cell* 68, 283–302. doi: 10.1016/0092-8674(92)90471-N

Mishra, B. P., Ansari, K. I., and Mandal, S. S. (2009). Dynamic association of MLL1, H3K4 trimethylation with chromatin and Hox gene expression during the cell cycle. *FEBS J.* 276, 1629–1640. doi: 10.1111/j.1742-4658.2009.06895.x

Mlodzik, M., Fjose, A., and Gehring, W. J. (1988). Molecular structure and spatial expression of a homeobox gene from the labial region of the Antennapedia-complex. *EMBO J.* 7, 2569–2578. doi: 10.1002/j.1460-2075.1988.tb03106.x

Mo, R., Rao, S. M., and Zhu, Y. J. (2006). Identification of the MLL2 complex as a coactivator for estrogen receptor alpha. *J. Biol. Chem.* 281, 15714–15720. doi: 10.1074/jbc.M513245200

Morgan, R., Simpson, G., Gray, S., Gillett, C., Tabi, Z., Spicer, J., et al. (2016). HOX transcription factors are potential targets and markers in malignant mesothelioma, *BMC Cancer* 16:85. doi: 10.1186/s12885-016-2106-7

Neville, S. E., Baigent, S. M., Bicknell, A. B., Lowry, P. J., and Gladwell, R. T. (2002). Hox gene expression in adult tissues with particular reference to the adrenal gland. *Endocr. Res.* 28, 669–673. doi: 10.1081/ERC-120016984

Nguyen Kovochich, A., Arensman, M., Lay, A. R., Rao, N. P., Donahue, T., Li, X., et al. (2013). HOXB7 promotes invasion and predicts survival in pancreatic adenocarcinoma. *Cancer* 119, 529–539. doi: 10.1002/cncr.27725

Nilsson, S., and Gustafsson, J. A. (2000). Estrogen receptor transcription and transactivation: basic aspects of estrogen action. *Breast Cancer Res.* 2, 360–366. doi: 10.1186/bcr81

Nilsson, S., and Gustafsson, J. A. (2002). Estrogen receptor action. *Crit. Rev. Eukar. Gene* 12, 237–257. doi: 10.1615/CritRevEukaryotGeneExpr.v12.i4.10

Nilsson, S., Makela, S., Treuter, E., Tujague, M., Thomsen, J., Andersson, G., et al. (2001). Mechanisms of estrogen action. *Physiol. Rev.* 81, 1535–1565. doi: 10.1152/physrev.2001.81.4.1535

Okada, Y., Jiang, Q., Lemieux, M., Jeannotte, L., Su, L., and Zhang, Y. (2006). Leukaemic transformation by CALM-AF10 involves upregulation of Hoxa5 by hDOT1L. *Nat. Cell Biol.* 8, 1017–1024. doi: 10.1038/ncb1464

Plowright, L., Harrington, K. J., Pandha, H. S., and Morgan, R. (2009). HOX transcription factors are potential therapeutic targets in non-small-cell lung cancer (targeting HOX genes in lung cancer). *Br. J. Cancer* 100, 470–475. doi: 10.1038/sj.bjc.6604857

Raman, V., Martensen, S. A., Reisman, D., Evron, E., Odenwald, W. F., Jaffee, E., et al. (2000a). Compromised HOXA5 function can limit p53 expression in human breast tumours. *Nature* 405, 974–978. doi: 10.1038/35016125

Raman, V., Tamori, A., Vali, M., Zeller, K., Korz, D., and Sukumar, S. (2000b). HOXA5 regulates expression of the progesterone receptor. *J. Biol. Chem.* 275, 26551–26555. doi: 10.1074/jbc.C000324200

Rux, D. R., and Wellik, D. M. (2017). Hox genes in the adult skeleton: Novel functions beyond embryonic development. *Dev. Dyn.* 246, 310–317. doi: 10.1002/dvdy.24482

Saijo, H., Hirohashi, Y., Torigoe, T., Horibe, R., Takaya, A., Murai, A., et al. (2016). Plasticity of lung cancer stem-like cells is regulated by the transcription factor HOXA5 that is induced by oxidative stress. *Oncotarget* 7, 50043–50056. doi: 10.18632/oncotarget.10571

Shah, N., and Sukumar, S. (2010). The Hox genes and their roles in oncogenesis. *Nat. Rev. Cancer* 10, 361–371. doi: 10.1038/nrc2826

Shrestha, B., Ansari, K. I., Bhan, A., Kasiri, S., Hussain, I., and Mandal, S. S. (2012). Homeodomain-containing protein HOXB9 regulates expression of growth and angiogenic factors, facilitates tumor growth *in vitro* and is overexpressed in breast cancer tissue. *FEBS J.* 279, 3715–3726. doi: 10.1111/j.1742-4658.2012.08733.x

Svingen, T., and Tonissen, K. F. (2006). Hox transcription factors and their elusive mammalian gene targets. *Heredity* 97, 88–96. doi: 10.1038/sj.hdy.6800847

Takahashi, Y., Hamada, J., Murakawa, K., Takada, M., Tada, M., Nogami, I., et al. (2004). Expression profiles of 39 HOX genes in normal human adult organs and anaplastic thyroid cancer cell lines by quantitative real-time RT-PCR system. *Exp. Cell Res.* 293, 144–153. doi: 10.1016/j.yexcr.2003.09.024

Taniguchi, Y. (2014). Hox transcription factors: modulators of cell-cell and cell-extracellular matrix adhesion. *BioMed Res. Int.* 2014:591374. doi: 10.1155/2014/591374

Taylor, H. S., Arici, A., Olive, D., and Igarashi, P. (1998). HOXA10 is expressed in response to sex steroids at the time of implantation in the human endometrium. *J. Clin. Invest.* 101, 1379–1384. doi: 10.1172/JCI1057

Teo, W. W., Merino, V. F., Cho, S., Korangath, P., Liang, X., Wu, R. C., et al. (2016). HOXA5 determines cell fate transition and impedes tumor initiation and progression in breast cancer through regulation of E-cadherin and CD24. *Oncogene* 35, 5539–5551. doi: 10.1038/onc.2016.95

Wang, F., Zhang, R., Wu, X., and Hankinson, O. (2010). Roles of coactivators in hypoxic induction of the erythropoietin gene. *PLoS ONE* 5:e10002. doi: 10.1371/journal.pone.0010002

Wang, Z., Yu, C., and Wang, H. (2019). HOXA5 inhibits the proliferation and induces the apoptosis of cervical cancer cells via regulation of protein kinase B and p27. *Oncol. Rep.* 41, 1122–1130. doi: 10.3892/or.2018.6874

Wu, X. Y., Chen, H. X., Parker, B., Rubin, E., Zhu, T., Lee, J. S., et al. (2006). HOXB7, a homeodomain protein, is overexpressed in breast cancer and confers epithelial-mesenchymal transition. *Cancer Res.* 66, 9527–9534. doi: 10.1158/0008-5472.CAN-05-4470

Xi, S., Zhu, H., Xu, H., Schmidtmann, A., Geiman, T. M., and Muegge, K. (2007). Lsh controls Hox gene silencing during development. *Proc. Natl. Acad. Sci. U.S.A.* 104, 14366–14371. doi: 10.1073/pnas.0703669104

Xu, M., Zhao, G. N., Lv, X., Liu, G., Wang, L. Y., Hao, D. L., et al. (2014). CTCF controls HOXA cluster silencing and mediates PRC2-repressive higher-order chromatin structure in NT2/D1 cells. *Mol. Cell Biol.* 34, 3867–3879. doi: 10.1128/MCB.00567-14

Yan, W., Liu, S., Xu, E., Zhang, J., Zhang, Y., Chen, X., et al. (2013). Histone deacetylase inhibitors suppress mutant p53 transcription via histone deacetylase 8. *Oncogene* 32, 599–609. doi: 10.1038/onc.2012.81

Zakany, J., and Duboule, D. (2007). The role of Hox genes during vertebrate limb development. *Curr. Opin. Genet. Dev.* 17, 359–366. doi: 10.1016/j.gde.2007.05.011

Zheng, C. G., Jin, F. Q. C., and Chalfie, M. (2015). Hox proteins act as transcriptional guarantors to ensure terminal differentiation. *Cell Rep.* 13, 1343–1352. doi: 10.1016/j.celrep.2015.10.044

Conflict of Interest: The authors declare that the research was conducted in the absence of any commercial or financial relationships that could be construed as a potential conflict of interest.

frontiers in Cell and Developmental Biology

REVIEW
published: 11 January 2021
doi: 10.3389/fcell.2020.615071

The Complex Roles and Therapeutic Implications of m^{6}A Modifications in Breast Cancer

Min Wei[1,2†], Jing-Wen Bai[2,3†], Lei Niu[1,2], Yong-Qu Zhang[1,2], Hong-Yu Chen[1,2] and Guo-Jun Zhang[1,2]*

[1] Department of Breast and Thyroid Surgery, Xiang'an Hospital of Xiamen University, School of Medicine, Xiamen University, Xiamen, China, [2] Cancer Research Center, School of Medicine, Xiamen University, Xiamen, China, [3] Department of Oncology, Xiang'an Hospital of Xiamen University, School of Medicine, Xiamen University, Xiamen, China

Accumulating evidence indicates that N^6-methyladenosine (m^{6}A), which directly regulates mRNA, is closely related to multiple biological processes and the progression of different malignancies, including breast cancer (BC). Studies of the aberrant expression of m^{6}A mediators in BC revealed that they were associated with different BC subtypes and functions, such as proliferation, apoptosis, stemness, the cell cycle, migration, and metastasis, through several factors and signaling pathways, such as Bcl-2 and the PI3K/Akt pathway, among others. Several regulators that target m^{6}A have been shown to have anticancer effects. Fat mass and obesity-associated protein (FTO) was identified as the first m^{6}A demethylase, and a series of inhibitors that target FTO were reported to have potential for the treatment of BC by inhibiting cell proliferation and promoting apoptosis. However, the exact mechanism by which m^{6}A modifications are regulated by FTO inhibitors remains unknown. m^{6}A modifications in BC have only been preliminarily studied, and their mechanisms require further investigation.

Keywords: N^6-methyladenosine, breast cancer, m^{6}A modification regulator, mechanism pathways, FTO inhibitor

OPEN ACCESS

Edited by:
Xiao Zhu,
Guangdong Medical University, China

Reviewed by:
Ruiqiong Guo,
Michigan State University, United States
Chao Mao,
University of Texas MD Anderson Cancer Center, United States

****Correspondence:***
Guo-Jun Zhang
gjzhang@xah.xmu.edu.cn;
guoj_zhang@yahoo.com

† These authors have contributed equally to this work

Specialty section:
This article was submitted to Epigenomics and Epigenetics, a section of the journal Frontiers in Cell and Developmental Biology

Received: *08 October 2020*
Accepted: *07 December 2020*
Published: *11 January 2021*

Citation:
Wei M, Bai J-W, Niu L, Zhang Y-Q, Chen H-Y and Zhang G-J (2021) The Complex Roles and Therapeutic Implications of m^{6}A Modifications in Breast Cancer. Front. Cell Dev. Biol. 8:615071. doi: 10.3389/fcell.2020.615071

INTRODUCTION

Understanding the origins of cancer has changed significantly in recent decades, from being considered solely a genetic disease to being considered a genetic and/or epigenetic disease. Traditional epigenetic modifications, including the dysregulation of DNA methylation and histone modification, are causes of cancer, but chemical modifications of RNA were recently discovered to also cause cancer (Esteve-Puig et al., 2020). Breast cancer (BC) is the most common malignancy among women in the world (Siegel et al., 2020). Aberrant RNA modifications open a new era for studying the development and progression of BC (Chen et al., 2019).

Since the first modified nucleotides in RNAs were discovered in 1960 (Cohn, 1960), more than 170 distinct cellular RNA chemical modifications have been identified (Esteve-Puig et al., 2020), including pseudouridine (Ψ), N1-methyladenosine (m^{1}A), 5-methylcytidine (m^{5}C), N^6-methyladenosine (m^{6}A), 5-hydroxymethylcytosine (hm^{5}C), etc. Among these, m^{6}A is the most common and abundant posttranscriptional modification of messenger RNA (mRNA) and non-coding RNA (ncRNA). High-throughput sequencing revealed that one-third to one-half of mRNA transcripts had m^{6}A modifications in human and mouse transcriptomes (Dominissini et al., 2012). Although m^{6}A was first reported in 1974 (Desrosiers et al., 1974), little progress was made

for decades (Reichel et al., 2019). Recently, the function of m^{6}A has been gradually unveiled through advances in m^{6}A detection techniques, such as liquid chromatography-tandem mass spectrometry (Fu et al., 2015), methylated RNA immunoprecipitation sequencing (Meyer et al., 2012), methylation individual nucleotide-resolution crosslinking immunoprecipitation (Linder et al., 2015), and single-molecule real-time sequencing (Zhu et al., 2016).

The m^{6}A modification mainly identifies the conserved sequence RRACH (R = G/A, H = A/C/U). GGACU is one of the most common motifs (Harper et al., 1990). m^{6}A modifications were previously believed to be mainly concentrated in the 3′-untranslated region (UTR), especially around the stop codon (Meyer et al., 2012). In recent years, researchers confirmed that the 5′-UTR (Meyer et al., 2015) and coding sequence (CDS; Mao et al., 2019) were also important for m^{6}A modifications. Many studies have shown that they can regulate almost every stage of RNA metabolism, including alternative RNA splicing (Bartosovic et al., 2017; Louloupi et al., 2018), localization (Roundtree et al., 2017), translation efficiency (Wang et al., 2015b), mRNA stability (Wang et al., 2014), and protein expression (Yue et al., 2015).

N^6-methyladenosine is involved in the regulation of many biological processes, such as the transition fate of mammalian embryonic stem cells (Batista et al., 2014) and circadian rhythms (Fustin et al., 2013; Zhong et al., 2018), and various diseases, such as obesity (Dina et al., 2007), infertility (Ding et al., 2018), type 2 diabetic mellitus (Shen et al., 2015), and many kinds of cancers (Chen et al., 2019). Compared with various studies that explored the interplay between m^{6}A modifications and several types of cancers, studies of the role of m^{6}A in BC are still in their infancy. Some conclusions of existing studies are controversial, thus underscoring the necessity to review and discuss the functions of m^{6}A modifications and therapeutic strategies for BC.

This review focuses on the mechanism of m^{6}A modifications, the roles of different m^{6}A modulators in BC, especially their effect on proliferation, apoptosis, the cell cycle, and stemness, and therapeutic strategies for BC. This review will advance our understanding of the role of m^{6}A modifications in the development and progression of BC.

MECHANISM OF m^{6}A MODIFICATION

There are mainly three kinds of mediator proteins that regulate m^{6}A modifications: methyltransferase (writer), demethylase (eraser), and binding protein (reader). The regulation of m^{6}A modifications is dynamically reversible, depending on the activity of the "writer" and "eraser."

m^{6}A Methyltransferase (Writer)

N^6-methyladenosine modification is installed by the methyltransferase complex (MTC), which mainly consists of the methyltransferase like 3 (METTL3)/METTL14 heterodimer and Wilms' tumor 1-associated protein (WTAP; Scholler et al., 2018; **Figure 1**). In this m^{6}A MTC, METTL3 acts as the core catalytic subunit and transfers the methyl donor *S*-adenosylmethionine (SAM) to the adenine acceptor within the RRACH consensus motif. METTL14 colocalizes with METTL3 in nuclear speckles at a stoichiometric 1:1 ratio (Liu et al., 2014). METTL14 is responsible for stabilizing the structure of MTC, recognizing the substrate RNA sequence, and providing a binding platform (Wang P. et al., 2016; Wang X. et al., 2016). Huang et al. recently demonstrated that METTL14 can also recognize and bind H3K36me3. Thus, METTL14 facilitates m^{6}A MTC binding to RNA polymerase II to mediate the m^{6}A methylation of nascent RNA during transcription elongation (Huang H. et al., 2019). The combination of these histone and RNA modifications opens up new directions for epigenetics research. WTAP alone does not have any catalytic activity because it lacks the catalytic methylation domain, but its knockdown prominently decreases m^{6}A levels (Liu et al., 2014). It regulates the level of m^{6}A modification by interacting with the METTL3–METTL14 complex and promoting accumulation of the complex into nuclear speckles to efficiently methylate target RNAs (Ping et al., 2014). Other identified regulatory factors of MTC include KIAA1429/VIRMA (Yue et al., 2018), RBM15/15B (Patil et al., 2016; Knuckles et al., 2018), HAKAI (Ruzicka et al., 2017), and ZC3H13 (Knuckles et al., 2018).

Some newly discovered methyltransferase, such as METTL16, METTL5, and zinc finger CCHC-type containing 4 (ZCCHC4), can work alone and catalyze m^{6}A on some structured RNAs, such as U6 snRNA (Aoyama et al., 2020), 18S rRNA (Leismann et al., 2020), and 28S rRNA (Ren et al., 2019), respectively (**Figure 1**).

m^{6}A Demethylase (Eraser)

N^6-methyladenosine demethylases, including Fat mass and obesity-associated protein (FTO; Jia et al., 2012) and ALKB family protein 5 (ALKBH5; Zheng et al., 2013), can selectively remove the m^{6}A modification and reverse the methylation process (**Figure 1**). The coordination between m^{6}A methyltransferase and demethylase indicates that the m^{6}A modification is dynamic and reversible. Although both FTO and ALKBH5 are members of the ALKB family, they have different substrates. Emerging evidence demonstrates that FTO is able to mediate the demethylation of m^{6}A, m^{6}Am, and m^{1}A in the cell nucleus and cytoplasm (Wei et al., 2018). To date, m^{6}A in mRNA was the main zymolytic substrate of FTO. Different from FTO, ALKBH5 is mainly localized in the nucleus and selectively removes the m^{6}A methyl group (Mauer et al., 2017). This phenomenon reflects the complexity and specificity of the mechanism of m^{6}A modifications. Additionally, ALKBH5 accelerated the process of both mRNA transfer from intranuclear to extranuclear and promoted translation initiation (Zheng et al., 2013), whereas METTL3 downregulation delayed this process (Fustin et al., 2013).

m^{6}A Binding Proteins (Reader)

Other types of m^{6}A regulatory proteins, including YT521-B homology domain-containing family protein 1/2/3 (YTHDF1/2/3), YTH domain-containing proteins 1/2 (YTHDC1/2) (Haussmann et al., 2016), eukaryotic initiation factor 3 (elF3; Meyer and Jaffrey, 2017), the insulin-like growth factor-2 mRNA-binding protein (IGF2BP) family (Muller et al., 2019), and heterogeneous nuclear ribonucleoprotein (hnRNP)

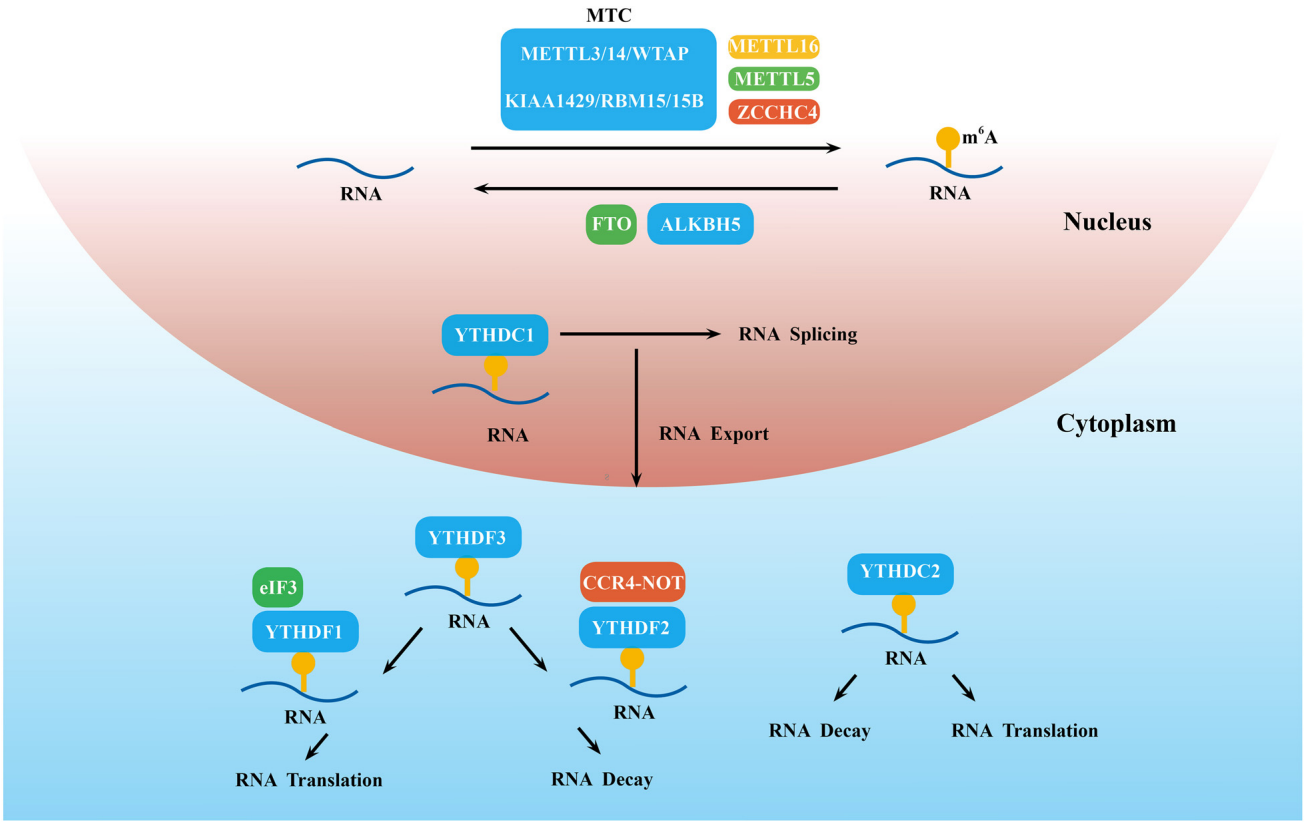

FIGURE 1 | Detailed molecular mechanism of m^{6}A modifications. These modifications are regulated by "writers" (the MTC, METTL5/16 and ZCCHC4), "erasers" (FTO and ALKBH5), and "readers" (YTHDC1-2 and YTHDF1-3), which install, remove, and recognize m^{6}A and thereby regulate RNA splicing, export, decay, translation, and so on.

family (Zhao et al., 2017), recognize the m^{6}A modification site and directly determine the fate of m^{6}A-modified RNA (Casella et al., 2019; **Figure 1**).

YT521-B homology domain-containing family protein 1/2/3 and YTHDC1/2 share the same YTH domain and have a 50-times higher affinity for m^{6}A mRNA than unmethylated mRNA (Theler et al., 2014). YTHDC1 was shown to be the major reader of nuclear m^{6}A modifications and accelerated mature mRNA transportation from the nucleus to the cytoplasm by affecting mRNA splicing (Roundtree et al., 2017). To date, however, little is known about the function of YTHDC2 in m^{6}A modifications. Hsu reported that YTHDC2 preferentially bound to m^{6}A-marked RNA with the RRACH consensus motif and then increased translation efficiency by 52% but also reduced mRNA abundance (Hsu et al., 2017).

When mRNA arrives at the cytoplasm, m^{6}A-methylated mRNA is mainly regulated by YTHDF1-3. YTHDF1 mainly binds to m^{6}A sites near the stop codon in the 3′-UTR and then interacts with the translation initiation factor eIF3 to improve the translation efficiency of target mRNA (Wang et al., 2015b). In 2019, Lin et al. (2019) reported that YTHDF1, by binding with eEF-2 at m^{6}A sites of the Snail CDS but not the 3′-UTR, promoted the translation of Snail. YTHDF2 was the first identified m^{6}A-binding protein, which triggered mRNA degradation by recruiting the CCR4-NOT deadenylase complex (Du et al., 2016). The role of YTHDF3 is more complex. YTHDF3 acts in concert with YTHDF2 to accelerate mRNA decay (Shi et al., 2017), but it promoted the translation of m^{6}A-modified RNA by cooperating with YTHDF1 (Li A. et al., 2017). IGF2BP family proteins (IGF2BP1, IGF2BP2, and IGF2BP3) are located in the cytoplasm and employ their K homology domains to identify the GG (m^{6}A) C sequence. They promote the stability and storage of target mRNAs under both normal and stress conditions (Huang et al., 2018). Some other m^{6}A readers, such as the HNRNP family and elF3, are under current exploration.

m^{6}A MODIFICATION IN THE DEVELOPMENT AND PROGRESSION OF BREAST CANCER

The majority of BC is sporadic and associated with alterations of genetics and epigenetics (Byler et al., 2014). Genetic alterations include mutations and copy number variations of certain genes. Conventional epigenetic remodeling consists of microRNA regulation, histone modification, and DNA methylation in BC (Rahman et al., 2019). m^{6}A modifications open new directions for studying epigenetics. An increasing number of studies

have revealed the importance of m^{6}A in the development and progression of BC.

The Role of m^{6}A Methyltransferase in Breast Cancer

m^6 A Methyltransferase Affects Breast Cancer Cells Through Several Molecular Mechanisms

In various cancer cells, the abnormal expression of METTL3 affects proliferation, invasion, metastasis, and the cell cycle (Zheng et al., 2019). In BC, METTL3 mainly acts as an oncogene (**Figure 2**). For example, METTL3 overexpression in transformed cells enhanced proliferation and migration ability, suggesting that the downregulation of m^{6}A modification acts as a brake during malignant transformation (Fry et al., 2018). B-cell lymphoma 2 (Bcl-2) is an anti-apoptotic protein (Konig et al., 2019) that has been shown to be a potential target of METTL3 in BC tissues and cells. The knockdown of METTL3 reduced the expression of Bcl-2, repressed the proliferation of MDA-MB-231 and MCF-7 cells, accelerated their apoptosis, and inhibited the growth of transplanted tumors *in vivo* (Wang et al., 2020).

A few studies have shown that hepatitis B x-interacting protein (HBXIP) is highly expressed in BC as an oncogene (Yue et al., 2013; Liu et al., 2014). METTL3 was positively linked with HBXIP in BC tissues and cells. In BC cells, HBXIP inhibited the expression of let-7g, which repressed the expression of METTL3 by targeting the 3′-UTR of METTL3 (Cai et al., 2018). Additionally, METTL3 upregulated the expression of HBXIP by stimulating the m^{6}A modification of HBXIP and thus formed a positive feedback regulatory loop of HBXIP/let-7g/METTL3/HBXIP, leading to the proliferation of BC cells (Cai et al., 2018). Cui et al. (2017) reported that the knockout of METTL3 and METTL14 promoted the growth, self-renewal, and tumorigenesis of glioblastoma stem cells (GCS) partly by upregulating BRCA2. BRCA2 was tightly related to hereditary BC (Paul and Paul, 2014). However, whether METTL3 and METTL14 regulate the development and progression of BC through BRCA2 is unknown. Altogether, Bcl-2, HBXIP, and BRCA2 are all potential targets of METTL3. We speculate that other targets of METTL3 will be uncovered as regulators of BC.

METTL14 is also closely related to the progression of BC (**Figure 2**). The knockdown of METTL14 reduced the long-term viability, migration, and invasion of BC cell lines (MDA-MB-231, MDA-MB-468, and BT549) and inhibited tumor growth in tumor xenograft models (Panneerdoss et al., 2018). BC cells were arrested in the G1–S phase when METTL14 was silenced. Mechanistically, METTL14 and the RNA-binding protein HuR form a potential positive feedback loop that regulates transforming growth factor-β (TGF-β) signaling pathway genes and cell cycle-associated genes (cyclin D1 and cyclin E1) and exhibit hyper m^{6}A with lower expression compared with scrambled control cells (Panneerdoss et al., 2018). m^6 A also affects BC cells through regulating the noncoding RNAs expression. Yi et al. found that METTL14 overexpression promoted the migration and invasion of MDA-MB-231 and MCF-7 cells through the upregulation of hsa-mir-146a-5p (Yi et al., 2020). However, Wu et al. reported that the overexpression of METTL14 in MDA-MB-231 cells inhibited cell viability, clone formation, and cell migration (Wu et al., 2019). METTL14 appears to play opposing roles in the same cell line. Whether other factors, such as the tumor microenvironment, impact METTL14 function deserves further exploration.

The role of methyltransferase KIAA1429 in BC had been preliminarily elucidated. A previous study (Qian et al., 2019)

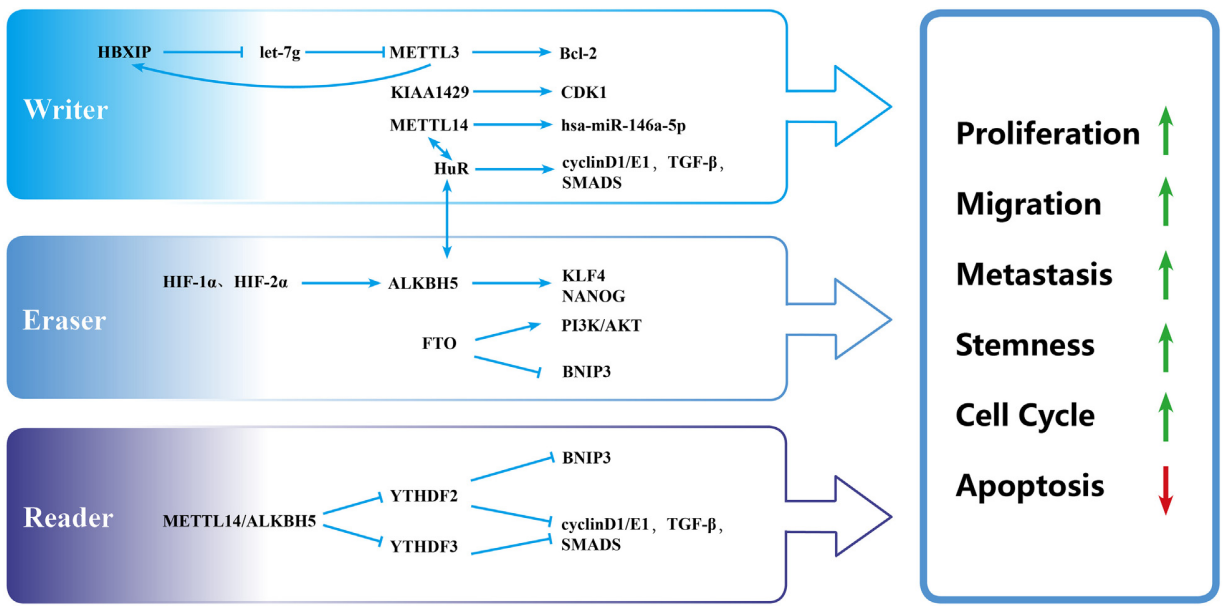

FIGURE 2 | Biological function of m^{6}A modulators in breast cancer. "Writers," "erasers," and "readers" promote cell proliferation, migration, metastasis, and stemness and inhibit apoptosis by regulating different targets.

showed that KIAA1429 promoted BC cell proliferation and the epithelial–mesenchymal transition (EMT) in MCF-7 and SUM1315 cell lines. This may be caused by an increase in stability of the cell cycle regulator cyclin-dependent kinase 1 (CDK1) mRNA in an m^{6}A-independent manner (Qian et al., 2019). The roles of other methyltransferases in BC have rarely been reported and deserve further study.

m^{6}A Methyltransferase Exhibits Abnormal Expression in Breast Cancer Tissues and Is Related to Certain BC Subtypes

Breast cancer tissues exhibit the dysregulation of m^{6}A methyltransferase compared with normal breast tissues, although m^{6}A methyltransferase levels vary (**Table 1**). The mRNA expression of classic methyltransferases (i.e., METTL3, METTL14, and WTAP) was reported to be either upregulated (Cai et al., 2018; Wang et al., 2020; Yi et al., 2020) or downregulated (Liu et al., 2019; Wu et al., 2019). Moreover, their mRNA levels were sometimes inconsistent with protein levels. Liu performed immunohistochemical staining in 20 matched BC and adjacent normal tissues with a BC tissue microarray (TMA) and found the upregulation of WTAP ($p = 0.002$), KIAA1429 ($p < 0.001$), and RBM15 ($p = 0.012$) but no significant changes in METTL3, METTL14, METTL16, or RBM15B in BC specimens (Liu et al., 2019), which was different from mRNA expression.

The expression of m^{6}A methyltransferase also correlated with molecular subtypes of BC (**Table 2**). METTL3 and METTL14 were highly expressed in normal breast-like and luminal A/B BC, but WTAP was mainly expressed in basal-like BC, based on results from the Oncomine and The Cancer Genome Atlas (TCGA) database (Wu et al., 2019). Inflammatory BC (IBC) is a rare and aggressive form of BC. The triple-negative subtype of IBC (TN-IBC) is substantially more metastatic and fatal than TN-non-IBC. In an analysis of differentially regulated genes in TN-IBC and TN-non-IBC, ZC3H13 (i.e., a member of the MTC) was among the top 10 genes and downregulated in TN-IBC (Funakoshi et al., 2019). These data are summarized in **Table 2**.

The Atypical Expression of m^{6}A Methyltransferase Is Closely Related to BC Prognosis

Studies have reported conflicting reports on the role of m^{6}A methyltransferase in the prognosis of BC (**Table 1**). Based on data from the TCGA-BC cohort, the higher expression of RBM15B ($p = 0.014$, 95% confidence interval: 0.48–0.94) significantly correlated with favorable overall survival (OS), whereas the high expression of KIAA1429 ($p = 0.032$, 95% confidence interval: 1.03–1.96) and METTL16 ($p = 0.02$, 95% confidence interval: 1.06–2.02) correlated with poor OS. With regard to relapse-free survival (RFS), the overexpression of RBM15B ($p = 0.021$, 95% confidence interval: 0.54–0.96) correlated with good RFS. However, other "writers" did not critically affect the survival rate (Liu et al., 2019). Another study, based on the bc-GenExMiner 4.0 database, found that the high expression of METTL3, METTL14, and WTAP correlated with good metastasis relapse (MR)-free survival in all BC patients (Wu et al., 2019). However, a separate study that conducted a Kaplan–Meier test revealed that BC patients with high METTL3 expression had unfavorable survival rates (Wang et al., 2020).

Role of m^{6}A Demethylase in Breast Cancer

m^{6}A Demethylases Affects Breast Cancer Cells via Different Molecules and Signaling Pathways

At the cellular level, FTO promoted the proliferation and mammosphere formation and suppressed cell apoptosis by inhibiting BCL2/adenovirus E1B 19-kDa protein-interacting protein 3 (BNIP3; i.e., a pro-apoptosis protein of the Bcl-2 family) in BC (Niu et al., 2019) (**Figure 2**). FTO demethylated the 3′-UTR of BNIP3 mRNA and promoted the degradation of BNIP3 mRNA in a YTHDF2-dependent manner. In MDA-MB-231 and MCF-7 cell lines, silencing BNIP3 alleviated the inhibition of cell proliferation that was mediated by FTO knocking down. In 4T1 cells, BNIP3 knockdown significantly weakened FTO-accelerated tumor growth and metastasis in a subcutaneous implantation model and tumor metastasis model in Balb/c mice. Additionally, FTO upregulated glycolysis and energy metabolism through the PI3K/AKT pathway in MDA-MB-231 and MCF-7 cells (Liu et al., 2017). The PI3K/AKT signaling pathway has a close relationship with proliferation, metabolism, immune response regulation, motility, and survival (Ortega et al., 2020). Therefore, FTO may exert important actions through the PI3K/AKT pathway, which deserves further study.

ALKB family protein 5 can promote the growth and metastasis of BC cells (**Figure 2**). The silencing of ALKBH5 inhibited the viability, migration, and invasion of BC cell lines and tumor growth in a tumor xenograft model in mice (Panneerdoss et al., 2018), similar to METTL14 knockdown that was mentioned above. In MDA-MB-231 cells, the knockdown of ALKBH5 promoted the m^{6}A modification of mRNA and inhibited the ability of survival, clone formation, and cell migration (Wu et al., 2019). In a mouse model of the orthotopic transplantation of BC tumors, ALKBH5-deficient MDA-MB-231 cells developed fewer tumors compared with the control group (43% vs. 100%), and only a few small lung metastases were found in the ALKBH5 knockdown group, thus confirming that ALKBH5 promoted the initiation of BC and lung metastasis (Zhang et al., 2016b). Under hypoxic conditions, hypoxia-inducible factor 1α (HIF-1α) and HIF-2α induced overexpression of the m^{6}A demethylase ALKBH5, which increased demethylation of the 3′-UTR of pluripotent factor NANOG mRNA and enhanced its protein stability (Zhang et al., 2016a). Therefore, ALKBH5 mediates BC stem cell (BCSC) transformation by NANOG in a HIF-dependent manner. Moreover, Zhang et al. (2016b) showed that hypoxia induced expression of the important oncogene ZNF217, which restrained m^{6}A RNA methylation by blocking METTL3. The knockdown of ZNF217 and ALKBH5 increased m^{6}A modification and inhibited hypoxia-induced expression of the pluripotent stem cell factors NANOG and KLF4, thereby suppressing the pluripotency of BC cells (Zhang et al., 2016b). Based on these studies, we speculate that silencing ALKBH5 may be an effective therapeutic strategy that can inhibit proliferation, metastasis, and stemness in BC.

TABLE 1 | Different expression levels and potential prognostic value of m^{6}A modulators in breast cancer (BC).

Genes	Up-/Down-regulation of expression	Methods of Detection	Correlation with prognosis	References
METTL3	Upregulated	GEPIA*/qRT-PCR/Western Blot	Unfavorable survival rate	Cai et al., 2018; Wang et al., 2020
	Downregulated	Oncomine*/TCGA*/qRT-PCR	Good RFS*	Wu et al., 2019
METTL14	Upregulated	qRT-PCR	Good RFS	Yi et al., 2020
	Downregulated	Oncomine/TCGA/		Liu et al., 2019; Wu et al., 2019
WTAP	Upregulated	IHC		Liu et al., 2019
	Downregulated	Oncomine/TCGA/		Wu et al., 2019; Liu et al., 2019
RBM15	Upregulated	TCGA/IHC		Liu et al., 2019
RBM15B	No significance	TCGA/IHC	Good OS*/good RFS	Liu et al., 2019
KIAA1429	Upregulated	TCGA/IHC	Poor OS	Liu et al., 2019
METTL16	Downregulated	TCGA	Poor OS	Liu et al., 2019
FTO	Upregulated	IHC	Poor OS, associated with the risk of BC	Tan et al., 2015; Chen et al., 2018; Gholamalizadeh et al., 2020
	Downregulated	Oncomine/TCGA/HPA*/qRT-PCR	Poor RFS	Liu et al., 2019; Wu et al., 2019
ALKBH5	Upregulated	TCGA/HPA/qRT-PCR/IHC		Liu et al., 2019; Wu et al., 2019
	Downregulated	Oncomine/TCGA	Poor RFS	Liu et al., 2019; Wu et al., 2019
YTHDF1	Upregulated	TCGA/IHC	Poor OS	Liu et al., 2019
YTHDF2	Upregulated	TCGA/IHC	oncogene	Chen et al., 2018; Liu et al., 2019
YTHDF3	Upregulated	IHC	Poor OS/independent predictor	Liu et al., 2019
YTHDC1	Downregulated	TCGA/HPA		Liu et al., 2019
HNRNPC	Upregulated	TCGA/IHC/HPA		Liu et al., 2019
HNRNPA2B1	Upregulated	TCGA/IHC		Liu et al., 2019

Note: GEPIA, Oncomine*, TCGA*, and HPA* are online databases. RFS*, relapse-free survival; OS*, overall survival.*

m^{6}A Demethylase Exhibits Abnormal Expression in Breast Cancer Tissues and Is Related to Certain BC Subtypes

To explore the clinical significance of FTO and ALKBH5 demethylases in BC, various studies have detected their expression levels based on three independent databases [Oncomine, TCGA, and the Human Protein Atlas (HPA)] in clinical BC specimens (**Table 1**). All of these databases indicated that FTO mRNA is significantly reduced in BC (Liu et al., 2019; Wu et al., 2019). ALKBH5 mRNA was either increased (Liu et al., 2019; Wu et al., 2019) or decreased (Wu et al., 2019) compared with normal tissue. At the protein level, immunohistochemical staining showed that ALKBH5 and FTO expression was high in BC (Tan et al., 2015; Liu et al., 2019; Niu et al., 2019). Notwithstanding these studies, no definitive conclusions can be drawn about the expression level of m^{6}A demethylase in BC. We briefly summarize these data in **Table 1**.

A correlation was found between the expression level of demethylase and molecular subtypes of BC (**Table 2**). ALKBH5 and FTO mRNA expression significantly increased in estrogen receptor (ER)-positive or progesterone receptor (PR)-positive patients, whereas FTO mRNA expression decreased in human epidermal growth factor receptor 2 (HER2)-positive patients, based on clinicopathological parameters from the bc-GenExMiner 4.0 database (Wu et al., 2019). Tan reported that FTO was highly expressed in hormone receptor (HR)-negative and HER2-positive BC patients, based on the immunohistochemical staining of specimens from 79 infiltrating ductal breast cancer (IDBC) patients (Tan et al., 2015). In another study that analyzed data from Gene Expression Omnibus (GEO) database (GSE9014), FTO expression was upregulated in HER2-positive BC (Niu et al., 2019).

The Atypical Expression of m^{6}A Demethylase Is Related to BC Prognosis

Findings of the prognostic value of FTO and ALKBH5 in BC have been variable (**Table 1**). Kaplan–Meier analysis, meta-analysis, and univariate Cox analysis indicated that decreases in FTO mRNA levels suggest poor RFS, based on data from the bc-GenExMiner 4.0 database, whereas ALKBH5 was not significantly related to prognosis (Wu et al., 2019). Another study found that high FTO expression was directly related to poor OS in ER-negative BC patients and advanced BC patients (Niu et al., 2019), based on the Genomics Analysis

TABLE 2 | Correlation between m^{6}A modulators and molecular typing of BC.

Gene (regulated expression)	Molecular subtypes	References
METTL3 (up)	Normal breast-like and luminal A/B	Wu et al., 2019
METTL14 (up)	Normal breast-like and luminal A/B	Wu et al., 2019
WTAP (up)	Basal-like	Wu et al., 2019
ZC3H13 (down)	TN-IBC*	Funakoshi et al., 2019
FTO (up)	ER (+)/PR (+) patients; Her2+; HR-/HER2+	Tan et al., 2015; Chen et al., 2018; Wu et al., 2019
FTO (down)	HER2 (+)	Wu et al., 2019
ALKBH5 (up)	ER (+) or PR (+) patients	Wu et al., 2019

TN-IBC, triple-negative inflammatory breast cancer.

and Visualization Platform.[1] FTO gene polymorphisms, such as rs9939609 and rs1477196, were associated with the risk of BC (Gholamalizadeh et al., 2020). This association may be affected by ER/PR status, tumor stage, and body mass index (BMI) (Gholamalizadeh et al., 2020).

The Role of m^{6}A-Binding Protein in Breast Cancer

Compared with other m^{6}A modulators, less research on the effect of m^{6}A-binding protein in BC has been conducted (**Tables 1**, **2**). Liu et al. (2019) reported that YTHDF1 ($p < 0.001$), YTHDF2 ($p = 0.022$), HNRNPC ($p < 0.001$), and HNRNPA2B1 ($p < 0.001$) were upregulated, and YTHDC1 ($p = 0.013$) was downregulated in BC samples, based on RNA-seq data from TCGA. At the protein level, immunohistochemical staining from 20 pairs of BC and adjacent matched normal breast tissue samples showed that YTHDF1-3, HNRNPC, and HNRNPA2B1 were significantly overexpressed in neoplastic tissues. No significant difference in YTHDC1 was found (Liu et al., 2019). However, HPA (without YTHDF1 or YTHDF3 data) analysis showed that HNRNPC and YTHDC1 expression was high in BC, whereas YTHDF2 and HNRNPA2B1 expression was not significantly different between normal and BC tissues (Liu et al., 2019). Further investigations of the prognostic value of m^{6}A-binding protein in BC revealed that the high expression of YTHDF1 ($p = 0.049$, 95% confidence interval: 1–1.91) and YTHDF3 ($p < 0.001$, 95% confidence interval: 1.28–2.49) was related to poor OS, based on clinical data from TCGA. Furthermore, YTHDF3 overexpression was deemed to be an independent predictor of poor OS in BC patients, based on univariate and multivariate analyses (Liu et al., 2019). Studies of the mechanism of regulation found that YTHDF2 participated in the degradation of BNIP3 by binding to potential m^{6}A sites in the 3′-UTR in BC (**Figure 2**). BNIP3 acts as a tumor suppressor, and YTHDF2 may play an oncogenic role by regulating BNIP3 (Niu et al., 2019).

Furthermore, significant crosstalk among YTHDF3, METTL14, and ALKBH5 has been reported (Panneerdoss et al., 2018). YTHDF3 levels significantly increased in BC cells with METTL14 and ALKBH5 knockdown, detected by RNA-seq and Western blot. It was further confirmed that such crosstalk regulated cancer cell growth and progression in rescue experiments in which YTHDF3 was knocked down in MRTTL14- and ALKBH5-depleted BC cells. We speculate that additional crosstalk exists among other m^{6}A molecules, which requires further study. Overall, m^{6}A modifications are involved in the development and progression of BC, the relevant mechanisms of which are summarized in **Figure 2**.

m^{6}A-TARGETING DRUGS SUPPRESS THE PROGRESSION OF BREAST CANCER

The dysregulation of m^{6}A modifications is linked to various diseases, especially cancer. The development of small-molecule m^{6}A-targeting drugs is an attractive therapeutic strategy. Some m^{6}A inhibitors, such as cycloleucine (Wang et al., 2015a) and 3-deazaadenosine (Chen et al., 2018; Yi et al., 2020), were shown to nonspecifically reduce m^{6}A levels by dose-dependently inhibiting SAM activity. During tumor progression, m^{6}A modification acts as a "dual-edged sword" with the controversial role of some m^{6}A modulators. The discovery of specific m^{6}A regulators may contribute to more effective treatment strategies for cancer.

Among the m^{6}A regulators, FTO was the first m^{6}A demethylase that was discovered in 2011 (Jia et al., 2011), which has attracted much interest because of its involvement in obesity and obesity-induced metabolic diseases (Zhao et al., 2014) and the occurrence, development, and prognosis of many kinds of cancer, such as melanoma (Yang et al., 2019), acute myeloid leukemia (AML; Li Z. et al., 2017), glioblastoma (Cui et al., 2017), lung carcinoma (Li et al., 2019a), hepatocellular carcinoma (Li et al., 2019b), and BC (Niu et al., 2019). FTO has been well studied, and several inhibitors of FTO have been developed with regard to their actions against m^{6}A modifications (Deng et al., 2018). To date, such FTO inhibitors include entacapone (which lowers fasting blood glucose levels and reduces body weight in diet-induced obese mice) (Peng et al., 2019), R-2HG (which inhibits proliferation/viability and promotes cell cycle arrest and apoptosis in FTO-high cancer cells) (Su et al., 2018), rhein (which suppresses axon elongation in axons) (Yu et al., 2018), meclofenamic acid (MA; which inhibits the proliferation of BC cells) (Kovala-Demertzi et al., 2009), MA2 (the ethyl ester form of MA; which arrests the G1/S transition and inhibits cell proliferation in germ cells) (Huang T. et al., 2019), FB23 and FB23-2 (which suppress proliferation and promote the differentiation and apoptosis of AML cells *in vitro* and *in vivo*) (Huang Y. et al., 2019), and CS1 and CS2 (which attenuate the self-renewal ability and reprograming immune response of leukemia cells) (Huang et al., 2015). These inhibitors have been shown to have different mechanisms of action, and the effects of rhein and MA have been explored in BC.

Rhein was the first discovered natural small-molecule inhibitor of FTO. It competitively binds the catalytic region of FTO and upregulates cellular m^{6}A levels *in vitro*

[1] https://hgserver1.amc.nl

(Chen et al., 2012). In axons, FTO inhibition by rhein or FTO knockdown by siRNA downregulated the local translation of GAP-43 mRNA and resulted in the suppression of axon elongation (Yu et al., 2018). Before rhein was found to be an inhibitor of FTO, it was shown to have antitumor effects. Rhein inhibited MCF-7 and MDA-MB-435 BC cell viability and growth by suppressing vascular endothelial growth factor (VEGF)- and endothelial growth factor (EGF)-induced activation of the PTEN/PI3K/AKT/mTOR and MAPK/ERK pathways in BC (Fernand et al., 2011). Rhein also had anti-proliferative and pro-apoptosis ability in MCF-7 cells and HER2-overexpressing MCF-7 cells (MCF-7/HER2). The rhein-induced inhibition of cell growth was associated with caspase-9-mediated apoptosis, and reactive oxygen species-mediated activation of the NF-κB and p53 signaling pathways also participated in this process (Chang et al., 2012). In 2019, one study evaluated rhein's function *in vivo*. Rhein enhanced the apoptotic effect of atezolizumab on 4T1 BC cells (Shen et al., 2019). Treatment with a combination of rhein (10 mg/kg) and atezolizumab (10 mg/kg) inhibited 4T1 xenograft tumor growth and increased serum levels of tumor necrosis factor α and interleukin-6, the $CD8^+$ T-cell ratio, apoptotic factors (e.g., caspase-3, caspase-8, and caspase-9), and Bax/Bcl-2 mRNA levels compared with rhein or atezolizumab treatment alone. However, these experiments did not clarify the role of m^{6}A modifications in the inhibitory effect of rhein in BC, which deserves further exploration.

Meclofenamic acid is a nonsteroidal anti-inflammatory drug that was originally approved by the United States Food and Drug Administration. It competes for FTO binding sites on single-stranded DNA (ssDNA) and directly interacts with FTO protein in HeLa cells to inhibit the catalytic activity of FTO and improve levels of m^{6}A modifications in RNA (Huang et al., 2015). Meclofenamic acid inhibited the proliferation of MCF-7 BC cells, with low toxicity (Kovala-Demertzi et al., 2009). However, whether this result can also be achieved by changing the level of m^{6}A modification remains unknown and requires further investigation.

Although numerous small-molecule m^{6}A regulators have been identified, further studies are needed to define their specificity and adverse effects for the treatment of BC *in vitro* and *in vivo*. Furthermore, multiple combinations of existing medical approaches with m^{6}A-targeting drugs may be viable options for the treatment of BC.

CONCLUSION

m^{6}A modifications are one of the most common modifications of mRNA and, most importantly, dynamically reversible. Several studies have shown that m^{6}A modifications are closely related to many human diseases, including cancer. However, the relationship between m^{6}A modifications and BC has not been fully elucidated. m^{6}A modifications play a complex role in expression levels, genotyping, prognosis, cell proliferation, and metastasis in BC. The controversial findings on the role of some m^{6}A modulators in BC may be attributable to the different test platforms that were employed or inconsistent proteomics and transcriptomics analyses or selective bias of clinical specimens. Most studies of m^{6}A modifications in BC have been performed *in vitro*. Therefore, more *in vivo* evidence is required to reveal the regulatory mechanism of m^{6}A modifications in BC.

Based on the significant role of m^{6}A modifications in oncogenesis and progression that has been reported, the development of novel m^{6}A regulators may be the new therapeutic options for malignant tumors. FTO, which was originally found to be involved in obesity and fat metabolism, was the first discovered m^{6}A demethylase. The antitumor effects of some agents that target FTO have been reported in BC. However, little is known about their exact mechanism of action and side effects. Whether these inhibitors influence other RNA modifications, such as m^1A, m^6Am, m^5C, and hm^5C, is unknown. More studies are also needed to demonstrate their effectiveness *in vivo*. Combination therapies, such as combining chemotherapy, radiotherapy, and immune checkpoint blockade with proper m^{6}A inhibitors, may hold promise for the treatment of BC, particularly those that have failed in routine treatment. Based on the oncogenic role of FTO in several cancers, inhibitors that target FTO have attracted scientific interests, but more information about its role in BC is needed. YTHDF3, an independent prognostic factor in BC, may be another target that merits further investigation.

N^6-methyladenosine modifications in the progression of BC are still being discovered. We expect that substantial progress will be made in further revealing the role of m^{6}A modifications in BC. Further advances in technology will likely contribute to the development of new, promising, and unexpected therapeutic strategies for the treatment of BC in coming years.

AUTHOR CONTRIBUTIONS

MW and J-WB designed the project and wrote the manuscript. Y-QZ, LN, and H-YC performed the literature searches in PubMed, Medline, and Google Scholar. G-JZ arranged and supervised the overall project. All authors contributed to the article and approved the submitted version.

FUNDING

This work was supported in part by grants from the National Natural Science Foundation of China (nos. 81602345 and 91859120), the Research Team Project of the Natural Science Foundation of Guangdong Province (no. 2016A030312008), Xiamen Science and Technology Bureau funded project (nos. 3502Z20194040 and 3502Z20209101). Xiamen's Key Laboratory of Precision Medicine for Endocrine-Related Cancers, start-up funds from Xiamen University, and the Youth Fund of Xiang'an Hospital of Xiamen University.

REFERENCES

Aoyama, T., Yamashita, S., and Tomita, K. (2020). Mechanistic insights into m6A modification of U6 snRNA by human METTL16. *Nucleic Acids Res.* 48, 5157–5168. doi: 10.1093/nar/gkaa227

Bartosovic, M., Molares, H. C., Gregorova, P., Hrossova, D., Kudla, G., and Vanacova, S. (2017). N6-methyladenosine demethylase FTO targets pre-mRNAs and regulates alternative splicing and 3′-end processing. *Nucleic Acids Res.* 45, 11356–11370. doi: 10.1093/nar/gkx778

Batista, P. J., Molinie, B., Wang, J., Qu, K., Zhang, J., Li, L., et al. (2014). m(6)A RNA modification controls cell fate transition in mammalian embryonic stem cells. *Cell Stem Cell* 15, 707–719. doi: 10.1016/j.stem.2014.09.019

Byler, S., Goldgar, S., Heerboth, S., Leary, M., Housman, G., Moulton, K., et al. (2014). Genetic and epigenetic aspects of breast cancer progression and therapy. *Anticancer Res.* 34, 1071–1077.

Cai, X., Wang, X., Cao, C., Gao, Y., Zhang, S., Yang, Z., et al. (2018). HBXIP-elevated methyltransferase METTL3 promotes the progression of breast cancer via inhibiting tumor suppressor let-7g. *Cancer Lett.* 415, 11–19. doi: 10.1016/j.canlet.2017.11.018

Casella, G., Tsitsipatis, D., Abdelmohsen, K., and Gorospe, M. (2019). mRNA methylation in cell senescence. *Wiley Interdiscip. Rev. RNA* 10:e1547.

Chang, C. Y., Chan, H. L., Lin, H. Y., Way, T. D., Kao, M. C., Song, M. Z., et al. (2012). Rhein induces apoptosis in human breast cancer cells. *Evid Based Comp. Altern. Med.* 2012:952504.

Chen, B., Ye, F., Yu, L., Jia, G., Huang, X., Zhang, X., et al. (2012). Development of cell-active N6-methyladenosine RNA demethylase FTO inhibitor. *J. Am. Chem. Soc.* 134, 17963–17971.

Chen, M., Wei, L., Law, C. T., Tsang, F. H., Shen, J., Cheng, C. L., et al. (2018). RNA N6-methyladenosine methyltransferase-like 3 promotes liver cancer progression through YTHDF2-dependent posttranscriptional silencing of SOCS2. *Hepatology* 67, 2254–2270. doi: 10.1002/hep.29683

Chen, X. Y., Zhang, J., and Zhu, J. S. (2019). The role of m(6)A RNA methylation in human cancer. *Mol. Cancer* 18:103.

Cohn, W. E. (1960). Pseudouridine, a carbon-carbon linked ribonucleoside in ribonucleic acids: isolation, structure, and chemical characteristics. *J. Biol. Chem.* 235, 1488–1498.

Cui, Q., Shi, H., Ye, P., Li, L., Qu, Q., Sun, G., et al. (2017). m(6)A RNA Methylation Regulates the self-renewal and tumorigenesis of glioblastoma stem cells. *Cell Rep.* 18, 2622–2634. doi: 10.1016/j.celrep.2017.02.059

Deng, X., Su, R., Stanford, S., and Chen, J. (2018). Critical enzymatic functions of FTO in obesity and cancer. *Front. Endocrinol.* 9:396. doi: 10.3389/fendo.2018.00396

Desrosiers, R., Friderici, K., and Rottman, F. (1974). Identification of methylated nucleosides in messenger RNA from Novikoff hepatoma cells. *Proc. Natl. Acad. Sci. U.S.A.* 71, 3971–3975. doi: 10.1073/pnas.71.10.3971

Dina, C., Meyre, D., Gallina, S., Durand, E., Korner, A., Jacobson, P., et al. (2007). Variation in FTO contributes to childhood obesity and severe adult obesity. *Nat. Genet.* 39, 724–726.

Ding, C., Zou, Q., Ding, J., Ling, M., Wang, W., Li, H., et al. (2018). Increased N6-methyladenosine causes infertility is associated with FTO expression. *J. Cell Physiol.* 233, 7055–7066. doi: 10.1002/jcp.26507

Dominissini, D., Moshitch-Moshkovitz, S., Schwartz, S., Salmon-Divon, M., Ungar, L., Osenberg, S., et al. (2012). Topology of the human and mouse m6A RNA methylomes revealed by m6A-seq. *Nature* 485, 201–206. doi: 10.1038/nature11112

Du, H., Zhao, Y., He, J., Zhang, Y., Xi, H., Liu, M., et al. (2016). YTHDF2 destabilizes m(6)A-containing RNA through direct recruitment of the CCR4-NOT deadenylase complex. *Nat. Commun.* 7:12626.

Esteve-Puig, R., Bueno-Costa, A., and Esteller, M. (2020). Writers, readers and erasers of RNA modifications in cancer. *Cancer Lett.* 474, 127–137. doi: 10.1016/j.canlet.2020.01.021

Fernand, V. E., Losso, J. N., Truax, R. E., Villar, E. E., Bwambok, D. K., Fakayode, S. O., et al. (2011). Rhein inhibits angiogenesis and the viability of hormone-dependent and -independent cancer cells under normoxic or hypoxic conditions in vitro. *Chem. Biol. Interact.* 192, 220–232. doi: 10.1016/j.cbi.2011.03.013

Fry, N. J., Law, B. A., Ilkayeva, O. R., Carraway, K. R., Holley, C. L., and Mansfield, K. D. N. (2018). (6)-methyladenosine contributes to cellular phenotype in a genetically-defined model of breast cancer progression. *Oncotarget* 9, 31231–31243. doi: 10.18632/oncotarget.25782

Fu, L., Amato, N. J., Wang, P., McGowan, S. J., Niedernhofer, L. J., and Wang, Y. (2015). Simultaneous quantification of methylated cytidine and adenosine in cellular and Tissue RNA by nano-flow liquid chromatography-tandem mass spectrometry coupled with the stable isotope-dilution method. *Anal. Chem.* 87, 7653–7659. doi: 10.1021/acs.analchem.5b00951

Funakoshi, Y., Wang, Y., Semba, T., Masuda, H., Hout, D., Ueno, N. T., et al. (2019). Comparison of molecular profile in triple-negative inflammatory and non-inflammatory breast cancer not of mesenchymal stem-like subtype. *PLoS One* 14:e0222336. doi: 10.1371/journal.pone.0222336

Fustin, J. M., Doi, M., Yamaguchi, Y., Hida, H., Nishimura, S., Yoshida, M., et al. (2013). RNA-methylation-dependent RNA processing controls the speed of the circadian clock. *Cell* 155, 793–806. doi: 10.1016/j.cell.2013.10.026

Gholamalizadeh, M., Jarrahi, A. M., Akbari, M. E., Bourbour, F., Mokhtari, Z., Salahshoornezhad, S., et al. (2020). Association between FTO gene polymorphisms and breast cancer: the role of estrogen. *Expert Rev. Endocrinol. Metab.* 15, 115–121. doi: 10.1080/17446651.2020.1730176

Harper, J. E., Miceli, S. M., Roberts, R. J., and Manley, J. L. (1990). Sequence specificity of the human mRNA N6-adenosine methylase in vitro. *Nucleic Acids Res.* 18, 5735–5741. doi: 10.1093/nar/18.19.5735

Haussmann, I. U., Bodi, Z., Sanchez-Moran, E., Mongan, N. P., Archer, N., Fray, R. G., et al. (2016). m(6)A potentiates Sxl alternative pre-mRNA splicing for robust *Drosophila* sex determination. *Nature* 540, 301–304. doi: 10.1038/nature20577

Hsu, P. J., Zhu, Y., Ma, H., Guo, Y., Shi, X., Liu, Y., et al. (2017). Ythdc2 is an N(6)-methyladenosine binding protein that regulates mammalian spermatogenesis. *Cell Res.* 27, 1115–1127. doi: 10.1038/cr.2017.99

Huang, H., Weng, H., Sun, W., Qin, X., Shi, H., Wu, H., et al. (2018). Recognition of RNA N(6)-methyladenosine by IGF2BP proteins enhances mRNA stability and translation. *Nat. Cell Biol.* 20, 285–295. doi: 10.1038/s41556-018-0045-z

Huang, H., Weng, H., Zhou, K., Wu, T., Zhao, B. S., Sun, M., et al. (2019). Histone H3 trimethylation at lysine 36 guides m(6)A RNA modification co-transcriptionally. *Nature* 567, 414–419. doi: 10.1038/s41586-019-1016-7

Huang, T., Guo, J., Lv, Y., Zheng, Y., Feng, T., Gao, Q., et al. (2019). Meclofenamic acid represses spermatogonial proliferation through modulating m(6)A RNA modification. *J. Anim. Sci. Biotechnol.* 10:63.

Huang, Y., Su, R., Sheng, Y., Dong, L., Dong, Z., Xu, H., et al. (2019). Small-molecule targeting of oncogenic FTO demethylase in acute myeloid leukemia. *Cancer Cell* 35, 677.e10–691.e10.

Huang, Y., Yan, J., Li, Q., Li, J., Gong, S., Zhou, H., et al. (2015). Meclofenamic acid selectively inhibits FTO demethylation of m6A over ALKBH5. *Nucleic Acids Res.* 43, 373–384. doi: 10.1093/nar/gku1276

Jia, G., Fu, Y., Zhao, X., Dai, Q., Zheng, G., Yang, Y., et al. (2011). N6-methyladenosine in nuclear RNA is a major substrate of the obesity-associated FTO. *Nat. Chem. Biol.* 7, 885–887. doi: 10.1038/nchembio.687

Jia, G. F., Fu, Y., Zhao, X., Dai, Q., Zheng, G. Q., Yang, Y., et al. (2012). N6-Methyladenosine in nuclear RNA is a major substrate of the obesity-associated FTO (vol 7, pg 885, 2011). *Nat. Chem. Biol.* 8:1008. doi: 10.1038/nchembio1212-1008a

Knuckles, P., Lence, T., Haussmann, I. U., Jacob, D., Kreim, N., Carl, S. H., et al. (2018). Zc3h13/Flacc is required for adenosine methylation by bridging the mRNA-binding factor Rbm15/Spenito to the m(6)A machinery component Wtap/Fl(2)d. *Genes Dev.* 32, 415–429. doi: 10.1101/gad.309146.117

Konig, S. M., Rissler, V., Terkelsen, T., Lambrughi, M., and Papaleo, E. (2019). Alterations of the interactome of Bcl-2 proteins in breast cancer at the transcriptional, mutational and structural level. *PLoS Comput. Biol.* 15:e1007485. doi: 10.1371/journal.pcbi.1007485

Kovala-Demertzi, D., Dokorou, V., Primikiri, A., Vargas, R., Silvestru, C., Russo, U., et al. (2009). Organotin meclofenamic complexes: synthesis, crystal structures and antiproliferative activity of the first complexes of meclofenamic acid - novel anti-tuberculosis agents. *J. Inorg. Biochem.* 103, 738–744. doi: 10.1016/j.jinorgbio.2009.01.014

Leismann, J., Spagnuolo, M., Pradhan, M., Wacheul, L., Vu, M. A., Musheev, M., et al. (2020). The 18S ribosomal RNA m(6) A methyltransferase Mettl5 is required for normal walking behavior in *Drosophila*. *EMBO Rep.* 21:e49443.

Li, A., Chen, Y. S., Ping, X. L., Yang, X., Xiao, W., Yang, Y., et al. (2017). Cytoplasmic m(6)A reader YTHDF3 promotes mRNA translation. *Cell Res.* 27, 444–447. doi: 10.1038/cr.2017.10

Li, J., Han, Y., Zhang, H., Qian, Z., Jia, W., Gao, Y., et al. (2019a). The m6A demethylase FTO promotes the growth of lung cancer cells by regulating the m6A level of USP7 mRNA. *Biochem. Biophys. Res. Commun.* 512, 479–485. doi: 10.1016/j.bbrc.2019.03.093

Li, J., Zhu, L., Shi, Y., Liu, J., Lin, L., and Chen, X. (2019b). m6A demethylase FTO promotes hepatocellular carcinoma tumorigenesis via mediating PKM2 demethylation. *Am. J. Transl. Res.* 11, 6084–6092.

Li, Z., Weng, H., Su, R., Weng, X., Zuo, Z., Li, C., et al. (2017). FTO plays an oncogenic role in acute myeloid leukemia as a N(6)-Methyladenosine RNA Demethylase. *Cancer Cell* 31, 127–141. doi: 10.1016/j.ccell.2016.11.017

Lin, X., Chai, G., Wu, Y., Li, J., Chen, F., Liu, J., et al. (2019). RNA m(6)A methylation regulates the epithelial mesenchymal transition of cancer cells and translation of Snail. *Nat. Commun.* 10:2065.

Linder, B., Grozhik, A. V., Olarerin-George, A. O., Meydan, C., Mason, C. E., and Jaffrey, S. R. (2015). Single-nucleotide-resolution mapping of m6A and m6Am throughout the transcriptome. *Nat. Methods* 12, 767–772. doi: 10.1038/nmeth.3453

Liu, F., You, X., Wang, Y., Liu, Q., Liu, Y., Zhang, S., et al. (2014). The oncoprotein HBXIP enhances angiogenesis and growth of breast cancer through modulating FGF8 and VEGF. *Carcinogenesis* 35, 1144–1153. doi: 10.1093/carcin/bgu021

Liu, J., Yue, Y., Han, D., Wang, X., Fu, Y., Zhang, L., et al. (2014). A METTL3-METTL14 complex mediates mammalian nuclear RNA N6-adenosine methylation. *Nat. Chem. Biol.* 10, 93–95. doi: 10.1038/nchembio.1432

Liu, L., Liu, X., Dong, Z., Li, J., Yu, Y., Chen, X., et al. (2019). N6-methyladenosine-related genomic targets are altered in breast cancer tissue and associated with poor survival. *J. Cancer* 10, 5447–5459. doi: 10.7150/jca.35053

Liu, Y., Wang, R., Zhang, L., Li, J., Lou, K., and Shi, B. (2017). The lipid metabolism gene FTO influences breast cancer cell energy metabolism via the PI3K/AKT signaling pathway. *Oncol. Lett.* 13, 4685–4690. doi: 10.3892/ol.2017.6038

Louloupi, A., Ntini, E., Conrad, T., and Orom, U. A. V. (2018). Transient N-6-Methyladenosine transcriptome sequencing reveals a regulatory role of m6A in splicing efficiency. *Cell Rep.* 23, 3429–3437. doi: 10.1016/j.celrep.2018.05.077

Mao, Y., Dong, L., Liu, X. M., Guo, J., Ma, H., Shen, B., et al. (2019). m(6)A in mRNA coding regions promotes translation via the RNA helicase-containing YTHDC2. *Nat. Commun.* 10:5332.

Mauer, J., Luo, X., Blanjoie, A., Jiao, X., Grozhik, A. V., Patil, D. P., et al. (2017). Reversible methylation of m(6)Am in the 5' cap controls mRNA stability. *Nature* 541, 371–375. doi: 10.1038/nature21022

Meyer, K. D., and Jaffrey, S. R. (2017). Rethinking m(6)a readers, writers, and erasers. *Annu. Rev. Cell Dev. Biol.* 33, 319–342. doi: 10.1146/annurev-cellbio-100616-060758

Meyer, K. D., Patil, D. P., Zhou, J., Zinoviev, A., Skabkin, M. A., Elemento, O., et al. (2015). 5'. UTR m(6)A promotes Cap-Independent translation. *Cell* 163, 999–1010. doi: 10.1016/j.cell.2015.10.012

Meyer, K. D., Saletore, Y., Zumbo, P., Elemento, O., Mason, C. E., and Jaffrey, S. R. (2012). Comprehensive analysis of mRNA methylation reveals enrichment in 3′ UTRs and near stop codons. *Cell* 149, 1635–1646. doi: 10.1016/j.cell.2012.05.003

Muller, S., Glass, M., Singh, A. K., Haase, J., Bley, N., Fuchs, T., et al. (2019). IGF2BP1 promotes SRF-dependent transcription in cancer in a m6A- and miRNA-dependent manner. *Nucleic Acids Res.* 47, 375–390. doi: 10.1093/nar/gky1012

Niu, Y., Lin, Z. Y., Wan, A., Chen, H. L., Liang, H., Sun, L., et al. (2019). RNA N6-methyladenosine demethylase FTO promotes breast tumor progression updates through inhibiting BNIP3. *Mol. Cancer* 18:46.

Ortega, M. A., Fraile-Martinez, O., Asunsolo, A., Bujan, J., Garcia-Honduvilla, N., and Coca, S. (2020). Signal transduction pathways in breast cancer: the important role of PI3K/Akt/mTOR. *J. Oncol.* 2020:9258396.

Panneerdoss, S., Eedunuri, V. K., Yadav, P., Timilsina, S., Rajamanickam, S., Viswanadhapalli, S., et al. (2018). Cross-talk among writers, readers, and erasers of m(6)A regulates cancer growth and progression. *Sci. Adv.* 4:eaar8263. doi: 10.1126/sciadv.aar8263

Patil, D. P., Chen, C. K., Pickering, B. F., Chow, A., Jackson, C., Guttman, M., et al. (2016). m(6)A RNA methylation promotes XIST-mediated transcriptional repression. *Nature* 537, 369–373. doi: 10.1038/nature19342

Paul, A., and Paul, S. (2014). The breast cancer susceptibility genes (BRCA) in breast and ovarian cancers. *Front. Biosci.* 19:605–618. doi: 10.2741/4230

Peng, S., Xiao, W., Ju, D., Sun, B., Hou, N., Liu, Q., et al. (2019). Identification of entacapone as a chemical inhibitor of FTO mediating metabolic regulation through FOXO1. *Sci. Transl. Med.* 11:eaau7116. doi: 10.1126/scitranslmed.aau7116

Ping, X. L., Sun, B. F., Wang, L., Xiao, W., Yang, X., Wang, W. J., et al. (2014). Mammalian WTAP is a regulatory subunit of the RNA N6-methyladenosine methyltransferase. *Cell Res.* 24, 177–189. doi: 10.1038/cr.2014.3

Qian, J. Y., Gao, J., Sun, X., Cao, M. D., Shi, L., Xia, T. S., et al. (2019). KIAA1429 acts as an oncogenic factor in breast cancer by regulating CDK1 in an N6-methyladenosine-independent manner. *Oncogene* 38, 6123–6141. doi: 10.1038/s41388-019-0861-z

Rahman, M. M., Brane, A. C., and Tollefsbol, T. O. (2019). MicroRNAs and epigenetics strategies to reverse Breast Cancer. *Cells* 8:1214. doi: 10.3390/cells8101214

Reichel, M., Koster, T., and Staiger, D. (2019). Marking RNA: m6A writers, readers, and functions in *Arabidopsis*. *J. Mol. Cell Biol.* 11, 899–910. doi: 10.1093/jmcb/mjz085

Ren, W., Lu, J., Huang, M., Gao, L., Li, D., Wang, G. G., et al. (2019). Structure and regulation of ZCCHC4 in m(6)A-methylation of 28S rRNA. *Nat. Commun.* 10:5042.

Roundtree, I. A., Luo, G. Z., Zhang, Z., Wang, X., Zhou, T., Cui, Y., et al. (2017). YTHDC1 mediates nuclear export of N(6)-methyladenosine methylated mRNAs. *eLife* 6:e31311.

Ruzicka, K., Zhang, M., Campilho, A., Bodi, Z., Kashif, M., Saleh, M., et al. (2017). Identification of factors required for m(6) A mRNA methylation in *Arabidopsis* reveals a role for the conserved E3 ubiquitin ligase HAKAI. *New Phytol.* 215, 157–172. doi: 10.1111/nph.14586

Scholler, E., Weichmann, F., Treiber, T., Ringle, S., Treiber, N., Flatley, A., et al. (2018). Interactions, localization, and phosphorylation of the m(6)A generating METTL3-METTL14-WTAP complex. *RNA* 24, 499–512. doi: 10.1261/rna.064063.117

Shen, F., Huang, W., Huang, J. T., Xiong, J., Yang, Y., Wu, K., et al. (2015). Decreased N(6)-methyladenosine in peripheral blood RNA from diabetic patients is associated with FTO expression rather than ALKBH5. *J. Clin. Endocrinol. Metab.* 100, E148–E154.

Shen, Z., Zhu, B., Li, J., and Qin, L. (2019). Rhein augments antiproliferative effects of atezolizumab based on Breast Cancer (4T1) regression. *Planta Med.* 85, 1143–1149. doi: 10.1055/a-1012-7034

Shi, H., Wang, X., Lu, Z., Zhao, B. S., Ma, H., Hsu, P. J., et al. (2017). YTHDF3 facilitates translation and decay of N(6)-methyladenosine-modified RNA. *Cell Res.* 27, 315–328. doi: 10.1038/cr.2017.15

Siegel, R. L., Miller, K. D., and Jemal, A. (2020). Cancer statistics, 2020. *CA Cancer J. Clin.* 70, 7–30.

Su, R., Dong, L., Li, C., Nachtergaele, S., Wunderlich, M., Qing, Y., et al. (2018). R-2HG exhibits anti-tumor activity by targeting FTO/m(6)A/MYC/CEBPA Signaling. *Cell* 172, 90.e23–105.e23.

Tan, A., Dang, Y., Chen, G., and Mo, Z. (2015). Overexpression of the fat mass and obesity associated gene (FTO) in breast cancer and its clinical implications. *Int. J. Clin. Exp. Pathol.* 8, 13405–13410.

Theler, D., Dominguez, C., Blatter, M., Boudet, J., and Allain, F. H. (2014). Solution structure of the YTH domain in complex with N6-methyladenosine RNA: a reader of methylated RNA. *Nucleic Acids Res.* 42, 13911–13919. doi: 10.1093/nar/gku1116

Wang, H., Xu, B., and Shi, J. (2020). N6-methyladenosine METTL3 promotes the breast cancer progression via targeting Bcl-2. *Gene* 722:144076. doi: 10.1016/j.gene.2019.144076

Wang, P., Doxtader, K. A., and Nam, Y. (2016). Structural basis for cooperative function of Mettl3 and Mettl14 methyltransferases. *Mo.l Cell* 63, 306–317. doi: 10.1016/j.molcel.2016.05.041

Wang, X., Feng, J., Xue, Y., Guan, Z., Zhang, D., Liu, Z., et al. (2016). Structural basis of N(6)-adenosine methylation by the METTL3-METTL14 complex. *Nature* 534, 575–578. doi: 10.1038/nature18298

Wang, X., Lu, Z., Gomez, A., Hon, G. C., Yue, Y., Han, D., et al. (2014). N6-methyladenosine-dependent regulation of messenger RNA stability. *Nature* 505, 117–120. doi: 10.1038/nature12730

Wang, X., Zhu, L., Chen, J., and Wang, Y. (2015a). mRNA m(6)A methylation downregulates adipogenesis in porcine adipocytes. *Biochem. Biophys. Res. Commun.* 459, 201–207. doi: 10.1016/j.bbrc.2015.02.048

Wang, X., Zhao, B. S., Roundtree, I. A., Lu, Z., Han, D., Ma, H., et al. (2015b). N(6)-methyladenosine modulates messenger RNA translation efficiency. *Cell* 161, 1388–1399. doi: 10.1016/j.cell.2015.05.014

Wei, J., Liu, F., Lu, Z., Fei, Q., Ai, Y., He, P. C., et al. (2018). Differential m(6)A, m(6)Am, and m(1)A demethylation mediated by FTO in the cell nucleus and cytoplasm. *Mol. Cell* 71, 973.e5–985.e5.

Wu, L., Wu, D., Ning, J., Liu, W., and Zhang, D. (2019). Changes of N6-methyladenosine modulators promote breast cancer progression. *BMC Cancer* 19:326. doi: 10.1186/s12885-019-5538-z

Yang, S., Wei, J., Cui, Y. H., Park, G., Shah, P., Deng, Y., et al. (2019). m(6)A mRNA demethylase FTO regulates melanoma tumorigenicity and response to anti-PD-1 blockade. *Nat. Commun.* 10:2782.

Yi, D., Wang, R., Shi, X., Xu, L., Yilihamu, Y., and Sang, J. (2020). METTL14 promotes the migration and invasion of breast cancer cells by modulating N6-methyladenosine and hsa-miR-146a-5p expression. *Oncol. Rep.* 43, 1375–1386.

Yu, J., Chen, M., Huang, H., Zhu, J., Song, H., Zhu, J., et al. (2018). Dynamic m6A modification regulates local translation of mRNA in axons. *Nucleic Acids Res.* 46, 1412–1423. doi: 10.1093/nar/gkx1182

Yue, L., Li, L., Liu, F., Hu, N., Zhang, W., Bai, X., et al. (2013). The oncoprotein HBXIP activates transcriptional coregulatory protein LMO4 via Sp1 to promote proliferation of breast cancer cells. *Carcinogenesis* 34, 927–935. doi: 10.1093/carcin/bgs399

Yue, Y., Liu, J., Cui, X., Cao, J., Luo, G., Zhang, Z., et al. (2018). VIRMA mediates preferential m(6)A mRNA methylation in 3′UTR and near stop codon and associates with alternative polyadenylation. *Cell Discov.* 4:10.

Yue, Y., Liu, J., and He, C. R. N. A. (2015). N6-methyladenosine methylation in post-transcriptional gene expression regulation. *Genes Dev.* 29, 1343–1355. doi: 10.1101/gad.262766.115

Zhang, C., Samanta, D., Lu, H., Bullen, J. W., Zhang, H., Chen, I., et al. (2016a). Hypoxia induces the breast cancer stem cell phenotype by HIF-dependent and ALKBH5-mediated m(6)A-demethylation of NANOG mRNA. *Proc. Natl. Acad. Sci. U.S.A.* 113, E2047–E2056.

Zhang, C., Zhi, W. I., Lu, H., Samanta, D., Chen, I., Gabrielson, E., et al. (2016b). Hypoxia-inducible factors regulate pluripotency factor expression by ZNF217- and ALKBH5-mediated modulation of RNA methylation in breast cancer cells. *Oncotarget* 7, 64527–64542. doi: 10.18632/oncotarget.11743

Zhao, B. S., Roundtree, I. A., and He, C. (2017). Post-transcriptional gene regulation by mRNA modifications. *Nat. Rev. Mol. Cell Biol.* 18, 31–42. doi: 10.1038/nrm.2016.132

Zhao, X., Yang, Y., Sun, B. F., Zhao, Y. L., and Yang, Y. G. (2014). FTO and obesity: mechanisms of association. *Curr. Diab. Rep.* 14:486.

Zheng, G. Q., Dahl, J. A., Niu, Y. M., Fedorcsak, P., Huang, C. M., Li, C. J., et al. (2013). ALKBH5 Is a mammalian RNA demethylase that impacts RNA metabolism and mouse fertility. *Mol. Cell* 49, 18–29. doi: 10.1016/j.molcel.2012.10.015

Zheng, W., Dong, X., Zhao, Y., Wang, S., Jiang, H., Zhang, M., et al. (2019). Multiple functions and mechanisms underlying the role of METTL3 in human cancers. *Front. Oncol.* 9:1403. doi: 10.3389/fonc.2019.01403

Zhong, X., Yu, J., Frazier, K., Weng, X., Li, Y., Cham, C. M., et al. (2018). Circadian clock regulation of hepatic lipid metabolism by modulation of m(6)A mRNA methylation. *Cell Rep.* 25, 1816.e4–1828.e4.

Zhu, L., Zhong, J., Jia, X., Liu, G., Kang, Y., Dong, M., et al. (2016). Precision methylome characterization of *Mycobacterium tuberculosis* complex (MTBC) using PacBio single-molecule real-time (SMRT) technology. *Nucleic Acids Res.* 44, 730–743. doi: 10.1093/nar/gkv1498

Conflict of Interest: The authors declare that the research was conducted in the absence of any commercial or financial relationships that could be construed as a potential conflict of interest.

frontiers in Genetics

REVIEW
published: 12 January 2021
doi: 10.3389/fgene.2020.562868

Epigenetic Alterations in Renal Cell Cancer With TKIs Resistance: From Mechanisms to Clinical Applications

Qinhan Li†, Zhenan Zhang†, Yu Fan and Qian Zhang**

Department of Urology, Peking University First Hospital, Institute of Urology, National Research Center for Genitourinary Oncology, Peking University, Beijing, China

The appearance of tyrosine kinase inhibitors (TKIs) has been a major breakthrough in renal cell carcinoma (RCC) therapy. Unfortunately, a portion of patients with TKIs resistance experience disease progression after TKIs therapy. Epigenetic alterations play an important role in the development of TKIs resistance. Current evidence suggests that epigenetic alterations occur frequently in RCC patients with poor response to TKIs therapy, and modulation of them could enhance the cytotoxic effect of antitumor therapy. In this review, we summarize the currently known epigenetic alterations relating to TKIs resistance in RCC, focusing on DNA methylation, non-coding RNAs (ncRNAs), histone modifications, and their interactions with TKIs treatment. In addition, we discuss application of epigenetic alteration analyses in the clinical setting to predict prognosis of patients with TKIs treatment, and the potential use of epigenetics-based therapies to surmount TKIs resistance.

Keywords: renal cell carcinoma, epigenetics, microRNA, long non-coding RNA, methylation, histone modification, target therapy, tyrosine kinase inhibitor

OPEN ACCESS

Edited by:
Xiao Zhu,
Guangdong Medical University, China

Reviewed by:
David Jim Martino,
University of Western Australia, Australia
Duo Xu,
Cornell University, United States

****Correspondence:***
Qian Zhang
zhangqianbjmu@126.com
Yu Fan
dantefanbmu@126.com

†These authors have contributed equally to this work

Specialty section:
This article was submitted to Epigenomics and Epigenetics, a section of the journal Frontiers in Genetics

Received: *29 June 2020*
Accepted: *10 December 2020*
Published: *12 January 2021*

Citation:
Li Q, Zhang Z, Fan Y and Zhang Q (2021) Epigenetic Alterations in Renal Cell Cancer With TKIs Resistance: From Mechanisms to Clinical Applications. Front. Genet. 11:562868. doi: 10.3389/fgene.2020.562868

INTRODUCTION

Renal cell carcinoma (RCC) is the most common type of renal cancer, causing more than 14,000 deaths yearly (Capitanio et al., 2019). For early stage of RCC, surgical excision is the recommended treatment. However, there are nearly 15% of patients with distant metastasis when diagnosed with RCC (Siegel et al., 2019).

Angiogenesis plays an important role in the biology and the pathogenesis of RCC. Loss of function of von Hippel–Lindau (VHL) tumor suppressor gene is a vital event in renal carcinogenesis and occurs in about 90% of all clear cell renal cell cancer (ccRCC; Nickerson et al., 2008). VHL encodes and forms a VHL protein complex, which acts as an essential factor in the oxygen-sensing pathway through ubiquitin-mediated degradation of hydroxylated hypoxia inducible factor 1 (HIF-1α) and HIF-2α (Maxwell et al., 1999; Kaelin, 2002). Loss of VHL function leads to the accumulation of HIF-1α and HIF-2α, which consequently facilitates transcription of the hypoxia response genes, such as genes in vascular endothelial growth factor (VEGF), platelet-derived growth factor (PDGF), and transforming growth factor alpha (TGF-α), eventually, resulting in angiogenesis and progression of tumor (Kourembanas et al., 1990; de Paulsen et al., 2001). The expression of VEGF and PDGF is significantly upregulated in RCC as a result of VHL inactivation, which, on the one hand, accelerates growth of tumor, on the other hand, is also its weakness. Tyrosine kinase inhibitors (TKIs), including sunitinib,

pazopanib, axitinib, sorafenib, and cabozanitinib are thought to exert their major therapeutic effects in RCC by antagonism of VEGF receptor (VEGFR) and PDGF receptor (PDGFR), leading to a reduction of tumor angiogenesis.

For metastatic RCC (mRCC), sunitinib, pazopanib, and cabozantinib are approved for first-line treatment, while axitinib and sorafenib are chosen as second-line treatment. Sunitinib is the most commonly used TKIs which can delay tumor progression and improve patient survival. However, only 20–30% of patients respond to sunitinib treatment initially, and almost all initial responders develop resistance in 2 years (Morais, 2014). Subsequent antitumor therapies are followed by immune-checkpoint inhibitor and mammalian target of rapamycin (mTOR), such as nivolumab and everolimus. TKIs resistance poses a great challenge for the TKIs treatment. Therefore, understanding the distinct molecular mechanisms underlying TKIs resistance is vital to find efficient biomarkers to predict the effect of TKIs and facilitate the development of novel antitumor drugs which overcome this resistance.

AN OVERVIEW OF EPIGENETIC MODIFICATION

Epigenetics refers to the study of molecules and mechanisms that can control chromatin structure and influence gene expression or the propensity for genes to be transcribed within organisms in the context of the same DNA sequence. The ability of cells to retain and transmit their special gene expression patterns to the progeny cells, referred to as epigenetic memory, is governed by epigenetic marks, such as DNA methylations, histone modifications, and non-coding RNAs (ncRNAs; Thiagalingam, 2020). Epigenetic modification is heritable but reversible (Cavalli and Heard, 2019). The unique epigenome defining the genetic code associated with each individual gene regulates the expression status of that gene. Defects in epigenetic factors and epigenetic modifications could act as pushers for various diseases including cancer.

Epigenetic modification is associated with drug resistance in numerous types of cancer, including RCC (Chekhun et al., 2007; Knoechel et al., 2014; Adelaiye-Ogala et al., 2017; Leonetti et al., 2019), which regulates gene expression at the protein level (histone modification and nucleosome remodeling), DNA level (DNA methylation), and RNA level (ncRNA). Histones are the central component of nucleosomal subunit, including four types of histone proteins [histone 2A (H2A), H2B, H3, and H4], which are wrapped by a 147-base-pair segment of DNA (Santos-Rosa and Caldas, 2005; Audia and Campbell, 2016). Histone modifications mainly take place at histone tails, which are densely populated with basic lysine and arginine residues (Audia and Campbell, 2016). The acetylation and methylation of lysine residues are well-known. Acetylation can alter the charge on the lysine residues and weaken the interaction of these histones with DNA, making the chromatin structure more open and accessible (Dawson and Kouzarides, 2012). This process is regulated by two enzymatic families with competing activities: promoted by histone lysine acetyltransferases (HATs) and inhibited by the histone deacetylases (HDACs; Li et al., 2019). Methylation of lysine residues in histone tails contains three forms: monomethylation (me1), demethylation (me2), and trimethylation (me3), making activation or repression of transcription (Kouzarides, 2007). This process is also competitively regulated by histone lysine methyltransferases (KMTs) and histone lysine demethylases (KDMs). Generally, acetylation of lysine 14 of H3 (H3K14), monmethylation of H3K4, H3K9, and H3K79, and phosphorylation of serine 10 (H3S10) are all linked with transcriptional activity (Cheung et al., 2000; Lo et al., 2000; Barski et al., 2007), while trimethylation of H3K9, H3K79, and H3K27 marks transcriptional repression (Boyer et al., 2006; Barski et al., 2007).

At the DNA level, the methylation of the 5-carbon on cytosine CpG dinucleotides is considered as an important epigenetic marker. Catalyzed by DNA methyltransferases (DNMTs), 5-carbon of the cytosine ring on promoter CpG islands gets a methyl from S-adenosylmethionine, converting to 5-methycytosine (5mc). 5mc attracts HDACs and methy-CpG-binding domain proteins (MBDs) to the site, resulting in removal of acetyl groups from histone proteins, compact conformation of nucleosome, and downregulation of gene transcription (Robert et al., 2003; Feinberg and Tycko, 2004; Wang et al., 2009). This process can be reversed by ten-eleven translocation (TET) proteins, which oxidize 5mc into 5-hydroxymethylcytosine (5hmc) and subsequently into 5-formylcytosine (5fC) and 5-carboxylcytosine (5caC) in an Fe(II)- and 2-oxoglutarate-dependent dioxygenases manner (Wu and Zhang, 2014; Rasmussen and Helin, 2016).

Non-coding RNAs regulate gene expression at RNA level, including mircoRNAs (miRNAs), small nucleolar RNAs (snoRNAs), piwiRNAs (piRNAs), and long ncRNA (lncRNA; Ma et al., 2013). In general, composed by about 19–25 nucleotides, miRNAs can lead to posttranscriptional gene silencing and translation stopping through binding to the 3'-untranslated region (3'-UTR) of the targeted messenger RNAs (mRNAs) and leading to its degradation or destabilization (Brennecke et al., 2005). lncRNAs are collectively defined as longer than 200 nucleotides in length, which modulate local or global gene expression in a neighboring (*cis*) or distal (*trans*) manner (Kopp and Mendell, 2018). For example, one classic *cis*-acting lncRNA is the X-inactive specific transcript (Xist) resulting in the X chromosome inaction (XCI) in mammals by recruiting various protein complexes to specific position (Lee and Bartolomei, 2013). Notably, lncRNAs can function as competing endogenous RNAs (ceRNAs) to compete with miRNAs by binding to their protein-coding transcripts, thereby antagonizing the repressive effects of miRNAs on mRNAs (Salmena et al., 2011; Du et al., 2016).

In this review, we summarize the currently known epigenetic alterations relating to TKIs resistance in RCC, focusing on DNA methylation, ncRNAs, histone modifications, and their interactions with TKIs treatment. In addition, we discuss the application of epigenetic alteration analyses in the clinical setting to predict prognosis of patients with TKIs treatment and develop new agents.

Mechanisms of Primary and Acquired Resistance to TKIs Treatment

There is no specific definition of TKIs resistance in RCC. Response to drug therapy is normally defined by the Response Evaluation Criteria In Solid Tumors (RECIST) criteria as evidence of tumor progression regardless of persistent treatment. Unfortunately, the current clinical studies depended on their own criteria to divide patients into responders and non-responders, which made their outcomes difficult to compare. Resistance to antiangiogenic therapy can be classified into intrinsic (primary) and acquired (secondary) resistance (Mollica et al., 2019). Intrinsic resistance is defined as an initial inefficacy of therapeutic agents, which may be attributed to the presence of resistant tumor clones prior to therapy due to inherited resistance or evolutionary clonal selection. Acquired resistance is classified as the progression of tumor after initial tumor regression during the therapy, which is often driven by the development of other pathways stimulating angiogenesis, such as AXL, MET, and PDGF/PDGFR, and thus the escape of cancer cells from VEGF/VEGFR blockade (Crawford et al., 2009; Zhou et al., 2016). While the explicit mechanisms of TKIs resistance are still being explored, several potential factors have been reported to be associated with TKIs resistance in RCC: lysosomal sequestration, mutations and modification of expression level, downstream signaling pathway activation, bypass or alternative pathway activation, ATP-binding cassette (ABC) efflux transporters, tumor microenvironment, epithelial-mesenchymal transition (EMT), and epigenetic modification (Housman et al., 2014; Makhov et al., 2018). Epigenetic regulation of the TKIs resistance is always linked to activation of downstream signaling pathways, promotion of EMT, and stimulation of alternative pathways.

Modulation of Downstream Signaling Pathways

Tyrosine kinase inhibitors exert their major antiangiogenic and antitumor effect in RCC by suppressing tyrosine kinase receptors on VEGFR and PDGFR and inhibiting their downstream signaling pathways. Therefore, RCC cells escape TKIs blockade through an important mechanism of activation of parallel downstream signaling pathways, among which PI3K/AKT and RAS/RAF/ERK are pivotal transduction cascades responsible for cell survival, proliferation, and invasion (Fresno Vara et al., 2004; Guo et al., 2015; Huang and Fu, 2015). The PI3K/AKT pathway is frequently activated in cancer and leads to the development and progression of numerous tumor types, including RCC (Samuels et al., 2004; Lawrence et al., 2014). PI3K, a family of lipid kinases, is normally activated by extracellular signals, such as growth factors, cytokines in physiologic conditions. Activated PI3K phosphorylates phosphatidylinositol 4,5-bisphosphate [Ptdlns(4,5)P2], propagating activation signals to downstream molecules (Hennessy et al., 2005). Phosphatase and tensin homolog deleted on chromosome 10 (PTEN) can turn off this pathway by inhibiting the phosphorylation of Ptdlns(4,5)P2 (Gewinner et al., 2009). AKT is the key mediator to respond to the PI3K signaling. The phosphorylated active AKT translocates from the cell membrane to other cell compartments to phosphorylate multiple downstream substrates, resulting in cell survival, growth, tumorigenesis, metastasis, and sunitinib resistance (Andjelković et al., 1997; Sakai et al., 2013; Fang et al., 2019). Activated by pAKT, mTOR complex 1 can lead to protein translation and lipid or nucleotide synthesis *via* phosphorylating numerous substrates, such as p70 ribosomal S6 kinase (p70S6K) and Eif4e-binding proteins (Manning and Cantley, 2003; Fruman and Rommel, 2014), eventually leading to the translation and accumulation of HIF-1α and HIF-2α. Acting as an inhibitory protein of the pathway, PTEN contributes to the downregulation of AKT activity, and loss of PTEN leads to sunitinib resistance due to lack of inhibitory input (Makhov et al., 2012). Sekino et al. (2019) identified miR-130 upregulation was associated with sunitinib resistance through suppression of PTEN.

Focal adhesion kinase (FAK) signaling plays an important role in activation of PI3K/AKT pathway by interacting with PI3K (Zhao and Guan, 2009; Poettler et al., 2013; Hung et al., 2017). Activation of FAK signaling contributes to the sorafenib and sunitinib resistance in a variety type of cancer, including RCC (Bai et al., 2012; Zhang et al., 2016; Zhou et al., 2017). The chromatin modifier enhancer of zeste homolog 2 (EZH2), a polycomb group protein homolog of Drosophila enhancer of zeste, is a histone methytransferase unit of polycomb repressive (PRC2), which can catalyze the trimethylation of H3K27, change chromatin configuration, and promote transcriptional silencing (Margueron and Reinberg, 2011; Di Croce and Helin, 2013). Adelaiye-Ogala et al. (2017) reported that increased EZH2 was associated with sunitinib resistance through redistribution in RCC cells, decreasingly binding to the *PTK2* gene, which encodes the FAK, and increasingly binding to *DAB2IP* and *PTPN2*, which act as tumor suppressors to inhibit RAS/RAF/ERK and P13K/AKT signaling pathways.

Ras/Raf/ERK signaling pathway is other important transduction cascade transmitting EGFR signaling, responsible for cancer development, maintenance, progression and thus, poorer prognosis and TKIs resistance (Bridgeman et al., 2016; Mandal et al., 2016). The methylation of *glutaminyl peptide cyclotransferase* (*QPCT*) gene had been reported to associate with sunitinib resistance through Ras/Raf/ERK signaling pathway (Zhao et al., 2019). The *QPCT* gene encodes glutaminyl cyclase (QC), an enzyme that is involved in the posttranslational modification by converting the N-terminal glutaminyl and glutamyl into pyroglutamate through cyclization, making the protein more resistant to protease degradation, more hydrophobic, and more prone to aggregation and neurotoxicity (Khan et al., 2016; Vijayan and Zhang, 2019). Hypomethylated *QPCT* gene increased the expression of QC, the process promoted by the NF-κB signaling (p65; Kehlen et al., 2013), leading to upregulation of HRAS and activation of the Ras/Raf/ERK signaling pathway (Herrero et al., 2016; Michael et al., 2016; Zhao et al., 2019). Zhai et al. (2017) had observed that lncRNA-SARCC could regulate androgen receptor (AR) to increase miR-143-3p expression and inhibit its downstream signals, including AKT, MMP-13, K-RAS, and P-ERK. The expression of lncRNA-SARCC was upregulated in RCC cells treated with sunitinib, which was associated with decreased resistance to sunitinib.

Modulation of Epithelial-to-Mesenchymal Transition

Epithelial-to-mesenchymal transition is a biologic process that epithelial cells lose their cell–cell basement membrane contacts and their structural polarity to become spindle-shaped and morphologically similar to mesenchymal cell (He and Magi-Galluzzi, 2014). While potential mechanisms are not fully explicit, numerous studies indicate that EMT constitutes a relevant resistance mechanism to TKI treatment (Fang et al., 2019; Hwang et al., 2019; Zhu et al., 2019), and relates to the development of metastases in cancer (Bastid, 2012). Signal transduction affects EMT through the TGF-beta 1 (TGF-β1) in different mechanisms (Wendt et al., 2009; Feldkoren et al., 2017; Fardi et al., 2019). Schematically, TGF-β1 activates zinc finger E-box binding 1 (ZEB1) and ZEB2, which are responsible for a key transcriptional repressor of the cadherin 1 gene (CDH1). CDH1 encodes the cell-adhesion glycoprotein E-cadherin whose downregulation is a pivotal hallmark of EMT (Loh et al., 2019). As an activator of EMT, the expression of ZEB2 is regulated by miR-141 (Berkers et al., 2013). In detail, miR-141 downregulation induces EMT and hypoxia resistance through the upregulation of ZEB2 and suppression of E-cadherin, resulting in an unfavorable response to sunitinib resistance and poor prognosis (Berkers et al., 2013; Fang et al., 2013).

The overexpression of EZH2 is beneficial to EMT by repression of E-cadherin (Crea et al., 2012; Liu et al., 2016). Adelaiye-Ogala et al. (2017) reported that EZH2 expression was linked to sunitinib resistance in RCC through an adaptive kinome reprograming, such as increased global tyrosine and serine phosphorylation as well as increased phosphorylated FAK. SOX5, one of SOX family involving in the regulation of tumor progression, is thought to contribute to EMT in different types of cancer (Grimm et al., 2019). Liu et al. (2019) reported lncRNA-GAS5 was responsible to sorafenib resistance by functioning as ceRNA to repress miR-21, which controlled its downstream target SOX5.

The Wnt/β-catenin pathway acts as one of the signaling pathways controlling EMT through directly or indirectly targeting several key transcription factors regulating E-cadherin expression and/or the fate of other epithelial molecules (Valenta et al., 2012). SET and MYND domain-containing protein 2 (SMYD2), which acts as one of the SMYD-methyltransferase protein family and specifically methylates H3K4 through its SET domain (Abu-Farha et al., 2008), is deemed to regulate the expression of miR-125b (Yan et al., 2019). miR-125b bind directly to the 3'-UTR of DKK3, a key regulatory factor in the Wnt/β-catenin pathway which acts as a tumor suppressor in RCC (Lu et al., 2017). Thus, the activation of SMYD2/miRNA-EMT pathway weakens the effect sunitinib treatment and accelerates the tumor growth (Yan et al., 2019).

Activation of Bypass Pathways

Extra activation of bypass pathways driving angiogenesis is also one of the most important processes driving TKIs resistance. The activation of MET and AXL confers to the stimulation of their downstream signal cascades, including PI3K and RAS signaling pathway, resulting in sunitinib resistance (Huang and Fu, 2015; Zhou et al., 2016). lncRNA Activated in RCC with Sunitinib Resistance (lncARSR) functions as a sponge and competes for binding of miR-34 and miR-449 to their transcripts, leading to the upregulation of AXL/MET and the activation of STAT3, AKT, and ERK signaling (Qu et al., 2016). miR-32-5p can increase the efficacy of sunitinib by suppressing the testicular nuclear receptor 4 (TR4), which plays an important role in activation of HGF/MET signaling pathway (Wang et al., 2018).

Inactivation of VHL leads to increased HIF-1*α* and HIF-2α. In renal carcinogenesis, HIF-1α functions more as a tumor suppressor than a tumor promoter, whereas HIF-2α is deemed to predominantly promote tumor growth and angiogenesis (Raval et al., 2005). Specifically, HIF-1α inhibits interaction of MYC with its DNA-binding partners by displacing the SP1 transcription factor from MYC, while HIF-2α could enhance MYC activity by forming a complex with MAX, and thus stabilizing the MYC-MAX and MYC-MAX-SP1 complexes (Keith et al., 2011). HIF-2α/C-MYC axis relates to progression and TKIs resistance in RCC (Zhai et al., 2016; Maroto et al., 2017). Beuselinck et al. (2015) segregated specific groups of patients with ccRCC, who presented sunitinib resistance into four molecular tumor subtypes based on their mRNA expression data: ccrcc1 (c-myc-up), ccrcc2 (classical), ccrcc3 (normal-like), and ccrcc4 (c-myc-up and immune-up). ccrcc1/ccrcc4 subtypes posed a hypomethylation of *MYC* gene and a global hypermethylation level, with overexpression of *MYC* and down-expression of corresponding genes, such as *PRC2* and *SUZ12*. Obviously, those two subgroups of patients experienced poor response to sunitinib treatment and shorter progression-free survival (PFS). Verbiest et al. (2018) reported the similar outcome in their study, which proved the resistance to pazopanib in ccrcc1/ccrcc4 subtypes.

In addition, lncRNA-SRLR overexpression is linked to sorafenib resistance through promotion of IL-6 transcription and activation of STAT3 (Xu et al., 2017). miR-942 is associated with sunitinib resistance by promoting the secretion of MMP9 and VEGF (Prior et al., 2014). miR-99a-3p, which targets ribonucleotide reductase regulatory subunit-M2 (RRM2), is downregulated in sunitinib-resistance RCC (Osako et al., 2019). Overexpression of breast cancer resistance protein BCRP/*ABCG2*, which is posttranscriptionally suppressed by miR-212-3p and miR-132-3p, is associated with superior response to sunitinib treatment in RCC patients (Reustle et al., 2018).

Some of the previously described epigenetic alterations associated with TKIs resistance are represented in **Figure 1**.

CLINICAL IMPLICATIONS OF EPIGENETICS ANALYSIS IN RCC

Tyrosine kinase inhibitors treatment has been established as first-line therapy for mRCC for a decade with 70–80% of disease control rate. However, approximately 20–30% of patients does not respond to TKIs treatment and experience disease progression within ≤3 months (Porta et al., 2012). Epigenetic alteration can act as a biomarker, which predicts the response

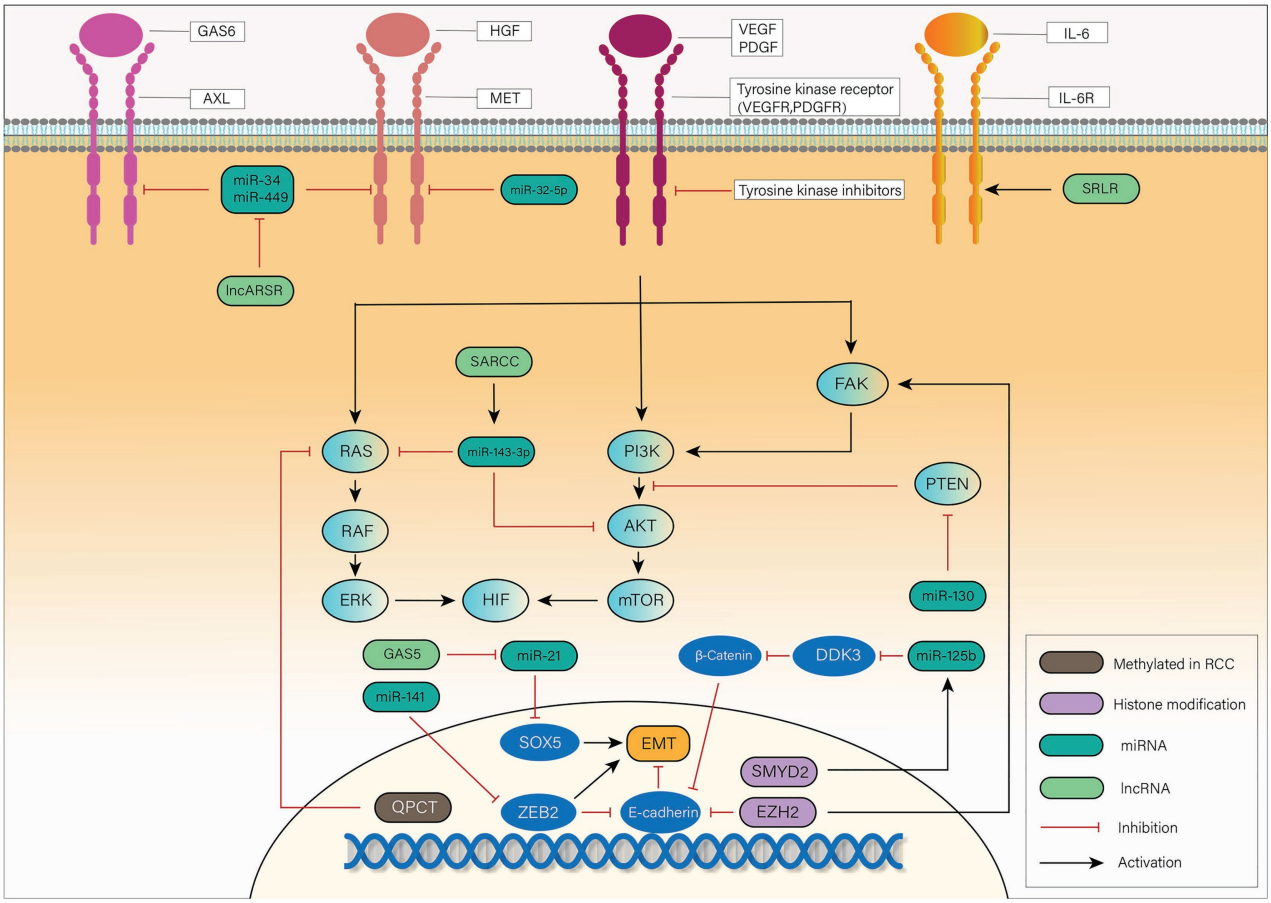

FIGURE 1 | Mechanisms of tyrosine kinase inhibitor (TKI) resistance mediated by epigenetic alterations in renal cell carcinoma (RCC): vascular endothelial growth factor (VEGF) and platelet-derived growth factor (PDGF) bind to a tyrosine kinase receptor and activate the downstream focal adhesion kinase (FAK), PI3K, and RAS pathways. Activated FAK, PI3K, and RAS phosphorylate their downstream signaling cascade, eventually leading to the translation and accumulation of hydroxylated hypoxia inducible factor 1 (HIF-1α) and HIF-2α. In RCC, TKIs exert their influence on antiangiogenesis through inhibition of tyrosine kinase receptor. Epithelial-mesenchymal transition (EMT), activation of downstream signaling pathways and bypass pathways mediated by epigenetic alterations are responsible for the TKIs resistance. Long non-coding RNA (lncRNA)-SARCC increases miR-143-3p expression, thus inhibiting its downstream signals, including AKT, RAS, and ERK. miR-130 enhances HIF signaling by inhibition of PTEN. Hypermethylated *QPCT* reduces its protein level, leading to inhibition of RAS. EMT, a key transformation in TKIs resistance, is promoted by SOX5, zinc finger E-box binding 2 (ZEB2), and β-Catenin while inhibited by E-cadherin. lncRNA-GAS5 promotes EMT by competing with miR-21 which suppresses the expression of SOX5. miR-141 suppresses the expression of ZEB2 to inhibit its promotion of EMT. SET and MYND domain-containing protein 2 (SMYD2) leads to EMT by promoting the expression of miR-125b, which inhibits DDK3 and activates Wnt/β-catenin signaling pathway. The chromatin modifier enhancer of zeste homolog 2 (EZH2) can not only inhibit E-cadherin but also activate FAK signaling pathway to exert its influence on TKIs resistance. Except for VEGF receptor (VEGFR) and PDGF receptor (PDGFR), activation of MET, AXL, and IL-6 pathways can also lead to phosphorylation of downstream transduction cascades, such as PI3K, STAT3, and RAS. lncRNA Activated in RCC with Sunitinib Resistance (lncARSR) inhibits miR-34 and miR-449, and thus activates MET/AXL pathway. miR-32-5p inhibits MET pathway while lncRNA-SRLR activates interleukin-6 (IL-6)R pathway. RCC, renal cell carcinoma; VEGF, vascular endothelial growth factor; PDGF, platelet-derived growth factor; TKI, tyrosine kinase inhibitor; QPCT, the methylation of glutaminyl peptide cyclotransferase; AR, androgen receptor; EMT, epithelial-to-mesenchymal transition; EZH2, the chromatin modifier enhancer of zeste homolog 2; ZEB2, zinc finger E-box binding 2; SMYD2, SET and MYND domain-containing protein 2; GAS6, growth-arrest-specific protein 6; HGF, hepatocyte growth factor; IL-6, interleukin-6.

of patient to antiangiogenic therapy, thus reducing unnecessary toxicities and costs and maximizing clinical benefit. Clinical investigations of a number of epigenetic alterations on FFPE/plasma samples and their correlation with response to TKIs therapies are listed in **Table 1**.

On the histone modification level, tissue low EZH2 expression was associated with increased overall survival (OS) in RCC treated with sunitinib (p = 0.005; Adelaiye-Ogala et al., 2017). On the DNA methylation level, tissue hypomethylation level in the CpG sites of *QPCT* promoter region showed a poor response to sunitinib therapy ($p < 0.05$; Zhao et al., 2019). Hypermethylation of *cystatin 6* (*CST6*), *ladinin 1* (*LAD1*) and *neurofilament heavy* (*NEFH*) were all linked to shortened PFS (p = 0.009, p = 0.011, and $p < 0.001$, respectively) and OS (p = 0.011, p = 0.043, and p = 0.028, respectively) for antiangiogenic therapy, including sunitinib, sorafenib, axitinib, and bevacizumab, among which methylation of *CST6* could predicted first-line therapy between response (0) and therapy

TABLE 1 | Epigenetic biomarkers in RCC patients treated with TKIs.

Classification	Epigenetic alteration	Study population	Sample source	TKIs treatment	Deregulation in TKI resistance	Reference
Histone	EZH2	16	tissue	sunitinib	↑	Adelaiye et al., 2015
DNA methylation	QPCT	10	tissue	sunitinib	↓	Zhao et al., 2019
	SYNPO2	63	tissue	Sunitinib, sorafenib, pazopanib	↓	Pompas-Veganzones et al., 2016
	NEFH	18	tissue	Sunitinib, sorafenib, axitinib, bevacizumab	↑	Dubrowinskaja et al., 2014
	CST6, LAD1	18	tissue	Sunitinib, sorafenib, axitinib, bevacizumab	↑	Peters et al., 2014
miRNA	miR-376b-3p	47	tissue	sunitinib	↓	Kovacova et al., 2019
	miR-9-5p	60	tissue	Sunitinib, pazopanib, sorafenib	↑	Ralla et al., 2018
	miR-489-3p	60	tissue	Sunitinib, pazopanib, sorafenib	↓	Ralla et al., 2018
	miR-628-5p	123	tissue	sunitinib	↓	Puente et al., 2017
	miR-27b	123	tissue	sunitinib	↓	Puente et al., 2017
	miR-99b-5p	40	tissue	Sunitinib, sorafenib, pazopanib	↓	Lukamowicz-Rajska et al., 2016
	miR-101	94	tissue	sunitinib	↓	Goto et al., 2016
	miR-155, miR-484	79	tissue	sunitinib	↑	Merhautova et al., 2015
	miR-942	20	tissue	sunitinib	↑	Prior et al., 2014
	miR-141, miR-144, miR-376b	20	tissue	sunitinib	↓	Berkers et al., 2013
	miR-520 g, miR-155, miR-526b,	20	tissue	sunitinib	↑	Berkers et al., 2013
	miR-424,	38	Plasma	sunitinib	↑	Gámez-Pozo et al., 2012
lncRNA	lncRNA-GAS5	15	tissue	sorafenib	↓	Liu et al., 2019
	lncRNA-SRLR	96	tissue	sorafenib	↑	Xu et al., 2017
	lncARSR	84	Plasma, tissue	sunitinib	↑	Qu et al., 2016

failure (1) with an AUC of 0.88 and a sensitivity and specificity of 82 and 86%, respectively (Dubrowinskaja et al., 2014; Peters et al., 2014). Methylation level of *VHL* was found to be significantly upregulated after sunitinib therapy ($p < 0.001$; Stewart et al., 2016), while there was no correlation between *VHL* methylation and response to pazopanib (Choueiri et al., 2013). Beuselinck et al. (2015) reported the patients with tissue *MYC* overexpression and global CpG hypermethylation received a shorter PFS and OS after sunitinib treatment ($p = 0.001$ and $p = 0.0003$, respectively). In contrast, tissue unmethylation *SYNPO2*, the gene that encoded myopodin, discriminated progressing patients after TKIs treatment (sunitinib, sorafenib, and pazopanib) from those free of disease, and remained as an independent predictive factor for progression, disease-specific survival, and OS ($p = 0.009$, $p = 0.006$, and $p = 0.01$, respectively; Pompas-Veganzones et al., 2016).

On the ncRNA level, both miRNA and lncRNA showed their influences on the response to TKIs treatment. In their original study, Berkers et al. (2013) described the upregulation of miR-520 g, miR-155, and miR-526b and downregulation of miR-141, miR-376b in tissue were linked to the poor responders to sunitinib ($p = 0.036$, $p = 0.04$, $p = 0.0067$, $p = 0.0098$, and $p = 0.032$, respectively). In an observational prospective study, blood samples from 38 patients and 287 miRNAs were taken and evaluated before initiation of therapy and 14 days later in patients receiving sunitinib treatment for advanced RCC. Twenty eight miRNAs of the 287 were found to be significant differences of expressions between the poor response and response groups, among which, downexpression of miR-424 was linked with prolonged response ($p = 0.016$; Gámez-Pozo et al., 2012). Other researchers (Prior et al., 2014) explored a putative role of miRNAs in influencing sunitinib resistance to RCC in tissue, identifying that tissue overexpressed miR-942 was associated with sunitinib resistance, reduced time to progression (TTP) and OS ($p = 0.0074$, $p = 0.003$, and $p = 0.0009$, respectively), and predicted sunitinib efficacy with an AUC of 0.798 and a sensitivity and specificity of 92 and 50%, respectively. Lukamowicz-Rajska et al. (2016) reported that tissue decreased miR-99b-5p was associated with TKIs non-responders (sunitinib, sorafenib, and pazopanib) with a shorter PFS (<3 months, $p < 0.0001$). Similarly, Puente et al. (2017) identified that the expression of miR-23b, miR-27b, and miR-628-5p in tumor tissue was upregulated in long-term responders to sunitinib ($p < 0.01$, each), among which high level of miR-27b and miR-628-5p were associated with increased disease specific survival ($p = 0.012$ and $p = 0.017$, respectively). Nineteen miRNAs were explored to have different expressions in tissue, and lower level of miR-155 and miR-484 were associated with increased TTP in patients on sunitinib treatment ($p < 0.01$ and $p < 0.05$, respectively; Merhautova et al., 2015). Among 40 miRNAs of 232 found to be downregulated in sunitinib-treated RCC specimens compared with those in normal kidney tissues, miR-101 showed the most dramatic downregulation ($p = 0.0013$; Goto et al., 2016). Increased miR-9-5p and decreased miR-489-3p were found in non-responder patients

of TKIs treatment, including sunitinib, sorafenib, and pazopanib compared to that in responder patients, and the AUC of miR-9-5p combined with clinicopathological variables to predict response(0)/non-response(1) to sunitinib treatment is 0.89 (Ralla et al., 2018). miR-212-3p and miR-132-30 were linked to shorter PFS of sunitinib therapy through interaction with BCRP/*ABCG2* expression (Reustle et al., 2018). In a more recent study, high-throughput miRNA microarray performed on FFPE tumor specimens from 47 patients treated with sunitinib, 158 miRNAs were identified to have different expressions in patient with good and poor response ($p < 0.05$). Moreover, miR-376b was significantly upregulated in patients with a long-term response to sunitinib and could identify patients with long-term response with a sensitivity of 83% and specificity of 67% ($p = 0.0002$, AUC = 0.758; Kovacova et al., 2019).

Regarding lncRNAs, relevant studies had disclosed their influences on TKIs therapy and prognosis. lncARSR was exposed in plasma and tissue separately by Qu et al. (2016), and was deemed to act as a sponge to compete with miR-34 and miR-449. High level of lncARSR in pre-surgery plasma was an independent prognostic factor for patients with sunitinib treatment, and was correlated with decreased PFS ($p = 0.02$ and $p = 0.014$, respectively). Intriguingly, low level of lncARSR in tissue exhibited a superior PFS after receiving sunitinib therapy ($p = 0.028$). A microarray analysis conducted by Xu et al. (2017) revealed the similar outcome in lncRNA-SRLR. Briefly, high tissue lncRNA-SRLR was associated with poor response to sorafenib, and patients with low lncRNA-SRLR expression had a more significant improvement in PFS after receiving sorafenib treatment ($p = 0.0198$ and $p = 0.0086$, respectively). lncRNA-GAS5 was also found to be downregulated in RCC patients with sorafenib resistance ($p < 0.01$; Liu et al., 2019).

Overall, these studies demonstrate that epigenetic alterations could be promising predictive biomarkers for TKIs response, as they function as important roles involved in mediating resistance through regulating important mechanisms. However, most of these studies are involved in a small number of patients, which limits their reliability. Moreover, there is no accepted criterion on how long a PFS of good response should last, so each study divides patients into good responders and poor responders based on its own standard. The different criteria limit the application of those epigenetic biomarkers in clinical setting.

EPIGENETIC ALTERATIONS AS THERAPEUTIC TARGETS

Besides the predictive value, epigenetic alterations have potential to become targets themselves for drug development, in order to overcome the TKIs resistance in RCC. Preclinical studies on RCC cell lines demonstrate that reversions of epigenetic alterations are effective strategies to re-sensitize resistant clones to TKIs treatment, including demethylation, restoration of miRNA function, and inhibition of HDAC. Therefore, implementing epigenetics-based therapeutic strategies in patients is the next step, and relevant clinical trials are under way. Generally, there are two classes of epigenetics-based drugs in clinical trials: broad reprogrammers, which have a broad effect, and targeted therapies, which focus on specific miRNA expression or histone modifications (Jones et al., 2016). The formers are represented by the DNMT inhibitors (DNMTi) and the HDAC inhibitors (HDACi), and the latters are represented by EZH2 inhibitors (Jones et al., 2016; Joosten et al., 2018). The outcomes of current clinical trials concerning combination of epigenetics-based therapy with TKIs are listed in **Table 2**. So far, HDACi and EZH2 inhibitors are the most promising agents to reverse the TKI resistance with a vast of clinical studies completed or ongoing. Combination of HDACi and antiangiogenic agents is the most common trial to reverse the acquired resistance and re-sensitize tumors to antiangiogenic therapy. A phase I study evaluated the safety, tolerability, and preliminary efficacy of HDACi vorinostat plus sorafenib in patients with RCC and non-small cell lung cancer (NSCLC) and showed poor tolerance and no confirmed responses (Dasari et al., 2013). Other study focused on the combination vorinostat with pazopanib in advanced solid tumors including RCC, and identified that the treatment achieved stable disease for at least 6 months or partial response (PR; SD $\geq$ 6 months/PR) in 19% of all patients ($n = 78$), median PFS of 2.2 months, and median OS of

TABLE 2 | Epigenetic drugs plus TKIs in treatment of RCC.

Drug	Combination agent	Tumor type	Trial phase	Result	Reference
Vorinostat	Sorafenib	RCC, NSCLC	I	Poorly tolerated, 1 unconfirmed PR and five of eight patients had durable minor responses (11–26%) in RCC subset	Dasari et al., 2013
Vorinostat	Pazopanib	Solid tumors including RCC	I	Stable disease at least 6 months or PR (SD $\geq$ 6 months/PR), median PFS of 3.5 months and median OS of 12.7 months	Fu et al., 2015
Vorinostat	Bevacizumab	ccRCC	I/II	6 OR (18%), including 1 CR and 5 PR. 5.7 months of median PFS and 13.9 months of OS	Pili et al., 2017
Abexinostat	Pazopanib	Solid tumor including RCC	I	27% of objective response rate, average 10.5 months of response duration in RCC subset	Aggarwal et al., 2017

RCC, renal cell carcinoma; NSCLC, non-small cell lung cancer; ccRCC, clear cell renal cell carcinoma; PR, partial response; CR, complete response; OS, overall survival; PFS, progression-free survival; SD, stable disease.

8.9 months (Fu et al., 2015). Furthermore, patients with detected hotspot *TP53* mutations had a superior rate of SD ≥ 6 months/PR, median PFS, and OS compared with those with undetected hotspot *TP53* mutations (45 vs. 16%, 3.5 vs. 2.0 months, and 12.7 vs. 7.4 months, respectively). In a phase I study, combination HDACi abexinostat with pazopanib in patient of RCC with tumor progression after received an average 2.5 lines of prior therapy and 1.6 lines of prior VEGF-targeting treatment received 27% of objective response rate and average 10.5 months of response duration (Aggarwal et al., 2017). Three patients with prior refractory disease to pazopanib monotherapy received durable minor or PR > 12 months treated with pazopanib plus abexinostat. Other clinical trial explored the effect of combination of HDACi with monoclonal antibody bevacizumab in advanced RCC. In a multicenter, single-arm phase I/II clinical trial, 33 patients with metastatic or unresectable ccRCC achieved 5.7 months of median PFS and 13.9 months of median OS, among which six patients achieved OR, including 1 CR and 5 PR (Pili et al., 2017). Regarding DNMTi, decitabine was the only agent tested by phase I trial and combination it with high-dose IL-2 achieved stable disease in three patients (Gollob et al., 2006). As the pharmacological defects of this DNMTi, such as short half-life and sensitivity to inactivation by cytidine deaminase, limit their clinical application, the second-generation DNMTi guadecitabine has been developed, which has shown promise in early preclinical models and clinical trial in patients with acute myeloid leukemia and myelodysplastic syndromes (Joosten et al., 2018).

The H3K27 histone N-methyltransferase EZH2 is a pusher of EMT leading to TKIs resistance, and its inhibitors may contribute to re-sensitize tumor to antiangiogenic treatment, which has been proven in preclinical test in RCC lines (Wagener et al., 2008; Adelaiye et al., 2015). The result of phase I trial that 64 patients including 21 with B-cell non-Hodgkin lymphoma and 43 with advanced solid tumors received EZH2 inhibitor tazemetostat showed the agent had a favorable safety profile and antitumor activity (Italiano et al., 2018).

Moreover, miRNAs also have the potential to become a target to reverse the TKIs resistance in RCC. Preclinical studies on RCC lines clearly demonstrated that both restoration of the tumor-suppressor miRNA function (by miRNA mimics) and inhibition of the oncogenic miRNAs (by antagomiRs) could re-sensitize resistance clones to TKIs. However, implementing miRNA-based therapies in clinic constitutes a significant challenge for clinicians and has not yet been realized. The main concerns fasten on the relative instability of miRNAs in body fluids and specific delivery of these miRNAs to tumor sites (Christopher et al., 2016; Leonetti et al., 2019). Recently, exosomes have been identified to function as carriers of miRNAs to deliver them from cell to extracellular milieu, which may become the sally port for miRNA-based therapy (Mathiyalagan and Sahoo, 2017; Rahbarghazi et al., 2019).

In addition, as epigenetic memory defines the ability of cells to retain and transmit their special gene expression status to the daughter cells, one differentiated somatic cell could become pluripotent and subsequently be reprogrammed into a different somatic cell through loss of its epigenetic memories responsible for its differentiated state. This process could serve as the basis for stem cell therapeutics by replacing one's affected cells with his/her own cells, which may become the potential target of new agents (Thiagalingam, 2020).

Although agents targeting the epigenome could be a promising therapy strategy for TKIs resistance in mRCC because of the widespread epigenetic deregulation in this tumor type, there are several problems of those agents limiting their clinical application. For example, clinical activity of a drug is not only related to the original rationale but also attribute to the off-target effects. Studies about patients treated with epigenetic agents such as DNMTi revealed acute genome-wide demethylation (Yang et al., 2006), which may not only restore abnormally silenced expression but also activate normally silenced expression, leading to adverse off-targets effects. The individual responses of epigenetic agents are variable in different tumor types. So far, hypomethylating drugs are generally more effective in myeloid malignancy than in RCC. Furthermore, the majority of patients have been treated with DNMTi or HDACi for a shortened period of time, the long-term effects of those agents are not explicit for us. In addition, combination treatment might bring more severe and dose-limiting toxicities than monotherapy. As a result, additional trials are urged to future elaborate the interaction of those agents with mechanism of TKIs resistance and to assess their use in RCC patients.

CONCLUSION

Although the advent of TKIs therapy indeed provides concrete hope for patients with advenced RCC, a part of patients with intrinsic or acquired resistance to TKIs benefit a little from the therapy and experience tumor progression after treatment. Epigenetic alterations are involved in the mechanisms underlying this event and could act as excellent biomakers to predict the response of patients to TKIs treatment. However, no epigenetic biomarker is currently applied in clinical setting regardless of numerous epigenetic biomarkers reported. Low efficiency and high cost of them may be the cause of this event. Therefore, for the purpose of translation them into clinical practice, more high-quality epigenetic biomarker studies are needed. In view, the criteria of TKIs resistance are ambiguous, uniform defination of TKIs resistance is urgent affair. Assay, statistical methods, and study designs also need be standardized to optimize their practice. In addition, epigenetics-based therapies are in full swing, which hold great promise and may optimize the management of patients with advanced RCC.

AUTHOR CONTRIBUTIONS

QL and ZZ searched the related published articles and wrote the manuscript. QZ and YF designed the work and instructed the progress of the review. All authors contributed to the article and approved the submitted version.

REFERENCES

Abu-Farha, M., Lambert, J. P., Al-Madhoun, A. S., Elisma, F., Skerjanc, I. S., and Figeys, D. (2008). The tale of two domains: proteomics and genomics analysis of SMYD2, a new histone methyltransferase. *Mol. Cell. Proteomics* 7, 560–572. doi: 10.1074/mcp.M700271-MCP200

Adelaiye, R., Ciamporcero, E., Miles, K. M., Sotomayor, P., Bard, J., Tsompana, M., et al. (2015). Sunitinib dose escalation overcomes transient resistance in clear cell renal cell carcinoma and is associated with epigenetic modifications. *Mol. Cancer Ther.* 14, 513–522. doi: 10.1158/1535-7163.mct-14-0208

Adelaiye-Ogala, R., Budka, J., Damayanti, N. P., Arrington, J., Ferris, M., Hsu, C. C., et al. (2017). EZH2 modifies sunitinib resistance in renal cell carcinoma by kinome reprogramming. *Cancer Res.* 77, 6651–6666. doi: 10.1158/0008-5472.can-17-0899

Aggarwal, R., Thomas, S., Pawlowska, N., Bartelink, I., Grabowsky, J., Jahan, T., et al. (2017). Inhibiting histone deacetylase as a means to reverse resistance to angiogenesis inhibitors: phase I study of abexinostat plus pazopanib in advanced solid tumor malignancies. *J. Clin. Oncol.* 35, 1231–1239. doi: 10.1200/jco.2016.70.5350

Andjelković, M., Alessi, D. R., Meier, R., Fernandez, A., Lamb, N. J., Frech, M., et al. (1997). Role of translocation in the activation and function of protein kinase B. *J. Biol. Chem.* 272, 31515–31524. doi: 10.1074/jbc.272.50.31515

Audia, J. E., and Campbell, R. M. (2016). Histone modifications and cancer. *Cold Spring Harb. Perspect. Biol.* 8:a019521. doi: 10.1101/cshperspect.a019521

Bai, L., Yang, J. C., Ok, J. H., Mack, P. C., Kung, H. J., and Evans, C. P. (2012). Simultaneous targeting of Src kinase and receptor tyrosine kinase results in synergistic inhibition of renal cell carcinoma proliferation and migration. *Int. J. Cancer* 130, 2693–2702. doi: 10.1002/ijc.26303

Barski, A., Cuddapah, S., Cui, K., Roh, T. Y., Schones, D. E., Wang, Z., et al. (2007). High-resolution profiling of histone methylations in the human genome. *Cell* 129, 823–837. doi: 10.1016/j.cell.2007.05.009

Bastid, J. (2012). EMT in carcinoma progression and dissemination: facts, unanswered questions, and clinical considerations. *Cancer Metastasis Rev.* 31, 277–283. doi: 10.1007/s10555-011-9344-6

Berkers, J., Govaere, O., Wolter, P., Beuselinck, B., Schöffski, P., van Kempen, L. C., et al. (2013). A possible role for microRNA-141 down-regulation in sunitinib resistant metastatic clear cell renal cell carcinoma through induction of epithelial-to-mesenchymal transition and hypoxia resistance. *J. Urol.* 189, 1930–1938. doi: 10.1016/j.juro.2012.11.133

Beuselinck, B., Job, S., Becht, E., Karadimou, A., Verkarre, V., Couchy, G., et al. (2015). Molecular subtypes of clear cell renal cell carcinoma are associated with sunitinib response in the metastatic setting. *Clin. Cancer Res.* 21, 1329–1339. doi: 10.1158/1078-0432.ccr-14-1128

Boyer, L. A., Plath, K., Zeitlinger, J., Brambrink, T., Medeiros, L. A., Lee, T. I., et al. (2006). Polycomb complexes repress developmental regulators in murine embryonic stem cells. *Nature* 441, 349–353. doi: 10.1038/nature04733

Brennecke, J., Stark, A., Russell, R. B., and Cohen, S. M. (2005). Principles of microRNA-target recognition. *PLoS Biol.* 3:e85. doi: 10.1371/journal.pbio.0030085

Bridgeman, V. L., Wan, E., Foo, S., Nathan, M. R., Welti, J. C., Frentzas, S., et al. (2016). Preclinical evidence that trametinib enhances the response to antiangiogenic tyrosine kinase inhibitors in renal cell carcinoma. *Mol. Cancer Ther.* 15, 172–183. doi: 10.1158/1535-7163.mct-15-0170

Capitanio, U., Bensalah, K., Bex, A., Boorjian, S. A., Bray, F., Coleman, J., et al. (2019). Epidemiology of renal cell carcinoma. *Eur. Urol.* 75, 74–84. doi: 10.1016/j.eururo.2018.08.036

Cavalli, G., and Heard, E. (2019). Advances in epigenetics link genetics to the environment and disease. *Nature* 571, 489–499. doi: 10.1038/s41586-019-1411-0

Chekhun, V. F., Lukyanova, N. Y., Kovalchuk, O., Tryndyak, V. P., and Pogribny, I. P. (2007). Epigenetic profiling of multidrug-resistant human MCF-7 breast adenocarcinoma cells reveals novel hyper- and hypomethylated targets. *Mol. Cancer Ther.* 6, 1089–1098. doi: 10.1158/1535-7163.mct-06-0663

Cheung, P., Tanner, K. G., Cheung, W. L., Sassone-Corsi, P., Denu, J. M., and Allis, C. D. (2000). Synergistic coupling of histone H3 phosphorylation and acetylation in response to epidermal growth factor stimulation. *Mol. Cell* 5, 905–915. doi: 10.1016/s1097-2765(00)80256-7

Choueiri, T. K., Fay, A. P., Gagnon, R., Lin, Y., Bahamon, B., Brown, V., et al. (2013). The role of aberrant VHL/HIF pathway elements in predicting clinical outcome to pazopanib therapy in patients with metastatic clear-cell renal cell carcinoma. *Clin. Cancer Res.* 19, 5218–5226. doi: 10.1158/1078-0432.ccr-13-0491

Christopher, A. F., Kaur, R. P., Kaur, G., Kaur, A., Gupta, V., and Bansal, P. (2016). MicroRNA therapeutics: discovering novel targets and developing specific therapy. *Perspect. Clin. Res.* 7, 68–74. doi: 10.4103/2229-3485.179431

Crawford, Y., Kasman, I., Yu, L., Zhong, C., Wu, X., Modrusan, Z., et al. (2009). PDGF-C mediates the angiogenic and tumorigenic properties of fibroblasts associated with tumors refractory to anti-VEGF treatment. *Cancer Cell* 15, 21–34. doi: 10.1016/j.ccr.2008.12.004

Crea, F., Fornaro, L., Bocci, G., Sun, L., Farrar, W. L., Falcone, A., et al. (2012). EZH2 inhibition: targeting the crossroad of tumor invasion and angiogenesis. *Cancer Metastasis Rev.* 31, 753–761. doi: 10.1007/s10555-012-9387-3

Dasari, A., Gore, L., Messersmith, W. A., Diab, S., Jimeno, A., Weekes, C. D., et al. (2013). A phase I study of sorafenib and vorinostat in patients with advanced solid tumors with expanded cohorts in renal cell carcinoma and non-small cell lung cancer. *Investig. New Drugs* 31, 115–125. doi: 10.1007/s10637-012-9812-z

Dawson, M. A., and Kouzarides, T. (2012). Cancer epigenetics: from mechanism to therapy. *Cell* 150, 12–27. doi: 10.1016/j.cell.2012.06.013

de Paulsen, N., Brychzy, A., Fournier, M. C., Klausner, R. D., Gnarra, J. R., Pause, A., et al. (2001). Role of transforming growth factor-alpha in von Hippel--Lindau (VHL)(−/−) clear cell renal carcinoma cell proliferation: a possible mechanism coupling VHL tumor suppressor inactivation and tumorigenesis. *Proc. Natl. Acad. Sci. U. S. A.* 98, 1387–1392. doi: 10.1073/pnas.031587498

Di Croce, L., and Helin, K. (2013). Transcriptional regulation by Polycomb group proteins. *Nat. Struct. Mol. Biol.* 20, 1147–1155. doi: 10.1038/nsmb.2669

Du, Z., Sun, T., Hacisuleyman, E., Fei, T., Wang, X., Brown, M., et al. (2016). Integrative analyses reveal a long noncoding RNA-mediated sponge regulatory network in prostate cancer. *Nat. Commun.* 7:10982. doi: 10.1038/ncomms10982

Dubrowinskaja, N., Gebauer, K., Peters, I., Hennenlotter, J., Abbas, M., Scherer, R., et al. (2014). Neurofilament heavy polypeptide CpG island methylation associates with prognosis of renal cell carcinoma and prediction of antivascular endothelial growth factor therapy response. *Cancer Med.* 3, 300–309. doi: 10.1002/cam4.181

Fang, Y., Wei, J., Cao, J., Zhao, H., Liao, B., Qiu, S., et al. (2013). Protein expression of ZEB2 in renal cell carcinoma and its prognostic significance in patient survival. *PLoS One* 8:e62558. doi: 10.1371/journal.pone.0062558

Fang, L., Zhang, Y., Zang, Y., Chai, R., Zhong, G., Li, Z., et al. (2019). HP-1 inhibits the progression of ccRCC and enhances sunitinib therapeutic effects by suppressing EMT. *Carbohydr. Polym.* 223:115109. doi: 10.1016/j.carbpol.2019.115109

Fardi, M., Alivand, M., Baradaran, B., Farshdousti Hagh, M., and Solali, S. (2019). The crucial role of ZEB2: from development to epithelial-to-mesenchymal transition and cancer complexity. *J. Cell. Physiol.* doi: 10.1002/jcp.28277 [Epub ahead of print]

Feinberg, A. P., and Tycko, B. (2004). The history of cancer epigenetics. *Nat. Rev. Cancer* 4, 143–153. doi: 10.1038/nrc1279

Feldkoren, B., Hutchinson, R., Rapoport, Y., Mahajan, A., and Margulis, V. (2017). Integrin signaling potentiates transforming growth factor-beta 1 (TGF-β1) dependent down-regulation of E-cadherin expression—important implications for epithelial to mesenchymal transition (EMT) in renal cell carcinoma. *Exp. Cell Res.* 355, 57–66. doi: 10.1016/j.yexcr.2017.03.051

Fresno Vara, J. A., Casado, E., de Castro, J., Cejas, P., Belda-Iniesta, C., and González-Barón, M. (2004). PI3K/Akt signalling pathway and cancer. *Cancer Treat. Rev.* 30, 193–204. doi: 10.1016/j.ctrv.2003.07.007

Fruman, D. A., and Rommel, C. (2014). PI3K and cancer: lessons, challenges and opportunities. *Nat. Rev. Drug Discov.* 13, 140–156. doi: 10.1038/nrd4204

Fu, S., Hou, M. M., Naing, A., Janku, F., Hess, K., Zinner, R., et al. (2015). Phase I study of pazopanib and vorinostat: a therapeutic approach for inhibiting mutant p53-mediated angiogenesis and facilitating mutant p53 degradation. *Ann. Oncol.* 26, 1012–1018. doi: 10.1093/annonc/mdv066

Gámez-Pozo, A., Antón-Aparicio, L. M., Bayona, C., Borrega, P., Gallegos Sancho, M. I., García-Domínguez, R., et al. (2012). MicroRNA expression profiling of peripheral blood samples predicts resistance to first-line sunitinib in advanced renal cell carcinoma patients. *Neoplasia* 14, 1144–1152. doi: 10.1593/neo.12734

Gewinner, C., Wang, Z. C., Richardson, A., Teruya-Feldstein, J., Etemadmoghadam, D., Bowtell, D., et al. (2009). Evidence that inositol polyphosphate 4-phosphatase type II is a tumor suppressor that inhibits PI3K signaling. *Cancer Cell* 16, 115–125. doi: 10.1016/j.ccr.2009.06.006

Gollob, J. A., Sciambi, C. J., Peterson, B. L., Richmond, T., Thoreson, M., Moran, K., et al. (2006). Phase I trial of sequential low-dose 5-aza-2'-deoxycytidine plus high-dose intravenous bolus interleukin-2 in patients with melanoma or renal cell carcinoma. *Clin. Cancer Res.* 12, 4619–4627. doi: 10.1158/1078-0432.ccr-06-0883

Goto, Y., Kurozumi, A., Nohata, N., Kojima, S., Matsushita, R., Yoshino, H., et al. (2016). The microRNA signature of patients with sunitinib failure: regulation of UHRF1 pathways by microRNA-101 in renal cell carcinoma. *Oncotarget* 7, 59070–59086. doi: 10.18632/oncotarget.10887

Grimm, D., Bauer, J., Wise, P., Krüger, M., Simonsen, U., Wehland, M., et al. (2019). The role of SOX family members in solid tumours and metastasis. *Semin. Cancer Biol.* 67, 122–153. doi: 10.1016/j.semcancer.2019.03.004

Guo, H., German, P., Bai, S., Barnes, S., Guo, W., Qi, X., et al. (2015). The PI3K/AKT pathway and renal cell carcinoma. *J. Genet. Genomics* 42, 343–353. doi: 10.1016/j.jgg.2015.03.003

He, H., and Magi-Galluzzi, C. (2014). Epithelial-to-mesenchymal transition in renal neoplasms. *Adv. Anat. Pathol.* 21, 174–180. doi: 10.1097/pap.0000000000000018

Hennessy, B. T., Smith, D. L., Ram, P. T., Lu, Y., and Mills, G. B. (2005). Exploiting the PI3K/AKT pathway for cancer drug discovery. *Nat. Rev. Drug Discov.* 4, 988–1004. doi: 10.1038/nrd1902

Herrero, A., Casar, B., Colon-Bolea, P., Agudo-Ibanez, L., and Crespo, P. (2016). Defined spatiotemporal features of RAS-ERK signals dictate cell fate in MCF-7 mammary epithelial cells. *Mol. Biol. Cell* 27, 1958–1968. doi: 10.1091/mbc.E15-02-0118

Housman, G., Byler, S., Heerboth, S., Lapinska, K., Longacre, M., Snyder, N., et al. (2014). Drug resistance in cancer: an overview. *Cancer* 6, 1769–1792. doi: 10.3390/cancers6031769

Huang, L., and Fu, L. (2015). Mechanisms of resistance to EGFR tyrosine kinase inhibitors. *Acta Pharm. Sin. B* 5, 390–401. doi: 10.1016/j.apsb.2015.07.001

Hung, T. W., Chen, P. N., Wu, H. C., Wu, S. W., Tsai, P. Y., Hsieh, Y. S., et al. (2017). Kaempferol inhibits the invasion and migration of renal cancer cells through the downregulation of AKT and FAK pathways. *Int. J. Med. Sci.* 14, 984–993. doi: 10.7150/ijms.20336

Hwang, H. S., Go, H., Park, J. M., Yoon, S. Y., Lee, J. L., Jeong, S. U., et al. (2019). Epithelial-mesenchymal transition as a mechanism of resistance to tyrosine kinase inhibitors in clear cell renal cell carcinoma. *Lab. Investig.* 99, 659–670. doi: 10.1038/s41374-019-0188-y

Italiano, A., Soria, J. C., Toulmonde, M., Michot, J. M., Lucchesi, C., Varga, A., et al. (2018). Tazemetostat, an EZH2 inhibitor, in relapsed or refractory B-cell non-Hodgkin lymphoma and advanced solid tumours: a first-in-human, open-label, phase 1 study. *Lancet Oncol.* 19, 649–659. doi: 10.1016/s1470-2045(18)30145-1

Jones, P. A., Issa, J. P., and Baylin, S. (2016). Targeting the cancer epigenome for therapy. *Nat. Rev. Genet.* 17, 630–641. doi: 10.1038/nrg.2016.93

Joosten, S. C., Smits, K. M., Aarts, M. J., Melotte, V., Koch, A., Tjan-Heijnen, V. C., et al. (2018). Epigenetics in renal cell cancer: mechanisms and clinical applications. *Nat. Rev. Urol.* 15, 430–451. doi: 10.1038/s41585-018-0023-z

Kaelin, W. G. (2002). Molecular basis of the VHL hereditary cancer syndrome. *Nat. Rev. Cancer* 2, 673–682. doi: 10.1038/nrc885

Kehlen, A., Haegele, M., Menge, K., Gans, K., Immel, U. D., Hoang-Vu, C., et al. (2013). Role of glutaminyl cyclases in thyroid carcinomas. *Endocr. Relat. Cancer* 20, 79–90. doi: 10.1530/erc-12-0053

Keith, B., Johnson, R. S., and Simon, M. C. (2011). HIF1alpha and HIF2alpha: sibling rivalry in hypoxic tumour growth and progression. *Nat. Rev. Cancer* 12, 9–22. doi: 10.1038/nrc3183

Khan, R. A., Chen, J., Shen, J., Li, Z., Wang, M., Wen, Z., et al. (2016). Common variants in QPCT gene confer risk of schizophrenia in the Han Chinese population. *Am. J. Med. Genet. B Neuropsychiatr. Genet.* 171b, 237–242. doi: 10.1002/ajmg.b.32397

Knoechel, B., Roderick, J. E., Williamson, K. E., Zhu, J., Lohr, J. G., Cotton, M. J., et al. (2014). An epigenetic mechanism of resistance to targeted therapy in T cell acute lymphoblastic leukemia. *Nat. Genet.* 46, 364–370. doi: 10.1038/ng.2913

Kopp, F., and Mendell, J. T. (2018). Functional classification and experimental dissection of long noncoding RNAs. *Cell* 172, 393–407. doi: 10.1016/j.cell.2018.01.011

Kourembanas, S., Hannan, R. L., and Faller, D. V. (1990). Oxygen tension regulates the expression of the platelet-derived growth factor-B chain gene in human endothelial cells. *J. Clin. Invest.* 86, 670–674. doi: 10.1172/jci114759

Kouzarides, T. (2007). Chromatin modifications and their function. *Cell* 128, 693–705. doi: 10.1016/j.cell.2007.02.005

Kovacova, J., Juracek, J., Poprach, A., Kopecky, J., Fiala, O., Svoboda, M., et al. (2019). MiR-376b-3p is associated with long-term response to sunitinib in metastatic renal cell carcinoma patients. *Cancer Genomics Proteomics* 16, 353–359. doi: 10.21873/cgp.20140

Lawrence, M. S., Stojanov, P., Mermel, C. H., Robinson, J. T., Garraway, L. A., Golub, T. R., et al. (2014). Discovery and saturation analysis of cancer genes across 21 tumour types. *Nature* 505, 495–501. doi: 10.1038/nature12912

Lee, J. T., and Bartolomei, M. S. (2013). X-inactivation, imprinting, and long noncoding RNAs in health and disease. *Cell* 152, 1308–1323. doi: 10.1016/j.cell.2013.02.016

Leonetti, A., Assaraf, Y. G., Veltsista, P. D., El Hassouni, B., Tiseo, M., and Giovannetti, E. (2019). MicroRNAs as a drug resistance mechanism to targeted therapies in EGFR-mutated NSCLC: current implications and future directions. *Drug Resist. Updat.* 42, 1–11. doi: 10.1016/j.drup.2018.11.002

Li, P., Ge, J., and Li, H. (2019). Lysine acetyltransferases and lysine deacetylases as targets for cardiovascular disease. *Nat. Rev. Cardiol.* 17, 96–115. doi: 10.1038/s41569-019-0235-9

Liu, L., Pang, X., Shang, W., Xie, H., Feng, Y., and Feng, G. (2019). Long non-coding RNA GAS5 sensitizes renal cell carcinoma to sorafenib via miR-21/SOX5 pathway. *Cell Cycle* 18, 257–263. doi: 10.1080/15384101.2018.1475826

Liu, L., Xu, Z., Zhong, L., Wang, H., Jiang, S., Long, Q., et al. (2016). Enhancer of zeste homolog 2 (EZH2) promotes tumour cell migration and invasion via epigenetic repression of E-cadherin in renal cell carcinoma. *BJU Int.* 117, 351–362. doi: 10.1111/bju.12702

Lo, W. S., Trievel, R. C., Rojas, J. R., Duggan, L., Hsu, J. Y., Allis, C. D., et al. (2000). Phosphorylation of serine 10 in histone H3 is functionally linked in vitro and in vivo to Gcn5-mediated acetylation at lysine 14. *Mol. Cell* 5, 917–926. doi: 10.1016/s1097-2765(00)80257-9

Loh, C. Y., Chai, J. Y., Tang, T. F., Wong, W. F., Sethi, G., Shanmugam, M. K., et al. (2019). The E-cadherin and N-cadherin switch in epithelial-to-mesenchymal transition: signaling, therapeutic implications, and challenges. *Cell* 8:1118. doi: 10.3390/cells8101118

Lu, Y., Zhao, X., Liu, Q., Li, C., Graves-Deal, R., Cao, Z., et al. (2017). lncRNA MIR100HG-derived miR-100 and miR-125b mediate cetuximab resistance via Wnt/β-catenin signaling. *Nat. Med.* 23, 1331–1341. doi: 10.1038/nm.4424

Lukamowicz-Rajska, M., Mittmann, C., Prummer, M., Zhong, Q., Bedke, J., Hennenlotter, J., et al. (2016). MiR-99b-5p expression and response to tyrosine kinase inhibitor treatment in clear cell renal cell carcinoma patients. *Oncotarget* 7, 78433–78447. doi: 10.18632/oncotarget.12618

Ma, L., Bajic, V. B., and Zhang, Z. (2013). On the classification of long non-coding RNAs. *RNA Biol.* 10, 925–933. doi: 10.4161/rna.24604

Makhov, P. B., Golovine, K., Kutikov, A., Teper, E., Canter, D. J., Simhan, J., et al. (2012). Modulation of Akt/mTOR signaling overcomes sunitinib resistance in renal and prostate cancer cells. *Mol. Cancer Ther.* 11, 1510–1517. doi: 10.1158/1535-7163.mct-11-0907

Makhov, P., Joshi, S., Ghatalia, P., Kutikov, A., Uzzo, R. G., and Kolenko, V. M. (2018). Resistance to systemic therapies in clear cell renal cell carcinoma: mechanisms and management strategies. *Mol. Cancer Ther.* 17, 1355–1364. doi: 10.1158/1535-7163.mct-17-1299

Mandal, R., Becker, S., and Strebhardt, K. (2016). Stamping out RAF and MEK1/2 to inhibit the ERK1/2 pathway: an emerging threat to anticancer therapy. *Oncogene* 35, 2547–2561. doi: 10.1038/onc.2015.329

Manning, B. D., and Cantley, L. C. (2003). Rheb fills a GAP between TSC and TOR. *Trends Biochem. Sci.* 28, 573–576. doi: 10.1016/j.tibs.2003.09.003

Margueron, R., and Reinberg, D. (2011). The Polycomb complex PRC2 and its mark in life. *Nature* 469, 343–349. doi: 10.1038/nature09784

Maroto, P., Esteban, E., Parra, E. F., Mendez-Vidal, M. J., Domenech, M., Pérez-Valderrama, B., et al. (2017). HIF pathway and c-Myc as biomarkers for response to sunitinib in metastatic clear-cell renal cell carcinoma. *Onco Targets Ther.* 10, 4635–4643. doi: 10.2147/OTT.S137677

Mathiyalagan, P., and Sahoo, S. (2017). Exosomes-based gene therapy for microRNA delivery. *Methods Mol. Biol.* 1521, 139–152. doi: 10.1007/978-1-4939-6588-5_9

Maxwell, P. H., Wiesener, M. S., Chang, G. W., Clifford, S. C., Vaux, E. C., Cockman, M. E., et al. (1999). The tumour suppressor protein VHL targets hypoxia-inducible factors for oxygen-dependent proteolysis. *Nature* 399, 271–275. doi: 10.1038/20459

Merhautova, J., Hezova, R., Poprach, A., Kovarikova, A., Radova, L., Svoboda, M., et al. (2015). miR-155 and miR-484 are associated with time to progression in metastatic renal cell carcinoma treated with sunitinib. *Biomed. Res. Int.* 2015:941980. doi: 10.1155/2015/941980

Michael, J. V., Wurtzel, J. G., and Goldfinger, L. E. (2016). Inhibition of galectin-1 sensitizes HRAS-driven tumor growth to rapamycin treatment. *Anticancer Res.* 36, 5053–5061. doi: 10.21873/anticanres.11074

Mollica, V., Di Nunno, V., Gatto, L., Santoni, M., Scarpelli, M., Cimadamore, A., et al. (2019). Resistance to systemic agents in renal cell carcinoma predict and overcome genomic strategies adopted by tumor. *Cancer* 11:830. doi: 10.3390/cancers11060830

Morais, C. (2014). Sunitinib resistance in renal cell carcinoma. *J. Kidney Cancer VHL* 1, 1–11. doi: 10.15586/jkcvhl.2014.7

Nickerson, M. L., Jaeger, E., Shi, Y., Durocher, J. A., Mahurkar, S., Zaridze, D., et al. (2008). Improved identification of von Hippel-Lindau gene alterations in clear cell renal tumors. *Clin. Cancer Res.* 14, 4726–4734. doi: 10.1158/1078-0432.ccr-07-4921

Osako, Y., Yoshino, H., Sakaguchi, T., Sugita, S., Yonemori, M., Nakagawa, M., et al. (2019). Potential tumor-suppressive role of microRNA-99a-3p in sunitinib-resistant renal cell carcinoma cells through the regulation of RRM2. *Int. J. Oncol.* 54, 1759–1770. doi: 10.3892/ijo.2019.4736

Peters, I., Dubrowinskaja, N., Abbas, M., Seidel, C., Kogosov, M., Scherer, R., et al. (2014). DNA methylation biomarkers predict progression-free and overall survival of metastatic renal cell cancer (mRCC) treated with antiangiogenic therapies. *PLoS One* 9:e91440. doi: 10.1371/journal.pone.0091440

Pili, R., Liu, G., Chintala, S., Verheul, H., Rehman, S., Attwood, K., et al. (2017). Combination of the histone deacetylase inhibitor vorinostat with bevacizumab in patients with clear-cell renal cell carcinoma: a multicentre, single-arm phase I/II clinical trial. *Br. J. Cancer* 116, 874–883. doi: 10.1038/bjc.2017.33

Poettler, M., Unseld, M., Braemswig, K., Haitel, A., Zielinski, C. C., and Prager, G. W. (2013). CD98hc (SLC3A2) drives integrin-dependent renal cancer cell behavior. *Mol. Cancer* 12:169. doi: 10.1186/1476-4598-12-169

Pompas-Veganzones, N., Sandonis, V., Perez-Lanzac, A., Beltran, M., Beardo, P., Juárez, A., et al. (2016). Myopodin methylation is a prognostic biomarker and predicts antiangiogenic response in advanced kidney cancer. *Tumour Biol.* 37, 14301–14310. doi: 10.1007/s13277-016-5267-8

Porta, C., Sabbatini, R., Procopio, G., Paglino, C., Galligioni, E., and Ortega, C. (2012). Primary resistance to tyrosine kinase inhibitors in patients with advanced renal cell carcinoma: state-of-the-science. *Expert. Rev. Anticancer. Ther.* 12, 1571–1577. doi: 10.1586/era.12.81

Prior, C., Perez-Gracia, J. L., Garcia-Donas, J., Rodriguez-Antona, C., Guruceaga, E., Esteban, E., et al. (2014). Identification of tissue microRNAs predictive of sunitinib activity in patients with metastatic renal cell carcinoma. *PLoS One* 9:e86263. doi: 10.1371/journal.pone.0086263

Puente, J., Laínez, N., Dueñas, M., Méndez-Vidal, M. J., Esteban, E., Castellano, D., et al. (2017). Novel potential predictive markers of sunitinib outcomes in long-term responders versus primary refractory patients with metastatic clear-cell renal cell carcinoma. *Oncotarget* 8, 30410–30421. doi: 10.18632/oncotarget.16494

Qu, L., Ding, J., Chen, C., Wu, Z. J., Liu, B., Gao, Y., et al. (2016). Exosome-transmitted lncARSR promotes sunitinib resistance in renal cancer by acting as a competing endogenous RNA. *Cancer Cell* 29, 653–668. doi: 10.1016/j.ccell.2016.03.004

Rahbarghazi, R., Jabbari, N., Sani, N. A., Asghari, R., Salimi, L., Kalashani, S. A., et al. (2019). Tumor-derived extracellular vesicles: reliable tools for cancer diagnosis and clinical applications. *Cell Commun. Signal* 17:73. doi: 10.1186/s12964-019-0390-y

Ralla, B., Busch, J., Flörcken, A., Westermann, J., Zhao, Z., Kilic, E., et al. (2018). miR-9-5p in nephrectomy specimens is a potential predictor of primary resistance to first-line treatment with tyrosine kinase inhibitors in patients with metastatic renal cell carcinoma. *Cancer* 10:321. doi: 10.3390/cancers10090321

Rasmussen, K. D., and Helin, K. (2016). Role of TET enzymes in DNA methylation, development, and cancer. *Genes Dev.* 30, 733–750. doi: 10.1101/gad.276568.115

Raval, R. R., Lau, K. W., Tran, M. G., Sowter, H. M., Mandriota, S. J., Li, J. L., et al. (2005). Contrasting properties of hypoxia-inducible factor 1 (HIF-1) and HIF-2 in von Hippel-Lindau-associated renal cell carcinoma. *Mol. Cell. Biol.* 25, 5675–5686. doi: 10.1128/mcb.25.13.5675-5686.2005

Reustle, A., Fisel, P., Renner, O., Büttner, F., Winter, S., Rausch, S., et al. (2018). Characterization of the breast cancer resistance protein (BCRP/ABCG2) in clear cell renal cell carcinoma. *Int. J. Cancer* 143, 3181–3193. doi: 10.1002/ijc.31741

Robert, M. F., Morin, S., Beaulieu, N., Gauthier, F., Chute, I. C., Barsalou, A., et al. (2003). DNMT1 is required to maintain CpG methylation and aberrant gene silencing in human cancer cells. *Nat. Genet.* 33, 61–65. doi: 10.1038/ng1068

Sakai, I., Miyake, H., and Fujisawa, M. (2013). Acquired resistance to sunitinib in human renal cell carcinoma cells is mediated by constitutive activation of signal transduction pathways associated with tumour cell proliferation. *BJU Int.* 112, E211–E220. doi: 10.1111/j.1464-410X.2012.11655.x

Salmena, L., Poliseno, L., Tay, Y., Kats, L., and Pandolfi, P. P. (2011). A ceRNA hypothesis: the rosetta stone of a hidden RNA language? *Cell* 146, 353–358. doi: 10.1016/j.cell.2011.07.014

Samuels, Y., Wang, Z., Bardelli, A., Silliman, N., Ptak, J., Szabo, S., et al. (2004). High frequency of mutations of the PIK3CA gene in human cancers. *Science* 304:554. doi: 10.1126/science.1096502

Santos-Rosa, H., and Caldas, C. (2005). Chromatin modifier enzymes, the histone code and cancer. *Eur. J. Cancer* 41, 2381–2402. doi: 10.1016/j.ejca.2005.08.010

Sekino, Y., Sakamoto, N., Sentani, K., Oue, N., Teishima, J., Matsubara, A., et al. (2019). miR-130b promotes sunitinib resistance through regulation of PTEN in renal cell carcinoma. *Oncology* 97, 164–172. doi: 10.1159/000500605

Siegel, R. L., Miller, K. D., and Jemal, A. (2019). Cancer statistics, 2019. *CA Cancer J. Clin.* 69, 7–34. doi: 10.3322/caac.21551

Stewart, G. D., Powles, T., Van Neste, C., Meynert, A., O'Mahony, F., Laird, A., et al. (2016). Dynamic epigenetic changes to VHL occur with sunitinib in metastatic clear cell renal cancer. *Oncotarget* 7, 25241–25250. doi: 10.18632/oncotarget.8308

Thiagalingam, S. (2020). Epigenetic memory in development and disease: unraveling the mechanism. *Biochim. Biophys. Acta Rev. Cancer* 1873:188349. doi: 10.1016/j.bbcan.2020.188349

Valenta, T., Hausmann, G., and Basler, K. (2012). The many faces and functions of β-catenin. *EMBO J.* 31, 2714–2736. doi: 10.1038/emboj.2012.150

Verbiest, A., Couchy, G., Job, S., Zucman-Rossi, J., Caruana, L., Lerut, E., et al. (2018). Molecular subtypes of clear cell renal cell carcinoma are associated with outcome during pazopanib therapy in the metastatic setting. *Clin. Genitourin. Cancer* 16, e605–e612. doi: 10.1016/j.clgc.2017.10.017

Vijayan, D. K., and Zhang, K. Y. J. (2019). Human glutaminyl cyclase: structure, function, inhibitors and involvement in Alzheimer's disease. *Pharmacol. Res.* 147:104342. doi: 10.1016/j.phrs.2019.104342

Wagener, N., Holland, D., Bulkescher, J., Crnkovic-Mertens, I., Hoppe-Seyler, K., Zentgraf, H., et al. (2008). The enhancer of zeste homolog 2 gene contributes to cell proliferation and apoptosis resistance in renal cell carcinoma cells. *Int. J. Cancer* 123, 1545–1550. doi: 10.1002/ijc.23683

Wang, M., Sun, Y., Xu, J., Lu, J., Wang, K., Yang, D. R., et al. (2018). Preclinical studies using miR-32-5p to suppress clear cell renal cell carcinoma metastasis via altering the miR-32-5p/TR4/HGF/met signaling. *Int. J. Cancer* 143, 100–112. doi: 10.1002/ijc.31289

Wang, Z., Zang, C., Cui, K., Schones, D. E., Barski, A., Peng, W., et al. (2009). Genome-wide mapping of HATs and HDACs reveals distinct functions in active and inactive genes. *Cell* 138, 1019–1031. doi: 10.1016/j.cell.2009.06.049

Wendt, M. K., Allington, T. M., and Schiemann, W. P. (2009). Mechanisms of the epithelial-mesenchymal transition by TGF-beta. *Future Oncol.* 5, 1145–1168. doi: 10.2217/fon.09.90

Wu, H., and Zhang, Y. (2014). Reversing DNA methylation: mechanisms, genomics, and biological functions. *Cell* 156, 45–68. doi: 10.1016/j.cell.2013.12.019

Xu, Z., Yang, F., Wei, D., Liu, B., Chen, C., Bao, Y., et al. (2017). Long noncoding RNA-SRLR elicits intrinsic sorafenib resistance via evoking IL-6/STAT3 axis in renal cell carcinoma. *Oncogene* 36, 1965–1977. doi: 10.1038/onc.2016.356

Yan, L., Ding, B., Liu, H., Zhang, Y., Zeng, J., Hu, J., et al. (2019). Inhibition of SMYD2 suppresses tumor progression by down-regulating microRNA-125b and attenuates multi-drug resistance in renal cell carcinoma. *Theranostics* 9, 8377–8391. doi: 10.7150/thno.37628

Yang, A. S., Doshi, K. D., Choi, S. W., Mason, J. B., Mannari, R. K., Gharybian, V., et al. (2006). DNA methylation changes after 5-aza-2'-deoxycytidine therapy in patients with leukemia. *Cancer Res.* 66, 5495–5503. doi: 10.1158/0008-5472.can-05-2385

Zhai, W., Sun, Y., Guo, C., Hu, G., Wang, M., Zheng, J., et al. (2017). LncRNA-SARCC suppresses renal cell carcinoma (RCC) progression via altering the androgen receptor(AR)/miRNA-143-3p signals. *Cell Death Differ.* 24, 1502–1517. doi: 10.1038/cdd.2017.74

Zhai, W., Sun, Y., Jiang, M., Wang, M., Gasiewicz, T. A., Zheng, J., et al. (2016). Differential regulation of LncRNA-SARCC suppresses VHL-mutant RCC cell proliferation yet promotes VHL-normal RCC cell proliferation via modulating androgen receptor/HIF-2α/C-MYC axis under hypoxia. *Oncogene* 35, 4866–4880. doi: 10.1038/onc.2016.19

Zhang, P. F., Li, K. S., Shen, Y. H., Gao, P. T., Dong, Z. R., Cai, J. B., et al. (2016). Galectin-1 induces hepatocellular carcinoma EMT and sorafenib resistance by activating FAK/PI3K/AKT signaling. *Cell Death Dis.* 7:e2201. doi: 10.1038/cddis.2015.324

Zhao, T., Bao, Y., Gan, X., Wang, J., Chen, Q., Dai, Z., et al. (2019). DNA methylation-regulated QPCT promotes sunitinib resistance by increasing HRAS stability in renal cell carcinoma. *Theranostics* 9, 6175–6190. doi: 10.7150/thno.35572

Zhao, J., and Guan, J. L. (2009). Signal transduction by focal adhesion kinase in cancer. *Cancer Metastasis Rev.* 28, 35–49. doi: 10.1007/s10555-008-9165-4

Zhou, Q., Guo, X., and Choksi, R. (2017). Activation of focal adhesion kinase and Src mediates acquired sorafenib resistance in A549 human lung adenocarcinoma xenografts. *J. Pharmacol. Exp. Ther.* 363, 428–443. doi: 10.1124/jpet.117.240507

Zhou, L., Liu, X. D., Sun, M., Zhang, X., German, P., Bai, S., et al. (2016). Targeting MET and AXL overcomes resistance to sunitinib therapy in renal cell carcinoma. *Oncogene* 35, 2687–2697. doi: 10.1038/onc.2015.343

Zhu, X., Chen, L., Liu, L., and Niu, X. (2019). EMT-mediated acquired EGFR-TKI resistance in NSCLC: mechanisms and strategies. *Front. Oncol.* 9:1044. doi: 10.3389/fonc.2019.01044

Conflict of Interest: The authors declare that the research was conducted in the absence of any commercial or financial relationships that could be construed as a potential conflict of interest.

frontiers in Cell and Developmental Biology

ORIGINAL RESEARCH
published: 15 January 2021
doi: 10.3389/fcell.2020.625056

MicroRNA-505, Suppressed by Oncogenic Long Non-coding RNA LINC01448, Acts as a Novel Suppressor of Glycolysis and Tumor Progression Through Inhibiting HK2 Expression in Pancreatic Cancer

Zhenglei Xu[1†], Dingguo Zhang[1†], Zhuliang Zhang[1], Weixiang Luo[2], Ruiyue Shi[1], Jun Yao[1], Defeng Li[1], Lisheng Wang[1] and Bihong Liao[3*]*

[1] The Second Clinical Medical College, Jinan University, Department of Gastroenterology, Shenzhen People's Hospital, Shenzhen, China, [2] Nursing Department, Shenzhen People's Hospital, The Second Affiliated Clinical Medical College of Jinan University, The First Affiliated Hospital of Southern University of Science and Technology, Shenzhen, China, [3] Department of Cardiology, Shenzhen People's Hospital, The Second Affiliated Clinical Medical College of Jinan University, The First Affiliated Hospital of Southern University of Science and Technology, Shenzhen, China

Background: MicroRNAs (miRNAs) and long non-coding RNAs (lncRNAs) play vital regulatory roles in pancreatic cancer (PC) initiation and progression. We aimed to explore the biological functions and underlying mechanisms of miR-505-3p (miR-505) in PC.

Methods: We first screened miRNA expression profiles using microarray in PC tissues and normal tissues, and then studied the function and underlying mechanism of miR-505. Moreover, we evaluated the regulatory effect of lncRNA LINC01448 on miR-505.

Results: We demonstrated miR-505 that was significantly downregulated in PC tissues. We further revealed that miR-505 significantly inhibited cell proliferation, invasion, sphere formation, glucose consumption, and lactate production by targeting HK2. In addition, overexpression of miR-505 led to tumor growth inhibition *in vivo*, demonstrating that it acts as a tumor suppressor in PC. LINC01448 was identified as an oncogenic lncRNA that could reduce miR-505 expression. Subsequent studies confirmed that LINC01448 enhanced cell proliferation, invasion, sphere formation, glucose consumption, and lactate production by regulating the miR-505/HK2 pathway.

Conclusions: These findings demonstrated that miR-505, suppressed by LINC01448, could function as a key tumor suppressor by targeting HK2 in PC, elucidating an important role of the LINC01448/miR-505/HK2 pathway in regulating PC glycolysis and progression.

Keywords: long non-coding RNA, microRNA, miR-505, HK2, pancreatic cancer

OPEN ACCESS

Edited by:
Xiao Zhu,
Guangdong Medical University, China

Reviewed by:
Chen Li,
Charité – Universitätsmedizin Berlin, Germany
Peixin Dong,
Hokkaido University, Japan

****Correspondence:***
Lisheng Wang
pouik256@163.com
Bihong Liao
tjwhy0909@163.com

[†]These authors have contributed equally to this work and share first authorship

Specialty section:
This article was submitted to Epigenomics and Epigenetics, a section of the journal Frontiers in Cell and Developmental Biology

Received: *02 November 2020*
Accepted: *21 December 2020*
Published: *15 January 2021*

Citation:
Xu Z, Zhang D, Zhang Z, Luo W, Shi R, Yao J, Li D, Wang L and Liao B (2021) MicroRNA-505, Suppressed by Oncogenic Long Non-coding RNA LINC01448, Acts as a Novel Suppressor of Glycolysis and Tumor Progression Through Inhibiting HK2 Expression in Pancreatic Cancer. Front. Cell Dev. Biol. 8:625056. doi: 10.3389/fcell.2020.625056

BACKGROUND

Pancreatic cancer (PC) is one of the most lethal malignancies worldwide (Garrido-Laguna and Hidalgo, 2015). The 5-year overall survival rate of PC has remained low at 6% (Garrido-Laguna and Hidalgo, 2015). PC is usually detected at advanced tumor stages when the disease has metastasized (Avula et al., 2020). Cancer metastasis is the leading cause of PC-related mortality (Sergeant et al., 2009; Avula et al., 2020). Thus, interventions to development and metastasis are critical for a favorable outcome. A growing body of evidence suggested that cancer stem cells constitute a distinct subpopulation in the tumor and play pivotal roles in tumor initiation and progression of PC (Sergeant et al., 2009; Avula et al., 2020). Moreover, most tumor cells highly rely on aerobic glycolysis to produce energy rather than mitochondrial oxidative phosphorylation even in the presence of oxygen, this is known as the "Warburg effect" (Avula et al., 2020). Hexokinase 2 (HK2) is a cancer-associated isoenzyme that catalyzes the first rate-limiting step of glucose metabolism, and depletion of HK2 in PC cell lines decreased lactate production, invasion, and metastasis (Anderson et al., 2016). However, the molecular mechanisms underlying the regulation of PC glycolysis and development are poorly understood.

Long non-coding RNAs (lncRNAs) are a group of RNA transcripts longer than 200 nucleotides without protein-coding potential (Huarte, 2015; Duguang et al., 2017). Recent studies have shown that lncRNAs are involved in the regulation of tumor cell's malignant behavior, including proliferation, invasion, and cancer stemness (Huarte, 2015; Duguang et al., 2017). Although the functions of most lncRNAs are largely unknown, lncRNAs have been shown to have important roles in affecting gene expression at both transcriptional and post-transcriptional levels (Huarte, 2015; Duguang et al., 2017). LncRNAs can function as guides, dynamic scaffolds, molecular decoys, and sponges *via* interaction with components of the cellular machinery, including DNA, RNA, and proteins (Balas and Johnson, 2018; Xu et al., 2020). Moreover, numerous lncRNAs are aberrantly expressed in PC and play essential roles in regulating the tumorigenesis, glycolysis, and metastasis of PC (Huarte, 2015; Duguang et al., 2017; Weidle et al., 2017).

MicroRNAs (miRNAs) are endogenous, small non-coding RNAs that regulate gene expression *via* inhibition of translation or the degradation of mRNA (Chan and Wang, 2015). MiRNAs are dysregulated in almost all types of cancers (including PC), and act as key regulators of cancer development and progression (Chan and Wang, 2015; Dong et al., 2018a). Previous studies have shown that miR-505-3p (miR-505) functions as a tumor suppressor in endometrial cancer (Chen S. et al., 2016), hepatocellular carcinoma (Lu et al., 2016), cervical cancer (Ma et al., 2017), osteosarcoma (Liu et al., 2018), glioma (Shi et al., 2018), and gastric cancer (Tian et al., 2018). Moreover, miR-505 inhibited the IGF-1R/AKT/GLUT-1 pathway and suppressed the glycolysis of hepatocellular carcinoma cells (Ren et al., 2019). Enhanced expression of miR-505 inhibited the expression of an oncogenic lncRNA ZEB1-AS1 in PC cells (Wei et al., 2020). However, the detailed functions and the underlying molecular mechanisms of miR-505 in PC remain unclear.

In this study, we found that miR-505 could significantly inhibit the proliferation, invasion, sphere formation, and glycolysis of PC cells by directly targeting HK2. Our results also revealed that miR-505 suppressed the growth of PC cells *in vivo*. Further mechanistic studies revealed that lncRNA LINC01448 could act as a suppressor of miR-505 to increase HK2 expression. Our findings provided new insights into the role of the LINC01448/miR-505/HK2 axis in PC progression, and this signaling pathway might represent a promising therapeutic target for PC treatment.

MATERIALS AND METHODS

Tissue Specimens

Specimens of PC tissues and corresponding adjacent normal tissues were obtained from 50 patients undergoing surgery at the Shenzhen People's Hospital, The Second Affiliated Clinical Medical College of Jinan University, The First Affiliated Hospital of Southern University of Science and Technology, China. These patients had not received prior treatment before surgery. This research was carried out in accordance with the Helsinki declaration and approved by the Research Ethics Committee of Shenzhen People's Hospital, The Second Affiliated Clinical Medical College of Jinan University, The First Affiliated Hospital of Southern University of Science and Technology. Written informed consent was obtained from each patient. All tissues were immediately frozen in liquid nitrogen and stored at −80°C for RNA extraction.

miRNA Microarray Analysis

The total RNA from five PC tissues and paired normal tissues was isolated using the TRIzol reagent (Invitrogen, Carlsbad, CA, USA). The expression profile of miRNAs was analyzed using the Agilent Human miRNA expression array (8 × 60K platform, Agilent, Inc., Santa Clara, CA, USA) following the manufacturer's instructions. In brief, 100 ng of total RNA from each specimen was labeled with cyanine 3-pCp (Cy3) using the miRNA Complete Labeling and Hyb kit (Agilent). Then, Cy3-labeled RNAs were hybridized to a miRNA microarray containing 1,887 human miRNAs. The miRNA microarray was scanned using the Agilent G2600D microarray scanner and analyzed using the Agilent Feature Extraction software package (v11.0.1.1).

Cell Lines and Transfection

Five PC cell lines (AsPC-1, PANC-1, BxPC-3, SW-1990, and PaCa-2) and a non-tumorous pancreatic cell line HPDE6-C7 were purchased from American Type Culture Collection (Manassas, VA, USA). These cells were cultured in RPMI1640 medium (Thermo Fisher Scientific, Waltham, MA, USA) supplemented with 10% fetal bovine serum (FBS, Thermo Fisher Scientific, Waltham, MA, USA) at 37°C in 5% CO_2.

The expression vectors expressing LINC01448 (or HK2) and the corresponding empty vector were purchased from Genepharma (Shanghai, China). The small-interfering RNAs (siRNAs) against LINC01448 (or HK2), the control siRNA,

miR-505 mimic, control mimic, miR-505 inhibitor, and control inhibitor were from Ribobio (Guangzhou, China). Transient transfection was conducted using the Lipofectamine 3000 reagent (Invitrogen, Carlsbad, CA, USA) in accordance with manufacturer's instructions.

RNA Extraction and Quantitative Real-Time PCR (qRT-PCR) Assays

Total RNA was isolated using the TRIzol reagent (Invitrogen, Carlsbad, CA, USA). The total RNA was then reverse transcribed using the M-MLV Reverse Transcriptase Kit (Invitrogen, Carlsbad, CA, USA) in accordance with manufacturer's protocol. The expression levels of mRNA were quantified with the SYBR Green quantitative PCR kit (Takara, Dalian, China) on a 7300 Real-Time PCR System (Applied Biosystems, Foster City, CA, USA). The primers were purchased from Genepharma (Shanghai, China). *GAPDH* was used as an internal control. The expression level of miR-505 was examined using the mirVanaTM qRT-PCR microRNA Detection Kit (Ambion, Austin, TX, USA) and normalized to U6.

Western Blotting Analysis

Cells were lysed with RIPA buffer (Beyotime, Beijing, China) containing 1% protease inhibitor cocktail (Selleck, Houston, TX, USA). An equal amount of protein was separated by SDS-polyacrylamide gel electrophoresis and transferred onto a PVDF membrane (Millipore, Bedford, MA, USA). After this, the membranes were incubated with the primary antibodies: HK2 (1:1,000, Cell Signaling, MA, USA) and GAPDH (1:5,000, Santa Cruz, CA, USA). After washing, the blots were incubated with HRP-conjugated secondary antibodies (Santa Cruz, CA, USA). The positive immunoreactivity was detected using the ECL detection system (Amersham Biosciences, Buckinghamshire, UK). GAPDH was used as the loading control.

Cell Proliferation Assays

Cell proliferation was assessed 72 h after transfection using the CCK-8 assay (Dojindo Laboratories, Kumamoto, Japan) according to the manufacturer's instructions. The absorbance was determined at the wavelength of 450 nm.

Transwell Invasion Assays

Cell invasion was assessed as previously reported (Dong et al., 2018b). Transfected cells were seeded into the upper chamber of an insert for invasion assays (8-μm pore size, Corning Costar Co, Lowell, CA, USA) with 500 μl serum-free media. The lower chambers were filled with 750 μl medium containing 10% FBS. After an incubation period of 24 h, the invaded cells were stained with Giemsa (Sigma, St. Louis, MO, USA) for 15 min. The number of cells was counted using an Olympus microscope.

Sphere Formation Assays

Single cells were cultured in serum-free medium supplemented with B27 (1:50; Invitrogen, Carlsbad, CA, USA), 20 ng/ml basic FGF (BD Biosciences, CA, USA) and 20 ng/ml EGF (Sigma, St. Louis, MO, USA). The cells were monitored for 14 days and the cell clusters that had grown to at least 50 μm in diameter were scored as a sphere.

Glucose Consumption and Lactate Production Assays

Glucose consumption and lactate production were measured using the Glucose Assay Kit-WST and Lactate Assay Kit-WST (Dojindo Laboratories, Kumamoto, Japan) as described previously (Matsuo et al., 2020).

In vivo Tumor Formation Assays

The experimental procedures involving animals were approved by the Shenzhen People's Hospital, The Second Affiliated Clinical Medical College of Jinan University, The First Affiliated Hospital of Southern University of Science and Technology, China. Four-week-old Nude mice ($n = 6$ per group) were obtained from Beijing HFK Bioscience (Beijing, China). PC cells (2×10^6 cells) were subcutaneously injected into the right flank of nude mice. The length and width of tumors were measured every 3 days, and tumor volume was calculated by the following formula: volume = length (mm) × width^2 (mm^2)/2. At 21 days after injection, the mice were sacrificed and tumor tissues were excised.

Luciferase Reporter Assays

The luciferase reporter plasmids containing wild-type (WT) LINC01448, mutant (MUT) LINC01448 with a mutated miR-505 binding site, WT *HK2* 3′-untranslated region (3′-UTR) fragment, and MUT *HK2* 3′-UTR fragment with a mutated miR-505 binding site, were obtained from Ribobio (Guangzhou, China). PC cells were co-transfected with the indicated reporter plasmids, together with miR-505 mimic, miR-505 inhibitor or the respective negative controls, using the Lipofectamine 3000 (Invitrogen, Carlsbad, CA, USA). After 48 h of incubation, the luciferase signal was quantified using a Dual-Luciferase Reporter Assay System (Promega, Madison, WI, USA) according to the manufacturer's directions.

RNA Immunoprecipitation (RIP) Assays

A Magna RIP RNA-Binding Protein Immunoprecipitation Kit (Millipore, Billerica, MA, USA) was utilized for the RIP assays. PC cells were lysed with RIP-lysis buffer and the cell extract was incubated with magnetic beads conjugated with anti-Ago2 antibody (Millipore, Bedford, MA, USA) or control anti-IgG antibody (Millipore, Bedford, MA, USA). The beads were incubated with proteinase K to remove proteins. Finally, extracted RNAs were subjected to the qRT-PCR analysis.

Statistical Analysis

Results are presented expressed as the mean ± standard deviation. The Student's *t*-tests, one-way ANOVA tests, Wilcoxon signed-rank tests, χ^2-tests and Fisher's exact tests were used to compare the mean values among groups. All experiments were done at least three times. $P < 0.05$ was considered statistically significant.

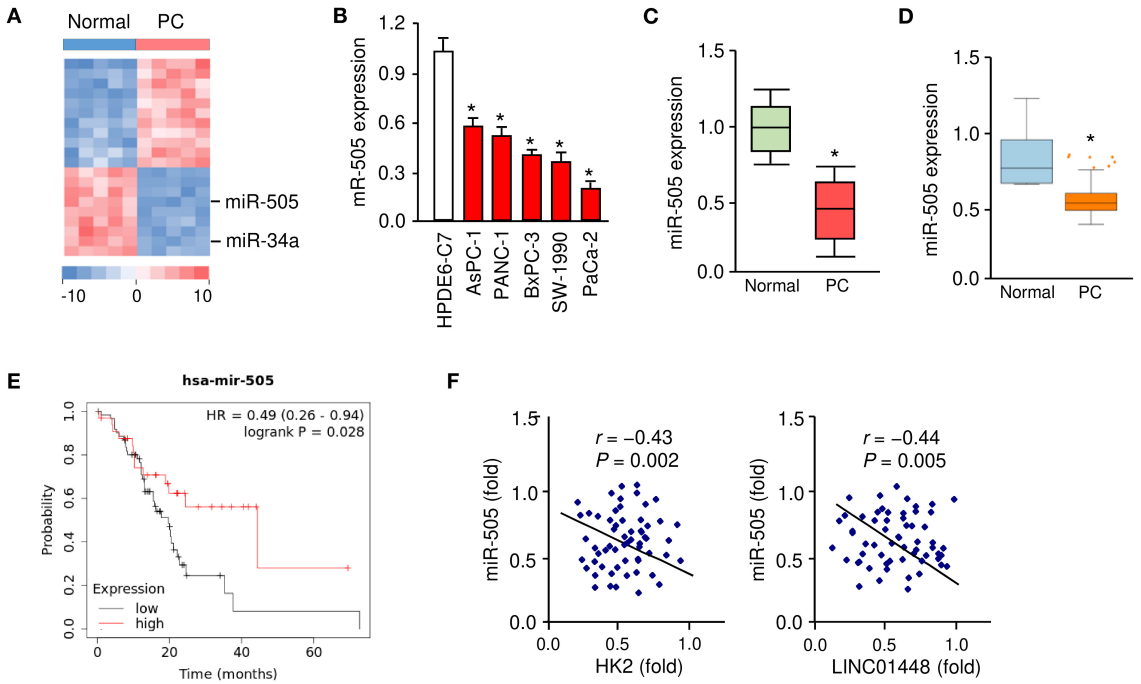

FIGURE 1 | Downregulation of miR-505 in PC tissues and cell lines. **(A)** The differentially expressed miRNAs between five PC tissues and their adjacent normal tissues were identified using a miRNA microarray analysis. **(B)** qRT-PCR analysis of miR-505 expression in PC cell lines and a normal pancreatic cell line HPDE6-C7. **(C)** miR-505 levels in PC tissues and normal tissues were examined using qRT-PCR assays. **(D)** Meta-profiling of differential expression of miR-505 in PC tissues and normal tissues (MIR-TV database). **(E)** Kaplan-Meier curves revealed that lower expression of miR-505 was related to poor overall survival in PC patients (KM Plotter database). **(F)** Correlative analysis of miR-505 and HK2/LINC01448 expression in PC tissues. *$P < 0.05$.

RESULTS

Downregulation of miR-505 in PC Tissues and Cell Lines

We applied miRNA microarray analysis to identify the miRNAs that are differentially expressed in PC tissues ($n = 5$) and their adjacent normal tissues ($n = 5$). MiR-34a is a known tumor suppressor downregulated in several types of malignancies including PC (Tang et al., 2017). As expected, miR-34a expression was significantly downregulated in PC samples compared with paired non-cancerous tissues (**Figure 1A**). We found that miR-505 was the most significantly downregulated miRNA in PC tissues (**Figure 1A**).

Our qRT-PCR assays revealed that the expression of miR-505 was significantly lower in the PC cell lines, whereas a normal pancreatic duct epithelial cell line HPDE6-C7 expressed a relatively higher expression level of miR-505 (**Figure 1B**). Furthermore, the qRT-PCR assays were used to determine the expression levels of miR-505 in 50 specimens of PC and normal tissues. miR-505 levels were significantly lower in PC tissues (**Figure 1C**). In addition, we analyzed the expression of miR-505 across different normal and cancer tissues using the MIR-TV database (http://mirtv.ibms.sinica.edu.tw/index.php). Compared with normal tissues, miR-505 was markedly downregulated in PC tissues (**Figure 1D**). We then accessed the prognostic value of miR-505 expression in the TCGA PC dataset using the KM Plotter database (http://kmplot.com/analysis/). Survival curves were plotted for PC patients ($n = 178$). High expression of miR-505 was positively associated with a favorable prognosis in PC patients (**Figure 1E**).

To further define the clinical significance of miR-505 expression in PC, we divided 50 PC tissues into two groups: cancers with below-median miR-505 expression and cancers with above-median miR-505 expression. The correlation of miR-505 expression with various clinical parameters was shown in **Table 1**. No significant association was found between miR-505 expression and age, tumor differentiation, or tumor size. Interestingly, lower miR-505 levels were significantly correlated with more advanced pathological stage and more lymph node metastasis (**Table 1**). Together, these results suggested that miR-505 might play a tumor suppressor role in PC.

miR-505 Inhibits the Proliferation, Invasion, Sphere Formation, and Glycolysis of PC Cells

To determine whether miR-505 could affect the malignant phenotypes in PC cells, we examined the effects of either miR-505 overexpression or knockdown on cell proliferation, invasion, sphere formation, and glycolysis. AsPC-1/PaCa-2 cells with relatively higher/lower miR-505 expression were used in subsequent functional assays (**Figure 2A**). The overexpression of miR-505 significantly suppressed the proliferation, invasion,

TABLE 1 | Correlation of miR-505 expression with clinical characteristics of patients with PC.

Characteristics	miR-505 expression		*P* values
	Below median	Above median	
Age (years)			
>60	14	11	0.778
≤60	12	13	
Differentiation			
Well/moderate	11	14	0.396
Poor	15	10	
Tumor size			
≤2 cm	15	16	0.57
>2 cm	11	8	
TNM stage			
I/II	5	16	0.0012
III/IV	21	8	
Lymph node metastasis			
Negative	4	21	0.0001
Positive	22	3	

sphere formation, glucose consumption, and lactate production of PaCa-2 cells (**Figures 2A–E**). We also transfected AsPC-1 cells that exhibit higher levels of miR-505 with miR-505 inhibitor and assessed the effects of miR-505 depletion on these malignant properties (**Figure 2A**). Cell proliferation, invasion, sphere formation, glucose consumption, and lactate production assays demonstrated that knockdown of miR-505 significantly induced the proliferation, invasion, sphere formation, glucose consumption, and lactate production of AsPC-1 cells (**Figures 2A–E**). Collectively, these data revealed that miR-505 overexpression significantly inhibits the proliferation, invasion, sphere formation, and glycolysis of PC cells.

miR-505 Represses Tumorigenesis of PC Cells *in vivo*

To further investigate the functional role of miR-505 in PC *in vivo*, we established nude mouse xenograft models by implanting PaCa-2 cells transfected with miR-505 mimic (or control mimic), or AsPC-1 cells transfected with miR-505 inhibitor (or control inhibitor), respectively (**Figure 3A**). The tumor growth was monitored, and we found that overexpression of miR-505 significantly decreased the tumor volumes and tumor weights, whereas silencing of miR-505 significantly enhanced the tumor volumes and tumor weights (**Figures 3B–D**). Taken together, these results demonstrated that miR-505 inhibits the tumorigenesis of PC cells *in vivo*.

miR-505 Directly Targets HK2 in PC Cells

We predicted the possible target genes of miR-505 using the TargetScan database (http://www.targetscan.org). According to this analysis, miR-505 could target the 3′-UTR of *HK2* mRNA (**Figure 4A**). To explore the potential role of HK2 in PC, we searched the UALCAN database (http://ualcan.path.uab.edu/index.html) for *HK2* expression in the TCGA PC tissues. This analysis revealed the significant upregulation of *HK2* in PC tissues compared with normal tissues (**Figure 4B**). Then, we performed qRT-PCR assays to analyze the level of *HK2* in PC cell lines (AsPC-1 and PaCa-2) and HPDE6-C7 cells. We found that *HK2* was overexpressed in PC cells compared with HPDE6-C7 cells (**Figure 4C**).

To analyze whether miR-505 directly represses HK2 expression by binding to its 3′-UTR, we performed the luciferase reporter assays by co-transfecting a reporter vector containing WT *HK2* 3′-UTR with miR-505 mimic (or miR-505 inhibitor) into PC cells. Transfection with miR-505 mimic significantly inhibited *HK2* luciferase activity in PaCa-2 cells, whereas transfection with miR-505 inhibitor significantly increased *HK2* luciferase activity in AsPC-1 cells (**Figure 4D**). However, transfection of miR-505 mimic or miR-505 inhibitor did not significantly alter the luciferase reporter activity of mutated *HK2* 3′-UTR (**Figure 4D**). Western blotting analysis confirmed that overexpression of miR-505 led to downregulation of HK2 in PaCa-2 cells (**Figure 4E**). On the contrary, knockdown of miR-505 increased HK2 protein levels in AsPC-1 cells (**Figure 4E**). These results verified that *HK2* is a target gene of miR-505.

We examined the effects of HK2 expression on PC cell proliferation, invasion, sphere formation, and glycolysis. Our cell functional assays suggested that overexpression of HK2 significantly induced the proliferation, invasion, sphere formation, glucose consumption, and lactate production of AsPC-1 cells (**Figures 4F,G**). However, silencing of HK2 significantly impaired the proliferation, invasion, sphere formation, glucose consumption, and lactate production of PaCa-2 cells (**Figures 4F,G**). Furthermore, Kaplan-Meier survival analysis using data from the KM Plotter database showed that those PC patients with high HK2 expression had worse overall survival (**Figure 4H**). These results have identified HK2 as a novel oncogene in PC cells and suggested that miR-505 negatively regulates the expression of HK2.

miR-505 Acts as a Tumor Suppressor by Inhibiting HK2 Expression in PC Cells

To explore whether miR-505 exerts its tumor suppressor functions through suppressing the expression of HK2. PaCa-2cells were co-transfected with miR-505 mimic (or control mimic), together with (or without) HK2 expression vector (**Figure 5A**). On the other hand, AsPC-1 cells were co-transfected with miR-505 inhibitor (or control inhibitor), together with (or without) HK2 siRNAs, respectively (**Figure 5A**). Our cell functional assays showed that overexpression of HK2 could restore miR-505 mimic-suppressed PC cell proliferation, invasion, sphere formation, and glycolysis (**Figure 5B**). In contrast, HK2 siRNA could prevent miR-505 knockdown-enhanced PC cell proliferation, invasion, sphere formation, and glycolysis (**Figures 5C,D**). Together, our data supported that miR-505 suppresses the malignant properties of PC cells by inhibiting HK2 expression.

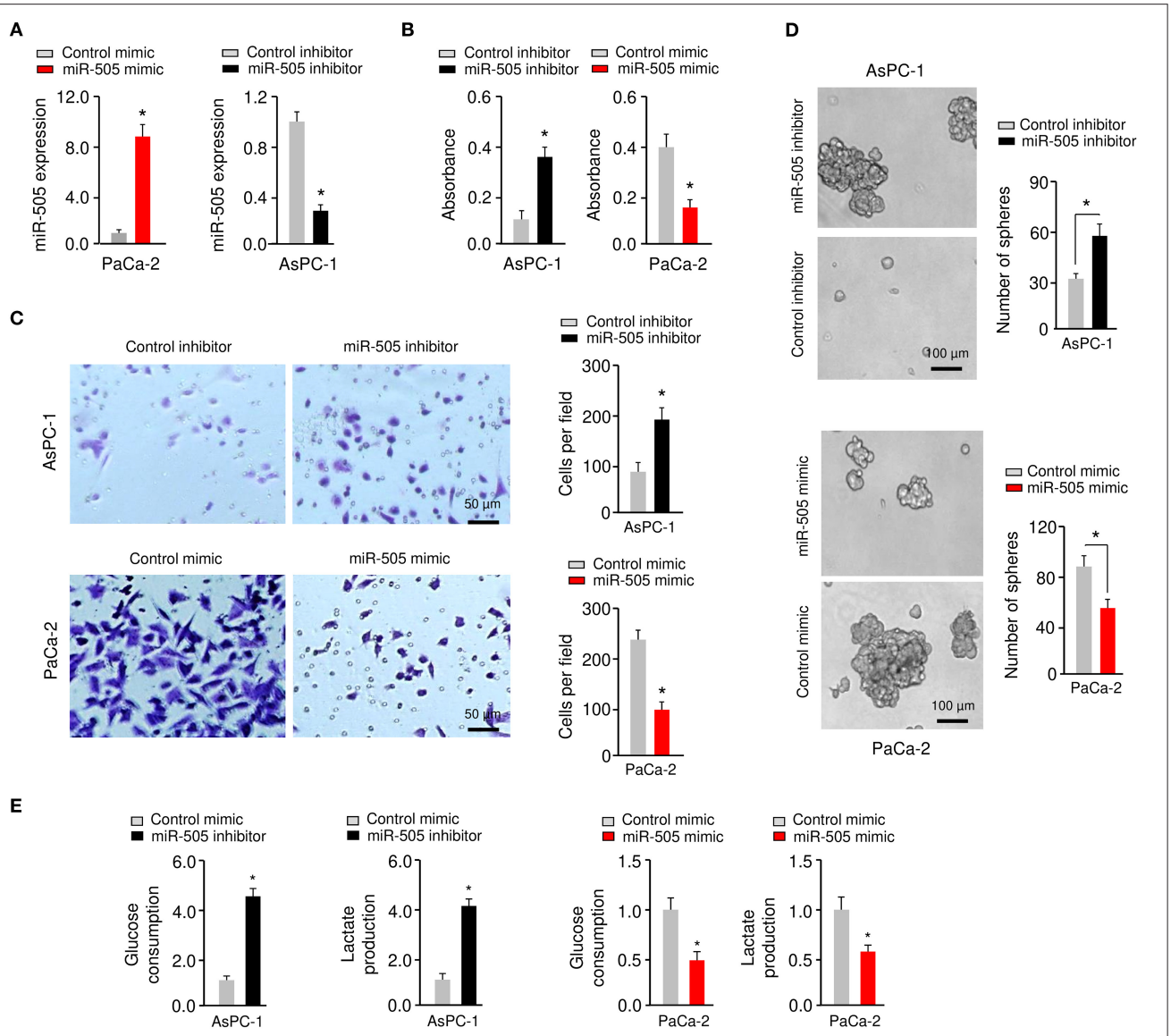

FIGURE 2 | miR-505 inhibits the proliferation, invasion, sphere formation, and glycolysis of PC cells. **(A)** Expression of miR-505 in PC cells transfected with miR-505 mimic, miR-505 inhibitor or their negative controls, respectively. **(B)** Cell proliferation was analyzed using CCK-8 assays. **(C)** Invasion of PaCa-2 (upper) cells was examined after miR-505 overexpression. Invasion of AsPC-1 (bottom) cells was examined after knockdown of miR-505. Scale bar: 50 μm. **(D)** PC cells were transfected as indicated, and sphere formation assays were conducted. Scale bar: 100 μm. **(E)** Glucose consumption and lactate production assays in PaCa-2 cells after overexpression of miR-505, and in AsPC-1 cells after knockdown of miR-505. *$P < 0.05$.

lncRNA LINC01448 Directly Binds to miR-505 and Represses Its Expression

Many lncRNAs were known to function as miRNA sponges, leading to the reduction of miRNA expression in tumor cells (Huarte, 2015). Using the NOCORI prediction program (http://starbase.sysu.edu.cn), lncRNA LINC01448 was found to contain one potential binding site for miR-505 (**Figure 6A**). Thus, we selected the lncRNA LINC01448 for our subsequent study.

The levels of LINC01448 were significantly increased in AsPC-1 and PaCa-2 cells when compared to HPDE6-C7 cells (**Figure 6B**). To assess the association between LINC01448 and miR-505, we performed the luciferase reporter assays. Overexpression of miR-505 suppressed the luciferase activities of WT LINC01448 reporter constructs, but this effect was abolished when the binding site for miR-505 within the LINC01448 sequence was mutated (**Figure 6C**). We further observed that the inhibition of miR-505 significantly increased the luciferase activities of WT LINC01448, but had no significant effect on the luciferase activities of MUT LINC01448 (**Figure 6C**). The qRT-PCR experiments suggested that silencing of LINC01448 in PaCa-2 cells led to a significant increase in miR-505 expression, while the overexpression of LINC01448 in AsPC-1

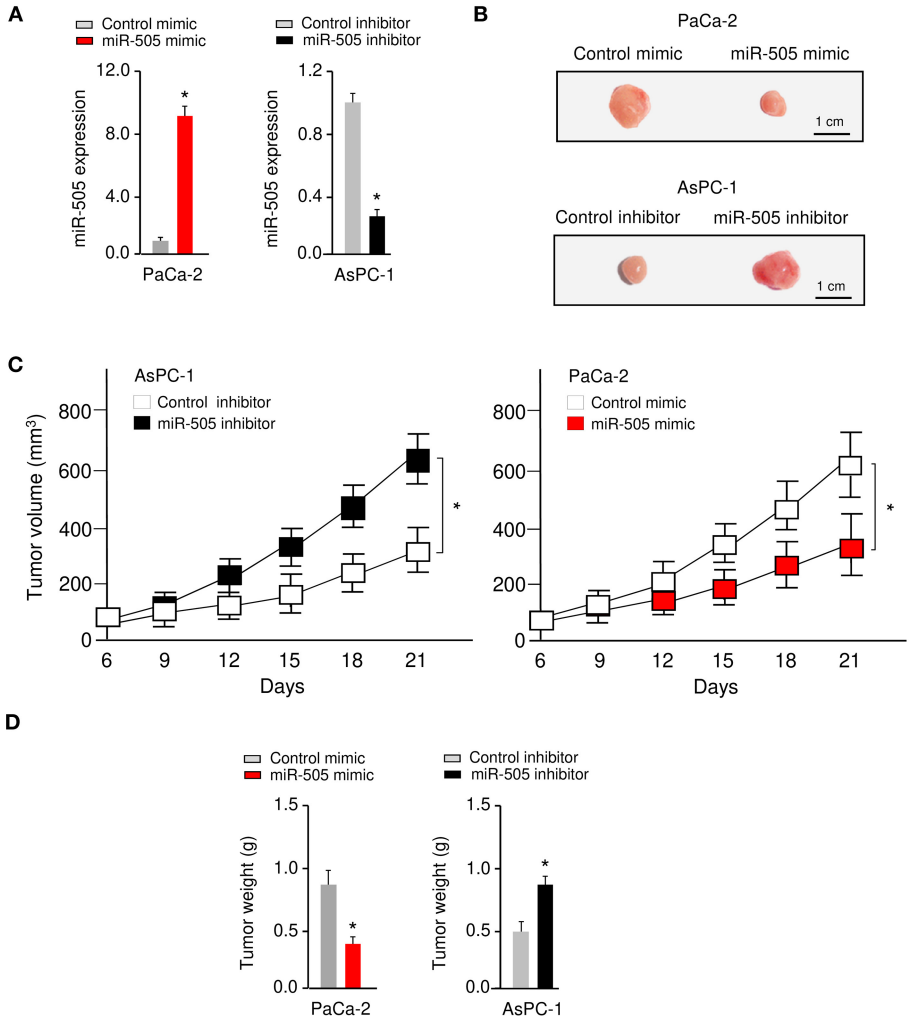

FIGURE 3 | miR-505 represses tumorigenesis of PC cells *in vivo*. **(A)** The levels of miR-505 in PC cells transfected with miR-505 mimic, miR-505 inhibitor or their negative controls, respectively. **(B–D)** Nude mouse xenograft model**s** were established by subcutaneously implanting PaCa-2 cells transfected with (or without) miR-505 mimic, or AsPC-1 cells transfected with (or without) miR-505 inhibitor, respectively. Representative images **(B)**, tumor volume growth curves **(C)**, and weight **(D)** of the formed tumors. Scale bar: 1 cm. *$P < 0.05$.

cells significantly reduced the levels of miR-505 (**Figure 6D**). We conducted RIP assays in PC cells that were transfected with miR-505 mimic or control mimic. Compared with the control group, the endogenous LINC01448 was efficiently pulled down by Ago2 in PC cells transfected with miR-505 mimic (**Figure 6E**).

Using qRT-PCR assays, we examined the expression of LINC01448 in PC tissues and adjacent normal tissues and found that the expression of LINC01448 was significantly increased in PC tissues (**Figure 6F**). Then, we explored the correlation between LINC01448 expression and PC patient survival using the KM Plotter database. PC patients were divided into high and low LINC01448 expression groups according to the median value. Kaplan–Meier survival analysis suggested that PC patients with low expression of LINC01448 displayed longer overall survival times than those with high expression of LINC01448 (**Figure 6G**). Collectively, these results demonstrated that LINC01448 may serve as a sponge for miR-505.

LINC01448 Promotes the Malignant Phenotypes of PC Cells *via* Repressing miR-505 Expression

To investigate whether LINC01448 modulates the malignant phenotypes of PC cells through repressing miR-505 expression, we conducted rescue experiments. AsPC-1 cells were transfected with a LINC01448 expression vector (or control vector), together with (or without) miR-505 mimic. Conversely, PaCa-2 cells were transfected with LINC01448 siRNA (or control siRNA), together with (or without) miR-505 inhibitor. Our cell functional assays showed that the overexpression of LINC01448 promoted the proliferation, invasion, sphere formation, glucose consumption, and lactate production of AsPC-1 cells, and

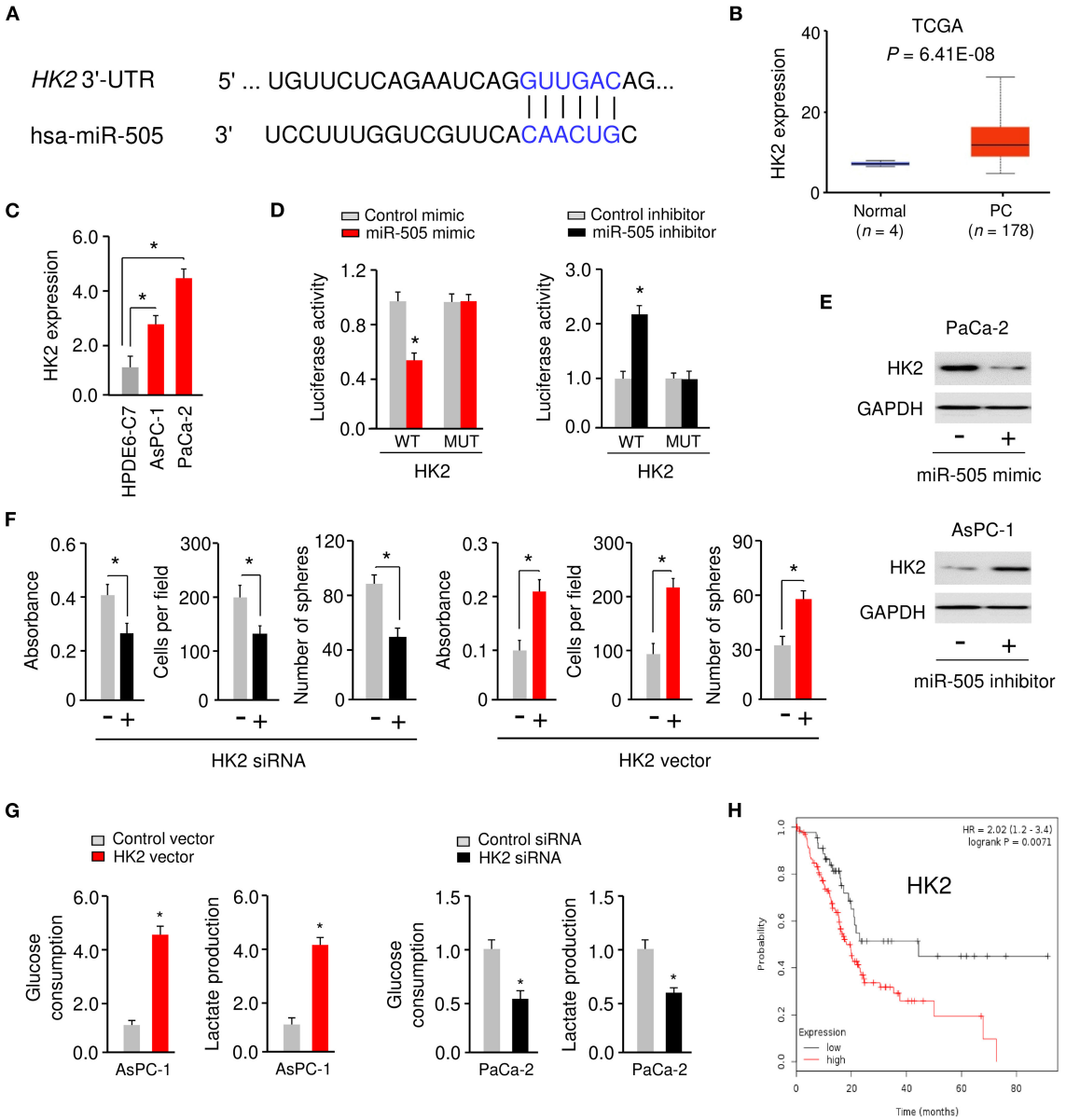

FIGURE 4 | miR-505 directly targets HK2 in PC cells. **(A)** The predicted miR-505 binding site in the *HK2* 3′-UTR sequence. **(B)** The expression of HK2 in PC tissues and normal tissues (UALCAN database). **(C)** qRT-PCR analysis of HK2 expression in PC cell lines and normal pancreatic cells. **(D)** PaCa-2 cells were transfected with luciferase reporter vectors containing wild-type (WT) or mutant (MUT) *HK2* 3′-UTR, along with (or without) miR-505 mimic, and AsPC-1 cells were transfected with luciferase reporter vectors containing WT or MUT *HK2* 3′-UTR, along with (or without) miR-505 inhibitor. The binding between miR-505 and HK2 was verified using luciferase reporter assays. **(E)** Western blotting analysis of HK2 expression in PaCa-2 cells transfected with (or without) miR-505 mimic, and in AsPC-1 cells transfected with (or without) miR-505 inhibitor. **(F)** PC cells were transfected with HK2 vector or HK2 siRNA as indicated, and cell proliferation, invasion and sphere formation assays were performed. **(G)** Glucose consumption and lactate production assays in PaCa-2 cells after knockdown of HK2 and in AsPC-1 cells after overexpression of HK2. **(H)** Kaplan-Meier curves for the overall survival of PC patients were compared between groups with high or low levels of HK2 based on the TCGA data from the KM Plotter database. $^*P < 0.05$.

these effects were partially reversed by the restoration of miR-505 expression (**Figure 7A**). Furthermore, the inhibition of miR-505 partially reversed the LINC01448 siRNA-reduced cell proliferation, invasion, sphere formation, glucose consumption, and lactate production (**Figure 7B**). The protein expression of HK2 was increased in LINC01448-overexpressing AsPC-1 cells, but was reduced in LINC01448-knockdown PaCa-2 cells (**Figure 7C**). Using qRT-PCR assays, we detected a significant negative association between miR-505 and *HK2*/LINC01448 expression in PC tissues (**Figure 1F**).

To further elucidate the mechanism underlying LINC01448 overexpression in PC, we investigated the involvement of transcription factors in regulating the expression of LINC01448. We used the UCSC database (http://genome.ucsc.edu/) to find

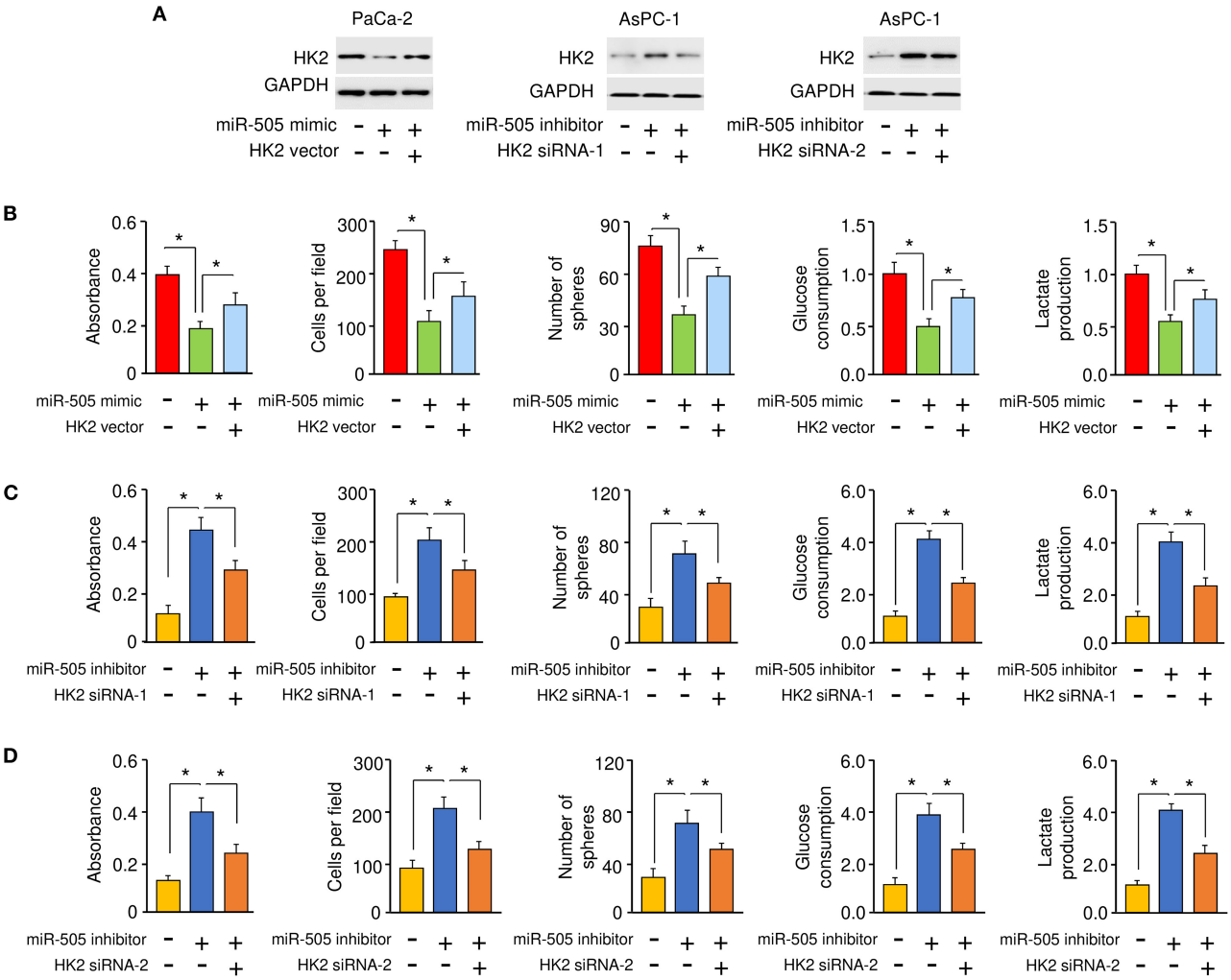

FIGURE 5 | miR-505 acts as a tumor suppressor by inhibiting HK2 expression in PC cells. **(A)** Western blotting analysis of HK2 expression in PaCa-2 cells transfected with or without miR-505 mimic, together with (or without) HK2 vector, or in AsPC-1 cells transfected with or without miR-505 inhibitor, together with (or without) HK2 siRNAs. **(B)** Cell functional assays were conducted in PaCa-2 cells transfected with (or without) miR-505 mimic, along with (or without) HK2 expression vector. **(C,D)** Cell functional assays were done in AsPC-1 cells transfected with (or without) miR-505 inhibitor, together with (or without) HK2 siRNA-1 **(C)** or HK2 siRNA-2 **(D)**. *$P < 0.05$.

possible transcription factors for LINC01448. Among these transcription factors, SOX2 has been recognized as a powerful oncogene in PC (Herreros-Villanueva et al., 2013), and it was reported as a transcription activator of lncRNAs (Wu et al., 2018). Consistent with this prediction, our qRT-PCR analysis showed that SOX2 expression was positively correlated with the levels of LINC01448 and HK2 in PC tissues (**Figure 8**). In contrast, the expression of SOX2 was negatively correlated with the expression of miR-505 in patients with PC (**Figure 8**). Taken together, these findings indicated a possibility that SOX2 might act as a transcription activator of LINC01448 in PC.

DISCUSSION

Although several studies have demonstrated that dysregulated miRNAs and lncRNAs could function as important regulators in PC through modulating cancer cell proliferation, migration, and invasion (Zhai et al., 2020), it remains unclear whether miR-505 and LINC00261 regulate the glycolysis and aggressive features of PC cells. To the best of our knowledge, for the first time, this study demonstrated that miR-505 functions as a tumor suppressor to attenuate glycolysis and aggressive phenotypes of PC cells through targeting HK2, and that oncogenic LINC01448 serves as an upstream inhibitor of miR-505 in PC cells (**Figure 9**).

In this study, we detected differentially expressed miRNAs in PC tissues. Of these miRNAs, miR-505 has been characterized as a tumor-suppressive miRNA in human endometrial cancer (Chen S. et al., 2016), hepatocellular carcinoma (Lu et al., 2016), cervical cancer (Ma et al., 2017), osteosarcoma (Liu et al., 2018), glioma (Shi et al., 2018), and gastric cancer (Tian et al., 2018). Very recently, one study showed that miR-505 inhibited the expression of an oncogenic lncRNA ZEB1-AS1 in PC cells (Ren et al.,

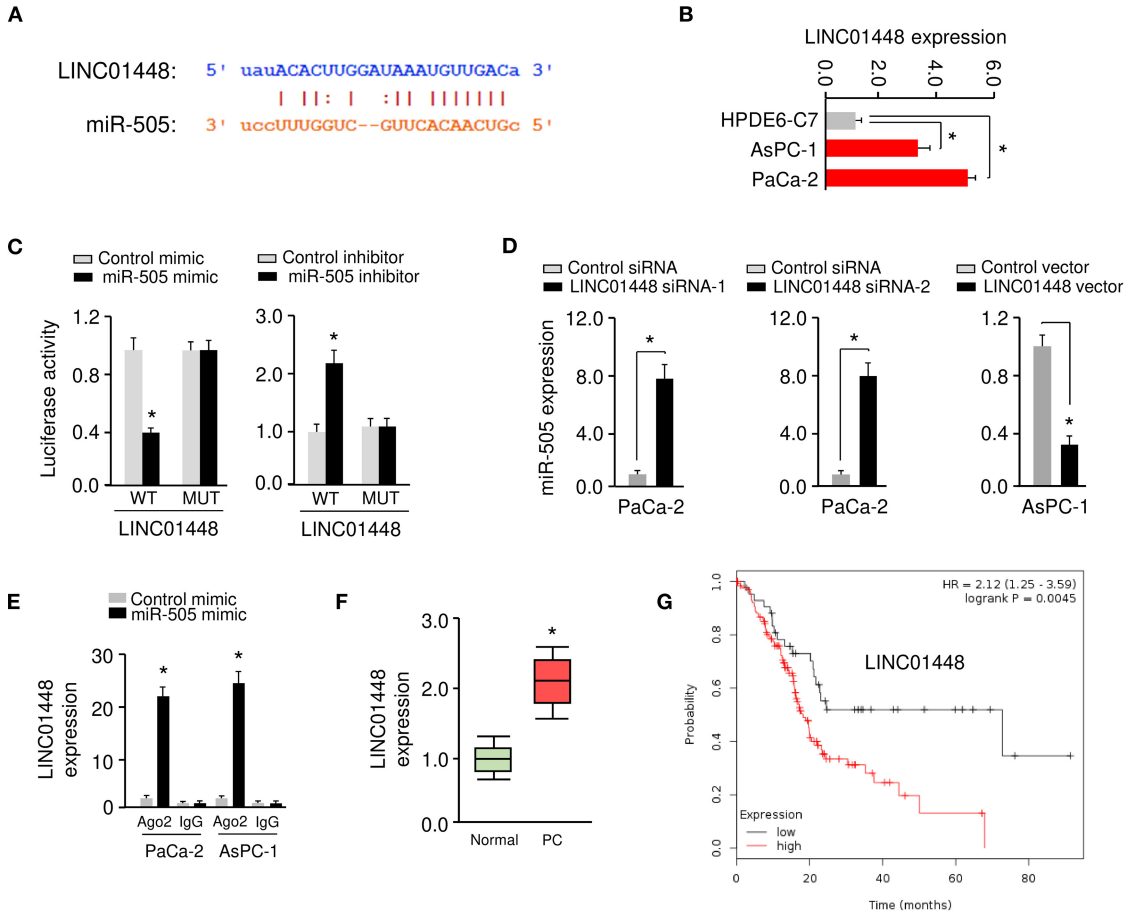

FIGURE 6 | LncRNA LINC01448 directly binds to miR-505 and represses its expression. **(A)** Putative binding sites between miR-505 and LINC01448. **(B)** qRT-PCR analysis of LINC01448 expression in PC cell lines and normal pancreatic cells using. **(C)** Luciferase activity in PaCa-2 cells transfected with WT or MUT LINC01448, along with (or without) miR-505 mimic, or in AsPC-1 cells transfected with WT or MUT LINC01448, along with (or without) miR-505 inhibitor. **(D)** miR-505 expression in PC cells after LINC01448 knockdown or overexpression of LINC01448. **(E)** RIP assays were conducted in PC cells transfected with control mimic and miR-505 mimic. LINC01448 expression was analyzed using qRT-PCR analysis. **(F)** qRT-PCR analysis of LINC01448 expression in PC tissues and normal tissues. **(G)** Kaplan-Meier curves for the overall survival of PC patients with high or low LINC01448 expression (KM Plotter database). $^*P < 0.05$.

2019), however the cellular role of miR-505 in the initiation and progression of PC remain to be elucidated. Here, our *in vitro* and *in vivo* experiments provided the first evidence that miR-505 can play a critical role in suppressing the glycolysis and progression of PC. The expression of miR-505 in PC tissues was significantly lower than that in corresponding normal tissues. Furthermore, the levels of miR-505 were positively associated with the favorable survival of patients with PC. These data suggested that miR-505 might be an effective prognostic biomarker and therapeutic target for PC patients.

A large number of oncogenes as target genes of miR-505 in tumor cells, including TGF-α (Chen S. et al., 2016), HMGB1 (Lu et al., 2016; Liu et al., 2018; Tian et al., 2018), FZD4 (Ma et al., 2017), IGF1R (Shi et al., 2018), WNT7B (Zhang et al., 2018), MAP3K3 (Tang et al., 2019), NRCAM (Ling et al., 2019), and RUNX2 (Zhao et al., 2019), have been recognized as direct target genes of miR-505. Among them, HMGB1 was found to promote cancer progression and metastasis in different cancers, such as hepatocellular carcinoma, lung cancer, breast cancer, colorectal cancer, prostate cancer, cervical cancer, and ovarian cancer (Tripathi et al., 2019). In this study, we proved that miR-505 regulated HK2 expression in PC cells at the post-transcriptional level. It would be possible that the restoration of miR-505 could effectively repress glycolysis and metastasis of PC by targeting other novel oncogenes. Further studies would be needed to explore this possibility.

Tumor cells are known for their increased glucose uptake rates even in the presence of abundant oxygen, defined as the Warburg effect (Avula et al., 2020). HK2 catalyzes the first committed step of glucose metabolism and is critically important for aerobic glycolysis in multiple cancer types (Stolfi et al., 2013). Moreover, knockdown of HK2 in ovarian cancer cells attenuated lactate production, cell invasion, and cancer cell stemness (Siu et al., 2019). Therefore, HK2 has been proposed as a therapeutic target for cancers (Chen X. S. et al., 2016; Garcia et al., 2019). In PC tissues, the expression of HK2 was significantly up-regulated and

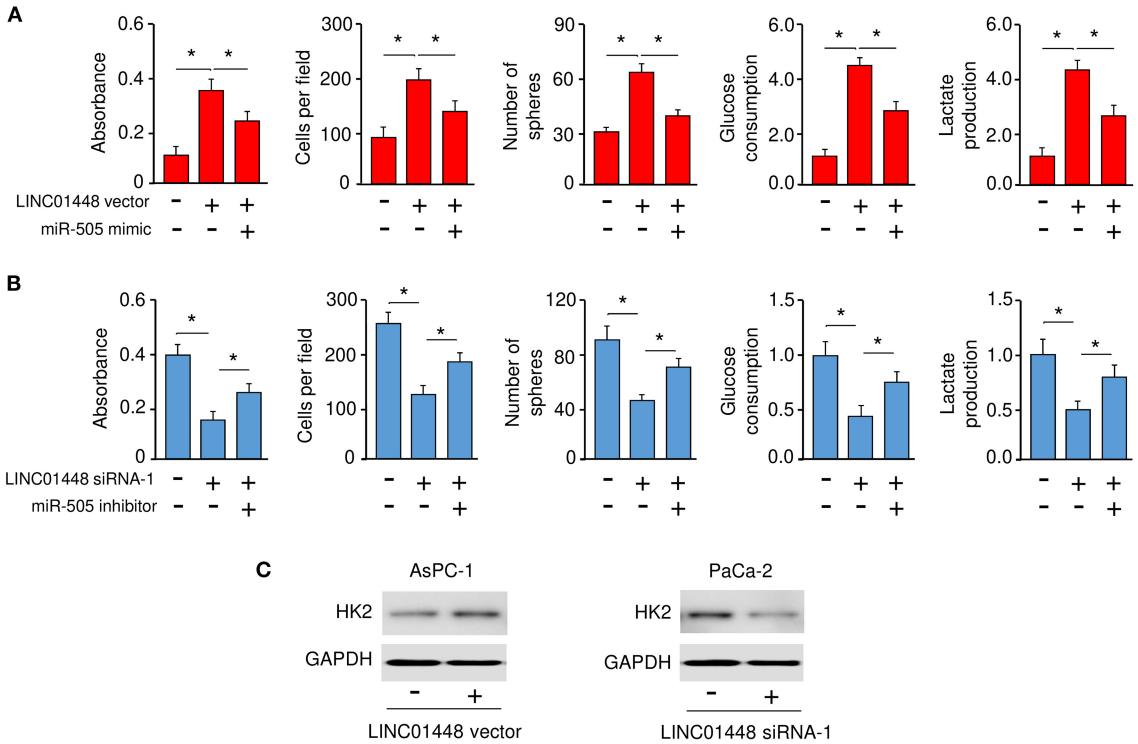

FIGURE 7 | LINC01448 promotes cell proliferation, invasion, sphere formation, and glycolysis by repressing miR-505 expression. **(A)** Cell functional assays were evaluated in AsPC-1 cells transfected with (or without) the LINC01448 expression vector, along with (or without) miR-505 mimic. **(B)** Cell functional assays in PaCa-2 cells transfected with (or without) LINC01448 siRNA-1, along with (or without) miR-505 inhibitor. **(C)** Western blotting analysis of HK2 expression in PaCa-2 cells transfected with (or without) LINC01448 siRNA-1, and in AsPC-1 cells transfected with (or without) LINC01448 expression vector. *$P < 0.05$.

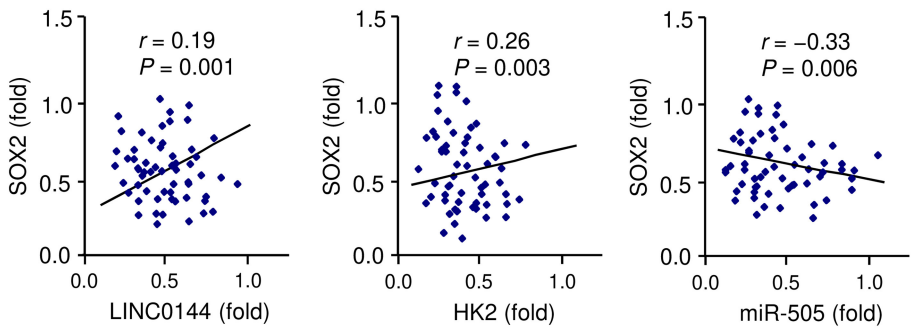

FIGURE 8 | Correlation between SOX2 and LINC01448/miR-505/HK2 expression in PC tissues, as determined by qRT-PCR assays.

increased HK2 expression was associated with shorter overall survival in patients with PC (Anderson et al., 2016). Furthermore, upregulation of HK2 can stimulate glycolysis and increase the proliferative and metastatic potential of PC cells (Anderson et al., 2016). Consistent with these previous findings, our current data verified that HK2 promoted glycolysis and facilitated the proliferation, invasion, and cancer stem cell-like properties of PC cells. In this study, we provided the first functional link between miR-505 and HK2, and have defined a new mechanism that drives overexpression of HK2 in PC. Previous papers reported that HK2 was a target of miR-143 (Peschiaroli et al., 2013), miR-199a-5p (Guo et al., 2015), miR-181b (Li et al., 2016), and miR-98 (Zhu et al., 2017). However, it remains largely unknown whether these miRNAs regulate HK2 expression in PC cells.

LncRNAs can act as sponges for miRNAs and thereby negatively regulate their expression (Dong et al., 2018c). For instance, lncRNA-CTS could function as a competing endogenous RNA for miR-505 in cervical cancer cells (Feng et al., 2019). LncRNA LEF-AS1 binds directly to miR-505 and suppressed its expression in colorectal cancer

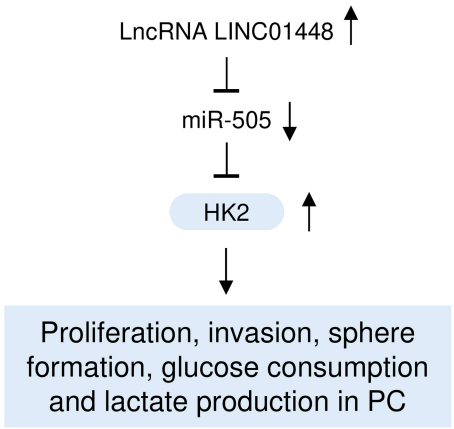

FIGURE 9 | A hypothetical model illustrating that the LINC01448/miR-505/HK2 axis modulates PC glycolysis and progression.

cells (Gong and Huang, 2019). Similarly, LINC00525 acted as a sponge for miR-505 in chordoma cells (Li et al., 2020). Up to now, the role and underlying mechanisms of LINC01448 in PC have not been previously reported. Our bioinformatic analysis, luciferase assay and RIP assay validated a direct interaction between miR-505 and LINC01448, identifying LINC01448 as a key upstream suppressor of miR-505 in PC cells. Our results account, at least in part, for the reduction of miR-505 expression observed in PC tissues. Importantly, we found that LINC01448 sponged miR-505 to facilitate the proliferation, invasion, sphere formation, and glycolysis of PC cells. Thus, our studies supported the notion that the therapeutic inhibition of LINC01448 may serve as a potential therapeutic strategy for PC treatment. Whether or how LINC01448 regulates the expression of other miRNAs in PC cells requires further investigation.

Many researchers have recognized that lncRNAs not only work as miRNA sponges, but also govern basic cellular processes by interacting with RNA-binding proteins (Huarte, 2015; Duguang et al., 2017). A recent study discovered that lncRNA LINC00261 exerted its function in PC cells, by binding to miR-222-3p to activate the HIPK2 pathway and by sequestering an RNA-binding protein IGF2BP1 to reduce c-Myc expression (Zhai et al., 2020). Whether LINC01448 could promote PC development by interacting with RNA-binding proteins should be investigated in our future research.

Multiple studies have shown that transcription factor, DNA methylation and EZH2-mediated H3K27 trimethylation represent important mechanisms that mediate the expression of miRNAs and lncRNAs (Lin et al., 2019; Zhai et al., 2020). For instance, downregulation of LINC00261 was caused by hypermethylation of the CpG islands in its promoter region and EZH2-mediated histone H3 lysine 27 trimethylation in PC cells (Zhai et al., 2020). In addition, p53, the most studied tumor suppressor, was shown to induce the expression of the lncRNA Pvt1b, leading to the suppression of lung tumorigenesis (Olivero et al., 2020). The transcription factor SOX2 induces the expression of lncRNA ANRIL by promoting its transcription in nasopharyngeal carcinoma cells (Wu et al., 2018). Interestingly, SOX2 might bind to the promoter region of LINC01448, and we have detected a positive correlation between the expression of SOX2 and LINC01448/HK2 expression, and an inverse correlation between the levels of SOX2 and miR-505 in PC tissues. Further studies will be needed to elucidate the possibility that SOX2 regulates the levels of LINC01448 in PC cells.

In summary, we found that miR-505 acted as a key tumor suppressor miRNA through targeting oncogene HK2 in PC cells. Our study further revealed that aberrant expression of LINC01448 could reduce the expression of miR-505 to promote proliferation, invasion, sphere formation, and glycolysis in PC cells. These findings provided new insights into the mechanisms that control glycolysis and aggressive phenotypes in PC, and highlighted LINC01448, miR-505 and HK2 as potential targets for therapeutic intervention in patients with PC.

DATA AVAILABILITY STATEMENT

The raw data supporting the conclusions of this article will be made available by the authors, without undue reservation.

ETHICS STATEMENT

The studies involving human participants were reviewed and approved by Shenzhen People's Hospital, the Second Affiliated Clinical Medical College of Jinan University, the First Affiliated Hospital of Southern University of Science and Technology, China. The patients/participants provided their written informed consent to participate in this study. The animal study was reviewed and approved by Shenzhen People's Hospital, the Second Affiliated Clinical Medical College of Jinan University, the First Affiliated Hospital of Southern University of Science and Technology, China.

AUTHOR CONTRIBUTIONS

LW and BL designed the experiments. ZX and DZ performed the experiments. ZZ, WL, RS, JY, and DL made significant revisions to the manuscript. All authors read and approved the final manuscript.

FUNDING

This study was supported by the Natural Science Foundation of Guangdong Province (No. 2018A0303130278).

REFERENCES

Anderson, M., Marayati, R., Moffitt, R., and Yeh, J. J. (2016). Hexokinase 2 promotes tumor growth and metastasis by regulating lactate production in pancreatic cancer. *Oncotarget* 8, 56081–56094. doi: 10.18632/oncotarget.9760

Avula, L. R., Hagerty, B., and Alewine, C. (2020). Molecular mediators of peritoneal metastasis in pancreatic cancer. *Cancer Metastasis Rev.* 39, 1223–1243. doi: 10.1007/s10555-020-09924-4

Balas, M. M., and Johnson, A. M. (2018). Exploring the mechanisms behind long noncoding RNAs and cancer. *Noncoding RNA Res.* 3, 108–117. doi: 10.1016/j.ncrna.2018.03.001

Chan, S. H., and Wang, L. H. (2015). Regulation of cancer metastasis by microRNAs. *J. Biomed. Sci.* 22:9. doi: 10.1186/s12929-015-0113-7

Chen, S., Sun, K. X., Liu, B. L., Zong, Z. H., and Zhao, Y. (2016). MicroRNA-505 functions as a tumor suppressor in endometrial cancer by targeting TGF-α. *Mol. Cancer*. 15:11. doi: 10.1186/s12943-016-0496-4

Chen, X. S., Li, L. Y., Guan, Y. D., Yang, J. M., and Cheng, Y. (2016). Anticancer strategies based on the metabolic profile of tumor cells: therapeutic targeting of the Warburg effect. *Acta Pharmacol. Sin.* 37, 1013–1019. doi: 10.1038/aps.2016.47

Dong, P., Xiong, Y., Yu, J., Chen, L., Tao, T., Yi, S., et al. (2018b). Control of PD-L1 expression by miR-140/142/340/383 and oncogenic activation of the OCT4-miR-18a pathway in cervical cancer. *Oncogene* 37, 5257–5268. doi: 10.1038/s41388-018-0347-4

Dong, P., Xiong, Y., Yue, J., Hanley, S. J. B., Kobayashi, N., Todo, Y., et al. (2018c). Long non-coding RNA NEAT1: a novel target for diagnosis and therapy in human tumors. *Front. Genet.* 9:471. doi: 10.3389/fgene.2018.00471

Dong, P., Xiong, Y., Yue, J., Hanley, S. J. B., and Watari, H. (2018a). miR-34a, miR-505 and miR-513 inhibit MMSET expression to repress endometrial cancer cell invasion and sphere formation. *Oncotarget* 9, 23253–23263. doi: 10.18632/oncotarget.25298

Duguang, L., Jin, H., Xiaowei, Q., Peng, X., Xiaodong, W., Zhennan, L., et al. (2017). The involvement of lncRNAs in the development and progression of pancreatic cancer. *Cancer Biol. Ther.* 18, 927–936. doi: 10.1080/15384047.2017.1385682

Feng, S., Liu, W., Bai, X., Pan, W., Jia, Z., Zhang, S., et al. (2019). LncRNA-CTS promotes metastasis and epithelial-to-mesenchymal transition through regulating miR-505/ZEB2 axis in cervical cancer. *Cancer Lett.* 465, 105–117. doi: 10.1016/j.canlet.2019.09.002

Garcia, S. N., Guedes, R. C., and Marques, M. M. (2019). Unlocking the potential of HK2 in cancer metabolism and therapeutics. *Curr. Med. Chem.* 26, 7285–7322. doi: 10.2174/0929867326666181213092652

Garrido-Laguna, I., and Hidalgo, M. (2015). Pancreatic cancer: from state-of-the-art treatments to promising novel therapies. *Nat. Rev. Clin. Oncol.* 12, 319–334. doi: 10.1038/nrclinonc.2015.53

Gong, X. Y., and Huang, A. L. (2019). LEF-AS1 participates in occurrence of colorectal cancer through adsorbing miR-505 and promoting KIF3B expression. *Eur. Rev. Med. Pharmacol. Sci.* 23, 9362–9370. doi: 10.26355/eurrev_201911_19429

Guo, W., Qiu, Z., Wang, Z., Wang, Q., Tan, N., Chen, T., et al. (2015). MiR-199a-5p is negatively associated with malignancies and regulates glycolysis and lactate production by targeting hexokinase 2 in liver cancer. *Hepatology* 62, 1132–1144. doi: 10.1002/hep.27929

Herreros-Villanueva, M., Zhang, J. S., Koenig, A., Abel, E. V., Smyrk, T. C., Bamlet, W. R., et al. (2013). SOX2 promotes dedifferentiation and imparts stem cell-like features to pancreatic cancer cells. *Oncogenesis* 2:e61. doi: 10.1038/oncsis.2013.23

Huarte, M. (2015). The emerging role of lncRNAs in cancer. *Nat. Med.* 21, 1253–1261. doi: 10.1038/nm.3981

Li, L., Lv, G., Wang, B., and Ma, H. (2020). Long noncoding RNA LINC00525 promotes the aggressive phenotype of chordoma through acting as a microRNA-505-3p sponge and consequently raising HMGB1 expression. *Onco. Targets Ther.* 13, 9015–9027. doi: 10.2147/OTT.S268678

Li, L. Q., Yang, Y., Chen, H., Zhang, L., Pan, D., and Xie, W. J. (2016). MicroRNA-181b inhibits glycolysis in gastric cancer cells via targeting hexokinase 2 gene. *Cancer Biomark.* 17, 75–81. doi: 10.3233/CBM-160619

Lin, T., Hou, P. F., Meng, S., Chen, F., Jiang, T., Li, M. L., et al. (2019). Emerging roles of p53 related lncRNAs in cancer progression: a systematic review. *Int. J. Biol. Sci.* 15, 1287–1298. doi: 10.7150/ijbs.33218

Ling, X. H., Fu, H., Chen, Z. Y., Lu, J. M., Zhuo, Y. J., Chen, J. H., et al. (2019). miR-505 suppresses prostate cancer progression by targeting NRCAM. *Oncol. Rep.* 42, 991–1004. doi: 10.3892/or.2019.7231

Liu, Y. J., Li, W., Chang, F., Liu, J. N., Lin, J. X., and Chen, D. X. (2018). MicroRNA-505 is downregulated in human osteosarcoma and regulates cell proliferation, migration and invasion. *Oncol. Rep.* 39, 491–500. doi: 10.3892/or.2017.6142

Lu, L., Qiu, C., Li, D., Bai, G., Liang, J., and Yang, Q. (2016). MicroRNA-505 suppresses proliferation and invasion in hepatoma cells by directly targeting high-mobility group box 1. *Life Sci.* 157, 12–18. doi: 10.1016/j.lfs.2016.05.039

Ma, C., Xu, B., Husaiyin, S., Wang, L., Wusainahong, K., Ma, J., et al. (2017). MicroRNA-505 predicts prognosis and acts as tumor inhibitor in cervical carcinoma with inverse association with FZD4. *Biomed. Pharmacother.* 92, 586–594. doi: 10.1016/j.biopha.2017.04.028

Matsuo, T., Konya, Y., Hirayama, E., and Sadzuka, Y. (2020). 2-Deoxy-D-glucose enhances the anti-cancer effects of idarubicin on idarubicin-resistant P388 leukemia cells. *Oncol. Lett.* 20, 962–966. doi: 10.3892/ol.2020.11616

Olivero, C. E., Martínez-Terroba, E., Zimmer, J., Liao, C., Tesfaye, E., Hooshdaran, N., et al. (2020). p53 Activates the long noncoding RNA Pvt1b to inhibit Myc and suppress tumorigenesis. *Mol. Cell.* 77, 761–774.e8. doi: 10.1016/j.molcel.2019.12.014

Peschiaroli, A., Giacobbe, A., Formosa, A., Markert, E. K., Bongiorno-Borbone, L., Levine, A. J., et al. (2013). miR-143 regulates hexokinase 2 expression in cancer cells. *Oncogene* 32, 797–802. doi: 10.1038/onc.2012.100

Ren, L., Yao, Y., Wang, Y., and Wang, S. (2019). miR-505 suppressed the growth of hepatocellular carcinoma cells via targeting IGF-1R. *Biosci. Rep.* 39:BSR20182442. doi: 10.1042/BSR20182442

Sergeant, G., Vankelecom, H., Gremeaux, L., and Topal, B. (2009). Role of cancer stem cells in pancreatic ductal adenocarcinoma. *Nat. Rev. Clin. Oncol.* 6, 580–586. doi: 10.1038/nrclinonc.2009.127

Shi, H., Yang, H., Xu, S., Zhao, Y., and Liu, J. (2018). miR-505 functions as a tumor suppressor in glioma by targeting insulin like growth factor 1 receptor expression. *Int. J. Clin. Exp. Pathol.* 11, 4405–4413.

Siu, M. K. Y., Jiang, Y. X., Wang, J. J., Leung, T. H. Y., Han, C. Y., Tsang, B. K., et al. (2019). Hexokinase 2 regulates ovarian cancer cell migration, invasion and stemness via FAK/ERK1/2/MMP9/NANOG/SOX9 signaling cascades. *Cancers* 11:813. doi: 10.3390/cancers11060813

Stolfi, C., Marafini, I., De Simone, V., Pallone, F., and Monteleone, G. (2013). The dual role of HK2 in the control of cancer growth and metastasis. *Int. J. Mol. Sci.* 14, 23774–23790. doi: 10.3390/ijms141223774

Tang, H., Lv, W., Sun, W., Bi, Q., and Hao, Y. (2019). miR-505 inhibits cell growth and EMT by targeting MAP3K3 through the AKT-NFκB pathway in NSCLC cells. *Int. J. Mol. Med.* 43, 1203–1216. doi: 10.3892/ijmm.2018.4041

Tang, Y., Tang, Y., and Cheng, Y. S. (2017). miR-34a inhibits pancreatic cancer progression through Snail1-mediated epithelial-mesenchymal transition and the Notch signaling pathway. *Sci. Rep.* 7:38232. doi: 10.1038/srep38232

Tian, L., Wang, Z. Y., Hao, J., and Zhang, X. Y. (2018). miR-505 acts as a tumor suppressor in gastric cancer progression through targeting HMGB1. *J. Cell Biochem.* doi: 10.1002/jcb.28082

Tripathi, A., Shrinet, K., and Kumar, A. (2019). HMGB1 protein as a novel target for cancer. *Toxicol. Rep.* 6:253–261. doi: 10.1016/j.toxrep.2019.03.002

Wei, G., Lu, T., Shen, J., and Wang, J. (2020). LncRNA ZEB1-AS1 promotes pancreatic cancer progression by regulating miR-505-3p/TRIB2 axis. *Biochem. Biophys. Res. Commun.* 528, 644–649. doi: 10.1016/j.bbrc.2020.05.105

Weidle, U. H., Birzele, F., Kollmorgen, G., and Rüger, R. (2017). Long non-coding RNAs and their role in metastasis. *Cancer Genomics Proteomics.* 14, 143–160. doi: 10.21873/cgp.20027

Wu, J. H., Tang, J. M., Li, J., and Li, X. W. (2018). Upregulation of SOX2-activated lncRNA ANRIL promotes nasopharyngeal carcinoma cell growth. *Sci. Rep.* 8:3333. doi: 10.1038/s41598-018-21708-z

Xu, D., Dong, P., Xiong, Y., Yue, J., Konno, Y., Ihira, K., et al. (2020). MicroRNA-361-mediated inhibition of HSP90 expression and EMT in cervical cancer is counteracted by oncogenic lncRNA NEAT1. *Cells* 9:632. doi: 10.3390/cells9030632

Zhai, S., Xu, Z., Xie, J., Zhang, J., Wang, X., Peng, C., et al. (2020). Epigenetic silencing of LncRNA LINC00261 promotes c-myc-mediated aerobic glycolysis by regulating miR-222-3p/HIPK2/ERK axis and sequestering IGF2BP1. *Oncogene*. doi: 10.1038/s41388-020-01525-3

Zhang, C., Yang, X., Fu, C., and Liu, X. (2018). Combination with TMZ and miR-505 inhibits the development of glioblastoma by regulating the WNT7B/Wnt/β-catenin signaling pathway. *Gene* 672, 172–179. doi: 10.1016/j.gene.2018.06.030

Zhao, P., Guan, H., Dai, Z., Ma, Y., Zhao, Y., and Liu, D. (2019). Long noncoding RNA DLX6-AS1 promotes breast cancer progression via miR-505-3p/RUNX2 axis. *Eur. J. Pharmacol.* 865:172778. doi: 10.1016/j.ejphar.2019.172778

Zhu, W., Huang, Y., Pan, Q., Xiang, P., Xie, N., and Yu, H. (2017). MicroRNA-98 suppress warburg effect by targeting HK2 in colon cancer cells. *Dig. Dis. Sci.* 62, 660–668. doi: 10.1007/s10620-016-4418-5

Conflict of Interest: The authors declare that the research was conducted in the absence of any commercial or financial relationships that could be construed as a potential conflict of interest.

frontiers in Genetics

ORIGINAL RESEARCH
published: 22 January 2021
doi: 10.3389/fgene.2020.583085

The Clinical Significance and Potential Molecular Mechanism of *PTTG1* in Esophageal Squamous Cell Carcinoma

Shang-Wei Chen[1†], Hua-Fu Zhou[1†], Han-Jie Zhang[2], Rong-Quan He[3], Zhi-Guang Huang[2], Yi-Wu Dang[2], Xia Yang[2], Jun Liu[1], Zong-Wang Fu[1], Jun-Xian Mo[4], Zhong-Qing Tang[5], Chang-Bo Li[4], Rong Li[3], Li-Hua Yang[3], Jie Ma[3], Lin-Jie Yang[2] and Gang Chen[2]**

[1] Department of Cardio-Thoracic Surgery, The First Affiliated Hospital of Guangxi Medical University, Nanning, China, [2] Department of Pathology, The First Affiliated Hospital of Guangxi Medical University, Nanning, China, [3] Department of Medical Oncology, First Affiliated Hospital of Guangxi Medical University, Nanning, China, [4] Department of Cardio-Thoracic Surgery, The Seventh Affiliated Hospital of Guangxi Medical University/Wuzhou Gongren Hospital, Wuzhou, China, [5] Department of Pathology, Wuzhou Gongren Hospital/The Seventh Affiliated Hospital of Guangxi Medical University, Wuzhou, China

Esophageal squamous cell carcinoma (ESCC) is the major histological type of esophageal cancers worldwide. Transcription factor *PTTG1* was seen highly expressed in a variety of tumors and was related to the degree of tumor differentiation, invasion, and metastasis. However, the clinical significance of *PTTG1* had yet to be verified, and the mechanism of abnormal *PTTG1* expression in ESCC was not clear. In this study, the comprehensive analysis and evaluation of *PTTG1* expression in ESCC were completed by synthesizing in-house immunohistochemistry (IHC), clinical sample tissue RNA-seq (in-house RNA-seq), public high-throughput data, and literature data. We also explored the possible signaling pathways and target genes of *PTTG1* in ESCC by combining the target genes of *PTTG1* (displayed by ChIP-seq), differentially expressed genes (DEGs) of ESCC, and *PTTG1*-related genes, revealing the potential molecular mechanism of *PTTG1* in ESCC. In the present study, *PTTG1* protein and mRNA expression levels in ESCC tissues were all significantly higher than in non-cancerous tissues. The pool standard mean difference (SMD) of the overall *PTTG1* expression was 1.17 (95% CI: 0.72–1.62, $P < 0.01$), and the area under curve (AUC) of the summary receiver operating characteristic (SROC) was 0.86 (95% CI: 0.83–0.89). By combining the target genes displayed by ChIP-seq of *PTTG1*, DEGs of ESCC, and *PTTG1*-related genes, it was observed that *PTTG1* may interact with these genes through chemokines and cytokine signaling pathways. By constructing a protein–protein interaction (PPI) network and combining ChIP-seq data, we obtained four *PTTG1* potential target genes, *SPTAN1*, *SLC25A17*, *IKBKB*, and *ERH*. The gene expression of *PTTG1* had a strong positive

OPEN ACCESS

Edited by:
Xiao Zhu,
Guangdong Medical University, China

Reviewed by:
Lin An,
Sanofi, United States
Renyuan Zhang,
University at Buffalo, United States

***Correspondence:**
Lin-Jie Yang
eyanglinjie@163.com
orcid.org/0000-0002-3353-0863
Gang Chen
chengang@gxmu.edu.cn
orcid.org/0000-0002-4864-1451

† These authors have contributed equally to this work

Specialty section:
This article was submitted to Epigenomics and Epigenetics, a section of the journal Frontiers in Genetics

Received: *14 July 2020*
Accepted: *30 November 2020*
Published: *22 January 2021*

Citation:
Chen S-W, Zhou H-F, Zhang H-J, He R-Q, Huang Z-G, Dang Y-W, Yang X, Liu J, Fu Z-W, Mo J-X, Tang Z-Q, Li C-B, Li R, Yang L-H, Ma J, Yang L-J and Chen G (2021) The Clinical Significance and Potential Molecular Mechanism of PTTG1 in Esophageal Squamous Cell Carcinoma. Front. Genet. 11:583085. doi: 10.3389/fgene.2020.583085

correlation with *SLC25A17* and *ERH*, which suggested that *PTTG1* might positively regulate the expression of these two genes. In summary, the high expression of *PTTG1* may play an important role in the formation of ESCC. These roles may be completed by *PTTG1* regulating the downstream target genes *SLC25A17* and *ERH*.

Keywords: *PTTG1*, esophageal squamous cell carcinoma, transcription factor, RNA sequencing, tissue microarray

INTRODUCTION

Esophageal cancer is the sixth leading cause of cancer-related deaths in the world and the eighth most common cancer globally; esophageal squamous cell carcinoma (ESCC) is the major histological type of esophageal cancers worldwide (Arnal et al., 2015). Despite the improved management and treatment of ESCC patients, the overall 5-year survival rate (10%) and 5-year survival rate following resection (15–40%) have remained low (Huang and Yu, 2018). The poor prognosis and rising morbidity of ESCC highlights the importance of improving detection methods, which is essential before treatment. As early clinical symptoms are not obvious, many ESCC patients are not diagnosed until the clinical symptoms appear in the late stage. In order to improve the prognosis of patients after surgery, patients were often treated with surgery combined with radiotherapy and chemotherapy, but this has not significantly increased the survival rate of ESCC patients. Since we have failed to fully understand the mechanism of the occurrence and development of ESCC, it is necessary and meaningful to explore its potential molecular mechanism to identify new prognostic biomarkers and potential ESCC therapeutic targets.

In recent years, studies have shown that transcription factors might play an important role in the occurrence and development of tumors, which has prompted us to study the clinical value and mechanism of transcription factor *PTTG1* in ESCC. *PTTG1* was the first proto-oncogene detected from rat pituitary tumor cells, encoding the securin protein—a protein that prevented separins from promoting the separation of sister chromatids (Pei and Melmed, 1997; Arenas et al., 2018). *PTTG1* was seen highly expressed in a variety of tumors and was related to the degree of tumor differentiation, invasion, and metastasis (Vlotides et al., 2007). It was shown that *PTTG1* played an essential role in the biological function of tumor cells. Its high expression in colorectal cancer promoted proliferation and metastasis (Ren and Jin, 2017). Its high expression in hepatocellular carcinoma, small cell lung carcinoma, and prostate cancer had value for clinical diagnosis and prognosis (Kong et al., 2019; Yang et al., 2019; Ersvær et al., 2020). Although studies found that *PTTG1* was likely to exhibit high expression in ESCC, the number of cases has been small and the research was based on a single center study, using a single detection method (Shibata et al., 2002; Ito et al., 2008; Feng et al., 2017). There have been only two reports on the mechanism of *PTTG1* in ESCC. It was found that *PTTG1* promoted the movement and migration of ESCC cells by activating related genes (Ito et al., 2008; Feng et al., 2017). The possible target genes of *PTTG1* as a transcription factor in ESCC had not been reported yet, and the practice of using integrated computational biology to mine ChIP-seq data to study the underlying molecular mechanism of *PTTG1* had not been reported.

Based on the existing research on *PTTG1* in ESCC, this study used clinical samples to make tissue chips, performed immunohistochemistry (IHC) to detect the expression level of *PTTG1* protein in ESCC tissues, and used our clinical sample tissues to conduct RNA sequencing (RNA-seq) to verify the expression of *PTTG1* mRNA. The comprehensive analysis and evaluation of *PTTG1* expression in ESCC were completed by synthesizing in-house IHC, clinical sample tissue RNA-seq (in-house RNA-seq), public high-throughput data, and literature data. We also explored the possible signaling pathways and target genes of *PTTG1* in ESCC by combining the target genes of *PTTG1* (displayed by ChIP-seq), differentially expressed genes (DEGs) of ESCC, and *PTTG1*-related genes (**Supplementary Figure 1**), revealing the potential molecular mechanism of *PTTG1* in ESCC and providing a new target for ESCC research.

MATERIALS AND METHODS

Expression Level of *PTTG1* Protein in Tissue Chip

A total of 302 cases were collected, including 159 ESCC tissues and 143 paracancerous tissues of 153 males and 18 females with a median age of 58 years. These chips (ESC242, ESC1503, and ESC1504) were produced by Fanpu Biotech, Inc. (Guilin, China). Two experienced pathologists read each case separately. *PTTG1* was a product of Biorbyt (Catalog No. orb3740037, Cambridge, United Kingdom). IHC was performed according to the instructions. The results were scored according to the IRS scoring system of 0–12 points (Lin et al., 2018). The scores of staining intensity were divided into 0, 1, 2, and 3, which represented negative, weak, medium, and strong, respectively. Positive staining proportion was classified as 0 for <10%, 1 for 11–25%, 2 for 26–50%, 3 for 51–75%, and 4 for 76–100%. The ultimate score was obtained based on the product of the positive proportion and the staining intensity. Then, the relationship between the *PTTG1* protein expression level and clinicopathological parameters was analyzed based on the IHC score.

RNA-Seq of Clinical Samples

We collected eight pairs of ESCC samples and corresponding adjacent normal esophageal tissues for RNA-seq from eight ESCC patients who underwent radical resection of EC from the First

Affiliated Hospital of Guangxi Medical University (Nanning, Guangxi, China), from April to August 2019. None of these ESCC patients received preoperative chemotherapy or radiotherapy. The tissue samples were stored at −80°C immediately after resection. These eight patients included six males and two females with a median age of 60 years. RNA-seq was executed by Wuhan Seqhealth Technology Co., LTD. (Wuhan, China). TRIzol reagent (Invitrogen, Carlsbad, CA, United States) was applied to extract and prepare total RNA from tumors and paired adjacent non-ESCC tissues. A total amount of 3 μg RNA per sample was used as initial material for the RNA sample preparations. Nanodrop™ 1000 spectrophotometer (Thermo Fisher Scientific, United States) was applied to examine RNA purity. RNA concentration was determined using a Qubit® 3.0 Fluorometer (Life Technologies, CA, United States). RNA integrity was determined using an RNA Nano 6000 Assay Kit and a Bioanalyzer 2100 system (Agilent Technologies, CA, United States). Afterward, the sequencing libraries were established using the NEBNext Ultra Directional RNA Library Prep Kit for Illumina (NEB, Ipswich, MA, United States) based on manufacturer's protocols. The 200 Illumina HiSeq X Ten platform was used to sequence the libraries. RNA-seq reads were aligned to the reference of homo_sapiens. GRCh38.[1] In the current study, we obtained the data on log2 (x + 0.001) conversion level 3 and reported RNA-seq data in transcripts per kilobase million (TPM). All enrolled patients signed an informed consent form, and the research including tissue chip and RNA-seq was approved by the ethics committee of the First Hospital Affiliated to Guangxi Medical University.

Collection of High-Throughput Data Sets

In order to compare the differences in gene expression between ESCC tissues and non-cancerous esophageal tissues, we used Gene Expression Omnibus (GEO), SRA, ArrayExpress, Oncomine, The Cancer Genome Atlas (TCGA), and various literature databases to extensively search ESCC-related data sets. The search formula is (Esophageal OR Esophagus) AND (maliganan* OR cancer OR tumor OR neoplas* OR carcinoma), AND "Homo sapiens" (porgn:_txid9606). All the information, including summary and overall design, of these data sets was then further evaluated.

Statistical Analysis

Student's *t*-test was performed using SPSS 22.0 to compare the differential expression of *PTTG1* between ESCC and non-cancerous tissues. The calculated results were presented in the form of the mean ± standard deviation (SD). GraphPad Prism 8.0 was applied to draw scatter plots and box plots. The area under curve (AUC) of receiver operating characteristic (ROC) was used to evaluate the ability of *PTTG1* levels to distinguish ESCC tissues from non-cancer tissues. In order to systematically analyze the expression level of *PTTG1*, we comprehensively analyzed in-house IHC, in-house RNA-seq, public RNA-seq, gene chip data, and published data. The standard mean difference (SMD) and 95% confidence interval (CI) were calculated by R 3.6.1, and the expression levels of *PTTG1* in ESCC and non-cancer tissues were compared. The funnel chart was employed to detect publication bias. Synthesizing all the data, the researchers used Stata12.0 to calculate the summary receiver operating characteristic (SROC) and further clarified the differential expression of *PTTG1* in ESCC and non-cancer tissues. Student's *t*-test was used to show the heterogeneity of the results. When $P < 0.05$ or $I^2 > 50\%$, there was heterogeneity, and a random effect model was used. When $P > 0.05$ or $I^2 < 50\%$, no obvious heterogeneity was detected, and a fixed-effect model was used. $P < 0.05$ was considered statistically significant.

Screening for *PTTG1* Target Genes, Esophageal Cancer Differentially Expressed Genes and *PTTG1*-Related Genes

Since *PTTG1* was a transcription factor, in order to obtain the key downstream target genes of *PTTG1*, we collected *PTTG1* target genes and potential binding sites proved by ChIP-seq through the Cistrome DB database[2] (Mei et al., 2017). Subsequently, we used the LIMMA package to process all gene chips containing *PTTG1* expression data and used LIMMA-VOOM to process DEGs of RNA-seq data [| log fold change (FC)| > 1, $P < 0.05$]. By calculating the correlation coefficient, the related genes were calculated in each high-throughput data set including *PTTG1* ($|r| > 0.5$, $P < 0.05$). Because each of the above steps contained multiple data sets, we researchers extracted genes that met the criteria in all data sets for intersection.

Functional Enrichment Analysis and Construction of Protein–Protein Interaction Networks to Screen Key Target Genes

In order to study the possible functions of these key target genes, the researchers carried out gene ontology (GO) functional enrichment analysis and Kyoto Encyclopedia of Genes and Genomes (KEGG) pathway enrichment analysis and visualization. We applied Cytoscape 3.7.1 to construct a protein–protein interaction (PPI) network of these genes and then used the MCODE algorithm to determine the hub gene of the protein densely connected neighborhood. The University of California, Santa Cruz (UCSC) Genome Browser on Human (GRCh38/hg38) Assembly was employed to display the binding position of the target gene and *PTTG1* in ChIP-seq.

RESULTS

Expression Level of *PTTG1* Protein in Tissue Microarray

The IHC scores of *PTTG1* in each ESCC and normal case based on two pathologists were presented in **Supplementary Table 1**. The intraclass correlation coefficients of IHC score in ESCC and

[1] ftp://ftp.ensembl.org/pub/relase-87/fasta/homo_sapiens/dna/

[2] http://cistrome.org/db/#/

normal tissues between two pathologists were 0.943 and 0.938, respectively. IHC staining of tissue chips showed that the *PTTG1* protein expression level in ESCC tissues was significantly higher than in non-cancerous tissues (10.410 ± 1.880 vs. 7.410 ± 2.153, $P < 0.0001$; AUC = 0.8405, $P < 0.0001$) (**Figure 1**). However, *PTTG1* expression did not show a significant correlation with various clinical parameters (**Supplementary Table 2**).

Expression Level of PTTG1 mRNA in In-House RNA-Seq

In order to confirm the high expression of *PTTG1* in ESCC tissues, we collected ESCC tissues and their matched non-cancer tissues from eight clinical patients with ESCC and obtained in-house RNA-seq data of these samples. It was found that the expression of *PTTG1* in ESCC tissues was significantly higher than in the adjacent tissues (5.6999 ± 0.6218 vs. 3.8690 ± 1.6307, $P = 0.0102$) (**Figures 2A,B**). ROC analysis showed that the expression of *PTTG1* was remarkably different between ESCC and non-cancerous tissues (AUC = 0.8906, $P = 0.0087$) (**Figure 2C**). These results further confirmed that *PTTG1* was overexpressed in ESCC.

Clinical Significance of *PTTG1* Expression Based on Public High-Throughput Data

To verify the results of our immunohistochemistry and RNA-seq experiments, a total of 15 GeneChips of ESCC tissues were gathered from public databases, namely, GSE45670GPL570, GSE77861GPL570, GSE26886GPL570, GSE69925GPL570, GSE100942GPL570, GSE33810GPL570, GSE17351GPL570, GSE20347GPL571, GSE38129GPL571, GSE29001GPL571, GSE33426GPL571, GSE23400GPL96, GSE32424, GSE45168,

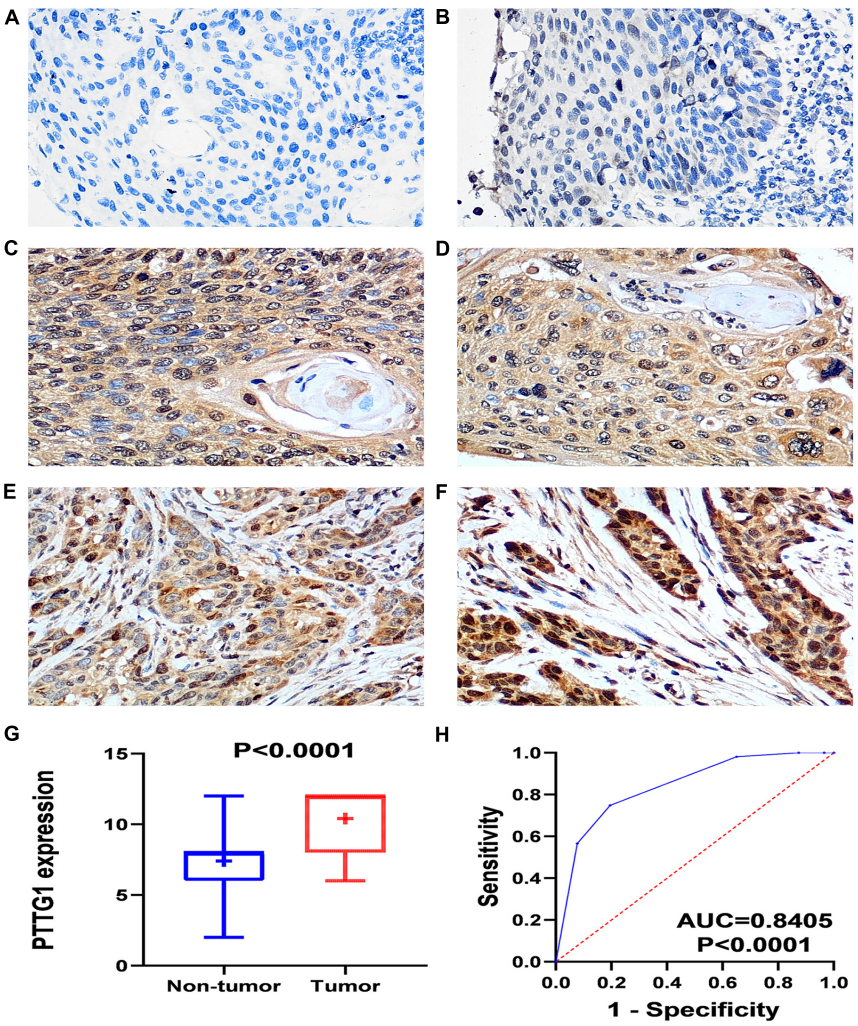

FIGURE 1 | *PTTG1* protein expression elevated in esophageal squamous cell carcinoma (ESCC) tissue chip assessed by in-house immunohistochemistry. **(A,B)** Immunohistochemical staining of *PTTG1* protein in non-cancerous esophageal tissues from different cases. Both cases were scored as 0 (×400); **(C–F)** ESCC tissues (×400). The scores of case **(C)** and case **(D)** were both 6. The score was recorded as 8 for case **(E)** and 12 for case **(F)**; **(G)** box diagram; **(H)** receiver operating characteristic (ROC) curve; AUC, area under the curve.

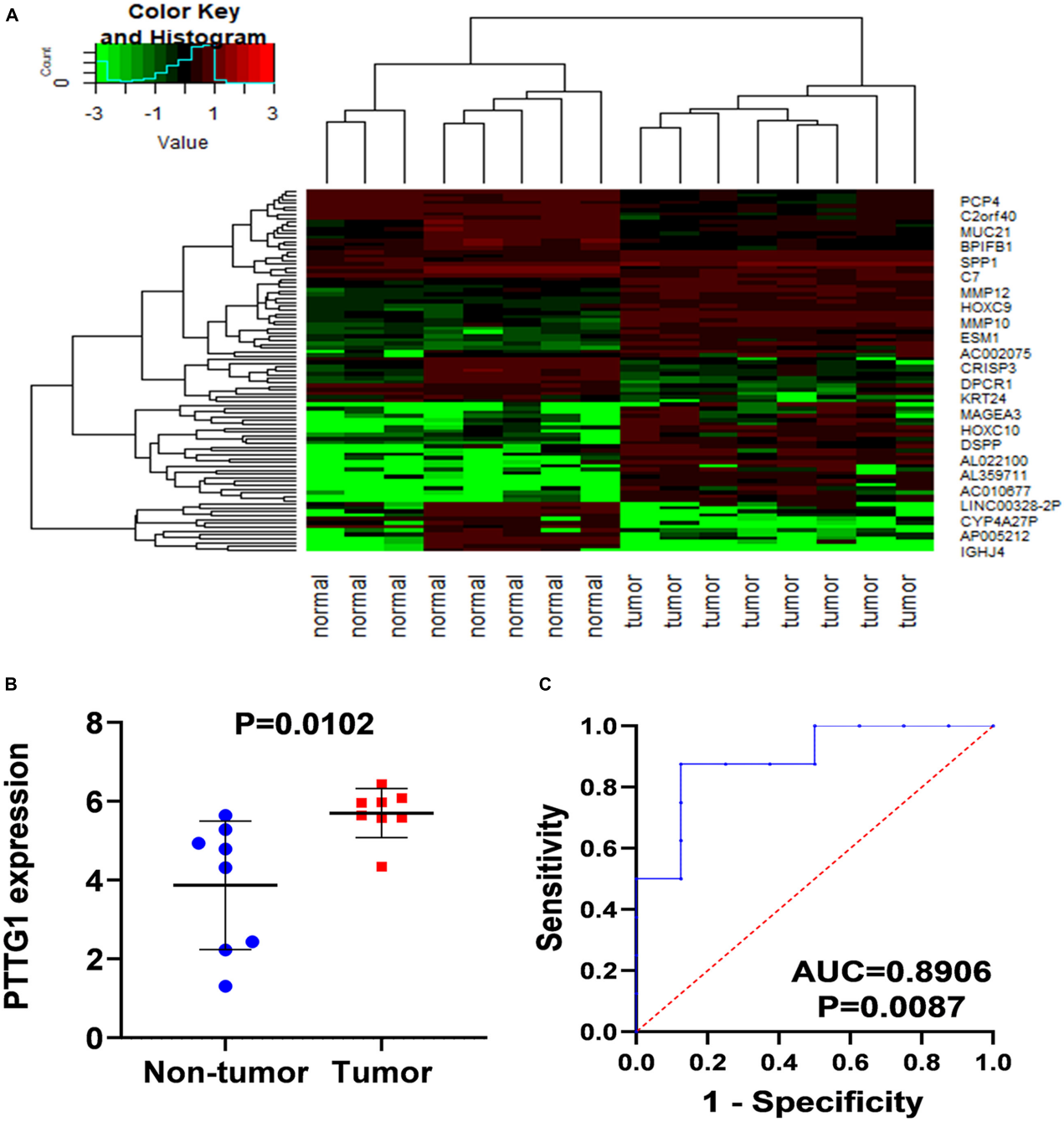

FIGURE 2 | In-house RNA-seq confirmed *PTTG1* overexpression in ESCC tissues. **(A)** Heatmap of differentially expressed genes (DEGs). **(B)** Scatter plot. **(C)** ROC curve.

and GSE70409. In order to avoid batch effects, the GPL570 and GPL571 from the same platform were combined. In order to improve the reliability of differential mRNA screening results, we downloaded the RNA-seq data and clinical follow-up information of ESCC. All data collection processes are shown in **Figure 3**. We used seven data sets, including six GeneChips (GPL570, GPL571, GSE23400, GSE32424, GSE45168, and GSE70409), and RNA-seq data (2,307 cases in total, with 620 cases of ESCC and 1,687 non-cancer cases) to investigate the expression of *PTTG1* in ESCC. After research, it was found that the expression of *PTTG1* in four high-throughput platforms (GPL570, GSE23400, GSE70409, and TCGA-GTEx) was significantly higher than in the non-cancer control group (**Figures 4A–F,M**). ROC analysis of all data sets showed that the expression of *PTTG1* had different degrees of significance for the clinical diagnosis of ESCC (**Figures 4G–L,N**). Further

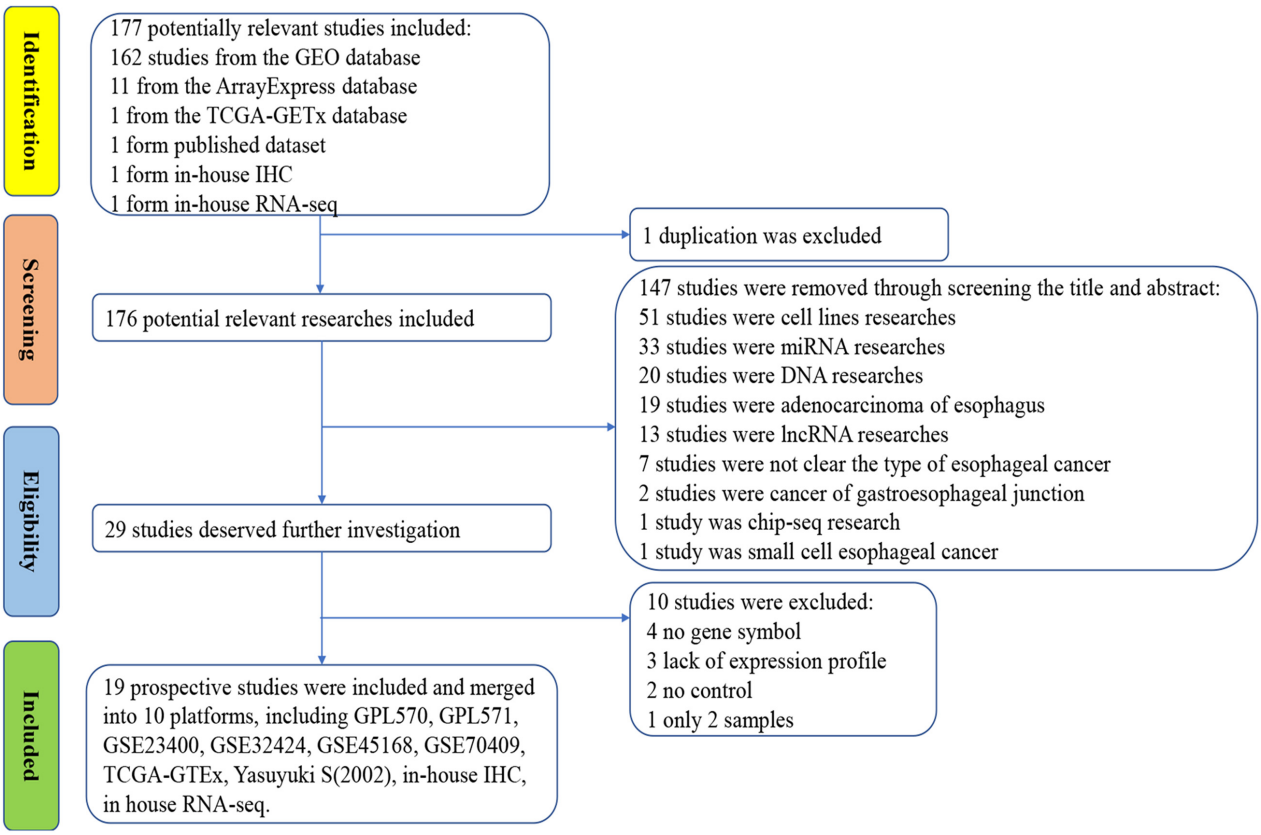

FIGURE 3 | Flow chart of data collection for this study.

analysis of public RNA-seq data showed that the average expression of *PTTG1* in ESCC was 11.5794 ± 0.7270, which was significantly higher than that of the non-cancer control group (7.5575 ± 2.5127, $P < 0.001$). We also analyzed the relationship between the expression of *PTTG1* and the clinical pathological parameters of ESCC patients. The expression of *PTTG1* was negatively correlated with the age of ESCC patients ($r = -0.3097$, $P = 0.004$), and the expression of *PTTG1* in young patients was higher (11.8 ± 0.7 vs. 11.3 ± 0.6, $P = 0.004$) (**Supplementary Table 3**). However, no significant difference in *PTTG1* expression was found in other clinicopathological parameters. The survival condition of patients with high *PTTG1* expression was worse than that of patients with low *PTTG1* expression (HR = 1.29), but no significant statistical difference was found (**Figure 4O**).

Comprehensive Analysis of *PTTG1* Expression

Because the research scale of a single data set was too small, it was difficult to draw effective conclusions. To make the results more reliable, we combined public RNA-seq, GeneChip, in-house IHC, in-house RNA-seq data, and published data (Shibata et al., 2002) for analysis. Our research included 835 cancer tissues and 1,886 non-cancer tissues. Considering the heterogeneity of our data, we chose a random effects model. The SMD of the overall *PTTG1* expression was 1.17 (95% CI: 0.72–1.62, $P < 0.01$, **Table 1**), which indicated that *PTTG1* was noticeably expressed in ESCC. The area under the SROC curve was 0.86 (95% CI: 0.83–0.89), with sensitivity being 0.75 (95% CI: 0.62–0.85), and specificity being 0.83 (95% CI: 0.77–0.87) (**Figure 5A** and **Supplementary Figure 2A**). The positive likelihood ratio was 4.31 (95% CI: 3.21–5.80), and the negative likelihood ratio was 0.30 (95% CI: 0.19–0.48) (**Supplementary Figure 2B**). The diagnostic odds ratio was 14.22 (95% CI: 7.60–26.62) (**Supplementary Figure 2C**). To visualize the publication bias, we performed Begg's funnel plot and Egger's test. The Begg's test showed no obvious publication bias ($P = 0.175$, **Figure 5B**). Egger's test also showed that the high expression of *PTTG1* in ESCC did not have a publication bias ($P = 0.844$). After a comprehensive analysis, *PTTG1* was confirmed to display high expression in ESCC.

Enrichment Analysis of Differentially Expressed Genes, *PTTG1*-Related Genes and Predicted Target Genes and Construction of Protein–Protein Interaction Network

Our researchers obtained a total of 23,872 DEGs, including 14,594 upregulated genes, 9,278 downregulated genes, and

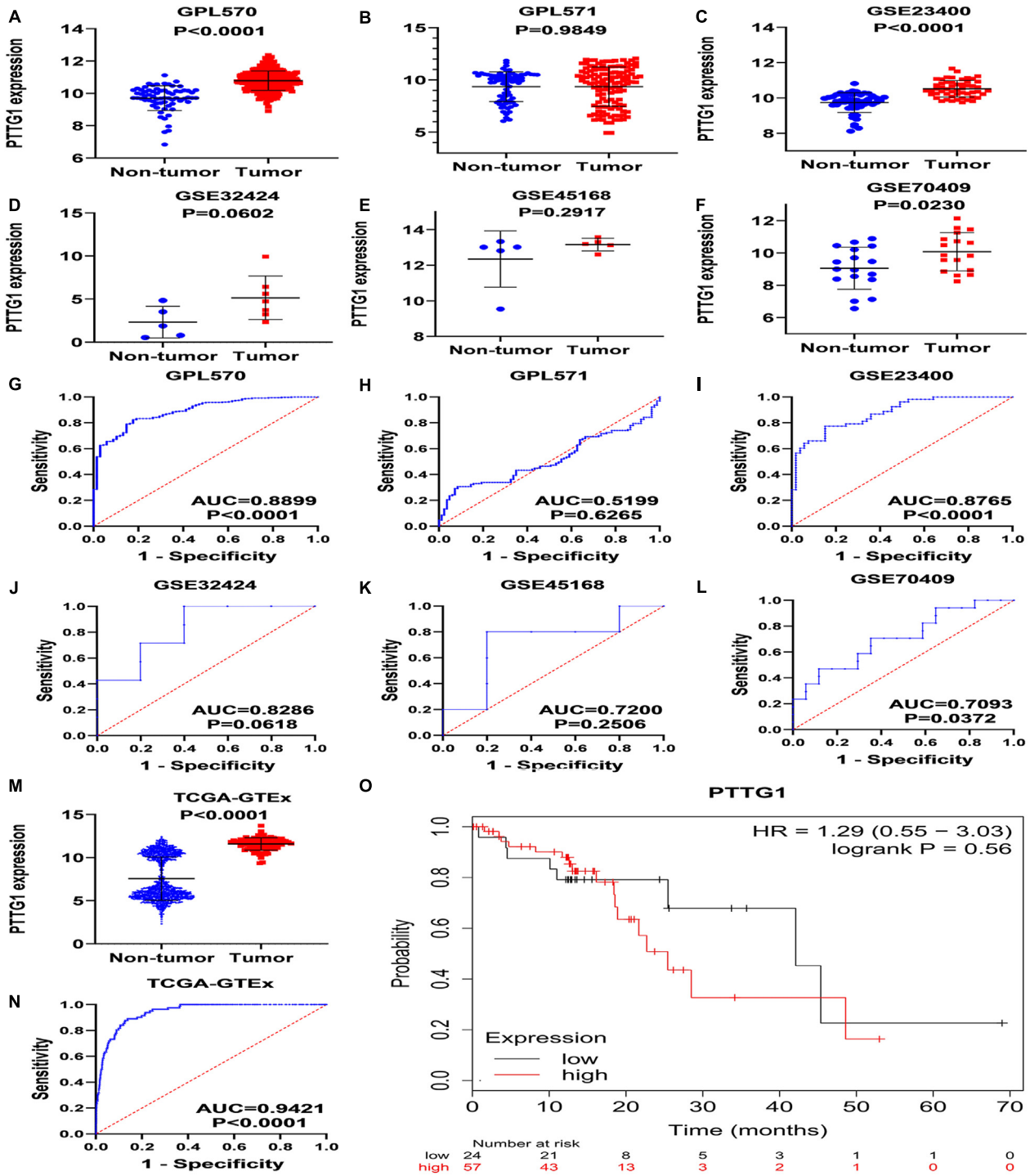

FIGURE 4 | Expression of *PTTG1* mRNA upregulates in ESCC based on high-throughput RNA-seq of public database. GPL570 **(A,G)**, GPL571 **(B,H)**, GSE23400 **(C,I)**, GSE32424 **(D,J)**, GSE45168 **(E,K)**, and GSE70409 **(F,L)**. The cancer genome atlas (TCGA) dot plot and ROC curve **(M–O)** KM survival analysis curve based on TCGA data from KMplot database; the median expression value of *PTTG1* was applied as cut-off value to classify patients into low and high expression groups.

11,450 related genes from six GeneChip platforms, TCGA-GTEx RNA-seq and in-house RNA-seq. The Cistrome DB database was used to predict *PTTG1* target genes, and 19,719 genes were acquired. We selected all the *PTTG1*-related genes to combine with 706 target genes with a score greater than 0.5 in the results of the Bistro DB ChIP-seq. We examined intersections with the upregulated and downregulated genes, respectively, and eventually gained 192 genes that crossed

TABLE 1 | Comprehensive analysis of *PTTG1* expression in esophageal squamous cell carcinoma (ESCC) based on gene microarrays, in-house immunohistochemistry (IHC), public RNA-seq, and in-house RNA-seq.

Study ID	ESCC			Normal			SMD	95% CI
	n	Mean	SD	*n*	Mean	SD		
GPL570	329	10.78	0.598	68	9.70	0.765	1.71	1.42; 2.00
GPL571	127	9.36	1.890	83	9.35	1.423	0.00	−0.27; 0.28
GSE23400	53	10.52	0.467	53	9.74	0.559	1.51	1.07; 1.94
GSE32424	7	2.52	0.566	5	1.54	0.829	1.32	0.00; 2.64
GSE45168	5	13.16	0.355	5	12.34	1.578	0.64	−0.65; 1.94
GSE70409	17	10.08	1.178	17	9.06	1.307	0.80	0.10; 1.50
TCGA-GTEx	82	11.58	0.727	1,456	7.56	2.512	1.64	1.41; 1.87
Yasuyuki S (2002)	48	0.10	0.068	48	0.05	0.041	1.01	0.58; 1.43
In-house IHC	159	10.41	1.880	143	7.41	2.153	1.49	1.23; 1.74
In-house RNA-seq	8	5.70	0.062	8	3.87	1.630	1.40	0.27; 2.53
Overall (I^2 = 0.92, P < 0.01)	835			1,886			1.17	0.72, 1.62

ESCC, esophageal squamous cell carcinoma; IHC, immunohistochemistry; n, number; SD, standard deviation; SMD, standard mean difference; CI, confidence interval.

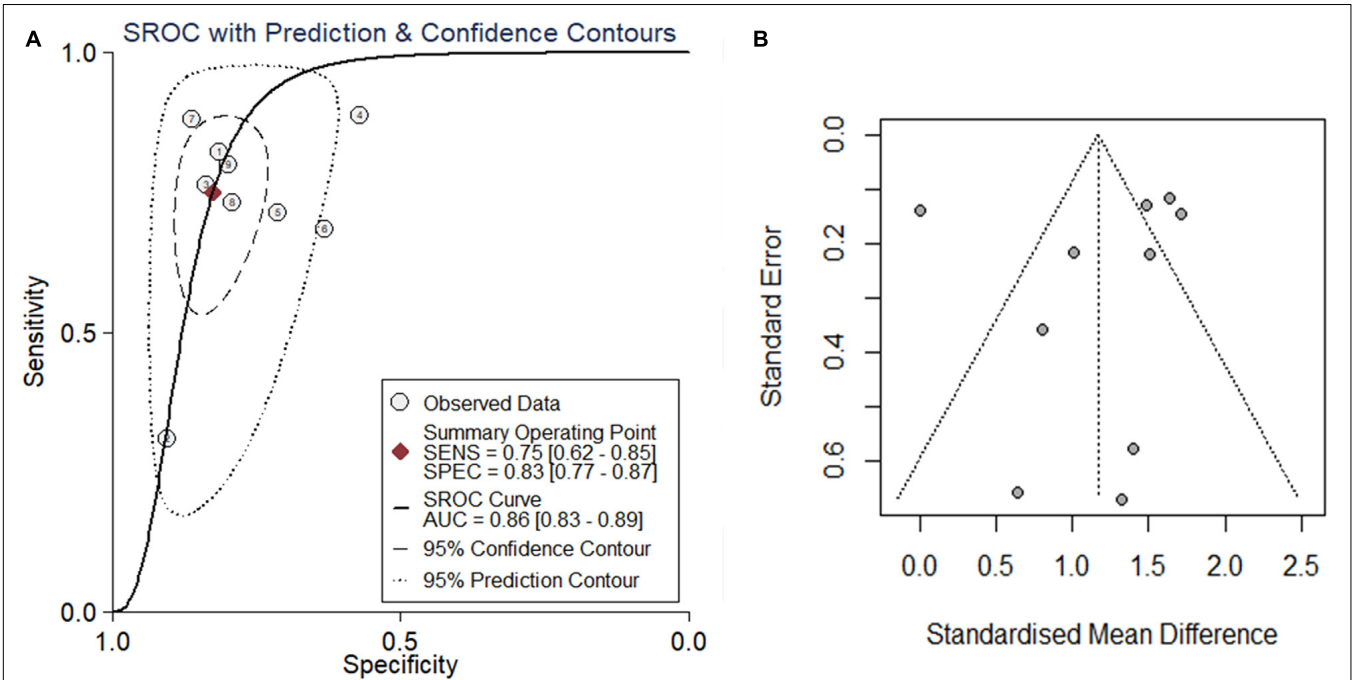

FIGURE 5 | Comprehensive analysis further confirmed that PTTG1 was significantly overexpressed in ESCC. **(A)** Summary receiver operating characteristic (SROC) curve. **(B)** Funnel chart of publication bias. AUC, area under curve.

with the upregulation and 139 genes that overlapped with downregulation (**Figures 6A,B**). Then, we conducted GO function enrichment, including biological process (BP), cellular component (CC), molecular function (MF), and KEGG pathway analysis. **Figures 7**, **8** illustrate the enrichment analysis of upregulated and downregulated overlapping genes, respectively. As shown in the figures, the results of gene enrichment of the two parts were similar. In the BP process, these genes were mainly enriched in cellular processes, metabolic processes, and biological regulation; in CC, they were largely enriched in organelles; in MF, they were mostly concentrated in functions such as catalytic activity, binding, and transportation activities; in KEGG pathway analysis, they were mainly enriched in inflammation mediated by chemokine and cytokine signaling pathway. The upregulated genes were also enriched in the ubiquitin proteasome pathway, while the downregulated genes were enriched in the apoptosis signaling pathway. This indicated that *PTTG1* may play a biological role in ESCC through these pathways. We also constructed a PPI network for these overlapping genes (**Figure 9**) and acquired the hub gene using MCODE. The

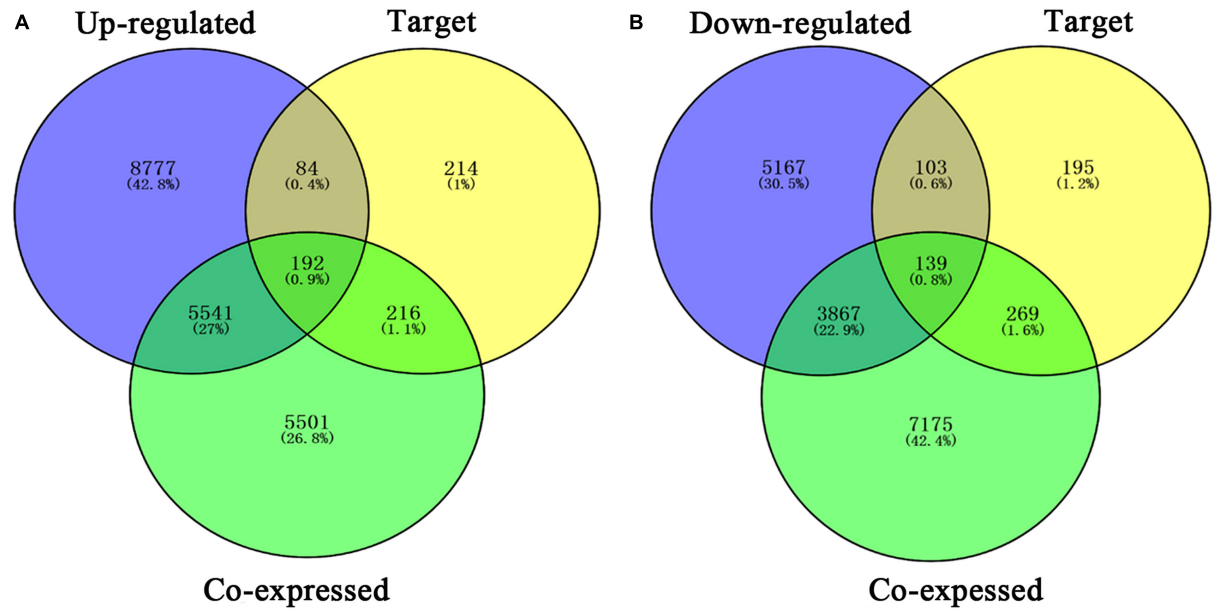

FIGURE 6 | Venn diagrams of overlapping *PTTG1*-related genes, target genes, and upregulated genes **(A)** and downregulated genes **(B)**. Upregulated, upregulated differential genes; downregulated, downregulated differential genes; target, target genes of *PTTG1* in ChIP-seq.

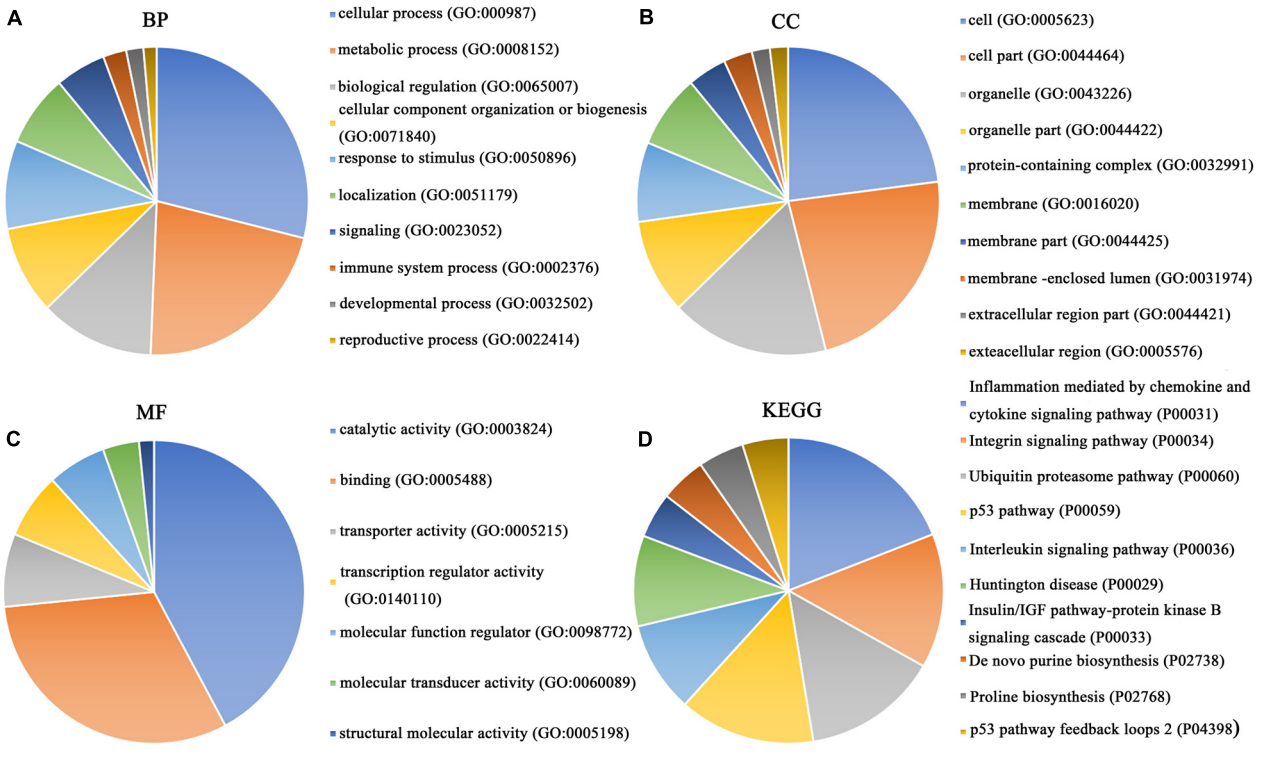

FIGURE 7 | Gene ontology (GO) function annotation and Kyoto Encyclopedia of Genes and Genomes (KEGG) pathway analysis of upregulated overlapping genes. **(A)** Biological process. **(B)** Cell composition. **(C)** Molecular function. **(D)** KEGG pathway analysis.

hub genes we obtained were *ARFGAP1*, *UBA6*, *STK4*, *ERCC4*, *SPTAN1*, *DDX24*, *RFC5*, *CHEK2*, *MAP1LC3B*, *ITCH*, *UBE2L3*, *MRPL20*, *MRPL22*, *RPL8*, *RPS14*, *PEX11A*, *ACSL1*, *SLC25A17*, *IKBKB*, *CFLAR*, *BCL10*, *CLNS1A*, *LSM3*, and *ERH*. These hub genes were entered into the Cistrome DB website. In the ChIP-seq track, each block represented a peak where the target gene

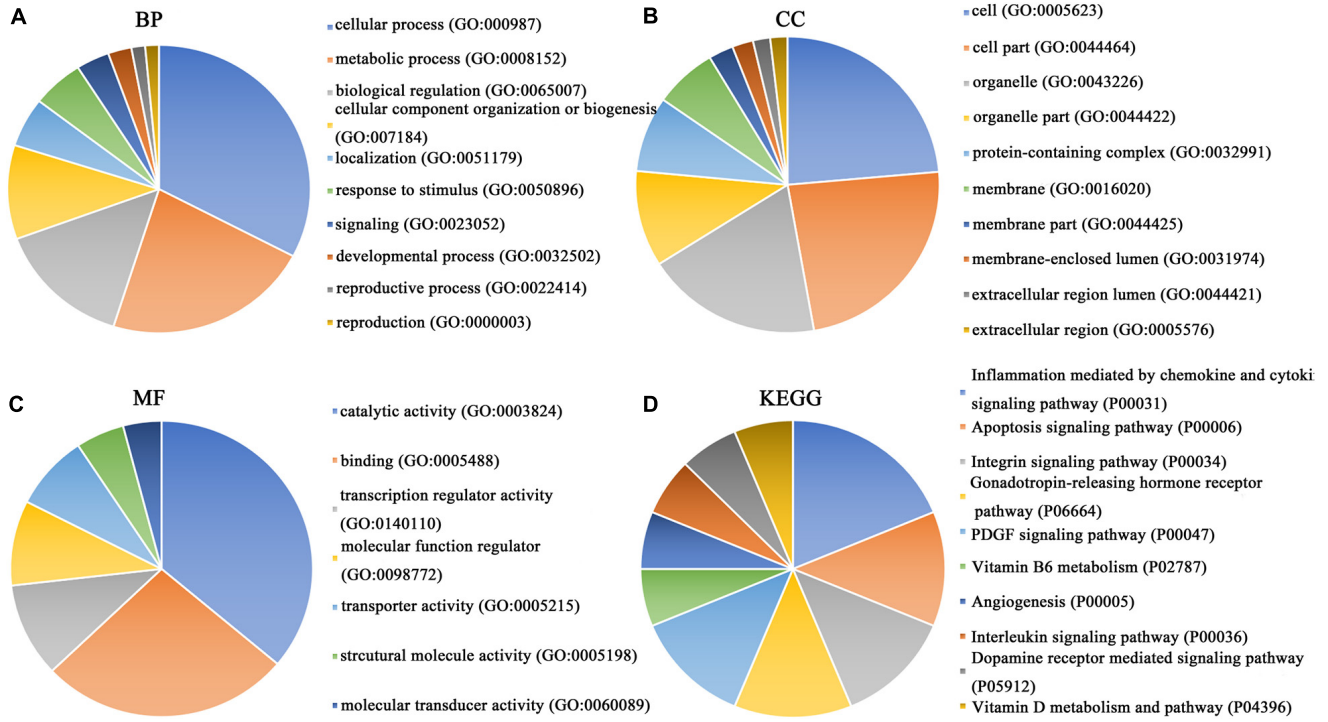

FIGURE 8 | GO function annotation and KEGG pathway analysis of downregulated overlapping genes. **(A)** Biological process. **(B)** Cell composition. **(C)** Molecular function. **(D)** KEGG pathway analysis.

would bind to the corresponding transcription factor. **Figure 10** shows that the *SPTAN1* and *PTTG1* binding peak could be seen at the site 278,308 bp away from the *PTTG1* transcription start site, *SLC25A17* was detected at 166,478 bp, *IKBKB* was discovered at 173,073 bp, and the overlapped peak of *ERH* and *PTTG1* was found at 96,965 bp. The transcription initiation sites of these genes were all integrated with *PTTG1* (**Figure 10**). To further explore the relationship between these target genes and *PTTG1*, we calculated the SMD of these genes and found that *SLC25A17* (SMD = 1.13, 95% CI: 0.04–2.22, $P < 0.01$; **Table 2**) and *ERH* (SMD = 1.20, 95% CI: 0.26–2.15, $P < 0.01$; **Table 3**) were significantly highly expressed. We also analyzed the correlation between *PTTG1* and these two target genes. The results showed that *PTTG1* and *SLC25A17* ($r = 0.5399$, $P < 0.0001$) (**Figure 11A**) and *ERH* ($r = 0.5498$, $P < 0.0001$) (**Figure 11B**) had a strong positive correlation, which suggested that *PTTG1* might positively regulate the expression of these two genes. These results indicated that *PTTG1* played an important part in regulating the functions of these proteins.

DISCUSSION

Although some studies reported on the expression level of *PTTG1* in ESCC, its clinical significance had yet to be verified, and the mechanism of abnormal *PTTG1* expression in ESCC was not clear. To address these issues, this study used a variety of detection methods to investigate the expression level of *PTTG1* in ESCC, including in-house IHC, in-house RNA-seq, gene chips, public RNA-seq, and a published study. We conducted a comprehensive integrated analysis of the expression data of 2,721 samples from independent studies to calculate SMD and SROC. This study on *PTTG1* expression in ESCC had the largest sample size of any related study by far. The analysis results showed that the expression of *PTTG1* in ESCC was upregulated. As a transcription factor, *PTTG1* could target and regulate specific genes to perform biological functions. Combining the analysis results of DEGs, *PTTG1*-related genes of ESCC, and ChIP-seq of *PTTG1*, we found for the first time that *SLC25A17* and *ERH* were likely to be the target genes of *PTTG1* in ESCC. These findings could help to study the key role of *PTTG1* in the regulation mechanism in ESCC.

So far, there have been only three reports on the clinical significance of *PTTG1* expression in ESCC. The sample size of these was relatively small, and they were based on a single center study. The use of a single detection method failed to fully represent the role of *PTTG1* in ESCC. At the time of these reports, the widely used high-throughput technology had not been adopted. Differences existed among the results of several studies. One study using RT-PCR of 48 cases of ESCC and its matched samples revealed that *PTTG1* expression was upregulated in ESCC, and the average expression level in tumor tissue was 2.19 times than that of normal tissue (0.105 vs. 0.048) (Shibata et al., 2002). In another study, the immunohistochemistry of 50 ESCC samples and normal esophageal tissues suggested that

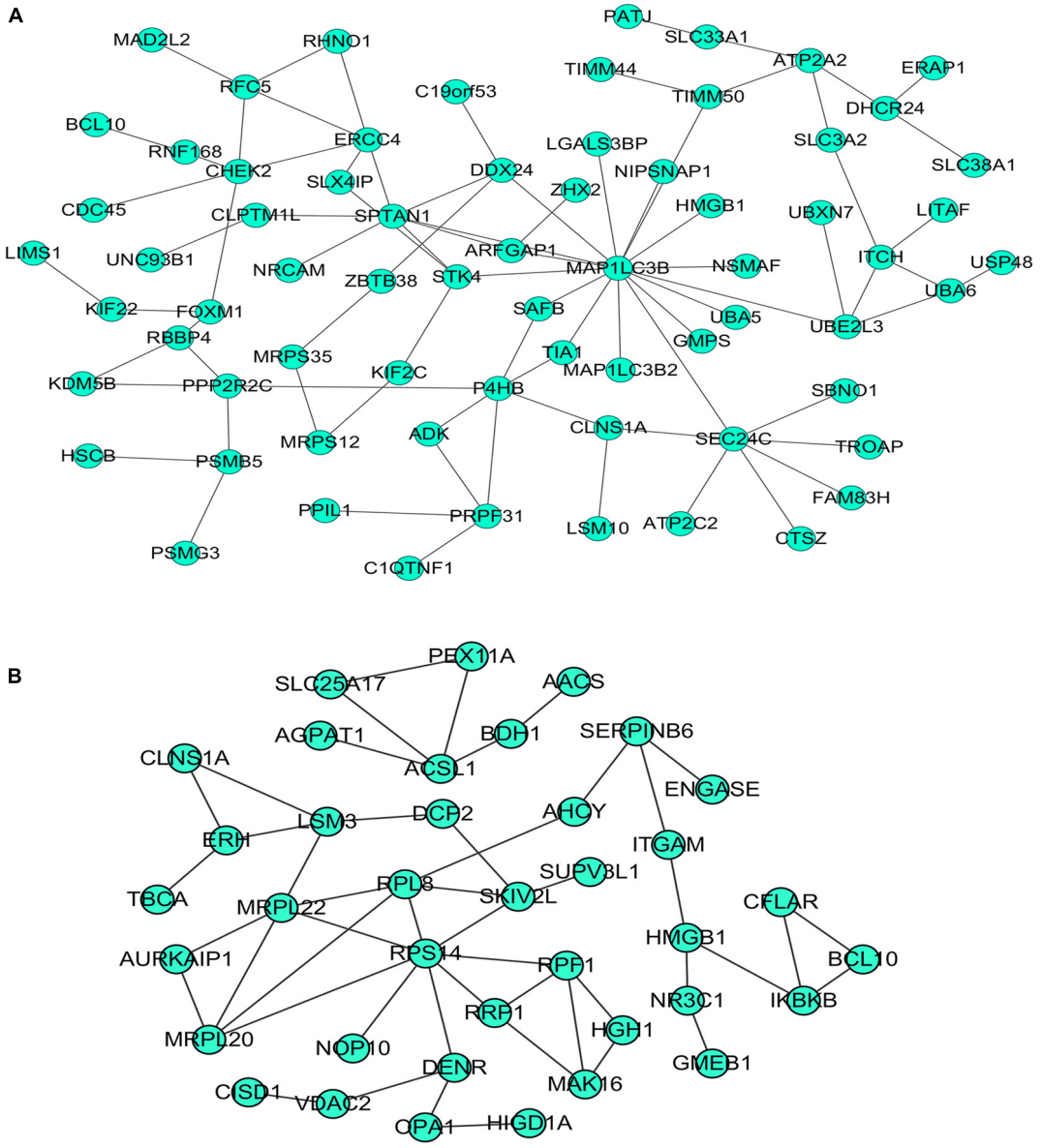

FIGURE 9 | Protein–protein interaction (PPI) network of overlapping genes. **(A)** PPI network of upregulated overlapping genes. **(B)** PPI network of downregulated overlapping genes.

PTTG1 was highly expressed in ESCC. Of 50 ESCC tissues, 31 (62%) were positive, while only 17 of 50 normal tissues (34%) were positive (Feng et al., 2017). Another study, using 113 cases of ESCC immunohistochemistry and immunoblotting, revealed the overexpression of *PTTG1*. It was found that 14 tumors in 113 cases were negatively expressed; 31 cases expressed 0–10% of tumor cells (1+), 52 cases showed 10–30% tumor cell expression (2+), and 16 cases showed 30% tumor cell expression (3+). *PTTG1* expression of 2+ or 3+ was determined as *PTTG1* positive (68/113, 60.2%), while *PTTG1* staining of normal esophageal epithelium showed no intracytoplasmic staining and occasionally intranuclear staining (about 10%) (Ito et al., 2008). In order to expand the sample size and integrate various detection methods and multi-center data, in this study, we employed various detection methods (immunohistochemistry of tissue chips, RNA-seq, microarrays, and RT-PCR) to study the clinical significance of *PTTG1* expression in ESCC tissues. The single detection method and the comprehensive results indicated that the *PTTG1* protein and mRNA were highly expressed in ESCC, which was consistent with the reported results (Shibata et al., 2002; Ito et al., 2008; Feng et al., 2017). In the study, SMD = 1.17 (95% CI: 0.72–1.62, $P < 0.01$), and this result was strongly supported by the SROC combined with AUC 0.86 (95% CI: 0.83–0.89). This study used a large sample to verify the upregulation of *PTTG1* in ESCC, suggesting that high expression of *PTTG1* might promote the occurrence of ESCC.

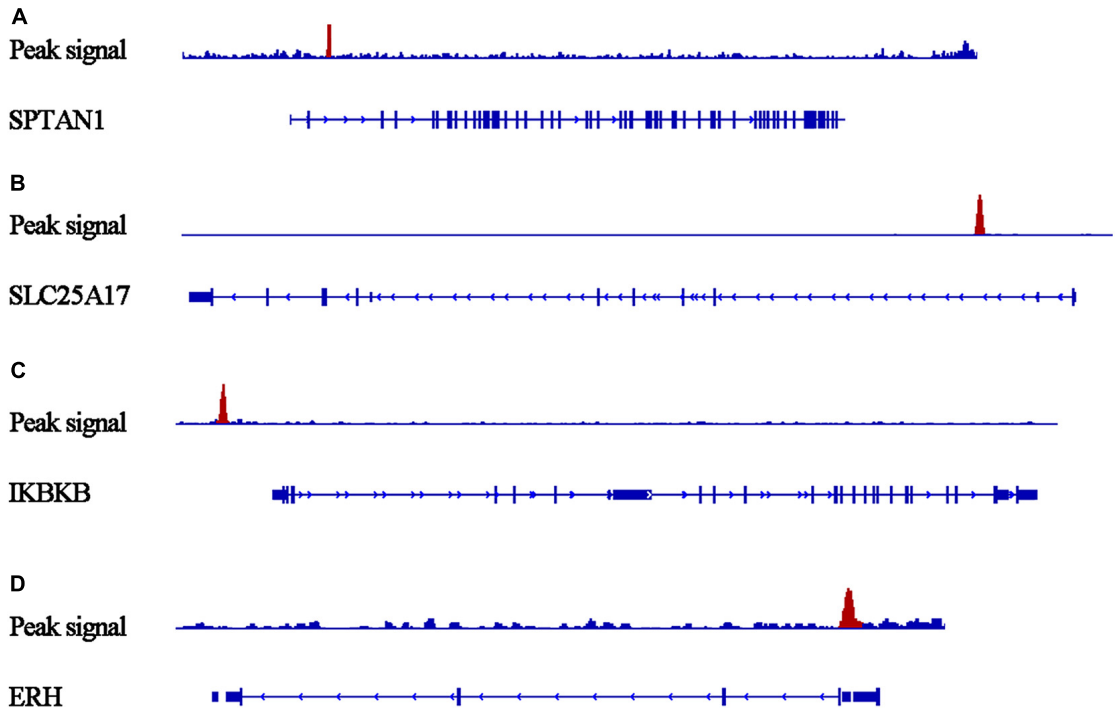

FIGURE 10 | Peaks of target genes binding to *PTTG1* in ChIP-seq based on the Cistrome DB database. The peak signals of each target genes are colored red. **(A)** *SPTAN1*; **(B)** *SLC25A17*; **(C)** *IKBKB*; **(D)** *ERH*.

TABLE 2 | Comprehensive analysis of *SLC25A17* expression in ESCC based on gene microarrays, public RNA-seq, and in-house RNA-seq.

Study ID	ESCC			Normal			SMD	95% CI
	n	Mean	SD	*n*	Mean	SD		
GPL570	329	630.1	247.1	68	649.4	104.5	−0.08	−0.34; 0.18
GPL571	127	176.6	188.6	83	253.9	169.1	−0.43	−0.70; 0.28
GSE23400	53	6.54	0.207	53	6.28	0.114	1.52	1.07; 1.94
GSE32424	7	3.14	0.172	5	1.56	0.532	4.02	1.75; 6.29
GSE45168	5	10.31	0.354	5	9.82	0.413	1.14	−0.25; 2.54
GSE70409	17	9.45	0.678	17	9.40	0.794	0.08	−0.60; 0.75
TCGA-GTEx	82	10.88	0.505	1,456	9.54	0.515	2.60	2.36; 2.84
In-house RNA-seq	8	4.19	0.498	8	3.64	0.348	1.21	0.12; 2.30
Overall (I^2 = 0.98, P < 0.01)	628			1,695			1.13	0.04; 2.22

ESCC, esophageal squamous cell carcinoma; n, number; SD, standard deviation; SMD, standard mean difference; CI, confidence interval.

In addition to its role in promoting ESCC, we also discussed the possibility of *PTTG1* advancing tumor progression. It was reported in the literature that the high expression of *PTTG1* was closely related to the pathological stage and lymph node metastasis (Shibata et al., 2002). *In vitro*, knocking down *PTTG1* in EC-1 and Eca-109 cell lines could inhibit EMT, migration, and metastasis (Ito et al., 2008; Feng et al., 2017). This study also examined the relationship between the progress of *PTTG1* and ESCC on a variety of data sets. In our study, we have confirmed that *PTTG1* was significantly overexpressed in ESCC tissues, and in the prognosis analysis, the survival condition of patients with high *PTTG1* expression was worse than that of patients with low *PTTG1* expression (HR = 1.29), but no significant statistical difference was found. The reason for this situation may be that overexpression of *PTTG1* plays an important role in the occurrence of ESCC, but it may have little effect on the development and progression of ESCC. Of course, this hypothesis needs to be further verified by our future experiments. We did not establish a relationship between the high expression of *PTTG1* and other pathological parameters that represented the clinical process; however, the expression of *PTTG1* in patients less than or equal to 60 years old was higher than that of patients older than 60, and a higher expression of *PTTG1* was correlated to a lower age. The mechanism of the relationship between *PTTG1* and the patient's age was unclear and requires further study.

TABLE 3 | Comprehensive analysis of *ERH* expression in ESCC based on gene microarrays, public RNA-seq, and in-house RNA-seq.

Study ID	ESCC			Normal			SMD	95% CI
	n	Mean	SD	*n*	Mean	SD		
GPL570	329	8,505	4,309	68	8,503	2,543	0.00	−0.26; 0.26
GPL571	127	3,905	4,576	83	5,676	3,759	−0.41	−0.69; −0.13
GSE23400	53	10.98	0.284	53	10.33	0.267	2.37	1.87; 2.87
GSE32424	7	6.58	0.356	5	5.22	0.358	3.52	1.46; 5.59
GSE45168	5	13.18	0.502	5	12.91	0.138	0.67	−0.63; 1.96
GSE70409	17	12.16	0.830	17	11.54	0.916	0.70	0.01; 1.40
TCGA-GTEx	82	12.27	0.533	1,456	11.27	0.495	2.00	1.77; 2.24
In-house RNA-seq	8	6.20	0.488	8	5.54	0.217	1.66	0.48; 2.84
Overall (I^2 = 0.97, P < 0.01)	628			1,695			1.20	0.26; 2.15

ESCC, esophageal squamous cell carcinoma; n, number; SD, standard deviation; SMD, standard mean difference; CI, confidence interval.

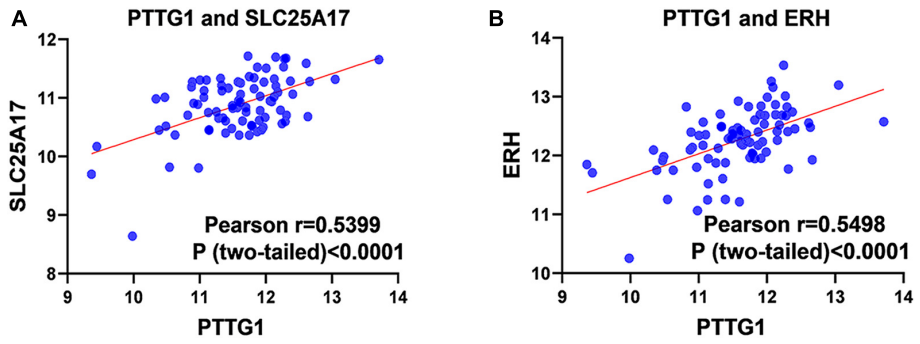

FIGURE 11 | Pearson correlation analysis of *PTTG1* and its target genes. **(A)** Pearson correlation between *PTTG1* and *SLC25A17*. **(B)** Pearson correlation between *PTTG1* and *ERH*.

We then investigated the reasons for the high expression of *PTTG1*. The mechanism of *PTTG1* in ESCC has been reported in previous studies. *PTTG1* induces EMT and metastasis in ESCC by activating GLI1 (Feng et al., 2017). *PTTG1* might also regulate the expression of multiple genes related to cell movement, including members of the Ras–Rho oncogene superfamily (Ito et al., 2008). As a transcription factor, *PTTG1* may achieve its biological function through targeted regulation of a certain set of genes. However, there was no report on the potential target genes of *PTTG1* in ESCC. By combining the target genes displayed by ChIP-seq of *PTTG1*, DEGs of ESCC, *PTTG1*-related genes, and the possible signaling pathways of *PTTG1*, it was observed that *PTTG1* may interact with these genes through chemokines and cytokine signaling pathways. The inflammatory response, integrin signaling pathway, ubiquitin proteasome pathway, and apoptosis signaling pathway played a role in ESCC. By constructing a PPI network and combining ChIP-seq data, we obtained four potential target genes, *SPTAN1*, *SLC25A17*, *IKBKB*, and *ERH*. These hub genes all had binding sites with *PTTG1*. Interestingly, these genes had been reported as tumor related, and *SPTAN1* was a family of filamentous cytoskeletal proteins that acted as an essential scaffold protein for stabilizing the plasma membrane and organizing intracellular organelles. The encoded protein had functions of DNA repair and cell cycle regulation. The expression of *SPTAN1* in metastatic colon cancer was lower than that in non-metastatic colon cancer. The low expression of *SPTAN1* reduced the ability of cell-to-cell contact, which facilitated the metastasis of colon cancer cells (Hinrichsen et al., 2014; Ackermann et al., 2019). It was found that *SPTAN1* expression increased in ovarian cancer after chemotherapy (L'Espérance et al., 2006). The *SLC25A17* gene was the only member of the mitochondrial carrier family that had previously been confirmed to be located in the peroxisomal membrane. It encoded a peroxisomal membrane protein of the mitochondrial solute carrier family and display varied expression levels in 21 human tissues (including brain, esophagus, lung, liver, and kidney tissues) (Agrimi et al., 2012). However, only one relevant study reported its role in tumors, showing that genetic changes in *SLC25A17* (CNV deletion) were closely associated with the overall survival rate and relapse-free survival rate of neuroblastoma patients (Khan et al., 2015). Because *SLC25A17* is positively correlated with TF *PTTG1* expression, it was worth further study. *IKBKB*, also known as IKKβ, is a nuclear factor κB kinase subunit β inhibitor, affecting cell physiology in many ways and phosphorylating proteins to regulate cellular processes from the cell cycle to metabolism and differentiation (Page et al., 2017). Excessive activity of *IKBKB* in oral and dental epithelial cells leads to changes in the composition of epithelial cells and the expression of several tumor suppressor proteins and miRNAs. This results

in cells in a pre-tumor state, and the lack of p53 or p16 tumor suppressor proteins and the loss of p19 would cause odontogenic tumors and metastases to local lymph nodes and lungs. *IKBKB* was observed in the areas of tumor ameloblasts that express keratin K5 at high levels (Page et al., 2020). *IKBKB* could be activated by α-KG produced by *GDH1* and then upregulate *GLUT1* to promote glucose uptake and tumor cell survival, thus accelerating the occurrence of glioma (Wang et al., 2019). *ERH* was an mRNA splicing and mitotic factor, and its function was related to pyrimidine biosynthesis and cell cycles (Gelsthorpe et al., 1997). The *ERH* gene might affect the apoptosis of bladder cancer T24 cells through TLR, NF-κB, TNF, or TGF-β signaling pathways, activating the growth of malignant tumors (Pang et al., 2020). The research team also proved that *ERH* knockdown could inhibit the transfer of BUC T24 cells *in vitro* and *in vivo* through nude mice tail vein metastasis experiments. They found that *ERH* gene knockdown suppressed MYC-mediated migration and invasion in bladder cancer T24 cells (Pang et al., 2019). In primary human breast cancer and breast cancer cell models, quantitative RT-PCR found that *ERH* expression was significantly more upregulated in tumorigenic breast cancer cell lines than in non-tumorigenic cell lines (Zafrakas et al., 2008). This study also found a significant positive correlation between *ERH* and *PTTG1* expression; the molecular relationship between these is also worthy of further study. These reports, to some extent, supported our hypothesis that *PTTG1* may play an important role in the occurrence and development of ESCC by upregulating *SLC25A17* and *ERH*.

Future research could continue this work and improve on the current deficiencies. First, extra research should be conducted on the relationship between *PTTG1* and ESCC progress and prognosis to explore whether *PTTG1* could act as a factor to evaluate the prognosis of ESCC. Second, the research should investigate whether *PTTG1* can be detected in body fluids and whether it contributes to the early diagnosis of ESCC. Third, a ChIP-seq of *PTTG1* using the ESCC cell line needs to be performed. Although the target genes of *PTTG1* in different tissue cells might partially overlap, they also have tumor specificity. Fourth, *in vivo* and *in vitro* experiments need to be carried out to study the biological functions and related molecular mechanisms of *PTTG1*. Fifth, related experiments need to demonstrate the function of the highlighted potential markers in our study.

CONCLUSION

This study combined multiple detection methods—IHC, RNA-seq, and gene chip data—to comprehensively demonstrate for the first time that *PTTG1* was highly expressed in ESCC tissues. This was true from the protein level to the mRNA level and from individual research to integrated analysis. The results were confirmed by a study based on 2,721 cases. It was found that the high expression of *PTTG1* may play an important role in the formation of ESCC. These roles may be completed by *PTTG1* regulating the downstream target genes *SLC25A17* and *ERH*; however, this hypothesis requires extra experiments to verify.

DATA AVAILABILITY STATEMENT

The data presented in the study are deposited in the Gene Expression Omnibus (GEO) (https://www.ncbi.nim.nih.gov/geo/) repository, accession number (GSE164158).

ETHICS STATEMENT

The studies involving human participants were reviewed and approved by the First Affiliated Hospital of Guangxi Medical University. The patients/participants provided their written informed consent to participate in this study.

AUTHOR CONTRIBUTIONS

All authors contributed to the study conception and design. H-FZ performed the data extraction and statistical analysis and drafted the manuscript. S-WC and H-JZ conceived and designed the study and edited the manuscript. L-JY, R-QH, and GC contributed to the design of the study, supervised all the experiments, and corrected the manuscript. Z-GH, XY, Y-WD, JL, and Z-WF collected, extracted, and analyzed the data. J-XM, Z-QT, C-BL, RL, L-HY, and JM critically revised the manuscript. All authors read and approved the final manuscript.

FUNDING

This study was supported by the Guangxi Degree and Postgraduate Education Reform and Development Research Projects, China (JGY2019050), Guangxi Medical University Training Program for Distinguished Young Scholars, Medical Excellence Award Funded by the Creative Research Development Grant from the First Affiliated Hospital of Guangxi Medical University, and Guangxi Zhuang Autonomous Region Health and Family Planning Commission Self-financed Scientific Research Project (Z20200928).

ACKNOWLEDGMENTS

The authors thank all the public data sources involved in the present study.

SUPPLEMENTARY MATERIAL

The Supplementary Material for this article can be found online at: https://www.frontiersin.org/articles/10.3389/fgene.2020.583085/full#supplementary-material

REFERENCES

Ackermann, A., Schrecker, C., Bon, D., Friedrichs, N., Bankov, K., Wild, P., et al. (2019). Downregulation of SPTAN1 is related to MLH1 deficiency and metastasis in colorectal cancer. *PLoS One* 14:e0213411. doi: 10.1371/journal.pone.0213411

Agrimi, G., Russo, A., Scarcia, P., and Palmieri, F. (2012). The human gene SLC25A17 encodes a peroxisomal transporter of coenzyme A, FAD and NAD+. *Biochem. J.* 443, 241–247. doi: 10.1042/bj20111420

Arenas, M. A. R., Whitsett, T. G., Aronova, A., Henderson, S. A., LoBello, J., Habra, M. A., et al. (2018). Protein Expression of PTTG1 as a Diagnostic Biomarker in Adrenocortical Carcinoma. *Ann. Surg. Oncol.* 25, 801–807. doi: 10.1245/s10434-017-6297-6291

Arnal, M. J. D., Arenas, Áf, Arbeloa, and Ál. (2015). Esophageal cancer: Risk factors, screening and endoscopic treatment in Western and Eastern countries. *World J. Gastroenterol.* 21, 7933–7943. doi: 10.3748/wjg.v21.i26.7933

Ersvær, E., Kildal, W., Vlatkovic, L., Cyll, K., Pradhan, M., Kleppe, A., et al. (2020). Prognostic value of mitotic checkpoint protein BUB3, cyclin B1, and pituitary tumor-transforming 1 expression in prostate cancer. *Mod. Pathol.* 33, 905–915. doi: 10.1038/s41379-019-0418-412

Feng, W., Xiaoyan, X., Shenglei, L., Hongtao, L., and Guozhong, J. (2017). PTTG1 cooperated with GLI1 leads to epithelial-mesenchymal transition in esophageal squamous cell cancer. *Oncotarget* 8, 92388–92400. doi: 10.18632/oncotarget.21343

Gelsthorpe, M., Pulumati, M., McCallum, C., Dang-Vu, K., and Tsubota, S. I. (1997). The putative cell cycle gene, enhancer of rudimentary, encodes a highly conserved protein found in plants and animals. *Gene* 186, 189–195. doi: 10.1016/s0378-1119(96)00701-709

Hinrichsen, I., Ernst, B. P., Nuber, F., Passmann, S., Schäfer, D., Steinke, V., et al. (2014). Reduced migration of MLH1 deficient colon cancer cells depends on SPTAN1. *Mol. Cancer.* 13:11. doi: 10.1186/1476-4598-13-11

Huang, F. L., and Yu, S. J. (2018). Esophageal cancer: Risk factors, genetic association, and treatment. *Asian J. Surg.* 41, 210–215. doi: 10.1016/j.asjsur.2016.10.005

Ito, T., Shimada, Y., Kan, T., David, S., Cheng, Y., Mori, Y., et al. (2008). Pituitary tumor-transforming 1 increases cell motility and promotes lymph node metastasis in esophageal squamous cell carcinoma. *Cancer Res.* 68, 3214–3224. doi: 10.1158/0008-5472.can-07-3043

Khan, F. H., Pandian, V., Ramraj, S., Natarajan, M., Aravindan, S., Herman, T. S., et al. (2015). Acquired genetic alterations in tumor cells dictate the development of high-risk neuroblastoma and clinical outcomes. *BMC Cancer* 15:514. doi: 10.1186/s12885-015-1463-y

Kong, J., Wang, T., Zhang, Z., Yang, X., Shen, S., and Wang, W. (2019). Five Core Genes Related to the Progression and Prognosis of Hepatocellular Carcinoma Identified by Analysis of a Coexpression Network. *DNA Cell Biol.* 38, 1564–1576. doi: 10.1089/dna.2019.4932

L'Espérance, S., Popa, I., Bachvarova, M., Plante, M., Patten, N., Wu, L., et al. (2006). Gene expression profiling of paired ovarian tumors obtained prior to and following adjuvant chemotherapy: molecular signatures of chemoresistant tumors. *Int. J. Oncol.* 29, 5–24.

Lin, P., Wen, D. Y., Dang, Y. W., He, Y., Yang, H., and Chen, G. (2018). Comprehensive and Integrative Analysis Reveals the Diagnostic, Clinicopathological and Prognostic Significance of Polo-Like Kinase 1 in Hepatocellular Carcinoma. *Cell Physiol. Biochem.* 47, 925–947. doi: 10.1159/000490135

Mei, S., Qin, Q., Wu, Q., Sun, H., Zheng, R., Zang, C., et al. (2017). Cistrome Data Browser: a data portal for ChIP-Seq and chromatin accessibility data in human and mouse. *Nucleic Acids Res.* 45, D658–D662. doi: 10.1093/nar/gkw983

Page, A., Bravo, A., Suarez-Cabrera, C., Sanchez-Baltasar, R., Oteo, M., Morcillo, M. A., et al. (2020). IKKβ overexpression together with a lack of tumour suppressor genes causes ameloblastic odontomas in mice. *Int. J. Oral. Sci.* 12:1. doi: 10.1038/s41368-019-0067-69

Page, A., Navarro, M., Suárez-Cabrera, C., Bravo, A., and Ramirez, A. (2017). Context-Dependent Role of IKKβ in Cancer. *Genes* 8:376. doi: 10.3390/genes8120376

Pang, K., Hao, L., Shi, Z., Chen, B., Pang, H., Dong, Y., et al. (2020). Comprehensive gene expression analysis after ERH gene knockdown in human bladder cancer T24 cell lines. *Gene* 738, 144475. doi: 10.1016/j.gene.2020.144475

Pang, K., Zhang, Z., Hao, L., Shi, Z., Chen, B., Zang, G., et al. (2019). The ERH gene regulates migration and invasion in 5637 and T24 bladder cancer cells. *BMC Cancer* 19:225. doi: 10.1186/s12885-019-5423-5429

Pei, L., and Melmed, S. (1997). Isolation and characterization of a pituitary tumor-transforming gene (PTTG). *Mol. Endocrinol.* 11, 433–441. doi: 10.1210/mend.11.4.9911

Ren, Q., and Jin, B. (2017). The clinical value and biological function of PTTG1 in colorectal cancer. *Biomed. Pharmacother.* 89, 108–115. doi: 10.1016/j.biopha.2017.01.115

Shibata, Y., Haruki, N., Kuwabara, Y., Nishiwaki, T., Kato, J., Shinoda, N., et al. (2002). Expression of PTTG (pituitary tumor transforming gene) in esophageal cancer. *JPN. J. Clin. Oncol.* 32, 233–237. doi: 10.1093/jjco/hyf058

Vlotides, G., Eigler, T., and Melmed, S. (2007). Pituitary tumor-transforming gene: physiology and implications for tumorigenesis. *Endocr. Rev.* 28, 165–186. doi: 10.1210/er.2006-2042

Wang, X., Liu, R., Qu, X., Yu, H., Chu, H., Zhang, Y., et al. (2019). α-Ketoglutarate-Activated NF-κB Signaling Promotes Compensatory Glucose Uptake and Brain Tumor Development. *Mol. Cell.* 76, 148–162e7. doi: 10.1016/j.molcel.2019.07.007

Yang, S., Wang, X., Liu, J., Ding, B., Shi, K., Chen, J., et al. (2019). Distinct expression pattern and prognostic values of pituitary tumor transforming gene family genes in non-small cell lung cancer. *Oncol. Lett.* 18, 4481–4494. doi: 10.3892/ol.2019.10844

Zafrakas, M., Losen, I., Knüchel, R., and Dahl, E. (2008). Enhancer of the rudimentary gene homologue (ERH) expression pattern in sporadic human breast cancer and normal breast tissue. *BMC Cancer* 8:145. doi: 10.1186/1471-2407-8-145

Conflict of Interest: The authors declare that the research was conducted in the absence of any commercial or financial relationships that could be construed as a potential conflict of interest.

frontiers in Cell and Developmental Biology

ORIGINAL RESEARCH
published: 18 February 2021
doi: 10.3389/fcell.2021.622198

Succinylation Regulators Promote Clear Cell Renal Cell Carcinoma by Immune Regulation and RNA N6-Methyladenosine Methylation

Wenqing Lu[1,2,3†], Xiaofang Che[1,2,3†], Xiujuan Qu[1,2,3], Chunlei Zheng[1,2,3], Xianghong Yang[4], Bowen Bao[1,2,3], Zhi Li[1,2,3], Duo Wang[1,2,3], Yue Jin[1,2,3], Yizhe Wang[5], Jiawen Xiao[6], Jianfei Qi[7] and Yunpeng Liu[1,2,3]**

[1] Department of Medical Oncology, The First Hospital of China Medical University, Shenyang, China, [2] Key Laboratory of Anticancer Drugs and Biotherapy of Liaoning Province, The First Hospital of China Medical University, Shenyang, China, [3] Liaoning Province Clinical Research Center for Cancer, Shenyang, China, [4] Department of Pathology, Shengjing Hospital of China Medical University, Shenyang, China, [5] Department of Respiratory and Infectious Disease of Geriatrics, The First Hospital of China Medical University, Shenyang, China, [6] Department of Medical Oncology, Shenyang Fifth People Hospital, Shenyang, China, [7] Marlene and Stewart Greenebaum Comprehensive Cancer Center, University of Maryland, Baltimore, MD, United States

OPEN ACCESS

Edited by:
Xiao Zhu,
Guangdong Medical University, China

Reviewed by:
Tatsuhiko Furukawa,
Kagoshima University, Japan
Helen Zhu,
Shanghai Jiao Tong University, China

***Correspondence:**
Jianfei Qi
JQi@som.umaryland.edu
Yunpeng Liu
ypliu@cmu.edu.cn

[†] These authors have contributed equally to this work and share first authorship

Specialty section:
This article was submitted to Epigenomics and Epigenetics, a section of the journal Frontiers in Cell and Developmental Biology

Received: 27 October 2020
Accepted: 28 January 2021
Published: 18 February 2021

Citation:
Lu W, Che X, Qu X, Zheng C, Yang X, Bao B, Li Z, Wang D, Jin Y, Wang Y, Xiao J, Qi J and Liu Y (2021) Succinylation Regulators Promote Clear Cell Renal Cell Carcinoma by Immune Regulation and RNA N6-Methyladenosine Methylation. Front. Cell Dev. Biol. 9:622198. doi: 10.3389/fcell.2021.622198

Succinylation is a newly discovered and multienzyme-regulated post-translational modification (PTM) that is associated with the initiation and progression of cancer. Currently, no systematic analyses on the role of succinylation regulators in tumors have been reported. In this study, we performed a comprehensive pan-cancer analysis on four well-known succinylation regulators (CPT1A, KAT2A, SIRT5, and SIRT7). We found that these regulators played specific and critical roles in the prognosis of clear cell renal cell carcinoma (ccRCC). We constructed a risk score (RS) based on two independent prognostic prediction factors, CPT1A and KAT2A, and subsequently developed a nomogram model containing the RS, which showed good accuracy in the prediction of overall survival (OS) in ccRCC patients. Furthermore, we used the similar expression pattern of four succinylation regulators according to consensus clustering analysis to divide the patients into three clusters that exhibited prominently different OS as well as clinicopathological characteristics. Differently expressed genes (DEGs) and pathway enrichment analyses of three clusters indicated that succinylation regulators might promote malignant progression of ccRCC by regulating the infiltration of immune cells and RNA N6-methyladenosine (m6A) methylation. Importantly, our data suggest that CPT1A and SIRT5 might up-regulate and down-regulate the expression of LRPPRC and EIF3B, respectively. Our study systematically analyzed the prognostic predictive values of four succinylation regulators and revealed their potential mechanisms in ccRCC aggressiveness. These data provide new insight into the understanding of succinylation modification and present clinical evidence for its role in ccRCC treatments.

Keywords: succinylation regulators, clear cell renal cell carcinoma, prognosis, immune, RNA N6-methyladenosine methylation

INTRODUCTION

Renal cell carcinoma (RCC) is one of the most common carcinomas with a continuously increasing incidence over several decades, in which clear cell renal cell carcinoma (ccRCC) accounts for approximately 75–80% (Shuch et al., 2015; Makhov et al., 2018). Curative resection is the most effective therapy for ccRCC. However, about 30% of patients could not be cured by surgical operation because of the local progression or distant metastasis at the first diagnosis, and around one third of patients suffered from recurrence after surgery (Li Q. K. et al., 2019). As ccRCC is not sensitive to radiotherapy or chemotherapy, the selection of appropriate therapeutic regimens for patients with advanced ccRCC remains challenging. The 5 years survival rate for patients with advanced ccRCC is only 11.7% (Siegel et al., 2017) and so there is an urgent need for the development of novel therapeutic options. Although new treatments such as anti-angiogenesis drugs and immune checkpoint inhibitors are recently recommended as first-line therapies, the objective response rate (ORR) is unsatisfactory yet (Angulo and Shapiro, 2019). It is necessary to develop novel prognostic biomarkers of ccRCC to screen out those patients with poor prognosis for more positive treatment.

Abbreviations: ccRCC, clear cell renal cell carcinoma; m6A, N6-methyladenosine; PTM, post-translational modification; RS, risk score; OS, overall survival; DEGs, differently expressed genes; RCC, renal cell carcinoma; ORR, objective response rate; CPT1A, carnitine palmitoyltransferase 1A; KAT2A, lysine acetyltransferase 2A; SIRT5, Sirtuin5; SIRT7, Sirtuin7; GC, gastric cancer; PDAC, pancreatic ductal adenocarcinoma; SOD1, superoxide dismutase; PKM2, pyruvate kinase M2; SHMT2, serine hydroxymethyltransferase2; GLS, glutaminase; SDHA; succinate dehydrogenase complex subunit A; ACOX1, acyl-CoA oxidase 1; TCGA, The Cancer Genome Atlas; CPTAC, Clinical Proteomic Tumor Analysis Consortium; ROC, receiver operating characteristic; IGP, in-group-proportion; PCA, principal component analysis; GO, gene ontology; KEEG, Kyoto Encyclopedia of Genes and Genomes; LASSO, least absolute shrinkage and selection operator; PLMD, Protein Lysine Modifications Database; FBS, fetal bovine serum; NC, negative control; ESCA, esophageal carcinoma; HNSCC, head and neck squamous cell carcinoma; LUSC, lung squamous cell carcinoma; LUAD, lung adenocarcinoma; LIHC, liver hepatocellular carcinoma; KIRP, kidney renal papillary cell carcinoma; KIRC, kidney renal clear cell carcinoma; COAD, colon adenocarcinoma; BRCA, breast invasive carcinoma; BLCA, bladder urothelial carcinoma; AUC, area under curve; CDF, cumulative distribution function; FC, fold change; BP, biological process; CC, cellular component; MF, molecular function; METTL3, methyltransferase like 3; METTL14, methyltransferase like 14; METTL16, methyltransferase like 16; WTAP, Wilms tumor 1 associated protein; VIRMA, Vir like m6A methyltransferase associated; RBM15, RNA binding motif protein 15; RBM15B, RNA binding motif protein 15B, ZC3H13, zinc finger CCCH-type containing 13, FTO, fat mass and obesity associated protein; ALKBH5, AlkB Homolog 5, RNA Demethylase; YTHDF1, YTH N(6)-methyladenosine RNA binding protein 1; YTHDF2, YTH N(6)-methyladenosine RNA binding protein 2; YTHDF3, YTH N(6)-methyladenosine RNA binding protein 3; YTHDC1, YTH domain containing 1; YTHDC2, YTH domain containing 2; AGO2, argonaute RISC catalytic component 2; RBMX, RNA binding motif protein, X-linked; ELAVL1, ELAV like RNA binding protein 1; HNRNPA2B1, heterogeneous nuclear ribonucleoprotein A2/B1; HNRNPC, heterogeneous nuclear ribonucleoprotein C (C1/C2), FMR1, fragile X mental retardation 1; LRPPRC, leucine-rich pentatricopeptide repeat containing; IGF2BP1, insulin-like growth factor 2 mRNA binding protein 1; IGF2BP2, insulin-like growth factor 2 mRNA binding protein 2; IGF2BP3, insulin-like growth factor 2 mRNA binding protein 3; EIF3A, eukaryotic translation initiation factor 3, subunit A; EIF3B, eukaryotic translation initiation factor 3, subunit B; EIF3C, eukaryotic translation initiation factor 3, subunit C; EIF3H, eukaryotic translation initiation factor 3, subunit H; ZCCHC4; zinc finger, CCHC domain containing 4; METTL5, methyltransferase like 5; TRMT112, tRNA methyltransferase 11-2 homolog.

Succinylation modification is a newly discovered post-translational modification (PTM) that regulates various physiological and pathological processes including tumor initiation and development. It is dynamically regulated by succinyl transferases including carnitine palmitoyltransferase 1A (CPT1A) (Kurmi et al., 2018) and lysine acetyltransferase 2A (KAT2A) (Wang Y. et al., 2017), and desuccinylases including Sirtuin5 (SIRT5) and Sirtuin7 (SIRT7). Accumulating evidence shows that succinylation regulators play important roles in tumor development by regulating the succinylation levels of substrate targets. CPT1A can promote the proliferation of breast cancer cells by succinylation of enolase 1 (Kurmi et al., 2018) and enhance metastasis of gastric cancer (GC) cells by succinylation of S100A10 (Wang et al., 2018). KAT2A has been shown to up-regulate 14-3-3ζ through its succinyltransferase activity which acts to promote proliferation, migration and invasion of human pancreatic ductal adenocarcinoma (PDAC) cells (Tong et al., 2020). SIRT5 can play a tumor-promoting role by desuccinylating substrates such as Cu/Zn superoxide dismutase (SOD1), pyruvate kinase M2 (PKM2), serine hydroxymethyltransferase2 (SHMT2), glutaminase (GLS), succinate dehydrogenase complex subunit A (SDHA) in the lung, liver, colon, breast and kidney cancers, respectively (Lin et al., 2013; Xiangyun et al., 2017; Chen et al., 2018; Greene et al., 2019; Ma et al., 2019). In particular, SIRT5 can promote breast cancer tumorigenesis in coordination with CTP1A (Kurmi et al., 2018; Greene et al., 2019). Also, SIRT5 can inhibit HCC tumorigenesis by regulating the activity of acyl-CoA oxidase 1 (ACOX1), or suppress GC invasion by desuccinylation of S100A10 (Wang et al., 2018). Based on these data, the roles of succinylation regulators in tumor development are complicated. Different succinylation regulators can have synergistic or antagonistic effects in specific tumors and the same succinylation regulator may have diverse functions in different types of tumors. There is a need to better understand the biology of succinylation regulators through a global analysis of their action in cancer development using the comprehensive bioinformatics approaches. However, such types of studies are not reported yet.

Succinylation regulators usually catalyze the succinylation modification of substrate proteins at lysine residues that are also frequently modified by other PTMs such as acetylation, ubiquitination and methylation. Compared to acetylation, succinylation can cause larger mass changes in substrate proteins due to the higher molecular weight of succinyl and can also have a greater effect on the charge of lysine residues from +1 to −1, resulting in more significant influences on the structure and function of target proteins (Kumar and Lombard, 2018). Moreover, competition between succinylation and other forms of PTMs at the same lysine residue can regulate the function of target proteins. For example, succinylation of S100A10 or GLS can increase the stability of these proteins by antagonizing ubiquitination and proteasome-dependent degradation (Wang et al., 2018; Zhao S. et al., 2019). The competitive relationship between succinylation and ubiquitination may regulate protein levels through the ubiquitin-proteasome pathway.

In this study, we conducted a pan-cancer analysis and identified a key role of succinylation regulators in ccRCC.

Mechanistically, our results suggested that succinylation regulators might promote the malignant progression of ccRCC by regulating tumor immunity and m6A methylation regulators. This study offers a novel perspective on the role of succinylation regulators in ccRCC, provides useful insight into the screening of ccRCC patients for immune therapy and reveals a potential regulatory relationship between succinylation modification and RNA m6A methylation.

MATERIALS AND METHODS

Study Design and Data Screening

All bioinformatics analyses in this study were performed following a flowchart as shown in **Supplementary Figure S1**. The RNA-seq transcriptome data and corresponding clinical information of pan-cancer including 33 tumors were acquired from the UCSC Xena Website[1]. The transcriptome data and more detailed clinical information of KIRC (also named ccRCC) were downloaded from The Cancer Genome Atlas (TCGA) database[2] and normalized using the R program. A total of 251 samples with integral clinicopathological parameters, including T stage, N stage, M stage, survival status, overall survival (OS), age and gender, were divided into dataset 1 and a total of 242 patients with integral clinicopathological parameters except for N stage were contained in dataset 2. The baseline characteristics were highly similar in dataset 1 and dataset 2 except for gender, which was shown in **Supplementary Materials** (**Supplementary Tables S1, S2** and **Supplementary Figures S2A–F**). The proteome data of ccRCC were obtained from The National Cancer Institute's Clinical Proteomic Tumor Analysis Consortium (CPTAC) database[3], in which 105 patients with expression information of CPT1A and KAT2A were screened to further analyze.

Construction of Multi-Succinylation-Regulator Risk Score Model

Univariate and subsequent multivariate Cox regression analyses were performed to pick out the independent prognostic predictors among four well-known succinylation regulators by "survival" package. The risk score (RS) based on succinylation regulators for each patient was calculated with the expression values of the selected genes weighted by their corresponding coefficients according to the multivariate Cox regression analysis. Patients were then divided into high-risk and low-risk group by the median of RS and difference between two groups was analyzed by log-rank test and visualized by Kaplan-Meier survival curve.

Establishment and Validation of Nomogram Prognostic Prediction Model

Multivariate Cox regression analysis was used to further pick out independent factors among RS and others clinical pathological characteristics, which were already screened by univariate Cox regression. According to the results of multivariate Cox regression analysis, the nomogram prognostic prediction model was established by the R package named "rms," and the C-index of this model was calculated by "survival" package. Calibration curve was used to evaluate the performance of this model, and receiver operating characteristic (ROC) analysis was utilized to assess the accuracy of the model for survival prediction by "timeROC" package.

Consensus Clustering on the Basis of Succinylation Regulators

To further investigate the function of succinylation regulators in ccRCC, patients in dataset 1 were separated into three clusters according to the best cut-off obtained from consensus clustering analysis using the R package named "ConsensusClusterPlus" (Wilkerson and Hayes, 2010). The in-group-proportion (IGP) statistic was used to evaluate the reproducibility of the consensus clustering by the "clusterRepro" package using data from dataset 2 (Kapp and Tibshirani, 2007; Li B. et al., 2019). Principal component analysis (PCA) within the R software was utilized to explore the expression patterns of genes in different clusters. Kaplan-Meier analysis was used to evaluate whether there was significant difference in OS among three clusters.

Function Analysis Among Different Clusters

Differentially expressed genes (DEGs) in cluster 2 or cluster 1 compared to cluster 3 were screened by the "Limma" package (Ritchie et al., 2015) with the criteria of adjusted $P < 0.05$ and $|\text{Log fold change (FC)}| > 0.585$. Gene ontology (GO) and Kyoto Encyclopedia of Genes and Genomes (KEGG) pathway enrichment were performed by the package called "clusterprofiler" based on DEGs mentioned above (Yu et al., 2012).

Immune Infiltration Analysis Among Different Clusters

The file of leukocyte gene signature matrix (LM22) and the corresponding source codes were downloaded from CIBERSORT website[4] to assess the abundance of immune cells among clusters of ccRCC (Newman et al., 2015), the immune infiltration analysis was performed by R software (v3.6.3), only samples with $P < 0.05$ were retained for subsequent analysis.

Construction of Immune Signature Underlining the Regulation of Succinylation

To explore the association of immune signature and succinylation regulators, a screening criteria was established as follows: (1) be up-regualted in cluster 2 as well as in clsuter1 in comparison with cluster 3; (2) be negatively correlated with OS of ccRCC patients (HR > 1, $P < 0.05$); (3) be

[1]http://xena.ucsc.edu/

[2]https://cancergenome.nih.gov/

[3]https://proteomics.cancer.gov/programs/cptac

[4]http://cibersort.stanford.edu

contained in the gene list downloaded from Immport Shared Data website[5]. Then more powerful prognostic predictors from genes conformed to the criteria were filtered by Least Absolute Shrinkage and Selection Operator (LASSO) algorithm using "glmnet" package in R (Friedman et al., 2010) and finally constructed the immune signature associated with the succinylation regulators. RS_immune was reckoned with the expression values of the each gene contained in immune signature weighted by their coefficients according to LASSO Cox regression analysis.

Succinylation Modification and Prognostic Value of m6A Regulators

The network of m6A regulators, which were reported by high-quality studies acquired from PubMed website[6], was constructed using Cytoscape software (v3.6.1). Online website Protein Lysine Modifications Database (PLMD)[7] was used to identify the succinylation and ubiquitination modified lysine residues within m6A regulators. In addition, the prediction value of m6A regulators in ccRCC was evaluated by univariate Cox regression analysis and LASSO.

Validation by Immunohistochemistry From Clinical Specimens of ccRCC

CcRCC tissues and matched adjacent normal kidney tissues from 42 ccRCC patients received radical nephrectomy and confirmed by pathological diagnosis from June 2015 to June 2016 were collected in Shengjing Hospital of China Medical University. The baseline characteristics of 42 ccRCC patients for immunohistochemistry are shown in **Supplementary Table S3**. This study was approved by Ethics Committee of the First Hospital of China Medical University (AF-SOP-07-1.1-01). The expression pattern of CPT1A, KAT2A, SIRT5, SIRT7, LRPPRC, and EIF3B was assessed by immunohistochemistry using the paraffin embedded tissues. The intensity of staining was classified on a scale of 0–3: 0 (negative), 1, (weak), 2 (moderate), 3 (strong); and the heterogeneity of staining was scored as 0 ($\leq$5%), 1 (6–25%), 2 (26–50%), 3 (51–75%), 4 (>75%). The protein expression of each molecule was calculated finally by the following formula: 3× scores of strongly staining cells + 2× scores of moderately staining cells + 1× scores of weakly staining cells. The expression pattern of each molecule was compared between normal and tumor tissues and then the correlation between CPT1A and LRPPRC, SIRT5 and EIF3B, CPT1A and EIF3B, SIRT5 and LRPPRC were calculated, respectively.

Cell Culture

Human renal adenocarcinoma cell lines ACHN (TCHu199) was purchased from the Chinese Academy of Sciences (Shanghai, China) and cultured in RPMI-1640 medium with 10% fetal bovine serum (FBS) and 100 U/ml penicillin-streptomycin, under the optimum culture condition of 37℃ and 5% CO_2.

[5]https://www.immport.org/shared/home

[6]https://pubmed.ncbi.nlm.nih.gov/

[7]http://plmd.biocuckoo.org/

Cell Transfection

The specific human siRNAs of CPT1A and SIRT5 were synthetized from JTS scientific (Wuhan, China). ACHN cells were inoculated into a six-well plate at the density of 1×10^5 and siRNAs were transfected into cells by jetPRIME® Transfection Reagent according to manufacturer's instructions. The coding strands of negative control (NC) and different siRNAs are listed as follows:

NC siRNA: 5′-UUCUCCGAACGUGUCACGU-3′
siCPT1A-2: 5′-GGAUGGGUAUGGUCAAGAU-3′
siCPT1A-3: 5′-GCCUUUACGUGGUGUCUAA-3′
siSIRT5-1: 5′-GCAGAUUUUCGAAAGUUUU-3′
siSIRT5-3: 5′-GAGUCCAAUUUGUCCAGCU-3′

Western Blotting

The protein samples were collected and quantified after transfected for 72 h. Samples were utilized to electrophoresis in an 8% SDS-polypropylene gel and then transferred onto PVDF membranes (Millipore, United States). After a 40 min-blocking with 5% skimmed milk, the membranes were incubated in primary antibodies for at least 6 h at room temperature and then washed by 1 × TBST buffer for 4 times. Finally, after incubation by secondary antibodies for 40 min and another washing for 4 times, the membranes were visualized using the Electrophoresis Gel Imaging Analysis System (DNR Bio-Imaging Systems, Israel).

Antibodies

Antibodies	Source	Identifier	Dilution Ratio	
			IHC	WB
CPT1A	Cell Signaling Technology	#12252		1:1,000
CPT1A	Proteintech	15184-1-AP	1:200	
KAT2A	Santa Cruz Biotechnology	sc-365321	1:50	
SIRT5	Sigma-Aldrich	HPA022002	1:800	1:500
SIRT7	Santa Cruz Biotechnology	12994-1-AP	1:50	
LRPPRC	Proteintech	21175-1-AP	1:400	1:1,000
EIF3β	Santa Cruz Biotechnology	sc-374156	1:50	1:2,000

Statistical Analyses

All statistical analyses in the whole study except for immunohistochemistry were performed using R software (v3.6.3). Wilcoxon test was used to compare the expression level of genes between tumor and normal tissues, and one-way ANOVA test was utilized to compare the expression pattern of succinylation regulators and m6A regulators as well as the infiltration pattern of immune cells in patients with different clusters. Overall survival between different groups was analyzed by Kaplan-Meier survival curve with log-rank test. Correlation between genes expression was analyzed by Spearman correlation analysis. Relationship between protein expression

and clinicopathological parameters was analyzed by chi-square test with package "stats" in R. Statistical analyses relating to immunohistochemistry was carried out by GraphPad Prism (v8.0.2), in which the unpaired Student's *t*-test was used to analyze the expression pattern of each molecule between normal and tumor tissues, Pearson correlation was utilized to identify the relationship between CPT1A and LRPPRC, SIRT5 and EIF3B, CPT1A and EIF3B, SIRT5 and LRPPRC. $P < 0.05$ was defined statistically significant in the whole study.

RESULTS

Altered Expression of Succinylation Regulators and Their Correlation With Clinicopathological Parameters of ccRCC Patients

To evaluate the roles of four well-known succinylation regulators (CPT1A, KAT2A, SIRT5, and SIRT7), we utilized the TCGA pan-cancer dataset to analyze the expression patterns and prognostic prediction values in 10 relatively common tumors including ESCA, STAD, LUSC, LUAD, LIHC, KIRP, KIRC, COAD, BRCA, and BLCA. We found that KAT2A was prominently up-regulated in all types of tumors compared to the corresponding normal tissues. SIRT7 was significantly up-regulated in 9 of 10 tumor types and down-regulated in COAD. The expression of CPT1A and SIRT5 showed significant differences between several tumors and normal tissues with a high level of heterogeneity in different tumors (**Figure 1A**). However, univariate Cox regression analysis showed that the overall survival (OS) of patients with KIRC (also named ccRCC), but not other tumor types, was associated with all four regulators ($P < 0.05$) (**Figure 1B** and **Supplementary Table S4**). Therefore, further analysis was focused on ccRCC. We performed correlation analysis between the expression of succinylation regulators and the clinicopathological parameters in dataset 1. Our results showed that expression of CPT1A or SIRT5 was negatively correlated with deeper tumor infiltration and distant metastasis, whereas the expression of SIRT7 exhibited opposite effect (**Supplementary Table S5**). The expression of KAT2A was not significantly correlated with any clinicopathological parameters.

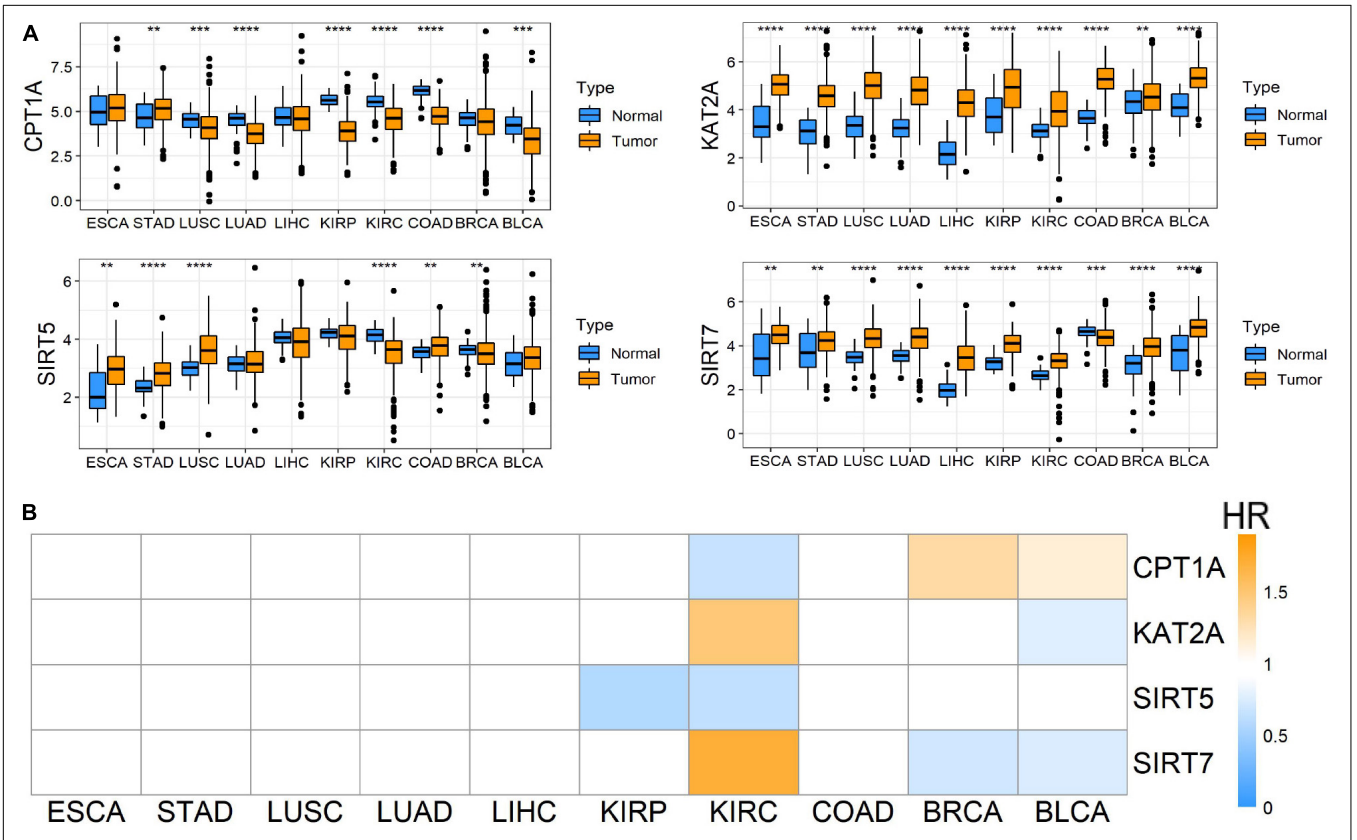

FIGURE 1 | Pan-cancer analysis among 10 common tumors. **(A)** Different mRNA expression patterns of four succinylation regulators, CPT1A, KAT2A, SIRT5 and SIRT7, between tumor and normal tissues among 10 common tumors, $^{*}P < 0.05$, $^{**}P < 0.01$, $^{***}P < 0.001$, and $^{****}P < 0.0001$. **(B)** Heatmap of HR illustrating the association between each succinylation regulator and survival status in different tumors. Orange modules mean statistically significant HR > 1, blue modules mean statistically significant HR < 1, and white modules represent for the regulators with no significant prognostic prediction value. HR, hazard ratios; ESCA, esophageal carcinoma; STAD, stomach adenocarcinoma; LUSC, lung squamous cell carcinoma; LUAD, lung adenocarcinoma; LIHC, liver hepatocellular carcinoma; KIRP, kidney renal papillary cell carcinoma; KIRC, kidney renal clear cell carcinoma; COAD, colon adenocarcinoma; BRCA, breast invasive carcinoma; BLCA, bladder urothelial carcinoma.

TABLE 1 | The univariate and multivariate Cox regression analysis between four well-known succinylation regulators and OS in dataset 1.

	Univariate cox				Multivariate cox			
Gene	**Coef**	**HR**	**95%CI**	**P**	**Coef**	**HR**	**95%CI**	***P***
CPT1A	−0.584	0.558	0.421–0.739	<0.001	−0.625	0.535	0.386–0.742	<0.001
KAT2A	0.740	2.095	1.624–2.702	<0.001	0.706	2.026	1.404–2.922	<0.001
SIRT5	−0.601	0.548	0.307–0.979	0.042	−0.004	0.996	0.555–1.787	0.988
SIRT7	1.322	3.749	2.265–6.205	<0.001	0.016	1.016	0.487–2.116	0.967

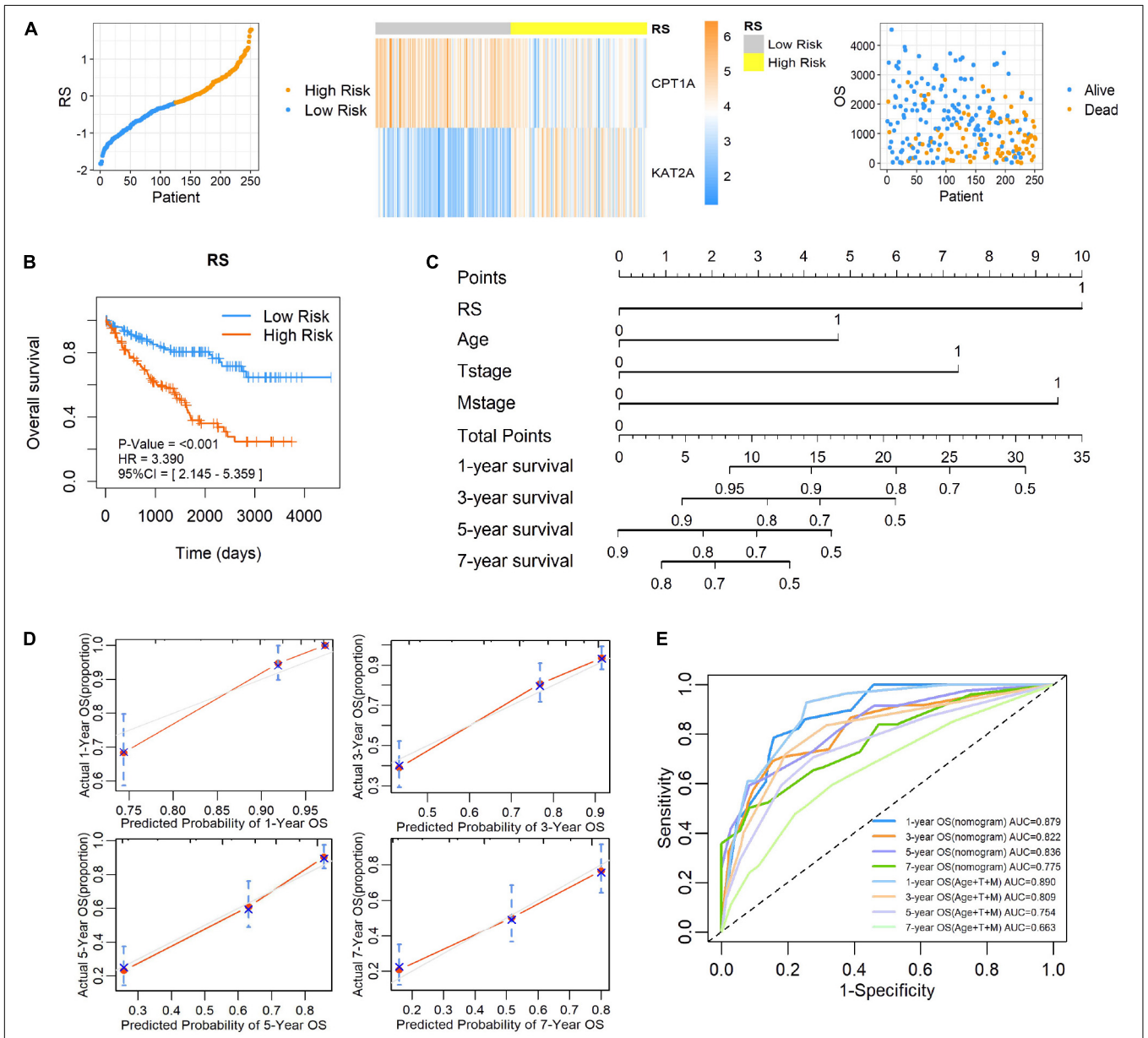

FIGURE 2 | Establishment and validation of a risk score and nomogram prognostic prediction model based on succinylation regulators in dataset 1. **(A)** Distribution of the RS, OS, survival status, and the relative expression of CPT1A and KAT2A among ccRCC patients in dataset 1. **(B)** Kaplan-Meier survival curve for ccRCC patients with high and low RS.**(C)** The nomogram prognosis prediction model containing RS, Age, T stage and M stage. **(D)** The calibration plots suggested the comparison between predicted and actual outcome for 1-, 3-, 5-, and 7-year survival probabilities in the nomogram model. **(E)** ROC curves described the predictive ability of nomogram model and traditional model only containing age, T stage and M stage for 1-, 3-, 5-, and 7-year survival probabilities. RS, risk score; OS, Overall Survival; ROC, Receiver Operating Characteristic.

TABLE 2 | The correlation between RS and clinicopathological parameters in dataset 1.

Parameter	Total	Low RS	High RS	*P*
T stage				0.012
T1 + T2	148	84	64	
T3 + T4	103	41	62	
N stage				0.073
N0	235	121	114	
N1	16	4	12	
M stage				0.004
M0	209	113	96	
M1	42	12	30	
Age				0.849
<Median	123	60	63	
≥Median	128	65	63	
Gender				0.034
Female	99	58	41	
Male	152	67	85	

The median age of ccRCC patients in dataset 1 is 62 years old.

Taken together, these data indicated that succinylation regulators might play a more important role in the development and progression of ccRCC.

Establishment of a Risk Score and Prognostic Predictive Nomogram Model Based on the Expression of Succinylation Regulators in ccRCC

To further clarify the prognostic predictive value of succinylation regulators in ccRCC, we performed univariate and multivariate Cox regression analyses. The results indicated that CPT1A (HR = 0.535, 95%CI = 0.386–0.742, $P < 0.001$) and KAT2A (HR = 2.026, 95%CI = 1.404–2.922, $P < 0.001$) were the independent prognostic predictors for ccRCC (**Table 1**). Then, a risk score (RS) was calculated for each patient according to the following formula: RS = 0.706 × EXP[KAT2A] − 0.625 × EXP[CPT1A]. The patients were then divided into high- and low-RS groups based on the median of RS compared to the low-RS group, the high-RS group exhibited low expression of CPT1A, high KAT2A expression and reduced survival (**Figure 2A**). The Kaplan-Meier curve analysis showed that the OS of the high-RS group was notably shorter than the low-RS group (HR = 3.390, 95%CI = 2.145–5.359, $P < 0.001$) (**Figure 2B**). Similar results were found in dataset 2 (**Supplementary Figures S3A,B**). Furthermore, the relationship between RS and different clinical parameters was analyzed by a Chi-square test and showed that a high RS was positively associated with T stage ($P = 0.012$), M stage ($P = 0.004$), as well as male ($P = 0.034$, **Table 2**).

To estimate the survival probabilities of ccRCC patients at 1, 3, 5, and 7 years, we established a nomogram prognostic prediction model based on all independent prognostic predictors recognized by the univariate and multivariate Cox regression analyses including RS (HR = 3.082, 95%CI = 1.913–4.966, $P < 0.001$), T stage (HR = 2.278, 95%CI = 1.447–3.588, $P < 0.001$), M stage (HR = 2.876, 95%CI = 1.788–4.625, $P < 0.001$) and age (HR = 1.729, 95%CI = 1.138–2.626, $P = 0.010$, **Table 3** and **Figure 2C**). The C-index of this model was 0.777, with a 95%CI ranging from 0.731 to 0.823. The overlapping of the calibration curve between the predictive values from the nomogram model and the actual observations demonstrated the accuracy of this model (**Figure 2D**). Next, we compared the performance of the nomogram model with the traditional model that only contained the clinical parameters (T stage, M stage and age) in the prognostic prediction. The results showed that the nomogram model was superior in predicting OS at 3, 5, and 7 years, whilst the traditional model had a larger area under the curve (AUC) for 1 year survival prediction (**Figure 2E**). These results suggested that the nomogram model was more powerful than the traditional model in predicting the long-term survival of ccRCC patients.

Cluster Identification Based on Consensus Clustering of Succinylation Regulators in ccRCC

To further ascertain the function of all succinylation regulators, consensus clustering analysis was performed to distinguish the expression similarities of four succinylation regulators. The patients in dataset 1 were separated into three clusters according to the minimum value of cumulative distribution function (CDF) ($k = 3$, **Figure 3A**). Significant differences in the expression patterns of the four regulators were found in clusters 1 ($CPT1A^{medium}$, $KAT2A^{medium}$, $SIRT5^{medium}$, $SIRT7^{medium}$), 2 ($CPT1A^{low}$, $KAT2A^{high}$, $SIRT5^{low}$, $SIRT7^{high}$), and 3 ($CPT1A^{high}$,

TABLE 3 | The univariate and multivariate Cox regression analysis between RS and other clinicopathological parameters and OS in dataset 1.

	Univariate cox				Multivariate cox			
Parameter	Coef	HR	95%CI	*P*	Coef	HR	95%CI	*P*
T stage	1.148	3.151	2.075–4.784	<0.001	0.823	2.278	1.447–3.588	<0.001
N stage	1.233	3.430	1.818–6.472	<0.001	0.334	1.397	0.707–2.758	0.336
M stage	1.444	4.237	2.752–6.524	<0.001	1.056	2.876	1.788–4.625	<0.001
Age	0.450	1.568	1.035–2.376	0.034	0.547	1.729	1.138–2.626	0.010
Gender	0.021	1.021	0.674–1.547	0.921				
RS	1.221	3.390	2.145–5.359	<0.001	1.126	3.082	1.913–4.966	<0.001

The median age of ccRCC patients in dataset 1 is 62 years old.

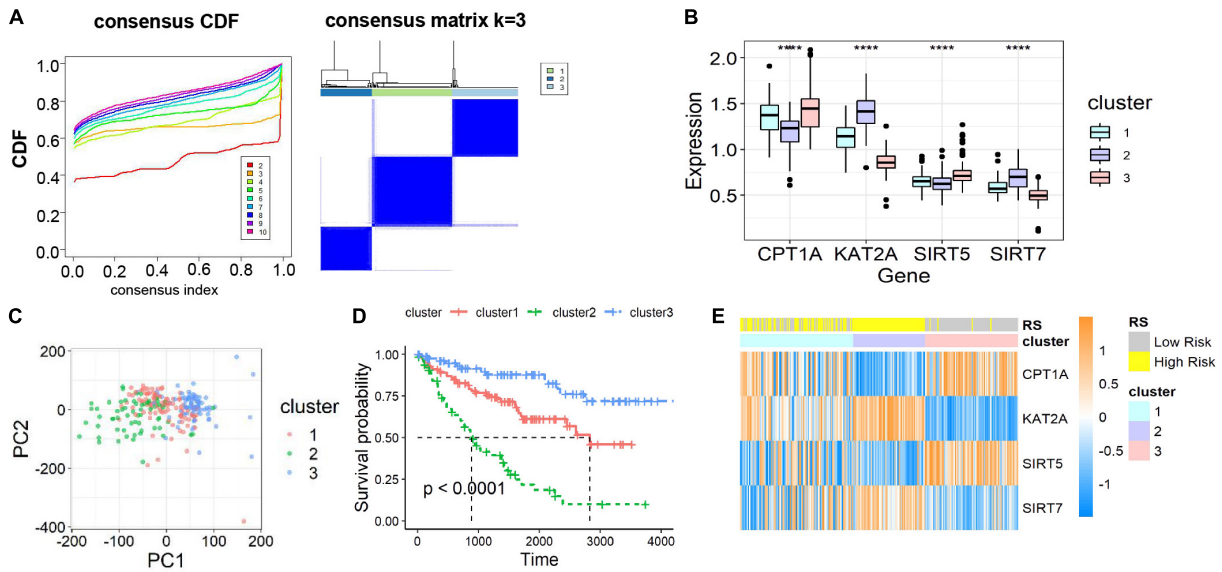

FIGURE 3 | Identification and characteristic description of the consensus clusters based on succinylation regulators in dataset 1. **(A)** Consensus clustering CDF for k = 2 to 10 and consensus clustering matrix for k = 3. **(B)** The different expression pattern of four succinylation regulators in three clusters at mRNA level, ****$P < 0.0001$. **(C)** PCA of the total mRNA expression profile in dataset 1. **(D)** Kaplan-Meier survival curve for ccRCC patients in different clusters. **(E)** The heatmap demonstrated the expression of four succinylation regulators in patients contained in dataset 1 as well as the association between RS and consensus clusters. CDF, cumulative distribution function; PCA, principal component analysis.

KAT2A^{low}, SIRT5^{high}, SIRT7^{low}) (**Figure 3B**). Patients in each cluster gathered well in sub-classes partitioned by principal component analysis (PCA), verifying the rationality of the consensus clustering (**Figure 3C**). The patients in cluster 2 had the shortest OS amongst the three clusters, while patients in cluster 3 showed the longest OS ($P < 0.001$, **Figure 3D**). When comparing groups were divided by the RS and clusters, we found that cluster 2 was completely contained in the high-RS subgroup (**Figure 3E**). For the clinicopathological features, cluster 2 was positively related to later T stage ($P < 0.001$) and M stage ($P = 0.001$) (**Table 4**). Taken together, ccRCC patients could be successfully separated by consensus clustering and cluster 2 accurately identified patients with more malignant characteristics in the high-RS group.

TABLE 4 | The correlation between clusters and clinicopathological parameters in dataset 1.

Parameter	Total	Cluster 1	Cluster 2	Cluster 3	*P*
T stage					<0.001
T1 + T2	148	63	24	61	
T3 + T4	103	39	41	23	
N stage					0.073
N0	235	98	57	80	
N1	16	4	8	4	
M stage					0.001
M0	209	87	45	77	
M1	42	15	20	7	
Age					0.854
<Median	123	48	32	43	
≥Median	128	54	33	41	
Gender					0.975
Female	99	41	25	33	
Male	152	61	40	51	
RS					<0.001
Low	125	45	0	80	
High	126	57	65	4	

The median age of ccRCC patients in dataset 1 is 62 years old.

The three-cluster classification was further verified using dataset 2. The in-group-proportion (IGP) values from cluster 1 to cluster 3 in dataset 2 were 0.972, 0.960 and 0.988, respectively (**Supplementary Figure S4A**). These values were much higher than a random partition into three clusters (IGP = 0.333). The three-clusters of dataset 2 highly resembled those of dataset 1 for the expression of four succinylation regulators (**Supplementary Figure S4B**), the distribution of patients in different principal components by PCA analysis (**Supplementary Figure S4C**), the relative length of OS time (**Supplementary Figure S4D**) and the relationship between cluster 2 and the high-RS group (**Supplementary Figure S4E**). In summary, ccRCC patients could be divided into three clusters according to the similarities in the expression of succinylation regulators. Poor prognosis was observed for clusters 1 or 2 and a good prognosis for cluster 3 was found.

Association of Succinylation Regulators With Immune Cell Infiltration in ccRCC

To assess the functions of the three clusters, we screened the differently expressed genes (DEGs) between the clusters and

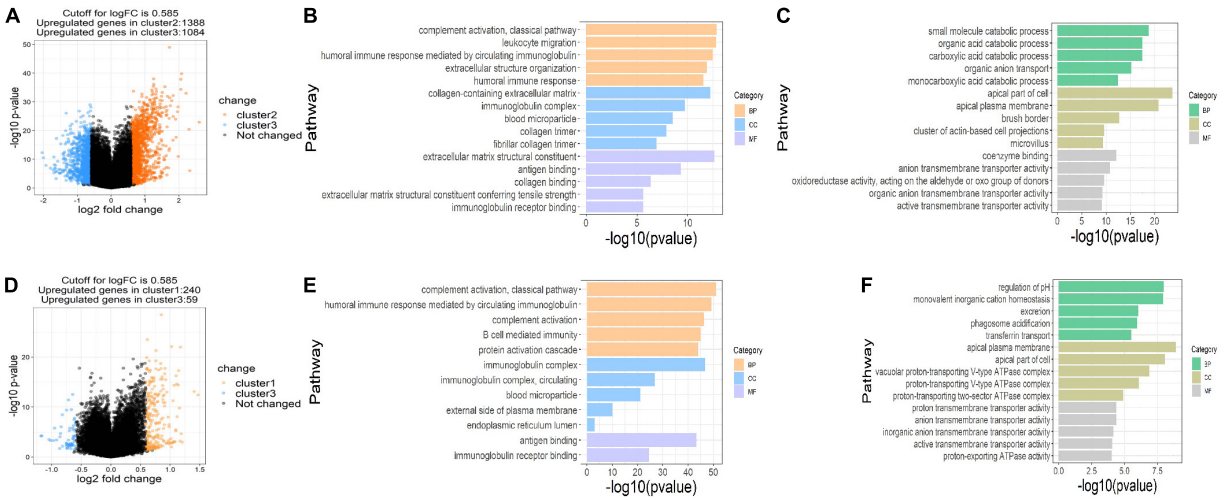

FIGURE 4 | DEGs and enriched pathways in clusters 1 and 2 in comparison with cluster 3. **(A)** Volcano plot of DEGs in cluster 2 ($n = 65$) compared to cluster 3 ($n = 84$), the cutoff is 0.585 in the absolute value of logFC and 0.05 in *P*-value. **(B,C)** The top 15 up-regulated GO pathways **(B)** and top 15 down-regulated GO pathways in cluster 2 compared to cluster 3 **(C)**. **(D)** Volcano plot of DEGs in cluster 1 ($n = 102$) compared to cluster 3, the cutoff is 0.585 in the absolute value of logFC and 0.05 in *P*-value. **(E,F)** The top 12 up-regulated GO pathways **(E)** and top 15 down-regulated GO pathways in cluster 1 compared to cluster 3 **(F)**. DEGs, differently expressed genes; FC, fold change; GO, Gene Ontology.

performed the gene ontology (GO) pathway enrichment analysis. The DEGs between the clusters were screened with the restriction of an adjusted $P < 0.05$ and a $|\log$ fold change (logFC)$| > 0.585$. 1,388 up-regulated and 1,084 down-regulated genes in cluster 2, 240 up-regulated genes and 59 down-regulated genes in cluster 1 were identified relative to cluster 3, respectively (**Figures 4A,D**). GO pathway enrichment analysis of DEGs demonstrated the top 15 up-regulated and down-regulated pathways in clusters 1 and 2 (**Figures 4B,C,E,F**). The top 15 pathways were defined as the sum of the top five pathways in biological process (BP), cellular component (CC) and molecular function (MF), respectively, among which only two pathways in MF were significantly up-regulated in cluster 1. Interestingly, we found that most of the up-regulated pathways were related to immune regulation and part of the pathways overlapped between clusters 1 and 2, suggesting that succinylation regulators might promote the ccRCC by regulating immune pathways (**Figures 4B,E**).

CIBERSORT was used to distinguish differences in immune infiltration among the three clusters. The result of 186 patients in dataset 1 met the requirements of CIBERSORT with a $P < 0.05$. The top 3 infiltrating immune cells were $CD8^+$ T cells, M0 macrophages and resting memory $CD4^+$ T cells, all of them showed no differences among the three clusters (**Figures 5A–C**). Interestingly, from a total of 22 immune cell types, three cell types were significantly different among the three clusters including regulatory T cells (Tregs, $P < 0.001$), M0 macrophages ($P < 0.05$) that exhibited an increasing trend with the promotion of malignancy, and resting mast cells ($P < 0.05$) that showed a decreasing tendency. The correlation analysis of 21 immune cell types (excluding naive $CD4^+$ T cells that show no infiltration in any patient) revealed that $CD8^+$ T cells were positively related to helper follicular T cells ($R = 0.59$, $P < 0.05$) and negatively related to resting memory $CD4^+$ T cells ($R = -0.7$, $P < 0.05$, **Figure 5D**). Kaplan-Meier analysis indicated that infiltration of Tregs was associated with the poor prognosis of OS (HR = 1.820, 95%CI = 1.140–2.906, $P = 0.011$) and infiltration of resting mast cells was associated with longer OS (HR = 0.462, 95%CI = 0.286–0.747, $P = 0.001$). The infiltration of M0 macrophages had no predictive effect on the OS of ccRCC patients (**Figure 5E**). The infiltration of Tregs was significantly more different amongst the three clusters compared to resting mast cells. These results suggested that succinylation regulators might contribute to malignancy of ccRCC by enhancing the infiltration of Tregs and inducing an immunosuppressive microenvironment. To determine which succinylation regulators play a major role in the infiltration of Tregs, we performed a correlation analysis between each regulator and FOXP3, an essential gene marker for Tregs. The expression of FOXP3 was positively related to SIRT7 ($R = 0.315$, $P = 0.007$) and negatively related to SIRT5 ($R = 0.331$, $P < 0.001$) and CPT1A ($R = -0.196$, $P < 0.001$) (**Figure 5F**). These results suggested that SIRT7-high, SIRT5-low or CTP1A-low might contribute to the infiltration of Tregs.

Establishment of a Succinylation Regulator-Related Prognostic Predictive Immune Signature in ccRCC

To further investigate the mechanism of succinylation regulators and immune regulation, we aimed to determine the key immune-related genes associated with succinylation regulators and ccRCC malignancy. Based on the criteria detailed in the "Materials and Methods" section, we identified a total of 34 immune-related genes that were up-regulated in clusters 1 and 2 and associated with poor prognosis (**Figures 6A–C**). Next, we performed the last absolute shrinkage and selection operator (LASSO) cox

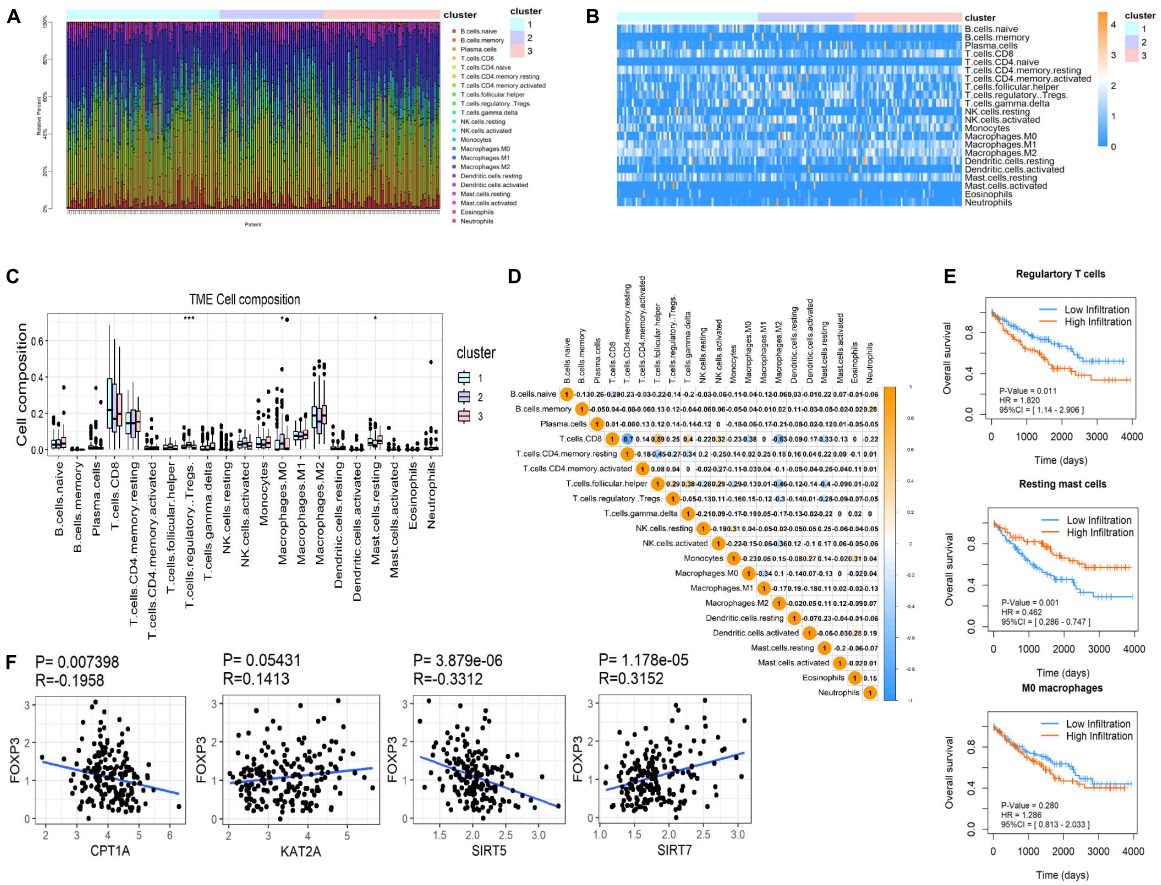

FIGURE 5 | Immune infiltration in ccRCC among the three clusters. **(A,B)** Both the stacked column chart **(A)** and the heatmap **(B)** exhibited the proportion of 22 immune cells in 186 patients screened by CIBERSORT with a significant *P*-value ($P < 0.05$). **(C)** The infiltration pattern of immune cells (except for CD4 naive T cells) in different clusters, $^{*}P < 0.05$ and $^{***}P < 0.001$. **(D)** Spearman correlation analysis of the 21 immune cells in 186 ccRCC patients. **(E)** Kaplan-Meier survival curves for patients with differently infiltrated Tregs, resting mast cells and M0 macrophages, respectively. **(F)** The Spearman correlation analysis between the expression of FOXP3 and the four succinylation regulators.

regression analysis to further identify six central immune factors as an immune signature (**Figure 6D**). Based on this immune signature, a RS was calculated according to the following formula: RS_immune = 0.148 × EXP[AGER] + 0.066 × EXP[IGLV3-21] + 0.038 × [IL20RB] + 0.283 × EXP[LTB4R] + 0.223 × EXP[NFKBIZ] + 0.018 × EXP[SAA1]. When separating the patients into the high- and low-risk groups based on the median of RS_immune, the OS of the two groups showed different trends (HR = 4.232, 95%CI = 2.614–6.850, $P < 0.001$) with the 5 and 7 years AUC larger than 0.8 (**Figures 6E,F**). Analysis of dataset 2 also showed similar results (**Supplementary Figures S5A,B**). All of these data indicated that succinylation regulators were associated with the expression of immune-related genes and a 6-gene immune signature could predict prognosis in ccRCC.

Association of Succinylation Regulators With N6-Methyladenosine RNA Methylation in ccRCC

In addition to the immune-related pathways, abundant GO pathways relating to RNA modification were shown to be up-regulated (**Figure 7A**). The pathway named "spliceosome" was enriched in the top 5 of KEGG pathways (**Figure 7B**) in cluster 2 compared to cluster 3. These results suggested that RNA modification might also be associated with succinylation regulators and ccRCC malignancy. N6-methyladenosine (m6A) methylation, one of the most common RNA-related modifications, is catalyzed by m6A regulators (Zaccara et al., 2019). We hypothesized that succinylation regulators might regulate m6A regulators to affect RNA-related pathways. To determine whether m6A regulators could be succinylated, we searched the protein lysine modification database (PLMD) to seek succinylation modified sites in 32 m6A regulators including METTL3, METTL14, METTL16, WTAP, VIRMA, RBM15, RBM15B, ZC3H13, FTO, ALKBH5, YTHDF1, YTHDF2, YTHDF3, YTHDC1, YTHDC2, AGO2, RBMX, ELAVL1, HNRNPA2B1, HNRNPC, FMR1, LRPPRC, IGF2BP1, IGF2BP2, IGF2BP3, EIF3A, EIF3B, EIF3C, EIF3H, ZCCHC4, METTL5, and TRMT112 (**Figure 7C**). In total, 23 lysine sites from five m6A readers including HNRNPA2B1, HNPNPC, HNRNPG, LRPPRC, and

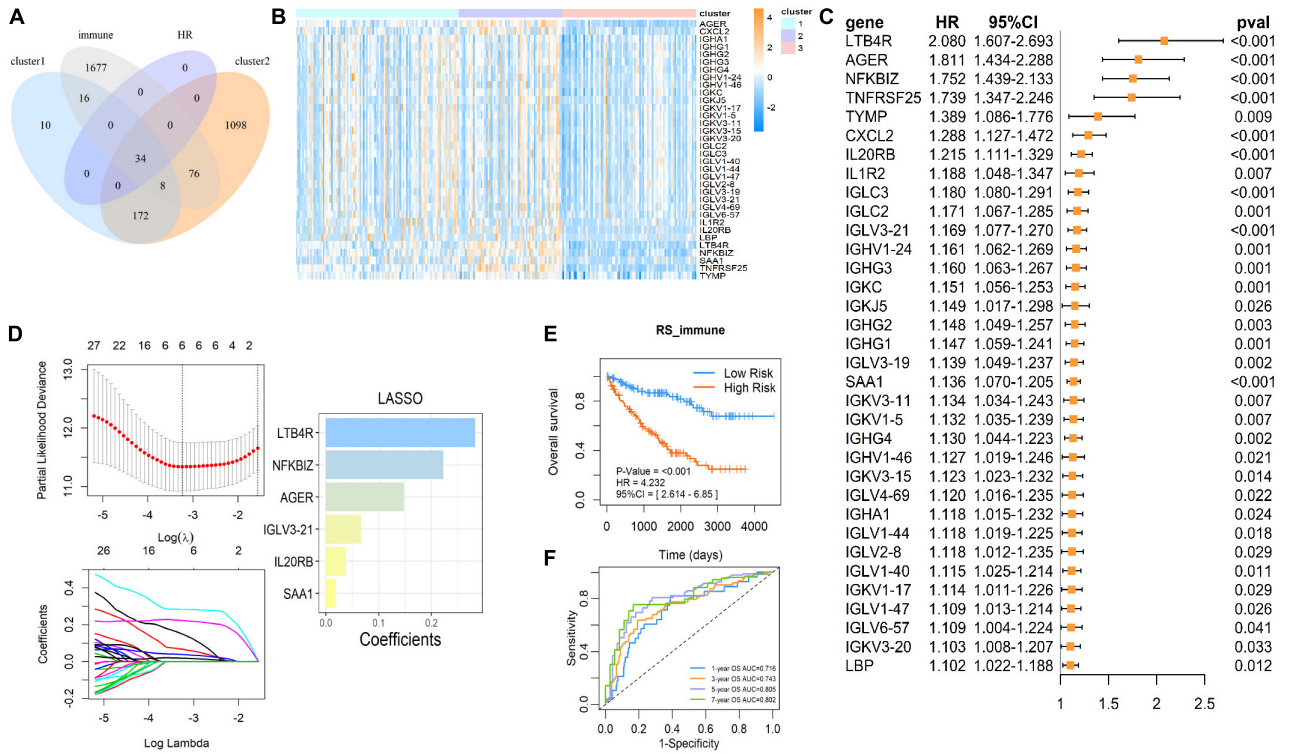

FIGURE 6 | The immune signature based on succinylation modification. **(A)** The Venn diagram showed 34 candidates contained in up-regulated genes in cluster 2 relative to cluster 3, up-regulated genes in cluster 1 relative to cluster 3 and the immune gene list form Immport Shared Data website at the same time, and all have a significant HR > 1 ($P < 0.05$). **(B)** The heatmap displayed relative mRNA expression of 34 candidate immune genes in three clusters. **(C)** Univariate Cox regression analysis of the association between the mRNA expression of 34 candidate immune genes and OS of patients with ccRCC in dataset 1. **(D)** The coefficients of important prognosis prediction factors calculated by multivariate Cox regression using LASSO. **(E)** Kaplan-Meier survival curves for patients with high and low RS based on immune signature. **(F)** The ROC curves based on immune signature for 1-, 3-, 5-, and 7-year survival probabilities. LASSO, least absolute shrinkage and selection operator.

EIF3B could potentially undergo succinylation modification (**Table 5**).

According to previous studies, succinylation regulators mainly regulate the activity or protein expression of their targeting molecules. We further analyzed the effects of succinylation regulators on the protein expression of the five m6A regulators using the ccRCC protein dataset from CPTAC. Based on their availability in the protein dataset, we selected CPT1A and SIRT5 as well as five m6A regulators (HNRNPA2B1, LRPPRC, RBMX, EIF3B, HNRNPC) for subsequent analyses. The protein expression of CPT1A and SIRT5 was lower in tumors compared to normal tissues (**Figure 7D**) and was highly similar to the mRNA expression patterns. The protein expression of the five m6A regulators was down-regulated or up-regulated in tumor tissues (**Figure 7D**). The CPT1A protein showed a positive correlation with HNRNPA2B1 ($R = 0.267$, $P = 0.006$) and LRPPRC ($R = 0.807$, $P < 0.001$), and was negatively correlated with RBMX ($R = -0.206$, $P = 0.035$) and EIF3B ($R = -0.562$, $P < 0.001$). CPT1A was not significantly correlated with HNRNPC (**Figure 7E**). The SIRT5 protein showed a negative correlation with HNRNPC ($R = -0.232$, $P = 0.017$), RBMX ($R = -0.447$, $P < 0.001$) and EIF3B ($R = -0.582$, $P < 0.001$), and a positive correlation with LRPPRC ($R = 0.853$, $P < 0.001$). SIRT5 was not significantly correlated with HNRNPA2B1 (**Figure 7F**). All the significant absolute *R*-values between CPT1A and LRPPRC, CPT1A and EIF3B, SIRT5 and EIF3B, SIRT5 and LRPPRC exceeded 0.5, suggesting that CPT1A and SIRT5 may regulate the expression of m6A regulators. From these data, we inferred that succinylation modification might promote malignant progression in ccRCC by regulating m6A regulators, at least partially by influencing protein expression levels.

Importance of Succinylation Modified m6A Regulators in the Prognosis of ccRCC

As many m6A regulators have been reported to be involved in the initiation and development of tumors, we aimed to test the prognostic predictive values of m6A regulators that may potentially be regulated by succinylation regulators in ccRCC. Global analysis using all 32 m6A regulators showed that 19 were significantly related to the OS of ccRCC patients (**Figure 8A**). To identify more powerful prognostic predictors amongst m6A regulators, we performed the LASSO Cox regression analysis and identified 11 genes

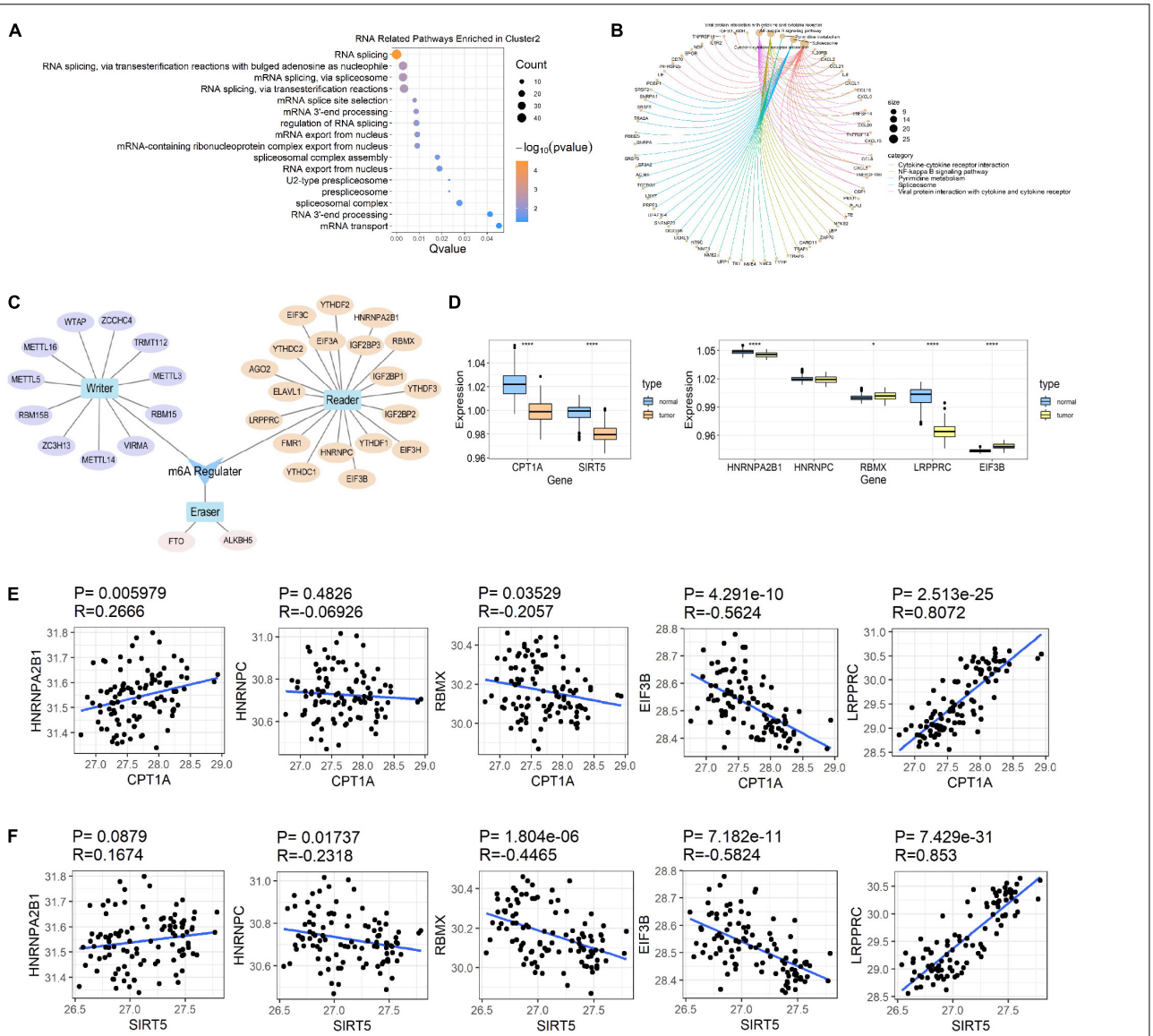

FIGURE 7 | Succinylation regulators might impact the expression of some m6A regulators. **(A)** The bubble diagram displayed of all RNA related GO pathways enriched by up-regulated genes in cluster 2 compared to cluster 3. **(B)** The circle chart showed top 5 KEGG pathways enriched by up-regulated genes in cluster 2 compared to cluster 3. **(C)** A brief summary of 32 m6A regulators reported by high-quality articles. **(D)** The expression patterns of CPT1A, SIRT5, and 5 m6A regulators at protein level between ccRCC and normal tissues (Wilcoxon test), $^{*}P < 0.05$, $^{****}P < 0.0001$. **(E)** The Spearman correlation analysis between the expression of CPT1A and 5 m6A regulators at protein level. **(F)** The Spearman correlation analysis between the protein expression of SIRT5 and 5 m6A regulators at protein level. GO, Gene Ontology; KEGG, Kyoto Encyclopedia of Genes and Genomes.

(LRPPRC, RBM15, YTHDC2, YTHDC1, METTL4, TIF2BP2, HNRNPA2B1, METTL3, IGFBP3, ELAVL1, EIF3B) whose expression levels were associated with prognosis of ccRCC patients (**Figures 8B,C**). Importantly, three m6A regulators modified by succinylation including LRPPRC, EIF3B, and HNRNPA2B1, were present in the 11-gene list. LRPPRC and EIF3B were identified as the most important protective and risk factors with the largest absolute value of coefficients. These results suggested that m6A regulators, particularly those potentially regulated by succinylation regulators, have important prognostic values in ccRCC.

Protein Level Validation of the Correlation Between Succinylation Regulators and Potential Downstream m6A Regulators

To clarify the clinical relevance of our findings, we examined the expression of four succinylation regulators and their potential downstream m6A regulators in 42 pairs of ccRCC tissues and adjacent normal tissues by immunohistochemistry. The staining of CPT1A, SIRT5, and LRPPRC was significantly lower in ccRCC tissues compared to normal tissues, while the staining

TABLE 5 | The succinylation and ubiquitination modified lysine residues among 5 m6A regulators.

Protein	Succinylation modified lysine residue	Overlapped by ubiquitination	Peptides
HNRNPA2B1	120	Yes	KLFVGGIKDTEEHH
HNRNPC	176	Yes	GKSGFNSKGQRGSS
	197	No	GDDLQAIKELTQIK
	204	Yes	KKELTQIKKVDSLL
	223	Yes	KIEKEQSKAVEMKN
	243	Yes	EQSSSSVKDETNVK
	8	Yes	MASNVTNKDPRSMN
RBMX	217	Yes	RDDGYSTKSYSSRD
	30	Yes	ALEAVFGKGRIVEV
LRPPRC	107	Yes	IPKKLLQKFNDTCR
	1121	No	QVRRDYLKAVTTLK
	1224	No	GLAYLFRKIEEQLE
	1326	No	EAYNSLMKYVSEKD
	1332	No	MKSYVSEKVTSAKA
	1357	No	KLDDLFLKYASLLK
	187	Yes	SPTDFLAKEEANIQ
	613	Yes	QYFHQLEKNVKIPE
	649	Yes	AHLLVESKLDFQKT
	750	No	SAVLDTGKVGLVRV
	772	No	QDAINILKMKEKDV
	868	No	VLCKLVEKETDLIQ
	966	Yes	YNLLKLYKNGDWQR
EIF3B	729	Yes	KDLKKYSKFEQKDR

of KAT2A, SIRT7, and EIF3B was higher in ccRCC tissues than in the normal tissues (**Figure 9A**). These observations agreed with our previous analyses (**Figures 1A**, **7D**). Importantly, a correlation analysis showed that the level of CPT1A was positively related to LRPPRC ($R = 0.3781$, $P = 0.0135$), whereas the level of SIRT5 was negatively related to EIF3B ($R = -0.4392$, $P = 0.0036$). No significant correlation was observed between CPT1A and EIF3B ($R = 0.0788$, $P = 0.6198$) or between SIRT5 and LRPPRC ($R = 0.2030$, $P = 0.1972$, **Figure 9B**). By combining the results from the CPTAC online dataset (**Figures 7E,F**) with our own data (**Figure 9B**), we deduced that CPT1A might increase the protein expression of LRPPRC whilst SIRT5 might inhibit the accumulation of EIF3B. Further validation was performed in the ACHN cell line by Western blotting, showing that LRPPRC was down-regulated following the silencing of CPT1A while EIF3B was prominently up-regulated by the knockdown of SIRT5 (**Figure 9C**). In sum, these results supported our bioinformatics analysis results that CPT1A might increase the expression of LRPPRC, while SIRT5 might decrease the expression of EIF3B in ccRCC.

DISCUSSION

In this research, we studied the prognostic predictive value of four succinylation regulators in ccRCC and explored the potential mechanisms of succinylation regulators in the progression of ccRCC. Until now, several studies have reported that CPT1A, SIRT5 and SIRT7 are individually related to the prognosis of ccRCC (Zhao Z. et al., 2019; Tan et al., 2020). Here, we took a comprehensive global analysis of the four succinylation regulators. According to our analyses, CPT1A and SIRT5 served as protective factors whereas SIRT7 acted as a risk factor for ccRCC, and these results were in agreement with previous studies (Zhao Z. et al., 2019; Tan et al., 2020). Also, we found that KAT2A could function as an independent risk factor for the prognosis of ccRCC. Importantly, the nomogram model involving both clinicopathological parameters and RS was superior in predicting long-term OS compared to a traditional model that only contains clinicopathological parameters. Therefore, succinylation regulators, in particular CPT1A and KAT2A, might serve as potential biomarkers for ccRCC due to their superior performance in OS estimation. Direct repression of CPT1A by HIF1 and HIF2 has been reported to reduce the transport of fatty acids into the mitochondria and force fatty acids to form lipid droplets for storage that can promote ccRCC (Du et al., 2017; Tan and Welford, 2020). The data reported in this study are consistent with previous reports, showing that CTP1A expression was down-regulated to promote ccRCC. SIRT5 has been reported to desuccinylate SDHA to promote ccRCC tumorigenesis (Ma et al., 2019). The findings in our study are inconsistent with this previous report as we found that SIRT5 was down-regulated in ccRCC. Nevertheless, succinylation modification is a multienzyme-regulated process in which the substrate protein might be simultaneously modified by several enzymes. Therefore, the investigation of a single succinylation regulator in previous studies may be insufficient to accurately reveal the role of succinylation modification in the development of ccRCC. To better understand the functions of succinylation modification in ccRCC, we analyzed all four succinylation regulators simultaneously to reveal their functions in ccRCC. We used the expression patterns of these regulators for consensus clustering analysis and divided ccRCC patients into three clusters. Similar to the nomogram prognostic model, the three clusters showed prominently different prognosis and clinicopathological characteristics. The patients in cluster 2 were completely included in the patients of the RS-high group, confirming the validity of the consensus clustering analysis. In contrast to the nomogram prognostic model using only CPT1A and KAT2A, the consensus clustering analysis considered the holistic effects of all the regulators and could more precisely reflect their functions in ccRCC. Furthermore, our pathway enrichment analyses of the three clusters suggested that succinylation regulators might play a role in the immune cell infiltration and m6A methylation in ccRCC.

We ascertained the prognostic value and the potential regulatory mechanism of succinylation regulators in ccRCC using a nomogram model and consensus clustering analysis. However, although this study suggested the comprehensive analysis of all the four regulators could help to find out some interesting discovery related to succinylation modification, bioinformatic analysis itself without experimental verification is hard to confirm if the prognostic prediction values of these molecules only

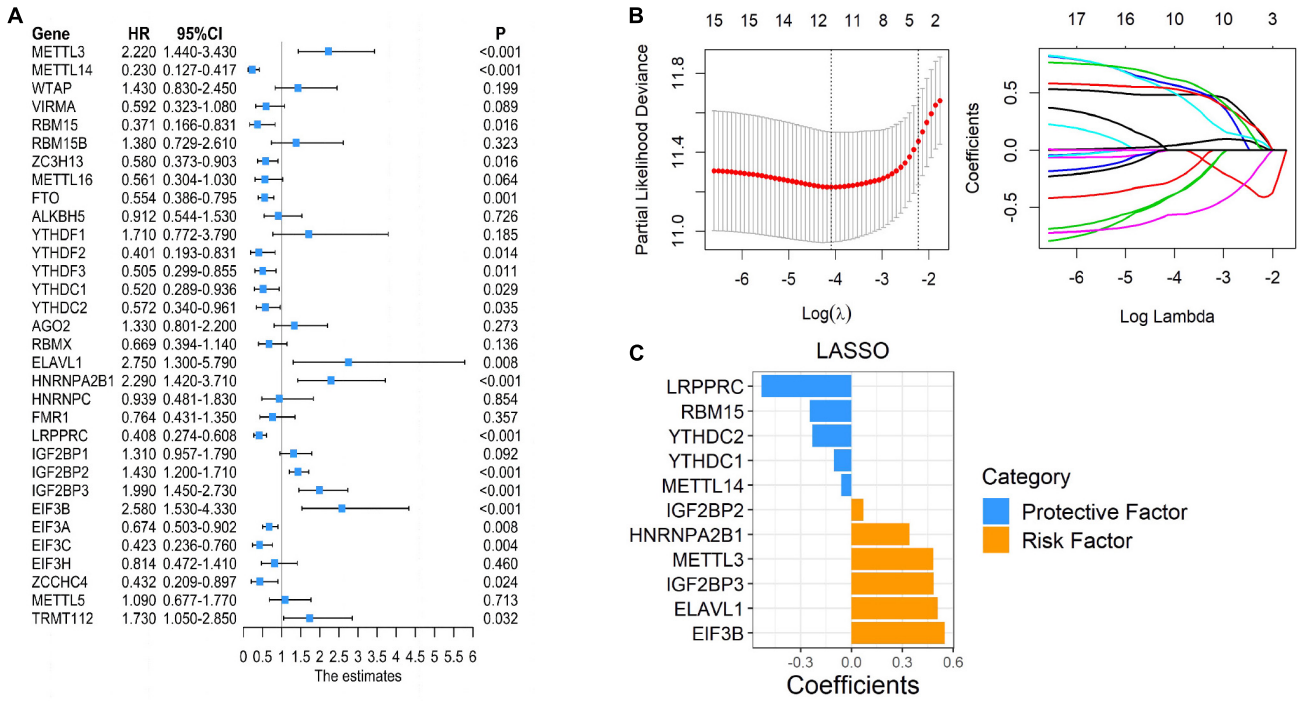

FIGURE 8 | Succinylation-modified m6A regulators play important roles in the prognosis of ccRCC. **(A)** Univariate Cox regression analysis of 32 m6A regulators. **(B,C)** The detailed coefficients calculated by multivariate Cox regression using LASSO.

depend on their succinylation regulatory activity. It is known that succinylation modification is not the only role of the four succinylation regulators. CPT1A is known to be able to regulate the oxidation of fatty acids (Tan and Welford, 2020); KAT2A is considered as classical acetylase both in histone and non-histone proteins, and its role of histone glutaryltransferase has also been discovered recently (Bao et al., 2019; Mutlu and Puigserver, 2020); SIRT5 is confirmed to own strong activity in demalonylase and deglutarylase while weak activity in deacetylase (Yang et al., 2017); SIRT7 acts as an deacetylase asl well as an "eraser" of the glutarylation of histone H4 lysine 91 (Bao et al., 2019). Therefore, more detailed investigations of these complex functions are required in future studies.

Our analyses suggested that the increased infiltration of Tregs in clusters 1 and 2 was associated with relatively short OS. The infiltration of Tregs was associated with poor prognosis and weak treatment response in ccRCC providing strong support for our results (Wang Y. et al., 2019; Pan et al., 2020). Moreover, our analyses implied that infiltration of Tregs in ccRCC might be associated with two desuccinylases, SIRT5 and SIRT7. Our results showed the positive relation of SIRT7 and negative relation of SIRT5 to FOXP3, which is an important marker of Tregs and critical for the immunosuppression function of Tregs. However, it remains unclear how SIRT5 and SIRT7 regulate the infiltration of Tregs. Loss of SIRT5 promotes the transcription of IL-1β in macrophages by increasing the succinylation level of PKM2 and forcing it to be translocated into the nucleus for the formation of the PKM2-HIF1α complex on the IL-1β promoter (Wang F. et al., 2017). As succinylation regulators do not directly regulate mRNA expression, SIRT5 might affect the infiltration of Tregs through immediate molecules such as the PKM2-IL-1β axis in ccRCC. As the accelerated proliferation of Tregs during immuno-therapy is known to reduce the efficacy of anti-PD-1 treatment (Kamada et al., 2019), SIRT5 and SIRT7 might have the potential to predict resistance to anti-PD-1 therapy. Also, the SIRT5 activator or SIRT7 inhibitor might have the potential to improve the efficacy of anti-PD-L1 therapy.

We identified a 6-immune gene signature that included LTB4R, NFKB2, AGER, IGLV3-21, IL20RB, and SAA1. These genes were overexpressed in clusters 1 and 2, and displayed excellent prognosis value in ccRCC. Among the six genes, SAA1 has been reported as a risk factor in ccRCC that can promote the proliferation of Tregs by inducing the secretion of IL-1β and IL-6 from monocyte (Nguyen et al., 2014; Wang Y. et al., 2019). Also, AGER and IL20RB have been reported as tumor promoters in ccRCC (Liu et al., 2020; Shen et al., 2020). LTB4R, NFKBIZ, and IGLV3-21 have not yet been explored in ccRCC. Our study revealed the excellent prognostic value of the 6-immune gene signature, highlighting the key role of succinylation regulators and immune regulation in ccRCC malignancy.

We found that RNA m6A methylation is another major pathway associated with succinylation regulators in ccRCC. RNA m6A methylation is the most widespread regulatory mechanism of RNA modification (Wang S. et al., 2017) and is dynamically regulated by three types of regulators containing "writers," "erasers," and "readers." Writers and erasers contribute to the

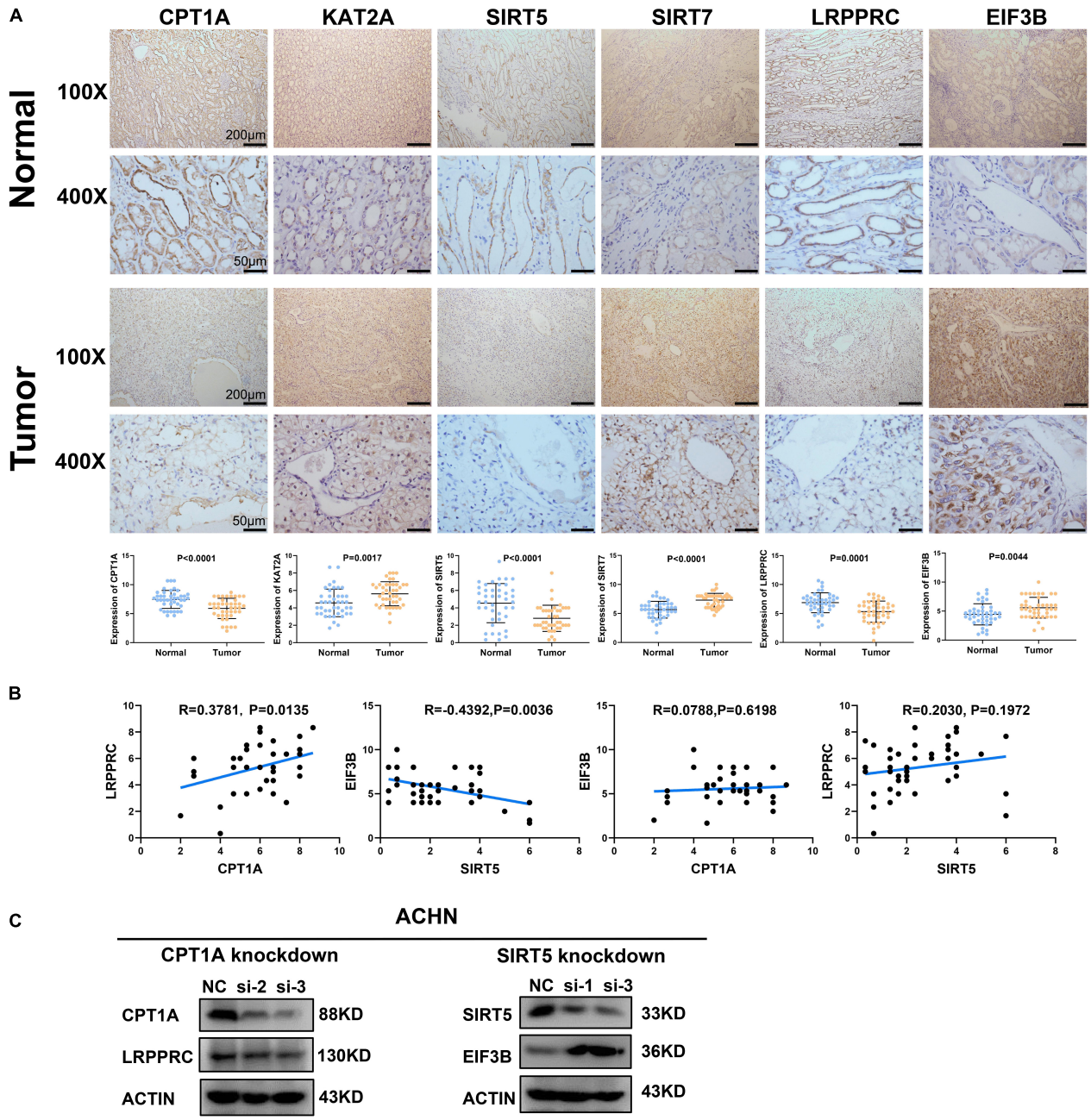

FIGURE 9 | Validation of the correlation between succinylation regulators and m6A regulators at protein level. **(A)** The expression pattern of CPT1A, KAT2A, SIRT5, SIRT7, LRPPRC, and EIF3B between ccRCC tissues and corresponding normal tissues by immunohistochemistry. Error bars show standard error of the mean, and the middle bar represents the median expression level of each molecule. **(B)** The correlation analysis between CPT1A and LRPPRC, SIRT5 and EIF3B, CPT1A and EIF3B, SIRT5 and LRPPRC according to immunohistochemistry scores in 42 ccRCC tissues. **(C)** In ACHN cells, the expression of LRPPRC and EIF3B were detected by western blotting after transient knockdown of CPT1A and SIRT5, respectively.

alteration of m6A methylation levels and readers control the regulatory effects of m6A modification on substrate molecules. RNA m6A methylation plays an important role in cancer development by regulating RNA splicing, stability, mRNA translational efficiency, secondary RNA structure, nuclear export and localization (Zaccara et al., 2019). Our results suggested that enrichment of RNA-related pathways in cluster 2 might be attributed to the regulation of m6A regulators by succinylation regulators. We identified 23 succinylation modified lysine residues among five m6A regulators including HNRHPA2B1, HNRNPC, RBMX, EIF3B, and LRPPRC. Interestingly, the five regulators all belonged to m6A "readers" in which HNRHPA2B1, HNRNPC, and RBMX mainly regulated the process of RNA splicing. These results were consistent with our findings that

RNA splicing and spliceosome ranked as top pathways related to RNA in the GO and KEGG pathway enrichment (**Figures 7A,B**). By correlation analysis using the online ccRCC protein dataset (**Figures 7E,F**), analysis of our tissue specimens (**Figure 9B**) and preliminary validation in the ACHN cell line (**Figure 9C**), we confirmed that CPT1A and SIRT5 could up-regulate and down-regulate the expression of LRPPRC and EIF3B in ccRCC, respectively. We found that 14 of the 23 succinylation-modified lysine residues were also modified by ubiquitination containing five residues in LRPPRC and one residue in EIF3B (**Table 5**). In previous studies, a site-competition mechanism between succinylation and ubiquitination has been reported. For example, succinylation modification of GLS could inhibit ubiquitination via competition for same lysine residues leading to decrescent protein degradation and increscent protein stability (Zhao S. et al., 2019). These data suggest that high succinylation levels might contribute to the stability of proteins. According to this mechanism, we speculated that CPT1A might increase the stability of LRPPRC, while SIRT5 might reduce the stability of EIF3B in a succinylation-ubiquitination competition mechanism. However, these predictions require extensive validation in the laboratory. Our global analysis of 32 m6A regulators is more integral than any other previously published report and showed that succinylation-modified m6A regulators, especially LRPPRC and EIF3B, are important for the prognosis of ccRCC. Our online website and bioinformatic analyses showed the potential connection between succinylation modification and m6A methylation, providing novel insight into the relationships between the two epigenetic modifications. These bioinformatic analyses offer strong clues for future experimental validation.

CONCLUSION

In conclusion, we discovered the prognostic value of succinylation regulators in ccRCC and established a nomogram prediction model, which showed good accuracy. Furthermore, the potential mechanism of succinylation regulators in ccRCC progression was revealed by regulating immune infiltration and RNA m6A methylation (**Supplementary Figure S6**). This study also provides clinical evidence for treatment options.

DATA AVAILABILITY STATEMENT

Publicly available datasets were analyzed in this study. This data can be found here: http://xena.ucsc.edu/, http://cancergemome.nih.gov/, https://proteomics.cancer.gov/programs/cptac.

ETHICS STATEMENT

The studies involving human participants were reviewed and approved by Ethics Committee of the First Hospital of China Medical University. The patients/participants provided their written informed consent to participate in this study.

AUTHOR CONTRIBUTIONS

WL and XC designed the study and performed most of the bioinformatic analyses with the help of YL, JQ, and XQ. CZ, XY, and DW performed the immunohistochemistry and accomplished corresponding analysis. BB and ZL downloaded the datasets and offered suggestions for statistical analysis. YJ, YW, and JX helped to prepare figures and tables. WL wrote the manuscript under the guidance from YL, XC, and JQ. All authors revised, read, and approved the final manuscript.

FUNDING

This study was supported by the National Natural Science Foundation of China (No. 81972751); the Key Research and Development Program of Liaoning Province (2018225060); the Natural Science Foundation of Liaoning Province (2019-ZD-777); Science and Technology Plan Project of Shenyang City (19-112-4-099).

SUPPLEMENTARY MATERIAL

The Supplementary Material for this article can be found online at: https://www.frontiersin.org/articles/10.3389/fcell.2021.622198/full#supplementary-material

REFERENCES

Angulo, J. C., and Shapiro, O. (2019). The changing therapeutic landscape of metastatic renal cancer. *Cancers (Basel).* 11:1227. doi: 10.3390/cancers11091227

Bao, X., Liu, Z., Zhang, W., Gladysz, K., Fung, Y. M. E., Tian, G., et al. (2019). Glutarylation of histone H4 lysine 91 regulates chromatin dynamics. *Mol. Cell* 76, 660–675 e669. doi: 10.1016/j.molcel.2019.08.018

Chen, X. F., Tian, M. X., Sun, R. Q., Zhang, M. L., Zhou, L. S., Jin, L., et al. (2018). SIRT5 inhibits peroxisomal ACOX1 to prevent oxidative damage and is downregulated in liver cancer. *EMBO Rep.* 19:e45124. doi: 10.15252/embr.201745124

Du, W., Zhang, L., Brett-Morris, A., Aguila, B., Kerner, J., Hoppel, C. L., et al. (2017). HIF drives lipid deposition and cancer in ccRCC via repression of fatty acid metabolism. *Nat. Commun.* 8:1769. doi: 10.1038/s41467-017-01965-8

Friedman, J., Hastie, T., and Tibshirani, R. (2010). Regularization paths for generalized linear models via coordinate descent. *J. Stat. Softw.* 33, 1–22. doi: 10.18637/jss.v033.i01

Greene, K. S., Lukey, M. J., Wang, X., Blank, B., Druso, J. E., Lin, M.-c. J., et al. (2019). SIRT5 stabilizes mitochondrial glutaminase and supports breast cancer tumorigenesis. *Proc. Natl. Acad. Sci. U.S.A* 116, 26625–26632. doi: 10.1073/pnas.1911954116

Kamada, T., Togashi, Y., Tay, C., Ha, D., Sasaki, A., Nakamura, Y., et al. (2019). PD-1(+) regulatory T cells amplified by PD-1 blockade promote hyperprogression of cancer. *Proc. Natl. Acad. Sci. U.S.A.* 116, 9999–10008. doi: 10.1073/pnas.1822001116

Kapp, A. V., and Tibshirani, R. (2007). Are clusters found in one dataset present in another dataset? *Biostatistics* 8, 9–31. doi: 10.1093/biostatistics/kxj029

Kumar, S., and Lombard, D. B. (2018). Functions of the sirtuin deacylase SIRT5 in normal physiology and pathobiology. *Crit. Rev.*

Biochem. Mol. Biol. 53, 311–334. doi: 10.1080/10409238.2018.1458071

Kurmi, K., Hitosugi, S., Wiese, E. K., Boakye-Agyeman, F., Gonsalves, W. I., Lou, Z., et al. (2018). Carnitine palmitoyltransferase 1A has a lysine succinyltransferase activity. *Cell Rep.* 22, 1365–1373. doi: 10.1016/j.celrep.2018.01.030

Li, B., Cui, Y., Nambiar, D. K., Sunwoo, J. B., and Li, R. (2019). The immune subtypes and landscape of squamous cell carcinoma. *Clin. Cancer Res.* 25, 3528–3537. doi: 10.1158/1078-0432.CCR-18-4085

Li, Q. K., Pavlovich, C. P., Zhang, H., Kinsinger, C. R., and Chan, D. W. (2019). Challenges and opportunities in the proteomic characterization of clear cell renal cell carcinoma (ccRCC): a critical step towards the personalized care of renal cancers. *Semin. Cancer Biol.* 55, 8–15. doi: 10.1016/j.semcancer.2018.06.004

Lin, Z. F., Xu, H. B., Wang, J. Y., Lin, Q., Ruan, Z., Liu, F. B., et al. (2013). SIRT5 desuccinylates and activates SOD1 to eliminate ROS. *Biochem. Biophys. Res. Commun.* 441, 191–195. doi: 10.1016/j.bbrc.2013.10.033

Liu, Q., Zhang, X., Tang, H., Liu, J., Fu, C., Sun, M., et al. (2020). Bioinformatics analysis suggests the combined expression of AURKB and KIF18B being an important event in the development of clear cell renal cell carcinoma. *Pathol. Oncol. Res.* 26, 1583–1594. doi: 10.1007/s12253-019-00740-y

Ma, Y., Qi, Y., Wang, L., Zheng, Z., Zhang, Y., and Zheng, J. (2019). SIRT5-mediated SDHA desuccinylation promotes clear cell renal cell carcinoma tumorigenesis. *Free Radic. Biol. Med.* 134, 458–467. doi: 10.1016/j.freeradbiomed.2019.01.030

Makhov, P., Joshi, S., Ghatalia, P., Kutikov, A., Uzzo, R. G., and Kolenko, V. M. (2018). Resistance to systemic therapies in clear cell renal cell carcinoma: mechanisms and management strategies. *Mol. Cancer Ther.* 17, 1355–1364. doi: 10.1158/1535-7163.MCT-17-1299

Mutlu, B., and Puigserver, P. (2020). GCN5 acetyltransferase in cellular energetic and metabolic processes. *Biochim. Biophys. Acta Gene Regul. Mech.* 1864:194626. doi: 10.1016/j.bbagrm.2020.194626

Newman, A. M., Liu, C. L., Green, M. R., Gentles, A. J., Feng, W., Xu, Y., et al. (2015). Robust enumeration of cell subsets from tissue expression profiles. *Nat Methods* 12, 453–457. doi: 10.1038/nmeth.3337

Nguyen, K. D., Macaubas, C., Truong, P., Wang, N., Hou, T., Yoon, T., et al. (2014). Serum amyloid A induces mitogenic signals in regulatory T cells via monocyte activation. *Mol. Immunol.* 59, 172–179. doi: 10.1016/j.molimm.2014.02.011

Pan, Q., Wang, L., Chai, S., Zhang, H., and Li, B. (2020). The immune infiltration in clear cell renal cell carcinoma and their clinical implications: a study based on TCGA and GEO databases. *J. Cancer* 11, 3207–3215. doi: 10.7150/jca.37285

Ritchie, M. E., Phipson, B., Wu, D., Hu, Y., Law, C. W., Shi, W., et al. (2015). limma powers differential expression analyses for RNA-sequencing and microarray studies. *Nucleic Acids Res.* 43:e47. doi: 10.1093/nar/gkv007

Shen, C., Liu, J., Wang, J., Zhong, X., Dong, D., Yang, X., et al. (2020). Development and validation of a prognostic immune-associated gene signature in clear cell renal cell carcinoma. *Int. Immunopharmacol.* 81:106274. doi: 10.1016/j.intimp.2020.106274

Shuch, B., Amin, A., Armstrong, A. J., Eble, J. N., Ficarra, V., Lopez-Beltran, A., et al. (2015). Understanding pathologic variants of renal cell carcinoma: distilling therapeutic opportunities from biologic complexity. *Eur. Urol.* 67, 85–97. doi: 10.1016/j.eururo.2014.04.029

Siegel, R. L., Miller, K. D., and Jemal, A. (2017). Cancer statistics, 2017. *CA Cancer J. Clin.* 67, 7–30. doi: 10.3322/caac.21387

Tan, S. K., and Welford, S. M. (2020). Lipid in renal carcinoma: queen bee to target? *Trends Cancer* 6, 448–450. doi: 10.1016/j.trecan.2020.02.017

Tan, Y., Li, B., Peng, F., Gong, G., and Li, N. (2020). Integrative analysis of sirtuins and their prognostic significance in clear cell renal cell carcinoma. *Front. Oncol.* 10:218. doi: 10.3389/fonc.2020.00218

Tong, Y., Guo, D., Yan, D., Ma, C., Shao, F., Wang, Y., et al. (2020). KAT2A succinyltransferase activity-mediated 14-3-3zeta upregulation promotes beta-catenin stabilization-dependent glycolysis and proliferation of pancreatic carcinoma cells. *Cancer Lett.* 469, 1–10. doi: 10.1016/j.canlet.2019.09.015

Wang, C., Zhang, C., Li, X., Shen, J., Xu, Y., Shi, H., et al. (2018). CPT1A-mediated succinylation of S100A10 increases human gastric cancer invasion. *J. Cell. Mol. Med.* 23, 293–305. doi: 10.1111/jcmm.13920

Wang, F., Wang, K., Xu, W., Zhao, S., Ye, D., Wang, Y., et al. (2017). SIRT5 desuccinylates and activates pyruvate kinase M2 to block macrophage IL-1beta production and to prevent DSS-induced colitis in mice. *Cell Rep.* 19, 2331–2344. doi: 10.1016/j.celrep.2017.05.065

Wang, S., Sun, C., Li, J., Zhang, E., Ma, Z., Xu, W., et al. (2017). Roles of RNA methylation by means of N(6)-methyladenosine (m(6)A) in human cancers. *Cancer Lett.* 408, 112–120. doi: 10.1016/j.canlet.2017.08.030

Wang, Y., Guo, Y. R., Liu, K., Yin, Z., Liu, R., Xia, Y., et al. (2017). KAT2A coupled with the alpha-KGDH complex acts as a histone H3 succinyltransferase. *Nature* 552, 273–277. doi: 10.1038/nature25003

Wang, Y., Yang, J., Zhang, Q., Xia, J., and Wang, Z. (2019). Extent and characteristics of immune infiltration in clear cell renal cell carcinoma and the prognostic value. *Transl. Androl. Urol.* 8, 609–618. doi: 10.21037/tau.2019.10.19

Wilkerson, M. D., and Hayes, D. N. (2010). ConsensusClusterPlus: a class discovery tool with confidence assessments and item tracking. *Bioinformatics* 26, 1572–1573. doi: 10.1093/bioinformatics/btq170

Xiangyun, Y., Xiaomin, N., linping, G., Yunhua, X., Ziming, L., Yongfeng, Y., et al. (2017). Desuccinylation of pyruvate kinase M2 by SIRT5 contributes to antioxidant response and tumor growth. *Oncotarget* 24, 6984–6993. doi: 10.18632/oncotarget.14346

Yang, L., Ma, X., He, Y., Yuan, C., Chen, Q., Li, G., et al. (2017). Sirtuin 5: a review of structure, known inhibitors and clues for developing new inhibitors. *Sci. China Life Sci.* 60, 249–256. doi: 10.1007/s11427-016-0060-7

Yu, G., Wang, L. G., Han, Y., and He, Q. Y. (2012). clusterProfiler: an R package for comparing biological themes among gene clusters. *OMICS* 16, 284–287. doi: 10.1089/omi.2011.0118

Zaccara, S., Ries, R. J., and Jaffrey, S. R. (2019). Reading, writing and erasing mRNA methylation. *Nat. Rev. Mol. Cell. Biol.* 20, 608–624. doi: 10.1038/s41580-019-0168-5

Zhao, S., Wang, J. M., Yan, J., Zhang, D. L., Liu, B. Q., Jiang, J. Y., et al. (2019). BAG3 promotes autophagy and glutaminolysis via stabilizing glutaminase. *Cell Death Dis.* 10:284. doi: 10.1038/s41419-019-1504-6

Zhao, Z., Liu, Y., Liu, Q., Wu, F., Liu, X., Qu, H., et al. (2019). The mRNA expression signature and prognostic analysis of multiple fatty acid metabolic enzymes in clear cell renal cell carcinoma. *J. Cancer* 10, 6599–6607. doi: 10.7150/jca.33024

Conflict of Interest: The authors declare that the research was conducted in the absence of any commercial or financial relationships that could be construed as a potential conflict of interest.

frontiers in Cell and Developmental Biology

REVIEW
published: 26 February 2021
doi: 10.3389/fcell.2021.656993

Critical Roles of PIWIL1 in Human Tumors: Expression, Functions, Mechanisms, and Potential Clinical Implications

Peixin Dong[1†], Ying Xiong[2†], Yosuke Konno[1*], Kei Ihira[1], Daozhi Xu[1], Noriko Kobayashi[1], Junming Yue[3,4] and Hidemichi Watari[1]*

[1] Department of Obstetrics and Gynecology, Hokkaido University School of Medicine, Hokkaido University, Sapporo, Japan, [2] State Key Laboratory of Oncology in South China, Department of Gynecology, Sun Yat-sen University Cancer Center, Guangzhou, China, [3] Department of Pathology and Laboratory Medicine, University of Tennessee Health Science Center, Memphis, TN, United States, [4] Center for Cancer Research, University of Tennessee Health Science Center, Memphis, TN, United States

OPEN ACCESS

Edited by:
Xiao Zhu,
Guangdong Medical University, China

Reviewed by:
Guoxin Zhang,
University of California, San Diego, United States
Xuan Cui,
Columbia University Irving Medical Center, United States

***Correspondence:**
Peixin Dong
dpx1cn@gmail.com
Yosuke Konno
konsuke013@gmail.com

[†] These authors have contributed equally to this work

Specialty section:
This article was submitted to Epigenomics and Epigenetics, a section of the journal Frontiers in Cell and Developmental Biology

Received: 21 January 2021
Accepted: 11 February 2021
Published: 26 February 2021

Citation:
Dong P, Xiong Y, Konno Y, Ihira K, Xu D, Kobayashi N, Yue J and Watari H (2021) Critical Roles of PIWIL1 in Human Tumors: Expression, Functions, Mechanisms, and Potential Clinical Implications. Front. Cell Dev. Biol. 9:656993. doi: 10.3389/fcell.2021.656993

P-element-induced wimpy testis (PIWI)-interacting RNAs (piRNAs) are a class of small non-coding RNA molecules that are 24–31 nucleotides in length. PiRNAs are thought to bind to PIWI proteins (PIWL1-4, a subfamily of Argonaute proteins), forming piRNA/PIWI complexes that influence gene expression at the transcriptional or post-transcriptional levels. However, it has been recently reported that the interaction of PIWI proteins with piRNAs does not encompass the entire function of PIWI proteins in human tumor cells. PIWIL1 (also called HIWI) is specifically expressed in the testis but not in other normal tissues. In tumor tissues, PIWIL1 is frequently overexpressed in tumor tissues compared with normal tissues. Its high expression is closely correlated with adverse clinicopathological features and shorter patient survival. Upregulation of PIWIL1 drastically induces tumor cell proliferation, epithelial-mesenchymal transition (EMT), invasion, cancer stem-like properties, tumorigenesis, metastasis and chemoresistance, probably via piRNA-independent mechanisms. In this article, we summarize the current existing literature on PIWIL1 in human tumors, including its expression, biological functions and regulatory mechanisms, providing new insights into how the dysregulation of PIWIL1 contributes to tumor initiation, development and chemoresistance through diverse signaling pathways. We also discuss the most recent findings on the potential clinical applications of PIWIL1 in cancer diagnosis and treatment.

Keywords: piRNA, PIWIL1, HIWI, tumorigenesis, cancer metastasis, prognostic biomarker, EMT, chemoresistance

INTRODUCTION

P-element-induced wimpy testis (PIWI)-interacting RNAs (piRNAs) are small (24–31 nucleotides), single-stranded non-coding RNAs with 2′-O-methylated at their 3′ ends (Ng et al., 2016; Wang et al., 2019; Yu et al., 2019). According to their origins, piRNAs can be divided into three classes: transposon-derived piRNAs, mRNA-derived piRNAs, and lncRNA-derived piRNAs (Weick and Miska, 2014; Ozata et al., 2019; Guo et al., 2020). Transposon-derived piRNAs are typically

transcribed from both genomic strands and silence transposons (Weick and Miska, 2014; Ozata et al., 2019; Guo et al., 2020). MRNA-derived piRNAs originate from the 3′-untranslated regions (3′-UTRs) of mRNAs (Weick and Miska, 2014; Ozata et al., 2019; Guo et al., 2020). Long non-coding RNA (lncRNA)-derived piRNAs often come from intergenic lncRNAs (Weick and Miska, 2014; Ozata et al., 2019; Guo et al., 2020). The biogenesis of piRNAs is involved in two major mechanisms: the primary synthesis mechanism and a secondary amplification pathway (also referred to as the "ping-pong" amplification cycle) (Weick and Miska, 2014; Ozata et al., 2019; Guo et al., 2020). The primary piRNAs are produced through the primary processing pathway, and the abundance of pre-existing piRNAs can be amplified through the "ping-pong" amplification cycle (Weick and Miska, 2014; Ozata et al., 2019; Guo et al., 2020).

PiRNAs are initially discovered in germline (Yu et al., 2019). Studies of animals suggested that silencing transposons in germline tissues is the ancestral function of piRNAs (Weick and Miska, 2014; Ozata et al., 2019; Guo et al., 2020). It was shown that piRNAs silence transposons transcriptionally by silencing transposon loci, as well as post-transcriptionally by triggering degradation of their transcripts (Weick and Miska, 2014; Ozata et al., 2019; Guo et al., 2020). However, many piRNAs expressed in the mammalian testis map to genome-unique sequences, which are not related to transposable elements (Weick and Miska, 2014; Ozata et al., 2019; Guo et al., 2020), indicating that the biological functions of piRNAs may extend beyond transposon control. In humans, more than 35,356 piRNAs have been found (Wang et al., 2019; Yu et al., 2019), and they are expressed in human somatic cells in a tissue-specific manner (Wang et al., 2019; Yu et al., 2019). Recent studies revealed that piRNAs post-transcriptionally regulate gene expression in microRNA (miRNA)-like manner, thereby participating in the pathogenesis of human cancer (Lu et al., 2010; Liu et al., 2019). The aberrant expression of piRNAs has been demonstrated in various cancer types (Cheng et al., 2011; Huang et al., 2013; Chu et al., 2015). Numerous studies have found that dysregulated piRNAs affect cancer hallmarks for tumor initiation and progression (Yu et al., 2019).

The Argonaute protein family members are ∼100 kDa highly basic proteins that are highly conserved between species (Carmell et al., 2002; Wu et al., 2020). Argonaute proteins can be separated according to the sequence into two subclasses: AGO and PIWI (Parker and Barford, 2006). Argonaute proteins regulate gene expression at both transcriptional and posttranscriptional levels by providing anchor sites for small regulatory RNAs (Parker and Barford, 2006; Wu et al., 2020). In contrast to AGO proteins that are ubiquitously expressed and interact with miRNAs and siRNAs, PIWI proteins (PIWIL1, PIWIL2, PIWIL3, and PIWIL4) are mainly expressed in germ cells, but usually absent in somatic tissues (Qiao et al., 2002; O'Donnell and Boeke, 2007). PIWI proteins use piRNAs as sequence-specific guides to form the piRNA-induced silencing complex, resulting in RNA degradation and epigenetic silencing (Tian et al., 2011; Meister, 2013).

The *PIWIL1* (also called HIWI) gene was first discovered in Drosophila (Cox et al., 1998) and fully identified in a human testis cDNA library (Qiao et al., 2002). *PIWIL1* is located on human chromosome 12q24.33 and encodes an 861-amino acid protein. The PIWIL1 protein contains two characteristic protein domains, namely PAZ domain and PIWI domains (Parker and Barford, 2006). In human testis, PIWIL1 was found to be expressed in late-pachytene spermatocytes and round/elongating spermatids (Hempfling et al., 2017), indicating a potential role for PIWIL1 in human spermatogenesis.

Importantly, overexpression of the *PIWIL1* gene is common to many tumor types (Suzuki et al., 2012), and its aberrant overexpression has been associated with tumorigenesis, tumor development and poor prognosis in different tumors (Suzuki et al., 2012; Tan et al., 2015). Growing evidence showed that PIWIL1 tends to exhibit tumor-promoting roles in sustaining tumor cell proliferation and activating invasion and metastasis (Suzuki et al., 2012; Tan et al., 2015). Although the molecular basis underlying the oncogenic functions of PIWIL1 remains largely unknown, PIWIL1 has been recently found to regulate the occurrence and progression of human cancers possibly through piRNA-independent mechanisms (Genzor et al., 2019; Li et al., 2020; Shi et al., 2020). Given that the expression of PIWIL1 is mostly restricted to the testis (Qiao et al., 2002) and broadly elevated in various tumors, PIWIL1 has the potential to be ideal targets for cancer diagnosis and therapy. Here, we review the most recent studies on PIWIL1, including its abnormal expression, cellular functions, mechanisms, along with its potentials as a biomarker for cancer diagnosis, prognosis evaluation, and a molecular target that enables the design of novel therapeutic strategies.

DYSREGULATION OF PIWIL1 IN TUMOR

Northern blot analysis of *PIWIL1* mRNA in a series of adult human normal tissues confirmed that *PIWIL1* is expressed abundantly in the testis, but undetectable in the spleen, thymus, prostate, ovary, small intestine, colon tissue and peripheral blood leukocytes (Qiao et al., 2002). Consistent with the proposed tumor-promoting role of PIWL1 during tumorigenesis and tumor progression, PIWIL1 can be overexpressed in many different types of tumor (**Table 1**), including gastric cancer (Liu et al., 2006; Wang et al., 2012; Gao et al., 2018), soft-tissue sarcoma (Taubert et al., 2007), esophageal squamous cell carcinoma (He et al., 2009), endometrial cancer (Liu et al., 2010b), colon cancer (Li L. et al., 2010; Litwin et al., 2015; Wang H.L. et al., 2015; Sun et al., 2017), cervical cancer (Li S. et al., 2010; Liu et al., 2010a), glioma (Sun et al., 2011), hepatocellular carcinoma (Jiang et al., 2011; Zhao et al., 2012), ovarian cancer (Li S. et al., 2010; Chen et al., 2013), breast cancer (Li S. et al., 2010; Wang D.W. et al., 2014; Cao et al., 2016; Litwin et al., 2018), bladder cancer (Eckstein et al., 2018), and renal cell carcinoma (Stöhr et al., 2019). However, real-time PCR analysis of renal cell carcinoma and non-tumor renal parenchyma tissues found a significant downregulation of *PIWIL1* in renal cell carcinoma tissues (Iliev et al., 2016).

TABLE 1 | The association between *PIWIL1* expression and clinicopathological factors of tumor.

Cancer type	No.	Method	Expression	Clinical factors					References
				Size	Stage/grade	Invasion depth	LN meta/recurrence	Survival	
Gastric cancer	50	IHC	Upregulation	–	–	–	–	–	Liu et al., 2006
Gastric cancer	182	Tissue microarray	Upregulation	–	–	–	–	Poor	Wang et al., 2012
Gastric cancer	120	IHC	Upregulation	–	+	+	+	Poor	Gao et al., 2018
Soft-tissue sarcoma	65	qPCR	–	–	–	–	–	Poor	Taubert et al., 2007
Esophageal squamous cell carcinoma	137	IHC	Upregulation	–	+	–	+	Poor	He et al., 2009
Endometrial cancer	64	IHC	Upregulation	–	–	–	–	–	Liu et al., 2010b
Colon cancer	75	IHC	Upregulation	–	–	–	–	–	Li L. et al., 2010
Colon cancer	178	IHC	Upregulation	–	+	–	+	–	Wang H.L. et al., 2015
Colon cancer	110	IHC	Upregulation	–	+	+	+	Poor	Sun et al., 2017
Colon cancer	72	qPCR	Upregulation	–	+	+	–	–	Litwin et al., 2015
Cervical cancer	59	IHC	Upregulation	–	+	–	+	–	Liu et al., 2010a
Cervical, breast, ovarian and endometrial cancer	–	IHC	Upregulation	–	–	–	–	–	Li S. et al., 2010
Glioma	66	IHC	–	–	+	–	–	Poor	Sun et al., 2011
Hepatocellular carcinoma	92	IHC	Upregulation	–	–	–	+	Poor	Jiang et al., 2011
Hepatocellular carcinoma	336	IHC	Upregulation	+	–	–	+	Poor	Zhao et al., 2012
Ovarian cancer	20	IHC	Upregulation	–	–	–	–	–	Chen et al., 2013
Breast cancer	240	Western blot	Upregulation	+	+	–	+	–	Wang D.W. et al., 2014
Breast cancer	27	qPCR/western blot	Upregulation	–	–	–	–	Poor	Cao et al., 2016
Breast cancer	101	IHC	Upregulation	–	–	–	–	–	Litwin et al., 2018
Bladder cancer	95	IHC	–	–	–	–	+	Poor	Eckstein et al., 2018
Renal cell carcinoma	610	Tissue microarray/IHC	–	–	+	+	+	Poor	Stöhr et al., 2019
Renal cell carcinoma	57	qPCR	Downregulation	–	–	–	–	Better	Iliev et al., 2016

LN meta, lymph node metastasis.

The mRNA expression of *PIWIL1* in different types of tumors was explored using the Oncomine database[1]. Twelve studies showed significant differences in *PIWIL1* mRNA expression between tumor and normal tissues (**Figure 1A**). The expression levels of *PIWIL1* were significantly increased in esophageal cancer, gastric cancer, head and neck cancer, kidney cancer, pancreatic cancer, and prostate cancer tissues compared with respective normal tissues (**Figure 1A**).

When looking at all cancer types in the TCGA data sets from the cBioPortal database[2], the *PIWIL1* gene is amplified in many tumors, in line with a tumor-promoting role (**Figure 1B**). Amplifications are more frequent in diffuse glioma, sarcoma, pheochromocytoma, ovarian cancer, bladder cancer, cervical cancer, esophageal squamous cell carcinoma, and renal non-clear cell carcinoma (**Figure 1B**). These results suggest that *PIWIL1* dysregulation is frequently occurring in human tumor tissues and *PIWIL1* might serve as a novel biomarker in several malignancies.

In melanoma, endometrial cancer, mature B-cell neoplasms, non-small cell lung cancer, colon cancer, bladder cancer, invasive breast cancer, esophagogastric adenocarcinoma and head and neck cancer, *PIWIL1* is often mutated (**Figure 1B**). Consistently, data from the IntOGen database[3] revealed that 362 *PIWIL1* mutations were found in 28,076 samples of various cancers, including a range of mutation types (such as missense and truncating mutations).

[1]https://www.oncomine.org

[2]https://www.cbioportal.org

[3]https://www.intogen.org/search

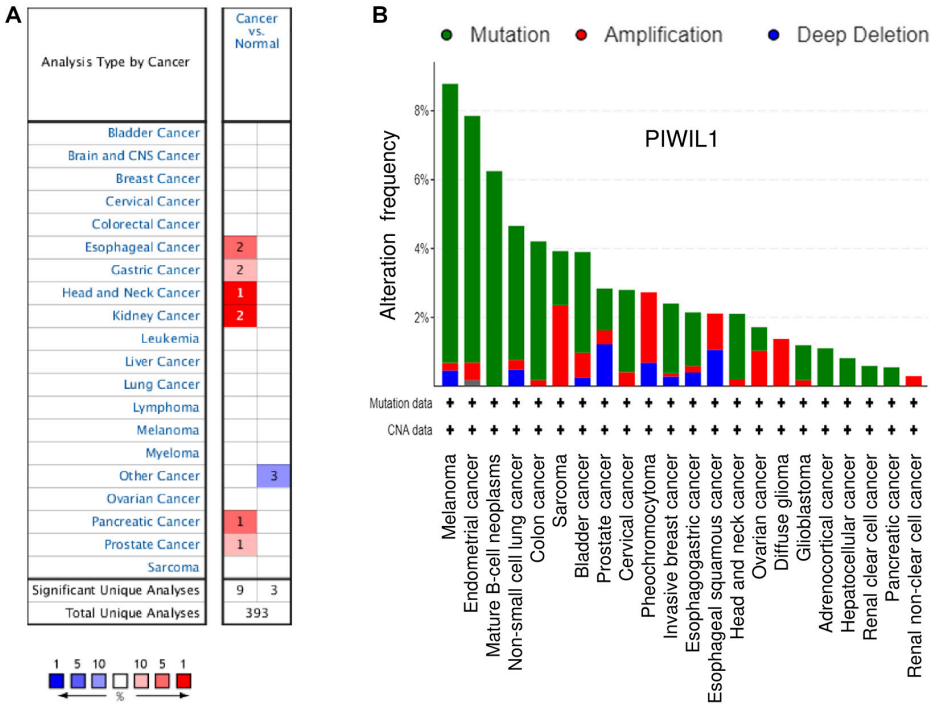

FIGURE 1 | The expression of *PIWIL1* in different types of tumors. **(A)** Comparison of *PIWIL1* mRNA levels in different tumors and in normal tissues according to the Oncomine database (https://www.oncomine.org). Red: upregulation; blue: downregulation. **(B)** Analysis of genetic alterations in *PIWIL1* in human tumor tissues using the Cancer Genome Atlas (TCGA) data retrieved from the cBioPortal database (https://www.cbioportal.org). Data are represented as a stacked histogram plot. Colors represent different types of alterations as indicated in the legend. Shown is the "Cancer Types Summary" where green indicates mutation, red indicates amplification, and blue indicates deletion.

IMPLICATIONS OF PIWIL1 EXPRESSION IN CANCER DIAGNOSIS AND PROGNOSTIC EVALUATION

Dysregulation of PIWIL1 occurs in a broad range of human cancers and is often associated with adverse clinicopathological features and shorter survival of cancer patients. For example, PIWIL1 expression is progressively increased in normal gastric tissues, atrophic gastritis, intestinal metaplasia and gastric cancer tissues (Liu et al., 2006), holding diagnostic potentials for improving early gastric cancer detection. Similarly, positive PIWIL1 expression in normal tissues, colonic adenoma and colon cancer was 11.1% (5/45), 53.7% (22/41), and 80.4% (74/92), respectively (Wang H.L. et al., 2015). Also, a study of normal cervical tissues, high-grade squamous intraepithelial lesions (HSILs) and cervical cancer samples showed a significantly higher frequency of PIWIL1 protein expression in HSILs and cervical cancer tissues when compared with that in the normal cervical epithelium (Liu et al., 2014). Another study observed that the protein levels of PIWIL1 increase in a stepwise manner in normal endometrium, endometrial atypical hyperplasia and endometrial cancer tissues (Chen et al., 2015a). Overexpression of PIWIL1 is an early event in colon carcinogenesis, since it is significantly upregulated from the earliest stages (I and II) of colon cancer progression compared to normal colon tissues (Sellitto et al., 2019). These studies indicate that PIWIL1 levels could be correlated with tumor progression and may be used to facilitate early cancer diagnosis.

High PIWIL1 expression was associated with higher histological grade and advanced tumor stage in different types of tumors, such as esophageal cancer (He et al., 2009), glioma (Sun et al., 2011), breast cancer (Wang D.W. et al., 2014), and renal cell carcinoma (Stöhr et al., 2019), linking its expression to de-differentiation and the progression of the tumor phenotypes. For several cancers, the expression of PIWIL1 expression at different stages of cancer has been examined (He et al., 2009; Liu et al., 2010a, 2014; Chen et al., 2015a; Wang H.L. et al., 2015; Sun et al., 2017; Stöhr et al., 2019). For instance, in esophageal cancer (He et al., 2009), colon cancer (Wang H.L. et al., 2015; Sun et al., 2017), cervical cancer (Liu et al., 2010a, 2014), renal cell carcinoma (Stöhr et al., 2019), and endometrial cancer (Chen et al., 2015a), PIWIL1 levels were significantly increased in late-stage tumors than in early stage tumors. Moreover, an induced expression of PIWIL1 has been linked to lymph node metastasis in patients with gastric cancer (Wang et al., 2012; Gao et al., 2018), colon cancer (Sun et al., 2017), hepatocellular carcinoma (Jiang et al., 2011; Zhao et al., 2012), breast cancer (Wang D.W. et al., 2014), bladder cancer (Eckstein et al., 2018), renal cell carcinoma (Stöhr et al., 2019), and endometrial cancer (Chen et al., 2015a). These findings demonstrate that high PIWIL1 expression might be considered as a useful marker for an aggressive phenotype of several malignancies.

Furthermore, PIWIL1 was found to be a poor prognostic factor in several tumors, including gastric cancer (Wang et al., 2012; Gao et al., 2018), soft-tissue sarcoma (Taubert et al., 2007), esophageal squamous cell carcinoma (He et al., 2009), colon cancer (Sun et al., 2017), glioma (Sun et al., 2011), hepatocellular carcinoma (Jiang et al., 2011; Zhao et al., 2012), breast cancer (Cao et al., 2016), bladder cancer (Eckstein et al., 2018), and renal cell carcinoma (Stöhr et al., 2019). However, a study in patients with renal cell carcinoma showed that high PIWIL1 expression is correlated with better prognosis (Iliev et al., 2016).

Our Kaplan-Meier analysis using the KM plotter database[4] established a close association of *PIWIL1* expression with unfavorable patient survival. Higher *PIWIL1* mRNA expression is significantly correlated to worsen overall survival for patients with breast cancer, renal cell carcinoma, rectum adenocarcinoma and sarcoma (**Figure 2**). Thus, the identification of aberrant PIWIL1 expression in tumor tissues might be useful in cancer diagnosis as well as in prognostic evaluation.

MECHANISMS OF *PIWIL1* DYSREGULATION IN TUMOR

Multiple transcriptional and post-transcriptional mechanisms by which PIWIL1 is inappropriately overexpressed in tumors have been summarized (**Figure 3**). Activation of the RASSF1C/MEK/ERK pathway has been shown to induce PIWIL1 expression in non-small cell lung cancer cells (Reeves et al., 2012). In addition, aberrant promoter DNA hypomethylation is one of the major mechanisms for PIWIL1 overexpression in lung cancer (Xie et al., 2018) and endometrial cancer (Chen et al., 2020). In endometrial cancer cells, estrogen was shown to enhance the transcription of *PIWIL1* by facilitating the binding of the ERα to the *PIWIL1* promoter (Chen et al., 2020). A positive correlation between HPV16 E7 and PIWIL1 was detected in cervical cancer tissues, although the related mechanism has not yet been described (Liu et al., 2010a).

Genome projects have shown that functional products encoded by the genome are not limited to proteins, but include a large number of biologically meaningful non-coding RNAs, such as miRNAs, circular RNAs (circRNAs) and lncRNAs (Anastasiadou et al., 2018; Yamamura et al., 2018). MiRNAs are known to target 3′-UTRs in mRNAs, thereby silencing gene expression at the post-transcriptional level (Anastasiadou et al., 2018; Yamamura et al., 2018; Xu et al., 2020). MiRNAs also interact with circRNAs and lncRNAs to regulate their stability (Anastasiadou et al., 2018; Yamamura et al., 2018). Owing to their functions in the regulation of gene expression, non-coding RNAs regulate multiple biological processes, such as cancer (Anastasiadou et al., 2018; Yamamura et al., 2018; Xu et al., 2020). The expression of PIWIL1 could be regulated by different miRNAs at the post-transcriptional level. MiR-154-5p directly targets PIWIL1 and decreases its expression in glioblastoma (Wang et al., 2017) and glioma (Zhou et al., 2020). In addition to miRNAs, lncRNA FALEC has been implicated in the regulation of PIWIL1 expression in colon cancer cells (Jiang et al., 2020). This study demonstrated that depletion of FALEC by shRNA could significantly decrease the proliferation, migration, invasion, angiogenesis and tumorigenesis of colon cancer cells, whereas these inhibitory effects were largely counteracted by ectopic PIWIL1 overexpression (Jiang et al., 2020). Furthermore, lncRNA FALEC induces PIWIL1 expression by serving as a molecular sponge for miR-2116-3p, which directly binds to the 3′-UTR of *PIWIL1* mRNA (Jiang et al., 2020).

[4]http://kmplot.com

ROLE OF PIWIL1 IN TUMORIGENESIS AND TUMOR PROGRESSION AND POSSIBLE MECHANISMS

Extensive studies have uncovered an important oncogenic role for PIWIL1 in cancer tumor initiation, progression and metastasis (Liu et al., 2006, 2014; Siddiqi et al., 2012; Wang et al., 2012, 2017; Zhao et al., 2012; Liang et al., 2013; Wang D.W. et al., 2014; Wang X. et al., 2014; Chen et al., 2015a; Li et al., 2015, 2020; Xie et al., 2015, 2018; Yang et al., 2015; Cao et al., 2016; Araújo et al., 2018; Gao et al., 2018; Jiang et al., 2020; Shi et al., 2020; Zhou et al., 2020; **Table 2** and **Figure 4**). Many studies have demonstrated that PIWIL1 drives tumorigenesis, malignant progression and metastasis by promoting cell migration, invasion, epithelial-mesenchymal transition (EMT), stem-like properties, tumorigenesis and metastasis, while inhibiting apoptosis.

Of note, controversies exist regarding the underlying mechanisms of PIWIL1 in tumors. In colon cancer cells, several piRNAs seem to be loaded into a complex consisting of PIWIL1 and specific mRNAs (Sellitto et al., 2019), indicating that the formation of PIWIL1/piRNA complex might exert biological roles in colon cancer. It will be of great interest to understand whether PIWI proteins could utilize piRNAs as targeting guides to influence the stability of specific mRNA targets in tumor cells (Mai et al., 2018). However, recent observations that PIWIL1 does not associate with piRNAs in pancreatic (Li et al., 2020) and gastric cancer cells (Shi et al., 2020) supported the hypothesis that upregulated PIWIL1 protein probably functions in a piRNA-independent manner in cancer cells.

In contrast to these oncogenic activities, previous studies suggested that PIWIL1 may have a tumor suppressor function in some cancer types, including chronic myeloid leukemia and acute myeloid leukemia (Sharma et al., 2001; Wang Y. et al., 2015). This tumor suppressor activity is thought to be controlled by some signaling pathways that decrease the expression of MMP-2/MMP-9 and increase cell apoptosis.

REGULATION OF CELL PROLIFERATION, INVASIVENESS, TUMORIGENESIS AND METASTASIS

A previous study using co-immunoprecipitation and next-generation sequencing analysis demonstrated that RNA fragments interacting with PIWIL1 were indistinguishable from

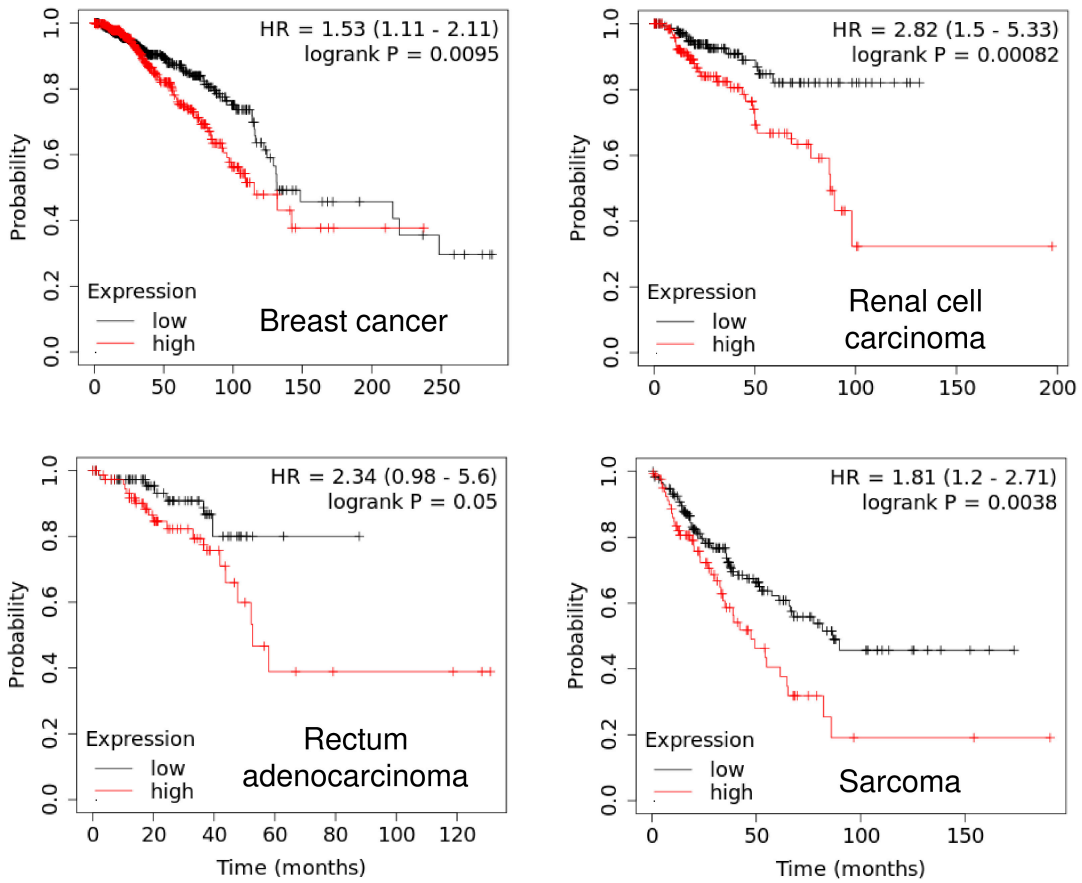

FIGURE 2 | High PIWIL1 expression predicts poor prognosis in patients with tumors. The probability of overall survival in patients with high or low *PIWIL1* expression in different tumors was assessed using the KM plotter database (http://kmplot.com).

background pull-down (Genzor et al., 2019). This provided the initial evidence for eliminating the formation of functional piRNA/PIWIL1 complexes in a colon cancer cell line COLO205 (Genzor et al., 2019). Consistently, a recent study revealed that piRNA expression was not detectable in several PIWIL1-expressing cancer cell lines, and co-immunoprecipitation assays failed to detect the association of PIWIL1 with small RNAs in pancreatic, breast, colon and gastric cancer cells that express PIWIL1 (Li et al., 2020). Comprehensive functional and mechanistic studies showed that, even in the absence of piRNA loading, PIWIL1 could still promote pancreatic cancer metastasis by acting as a co-activator of the anaphase-promoting complex/cyclosome to degrade a critical cell adhesion-related protein, Pinin (Li et al., 2020). Furthermore, a piRNA-independent mechanism has been proposed to account for the oncogenic functions of PIWIL1 in gastric cancer cells (Shi et al., 2020). Their results suggested that *PIWIL1* can significantly boost cell proliferation, migration, tumorigenesis and metastasis by forming a complex with UPF1, UPF2, SMG1 and other components to degrade mRNAs and lncRNAs with tumor suppressor potential (Shi et al., 2020).

Another major mechanism by which PIWIL1 promotes endometrial cancer progression might be through the induction of DNA methylation at *PTEN* CpG islands (Chen et al., 2015b). PIWIL1 causes epigenetic silencing of *PTEN* gene via the upregulation of DNA methyltransferase DNMT1 in endometrial cancer cells (Chen et al., 2015b). Using a mouse model, it was demonstrated that overexpression of PIWIL1 in sarcoma cells was sufficient to promote tumorigenesis, possibly through inducing global DNA methylation (Siddiqi et al., 2012). In addition, PIWIL1 overexpression with an adenovirus vector significantly increases the proliferation of colon cancer cells by increasing global DNA methylation levels (Yang et al., 2015).

REGULATION OF EMT, CANCER STEM CELL-LIKE PROPERTIES AND DRUG RESISTANCE

In cervical cancer, PIWIL1 has been associated with enhanced sphere formation and tumorigenesis, increased resistance to cisplatin, and elevated expression of several stem cell self-renewal-genes (*OCT4*, *NANOG* and *BMI1*) (Liu et al., 2014). PIWIL1 can drive EMT in endometrial cancer cells by upregulating the expression of Vimentin and N-cadherin and by decreasing E-cadherin expression (Chen et al., 2015a). This

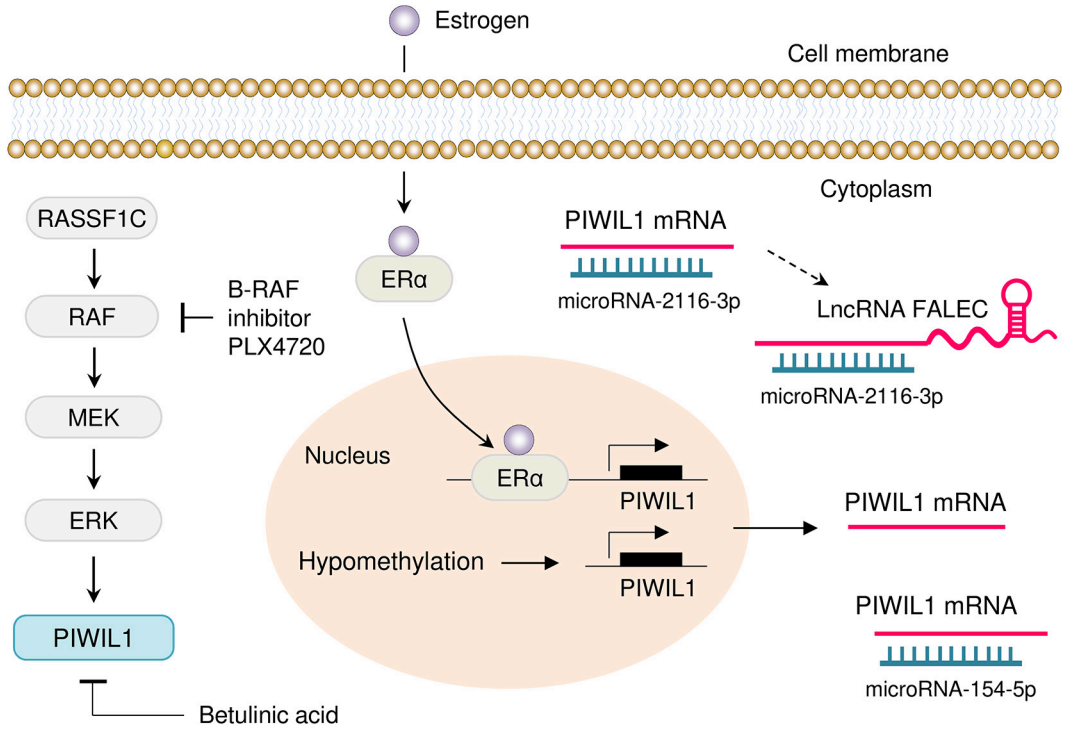

FIGURE 3 | Mechanisms of PIWIL1 dysregulation in tumor. Several mechanisms that drive overexpression of PIWIL1 have been discovered, including activation of the RASSF1C/MEK/ERK pathway, hypomethylation of the *PIWIL1* promoter and enhanced binding of ERα to the *PIWIL1* promoter. Also, PIWIL1 is targeted by miR-154-5p and miR-2116-3p in tumor cells. Moreover, lncRNA FALEC indirectly induces PIWIL1 expression by sponging miR-2116-3p. Inhibition of B-RAF with PLX4720 (a selective B-RAF inhibitor) and treatment with Betulinic acid (a plant secondary metabolite isolated from birch trees), causes downregulation of PIWIL1 in cancer cells.

study also suggested that the pro-cancer stem cell activities of PIWIL1 might be mediated by the induction of two stem cell-related genes (*CD44* and *ALDH1*) (Chen et al., 2015a). Recently, it was shown that PIWIL1 is enriched in glioma stem-like cells (GSCs) and silencing PIWIL1 in GSCs impaired their self-renewal and triggered senescence or apoptosis (Huang et al., 2021). PIWIL1 knockdown strongly increased the expression of BTG2 and FBXW7, but reduced the levels of c-MYC, Olig2 and Nestin in GSCs (Huang et al., 2021). These results supported that PIWIL1 is important for multiple aspects of tumor biology, including EMT-driven metastatic growth, the maintenance of cancer stem cell-like phenotypes, and resistance to therapeutic agents.

TARGETING PIWIL1 FOR CANCER THERAPY

The potential use of PIWIL1 as a therapeutic target for human cancers has been studied previously (Li et al., 2020; Shi et al., 2020). Several strategies have been developed to target PIWIL1 in tumor cells either directly or indirectly.

RNA interference (RNAi)-mediated suppression of PIWIL1 expression in tumor cells reduced proliferation, migration, invasion, EMT, sphere formation and angiogenesis (Zhao et al., 2012; Wang D.W. et al., 2014; Wang X. et al., 2014; Li et al., 2020; Shi et al., 2020). Inactivation of PIWIL1 in mouse models of pancreatic cancer leads to significant tumor shrinkage and a dramatic reduction in metastatic growth (Li et al., 2020). Knockout of *PIWIL1* using the CRISPR/Cas9 system markedly attenuates the tumor growth of gastric cancer *in vivo* (Shi et al., 2020). Therefore, RNAi and CRISPR/Cas9 techniques can be explored as a potential therapeutic strategy for tumors overexpressing PIWIL1.

Since small molecules that bind directly to PIWIL1 and alter its function have not yet been achieved, targeting the signaling pathways that contribute to PIWIL1 dysregulation has been exploited as new approaches to treat PIWIL1-expressing cancers (Reeves et al., 2012; Herr et al., 2015). One of these pathways is the RAS/RAF/MEK/ERK pathway, and several MEK inhibitors have been developed. For example, PLX4720 is a selective B-RAF inhibitor, and treatment with this drug strongly downregulates the expression of PIWIL1 in colon cancer cells (Herr et al., 2015). Betulinic acid, a plant secondary metabolite isolated from birch trees, was shown to inhibit cell proliferation and reduce the levels of PIWIL1 in gastric cancer and lung cancer (Yang et al., 2010; Reeves et al., 2014). Other targets that have been explored in PIWIL1-expressing tumors include miR-154-5p (Wang et al., 2017; Zhou et al., 2020) and miR-2116-3p (Jiang et al., 2020). Therefore, suppression of PIWIL1 expression via introducing miR-154-5p/miR-2116-3p mimics or downregulating the levels

TABLE 2 | Roles, cellular functions and underlying mechanisms of PIWIL1 in tumor cells.

Tumor type	Role	Function	Mechanism	References
Pancreatic cancer	Oncogene	Proliferation, migration, invasion, tumorigenesis, metastasis	Acting as a co-activator of APC/C to degrade the cell-adhesion protein Pinin	Li et al., 2020
Gastric cancer	Oncogene	Proliferation, migration, tumorigenesis, metastasis	Forming a complex with UPF1, UPF2 and SMG1 to degrade its target mRNAs and lncRNAs	Shi et al., 2020
Gastric cancer	Oncogene	Proliferation	Cell cycle regulation	Liu et al., 2006
Gastric cancer	Oncogene	Proliferation, migration, invasion	–	Gao et al., 2018
Hepatocellular carcinoma	Oncogene	Proliferation, invasion	–	Zhao et al., 2012
Breast cancer	Oncogene	Proliferation	–	Wang D.W. et al., 2014
Breast cancer	Oncogene	Apoptosis, cell cycle arrest	Possibly regulating transforming growth factor-β receptors and cyclin-dependent kinases	Cao et al., 2016
Cervical cancer	Oncogene	Sphere formation, tumorigenesis, resistance to cisplatin	Possibly increasing OCT4, NANOG and BMI1 expression	Liu et al., 2014
Endometrial cancer	Oncogene	EMT, stem-like properties	Decreasing E-cadherin expression, while the increasing Vimentin, N-cadherin, CD44 and ALDH1 expression	Chen et al., 2015a
Lung adenocarcinoma	Oncogene	Proliferation, migration, invasion	–	Xie et al., 2018
Glioblastoma	Oncogene	Proliferation, apoptosis, invasion	–	Wang et al., 2017
Glioma	Oncogene	Proliferation, invasion	–	Zhou et al., 2020
Colon cancer	Oncogene	Proliferation, migration, invasion, angiogenesis, tumorigenesis	–	Jiang et al., 2020
Lung cancer stem cells	Oncogene	Tumorigenesis	–	Liang et al., 2013
Gastric cancer	Oncogene	Migration, invasion	Possibly regulating several genes involved in migration and invasion processes	Araújo et al., 2018
Sarcoma	Oncogene	Proliferation, tumorigenesis	Promoting global DNA methylation	Siddiqi et al., 2012
Colon cancer	Oncogene	Proliferation	Promoting global DNA methylation	Yang et al., 2015
Glioma	Oncogene	Proliferation, migration, invasion, tumorigenesis	Possibly increasing Cyclin D1, MMP-2 and MMP-9 expression, whereas decreasing p21 expression	Wang X. et al., 2014
Hepatocellular carcinoma	Oncogene	Proliferation, migration	–	Xie et al., 2015
Hepatocellular carcinoma, cervical cancer	Oncogene	Proliferation, migration, invasion	Inducing STMN1 expression	Li et al., 2015
Chronic myeloid leukemia	Tumor suppressor	Proliferation, migration, tumorigenesis	Decreasing MMP-2 and MMP-9 expression	Wang Y. et al., 2015
Acute myeloid leukemia	Tumor suppressor	Proliferation, apoptosis	–	Sharma et al., 2001
Glioblastoma	Oncogene	Apoptosis, senescence, stem-like properties	Decreasing BTG2 and FBXW7 expression, whereas increasing c-MYC, Olig2 and Nestin expression	Huang et al., 2021

of lncRNA FALEC might be additional strategies in PIWIL1-positive tumors.

The acquisition of EMT and cancer stem-cell properties is a possible mechanistic basis for anti-cancer drug resistance (Shibue and Weinberg, 2017). After knocking down PIWIL1 in cervical cancer cells by shRNA, increased sensitivity to cisplatin was observed (Liu et al., 2014). In endometrial cancer, PIWIL1 has been associated with EMT and cancer stem cell-like characteristics (Chen et al., 2015a). These results suggest that, in the future, it could be useful to combine inhibitors against PIWIL1 with other cytotoxic drugs.

PERSPECTIVES

PIWIL1 has a critical role in the initiation, growth, progression, local and distant invasion, and treatment resistance. However, evidence also supports a tumor suppressor role for PIWIL1

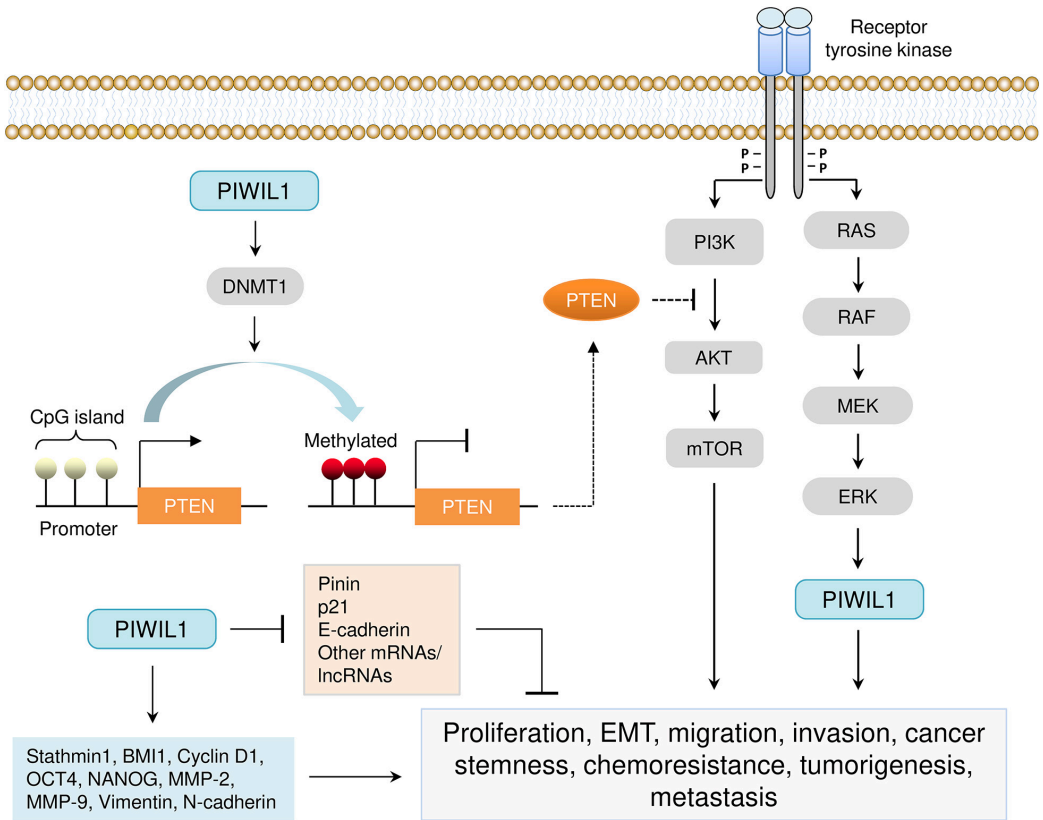

FIGURE 4 | Aberrant expression of *PIWIL1* mediates tumorigenesis and progression. PIWIL1 controls the expression of numerous downstream targets (such as PTEN, DNMT1, Pinin, p21, E-cadherin, BMI1, Stathmin1, Cyclin D1, OCT4, NANOG, MMP-2, MMP-9, Vimentin, and N-cadherin) involved in biological processes that are crucial for PIWIL1-dependent tumor promotion (including cell proliferation, EMT, migration, invasion, cancer stem-like properties, chemoresistance, tumorigenesis and metastasis). PIWIL1 epigenetically silences the expression of PTEN (a novel inhibitor of the PI3K/AKT pathway) by promoting DNA hypermethylation of the promoter of *PTEN*.

in some cell types. Whether PIWIL1 has a context-dependent function in different cancers, and whether PIWIL1 expression may serve as a biomarker for cancer subtyping and re-classification needs to be explored. Whether genomic mutations in *PIWIL1* gene are associated with induced PIWIL1 expression remains unclear, and the functional consequences of such mutations in tumor cells are not well understood. In addition, despite the recent advances in our understanding of PIWIL1, upstream regulators of PIWIL1 as well as its downstream signaling pathways in human tumors remain largely elusive. Furthermore, it would be better to use PIWIL1 inhibitors as an adjuvant to chemotherapy or other treatments. A deeper understanding of the crosstalk between PIWIL1 and other signaling pathways would be important to design effective therapeutic strategies that could sensitize PIWIL1-expressing tumor cells to chemotherapeutic agents or targeted therapies.

CONCLUSION

In sum, PIWIL1 has proven its tumor-promoting roles in various aspects of cancer biology. The restricted expression of PIWIL1 in normal adult tissues, and its overexpression in a broad spectrum of malignancies, has led to the consideration of PIWIL1 as an ideal target for cancer diagnosis and treatment.

AUTHOR CONTRIBUTIONS

PD wrote the manuscript. All authors contributed to the article and approved the submitted version.

FUNDING

This work was supported by a grant from JSPS Grant-in-Aid for Scientific Research (C) (18K09278 and 19K09769), China Scholarship Council (202008050143) to DX, and an NIH/NCI grant 1R21CA216585-01A1 to JY.

ACKNOWLEDGMENTS

We thank Dr. Zhujie Xu for excellent assistance. We wish to thank Dr. Mo-Fang Liu from Shanghai Institute of Biochemistry and Cell Biology for giving critical comments on this manuscript.

REFERENCES

Anastasiadou, E., Jacob, L. S., and Slack, F. J. (2018). Non-coding RNA networks in cancer. *Nat. Rev. Cancer.* 18, 5–18. doi: 10.1038/nrc.2017.99

Araújo, T., Khayat, A., Quintana, L., Calcagno, D., Mourão, R., Modesto, A., et al. (2018). Piwi like RNA-mediated gene silencing 1 gene as a possible major player in gastric cancer. *World J. Gastroenterol.* 24, 5338–5350. doi: 10.3748/wjg.v24.i47.5338

Cao, J., Xu, G., Lan, J., Huang, Q., Tang, Z., and Tian, L. (2016). High expression of piwi-like RNA-mediated gene silencing 1 is associated with poor prognosis via regulating transforming growth factor-β receptors and cyclin-dependent kinases in breast cancer. *Mol. Med. Rep.* 13, 2829–2835. doi: 10.3892/mmr.2016.4842

Carmell, M. A., Xuan, Z., Zhang, M. Q., and Hannon, G. J. (2002). The argonaute family: tentacles that reach into RNAi, developmental control, stem cell maintenance, and tumorigenesis. *Genes Dev.* 16, 2733–2742. doi: 10.1101/gad.1026102

Chen, C., Liu, J., and Xu, G. (2013). Overexpression of PIWI proteins in human stage III epithelial ovarian cancer with lymph node metastasis. *Cancer Biomark.* 13, 315–321. doi: 10.3233/CBM-130360

Chen, Z., Che, Q., He, X., Wang, F., Wang, H., Zhu, M., et al. (2015a). Stem cell protein Piwil1 endowed endometrial cancer cells with stem-like properties via inducing epithelial-mesenchymal transition. *BMC Cancer* 15:811. doi: 10.1186/s12885-015-1794-8

Chen, Z., Che, Q., Jiang, F. Z., Wang, H. H., Wang, F. Y., Liao, Y., et al. (2015b). Piwil1 causes epigenetic alteration of PTEN gene via upregulation of DNA methyltransferase in type I endometrial cancer. *Biochem. Biophys. Res. Commun.* 463, 876–880. doi: 10.1016/j.bbrc.2015.06.028

Chen, Z., Yang, H. J., Lin, Q., Zhu, M. J., Yu, Y. Y., He, X. Y., et al. (2020). Estrogen-ERα signaling and DNA hypomethylation co-regulate expression of stem cell protein PIWIL1 in ERα-positive endometrial cancer cells. *Cell Commun. Signal.* 18:84. doi: 10.1186/s12964-020-00563-4

Cheng, J., Guo, J. M., Xiao, B. X., Miao, Y., Jiang, Z., Zhou, H., et al. (2011). piRNA, the new non-coding RNA, is aberrantly expressed in human cancer cells. *Clin. Chim. Acta.* 412, 1621–1625. doi: 10.1016/j.cca.2011.05.015

Chu, H., Hui, G., Yuan, L., Shi, D., Wang, Y., Du, M., et al. (2015). Identification of novel piRNAs in bladder cancer. *Cancer Lett.* 356(2 Pt B), 561–567. doi: 10.1016/j.canlet.2014.10.004

Cox, D. N., Chao, A., Baker, J., Chang, L., Qiao, D., and Lin, H. (1998). A novel class of evolutionarily conserved genes defined by piwi are essential for stem cell self-renewal. *Genes Dev.* 12, 3715–3727. doi: 10.1101/gad.12.23.3715

Eckstein, M., Jung, R., Weigelt, K., Sikic, D., Stöhr, R., Geppert, C., et al. (2018). Piwi-like 1 and -2 protein expression levels are prognostic factors for muscle invasive urothelial bladder cancer patients. *Sci. Rep.* 8:17693. doi: 10.1038/s41598-018-35637-4

Gao, C. L., Sun, R., Li, D. H., and Gong, F. (2018). PIWI-like protein 1 upregulation promotes gastric cancer invasion and metastasis. *Onco Targets Ther.* 11, 8783–8789. doi: 10.2147/OTT.S186827

Genzor, P., Cordts, S. C., Bokil, N. V., and Haase, A. D. (2019). Aberrant expression of select piRNA-pathway genes does not reactivate piRNA silencing in cancer cells. *Proc. Natl. Acad. Sci. U. S. A.* 116, 11111–11112. doi: 10.1073/pnas.1904498116

Guo, B., Li, D., Du, L., and Zhu, X. (2020). piRNAs: biogenesis and their potential roles in cancer. *Cancer Metastasis Rev.* 39, 567–575. doi: 10.1007/s10555-020-09863-0

He, W., Wang, Z., Wang, Q., Fan, Q., Shou, C., Wang, J., et al. (2009). Expression of HIWI in human esophageal squamous cell carcinoma is significantly associated with poorer prognosis. *BMC Cancer* 9:426. doi: 10.1186/1471-2407-9-426

Hempfling, A. L., Lim, S. L., Adelson, D. L., Evans, J., O'Connor, A. E., Qu, Z. P., et al. (2017). Expression patterns of HENMT1 and PIWIL1 in human testis: implications for transposon expression. *Reproduction* 154, 363–374. doi: 10.1530/REP-16-0586

Herr, R., Köhler, M., Andrlová, H., Weinberg, F., Möller, Y., Halbach, S., et al. (2015). B-Raf inhibitors induce epithelial differentiation in BRAF-mutant colorectal cancer cells. *Cancer Res.* 75, 216–229. doi: 10.1158/0008-5472.CAN-13-3686

Huang, G., Hu, H., Xue, X., Shen, S., Gao, E., Guo, G., et al. (2013). Altered expression of piRNAs and their relation with clinicopathologic features of breast cancer. *Clin. Transl. Oncol.* 15, 563–568. doi: 10.1007/s12094-012-0966-0

Huang, H., Yu, X., Han, X., Hao, J., Zhao, J., Bebek, G., et al. (2021). Piwil1 regulates glioma stem cell maintenance and glioblastoma progression. *Cell. Rep.* 34:108522. doi: 10.1016/j.celrep.2020.108522

Iliev, R., Stanik, M., Fedorko, M., Poprach, A., Vychytilova-Faltejskova, P., Slaba, K., et al. (2016). Decreased expression levels of PIWIL1, PIWIL2, and PIWIL4 are associated with worse survival in renal cell carcinoma patients. *Onco Targets Ther.* 9, 217–222. doi: 10.2147/OTT.S91295

Jiang, H., Liu, H., and Jiang, B. (2020). Long non-coding RNA FALEC promotes colorectal cancer progression via regulating miR-2116-3p-targeted PIWIL1. *Cancer Biol. Ther.* 21, 1025–1032. doi: 10.1080/15384047.2020.1824514

Jiang, J., Zhang, H., Tang, Q., Hao, B., and Shi, R. (2011). Expression of HIWI in human hepatocellular carcinoma. *Cell Biochem. Biophys.* 61, 53–58. doi: 10.1007/s12013-011-9160-1

Li, C., Zhou, X., Chen, J., Lu, Y., Sun, Q., Tao, D., et al. (2015). PIWIL1 destabilizes microtubule by suppressing phosphorylation at Ser16 and RLIM-mediated degradation of Stathmin1. *Oncotarget* 6, 27794–27804. doi: 10.18632/oncotarget.4533

Li, F., Yuan, P., Rao, M., Jin, C. H., Tang, W., Rong, Y. F., et al. (2020). piRNA-independent function of PIWIL1 as a co-activator for anaphase promoting complex/cyclosome to drive pancreatic cancer metastasis. *Nat. Cell Biol.* 22, 425–438. doi: 10.1038/s41556-020-0486-z

Li, L., Yu, C., Gao, H., and Li, Y. (2010). Argonaute proteins: potential biomarkers for human colon cancer. *BMC Cancer* 10:38. doi: 10.1186/1471-2407-10-38

Li, S., Meng, L., Zhu, C., Wu, L., Bai, X., Wei, J., et al. (2010). The universal overexpression of a cancer testis antigen hiwi is associated with cancer angiogenesis. *Oncol. Rep.* 23, 1063–1068.

Liang, D., Dong, M., Hu, L. J., Fang, Z. H., Xu, X., Shi, E. H., et al. (2013). Hiwi knockdown inhibits the growth of lung cancer in nude mice. *Asian Pac. J. Cancer Prev.* 14, 1067–1072. doi: 10.7314/apjcp.2013.14.2.1067

Litwin, M., Dubis, J., Arczyńska, K., Piotrowska, A., Frydlewicz, A., Karczewski, M., et al. (2015). Correlation of HIWI and HILI expression with cancer stem cell markers in colorectal cancer. *Anticancer Res.* 35, 3317–3324.

Litwin, M., Szczepańska-Buda, A., Michałowska, D., Grzegrzółka, J., Piotrowska, A., Gomułkiewicz, A., et al. (2018). Aberrant expression of PIWIL1 and PIWIL2 and their clinical significance in ductal breast carcinoma. *Anticancer Res.* 38, 2021–2030. doi: 10.21873/anticanres.12441

Liu, W., Gao, Q., Chen, K., Xue, X., Li, M., Chen, Q., et al. (2014). Hiwi facilitates chemoresistance as a cancer stem cell marker in cervical cancer. *Oncol. Rep.* 32, 1853–1860. doi: 10.3892/or.2014.3401

Liu, W. K., Jiang, X. Y., and Zhang, Z. X. (2010b). Expression of PSCA, PIWIL1, and TBX2 in endometrial adenocarcinoma. *Onkologie* 33, 241–245. doi: 10.1159/000305098

Liu, W. K., Jiang, X. Y., and Zhang, Z. X. (2010a). Expression of PSCA, PIWIL1 and TBX2 and its correlation with HPV16 infection in formalin-fixed, paraffin-embedded cervical squamous cell carcinoma specimens. *Arch. Virol.* 155, 657–663. doi: 10.1007/s00705-010-0635-y

Liu, X., Sun, Y., Guo, J., Ma, H., Li, J., Dong, B., et al. (2006). Expression of hiwi gene in human gastric cancer was associated with proliferation of cancer cells. *Int. J. Cancer* 118, 1922–1929. doi: 10.1002/ijc.21575

Liu, Y., Dou, M., Song, X., Dong, Y., Liu, S., Liu, H., et al. (2019). The emerging role of the piRNA/piwi complex in cancer. *Mol. Cancer* 18:123. doi: 10.1186/s12943-019-1052-9

Lu, Y., Li, C., Zhang, K., Sun, H., Tao, D., Liu, Y., et al. (2010). Identification of piRNAs in Hela cells by massive parallel sequencing. *BMB Rep.* 43, 635–641. doi: 10.5483/BMBRep.2010.43.9.635

Mai, D., Ding, P., Tan, L., Zhang, J., Pan, Z., Bai, R., et al. (2018). PIWI-interacting RNA-54265 is oncogenic and a potential therapeutic target in colorectal adenocarcinoma. *Theranostics* 8, 5213–5230. doi: 10.7150/thno.28001

Meister, G. (2013). Argonaute proteins: functional insights and emerging roles. *Nat. Rev. Genet.* 14, 447–459. doi: 10.1038/nrg3462

Ng, K. W., Anderson, C., Marshall, E. A., Minatel, B. C., Enfield, K. S., Saprunoff, H. L., et al. (2016). Piwi-interacting RNAs in cancer: emerging functions and clinical utility. *Mol. Cancer* 15:5. doi: 10.1186/s12943-016-0491-9

O'Donnell, K. A., and Boeke, J. D. (2007). Mighty piwis defend the germline against genome intruders. *Cell* 129, 37–44. doi: 10.1016/j.cell.2007.03.028

Ozata, D. M., Gainetdinov, I., Zoch, A., O'Carroll, D., and Zamore, P. D. (2019). PIWI-interacting RNAs: small RNAs with big functions. *Nat. Rev. Genet.* 20, 89–108. doi: 10.1038/s41576-018-0073-3

Parker, J. S., and Barford, D. (2006). Argonaute: a scaffold for the function of short regulatory RNAs. *Trends Biochem. Sci.* 31, 622–630. doi: 10.1016/j.tibs.2006.09.010

Qiao, D., Zeeman, A. M., Deng, W., Looijenga, L. H., and Lin, H. (2002). Molecular characterization of hiwi, a human member of the piwi gene family whose overexpression is correlated to seminomas. *Oncogene* 21, 3988–3999. doi: 10.1038/sj.onc.1205505

Reeves, M. E., Baldwin, M. L., Aragon, R., Baldwin, S., Chen, S. T., Li, X., et al. (2012). RASSF1C modulates the expression of a stem cell renewal gene, PIWIL1. *BMC Res. Notes* 5:239. doi: 10.1186/1756-0500-5-239

Reeves, M. E., Firek, M., Chen, S. T., and Amaar, Y. G. (2014). Evidence that RASSF1C stimulation of lung cancer cell proliferation depends on IGFBP-5 and PIWIL1 expression levels. *PLoS One* 9:e101679. doi: 10.1371/journal.pone.0101679

Sellitto, A., Geles, K., D'Agostino, Y., Conte, M., Alexandrova, E., Rocco, D., et al. (2019). Molecular and functional characterization of the somatic PIWIL1/piRNA pathway in colorectal cancer cells. *Cells* 8:1390. doi: 10.3390/cells8111390

Sharma, A. K., Nelson, M. C., Brandt, J. E., Wessman, M., Mahmud, N., Weller, K. P., et al. (2001). Human CD34(+) stem cells express the hiwi gene, a human homologue of the *Drosophila* gene piwi. *Blood* 97, 426–434. doi: 10.1182/blood.v97.2.426

Shi, S., Yang, Z. Z., Liu, S., Yang, F., and Lin, H. (2020). PIWIL1 promotes gastric cancer via a piRNA-independent mechanism. *Proc. Natl. Acad. Sci. U. S. A.* 117, 22390–22401. doi: 10.1073/pnas.2008724117

Shibue, T., and Weinberg, R. A. (2017). EMT, CSCs, and drug resistance: the mechanistic link and clinical implications. *Nat. Rev. Clin. Oncol.* 14, 611–629. doi: 10.1038/nrclinonc.2017.44

Siddiqi, S., Terry, M., and Matushansky, I. (2012). Hiwi mediated tumorigenesis is associated with DNA hypermethylation. *PLoS One* 7:e33711. doi: 10.1371/journal.pone.0033711

Stöhr, C. G., Steffens, S., Polifka, I., Jung, R., Kahlmeyer, A., Ivanyi, P., et al. (2019). Piwi-like 1 protein expression is a prognostic factor for renal cell carcinoma patients. *Sci. Rep.* 9:1741. doi: 10.1038/s41598-018-38254-3

Sun, G., Wang, Y., Sun, L., Luo, H., Liu, N., Fu, Z., et al. (2011). Clinical significance of Hiwi gene expression in gliomas. *Brain Res.* 1373, 183–188. doi: 10.1016/j.brainres.2010.11.097

Sun, R., Gao, C. L., Li, D. H., Li, B. J., and Ding, Y. H. (2017). Expression status of PIWIL1 as a prognostic marker of colorectal cancer. *Dis. Markers* 2017:1204937. doi: 10.1155/2017/1204937

Suzuki, R., Honda, S., and Kirino, Y. (2012). PIWI expression and function in cancer. *Front. Genet.* 3:204. doi: 10.3389/fgene.2012.00204

Tan, Y., Liu, L., Liao, M., Zhang, C., Hu, S., Zou, M., et al. (2015). Emerging roles for PIWI proteins in cancer. *Acta Biochim. Biophys. Sin. (Shanghai)* 47, 315–324. doi: 10.1093/abbs/gmv018

Taubert, H., Greither, T., Kaushal, D., Würl, P., Bache, M., Bartel, F., et al. (2007). Expression of the stem cell self-renewal gene Hiwi and risk of tumour-related death in patients with soft-tissue sarcoma. *Oncogene* 26, 1098–1100. doi: 10.1038/sj.onc.1209880

Tian, Y., Simanshu, D. K., Ma, J. B., and Patel, D. J. (2011). Structural basis for piRNA 2'-O-methylated 3'-end recognition by Piwi PAZ (Piwi/Argonaute/Zwille) domains. *Proc. Natl. Acad. Sci. U. S. A.* 108, 903–910. doi: 10.1073/pnas.1017762108

Wang, D. W., Wang, Z. H., Wang, L. L., Song, Y., and Zhang, G. Z. (2014). Overexpression of hiwi promotes growth of human breast cancer cells. *Asian Pac. J. Cancer Prev.* 15, 7553–7558. doi: 10.7314/apjcp.2014.15.18.7553

Wang, H. L., Chen, B. B., Cao, X. G., Wang, J., Hu, X. F., Mu, X. Q., et al. (2015). The clinical significances of the abnormal expressions of Piwil1 and Piwil2 in colonic adenoma and adenocarcinoma. *Onco Targets Ther.* 8, 1259–1264. doi: 10.2147/OTT.S77003

Wang, J., Zhang, P., Lu, Y., Li, Y., Zheng, Y., Kan, Y., et al. (2019). piRBase: a comprehensive database of piRNA sequences. *Nucleic Acids Res.* 47, D175–D180. doi: 10.1093/nar/gky1043

Wang, X., Sun, S., Tong, X., Ma, Q., Di, H., Fu, T., et al. (2017). MiRNA-154-5p inhibits cell proliferation and metastasis by targeting PIWIL1 in glioblastoma. *Brain Res.* 1676, 69–76. doi: 10.1016/j.brainres.2017.08.014

Wang, X., Tong, X., Gao, H., Yan, X., Xu, X., Sun, S., et al. (2014). Silencing HIWI suppresses the growth, invasion and migration of glioma cells. *Int. J. Oncol.* 45, 2385–2392. doi: 10.3892/ijo.2014.2673

Wang, Y., Jiang, Y., Ma, N., Sang, B., Hu, X., Cong, X., et al. (2015). Overexpression of Hiwi inhibits the growth and migration of chronic myeloid leukemia cells. *Cell Biochem. Biophys.* 73, 117–124. doi: 10.1007/s12013-015-0651-3

Wang, Y., Liu, Y., Shen, X., Zhang, X., Chen, X., Yang, C., et al. (2012). The PIWI protein acts as a predictive marker for human gastric cancer. *Int. J. Clin. Exp. Pathol.* 5, 315–325.

Weick, E. M., and Miska, E. A. (2014). piRNAs: from biogenesis to function. *Development* 141, 3458–3471. doi: 10.1242/dev.094037

Wu, J., Yang, J., Cho, W. C., and Zheng, Y. (2020). Argonaute proteins: structural features, functions and emerging roles. *J. Adv. Res.* 24, 317–324. doi: 10.1016/j.jare.2020.04.017

Xie, K., Zhang, K., Kong, J., Wang, C., Gu, Y., Liang, C., et al. (2018). Cancer-testis gene PIWIL1 promotes cell proliferation, migration, and invasion in lung adenocarcinoma. *Cancer Med.* 7, 157–166. doi: 10.1002/cam4.1248

Xie, Y., Yang, Y., Ji, D., Zhang, D., Yao, X., and Zhang, X. (2015). Hiwi downregulation, mediated by shRNA, reduces the proliferation and migration of human hepatocellular carcinoma cells. *Mol. Med. Rep.* 11, 1455–1461. doi: 10.3892/mmr.2014.2847

Xu, D., Dong, P., Xiong, Y., Chen, R., Konno, Y., Ihira, K., et al. (2020). PD-L1 Is a tumor suppressor in aggressive endometrial cancer cells and its expression is regulated by miR-216a and lncRNA MEG3. *Front. Cell Dev. Biol.* 8:598205. doi: 10.3389/fcell.2020.598205

Yamamura, S., Imai-Sumida, M., Tanaka, Y., and Dahiya, R. (2018). Interaction and cross-talk between non-coding RNAs. *Cell. Mol. Life Sci.* 75, 467–484. doi: 10.1007/s00018-017-2626-6

Yang, L., Bi, L., Liu, Q., Zhao, M., Cao, B., Li, D., et al. (2015). Hiwi promotes the proliferation of colorectal cancer cells via upregulating global DNA methylation. *Dis. Markers* 2015:383056. doi: 10.1155/2015/383056

Yang, L. J., Chen, Y., Ma, Q., Fang, J., He, J., Cheng, Y. Q., et al. (2010). Effect of betulinic acid on the regulation of Hiwi and cyclin B1 in human gastric adenocarcinoma AGS cells. *Acta Pharmacol. Sin.* 31, 66–72. doi: 10.1038/aps.2009.177

Yu, Y., Xiao, J., and Hann, S. S. (2019). The emerging roles of PIWI-interacting RNA in human cancers. *Cancer Manag. Res.* 11, 5895–5909. doi: 10.2147/CMAR.S209300

Zhao, Y. M., Zhou, J. M., Wang, L. R., He, H. W., Wang, X. L., Tao, Z. H., et al. (2012). HIWI is associated with prognosis in patients with hepatocellular carcinoma after curative resection. *Cancer* 118, 2708–2717. doi: 10.1002/cncr.26524

Zhou, H., Zhang, Y., Lai, Y., Xu, C., and Cheng, Y. (2020). Circ_101064 regulates the proliferation, invasion and migration of glioma cells through miR-154-5p/PIWIL1 axis. *Biochem. Biophys. Res. Commun.* 523, 608–614. doi: 10.1016/j.bbrc.2019.12.096

Conflict of Interest: The authors declare that the research was conducted in the absence of any commercial or financial relationships that could be construed as a potential conflict of interest.

frontiers in Cell and Developmental Biology

SYSTEMATIC REVIEW
published: 11 March 2021
doi: 10.3389/fcell.2021.570898

OPCML Methylation and the Risk of Ovarian Cancer: A Meta and Bioinformatics Analysis

Yang Shao[1,2†], Jing Kong[1†], Hanzi Xu[3], Xiaoli Wu[1], YuePeng Cao[1], Weijian Li[1], Jing Han[4], Dake Li[1], Kaipeng Xie[1] and Jiangping Wu[1*]*

[1] Nanjing Maternity and Child Health Care Institute, Nanjing Maternity and Child Health Care Hospital, Women's Hospital of Nanjing Medical University, Nanjing, China, [2] The First People's Hospital of Zhangjiagang City, The Zhangjiagang Affiliated Hospital of Soochow University, Suzhou, China, [3] Department of Radiotherapy, The Affiliated Cancer Hospital of Nanjing Medical University, Nanjing, China, [4] Jiangsu Institute of Cancer Research, The Affiliated Cancer Hospital of Nanjing Medical University, Nanjing, China

OPEN ACCESS

Edited by:
Xiao Zhu,
Guangdong Medical University, China

Reviewed by:
Abhijit Shukla,
Memorial Sloan Kettering Cancer Center, United States
Mingzhi Han,
University of Bergen, Norway

***Correspondence:**
Jiangping Wu
wujiangping@njmu.edu.cn
Kaipeng Xie
kaipengxie@njmu.edu.cn

[†] These authors have contributed equally to this work

Specialty section:
This article was submitted to Epigenomics and Epigenetics, a section of the journal Frontiers in Cell and Developmental Biology

Received: 01 July 2020
Accepted: 08 February 2021
Published: 11 March 2021

Citation:
Shao Y, Kong J, Xu H, Wu X, Cao Y, Li W, Han J, Li D, Xie K and Wu J (2021) OPCML Methylation and the Risk of Ovarian Cancer: A Meta and Bioinformatics Analysis. Front. Cell Dev. Biol. 9:570898. doi: 10.3389/fcell.2021.570898

Background: The association of opioid binding protein cell adhesion molecule-like (OPCML) gene methylation with ovarian cancer risk remains unclear.

Methods: We identified eligible studies by searching the PubMed, Web of Science, ScienceDirect, and Wanfang databases. Odds ratios (ORs) and 95% confidence intervals (95% CIs) were used to determine the association of OPCML methylation with ovarian cancer risk. Meta-regression and subgroup analysis were used to assess the sources of heterogeneity. Additionally, we analyzed the Gene Expression Omnibus (GEO) and The Cancer Genome Atlas (TCGA) datasets to validate our findings.

Results: Our study included 476 ovarian cancer patients and 385 controls from eight eligible studies. The pooled OR was 33.47 (95% CI = 12.43–90.16) in the cancer group vs. the control group under the random-effects model. The association was still significant in subgroups according to sample type, control type, methods, and sample sizes (all $P < 0.05$). Sensitivity analysis showed that the finding was robust. No publication bias was observed in Begg's ($P = 0.458$) and Egger's tests ($P = 0.261$). We further found that OPCML methylation was related to III/IV (OR = 4.20, 95% CI = 1.59–11.14) and poorly differentiated grade (OR = 4.37; 95% CI = 1.14–16.78). Based on GSE146552 and GSE155760, we validated that three CpG sites (cg16639665, cg23236270, cg15964611) in OPCML promoter region were significantly higher in cancer tissues compared to normal tissues. However, we did not observe the associations of OPCML methylation with clinicopathological parameters and overall survival based on TCGA ovarian cancer data.

Conclusion: Our findings support that OPCML methylation is associated with an increased risk of ovarian cancer.

Keywords: OPCML, methylation, ovarian cancer, risk, progression

INTRODUCTION

Ovarian cancer is the most frequent cause of death in women with gynecological malignancies. In 2020, 313,959 new ovarian cancer cases were diagnosed and 207,252 new deaths occurred from ovarian cancer in the world (Sung et al., 2021). Most patients are diagnosed at an advanced or incurable stage because of asymptomatic development (Lheureux et al., 2019). Therefore, identifying novel biomarkers for early diagnosis and research on treatment strategies could reduce the incidence of ovarian cancer and improve the survival rate in advanced ovarian cancer patients.

Aberrant gene expression, including the activation of oncogenes and inactivation of tumor suppressor genes (TSGs), plays a vital role in tumorigenesis (Ehrlich, 2002). Emerging studies have shown that DNA methylation is a key mechanism of epigenetic variability in gene expression (Wilson et al., 2007). Compared with normal cells, cancer cells exhibit extensive changes in DNA methylation patterns (Vidal et al., 2017). Cancer cells undergo alterations in 5-methylcytosine distribution including global DNA hypomethylation and hypermethylation of CpG islands (Jones, 2012). Notably, aberrant DNA methylation is not only a well-known mechanism of TSG inactivation but also one of the earliest events in carcinogenesis (Rauscher et al., 2015; Widschwendter et al., 2017). DNA methylation is considered a promising biomarker for cancer diagnosis and the prediction of treatment and prognosis (Szyf, 2012; Widschwendter et al., 2017). Intriguingly, the Food and Drug Administration (FDA) has approved the first methylation-based assay in colorectal cancer screening and early detection (Song et al., 2017; Widschwendter et al., 2018). Therefore, evaluating the alteration of DNA methylation in ovarian cancer is urgent.

Opioid binding protein cell adhesion molecule-like (OPCML) gene at 11q25 is a glycosyl-phosphatidylinositol (GPI)-anchored cell adhesion-like molecule and belongs to the IgLON family (Wu and Sood, 2012). OPCML demonstrates tumor-suppressor function in epithelial ovarian cancer both *in vitro* and *in vivo* (Sellar et al., 2003). Subsequently, the same team described the mechanism underlying the phenotype of OPCML. It negatively regulates a specific receptor tyrosine kinase (RTK) repertoire comprising erythropoietin-producing hepatocellular receptor-2 (EPHA2), fibroblast growth factor receptor-1 (FGFR1), fibroblast growth factor receptor-3 (FGFR3), human epidermal growth factor receptor-2 (HER2), and human epidermal growth factor receptor-4 (HER4) receptors by binding to the extracellular domains of RTKs, thus promoting their degradation *via* a polyubiquitination-associated proteasomal mechanism and leading to growth inhibition (McKie et al., 2012). Additionally, they revealed that a recombinant protein based on OPCML is an active anticancer agent preclinical *in vivo*. Another study showed that OPCML restoration interfered with HER2-EGFR heterodimer formation and potentiated lapatinib and erlotinib

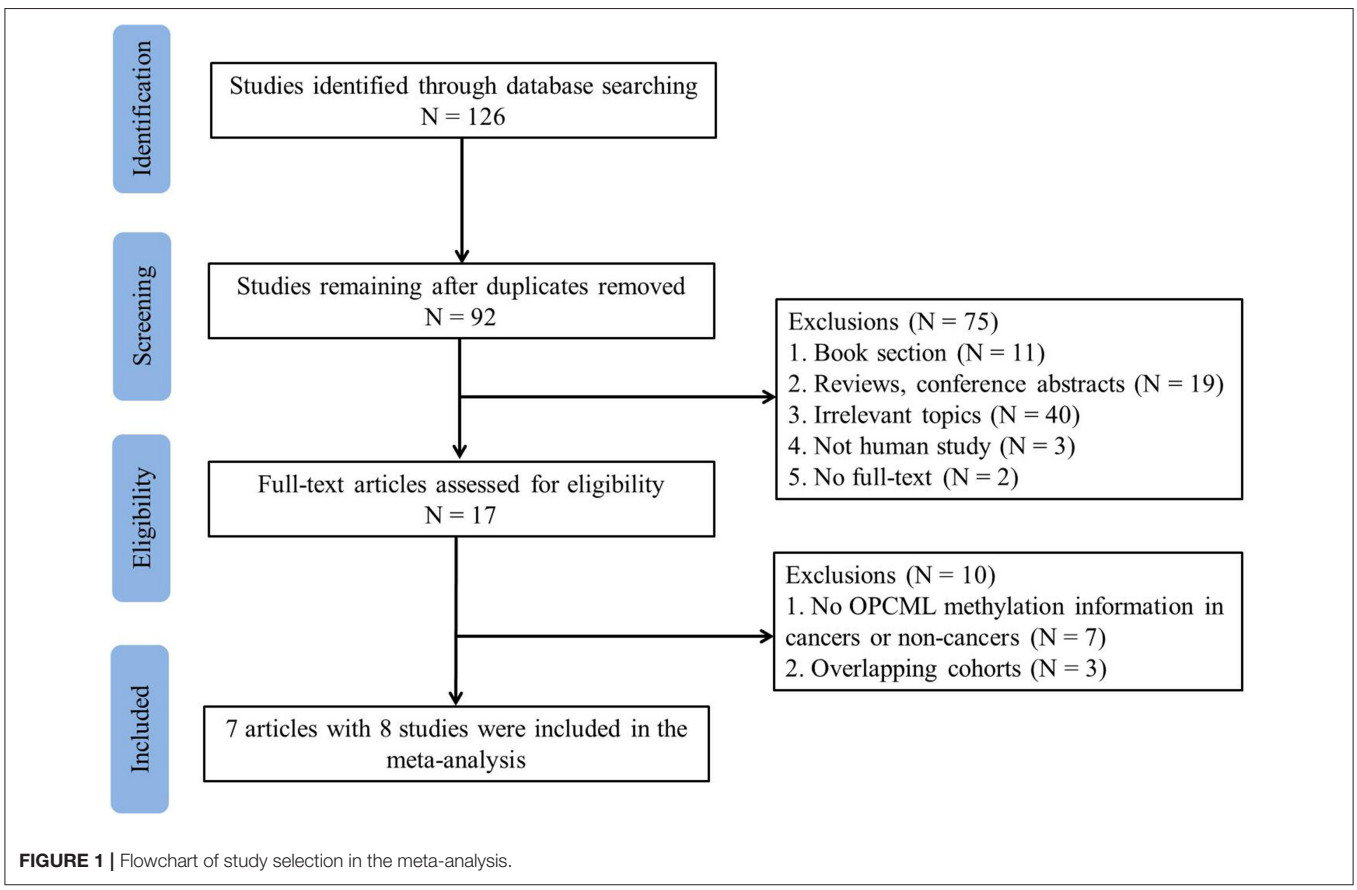

FIGURE 1 | Flowchart of study selection in the meta-analysis.

TABLE 1 | Characteristics of included studies.

References	Country	Age (mean or median)	Cancer group		Control group		Sample type	Control type	Method	Methylation frequency of OPCML associated with other clinicopathological parameters
			M	U	M	U				
Wang et al. (2015)	China	Cancer, 54.06 years. Benign, 33.95 years. Healthy, 46.17 years.	64	7	11[a]	112[a]	Serum	BOT&NT	MSP	FIGO stage: I/II (33/39), III/IV (30/32).
Xing et al. (2015)	China	NR	27	8	2	9	Tissues	NT	CCP-based FRET	Age: <60 years (23/28), ≥60 years (4/7). FIGO stage: I/II (5/11), III/IV (22/24). Histological type: serous (22/26), others (5/9)[b]. Grade of differentiation[c]: High-grade serous (19/21), others (8/14) Ascites: positive (21/24), Negative (6/11). CA125: >200 U/mL (21/25), <200 U/mL (6/10)
Zhou et al. (2014a)	China	Cancer and normal, 50 years.	39	6	0[d]	40[d]	Tissues	NT	MSRE-PCR	Tissues FIGO stage: I/II (5/10), III/IV (34/35). Histological type: serous (18/20), others (21/25)[e]. Tumor differentiation: Well and moderately differentiated (10/16), Poorly differentiated (29/29).
		Healthy, 50 years.	36	9	0[d]	20[d]	Serum	NT	MSRE-PCR	Serum FIGO stage: I/II (5/10), III/IV (31/35). Histological type: serous (17/20), others (19/25)[e]. Tumor differentiation: Well and moderately differentiated (9/16), Poorly differentiated (27/29).
Zhou et al. (2014b)	China	Cancer, 54 years. Benign, 53 years. Normal, 54 years.	80	22	0[f]	30[f]	Tissues	NT	MSP	Age: <55 years (39/54), ≥55 years (41/48). Pathological stage*: I/II (31/44), III/IV (49/58). Histological type[b]: serous (42/57), others (38/45).
			–	–	28[f]	57[f]	Tissues	BOT	MSP	
Czekierdowski et al. (2006)	Poland	NR[g]	20	23	0	4	Tissues	NT	MSP	FIGO stage: I/II (4/5), III/IV (16/38). Histological type: serous (8/15), others (12/28)[h]. Histological Grading: G1+G2 (11/20), G3 (9/23)[k]
Zhang et al. (2006)	China	Cancer, 51.5 years. Benign, 39.0 years. Normal, 46.5 years.	32	40	0	20	Tissues	NT	Restriction enzyme cut	
					0	17	Tissues	BOT	Restriction enzyme cut	
Liu et al. (2008)[i]	China	Cancer, 53.8 years. Normal, 53.2 years.	30	33	0	20	Tissues	NT	MSP	FIGO stage: I/II (2/22), III/IV (16/41). Histological type: serous (20/34), others (10/29)[j]. Grading: Well and Moderately differentiated (6/36), Poorly differentiated (12/27)
					2	13	Tissues	AT		

M, methylation; U, unmethylation; BOT, benign ovarian tissues or blood; NT, normal ovarian tissues or blood of cancer-free patients or healthy people; AT, Adjacent non-cancerous ovarian tissues; MSP, methylation-specific polymerase chain reaction; MSRE-PCR, methylation-sensitive restriction enzyme-polymerase chain reaction; CCP-based FRET, cationic conjugated polymer (CCP)-based fluorescence resonance energy transfer (FRET); FIGO, International Federation of Gynecology and Obstetrics. NR, not reported the median or mean age in all patients.

[a] *The control group include 43 benign ovarian carcinoma and 80 healthy women in this study.*

[b] *Others included Mucinous, Clear cell, and Endometrioid carcinomas.*

[c] *In further analysis, we regarded the high-grade serous as Poorly differentiated., others as well and moderately differentiated.*

[d] *This study include 45 ovarian tumor tissues, 40 normal ovarian tissues, and 20 serum samples.*

[e] *Others included Mucinous, Clear cell, Endometrioid, and undifferentiated carcinomas.*

[f] *This study include 102 ovarian cancer tissues, 85 benign ovarian tumor, and 30 normal ovarian.*

[*] *Pathological stage was classified according to the tumor, lymph node, and metastasis (TNM) classification of the American Joint Committee on Cancer (AJCC).*

[g] *This study only reported the mean ages of different histological type, but not reported the mean age of cancer in tumor and normal tissue.*

[h] *Others included Mucinous, Clear cell, Endometrioid, undifferentiated, metastatic, and other carcinomas.*

[i] *This study include 63 epithelial ovarian cancer tissues, 41 Metastatic tissues of pelvic and abdomen cavity, 15 Adjacent non-cancerous ovarian tissues, 20 Normal ovairan tissues.*

[j] *Others included Mucinous, Clear cell, and Endometrioid carcinomas.*

[k] *In further analysis, we regarded the G1+G2 as well and moderately differentiated, G3 as poorly differentiated.*

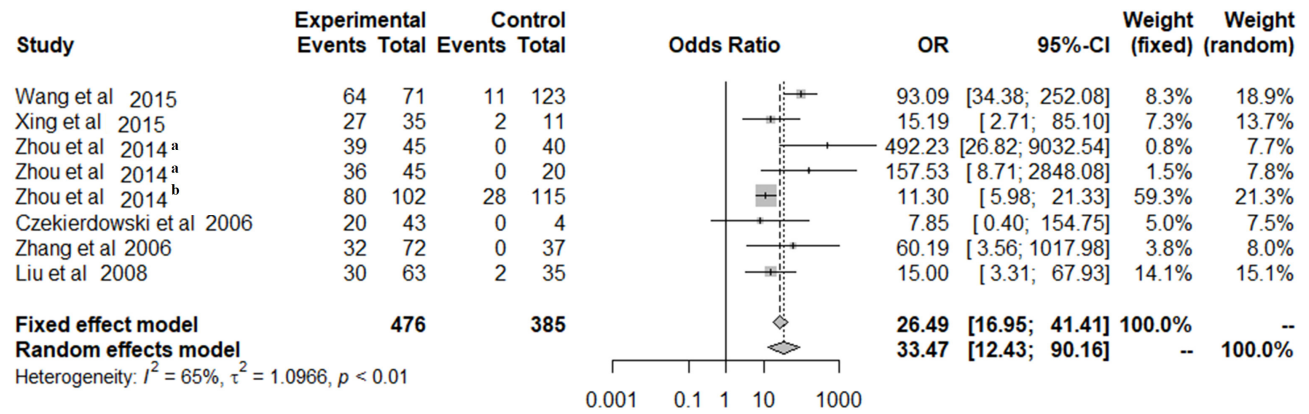

FIGURE 2 | The summary estimates for OPCML methylation frequency associated with ovarian cancer in the meta-analysis.

therapy in ovarian and breast cancer cell lines overexpressing HER2 (Zanini et al., 2017). Recent researches on OPCML protein reveal that OPCML is a potential anti-cancer therapy (Birtley et al., 2019; Simovic et al., 2019). Considering the biological and clinical effects of OPCML, research on the mechanism of aberrant expression patterns may benefit ovarian cancer patients from OPCML-based therapy.

Many studies have indicated that OPCML DNA hypermethylation frequently occurs in ovarian cancers. However, the findings remain unclear regarding the small population and different methods in previous studies (Czekierdowski et al., 2006; Zhang et al., 2006, 2014; Chen et al., 2007; Liu et al., 2008; Zhou et al., 2011, 2014a,b; Wang et al., 2015, 2017; Xing et al., 2015). Therefore, we performed a meta-analysis to identify the association of OPCML methylation with ovarian cancer risk. We further assessed whether OPCML methylation was associated with other clinicopathological parameters in eligible studies, such as age, stage, histological type, and tumor differentiation. Additionally, we validated our results based on the Gene Expression Omnibus (GEO) and The Cancer Genome Atlas (TCGA) ovarian cancer datasets.

MATERIALS AND METHODS

Literature Search Strategy

A systematic literature search was performed in the PubMed, Web of Science, ScienceDirect, and Wanfang databases using the following keywords and search items: (ovarian OR ovary) AND (cancer OR carcinoma OR tumor) AND (OPCML methylation). The search was updated until November 17, 2020.

Study Selection

The inclusion criteria were as follows: (1) studies primarily evaluating the association between OPCML methylation and ovarian cancer, (2) studies including case and control populations, (3) the incidence of OPCML methylation in case and control groups, and (4) studies using human tissues or blood. Based on the inclusion criteria, the titles and abstracts from the preliminary search were evaluated. Subsequently, all related studies were evaluated as full-text papers. Exclusion criteria were (1) book section, conference abstracts, and reviews, (2) studies with insufficient data to provide the methylation frequencies in cancer and control groups, and (3) studies without human samples. In the case of duplicated publications from the shared cohort, we selected the most complete information to be included in the meta-analysis.

TABLE 2 | Meta-regression analysis.

Heterogeneity sources	Coefficient	95% CI	*P*
Publication year	0.814	(−0.751, 2.380)	0.308
Country	10.538	(−9.721, 30.795)	0.308
Sample type	−0.716	(−3.370, 1.939)	0.597
Control type	4.851	(−4.042,13.744)	0.285
Method	3.748	(−1.419, 8.916)	0.155
Sample size	−0.001	(−0.020, 0.018)	0.889

Data Extraction and Quality Assessment

The following information was extracted for each eligible study: the first author's name, publication year, country, age, number of methylated and unmethylated samples in cancer and control groups, sample type, control type, methylation detection methods, and other clinicopathological parameters. In our study, controls included adjacent non-cancerous ovarian tissues (AT), tissue and blood samples from benign ovarian tumor (BOT) and other cancer-free patients (NT). Additionally, we used the Newcastle-Ottawa Scale (NOS) to assess the quality. The NOS includes the selection of the research groups (four stars), comparison of the groups (two stars), and ascertainment of the outcome (three stars).

Bioinformatics Analysis

Two DNA methylation data were downloaded from the Gene Expression Omnibus (GEO) database: GSE146552 (20 high grade serous ovarian cancers, 16 epithelial layer by mechanical scraping of resected fimbriae fallopian tubes and ovaries)

TABLE 3 | Subgroup analysis of associations between *OPCML* methylation and ovarian cancer risk.

Group	Studies	Case		Control		Fixed effects model	Random effects model	Heterogeneity	
	n	M	U	M	U	OR (95% CI)	OR (95% CI)	I^2 (%)	*P*
Country									
China	7	308	125	43	338	27.47 (17.52, 43.08)	38.17 (13.21, 110.28)	70	<0.01
Poland	1	20	23	0	4	7.85 (0.40, 154.75)	7.85 (0.40, 154.75)	–	–
Sample type									
Serum	2	100	16	11	132	102.86 (39.37, 268.74)	98.42 (38.37, 252.45)	0	0.73
Tissues	6	228	132	32	210	18.22 (10.93, 30.36)	19.13 (7.71, 47.44)	39	0.15
Control type									
NT	4	122	46	2	73	52.77 (16.92, 164.55)	47.94 (7.38, 311.27)	53	0.09
NT&BOT	3	176	69	39	236	23.41 (13.96, 39.25)	35.50 (6.38, 197.47)	84	<0.01
AT&NT	1	30	33	2	33	15.00 (3.31, 67.93)	15.00 (3.31, 67.93)	–	–
Methods									
MSP	4	194	85	41	236	19.52 (11.94, 31.92)	21.78 (6.10, 77.79)	76	<0.01
CCP-based FRET	1	27	8	2	9	15.19 (2.71, 85.10)	15.19 (2.71, 85.10)	–	–
Restriction enzyme related methods	3	107	55	0	97	139.45 (24.06, 808.26)	163.86 (31.13, 862.61)	0	0.59
Sample size									
<100	5	152	79	4	106	34.19 (14.11, 82.86)	32.63 (8.42, 126.53)	45	0.12
≥100	3	176	69	39	236	23.41 (13.96, 39.25)	35.50 (6.38, 197.47)	84	<0.01

M, methylation; U, unmethylation; BOT, benign ovarian tissues; NT, normal ovarian tissues of cancer-free patients or healthy people; AT, Adjacent non-cancerous ovarian tissues; MSP, methylation-specific polymerase chain reaction; CCP-based FRET, a cationic conjugated polymer (CCP)-based fluorescence resonance energy transfer (FRET); Restriction enzyme related methods include methylation-sensitive restriction enzyme-polymerase chain reaction and restriction enzyme cut analysis.

and GSE155760 (23 high-grade serous ovarian carcinoma, 11 fallopian tube mucosa from cancer-free normal control). The GEO2R online analysis tool (https://www.ncbi.nlm.nih.gov/geo/geo2r/) was used to identify the differential DNA methylated sites ($P < 0.05$) between cancer tissues and normal tissues. For the cancer genome atlas (TCGA) ovarian serous cystadenocarcinoma (OV) data, we downloaded the OPCML expression data (log2-transformed RSEM normalized count) based on RNA sequencing (RNA-Seq), OPCML-associated DNA methylation data (cg03923934, cg25853078) based on HumanMethylation27 and the clinical data including age, stage, grade, and overall survival from the website (https://xena.ucsc.edu/).

Statistical Analysis

We calculated the pooled odds ratios (ORs) and 95% confidence intervals (95% CIs) to evaluate the association between OPCML methylation and ovarian cancer risk. The heterogeneity of studies was evaluated by the χ^2-based *Q*-test. When the $P > 0.05$, the fixed-effects model was used to combine the effect size; otherwise, the random-effects model was adopted. We conducted meta-regression to explore sources of heterogeneity and further performed a subgroup analysis to evaluate the source of the heterogeneity. The contribution of each study to our findings was examined according to sensitivity analysis. We used the Begg's rank correlation method (Begg and Mazumdar, 1994) and a funnel plot for Egger's test (Egger et al., 1997) to evaluate publication bias.

The correlation between OPCML methylation and its expression in TCGA was calculated by Spearman's rank correlation. Kruskal-Wallis and Wilcoxon-Mann-Whitney *U* tests were applied for comparisons, as appropriate. Survival analysis was performed using the log-rank test and a Cox regression model. Hazard ratios (HRs) and corresponding 95% CIs were calculated to assess the associations of factors with overall survival. All statistical tests were two-sided and performed using the R software (version 3.6). *P*-value < 0.05 were considered statistically significant.

RESULTS

Study Characteristics

The detailed information of how we selected relevant articles is shown in **Figure 1**. We initially identified 126 articles from PubMed, Web of Science, ScienceDirect, and Wanfang databases and excluded 34 duplicated articles. After reviewing 92 articles based on titles and abstracts, 75 articles did not meet the selection criteria, leaving 17 studies for detailed full-text evaluation. Seven articles were excluded because they did not report the methylation frequencies in cancers or controls. Three articles were excluded because of overlapping cohorts (Zhou et al., 2011; Zhang et al., 2014; Wang et al., 2017). The study performed by Zhou et al. (2014a) included two sample types, tissue and serum. Thus, we considered this paper as two separate studies. Therefore, seven eligible articles with eight studies including 476 ovarian cancer patients and 385 controls were included in the meta-analysis.

The characteristics of the eight studies are summarized in **Table 1**. Seven studies were performed in China and one study was performed in Poland. The cases comprised of cancer

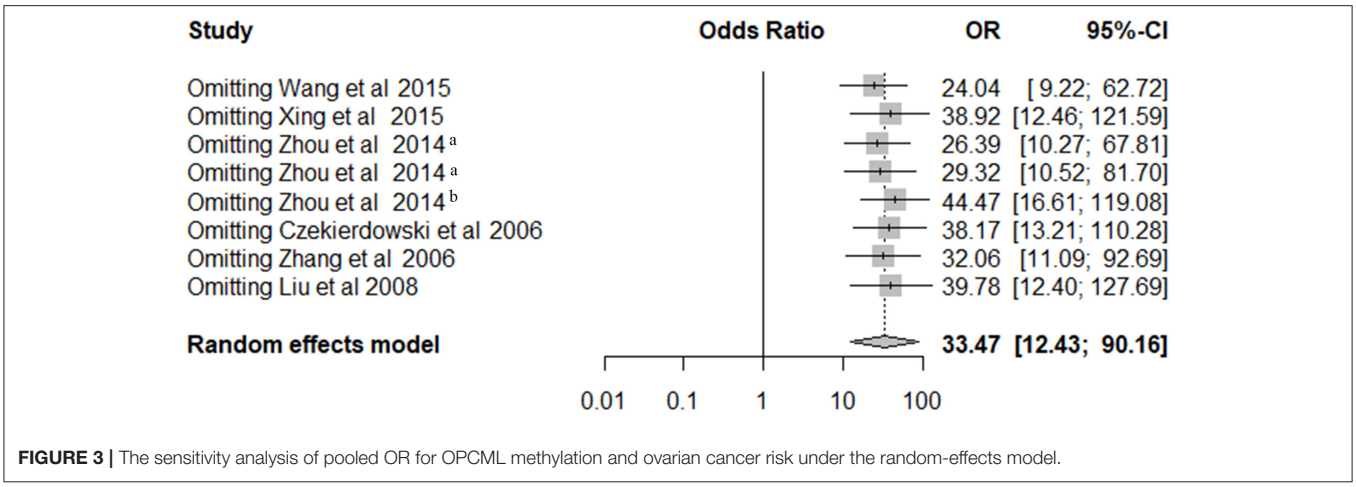

FIGURE 3 | The sensitivity analysis of pooled OR for OPCML methylation and ovarian cancer risk under the random-effects model.

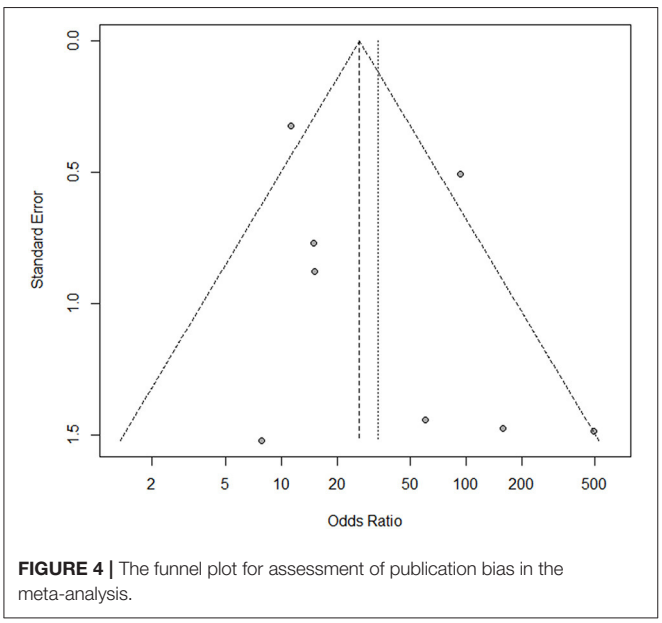

FIGURE 4 | The funnel plot for assessment of publication bias in the meta-analysis.

tissues and blood from ovarian cancer patients. Among the eight included studies, six studies clearly described that the cases were primary tumor patients whereas two studies (Wang et al., 2015; Xing et al., 2015) did not. In the study performed by Liu et al. (2008), there are 41 metastatic tissues of pelvic and abdomen cavity. We provided this in **Table 1**. However, we did not include these samples when we calculated the pooled OR. The controls in these studies were not matched to cases for any features. OPCML promoter methylation was detected in all eligible articles. There are four studies that used methylation-specific polymerase chain reaction (MSP), three used restriction enzyme-related analysis [methylation-sensitive restriction enzyme-polymerase chain reaction (MSRE-PCR) and restriction enzyme cut analysis], and one study used cationic conjugated polymer (CCP)-based fluorescence resonance energy transfer (FRET) to detect OPCML methylation in ovarian cancer and controls. According to the NOS criteria, the quality of these studies was six, indicating a relatively high quality. Detailed features are shown in **Supplementary Table 1**.

Relationship Between OPCML Methylation and Ovarian Cancer Risk

Because of significant heterogeneity among the included studies, a random-effects model was used to evaluate the effect size ($P < 0.01$; $I^2 = 65\%$; **Figure 2**). In the overall meta-analysis, the OPCML methylation frequency was significantly associated with an increased risk of ovarian cancer (summary OR: 33.47; 95% CI = 12.43–90.16; $P < 0.001$; **Figure 2**).

Meta-Regression and Subgroup Analysis

To explore the potential sources of heterogeneity, we performed multiple regression model using six variables (publication year, country, sample type, control type, methods, and sample size). However, the source of heterogeneity was not observed among these factors (all $P > 0.05$; **Table 2**). We also conducted subgroup analysis to assess the source of the heterogeneity according to country, sample type, sample size, control type, and method (**Table 3**). In the subgroup analysis of country, the OR was 38.17 (95% CI = 13.21–110.28) in China under the random-effects model. The OR was 102.86 (95% CI = 39.37–268.74) under the fixed-effects model in the serum subgroup, and 18.22 (95% CI = 10.93–30.36) under the fixed-effects model in the tissues subgroup. In the subgroup analysis based on the control type, the OR was 52.77 (95% CI = 16.92–164.55) in the NT group under the fixed-effects model and 35.50 (95% CI = 6.83–197.47) in the NT and BOT groups under the random-effects model. In the subgroup analysis of methods, the OR was 21.78 (95% CI = 6.10–77.79) in the MSP group under the random-effects model and 139.45 (95% CI = 24.06–808.26) in the restriction enzyme-related analysis group under the fixed-effects model. The OR for the sample size subgroup was 34.19 (95% CI = 14.11–82.86) in the <100 subgroup under the fixed-effects model and 35.50 (95% CI = 6.38–197.47) in the ≥100 subgroup under the random-effects model.

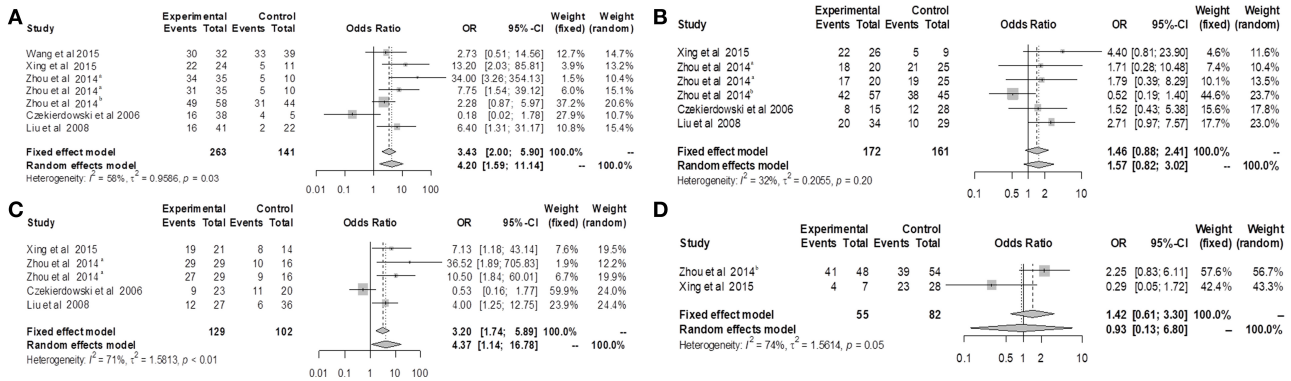

FIGURE 5 | Forest plots for OPCML methylation and clinicopathological features of ovarian cancer patients. **(A)** Forest plot for the relationship between OPCML methylation and III/IV stage. **(B)** Forest plot for the relationship between OPCML methylation and serous ovarian cancer. **(C)** Forest plot for the relationship between OPCML methylation and poorly differentiated tumor. **(D)** Forest plot for the relationship between OPCML methylation and older age.

Sensitivity Analysis

As shown in **Figure 3**, leave-one-out sensitivity analysis was performed by removing a single study at a time under the random-effects model to assess the stability of the results. Our results showed that the ORs ranged from 24.04 (95% CI = 9.22–62.72) to 44.47 (95% CI = 16.61–119.08).

Publication Bias

Begg's and Egger's tests were performed to estimate the publication bias of the included studies. The funnel plot was approximately symmetric (**Figure 4**), indicating no publication bias in Begg's ($P = 0.458$) or Egger's tests ($P = 0.261$).

Relationship Between OPCML Methylation and Clinicopathological Features

We divided the ovarian cancer patients into groups based on clinical features including stage, histological type, tumor differentiation, and age, and then further valuated the associations between other variables and OPCML methylation (**Figure 5**). The findings suggested that methylation was related to III/IV (OR = 4.20; 95% CI = 1.59–11.14) and poorly differentiated tumor (OR = 4.37; 95% CI = 1.14–16.78), while methylation was not related to serous histology (OR = 1.46; 95% CI = 0.88–2.41) or older age (OR = 1.42; 95% CI = 0.61–3.30).

Validation of the Results in Multiple Public Databases

Based on GSE146552 and GSE155760 datasets, we evaluated the DNA methylation profiling in ovarian cancer tissues and normal tissues (**Figure 6A**). We firstly analyzed the differential methylated sites between cancer tissues and normal tissues (**Figure 6B**). Then, we found that methylation levels of 55 differential methylated CpG sites were consistent in two datasets (**Table 4**). Among them, three CpG sites (cg16639665, cg23236270, cg15964611) were located in OPCML promoter regions (**Figures 6C,D**, all $P < 0.05$). In consistent with the results of meta-analysis, the methylation levels of three CpG sites were significantly higher in cancer tissues compared to normal tissues. Based on the TCGA ovarian cancer datasets, two OPCML-associated CpG sites (cg03923934, cg25853078, **Figures 7A,B**) were significantly associated with OPCML expression (rho = 0.261, $P = 5.97 \times 10^{-6}$; rho = 0.211, $P = 2.75 \times 10^{-4}$). However, we did not observe the significant associations for the clinicopathological parameters and overall survival time (**Figures 7C–F**).

DISCUSSION

In the present study, we pooled eight studies together and compared the frequency of OPCML methylation in 476 ovarian cancers with 385 non-malignant tissues or blood samples. The results indicated that OPCML methylation was associated with ovarian cancer risk. The association was still significant in subgroups according to sample type, control type, methods, and sample size. Additionally, we observed significant associations between OPCML methylation and clinical stages and the grade of differentiation in ovarian cancer based on meta-analysis.

OPCML widely downregulated in many tumor types including brain tumors (Reed et al., 2007), non-small cell lung carcinoma (Tsou et al., 2007), bladder cancer (Duarte-Pereira et al., 2011), cholangiocarcinoma (Sriraksa et al., 2011), nasopharyngeal, esophageal, gastric, hepatocellular, colorectal, breast, cervical cancers, and ovarian cancer (Cui et al., 2008). Zanini et al. (2017) found that OPCML expression is associated with better progression free survival in HER2-positive ovarian cancer patients. Notably, exogenous recombinant OPCML protein inhibited ovarian cancer cell growth *in vitro* and *in vivo* (McKie et al., 2012; Wu and Sood, 2012). Recently, the advances in structure-function relationships of OPCML give rise to its potential as an anti-cancer therapy (Birtley et al., 2019). DNA methylation is the most common epigenetic modification and is widely reported for the transcriptional silencing of tumor suppressor genes in ovarian cancer. Previous studies

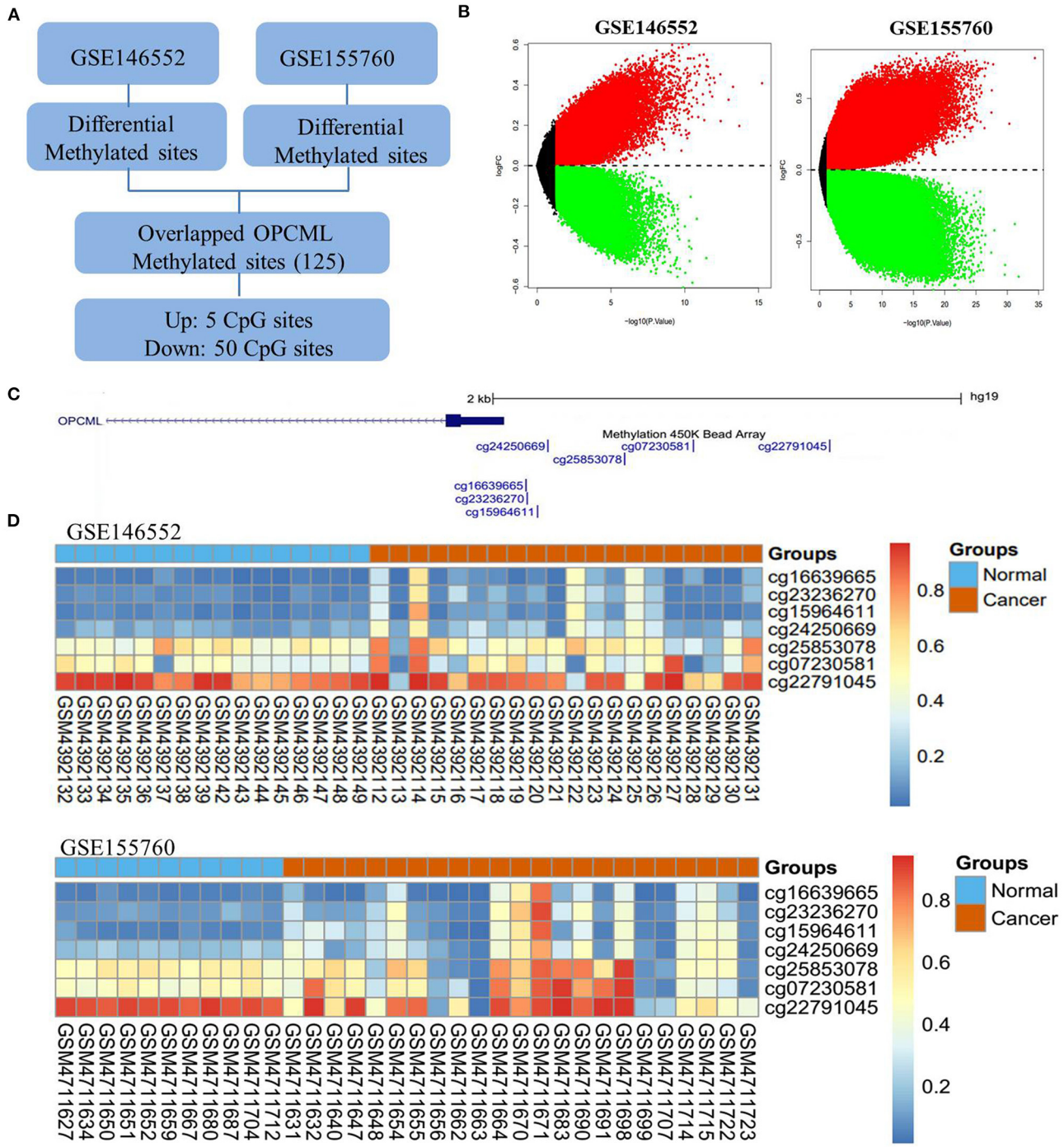

FIGURE 6 | The OPCML methylation status in ovarian cancer tissues and normal tissues. **(A)** The workflow of differential methylated sites in GSE146552 and GSE155760. **(B)** Volcano plots of differential methylated sites based on GSE146552 and GSE155760. **(C)** There are seven CpG sites in OPCML promoter regions. **(D)** The methylation status of seven CpG sites in GSE146552 and GSE155760. Among them, three differential methylated sites (cg16639665, cg23236270, cg15964611) were observed in both GSE146552 and GSE155760.

have indicated that OPCML methylation is associated with the inactivation of OPCML, which has a tumor suppressor function in ovarian cancer (Simovic et al., 2019). However, studies with small sample sizes and different control types and methylation methods might produce inconsistent results. For example, in the study performed by Czekierdowski et al. (2006) OPCML methylation was observed in 20 out of 43 cases of ovarian cancer, but no methylation was found in four

TABLE 4 | Consistently differential DNA methylated sites ($P < 0.05$ and the same direction of logFC in both datasets) between ovarian cancer tissues and normal tissues based on GEO DNA methylation datasets.

ID	chrom	chromStart	chromEnd	GSE155760		GSE146552		Gene
				logFC	*P*-value	logFC	*P*-value	
cg01875106	chr11	132287341	132287343	−0.6360	1.050×10^{-12}	−0.2740	1.500×10^{-4}	OPCML
cg11500790	chr11	132321480	132321482	−0.5980	1.400×10^{-7}	−0.3440	8.150×10^{-5}	OPCML
cg05806819	chr11	132432636	132432638	−0.0195	3.980×10^{-2}	−0.0523	3.340×10^{-2}	OPCML
cg03784083	chr11	132513894	132513896	−0.4300	4.610×10^{-4}	−0.2160	4.350×10^{-3}	OPCML
cg08080489	chr11	132526946	132526948	−0.5720	6.510×10^{-8}	−0.2800	1.240×10^{-4}	OPCML
cg17242596	chr11	132527295	132527297	−0.6000	3.930×10^{-8}	−0.3990	1.650×10^{-5}	OPCML
cg06967998	chr11	132527437	132527439	−0.6200	1.490×10^{-7}	−0.3880	2.850×10^{-5}	OPCML
cg10376306	chr11	132588617	132588619	−0.3060	7.050×10^{-4}	−0.1590	5.340×10^{-3}	OPCML
cg12156287	chr11	132662865	132662867	−0.4030	3.800×10^{-12}	−0.1600	2.330×10^{-2}	OPCML
cg18944144	chr11	132673498	132673500	−0.5470	1.730×10^{-6}	−0.2650	1.120×10^{-3}	OPCML
cg05035315	chr11	132691483	132691485	−0.6190	2.010×10^{-9}	−0.3730	7.990×10^{-6}	OPCML
cg13136241	chr11	132709827	132709829	−0.3190	1.080×10^{-3}	−0.1770	1.210×10^{-2}	OPCML
cg26824847	chr11	132728087	132728089	−0.5170	2.470×10^{-10}	−0.3810	1.270×10^{-6}	OPCML
cg19743254	chr11	132735813	132735815	−0.3410	1.090×10^{-3}	−0.1950	1.950×10^{-2}	OPCML
cg10966440	chr11	132745700	132745702	−0.6570	7.910×10^{-11}	−0.4670	8.810×10^{-7}	OPCML
cg23813681	chr11	132772322	132772324	−0.4060	1.880×10^{-4}	−0.1810	2.100×10^{-2}	OPCML
cg16813466	chr11	132811377	132811379	−0.4090	6.750×10^{-5}	−0.2440	1.190×10^{-3}	OPCML
cg07649562	chr11	132813503	132813505	0.0662	4.840×10^{-2}	0.0419	2.210×10^{-2}	OPCML
cg18710784	chr11	132813562	132813564	0.2530	9.680×10^{-3}	0.2100	1.020×10^{-3}	OPCML
cg15618210	chr11	132816802	132816804	−0.6010	9.760×10^{-8}	−0.3020	5.000×10^{-4}	OPCML
cg02993944	chr11	132831380	132831382	−0.3230	1.030×10^{-3}	−0.1520	1.250×10^{-2}	OPCML
cg16123848	chr11	132853100	132853102	−0.4960	9.470×10^{-6}	−0.3320	3.560×10^{-4}	OPCML
cg11747462	chr11	132869599	132869601	−0.2650	6.650×10^{-4}	−0.1320	2.100×10^{-2}	OPCML
cg03887438	chr11	132910641	132910643	−0.3410	3.090×10^{-13}	−0.1540	5.610×10^{-3}	OPCML
cg18413062	chr11	132931731	132931733	−0.4250	1.660×10^{-9}	−0.2350	5.720×10^{-4}	OPCML
cg13296579	chr11	132934961	132934963	−0.1630	3.160×10^{-2}	−0.0885	3.160×10^{-2}	OPCML, AP004782.1
cg20417723	chr11	132935119	132935121	−0.2570	4.250×10^{-3}	−0.1440	1.560×10^{-2}	OPCML, AP004782.1
cg26906285	chr11	132935462	132935464	−0.1720	1.820×10^{-2}	−0.1560	3.880×10^{-3}	OPCML, AP004782.1
cg05886537	chr11	132936427	132936429	−0.3250	2.030×10^{-3}	−0.1770	3.810×10^{-3}	OPCML, AP004782.1
cg08945802	chr11	132946454	132946456	−0.1980	1.710×10^{-2}	−0.0864	4.530×10^{-2}	OPCML
cg05807849	chr11	132946691	132946693	−0.4100	2.210×10^{-5}	−0.2090	7.820×10^{-3}	OPCML
cg11983942	chr11	132946933	132946935	−0.3910	8.510×10^{-8}	−0.1930	8.810×10^{-4}	OPCML
cg08357627	chr11	132949125	132949127	−0.5150	3.900×10^{-11}	−0.2480	3.460×10^{-4}	OPCML
cg11515095	chr11	132949436	132949438	−0.3320	1.500×10^{-3}	−0.1840	8.340×10^{-3}	OPCML
cg10335834	chr11	132949780	132949782	−0.2800	1.370×10^{-3}	−0.1570	1.030×10^{-2}	OPCML
cg15702349	chr11	132950103	132950105	−0.1970	4.550×10^{-3}	−0.0989	1.620×10^{-2}	OPCML
cg26237595	chr11	132955641	132955643	−0.2940	6.960×10^{-3}	−0.1910	6.130×10^{-3}	OPCML
cg01311955	chr11	132965249	132965251	−0.2780	1.140×10^{-4}	−0.2670	1.270×10^{-3}	OPCML
cg20972294	chr11	133005918	133005920	−0.3710	9.260×10^{-4}	−0.1940	1.420×10^{-2}	OPCML
cg12697833	chr11	133085432	133085434	−0.5370	9.690×10^{-8}	−0.2850	1.670×10^{-3}	OPCML
cg26311804	chr11	133155302	133155304	−0.3740	4.070×10^{-4}	−0.1680	6.610×10^{-3}	OPCML
cg04913291	chr11	133187955	133187957	−0.4150	9.420×10^{-6}	−0.2830	1.090×10^{-3}	OPCML
cg22209355	chr11	133208306	133208308	−0.3650	6.770×10^{-4}	−0.2050	6.410×10^{-4}	OPCML
cg05131064	chr11	133228365	133228367	−0.2820	2.300×10^{-3}	−0.1370	2.400×10^{-2}	OPCML
cg08872013	chr11	133229156	133229158	−0.2390	3.790×10^{-3}	−0.1100	2.460×10^{-2}	OPCML
cg20886183	chr11	133230390	133230392	−0.2530	4.390×10^{-3}	−0.1980	1.230×10^{-2}	OPCML, OPCML-IT1
cg01880176	chr11	133230949	133230951	−0.3070	7.980×10^{-5}	−0.1540	4.180×10^{-3}	OPCML, OPCML-IT1
cg06379368	chr11	133231146	133231148	−0.2650	1.750×10^{-3}	−0.1630	1.330×10^{-2}	OPCML, OPCML-IT1
cg13974487	chr11	133231880	133231882	−0.2720	1.790×10^{-3}	−0.1710	1.340×10^{-3}	OPCML, OPCML-IT1
cg18204273	chr11	133232926	133232928	−0.1850	2.260×10^{-2}	−0.1540	1.490×10^{-2}	OPCML, OPCML-IT1
cg01140660	chr11	133233199	133233201	−0.4660	1.190×10^{-4}	−0.2160	5.430×10^{-3}	OPCML, OPCML-IT1

(Continued)

TABLE 4 | Continued

ID	chrom	chromStart	chromEnd	GSE155760		GSE146552		Gene
				logFC	*P*-value	logFC	*P*-value	
cg09531376	chr11	133234072	133234074	−0.3370	1.850×10^{-3}	−0.1560	4.630×10^{-3}	OPCML, OPCML-IT1
cg16639665	chr11	133402496	133402498	0.1380	3.450×10^{-2}	0.1130	1.090×10^{-2}	OPCML
cg23236270	chr11	133402499	133402501	0.1630	2.090×10^{-2}	0.1150	4.540×10^{-3}	OPCML
cg15964611	chr11	133402544	133402546	0.2070	2.630×10^{-3}	0.1080	3.180×10^{-2}	OPCML

Bold values represent CpG sites in OPCML promoter region.

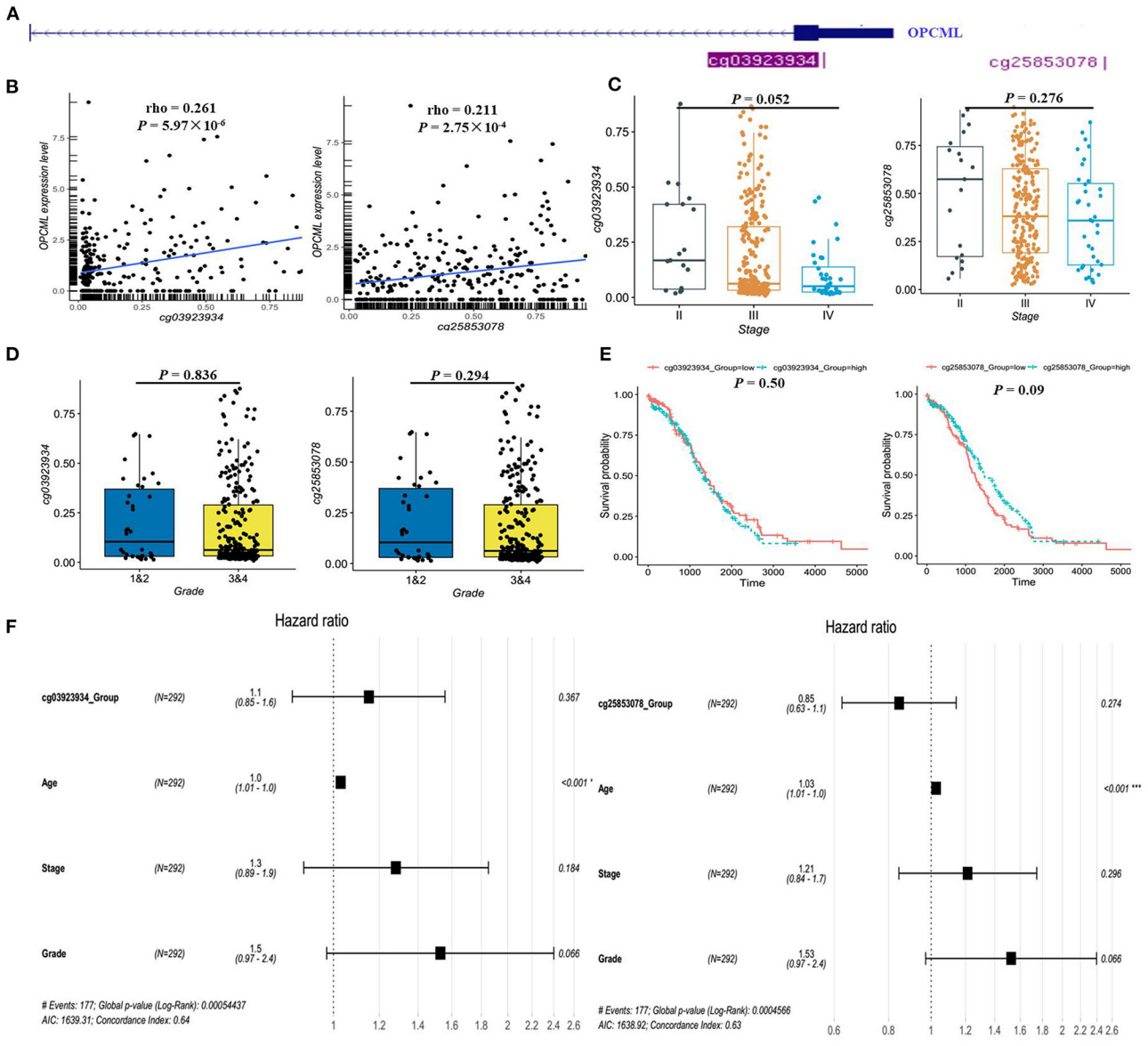

FIGURE 7 | The methylation status of OPCML-associated CpG sites in the TCGA dataset. **(A)** There are only two CpG sites from HumanMethylation27k, and the location of two CpG sites in OPCML. **(B)** There are significantly positive associations between two CpG sites and OPCML expression. **(C)** The methylation levels were not significantly associated with clinical stage. **(D)** The methylation levels were not significantly associated with clinical grade. **(E)** No significant associations were observed in patient with different methylation levels using log-rank analysis. **(F)** No significant associations were observed in patient with different methylation levels using cox analysis.

normal ovaries. No significant association was observed in this study. The control sample size in this study was small. Additionally, most previous studies reported the methylation frequency of OPCML in tumor and non-tumor tissues or serum, but the precise estimates for the associations were unclear. In the present study, we attempted to consolidate the available data and found that OPCML methylation was associated with an increased risk of ovarian cancer. The findings from the sensitivity analysis showed that our results are reliable and stable. Overall, given the TSG role and frequent methylation inactivation of OPCML in ovarian cancer, the restoration of OPCML expression could be a promising approach for ovarian cancer treatment.

In the subgroup analysis, the OR was 38.17 in China but 7.85 in Poland. The cause may be due to the limited studies in Poland. Therefore, more studies should be performed to confirm these observations in Europeans. In the serum subgroup, the OR value was highest (OR = 102.86) than that in the tissue subgroup (OR = 18.22). The results should be interpreted with caution because of the relatively small number of subjects included in the serum subgroup. Given that serum is a promising biomarker for non-invasive ovarian cancer diagnosis, further well-designed studies are warranted to explore the diagnostic performance of OPCML methylation in serum. Regarding the methods, the OR was 21.78 in the MSP group and 139.45 in the restriction enzyme-related analysis group. Technically, MSP amplify either methylated (M) or unmethylated (U) alleles after bisulfite conversion and evaluate methylation status in CpG regions (Herman et al., 1996). MSRE-PCR can recognize and degrade unmethylated DNA sequences whereas the methylated DNA sequences remain intact (Ramsahoye et al., 1997).Taken together, the results of subgroup analyses showed that OPCML methylation was significantly associated with an increased risk of ovarian cancer, regardless of the sample size, sample type, control type, and methods. Additionally, we found that the methylation status was associated with III/IV stage and poorly differentiated tumors. This finding suggests that OPCML is related to the malignant progression of ovarian cancer.

Based on publicly available datasets, we observed that the DNA methylation levels of cg16639665, cg23236270, and cg15964611 were consistently higher in cancer tissues than that in normal tissues, which validated some results of our meta-analysis. However, we did not confirm the difference of the OPCML methylation levels in different groups of clinical stage, grade, and so on. We found the positive association between DNA methylation level of cg25853078 in OPCML promoter region and OPCML expression. This positive association did not fit the hypothesis that DNA methylation levels in promoter region suppress the expression and contribute to ovarian cancer development. The DNA methylation levels in previous published papers were regions but not one CpG site. There are some CpG sites in OPCML promoter region, but we only assessed one CpG site in the promoter region based on the HumanMethylation27 platform. Therefore, other CpG sites were not calculated based on the TCGA data, which may have significant roles in the regulation of OPCML expression. Our study possessed several limitations. First, the total sample size in our study was relatively small and enrolled studies had low quality. Second, all the eligible studies were case-control designs and we could not explore the causation between OPCML methylation and ovarian cancer risk. Additionally, we used the incidence of OPCML methylation in the case and control groups to evaluate the pooled estimates because the adjusted ORs were not reported in the original studies. Further prospective studies with large samples are warranted to determine the role of OPCML in ovarian cancer risk and progression.

DATA AVAILABILITY STATEMENT

The original contributions presented in the study are included in the article/**Supplementary Material**, further inquiries can be directed to the corresponding authors.

AUTHOR CONTRIBUTIONS

YS, KX, and JW: conception and design. YS and JK: acquisition of data. HX, XW, YC, WL, JH, and DL: analysis and interpretation of data. YS, KX, and JW: manuscript drafting or revising. All authors contributed to the article and approved the submitted version.

FUNDING

This work was financially supported by the Nanjing Medical Science and Technique Development Foundation (JQX18009) and National Natural Science Foundation of China (81702569).

ACKNOWLEDGMENTS

We are thankful to the publicly available datasets (TCGA, GEO).

SUPPLEMENTARY MATERIAL

The Supplementary Material for this article can be found online at: https://www.frontiersin.org/articles/10.3389/fcell.2021.570898/full#supplementary-material

REFERENCES

Begg, C. B., and Mazumdar, M. (1994). Operating characteristics of a rank correlation test for publication bias. *Biometrics* 50, 1088–1101. doi: 10.2307/2533446

Birtley, J. R., Alomary, M., Zanini, E., Antony, J., Maben, Z., Weaver, G. C., et al. (2019). Inactivating mutations and X-ray crystal structure of the tumor suppressor OPCML reveal cancer-associated functions. *Nat. Commun.* 10:3134. doi: 10.1038/s41467-019-10966-8

Chen, H., Ye, F., Zhang, J., Lu, W., Cheng, Q., and Xie, X. (2007). Loss of OPCML expression and the correlation with CpG island methylation and LOH in ovarian serous carcinoma. *Eur. J. Gynaecol. Oncol.* 28, 464–467.

Cui, Y., Ying, Y., van Hasselt, A., Ng, K. M., Yu, J., Zhang, Q., et al. (2008). OPCML is a broad tumor suppressor for multiple carcinomas and

lymphomas with frequently epigenetic inactivation. *PLoS ONE* 3:e2990. doi: 10.1371/journal.pone.0002990

Czekierdowski, A., Czekierdowska, S., Szymanski, M., Wielgos, M., Kaminski, P., and Kotarski, J. (2006). Opioid-binding protein/cell adhesion molecule-like (OPCML) gene and promoter methylation status in women with ovarian cancer. *Neuro Endocrinol. Lett*. 27, 609–613.

Duarte-Pereira, S., Paiva, F., Costa, V. L., Ramalho-Carvalho, J., Savva-Bordalo, J., Rodrigues, A., et al. (2011). Prognostic value of opioid binding protein/cell adhesion molecule-like promoter methylation in bladder carcinoma. *Eur. J. Cancer*. 47, 1106–1114. doi: 10.1016/j.ejca.2010.12.025

Egger, M., Davey Smith, G., Schneider, M., and Minder, C. (1997). Bias in meta-analysis detected by a simple, graphical test. *BMJ* 315, 629–634. doi: 10.1136/bmj.315.7109.629

Ehrlich, M. (2002). DNA methylation in cancer: too much, but also too little. *Oncogene* 21, 5400–5413. doi: 10.1038/sj.onc.1205651

Herman, J. G., Graff, J. R., Myöhänen, S., Nelkin, B. D., and Baylin, S. B. (1996). Methylation-specific PCR: a novel PCR assay for methylation status of CpG islands. *Proc. Natl. Acad. Sci. U.S.A*. 93, 9821–9826. doi: 10.1073/pnas.93.18.9821

Jones, P. A. (2012). Functions of DNA methylation: islands, start sites, gene bodies and beyond. *Nat. Rev. Genet*. 13, 484–492. doi: 10.1038/nrg3230

Lheureux, S., Gourley, C., Vergote, I., and Oza, A. M. (2019). Epithelial ovarian cancer. *Lancet* 393, 1240–1253. doi: 10.1016/S0140-6736(18)32552-2

Liu, M., Wang, Y., Cao, X., Zhou, F., Qiao, H., Lu, X., et al. (2008). The relationship between the incidence of OPCML methylation and the development of epithelial ovarian cancer (in Chinese). *China Oncol*. 18, 950–952.

McKie, A. B., Vaughan, S., Zanini, E., Okon, I. S., Louis, L., de Sousa, C., et al. (2012). The OPCML tumor suppressor functions as a cell surface repressor-adaptor, negatively regulating receptor tyrosine kinases in epithelial ovarian cancer. *Cancer Discov*. 2, 156–171. doi: 10.1158/2159-8290.CD-11-0256

Ramsahoye, B. H., Burnett, A. K., and Taylor, C. (1997). Restriction endonuclease isoschizomers ItaI, BsoFI and Fsp4HI are characterised by differences in their sensitivities to CpG methylation. *Nucl. Acids Res*. 25, 3196–3198. doi: 10.1093/nar/25.16.3196

Rauscher, G. H., Kresovich, J. K., Poulin, M., Yan, L., Macias, V., Mahmoud, A. M., et al. (2015). Exploring DNA methylation changes in promoter, intragenic, and intergenic regions as early and late events in breast cancer formation. *BMC Cancer* 15:816. doi: 10.1186/s12885-015-1777-9

Reed, J. E., Dunn, J. R., du Plessis, D. G., Shaw, E. J., Reeves, P., Gee, A. L., et al. (2007). Expression of cellular adhesion molecule 'OPCML' is down-regulated in gliomas and other brain tumours. *Neuropathol. Appl. Neurobiol*. 33, 77–85. doi: 10.1111/j.1365-2990.2006.00786.x

Sellar, G. C., Watt, K. P., Rabiasz, G. J., Stronach, E. A., Li, L., Miller, E. P., et al. (2003). OPCML at 11q25 is epigenetically inactivated and has tumor-suppressor function in epithelial ovarian cancer. *Nat. Genet*. 34, 337–343. doi: 10.1038/ng1183

Simovic, I., Castaño-Rodríguez, N., and Kaakoush, N. O. (2019). OPCML: a promising biomarker and therapeutic avenue. *Trends Cancer* 5, 463–466. doi: 10.1016/j.trecan.2019.06.002

Song, L., Jia, J., Peng, X., Xiao, W., and Li, Y. (2017). The performance of the SEPT9 gene methylation assay and a comparison with other CRC screening tests: a meta-analysis. *Sci. Rep*. 7:3032. doi: 10.1038/s41598-017-03321-8

Sriraksa, R., Zeller, C., El-Bahrawy, M. A., Dai, W., Daduang, J., Jearanaikoon, P., et al. (2011). CpG-island methylation study of liver fluke-related cholangiocarcinoma. *Br. J. Cancer* 104, 1313–1318. doi: 10.1038/bjc.2011.102

Sung, H., Ferlay, J., Siegel, R. L., Laversanne, M., Soerjomataram, I., Jemal, A., et al. (2021). Global cancer statistics 2020: GLOBOCAN estimates of incidence and mortality worldwide for 36 cancers in 185 countries. *CA Cancer J. Clin*. doi: 10.3322/caac.21660. [Epub ahead of print].

Szyf, M. (2012). DNA methylation signatures for breast cancer classification and prognosis. *Genome Med*. 4:26. doi: 10.1186/gm325

Tsou, J. A., Galler, J. S., Siegmund, K. D., Laird, P. W., Turla, S., Cozen, W., et al. (2007). Identification of a panel of sensitive and specific DNA methylation markers for lung adenocarcinoma. *Mol. Cancer* 6:70. doi: 10.1186/1476-4598-6-70

Vidal, E., Sayols, S., Moran, S., Guillaumet-Adkins, A., Schroeder, M. P., Royo, R., et al. (2017). A DNA methylation map of human cancer at single base-pair resolution. *Oncogene* 36, 5648–5657. doi: 10.1038/onc.2017.176

Wang, B., Yu, L., Luo, X., Huang, L., Li, Q. S., Shao, X. S., et al. (2017). Detection of OPCML methylation, a possible epigenetic marker, from free serum circulating DNA to improve the diagnosis of early-stage ovarian epithelial cancer. *Oncol. Lett*. 14, 217–223. doi: 10.3892/ol.2017.6111

Wang, B., Yu, L., Yang, G. Z., Luo, X., and Huang, L. (2015). Application of multiplex nested methylated specific PCR in early diagnosis of epithelial ovarian cancer. *Asian Pa.c J. Cancer Prev*. 16, 3003–3007. doi: 10.7314/APJCP.2015.16.7.3003

Widschwendter, M., Jones, A., Evans, I., Reisel, D., Dillner, J., Sundström, K., et al. (2018). Epigenome-based cancer risk prediction: rationale, opportunities and challenges. *Nat. Rev. Clin. Oncol*. 15, 292–309. doi: 10.1038/nrclinonc.2018.30

Widschwendter, M., Zikan, M., Wahl, B., Lempiäinen, H., Paprotka, T., Evans, I., et al. (2017). The potential of circulating tumor DNA methylation analysis for the early detection and management of ovarian cancer. *Genome Med*. 9:116. doi: 10.1186/s13073-017-0500-7

Wilson, A. S., Power, B. E., and Molloy, P. L. (2007). DNA hypomethylation and human diseases. *Biochim. Biophys. Acta* 1775, 138–162. doi: 10.1016/j.bbcan.2006.08.007

Wu, S. Y., and Sood, A. K. (2012). New roles opined for OPCML. *Cancer Discov*. 2, 115–116. doi: 10.1158/2159-8290.CD-11-0356

Xing, B. L., Li, T., Tang, Z. H., Jiao, L., Ge, S. M., Qiang, X., et al. (2015). Cumulative methylation alternations of gene promoters and protein markers for diagnosis of epithelial ovarian cancer. *Genet. Mol. Res*. 14, 4532–4540. doi: 10.4238/2015.May.4.11

Zanini, E., Louis, L. S., Antony, J., Karali, E., Okon, I. S., McKie, A. B., et al. (2017). The tumor-suppressor protein OPCML potentiates anti-EGFR- and anti-HER2-targeted therapy in HER2-positive ovarian and breast cancer. *Mol Cancer Ther*. 16, 2246–2256. doi: 10.1158/1535-7163.MCT-17-0081

Zhang, J., Xing, B., Song, J., Zhang, F., Nie, C., Jiao, L., et al. (2014). Associated analysis of DNA methylation for cancer detection using CCP-based FRET technique. *Anal. Chem*. 86, 346–350. doi: 10.1021/ac402720g

Zhang, J., Ye, F., Chen, H. Z., Ye, D. F., Lu, W. G., and Xie, X. (2006). Deletion of OPCML gene and promoter methylation in ovarian epithelial carcinoma (in Chinese). *Zhongguo Yi Xue Ke Xue Yuan Xue Bao* 28, 173–177.

Zhou, F., Cao, X., Ma, M., Liu, M., and Tao, G. (2011). Detection of OPCML methylation in tissues of ovarian cancer by MSRE-PCR. *Chin. J. Clin. Lab. Sci*. 29, 427–429.

Zhou, F., Ma, M., Tao, G., Chen, X., Xie, W., Wang, Y., et al. (2014a). Detection of circulating methylated opioid binding protein/cell adhesion molecule-like gene as a biomarker for ovarian carcinoma. *Clin. Lab*. 60, 759–765. doi: 10.7754/Clin.Lab.2013.130446

Zhou, F., Tao, G., Chen, X., Xie, W., Liu, M., and Cao, X. (2014b). Methylation of OPCML promoter in ovarian cancer tissues predicts poor patient survival. *Clin. Chem. Lab. Med*. 52, 735–742. doi: 10.1515/cclm-2013-0736

Conflict of Interest: The authors declare that the research was conducted in the absence of any commercial or financial relationships that could be construed as a potential conflict of interest.

frontiers in Cell and Developmental Biology

ORIGINAL RESEARCH
published: 11 June 2021
doi: 10.3389/fcell.2021.682561

Genome-Wide Histone H3K27 Acetylation Profiling Identified Genes Correlated With Prognosis in Papillary Thyroid Carcinoma

Luyao Zhang[1†], Dan Xiong[2†], Qian Liu[3], Yiling Luo[3], Yuhan Tian[2], Xi Xiao[1], Ye Sang[4], Yihao Liu[5], Shubin Hong[1], Shuang Yu[1], Jie Li[6], Weiming Lv[6], Yanbing Li[1], Zhonghui Tang[2], Rengyun Liu[4], Qian Zhong[3]* and Haipeng Xiao[1]**

[1] Department of Endocrinology, The First Affiliated Hospital, Sun Yat-sen University, Guangzhou, China, [2] Zhongshan School of Medicine, Sun Yat-sen University, Guangzhou, China, [3] Sun Yat-sen University Cancer Center, State Key Laboratory of Oncology in South China, Collaborative Innovation Center for Cancer Medicine, Guangzhou, China, [4] Institute of Precision Medicine, The First Affiliated Hospital, Sun Yat-sen University, Guangzhou, China, [5] Clinical Trials Unit, The First Affiliated Hospital, Sun Yat-sen University, Guangzhou, China, [6] Department of Breast and Thyroid Surgery, The First Affiliated Hospital, Sun Yat-sen University, Guangzhou, China

OPEN ACCESS

Edited by:
Xiao Zhu,
Guangdong Medical University, China

Reviewed by:
Yanqiang Li,
Boston Children's Hospital and Harvard Medical School, United States
Chongming Jiang,
Baylor College of Medicine, United States

***Correspondence:**
Haipeng Xiao
xiaohp@mail.sysu.edu.cn
Qian Zhong
zhongqian@sysucc.org.cn
Rengyun Liu
liury9@mail.sysu.edu.cn

[†] These authors have contributed equally to this work

Specialty section:
This article was submitted to Epigenomics and Epigenetics, a section of the journal Frontiers in Cell and Developmental Biology

Received: 18 March 2021
Accepted: 14 May 2021
Published: 11 June 2021

Citation:
Zhang L, Xiong D, Liu Q, Luo Y, Tian Y, Xiao X, Sang Y, Liu Y, Hong S, Yu S, Li J, Lv W, Li Y, Tang Z, Liu R, Zhong Q and Xiao H (2021) Genome-Wide Histone H3K27 Acetylation Profiling Identified Genes Correlated With Prognosis in Papillary Thyroid Carcinoma. Front. Cell Dev. Biol. 9:682561. doi: 10.3389/fcell.2021.682561

Thyroid carcinoma (TC) is the most common endocrine malignancy, and papillary TC (PTC) is the most frequent subtype of TC, accounting for 85–90% of all the cases. Aberrant histone acetylation contributes to carcinogenesis by inducing the dysregulation of certain cancer-related genes. However, the histone acetylation landscape in PTC remains elusive. Here, we interrogated the epigenomes of PTC and benign thyroid nodule (BTN) tissues by applying H3K27ac chromatin immunoprecipitation followed by deep sequencing (ChIP-seq) along with RNA-sequencing. By comparing the epigenomic features between PTC and BTN, we detected changes in H3K27ac levels at active regulatory regions, identified PTC-specific super-enhancer-associated genes involving immune-response and cancer-related pathways, and uncovered several genes that associated with disease-free survival of PTC. In summary, our data provided a genome-wide landscape of histone modification in PTC and demonstrated the role of enhancers in transcriptional regulations associated with prognosis of PTC.

Keywords: papillary thyroid carcinoma, benign thyroid nodule, enhancer, H3K27ac, transcriptome, epigenetics

INTRODUCTION

Thyroid carcinoma (TC) is the most common endocrine malignancy with an increasing incidence during the past decades (Kilfoy et al., 2009). Papillary TC (PTC) is the most frequent subtype, which accounts for 85–90% of all the TC cases and occurs three times more frequently in women than in men (Jemal et al., 2010). It is now well accepted that both genetic alterations and epigenetic changes contribute to PTC development and progression. Some somatic driver mutations, such as the *BRAF* V600E and *TERT* promoter mutations (Liu et al., 2017), and epigenetic alterations, such as specific non-coding RNAs and DNA methylation modifications (Yu et al., 2012; Yim et al., 2019), have been well established as diagnostic and prognostic markers of PTC.

Histones are subject to a variety of post-transcriptional modifications including methylation, acetylation, phosphorylation, and ubiquitination (Bártová et al., 2008; Matsuda et al., 2015), which influence interactions between DNA and histones, resulting in global regulation of gene expression. Typically, histone acetylation is related to active transcription, while deacetylation

induced transcriptional silencing. Histone modifications control gene expression, and numerous studies have found that dysregulation of this modification functionally impacts transcriptome in carcinogenesis. Several histone deacetylated inhibitors such as vorinostat (SAHA), a suberoylanilide hydroxamic acid that inhibits deacetylase enzymatic activity, had been used in clinical trials treating TC patients. Moreover, it was reported that SAHA induced apoptosis in PTC cell lines (Brest et al., 2011). Recently, one study reported global levels of histone modifications in four thyroid tissues (Siu et al., 2017). Studies reported histone acetylation increment at the promoters of *NIS* and *ECAD* in TC cells (Federico et al., 2009; Zhang et al., 2014).

It is now recognized that enhancers and super-enhancers (SEs) are crucial components of genetic transcription regulators in cancers. Enhancer, a DNA region that transcription factors can bind, could positively regulate gene expression in *cis*- or *trans*- manner. It has been proposed that tumorigenesis is usually accompanied by dysregulation of enhancer activities (Bulger and Groudine, 2011). SEs, defined as clusters of enhancers densely occupied with mediators and chromatin regulators, can facilitate expressions of important genes in determining cell identity and fate (Whyte et al., 2013). Characterized by high levels of H3K27ac, enhancers can be readily identified by chromatin immunoprecipitation followed by deep-sequencing (CHIP-seq). Moreover, SEs are more prone to perturbations than typical enhancers (Zhou et al., 2015). One of the mechanisms that histone acetylation mediates RNA transcriptions is to interact with the bromodomain and extra-terminal domain (BET) protein BRD4 (Dey et al., 2003), which could serve as potential therapeutic targets of cancers. BET inhibitor JQ1 inhibits interactions between BET protein and acetylated histones, resulting in downregulation of a number of genes and related signaling pathways (Filippakopoulos et al., 2010). It has been reported that JQ1 inhibited the tumor growth in differentiated and undifferentiated TC (Gao et al., 2016; Zhu et al., 2017).

Accumulating evidence underscored the role of enhancer-driven transcriptional programs in tumor pathogenesis. However, the H3K27ac landscape and enhancer pattern of PTC remained unclear. Here, we generated reference epigenome data for PTC and benign thyroid nodule (BTN) tissues using H3K27ac ChIP-seq along with global transcriptome, comparing epigenomic features and SEs between these two groups. This study provided an epigenetic insight for understanding the development of PTC, revealing regulations of epigenomic modifications on the transcription level, and identified several enhancer-regulated genes that hold the potential to serve as diagnostic and prognostic markers for PTC.

MATERIALS AND METHODS

Thyroid Tissues

This study included eight PTC and four BTN female cases who were treated at The First Affiliated Hospital of Sun Yat-sen University. The diagnosis of PTC was performed according to the WHO criteria. The thyroid specimens and clinicopathologic data were collected after our institutional review board approval.

H3K27ac ChIP-seq and Library Preparation

Primary PTC and BTN were pulverized in liquid nitrogen with mortar. Tissue powder was then cross-linked with 1% formaldehyde and lysed with lysis buffer. Genomic DNA was then sonicated into 200 to 500 bp fragments using ultrasonicator in lysis buffer. The supernatant was diluted, and the lysates were incubated with anti-H3K27ac antibody (ab4729; Abcam, Cambridge, United Kingdom) overnight at 4°C. Protein–DNA complexes were captured with protein A agarose beads. After extensive washing, protein–DNA complexes were eluted and reverse cross-linked. DNA was purified with QIAGEN (Hilden, Germany) PCR purification kit (Cat No. 28106). Ten nanograms of purified DNA was used for downstream library-prep with NEBNext Ultra II DNA Library Prep Kit for Illumina (NEB #E7103; New England Biolabs, Ipswich, MA, United States), following the manufacturer's instructions. The quality of sequencing libraries was analyzed with bioanalyzer (Agilent Technologies, Santa Clara, CA, United States) and then sequenced by Illumina NovaSeq 6000 platform. Input DNA from each sample were sequenced using different bar codes.

Processing of Raw ChIP-seq Data

The clean ChIP-seq reads were aligned to the human genome (hg38) using BWA with default parameters. Then, the unmapped reads and non-uniquely mapped reads (mapping quality < 20) were removed by SAMtools, while the PCR duplicate reads were filtered by Picard. The H3K27ac modification regions were defined using MACS. To find out the differential H3K27ac modification region, the modification regions were merged by BEDtools, and the reads of the merged regions were estimated by HTSeq. Finally, DESeq2 was performed to normalize the counts and to detect differential H3K27ac regions ($|$ fold change$| \geq 2$ and p value < 0.05).

RNA-seq and Library Preparation

Primary tissues were pulverized in liquid nitrogen, and RNA was extracted with TRIzol (Invitrogen, Carlsbad, CA, United States) following manufacturer's protocol. RNA-seq was performed by Berry Genomics Co., China. Briefly, RNA degradation and contamination were monitored on 1% agarose gels, and purity was checked with NanoPhotometer spectrophotometer (IMPLEN, Westlake Village, CA, United States). RNA integrity was assessed with RNA Nano 6000 Assay Kit of the Bioanalyzer 2100 system (Agilent Technologies, Santa Clara, CA, United States). A total amount of 1 μg of RNA per sample was used as input material for the RNA preparations. Sequencing libraries were generated with NEBNext Ultra RNA Library Prep Kit for Illumina (NEB, United States) following manufacturer's recommendations, and index codes were added to attribute sequences to corresponding sample. Library quality was assessed on the Agilent Bioanalyzer 2100 system. After cluster generation, the library preparations were sequenced on an Illumina NovaSeq 6000 platform.

Processing of Raw RNA-seq Data

Differential expression analysis was performed with DESeq; the clean RNA-seq reads were aligned to the human genome (hg38) using HISAT with default parameters. Then, the reads overlapped with genes were estimated by HTseq. The normalization, counts, and detection of differentially expressed genes were performed by DEseq2 ($|$ fold change$| \geq 2$ and p value < 0.05).

Pathway Enrichment Analysis

Genomic Regions Enrichment of Annotations Tool (GREAT)[1] was used to analyze the functional significance of differentiated H3K27ac-modified regions (McLean et al., 2010). Pathway analysis was performed with gene names using DAVID. Selected Kyoto Encyclopedia of Genes and Genomes (KEGG) pathways that have p values of less than 0.05 were reported. Pathway enrichment analysis was performed using gene set enrichment analysis (GSEA)[2] (Liao et al., 2019).

Identification of Enhancer

Enhancers and promoters were identified by MACS (Liu, 2014). To identify SEs, all enhancers were ranked according to their total ChIP-seq signal using ROSE (Zhou et al., 2015). Enhancers were sorted and plotted based on H3K27ac signals in ascending order. The cutoff value was set to distinguish SEs from typical enhancers, in which enhancers were assigned as SEs if their H3K27ac signals exceeded this threshold level.

Cell Culture

BCPAP and KTC-1 cells were cultured in RPMI-1640 media supplemented with 10% fetal bovine serum (FBS; #10270-106; Gibco, Thermo Fisher Scientific, Waltham, MA, United States). TPC-1 cells were cultured with Dulbecco modified Eagle medium supplemented with 10% FBS (Gibco). All the cells were maintained at 37°C in a 5% CO_2 humidified chamber.

SAHA/JQ1 Treatment

BCPAP, KTC-1, and TPC-1 cells were seeded on day 0 and treated with JQ1 (S7110; Selleck, Houston, TX, United States) or Vorinostat (SAHA) (S1047; Selleck) or vehicle for 48 h with indicated concentrations on day 1. Fresh culture medium with drugs or vehicle was replenished every 24 h.

qRT-PCR

Total mRNAs were extracted using RNAsimple Total RNA Kit (#DP419; TIANGEN Biotech, Beijing, China). Five hundred nanograms of mRNA was used as template for reverse transcription with PrimeScript RT Master Mix (RR036A; Takara, Dalian, China). cDNAs were then amplified on ABI QuantStudio 5 Real-Time PCR System (Thermo Fisher), and SYBR Green Master Mix (A25742; Thermo Fisher Scientific, Waltham, MA, United States) was used to detect cDNA amplification. GAPDH was used to normalize gene expression. RNA relative expression was calculated using the $2^{-\Delta\Delta CT}$ method.

[1] http://great.stanford.edu/

[2] http://www.webgestalt.org/

Statistical Analysis

Statistical analyses were performed using R and GraphPad Prism software. Student's t-test was performed to compare two groups of the continuous variables. All the p values were two-sided, and $p < 0.05$ was regarded as statistically significant.

RESULTS

Epigenetic Landscapes of Papillary Thyroid Carcinoma and Benign Thyroid Nodule

To identify histotype-specific landscapes of active chromatin in thyroid tissues, ChIP-seq using H3K27ac (acetylated lysine 27 of histone H3) antibody was performed on eight PTC and four BTN samples from 12 Chinese females (**Supplementary Data**). Model-based analysis for ChIP-seq (MACS) was used to analyze and identify significant peaks from the samples. Principal component analysis (PCA) indicated that PTC and BTN samples grouped into two clusters according to their genome-wide H3K27ac profiles, suggesting that the differences were etiology specific (**Figure 1A**). When comparing H3K27ac peaks between PTC and BTN, 395 peaks were unique to PTC samples, while 437 peaks were unique to BTN. With all the differentiated peaks, PTC and BTN samples segregated well on hierarchical clustering (**Figure 1B**). Differentiated H3K27ac peaks distributed across different regions genome-wide, which showed a greater distribution in intron and intergenic regions with 8.6% PTC-specific and 14.8% BTN-unique peaks located at promoter–transcription start site (TSS) regions (**Figure 1C**). After the differentiated peaks were annotated with GREAT, we found that gene ontology (GO) terms enriched with PTC-specific peaks included T-cell activation, regulation of lymphocyte activation, leukocyte cell–cell adhesion, and interferon-gamma secretion. Vasculature development, vascular endothelial growth factor signaling pathway, tube morphogenesis, etc., were enriched with BTN-unique peaks (**Figure 1D**).

Super-Enhancer-Regulated Genes Differed in Papillary Thyroid Carcinoma and Benign Thyroid Nodule

Super-enhancers are clusters of enhancers and are critically important in development, differentiation, and oncogenesis (Whyte et al., 2013). To identify SEs, H3K27ac signals from sliding windows containing enhancers were ranked using ROSE (Zhou et al., 2015). We first identified the SEs in the tumor and BTN tissues, and enhancers in each sample were annotated (**Supplementary Data**). A total of 3,369 SEs were identified in PTC and 3,366 SEs in BTN samples, among which 367 and 364 SEs were specific to PTC and BTN, respectively (**Figure 2A**). SE genomic sites were categorized into PTC-specific and BTN-specific SE sites. H3K27ac signaling of BTN SEs at PTC-specific genomic sites was significantly lower than that of PTC, contrary to the situation at BTN-specific SE genomic sites (**Figure 2B**).

Enhancers were ranked based on their H3K27ac signals (**Figure 2C**). Some SE-adjacent genes in PTC were known to

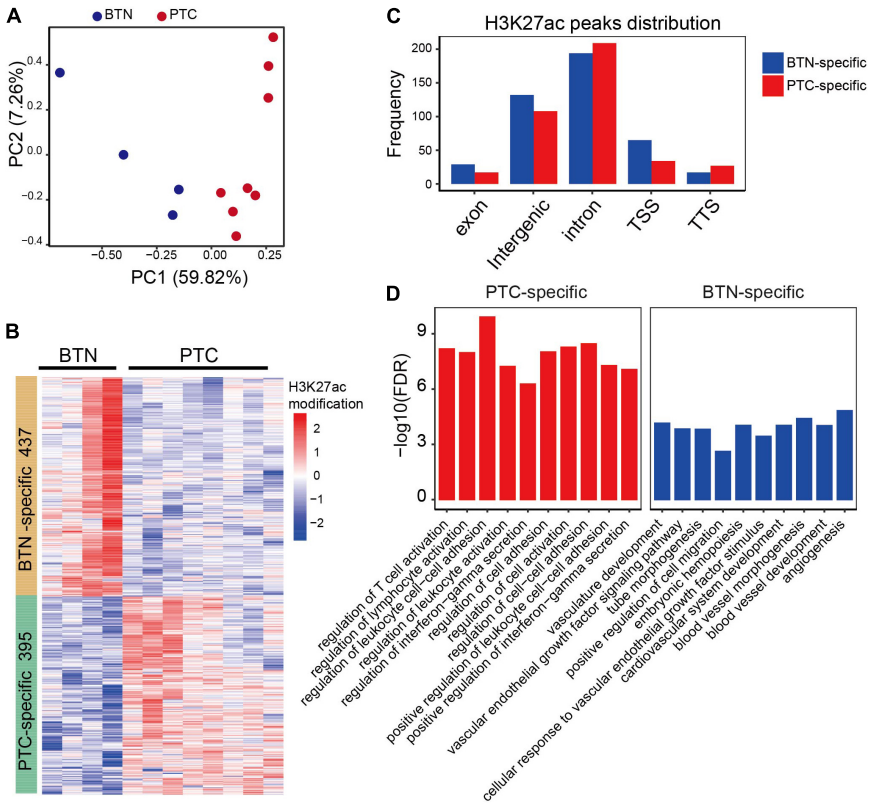

FIGURE 1 | Characterization of H3K27ac landscapes in PTC and BTN. **(A)** Principal component analysis of normalized PTC and BTN H3K27ac peaks. **(B)** Heatmap of differentiated H3K27ac-modified peaks between PTC and BTN. **(C)** Distribution of differentiated histone H3K27ac marks in genome. TSS, transcription start sites; TTS, transcription termination sites. **(D)** Bar plots showing top gene ontology (GO) terms of PTC and BTN-specific H3K27ac peaks. PTC, papillary thyroid carcinoma; BTN, benign thyroid nodule.

be involved in TC or play a part in oncogenesis, such as *EPHB3*, *ALOX5*, and *ELF3*. In contrast, SEs in BTN included some tumor suppressor genes, which were previously reported in various cancers, such as *ARHGAP24* and *CA4*. SEs were assigned to their putative target genes and were then subjected to pathway enrichment analysis to determine their biological functional classifications (**Supplementary Data**). As is shown in GO analyses, these SE-adjacent genes of PTC uncovered some immune-related pathways such as immune cell activation and immune response, and other related pathways included positive regulation of ERK1 and ERK2 cascades, and regulation of NF-kappa B transcription factor activity. BTN-specific GO terms revealed pathways of negative regulation of transcription, cell migration, cell growth, etc. (**Figure 2D**). KEGG pathway analysis indicated some immune-related and cancer-related pathways in SE-adjacent genes of PTC (**Figure 2E**).

Transcriptome Features of Papillary Thyroid Carcinoma and Benign Thyroid Nodule

Global transcriptomic features were analyzed in thyroid samples, and histotype-specific patterns of gene expression for the two groups were identified. There were 2,019 differentially expressed genes specific to PTC, while 800 genes showed a higher expression in BTN (**Figures 3A,B** and **Supplementary Data**). KEGG enrichment analysis of differentiated genes revealed that genes with higher expressions in PTC were mostly enriched in immune functions such as T-cell receptor signaling pathway, chemokine signaling pathway, antigen processing, and presentation, while BTN-specific genes were over-represented in Rap1 signaling pathway, calcium signaling pathway, mineral absorption, etc. GO annotations also revealed that genes with a higher expression in PTC were mainly involved in pathways such as immune response and inflammatory response. In contrast, BTN samples had a higher expression in metabolism pathways such as oxidation-reduction process, cellular response to hypoxia, and cellular response to zinc ion (**Figures 3C,D** and **Supplementary Data**).

The differentiated genes between the two groups were depicted (**Figure 3E**). Some known oncogenes and tumor suppressor genes were found in PTC-specific or BTN-specific genes, respectively (**Figure 3E**). GSEA was conducted and showed significant enrichment of PTC-specific genes in cancer-related pathways, such as NF-kappa B, while BTN-specific genes were enriched in metabolism-related pathways (**Figure 3F**). Besides, GSEA indicated enrichment of immune-related pathways in PTC-specific genes (**Figure 3G**).

The SEs were assigned to the most adjacent genes, and the expressions of SE-associated genes were higher in the

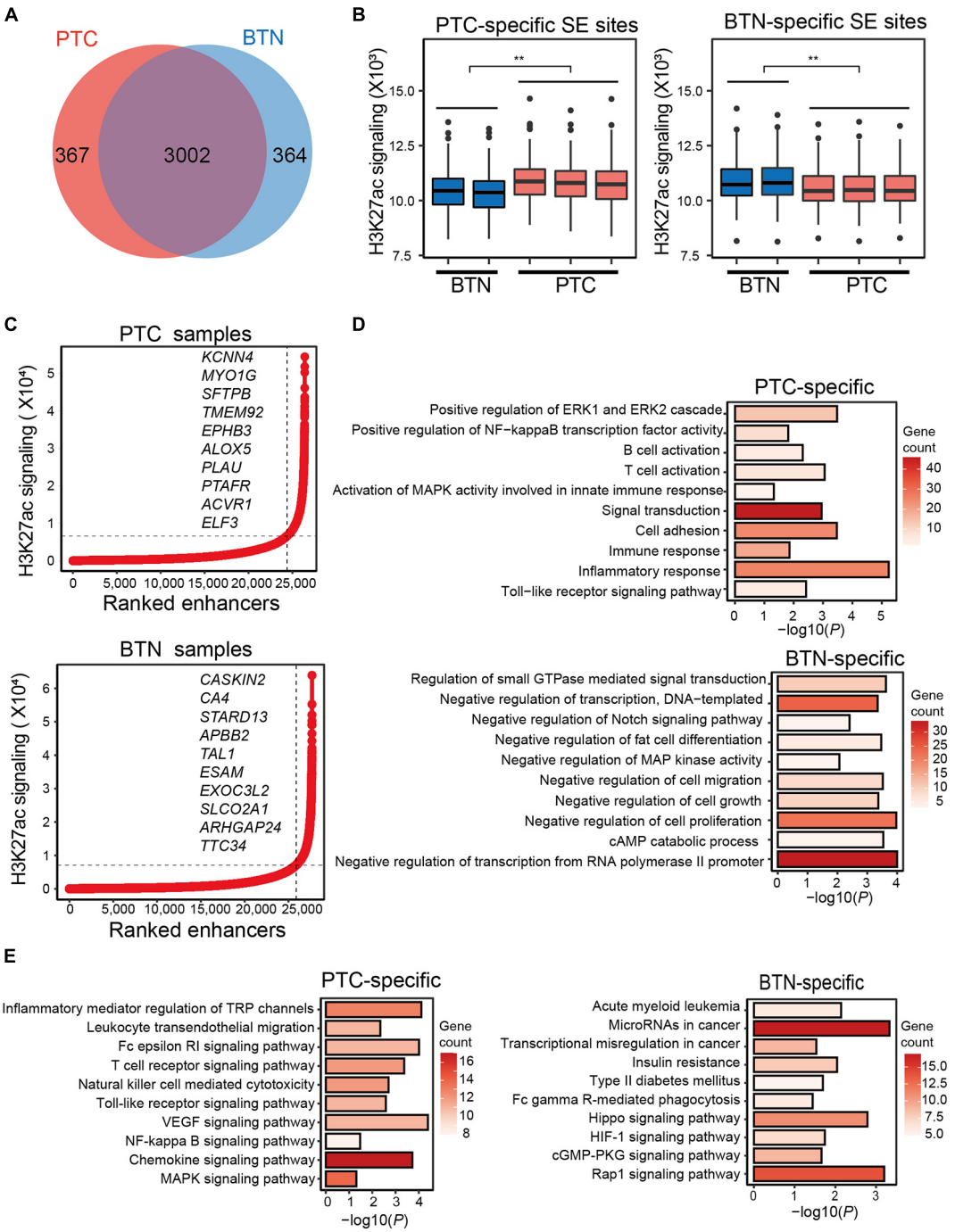

FIGURE 2 | Characterization of super-enhancers in PTC and BTN. **(A)** Venn diagram showing SE numbers of PTC-specific, BTN-specific, and overlapped SEs. **(B)** Histotype-specific genomic SEs showed significantly different H3K27ac signaling levels at PTC-specific or BTN-specific SE genomic sites. $^{**}p < 0.01$. **(C)** Enhancers of representative PTC and BTN sample were ranked by their H3K27ac signaling. Important genes were indicated by their ranks. **(D)** Bar plots showing GO terms of PTC- and BTN-specific SE-associated genes. **(E)** Bar plots showing KEGG pathway analysis in PTC and BTN. PTC, papillary thyroid carcinoma; BTN, benign thyroid nodule; SE, super-enhancer; GO, gene ontology; KEGG, Kyoto Encyclopedia of Genes and Genomes.

histotype of interest. As exemplified in SE-associated genes in PTC (**Figures 4A,C**), oncogenes *ALOX5* and *ELF3* were more highly expressed in PTC compared with BTN tissues. Moreover, The Cancer Genome Atlas (TCGA) and Genotype-Tissue Expression (GTEx) data indicated higher levels of *ALOX5* and *ELF3* in TC compared with adjacent and normal thyroid tissues (**Figures 4B,D**). The tracks of ChIP-seq and RNA-seq signals of *SLCO2A1* and *ARHGAP24* were shown to present

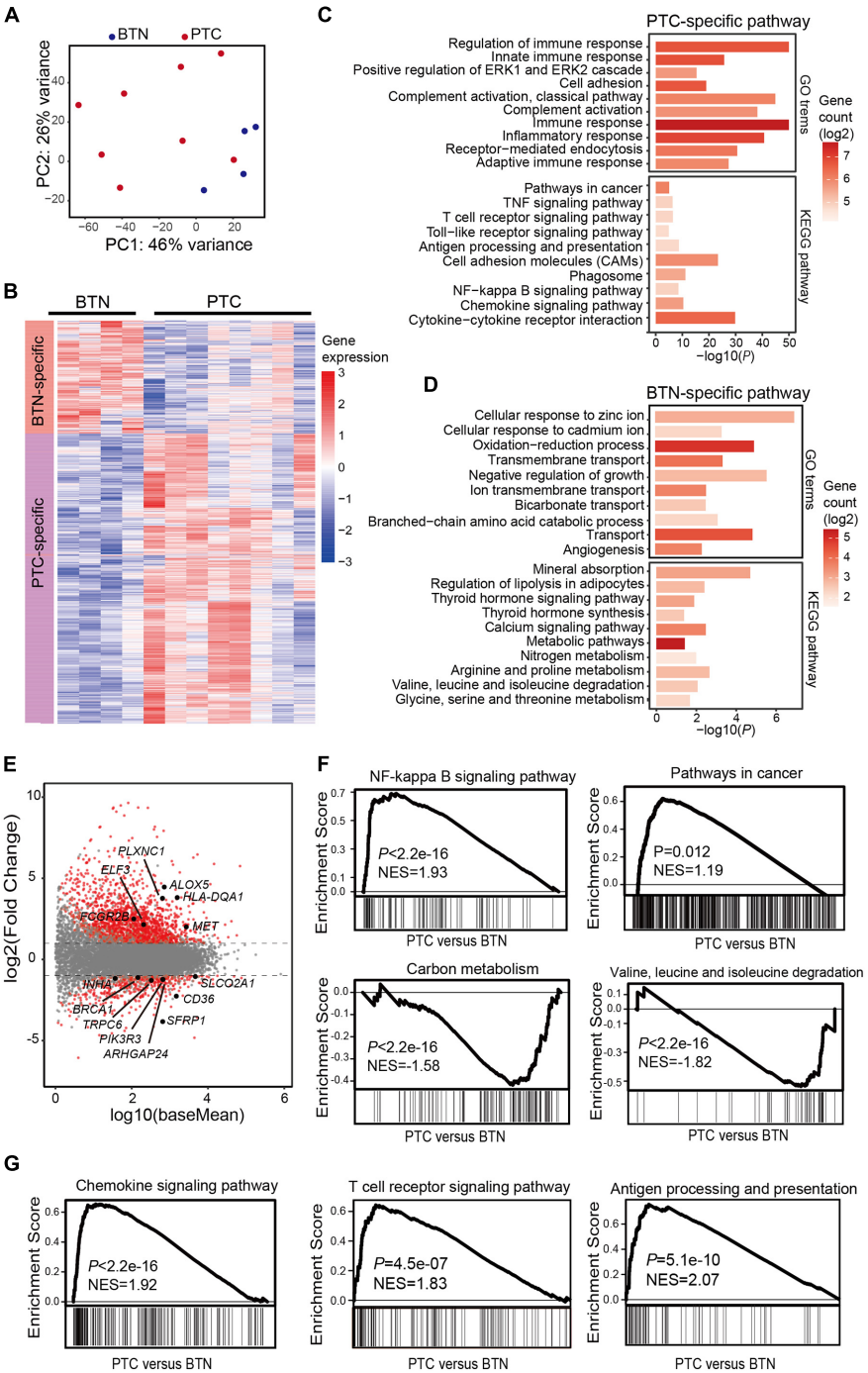

FIGURE 3 | Transcriptome characterization of PTC and BTN tissues. **(A)** Principal component analysis of transcriptomes in PTC and BTN. **(B)** Heatmap of gene expression values in PTC and BTN. **(C,D)** Enrichment analysis for GO terms and KEGG pathway. Top pathways for PTC-upregulated and BTN-upregulated genes are shown. **(E)** MA plot for differentiated analysis of gene expression between PTC and nodule tissues. The red plots at the upper side of the line represent PTC-specific genes, while plots at the opposite side represent nodule-specific genes. **(F)** GSEA plots indicated cancer-related and metabolism-related genes in PTC and BTN samples. **(G)** GSEA plots showed PTC-upregulated genes enriched in immune-related pathways. PTC, papillary thyroid carcinoma; BTN, benign thyroid nodule; GO, gene ontology; KEGG, Kyoto Encyclopedia of Genes and Genomes; GSEA, gene set enrichment analysis.

wide BTN-specific SEs (**Figures 4E,G**), coinciding with their higher expressions in BTN and in normal thyroid tissues compared with PTC and TC, respectively (**Figures 4F,H**). Notably, lower transcription level of *SLCO2A1* was observed in advanced TC stages and associated with poor disease-free survival (**Supplementary Figure 1**).

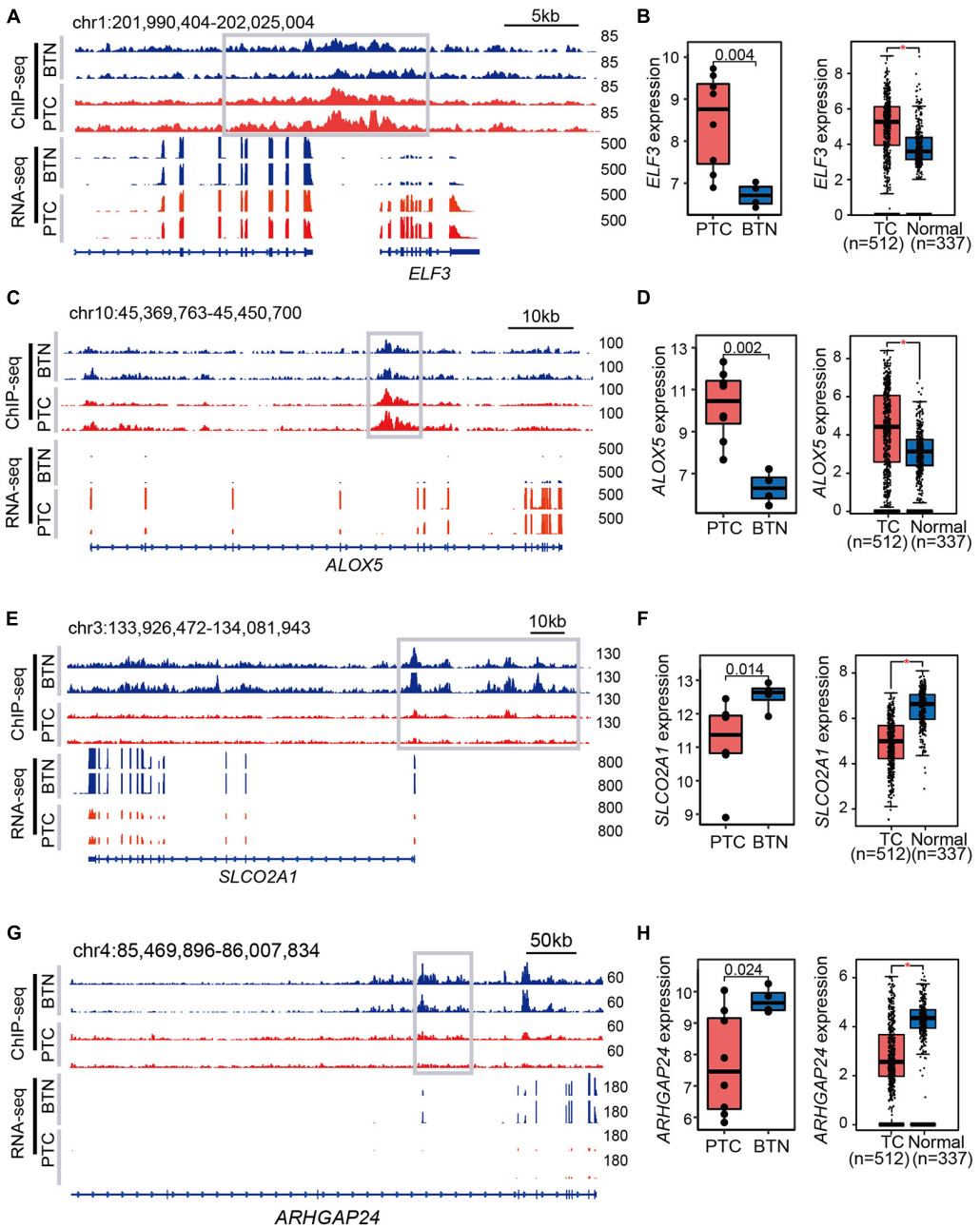

FIGURE 4 | Examples of histotype-specific SE-associated genes. **(A,C)** Gene tracks of PTC-specific SEs. The adjacent genes *ELF3* and *ALOX5* showed strong SE peaks and RNA-seq signals in PTC tissues. **(B,D)** Expression profiles in PTC-specific SEs. Relative expression levels between PTC and BTN are shown in the left panel, while the right box plots indicate expression analysis of TC and normal samples from TCGA and GTEx datasets. **(E,G)** BTN-specific SE tracks and RNA-seq signals. **(F,H)** High expression levels of *SLCO2A1* and *ARHGAP24* in BTN tissues, and similar trends were observed in TCGA and GTEx databases. *$p < 0.05$. SE, super-enhancer; PTC, papillary thyroid carcinoma; BTN, benign thyroid nodule; TCGA, The Cancer Genome Atlas; GTEx, Genotype-Tissue Expression.

Identification of Genes That Are Sensitive to Epigenetic Drugs and Associate With Prognosis of Papillary Thyroid Carcinoma

We integrated H3K27ac ChIP-seq and RNA-seq data to map typical enhancers and promoters to their putative targets. As shown in **Figure 5A**, PTC samples had stronger H3K27ac signals than BTN samples in the genome location of the *PLXNC1* gene. After a comparison of active chromatin regions of *PLXNC1* with an available database to infer potential enhancers, predicted enhancer–promoter associations were found (**Supplementary Figure 2**). The RNA-seq revealed that the *PLXNC1* was expressed higher in PTC than BTN

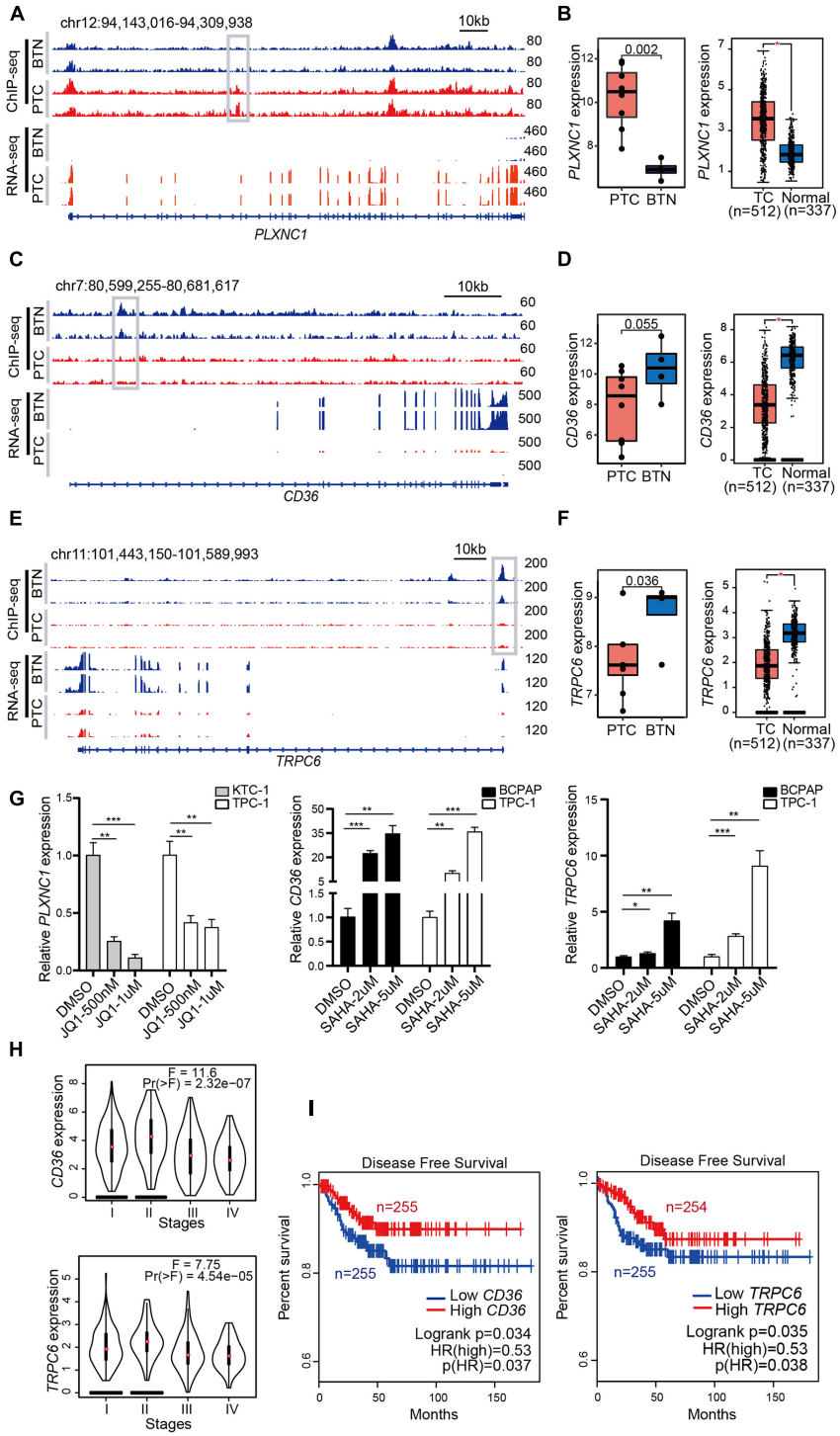

FIGURE 5 | Identification of H3K27ac modification-related genes that are sensitive to epigenetic drugs and associated with the prognosis of PTC. **(A)** H3K27ac ChIP-seq signals and RNA-seq tracks of *PLXNC1*. **(B)** High expressions of *PLXNC1* in PTC (left box plot), and transcriptome data from TCGA and GTEx exhibited consistent difference (right box plot). *$p < 0.05$. **(C,E)** Strong H3K27ac peaks and RNA-seq signals in *CD36* and *TRPC6* in BTN tissues. **(D,F)** Higher expressions of *CD36* and *TRPC6* in BTN (left box plots) and normal tissues (right box plots). *$p < 0.05$. **(G)** Treatment with JQ1 or vehicles as control at indicated concentrations for 48 h greatly reduced *PLXNC1* expression levels in KTC-1 and TPC-1 cell lines. SAHA treatment induced a significant higher expression of *CD36* and *TRPC6* in BCPAP and TPC-1 cells. Expression analysis was normalized against GAPDH. *$p < 0.05$, **$p < 0.01$, ***$p < 0.001$. **(H)** Lower levels of *CD36* and *TRPC6* transcription were observed in stage III and IV in TCGA (THCA) datasets. **(I)** Higher levels of *CD36* and *TRPC6* transcription associated with higher disease-free survival rate in patients with thyroid cancers. Analysis was performed with TCGA (THCA) datasets. PTC, papillary thyroid carcinoma; TCGA, The Cancer Genome Atlas; GTEx, Genotype-Tissue Expression.

samples (**Figure 5A**). Consistently, a higher expression of *PLXNC1* in PTC than normal controls was found when analyzing data from TCGA and GTEx samples (**Figure 5B**). In contrast, *CD36* and *TRPC6* showed significantly stronger H3K27ac signals and higher expressions in BTN than PTC (**Figures 5C–F**). Importantly, treatment of thyroid cancer cells with BRD4 inhibitor JQ1 significantly downregulated the expression of *PLXNC1* and some PTC-specific genes, while the histone deacetylase inhibitors (HDACi) SAHA treatment induced robust increases of *CD36* and *TRPC6* expressions in thyroid cancer cell lines (**Figure 5G** and **Supplementary Figure 3**). Furthermore, low expression levels of *CD36* and *TRPC6* were observed in advanced stages of PTC (**Figure 5H**) and correlated with poor disease-free survival in patients with PTC (**Figure 5I**), suggesting that these genes are potential predictors for PTC recurrence.

DISCUSSION

Accumulating evidence suggested that epigenome alterations greatly impact cancer development (Hamdane et al., 2019). In this study, we revealed histone modification features by comparing PTC and BTN, facilitating the knowledge of active regulatory patterns and global expression profiles in thyroid tissues. H3K27ac is an established mark of transcriptional activation. Our data presented differentiated epigenomes between PTC and BTN, with an epigenetic landscape for the PTC progression compared with BTN, and provided references for novel biomarkers for the prognosis of thyroid tumors.

It was recognized that SEs have great impact on tumor pathogenesis and cell identity (Hnisz et al., 2013). The common histone features indicated the common epigenetic modulations between PTC and BTN. Different enhancers might underline specific gene expression patterns in these two groups. In the present study, we found that PTC-specific SE-adjacent genes showed higher expression levels than those in BTN, such as *ALOX5* and *ELF3*. *ALOX5* had been reported to be highly expressed in PTC compared with normal tissues and was related to PTC tumor invasion (Kummer et al., 2012; Reyes et al., 2019). *ELF3* was reported to be overexpressed with poor prognosis in PTC patients and likely function as an oncogene in TC (Chen et al., 2019). As for BTN-specific SE-adjacent genes identified in this study, *SLCO2A1* was reported to be downregulated in follicular thyroid cancer than benign adenoma (Pfeifer et al., 2013), suggesting its role in thyroid tumor pathogenesis. Several studies reported *ARHGAP24* as a tumor suppressor gene in various malignant tumors, including malignant lymphomas (Nishi et al., 2015), breast cancer (Saito et al., 2012), renal cancer (Wang et al., 2017), lung cancer (Wang et al., 2020), and colorectal cancer (Zhang et al., 2018). However, no study was performed on the functions of *ARHGAP24* in thyroid tumors so far. Though the H3K27ac profile and TCGA database pinpointed that *SLCO2A1* and *ARHGAP24* could be potential predictors for PTC recurrence, their post-transcriptional modification and biological functions require further validation in PTC.

Principal component analysis of PTC and BTN showed two distinct clusters, suggesting etiology-specific epigenetic profiles in these two groups. Interestingly, pathway analysis showed that PTC-specific peaks and genes are enriched in immune-response pathways, indicating that immunoreactions might get involved in thyroid tumor pathogenesis. Whereas the H3K27ac patterns in the two histotypes could not explain all the differentiated gene expressions, one explanation could be that hypomethylation also plays a role in the upregulation of cancer-related genes (Rodríguez-Rodero et al., 2013).

The overexpression of oncogene and silencing of tumor suppressor genes caused by epigenetic modifications were usually reversible with epigenetic enzyme inhibitors. JQ1/SAHA had been assessed in numerous malignancies including TC in clinical trials, and previous studies showed their anti-tumorigenesis functions in TC (Tan et al., 2010). SAHA inhibits deacetylase enzymatic activity. BRD4 inhibitor JQ1 could induce cell growth arrest and apoptosis. The expression levels of certain genes altered following treatment of JQ1 and SAHA, indicating that these drugs might inhibit tumor growth by regulating the expression of some key genes. *PLXNC1* is reported as an oncogene in liver carcinoma (Odabas et al., 2018) and gastric cancer (Chen et al., 2020) and also played a part in TC progression. MiR-4500 repressed PTC development by decreasing *PLXNC1* expression (Li et al., 2019). Besides, it was found that *PLXNC1* was highly expressed in TC (Chen et al., 2013), and the expression level was higher in PTC tissues compared with their paired normal tissues (Qu et al., 2016). Among the genes regulated by SAHA, *CD36* low expression was associated with higher metastasis grade and poor prognosis in colon, breast, and ovarian cancers (Tanase et al., 2020) and pancreatic ductal adenocarcinoma (Jia et al., 2018). *TRPC6* is an important member of the transient receptor potential channels superfamily, participating in the various biological processes (Dietrich and Gudermann, 2014; Jardin et al., 2020). Though it remained unclear if these genes were sufficient to promote or inhibit PTC pathogenesis, their higher transcription levels were related to favorable disease-free rate in TC. Our results suggested the potential roles of these genes in PTC, and their molecular and biological functions warrant further investigation.

While it remained to be elucidated whether epigenetic dysregulation precedes the tumorigenesis, the different histone modification and expression levels in PTC and BTN provided evidence that histone modifications differed in disease states. Though heterogeneity existed in these samples, the results obtained from clustering and statistical algorithm along with supporting evidence from population database and previous biological studies allowed arresting conclusions.

CONCLUSION

In summary, our results presented different epigenomic features of PTC and BTN, and dysregulation of enhancers and their targeted genes provide new insights into the pathogenesis and

development of PTC. Some enhancer-regulated genes were associated with disease-free survival of PTC, which may hold potential as markers for the prognosis of the disease.

DATA AVAILABILITY STATEMENT

The original contributions presented in the study are publicly available. This data can be found here: Genome Sequence Archive in National Genomics Data Center, China National Center for Bioinformation/Beijing Institute of Genomics, Chinese Academy of Sciences, under accession number HRA000779.

ETHICS STATEMENT

The studies involving human participants were reviewed and approved by the Institutional Ethics Committee of The First Affiliated Hospital of Sun Yat-sen University. The ethics committee waived the requirement of written informed consent for participation.

AUTHOR CONTRIBUTIONS

HX, QZ, RL, and ZT designed the study. WL, JL, YaL, YLi, SH, and SY collected the tissue samples and clinical information. LZ, QL, YLu, XX, and YS performed the experiments. LZ, DX, ZT, YT, XX, RL, and QZ analyzed the data. LZ and DX drafted the manuscript. All authors contributed to the manuscript revision and approved the final version of the manuscript.

FUNDING

This study was supported by the National Natural Science Foundation of China (Nos. 81772850, 82072982, and 82072952) and the Guangzhou Science and Technology Project (No. 201803010057).

SUPPLEMENTARY MATERIAL

The Supplementary Material for this article can be found online at: https://www.frontiersin.org/articles/10.3389/fcell.2021.682561/full#supplementary-material

REFERENCES

Bártová, E., Krejcí, J., Harnicarová, A., Galiová, G., and Kozubek, S. (2008). Histone modifications and nuclear architecture: a review. *J. Histochem. Cytochem.* 56, 711–721. doi: 10.1369/jhc.2008.951251

Brest, P., Lassalle, S., Hofman, V., Bordone, O., Gavric, T. V., Bonnetaud, C., et al. (2011). MiR-129-5p is required for histone deacetylase inhibitor-induced cell death in thyroid cancer cells. *Endocr. Relat. Cancer* 18, 711–719. doi: 10.1530/ERC-10-0257

Bulger, M., and Groudine, M. (2011). Functional and mechanistic diversity of distal transcription enhancers. *Cell* 144, 327–339. doi: 10.1016/j.cell.2011.01.024

Chen, H., Chen, W., Zhang, X., Hu, L., Tang, G., Kong, J., et al. (2019). E26 transformation (ETS)-specific related transcription factor-3 (ELF3) orchestrates a positive feedback loop that constitutively activates the MAPK/Erk pathway to drive thyroid cancer. *Oncol. Rep.* 41, 570–578. doi: 10.3892/or.2018.6807

Chen, J., Liu, H., Chen, J., Sun, B., Wu, J., and Du, C. (2020). PLXNC1 enhances carcinogenesis through transcriptional activation of IL6ST in gastric cancer. *Front. Oncol.* 10:33. doi: 10.3389/fonc.2020.00033

Chen, Y., Soong, J., Mohanty, S., Xu, L., and Scott, G. (2013). The neural guidance receptor Plexin C1 delays melanoma progression. *Oncogene* 32, 4941–4949. doi: 10.1038/onc.2012.511

Dey, A., Chitsaz, F., Abbasi, A., Misteli, T., and Ozato, K. (2003). The double bromodomain protein Brd4 binds to acetylated chromatin during interphase and mitosis. *Proc. Natl. Acad. Sci. U.S.A.* 100, 8758–8763. doi: 10.1073/pnas.1433065100

Dietrich, A., and Gudermann, T. (2014). TRPC6: physiological function and pathophysiological relevance. *Handb. Exp. Pharmacol.* 222, 157–188. doi: 10.1007/978-3-642-54215-2_7

Federico, A., Pallante, P., Bianco, M., Ferraro, A., Esposito, F., Monti, M., et al. (2009). Chromobox protein homologue 7 protein, with decreased expression in human carcinomas, positively regulates E-cadherin expression by interacting with the histone deacetylase 2 protein. *Cancer Res.* 69, 7079–7087. doi: 10.1158/0008-5472.CAN-09-1542

Filippakopoulos, P., Qi, J., Picaud, S., Shen, Y., Smith, W. B., Fedorov, O., et al. (2010). Selective inhibition of BET bromodomains. *Nature* 468, 1067–1073. doi: 10.1038/nature09504

Gao, X., Wu, X., Zhang, X., Hua, W., Zhang, Y., Maimaiti, Y., et al. (2016). Inhibition of BRD4 suppresses tumor growth and enhances iodine uptake in thyroid cancer. *Biochem. Biophys. Res. Commun.* 469, 679–685. doi: 10.1016/j.bbrc.2015.12.008

Hamdane, N., Jühling, F., Crouchet, E., El, S. H., Thumann, C., Oudot, M. A., et al. (2019). HCV-Induced epigenetic changes associated with liver cancer risk persist after sustained virologic response. *Gastroenterology* 156, 2313–2329. doi: 10.1053/j.gastro.2019.02.038

Hnisz, D., Abraham, B. J., Lee, T. I., Lau, A., Saint-André, V., Sigova, A. A., et al. (2013). Super-enhancers in the control of cell identity and disease. *Cell* 155, 934–947. doi: 10.1016/j.cell.2013.09.053

Jardin, I., Nieto, J., Salido, G. M., and Rosado, J. A. (2020). TRPC6 channel and its implications in breast cancer: an overview. *Biochim. Biophys. Acta Mol. Cell Res.* 1867:118828. doi: 10.1016/j.bbamcr.2020.118828

Jemal, A., Siegel, R., Xu, J., and Ward, E. (2010). Cancer statistics, 2010. *CA Cancer J. Clin.* 60, 277–300. doi: 10.3322/caac.20073

Jia, S., Zhou, L., Shen, T., Zhou, S., Ding, G., and Cao, L. (2018). Down-expression of CD36 in pancreatic adenocarcinoma and its correlation with clinicopathological features and prognosis. *J. Cancer* 9, 578–583. doi: 10.7150/jca.21046

Kilfoy, B. A., Zheng, T., Holford, T. R., Han, X., Ward, M. H., Sjodin, A., et al. (2009). International patterns and trends in thyroid cancer incidence, 1973-2002. *Cancer Causes Control* 20, 525–531. doi: 10.1007/s10552-008-9260-4

Kummer, N. T., Nowicki, T. S., Azzi, J. P., Reyes, I., Iacob, C., Xie, S., et al. (2012). Arachidonate 5 lipoxygenase expression in papillary thyroid carcinoma promotes invasion via MMP-9 induction. *J. Cell. Biochem.* 113, 1998–2008. doi: 10.1002/jcb.24069

Li, R., Teng, X., Zhu, H., Han, T., and Liu, Q. (2019). MiR-4500 regulates PLXNC1 and inhibits papillary thyroid cancer progression. *Horm Cancer* 10, 150–160. doi: 10.1007/s12672-019-00366-1

Liao, Y., Wang, J., Jaehnig, E. J., Shi, Z., and Zhang, B. (2019). WebGestalt 2019: gene set analysis toolkit with revamped UIs and APIs. *Nucleic Acids Res.* 47, W199–W205. doi: 10.1093/nar/gkz401

Liu, R., Bishop, J., Zhu, G., Zhang, T., Ladenson, P. W., and Xing, M. (2017). Mortality risk stratification by combining BRAF V600E and TERT promoter mutations in papillary thyroid cancer: genetic duet of BRAF and TERT promoter mutations in thyroid cancer mortality. *JAMA Oncol.* 3, 202–208. doi: 10.1001/jamaoncol.2016.3288

Liu, T. (2014). Use model-based Analysis of ChIP-Seq (MACS) to analyze short reads generated by sequencing protein-DNA interactions in embryonic stem cells. *Methods Mol. Biol.* 1150, 81–95. doi: 10.1007/978-1-4939-0512-6_4

Matsuda, S., Furuya, K., Ikura, M., Matsuda, T., and Ikura, T. (2015). Absolute quantification of acetylation and phosphorylation of the histone variant H2AX upon ionizing radiation reveals distinct cellular responses in two cancer cell lines. *Radiat. Environ. Biophys.* 54, 403–411. doi: 10.1007/s00411-015-0608-3

McLean, C. Y., Bristor, D., Hiller, M., Clarke, S. L., Schaar, B. T., Lowe, C. B., et al. (2010). GREAT improves functional interpretation of cis-regulatory regions. *Nat. Biotechnol.* 28, 495–501. doi: 10.1038/nbt.1630

Nishi, T., Takahashi, H., Hashimura, M., Yoshida, T., Ohta, Y., and Saegusa, M. (2015). FilGAP, a Rac-specific Rho GTPase-activating protein, is a novel prognostic factor for follicular lymphoma. *Cancer Med.* 4, 808–818. doi: 10.1002/cam4.423

Odabas, G., Cetin, M., Turhal, S., Baloglu, H., Sayan, A. E., and Yagci, T. (2018). Plexin c1 marks liver cancer cells with epithelial phenotype and is overexpressed in hepatocellular carcinoma. *Can. J. Gastroenterol. Hepatol.* 2018:4040787. doi: 10.1155/2018/4040787

Pfeifer, A., Wojtas, B., Oczko-Wojciechowska, M., Kukulska, A., Czarniecka, A., Eszlinger, M., et al. (2013). Molecular differential diagnosis of follicular thyroid carcinoma and adenoma based on gene expression profiling by using formalin-fixed paraffin-embedded tissues. *BMC Med. Genomics* 6:38. doi: 10.1186/1755-8794-6-38

Qu, T., Li, Y. P., Li, X. H., and Chen, Y. (2016). Identification of potential biomarkers and drugs for papillary thyroid cancer based on gene expression profile analysis. *Mol. Med. Rep.* 14, 5041–5048. doi: 10.3892/mmr.2016.5855

Reyes, I., Reyes, N., Suriano, R., Iacob, C., Suslina, N., Policastro, A., et al. (2019). Gene expression profiling identifies potential molecular markers of papillary thyroid carcinoma. *Cancer Biomark.* 24, 71–83. doi: 10.3233/CBM-181758

Rodríguez-Rodero, S., Fernández, A. F., Fernández-Morera, J. L., Castro-Santos, P., Bayon, G. F., Ferrero, C., et al. (2013). DNA methylation signatures identify biologically distinct thyroid cancer subtypes. *J. Clin. Endocrinol. Metab.* 98, 2811–2821. doi: 10.1210/jc.2012-3566

Saito, K., Ozawa, Y., Hibino, K., and Ohta, Y. (2012). FilGAP, a Rho/Rho-associated protein kinase-regulated GTPase-activating protein for Rac, controls tumor cell migration. *Mol. Biol. Cell.* 23, 4739–4750. doi: 10.1091/mbc.E12-04-0310

Siu, C., Wiseman, S., Gakkhar, S., Heravi-Moussavi, A., Bilenky, M., Carles, A., et al. (2017). Characterization of the human thyroid epigenome. *J. Endocrinol.* 235, 153–165. doi: 10.1530/JOE-17-0145

Tan, J., Cang, S., Ma, Y., Petrillo, R. L., and Liu, D. (2010). Novel histone deacetylase inhibitors in clinical trials as anti-cancer agents. *J. Hematol. Oncol.* 3:5. doi: 10.1186/1756-8722-3-5

Tanase, C., Gheorghisan-Galateanu, A. A., Popescu, I. D., Mihai, S., Codrici, E., Albulescu, R., et al. (2020). CD36 and CD97 in pancreatic cancer versus other malignancies. *Int. J. Mol. Sci.* 21:5656. doi: 10.3390/ijms21165656

Wang, L., Shen, S., Xiao, H., Ding, F., Wang, M., Li, G., et al. (2020). ARHGAP24 inhibits cell proliferation and cell cycle progression and induces apoptosis of lung cancer via a STAT6-WWP2-p27 axis. *Carcinogenesis* 41, 711–721. doi: 10.1093/carcin/bgz144

Wang, L., Wei, W. Q., Wu, Z. Y., and Wang, G. C. (2017). MicroRNA-590-5p regulates cell viability, apoptosis, migration and invasion of renal cell carcinoma cell lines through targeting ARHGAP24. *Mol. Biosyst.* 13, 2564–2573. doi: 10.1039/c7mb00406k

Whyte, W. A., Orlando, D. A., Hnisz, D., Abraham, B. J., Lin, C. Y., Kagey, M. H., et al. (2013). Master transcription factors and mediator establish super-enhancers at key cell identity genes. *Cell* 153, 307–319. doi: 10.1016/j.cell.2013.03.035

Yim, J. H., Choi, A. H., Li, A. X., Qin, H., Chang, S., Tong, S. T., et al. (2019). Identification of Tissue-Specific DNA methylation signatures for thyroid nodule diagnostics. *Clin. Cancer Res.* 25, 544–551. doi: 10.1158/1078-0432.CCR-18-0841

Yu, S., Liu, Y., Wang, J., Guo, Z., Zhang, Q., Yu, F., et al. (2012). Circulating microRNA profiles as potential biomarkers for diagnosis of papillary thyroid carcinoma. *J. Clin. Endocrinol. Metab.* 97, 2084–2092. doi: 10.1210/jc.2011-3059

Zhang, S., Sui, L., Zhuang, J., He, S., Song, Y., Ye, Y., et al. (2018). ARHGAP24 regulates cell ability and apoptosis of colorectal cancer cells via the regulation of P53. *Oncol. Lett.* 16, 3517–3524. doi: 10.3892/ol.2018.9075

Zhang, Z., Liu, D., Murugan, A. K., Liu, Z., and Xing, M. (2014). Histone deacetylation of NIS promoter underlies BRAF V600E-promoted NIS silencing in thyroid cancer. *Endocr. Relat. Cancer* 21, 161–173. doi: 10.1530/ERC-13-0399

Zhou, H., Schmidt, S. C., Jiang, S., Willox, B., Bernhardt, K., Liang, J., et al. (2015). Epstein-Barr virus oncoprotein super-enhancers control B cell growth. *Cell Host Microbe* 17, 205–216. doi: 10.1016/j.chom.2014.12.013

Zhu, X., Enomoto, K., Zhao, L., Zhu, Y. J., Willingham, M. C., Meltzer, P., et al. (2017). Bromodomain and extraterminal protein inhibitor JQ1 suppresses thyroid tumor growth in a mouse model. *Clin. Cancer Res.* 23, 430–440. doi: 10.1158/1078-0432.CCR-16-0914

Conflict of Interest: The authors declare that the research was conducted in the absence of any commercial or financial relationships that could be construed as a potential conflict of interest.

frontiers in Cell and Developmental Biology

BRIEF RESEARCH REPORT
published: 29 June 2021
doi: 10.3389/fcell.2021.708038

CHK Methylation Is Elevated in Colon Cancer Cells and Contributes to the Oncogenic Properties

Shudong Zhu[1,2,3†], Yan Zhu[1,3†], Qiuwen Wang[2†], Yi Zhang[4] and Xialing Guo[5]*

[1] School of Medicine, Nantong University, Nantong, China, [2] Department of Biochemistry and Molecular Biology, School of Life Science, Central South University, Changsha, China, [3] Xuzhou Health Research Institute, Xuzhou, China, [4] Department of Gastrointestinal Surgery, The Third Xiangya Hospital, School of Life Science, Central South University, Changsha, China, [5] Argus Pharmaceuticals, Changsha, China

Src is an important oncogene that plays key roles in multiple signal transduction pathways. Csk-homologous kinase (CHK) is a kinase whose molecular roles are largely uncharacterized. We previously reported expression of CHK in normal human colon cells, and decreased levels of CHK protein in colon cancer cells leads to the activation of Src (Zhu et al., 2008). However, how CHK protein expression is downregulated in colon cancer cells has been unknown. We report herein that CHK mRNA was decreased in colon cancer cells as compared to normal colon cells, and similarly in human tissues of normal colon and colon cancer. Increased levels of DNA methylation at promotor CpG islands of CHK gene were observed in colon cancer cells and human colon cancer tissues as compared to their normal healthy counterparts. Increased levels of DNA methyltransferases (DNMTs) were also observed in colon cancer cells and tissues. DNA methylation and decreased expression of CHK mRNA were inhibited by DNMT inhibitor 5-Aza-CdR. Cell proliferation, colony growth, wound healing, and Matrigel invasion were all decreased in the presence of 5-Aza-CdR. These results suggest that increased levels of DNA methylation, possibly induced by enhanced levels of DNMT, leads to decreased expression of CHK mRNA and CHK protein, promoting increased oncogenic properties in colon cancer cells.

Keywords: CHK, colon cancer, DNA methylation, FHC, drug resistance

OPEN ACCESS

Edited by:
Xiao Zhu,
Guangdong Medical University, China

Reviewed by:
Qi Zhao,
University of Macau, China
Songshu Meng,
Dalian Medical University, China

****Correspondence:***
Shudong Zhu
1125537080@qq.com

† These authors have contributed equally to this work and share first authorship

Specialty section:
This article was submitted to Epigenomics and Epigenetics, a section of the journal Frontiers in Cell and Developmental Biology

Received: *11 May 2021*
Accepted: *09 June 2021*
Published: *29 June 2021*

Citation:
Zhu S, Zhu Y, Wang Q, Zhang Y and Guo X (2021) CHK Methylation Is Elevated in Colon Cancer Cells and Contributes to the Oncogenic Properties. Front. Cell Dev. Biol. 9:708038. doi: 10.3389/fcell.2021.708038

INTRODUCTION

Src is an important oncogene that plays key roles in multiple signal transduction pathways (Yeatman, 2004). Csk-homologous kinase (CHK) sharing 53% amino acid identity with c-Src tyrosine kinase (Csk). CHK has been reported to be expressed primarily in brain and hematopoietic cells (Chow et al., 1994). Unlike Csk, which phosphorylates and inhibits Src effectively, CHK is not capable of phosphorylating Src Y530 effectively (Advani et al., 2017). The molecular and functional roles of CHK are largely uncharacterized.

We previously reported that CHK expression was not restricted to brain and hematopoietic cells, instead, CHK is also expressed in normal colon cells and its protein levels were decreased in colon

Abbreviations: CHK, Csk-homologous kinase; Csk, c-Src tyrosine kinase; Ct, cycle threshold; DNMT, DNA methyltransferase; MTT, methyl-thiazolyldiphenyl-tetrazoliumbromide; SFKs, Src family kinases.

cancer cells, leading to the activation of Src *via* a mechanism irrelevant of Src Y530 phosphorylation (Zhu et al., 2008). We also showed that CHK acts additively with Csk in suppressing Src kinase activity in colon cells (Zhu et al., 2008). Recently, it is also shown that CHK plays an auxiliary role to Csk in hematopoietic cells (Nagy et al., 2020).

The main objective of this current study was to explore the mechanisms of how CHK protein levels are downregulated in colon cancer cells. Here, we reported CHK mRNA was also decreased in colon cancer cells as compared to normal colon cells, and decreased in human colon cancer tissues as compared to normal colon tissues. Underlying molecular mechanism was studied. Biological effects were also studied in the presence of 5-Aza-CdR. The results suggest that increased levels of DNA methylation, possibly induced by enhanced levels of DNA methyltransferases (DNMTs), leads to decreased expression of CHK mRNA and therefore CHK protein, promoting increased oncogenic properties, revealing an important CHK regulatory mechanism in contributing to the tumorigenesis of colon cancer.

MATERIALS AND METHODS

Materials

5-Aza-CdR was purchased from Sigma. GAPDH antibody was from Cell Signaling. DNMT3a and DNMT3b antibodies were from Cellclonal, China. DNMT1 antibody was from Wanlei, China.

Cell Culture

SW48, SW480, RKO, LoVo, HCT-15, HCT 116, HT-29, FHC, and K562 (ATCC) were cultured in the complete growth medium according to ATCC. Primary normal colon epithelial cells were obtained from normal colon tissues and cultured in DMEM/F12 complete medium.

Preparation of Lysates

Subconfluent cells in tissue culture were lysed in RIPA lysis buffer supplemented with phosphatase inhibitors and protease inhibitors (Zhu et al., 2007). Lysates were clarified by centrifugation at 10,000 *g* for 20 min. Protein was quantified with the BCA assay. Tumor tissues were homogenized in RIPA lysis buffer with a Dounce homogenizer for 50 strokes first before centrifugation (Bjorge et al., 2000).

Immunoblotting

Proteins were separated on SDS-PAGE followed by transfer to PVDF membranes. Blots were incubated with the primary antibodies in TBST at room temperature for 1 h. Following incubation with secondary antibody conjugated to horseradish peroxidase, the blots were visualized with ECL.

Quantitative Real-Time PCR

Total RNA from cell or tissue samples were isolated using TRIzol reagent (Invitrogen) and reverse transcription was done using HiScript IIQ RT superMix (Vazyme, China) following instructions of the manufacture. cDNA was amplified using PCR primers as follows: forward 5′-CTGTCCTGCAGGGTGAGTACCT -3′ and reverse 5′-GTCATGACGGCCGTCTCGTCC -3′. RT-qPCR results were analyzed using comparative cycle threshold (Ct), followed by gene expressions normalized to that of GAPDH.

Methylation-Specific PCR

Total DNA of the cells or tissues was extracted using TIANamp Genomic DNA kit (TianGen Biotech, China) according to instructions of the manufacturer. Bisulfite conversion of the DNA was done using EZ DNA Methylation – Gold Kit (Zymo, United States). Methylation-specific PCR primers were as follows: (Methylation) forward 5′- AGGTGTGCGTATACGTTTTC -3′ and reverse 5′-TATACGCGACCCTACGTAAC -3′. (Unmethylation) forward 5′- AATAGGTGTGTATATGTTTTT -3′ and reverse 5′-TATACACAACCCTACATAACACC -3′. PCR products were examined using agarose gel electrophoresis followed by images captured with Gel Doc XR + (Bio-Rad).

Methyl-thiazolyldiphenyl-tetrazoliumbromide Assay

Cells were treated with 5-Aza-CdR for various hours as stated in the figure legends. Methyl-thiazolyldiphenyl-tetrazoliumbromide (MTT) assay of Succinate Dehydrogenase (SDH) activity was performed as described (Molenaar et al., 2012).

Clonogenic Growth Assay

Thousand cells were plated in 6-well plates and cultured for 14 days in presence or absence of 5-Aza-CdR, with medium changed every three days until colonies were evident. The plates were washed with PBS, fixed with paraformaldehyde and stained with hematoxylin. Images were taken by the inverted microscopy. Colonies were counted manually in a blinded fashion.

Wound Healing Assay

Cells were plated in 6-well plates to a density of about 80–90% confluence. A linear wound was generated with a 200 μl pipette tip straightly. Cell fragments were immediately removed by using PBS and then cells were cultured in medium supplement with 1% FBS. Images were taken at 0, 24, and 48 h of wound formation by the inverted microscopy and the width of the scratch was measured using ImageJ software.

Cell Invasion Assay

This was done by Matrigel Invasion Chamber (BD Biosciences) and stained with Diff Quik, according to the protocols of the manufacturer.

Statistical Analysis

The results were expressed as means ± SD. Experiments were repeated for three independent times unless stated otherwise.

The difference of two groups was assessed by analysis of variance (ANOVA) and *t* test.

RESULTS

Downregulation of CHK protein levels activates Src in colon cancer cells (Zhu et al., 2008). To explore if transcriptional regulation led to this downregulation of CHK protein, we examined the mRNA levels of CHK in various colon cell lines using qPCR. Results show that mRNA levels in all the colon cancer cell lines examined, including HT-29, HCT 116, HCT-15, SW48, SW480, RKO, and LoVo, were all significantly decreased as compared to those in normal colon epithelial cell strain FHC (**Figure 1A**). To further verify the results, we also employed primary colon epithelial cells from human normal colon tissues of three individuals, and found similar downregulation of CHK mRNA as compared to these primary normal colon epithelial cells (**Figure 1A**).

Tumor tissues and adjacent normal tissues of five colorectal cancer patients have also been collected for examination of the CHK mRNA levels. Levels of CHK mRNA in tumor tissues were significantly lower than those in corresponding normal tissues (**Figure 1B**).

To investigate if the mRNA decrease is due to epigenetic regulation, we examined methylation of CpG islands at CHK promoter region. In all colorectal cancer cells examined, including HT-29, HCT 116, HCT-15, SW48, SW480, RKO and LoVo, and CpG islands were heavily methylated, suggesting CHK mRNA were poorly expressed. In contrast, in the three control primary normal colon epithelial cells, methylation of CpG islands were undetectable, suggesting high levels of CHK mRNA expression (**Figure 2A**). On the other hand, although FHC was methylated at CpG islands, the level of unmethylation is higher than those of the colon cancer cell lines, in line with that the level of CHK mRNA in FHC is higher than those in the colon cancer cell lines.

The change of methylation of CpG islands of the CHK gene were also examined in colorectal cancer tissues and adjacent tissues and showed similar pattern (**Figure 2B**). In #1 and #5 patients, CHK gene was fully methylated or nearly fully methylated in the cancer tissues, in contrast to full unmethylation or almost full unmethylation in the adjacent normal colon tissues. In #2, #3, and #4 patients, although unmethylation was detected in colon cancer tissues, the percentages of unmethylated CHK in the total CHK in normal colon tissues were much higher than that in colon cancer tissues (**Figure 2B**).

These data show consistent upregulation of methylation at CHK CpG island in the colon cancer cell lines and cancer tissues.

The down-regulation of CHK mRNA and the upregulation of the CHK CpG methylation suggest that the downregulation of CHK protein in colorectal cancer cells may be caused by downregulation of CHK mRNA, and the downregulation of CHK mRNA in colorectal cancer cells may be caused by the methylation of the CpG island of the CHK gene.

CpG methylation is mediated by DNMTs. We next examined the levels of expression of various DNMTs, including DNMT1, DNMT3a, and DNMT3b. Immunoblotting results indicate that the expression of DNMT1 protein in all the colon cancer cells including HT-29, HCT 116, HCT-15, SW48, SW480, RKO (except LoVo) were all elevated compared with normal colonic epithelial cells including primary cells of normal colon (primary

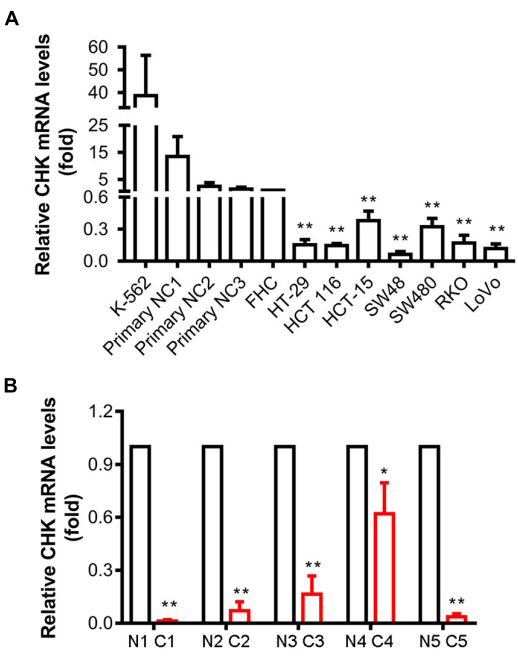

FIGURE 1 | Expression of CHK mRNA is downregulated in human colon cancer cell lines and colon cancer tissues. mRNA levels were measured using qPCR. **(A)** Cell lines. FHC was control normal colon cell strain. K562 was a positive control of CHK mRNA expression. NC, normal colon. **(B)** Tissues. C, cancer tissue; N, adjacent normal tissue. #, patient number. The relative expression level was calculated according to the Ct value. *t*-test, $^{*}P < 0.05$, $^{**}P < 0.01$. Error bars represent the SD from three independent experiments.

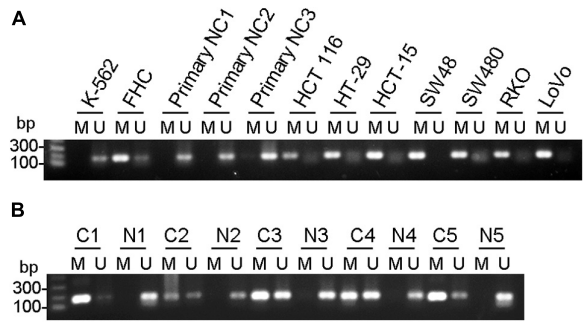

FIGURE 2 | CHK gene was methylated in colon cancer cell lines and colon cancer tissues. Detection of the 196-bp product specific for a bisulfite conversion of genomic DNA was shown. U and M indicate the presence of unmethylated and methylated PCR products, respectively. **(A)** Cells. FHC was control normal colon cell strain. K562 was a positive control of CHK unmethylation. NC, normal colon. **(B)** Tissues. C, cancer tissue; N, adjacent normal tissue. #, patient number. Results are representative of three independent experiments.

cell #1, 2, and 3), and normal colon epithelial cells FHC (**Supplementary Figure 1A**). Although DNMT1 level in LoVo cells appear to be similar to that in the FHC and primary normal colon 2, and 3 cells, it is in fact higher than that in these cells after normalization with GAPDH.

On the other hand, The expression of DNMT3a is low in normal colonic epithelial cells FHC and primary normal colon epithelial cells 1, 2, and 3, and relatively higher in colon cancer cells (HT-29, HCT 116, HCT-15, SW48, SW480, RKO, and LoVo). This is also true for DNMT3b (**Supplementary Figure 1A**). Taken together, the expression levels of DNMTs are higher in colon cancer cells than that in normal colon cells.

Furthermore, the expression of DNMT1 and DNMT3b were all elevated in human colon cancer tissues as compared to the adjacent normal colon tissues (**Supplementary Figure 1B**). Although the DNMT3a protein levels appears to be elevated in cancer tissues as compared with the adjacent normal colon tissues as well, the image quality of immunoblotting results appears low, probably due to low abundance and degradation of DNMT3a in the tissues (data not shown).

The expression of CHK mRNA was increased, after treatment of the cells with DNMT inhibitor 5-Aza-CdR (**Figure 3A**). Furthermore, the methylation levels of CHK gene were decreased after treatment of the cells with 5-Aza-CdR (**Figure 3B**). These results are in line with the observed differences of CHK gene methylation and expression of CHK mRNA in between colon cancer cells and normal colon cells, suggesting that DNA methylation plays an important role in silencing CHK mRNA expression in the colon cancer cells.

Lastly, we examined the biological effects of methylation inhibition. Results show that cell proliferation, clonegenic growth, cell migration, cell invasion were all decreased in presence of 5-Aza-CdR (**Figure 4**), indicating that the epigenetic suppression of CHK expression contributes to the oncogenic properties of colon cancer cells.

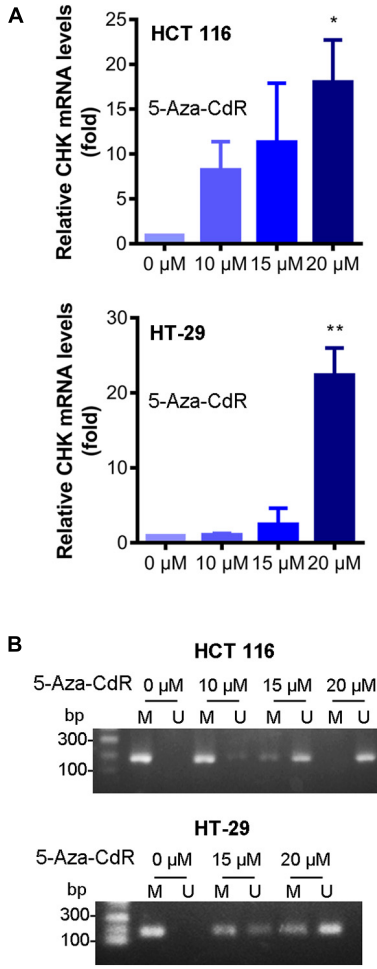

FIGURE 3 | 5-Aza-CdR reversed CHK methylation and expression of CHK mRNA. HCT 116 and HT-29 cells were treated with indicated concentrations of 5-Aza-CdR. mRNA levels were measured using qPCR **(A)**. The relative expression level was calculated according to the Ct value. *t*-test, $^{*}P < 0.05$, $^{**}P < 0.01$. $N = 3$ independent experiments. Methylation of CHK gene in colon cancer cell lines was measured **(B)**. Detection of the 196-bp product specific for a bisulfite conversion of genomic DNA was shown. U and M indicate the presence of unmethylated and methylated PCR products, respectively. Results are representative of three independent experiments.

DISCUSSION

The fact that Csk was not able to fully inhibit Src kinase activity, and CHK siRNA work additively with Csk siRNA in upregulating Src activity in colon cells (Zhu et al., 2008) suggests that upregulation of CHK protein levels could collaborate with Csk upregulation in maximizing downregulating Src kinase activity. Our work in this report suggests that this could be done by epigenetically upregulating CHK transcript expression, including but not limited to downregulation of DNMTs such as employing DNMT inhibitors or decreasing DNMT protein levels.

The recent study also demonstrates interplay between CHK and Csk in hematopoietic cells (Nagy et al., 2020). The feedback upregulation of CHK expression induced by absence of Csk suggests an auxiliary role of CHK in the hematopoietic cells. Therefore, it's possible that upregulation of CHK could reduce the drug resistance effect of cancer treatment with Csk upregulation.

Src inhibitors have been used for clinical studies, and clinical trials showed that the efficacy of several Src inhibitors in solid tumor as modest (Elias and Ditzel, 2015). The underlying reason is not known, but it is very likely the drug resistance mechanism(s) play important roles in this regard. It is possible that epigenetic CHK upregulation could also help in overcoming the drug resistance of Src kinase inhibitors, especially considering the fact that CHK inhibits Src activity mainly not *via* phosphorylating Src. Furthermore, the fact that CHK inhibits members of Src family kinases (SFKs) may also help overcome the potential drug resistance due to the feedback upregulation of other members of SFKs induced by specific Src inhibitor(s). Therefore, although novel Src inhibitors are still being developed (Yang et al., 2019; Weng et al., 2020), the role of CHK in cancer treatment with Src inhibitor(s) should be considered.

Levels of DNMT proteins were found upregulated in colon cancer cells in our study. It has been reported that knocking down

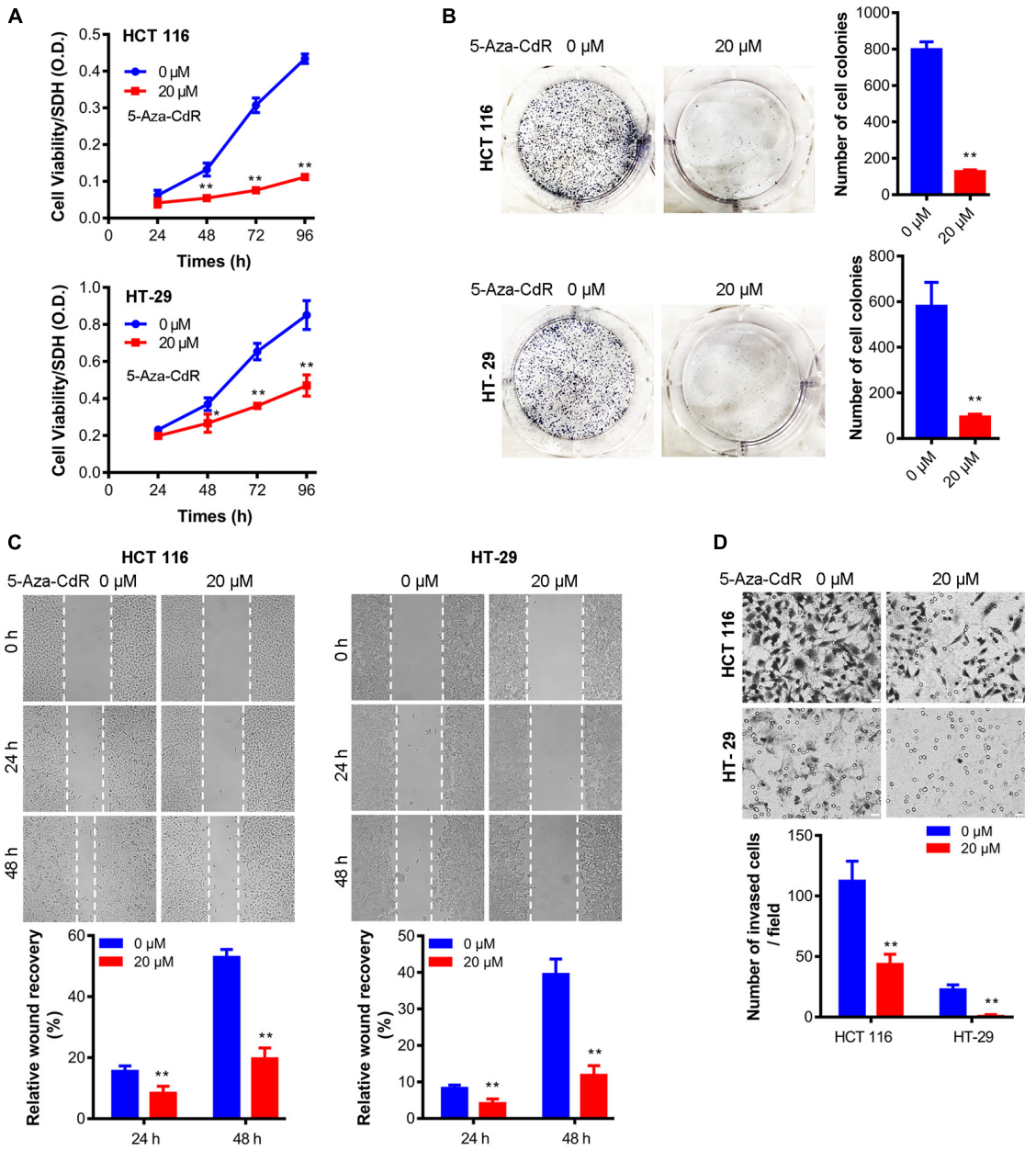

FIGURE 4 | 5-Aza-CdR suppressed oncogenic properties of colon cancer cells. Cell was treated with 5-Aza-CdR at indicated concentrations for indicated hours. MTT cell proliferation assay **(A)**, clonogenic growth at 14 days **(B)**, wound healing assay **(C)**, and cell invasion at 48 h **(D)** were measured. $N = 3$ independent experiments. t-test, $^{*}P < 0.05$, $^{**}P < 0.01$. Representative images were shown.

of DNMT1 in colon cancer cells resulted in global demethylation of CpG sites, suggesting that DNMT1 is important for global methylation of CpG sites (Robert et al., 2003). Therefore, DNMT1 is likely important for the methylation of CpG sites of CHK in colon cancer cells we reported. Meanwhile, knocking down of DNMT1 in colon cancer cells significantly increased the ability of 5-Aza-CdR to increase expression of CDKN2A, indicating that DNMT1 may work additively or synergistically with other members of DNMT in regulating DNA methylation (Robert et al., 2003). These results are in line with our observation of the elevated levels of multiple members of DNMT in colon cancer cells, and suggest that the elevation of multiple members of DNMT may cooperate to increase the methylation of CHK gene, leading to the downregulation of CHK expression in the cells. It would also be interesting to find out the underlying mechanism of DNMT upregulation. This mechanism may also be a plausible strategy in further upregulating CHK levels. On the other hand, although epigenetics appears to be involved in regulating CHK expression, other regulating mechanism should not be excluded, for example, degradation of CHK mRNA or protein.

The significant biological effects associated with the epigenetic regulation of CHK expression in colon cancer cells including cell proliferation, wound healing, and cell invasion, support further exploration of the molecular roles and regulation of CHK.

DATA AVAILABILITY STATEMENT

The original contributions presented in the study are included in the article/**Supplementary Material**, further inquiries can be directed to the corresponding author.

AUTHOR CONTRIBUTIONS

SZ conceived and designed the study. QW and YaZ conducted the experiments and performed statistical analysis with help from others. SZ, YaZ, and QW wrote the manuscript with input from all co-authors. YiZ conducted surgery for clinical samples, and contributed to manuscript preparation with XG. All authors contributed to the article and approved the submitted version.

FUNDING

This work was supported in part by NTU University (SZ, NTU03083068), CSU University (SZ, CSU996010197), Hunan Province BRJH Foundation (SZ, HNBRJH2015ZSD), and XUZHOU SCJH Foundation (SZ, XZSCJH2020ZSD).

SUPPLEMENTARY MATERIAL

The Supplementary Material for this article can be found online at: https://www.frontiersin.org/articles/10.3389/fcell.2021.708038/full#supplementary-material

REFERENCES

Advani, G., Lim, Y. C., Catimel, B., Lio, D., Ng, N., Chüeh, A. C., et al. (2017). Csk-homologous kinase (Chk) is an efficient inhibitor of Src-family kinases but a poor catalyst of phosphorylation of their C-terminal regulatory tyrosine. *Cell Commun. Signal.* 15:29. doi: 10.1186/s12964-017-0186-x

Bjorge, J. D., Pang, A., and Fujita, D. J. (2000). Identification of protein-tyrosine phosphatase 1B as the major tyrosine phosphatase activity capable of dephosphorylating and activating c-Src in several human breast cancer cell lines. *J. Biol. Chem.* 275, 41439–41446. doi: 10.1074/jbc.M004852200

Chow, L. M., Jarvis, C., Hu, Q., Nye, S. H., Gervais, F. G., Veillette, A., et al. (1994). Ntk: a Csk-related protein-tyrosine kinase expressed in brain and T lymphocytes. *Proc. Natl. Acad. Sci. U.S.A.* 91, 4975–4979. doi: 10.1073/pnas.91.11.4975

Elias, D., and Ditzel, H. J. (2015). The potential of Src inhibitors. *Aging* 7, 734–735. doi: 10.18632/aging.100821

Molenaar, J. J., Domingo-Fernández, R., Ebus, M. E., Lindner, S., Koster, J., Drabek, K., et al. (2012). LIN28B induces neuroblastoma and enhances MYCN levels via let-7 suppression. *Nat. Genet.* 44, 1199–1206. doi: 10.1038/ng.2436

Nagy, Z., Mori, J., Ivanova, V. S., Mazharian, A., and Senis, Y. A. (2020). Interplay between the tyrosine kinases Chk and Csk and phosphatase PTPRJ is critical for regulating platelets in mice. *Blood* 135, 1574–1587. doi: 10.1182/blood.2019002848

Robert, M. F., Morin, S., Beaulieu, N., Gauthier, F., Chute, I. C., Barsalou, A., et al. (2003). DNMT1 is required to maintain CpG methylation and aberrant gene silencing in human cancer cells. *Nat. Genet.* 33, 61–65. doi: 10.1038/ng1068

Weng, C. W., Li, J. H., Tsai, J. Y., Lin, S. H., Chang, G. C., and Liu, C. C. (2020). Pharmacophore-based virtual screening for the identification of the novel Src inhibitor SJG-136 against lung cancer cell growth and motility. *Am. J. Cancer Res.* 10, 1668–1690.

Yang, W., Meng, L., Chen, K., Tian, C., Peng, B., Zhong, L., et al. (2019). Preclinical pharmacodynamic evaluation of a new Src/FOSL1 inhibitor, LY-1816, in pancreatic ductal adenocarcinoma. *Cancer Sci.* 110, 1408–1419. doi: 10.1111/cas.13929

Yeatman, T. J. (2004). A renaissance for SRC. *Nat. Rev. Cancer* 4, 470–480. doi: 10.1038/nrc1366

Zhu, S., Bjorge, J. D., Cheng, H. C., and Fujita, D. J. (2008). Decreased CHK protein levels are associated with Src activation in colon cancer cells. *Oncogene* 27, 2027–2034. doi: 10.1038/sj.onc.1210838

Zhu, S., Bjorge, J. D., and Fujita, D. J. (2007). PTP1B contributes to the oncogenic properties of colon cancer cells through Src activation. *Cancer Res.* 67, 10129–10137. doi: 10.1158/0008-5472.CAN-06-4338

Conflict of Interest: The authors declare that the research was conducted in the absence of any commercial or financial relationships that could be construed as a potential conflict of interest.

frontiers in Genetics

ORIGINAL RESEARCH
published: 01 September 2021
doi: 10.3389/fgene.2021.720979

Identification of a Novel Epigenetic Signature CHFR as a Potential Prognostic Gene Involved in Metastatic Clear Cell Renal Cell Carcinoma

Xiangling Chen[1,2,3†], Jiatian Lin[4†], Qiaoling Chen[5†], Ximian Liao[1,2], Tongyu Wang[1,2], Shi Li[1,2], Longyi Mao[1,2] and Zesong Li[1,2]*

[1] Guangdong Provincial Key Laboratory of Systems Biology and Synthetic Biology for Urogenital Tumors, Department of Urology, The First Affiliated Hospital of Shenzhen University, Shenzhen Second People's Hospital (Shenzhen Institute of Translational Medicine), Shenzhen, China, [2] Shenzhen Key Laboratory of Genitourinary Tumor, Department of Urology, The First Affiliated Hospital of Shenzhen University, Shenzhen Second People's Hospital (Shenzhen Institute of Translational Medicine), Shenzhen, China, [3] Shenzhen Institutes of Advanced Technology, Chinese Academy of Sciences, Shenzhen, China, [4] Department of Minimally Invasive Intervention, Peking University Shenzhen Hospital, Shenzhen, China, [5] NO.6 Middle School of Changsha, Changsha, China

OPEN ACCESS

Edited by:
Zhenhua Xu,
Children's National Hospital,
United States

Reviewed by:
Jun Pang,
Sun Yat-sen University, China
Wenzhi Li,
Shanghai Jiao Tong University, China

***Correspondence:**
Zesong Li
lzssc@yahoo.com

[†] These authors have contributed equally to this work

Specialty section:
This article was submitted to Epigenomics and Epigenetics, a section of the journal Frontiers in Genetics

Received: 05 June 2021
Accepted: 02 August 2021
Published: 01 September 2021

Citation:
Chen X, Lin J, Chen Q, Liao X, Wang T, Li S, Mao L and Li Z (2021) Identification of a Novel Epigenetic Signature CHFR as a Potential Prognostic Gene Involved in Metastatic Clear Cell Renal Cell Carcinoma. Front. Genet. 12:720979. doi: 10.3389/fgene.2021.720979

Metastasis is the main cause of clear cell renal cell carcinoma (ccRCC) treatment failure, and the key genes involved in ccRCC metastasis remain largely unknown. We analyzed the ccRCC datasets in The Cancer Genome Atlas database, comparing primary and metastatic ccRCC tumor records in search of tumor metastasis–associated genes, and then carried out overall survival, Cox regression, and receiver operating characteristic (ROC) analyses to obtain potential prognostic markers. Comprehensive bioinformatics analysis was performed to verify that the checkpoint with forkhead associated and ring finger domains (*CHFR*) gene is a reliable candidate oncogene, which is overexpressed in ccRCC metastatic tumor tissue, and that high expression levels of *CHFR* indicate a poor prognosis. A detailed analysis of the methylation of *CHFR* in ccRCC tumors showed that three sites within 200 bp of the transcription initiation site were significantly associated with prognosis and that hypomethylation was associated with increased *CHFR* gene expression levels. Knockdown of *CHFR* in ccRCC cells inhibited cell proliferation, colony formation, and migration ability. In summary, our findings suggest that the epigenetic signature on *CHFR* gene is a novel prognostic feature; furthermore, our findings offer theoretical support for the study of metastasis-related genes in ccRCC and provided new insights for the clinical treatment of the disease.

Keywords: clear cell renal cell carcinoma, metastasis, CHFR, methylation, epigenetic

INTRODUCTION

Renal cell carcinoma (RCC) is the most common (~90%) and lethal type of kidney cancer, with clear cell RCC (ccRCC) being the most prevalent and aggressive subtype (~75%) (Hsieh et al., 2017; Capitanio et al., 2019). Surgical excision for localized RCC, in the form of partial or radical nephrectomy, offers the chance of cure in these patients. However, approximately 30%

of the patients show local recurrence or distant metastasis, along with a poor 5-year survival rate (Kunath et al., 2017; Wiechno et al., 2018). The most common sites of RCC metastasis are lungs and bones (Ho et al., 2017), and metastasis is the main reason of mortality associated with RCC. Thus, identification of the molecular characteristics underlying ccRCC tumor metastasis is urgently needed. Transcriptional profiling is an effective tool for discovering the molecular mechanisms underlying the metastasis or progression of ccRCC and predicting clinical outcomes. A comprehensive overview of the transcriptomic profiles of ccRCC was available from The Cancer Genome Atlas (TCGA) project. Using these data, we identified genes that support ccRCC metastases by comparing the gene expression profiles of metastatic tumors and primary tumor. Our study aimed to identify more genes associated with ccRCC tumor metastasis, thereby supporting the development of new gene targeted drugs for aggressive ccRCC.

We identified 4,933 differentially expressed genes (DEGs) between ccRCC tumor tissues and normal tissues as reported in TCGA and 86 metastatic phenotype-associated genes. To obtain the interactions between these 86 DEGs, we constructed a protein–protein interaction (PPI) network and obtained 22 seeds, of which 13 genes were associated with overall survival (OS). The checkpoint with forkhead-associated and ring finger domain (*CHFR*) gene stood out. It encodes the E3 ubiquitin ligase enzyme, an important checkpoint protein, which has been reported to inhibit tumorigenesis in a variety of tumors (Privette and Petty, 2008; Sanbhnani and Yeong, 2012). CHFR plays an important role in cell cycle regulation by delaying entry into metaphase in response to microtubular stress, by affecting substrates *via* both proteasome-dependent and independent process. CHFR could act as an E3 ubiquitin ligase that ubiquitinates and degrades the substrates. Yu et al. (2005) found that CHFR is a tumor suppressor that ensures chromosomal stability by controlling the expression levels of key mitotic proteins, such as Aurora A. Oh et al. (2009) reported that CHFR binds and downregulates HDAC1 by inducing its polyubiquitylation both *in vitro* and *in vivo* to suppress tumorigenesis. Other substrates of CHFR include, but are not limited to Kif22 (Maddika et al., 2009), PLK1 (Kang et al., 2002), poly(ADP-ribose) 1 PARP1 (Kashima et al., 2012), and TOPK (Shinde et al., 2013). CHFR can also target proteins not for degradation but to activate signal transduction. For example, CHFR binds to MAD2 to enable its activation and transport to the kinetochore; MAD2 is not able to inhibit anaphase progression without the help of CHFR, so CHFR abnormalities result in mitotic defects (Keller and Petty, 2011). Recent studies have shown that mitotic abnormalities are closely related to tumorigenesis (Funk et al., 2016). Thus, substantial evidence suggests that the mitotic checkpoint protein CHFR could serve as a biomarker for tumorigenesis, as well as a potential therapeutic target (Derks et al., 2014).

DNA methylation is found in the dinucleotides of nearly 80% of the CpG islands in the genome (Craig and Bickmore, 1994) and controls various cell functions, such as proliferation, differentiation, and apoptosis (Cao et al., 2020). In human cancers, the abnormal methylation of promoters could lead to the silencing or activation of target genes, affecting transcriptional pathways, and resulting in cancer development (Antequera and Bird, 1993). Genes can be regulated by methylation at a single site; for example, *CMTM3* is involved in the pathogenesis of testicular cancer, and is often silenced, at least partially, by methylation at a single specific CpG site in tumor tissue (Li et al., 2014). Fleischer et al. (2014) demonstrated the role of DNA methylation–based markers in clinical diagnosis and highlighted the importance of epigenetic changes in cancer. Some studies have shown that the downregulation of *CHFR* expression in some cancers is caused by hypermethylation of its promoter (Sanbhnani and Yeong, 2012; Derks et al., 2014). In ccRCC, *CHFR* hypermethylation is accompanied by elevated gene expression levels, but the cause is unknown. The classification of methylation states of *CHFR* may not be sufficiently detailed, and the specific sites associated with each category are unclear.

In our study, we found that *CHFR* can be used as a prognostic marker for malignant ccRCC, and the identification of three methylation sites near transcription initiation sites can predict patient prognosis by using comprehensive analysis; no previously identified markers can achieve this. Functional assays, including Cell Counting Kit 8 (CCK8), colony formation, and Transwell assays, indicate that CHFR is related to the malignant behavior of ccRCC cells. Taken together, our findings suggest that the epigenetic signature of *CHFR* is a novel prognostic gene involved in metastatic ccRCC.

RESULTS

DEG Screening, Gene Ontology, Kyoto Encyclopedia of Genes and Genomes, and PPI Functions Analysis

We selected DEGs in ccRCC normal and tumor tissues from TCGA database. Genes were considered upregulated or downregulated between normal and tumor tissues when their absolute fold change (tumor/normal) was greater than 2 ($|FC| > 2$) and their p value was less than 0.01 ($p < 0.01$). A total of 4,933 genes were identified as DEGs (**Figure 1A** and **Supplementary Table 1**). To obtain novel insight into the biology of metastatic ccRCC, the expression levels of 4,933 DEGs were compared further between the lymph node metastasis tissue (pathological_N1) and no lymph node metastasis tissue (pathological_N0), distant metastatic ccRCC tissues (pathological_M1) and primary tissues (pathological_M0), and different TNM stage tissues (pathological stage). Clinical characteristics are shown in **Table 1**. The Venn diagram showed that 86 genes were significantly associated with pathological N ($p < 0.05$), pathological M ($p <$ 1E-5), and pathological stage ($p <$ 1E-10) (**Figure 1B** and **Supplementary Table 2**). The 86 overlapped metastasis-associated genes were investigated using functional enrichment analysis, specifically Gene Ontology (GO) and Kyoto Encyclopedia of Genes and Genomes (KEGG). It is interesting that many cell cycle–related processes were enriched in biological process (BP), cell components (CC), molecular function (MF), and KEGG. This

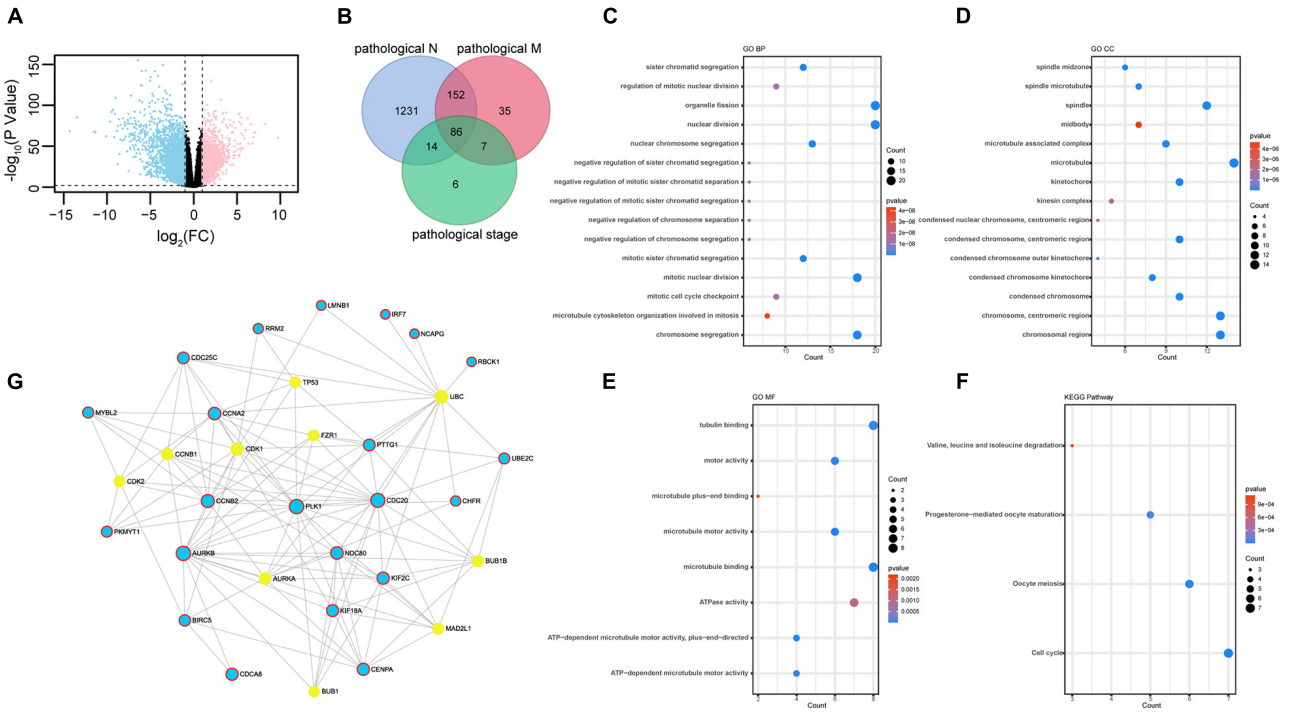

FIGURE 1 | Identification of differently expressed genes: **(A)** 4,933 DEGs identified in ccRCC TCGA dataset plotted in the volcano plot, in which the logarithmic ratio of FC of the tumor/normal are plotted against negative logarithmic *P*-values; 2,571 genes were significantly downregulated (blue); 2,362 genes were upregulated (red) (| fold change| > 2, $p < 0.01$). **(B)** Venn diagram of metastasis-related genes in ccRCC in TCGA dataset. A total of 86 genes showed significant association with pathological M ($p < 0.05$), pathological N ($p <$ 1E-5), and pathological stage ($p <$ 1E-10). **(C–F)** GO terms representing BP, CC, and MF and KEGG pathway analysis. **(G)** PPI network of 86 DEGs. The 22 seeds genes are shown in blue. The STRING Interactome database was selected to construct PPI, and the confidence score cutoff was set as 900; degree filter threshold values > 5.

analysis indicated that in ccRCC metastatic process of ccRCC, cell cycle–related genes play important roles (**Figures 1C–F**). To obtain the interactions between the 86 DEGs, we constructed the PPI network using online Networkanalyst software. As shown in **Figure 1G**, the subnetwork included 32 nodes and 22 seeds. Detailed information concerning the seeds is provided in **Supplementary Table 3**.

Survival Analysis of Hub Genes

Next, we analyzed all 22 seed genes associated with ccRCC from TCGA cohort. Thirteen genes were significantly associated with OS ($p < 0.001$) (**Figures 2**, **3A**). Increased expression of all 13 genes correlated with higher risks, most notably in the case of *CHFR* (**Figure 3A**). The expression of *CHFR* in other cancers has also been investigated. Compared to the normal control, *CHFR* was also overexpressed in cancers, including bladder urothelial carcinoma, breast invasive carcinoma, cervical squamous cell carcinoma and endocervical adenocarcinoma, cholangiocarcinoma, glioblastoma multiforme, head and neck squamous carcinoma, kidney renal papillary cell carcinoma, liver hepatocellular carcinoma (LIHC), lung adenocarcinoma, lung squamous carcinoma, pheochromocytoma and paraganglioma, prostate adenocarcinoma (PRAD), and uterine corpus endometrial carcinoma (**Supplementary Figure 1A**). In addition, high *CHFR* expression was significantly associated with worse OS rates among PRAD, LIHC, and KIRC (ccRCC) patients (**Figures 3A–C** and **Supplementary Figures 1B–D**).

TABLE 1 | TNM clinical characters.

Characteristics		No. of patients
Pathological N	N0	240
	N1	17
Pathological M	M0	426
	M1	79
Pathological stage	I	269
	II	57
	III	125
	IV	84

CHFR Was Associated With Various Clinicopathological Variables

Next, we will focus on the clinical value of *CHFR* status in ccRCC. As previously mentioned, significantly worse OS rates, progression-free intervals (PFIs), and disease-specific survival (DSS) rates were observed in the ccRCC patients with high *CHFR* expression than those with low *CHFR* expression (**Figures 3A–C**). Univariate and multivariate Cox regression analyses showed that expression level could serve as an attractive predictor

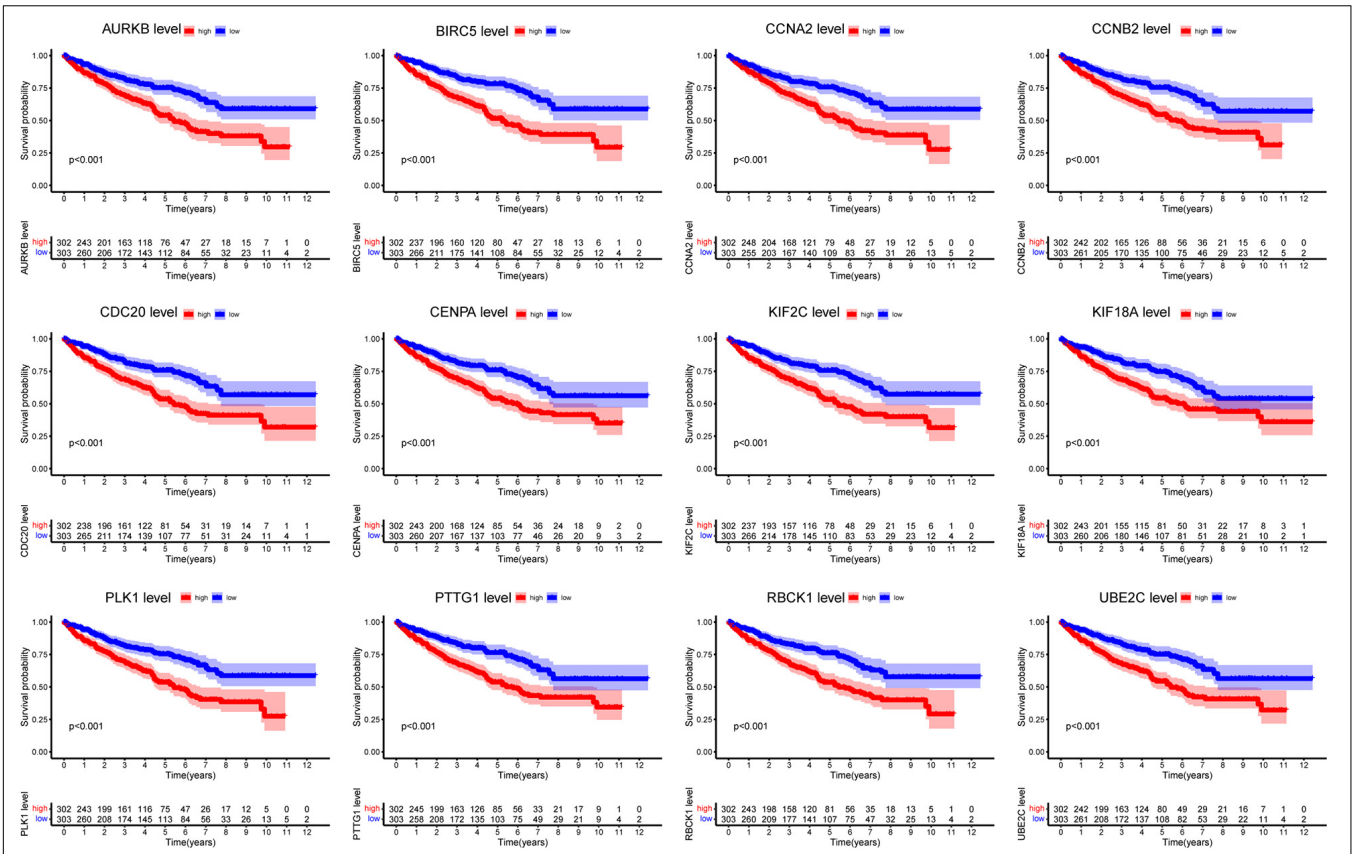

FIGURE 2 | Overall survival analysis of all seed genes.

of prognosis in metastatic ccRCC patients (**Table 2**). Time-dependent receiver operating characteristic (ROC) analysis was used to determine the diagnostic value of *CHFR* expression, and the results showed that *CHFR* areas under the curves (AUCs) for the 1-, 3-, and 5-year OS prediction were 0.698, 0.684, and 0.726, respectively (**Figure 3D**). Our systematic analysis indicated that *CHFR* is a reliable prognostic gene in ccRCC. Next, we explored the role of *CHFR* in ccRCC metastasis. Based on TCGA datasets, *CHFR* gene expression levels were significantly upregulated in tumor tissue compared with those in adjacent control normal tissue (**Figure 3E**). In many other datasets, we obtained similar results; CHFR gene expression level was significantly upregulated in kidney tumor tissue compared with adjacent control normal tissue, as shown in **Supplementary Figure 2**. The TCGA dataset revealed that *CHFR* was highly expressed in the tissues of patients with higher tumor histological grades (**Figure 3F**), advanced primary tumor pathological stages (**Figure 3G**), lymph node metastasis (**Figure 3H**), distant metastasis (**Figure 3I**), and advanced pathological stages (**Figure 3J**). Moreover, ROC analysis was performed to evaluate the diagnostic accuracy of *CHFR* in differentiating the metastatic-related clinical characteristics of ccRCC patients. As expected, the results showed that *CHFR* was highly accurate in discriminating distant metastasis from no distant metastasis as well as advanced stages (III and IV) from early stages (I and II) (**Figures 3K,L**). These results indicate that *CHFR* can be used as a potential diagnostic parameter to distinguish high-risk from low-risk ccRCC patients.

Downregulation of CHFR Significantly Suppressed Proliferation and Migration of ccRCC Cells

To clarify the expression of CHFR, we detected CHFR levels in ccRCC cells using Western blotting. The levels were upregulated in ACHN, 786-O, 769-P, and CAKI-1 ccRCC cell lines (**Figure 4A**). Real-time polymerase chain reaction (PCR) and Western blot assays established that *CHFR* mRNA and protein expression levels were significantly downregulated in 769-P and ACHN cells after treatment with targeted siRNAs (**Figures 4B,C**). The CCK8 assay indicated that cell proliferation was significantly lower for the cancer cells with *CHFR* knockdown than those with control siRNA transfection (**Figure 4D**). In addition, a significantly lower number of colonies were formed when *CHFR* was knocked down in 769-P and ACHN cells (**Figure 4E**). The results indicated that cellular proliferation capacity was suppressed when CHFR expression was reduced. The migratory ability of ccRCC cells in which CHFR deficiency occurred was also tested. Transwell analysis showed that knockdown of CHFR significantly inhibited the migration of 769-P and ACHN cells

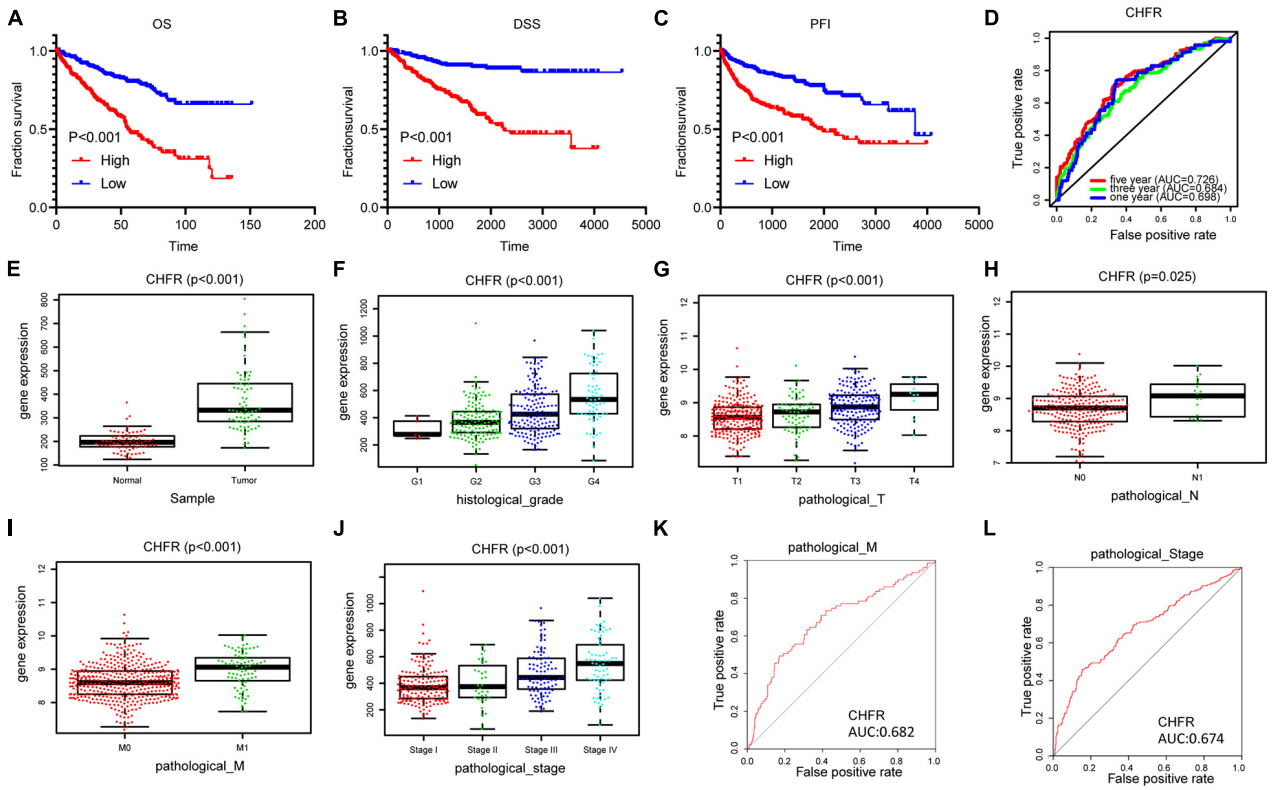

FIGURE 3 | Identification of CHFR overexpression is associated with poor prognosis of ccRCC: **(A–C)** *CHFR* that was upregulated in ccRCC patients related to a shorter OS, PFI, and DSS survival based on TCGA dataset. **(D)** The time-dependent ROC for 1-, 3-, and 5-year OS predictions for the *CHFR* prognostic signature. **(E)** *CHFR* gene expression in ccRCC adjacent normal tissues and tumor tissues according TCGA dataset. **(F–J)** CHFR expression was analyzed in ccRCC patients regarding histological grade, pathological T, pathological N, pathological M, and pathological stage. **(K)** ROC curve analysis of *CHFR* as individual biomarkers to discriminate ccRCC patients with distant metastasis form patients without distant metastasis. **(L)** ROC curve analysis of *CHFR* as individual biomarkers to discriminate ccRCC patients in pathological stages III and IV from patients in pathological stages I and II.

TABLE 2 | Univariate and multivariate Cox analyses.

	Univariate analysis				Multivariate analysis			
Characteristics	**HR**	**HR.95L**	**HR.95H**	***p***	**HR**	**HR.95L**	**HR.95H**	***p***
Histological grade 1 + 2 vs. 3 + 4	2.634	1.876	3.700	<0.001				
Pathological T T1 + T2 vs. T3 + T4	3.179	2.107	4.797	<0.001				
Pathological N Yes vs. no	3.392	1.801	6.389	<0.001				
Pathological M Yes vs. no	4.351	3.190	5.935	<0.001	2.393	1.450	3.951	0.001
Pathological stage I + II vs. III + IV	3.550	2.307	5.461	<0.001	1.945	1.174	3.221	0.010
CHFR High vs. low	3.068	2.214	4.252	<0.001	3.402	2.093	5.530	<0.001

(**Figure 4F**). The above results demonstrated that CHFR had a critical effect on the proliferation and migration of ccRCC cells.

Identifying Specific Prognostic Methylation Sites in CHFR

CHFR expression levels have been reported to be regulated by methylation modifications. In ccRCC tumor tissues, although the overall methylation level of CHFR increased, the gene expression level was also significantly increased. Therefore, we analyzed the data related to methylation modification in TCGA database in detail and found that 73 sites on the CHFR gene were modified by methylation (**Supplementary Table 4**, methylation site and Cox analysis). Because DNA methylation in the promoter regions strongly influences gene expression, we selected CpGs in the promoter regions. Promoter regions were defined as 2 kb upstream to 0.5 kb downstream from the transcription start sites. Finally, we screened 23 methylation modification sites from these promoter regions (**Supplementary Table 4, 23** TSS200-1500 sites). Next, in order to determine the methylation sites associated with survival outcomes, we selected prognosis-associated CpGs sites from the 23 methylation modification sites.

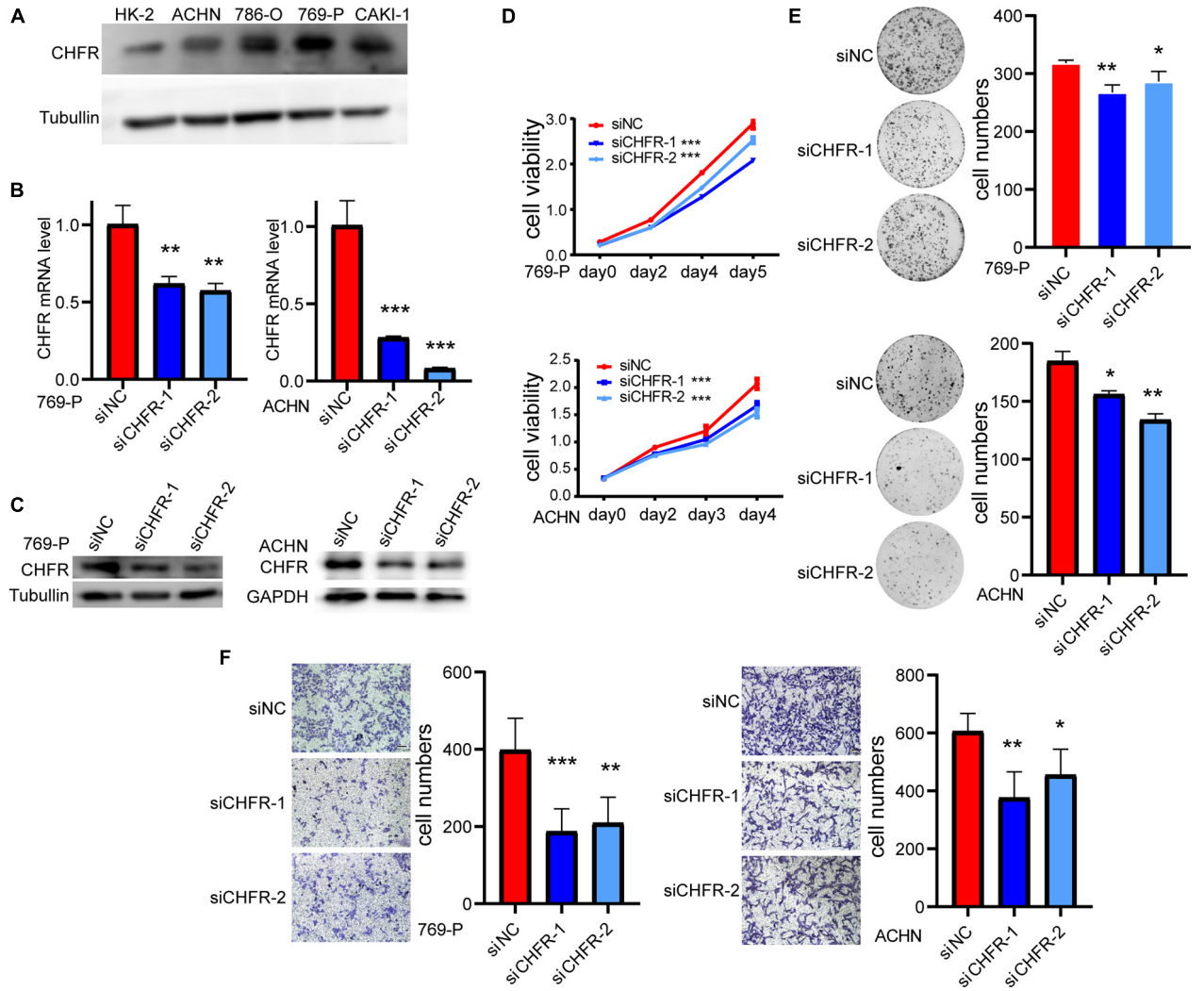

FIGURE 4 | Depletion of CHFR suppresses ccRCC growth and metastasis: **(A)** Western blot: CHFR protein level was higher in ccRCC carcinoma cells than that in normal kidney cell line HK-2. **(B,C)** The knockdown efficiency of CHFR in 769-P and ACHN cells transfected with CHFR siRNA or control siRNA was verified by RT-PCR assay and Western blot assay. **(D)** CCK8 assay of ACHN and 769-P cells transfected with CHFR siRNA or control siRNA. The proliferation rates transfected with siCHFR were significantly lower than the control cells. **(E)** Colony formation assay. CHFR knockdown suppressed the colony formation. **(F)** Transwell assays were used to evaluate cell migration ability. Scale bar: 100 μm. All values are expressed as the mean ± SD (*$p < 0.05$, **$p < 0.01$, ***$p < 0.001$).

We obtained 10 survival-associated methylation sites, of which seven predicted a poor prognosis when hypomethylated and three did so when hypermethylated (**Supplementary Figure 3**). Moreover, among these sites, only the top three were not based on optimal grouping, and these were within the range of 200 bp upstream of the transcription initiation region (**Supplementary Figure 3**). Therefore, we focused on the regulation of gene expression by these three prognostic sites. Patients were divided into hypermethylated and hypomethylated groups according to the three different prognostic sites' methylation levels (calculated as reference ratios to medians). In all three sites, we found that the expression level of *CHFR* in the hypomethylated group was significantly increased (**Figure 5A**), and the hypomethylated group predicted a poor prognosis in terms of OS (**Figure 5B**) and DSS (**Figure 5C**). Therefore, the increase in *CHFR* gene expression levels in ccRCC may be mainly regulated by three methylation modification sites near the transcription initiation site, and our findings indicate their predictive and prognostic value as methylation-based biomarkers in the diagnosis and treatment of ccRCC.

DISCUSSION

Nearly 20% of ccRCC cases are at an advanced stage at the time of diagnosis (Mitchell et al., 2018). Even with surgical excision, 30% of localized ccRCC cases tend to show subsequent recurrence and metastases, and the 5-year survival rate of patients with distant metastases is approximately only 8–10% (Choueiri and Motzer, 2017; Miao et al., 2018). Therefore, there is an

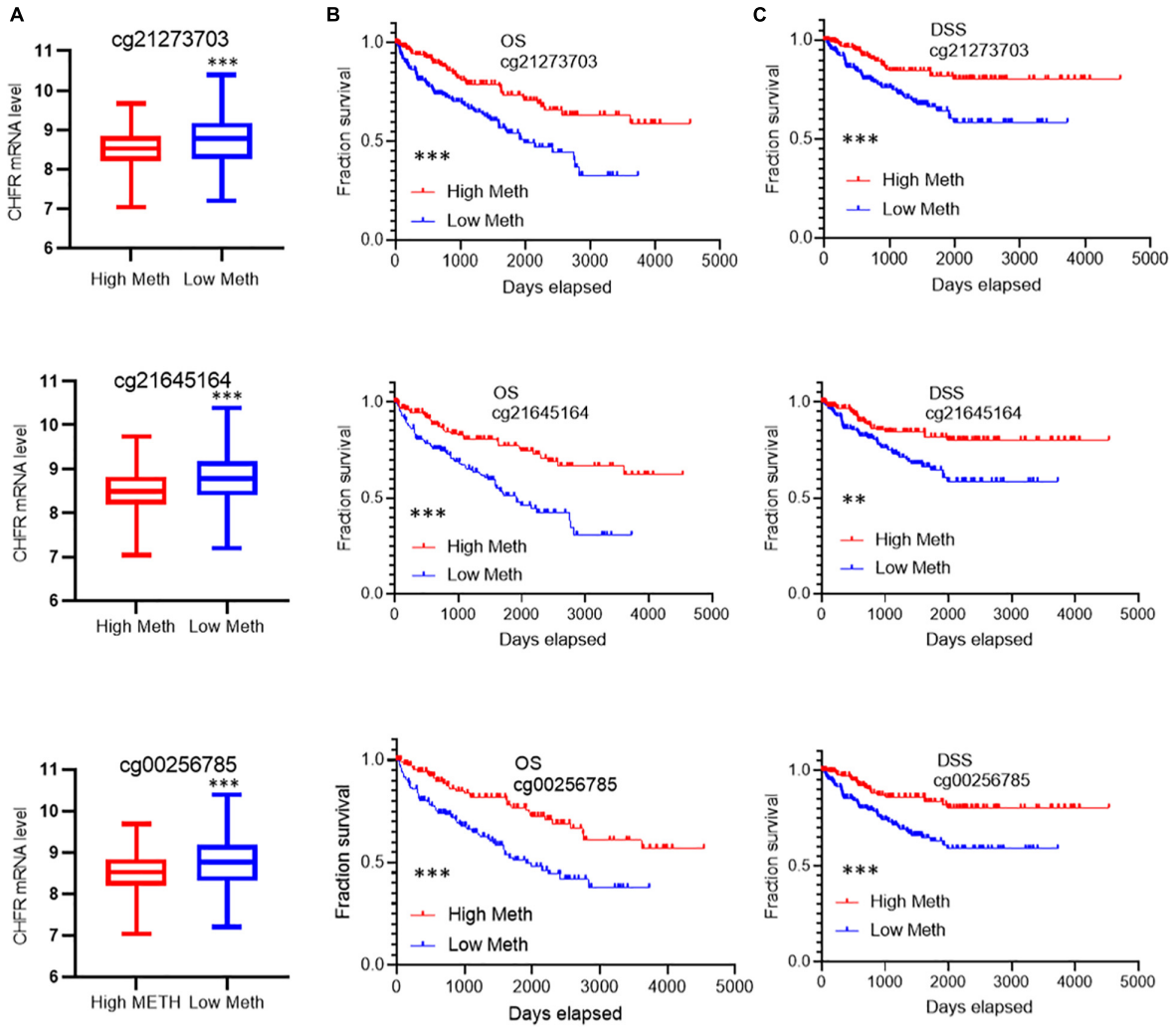

FIGURE 5 | Correlation of the top 3 methylation sites with prognosis and *CHFR* expression: **(A)** Low levels of methylation at all three modification sites are associated with high gene expression **(B,C)** and associated with poor prognosis including overall survival and disease-specific survival $^{*}p < 0.05$, $^{**}p < 0.01$, $^{***}p < 0.001$.

urgent need to further understand the molecular mechanisms that drive ccRCC metastasis to support the development of more effective therapeutic strategies. Rapid advances in genomics and transcriptomics have provided valuable opportunities to explore potential metastasis-related drivers.

In our study, in order to mine metastasis-related genes, we compared patient tissues with and without lymph node metastasis, tissues with and without distal metastasis, and tissues with high- and low-progression TNM stages, respectively, by using TCGA transcriptional profiling database. We suggest that genes that differ significantly in lymph node metastasis tissues, distal tumor metastasis tissues, and different pathological grades tissues are more likely to be markers of metastatic renal clear cell carcinoma, and thus, we further screened out the intersection genes of the three datasets. Through the above screening, a total of 86 genes were obtained, and the function and interaction analysis of 86 genes showed that, interestingly, many cell cycle–related genes were enriched. Many mitosis-related genes do play an important role in tumor development. For example, *UBE2C*, directly targeted by miR-548e-5p, increases cellular growth and invasive abilities of non–small cell lung cancer cells (Jin et al., 2019), *CDK1* interacts with *Sox2* and promotes tumor initiation in human melanoma (Ravindran Menon et al., 2018), and silencing CDCA8 suppresses hepatocellular carcinoma growth and stemness *via* restoration of the *ATF3* tumor suppressor (Jeon et al., 2021).

In particular, the checkpoint protein CHFR has attracted our attention. We found that CHFR was significantly overexpressed in ccRCC tissue samples with higher TNM grade and that CHFR overexpression predicted a poor prognosis and a higher risk of death. Several studies have suggested that CHFR expression is downregulated and inhibited by promoter hypermethylation in different types of cancer (Sanbhnani and Yeong, 2012; Derks et al., 2014). As a tumor suppressor gene, CHFR plays an important role in tumor progression and metastasis, as seen in gastric cancer (Hu et al., 2011), pancreatic cancer

(Zhang et al., 2017), and esophageal adenocarcinoma (Soutto et al., 2010). We therefore evaluated the expression of *CHFR* in 33 different types of cancer from TCGA database and its relationship with prognosis. We found that *CHFR* was upregulated in many cancers, and high expression of *CHFR* in PRAD and LIHC also predicted poor prognosis. Our findings suggest a complex role for *CHFR* in different cancers. A detailed analysis of the methylation of *CHFR* at 73 sites in ccRCC tumors showed that three sites located within approximately 200 bp of the transcription initiation site were significantly associated with prognosis and that hypomethylation was associated with increased gene expression levels. We performed a series of functional experiments on ccRCC cells. The results showed that knockdown of *CHFR* inhibited the proliferation, invasion, and metastasis of ccRCC cells. Taken together, our findings suggest that the epigenetic signature of the *CHFR* gene is a novel prognostic feature involved in metastatic ccRCC.

Our study had a few limitations. First, we used public databases, and these findings need to be validated in prospective clinical trials. Second, although we have demonstrated the role of *CHFR* in ccRCC cells *in vitro*, its effect on ccRCC development needs to be further studied *in vivo*. Concurrently, it is necessary to explore the molecular mechanisms of *CHFR* in ccRCC. In conclusion, this study has increased our understanding of the metastatic mechanism in ccRCC, suggesting that *CHFR* expression can be used as a biomarker for the prognosis of ccRCC, although further study of the related molecular pathways of *CHFR* in ccRCC is needed.

MATERIALS AND METHODS

Cell Culture

ccRCC cell lines were purchased from the Cell Bank of the Chinese Academy of Sciences (Shanghai, China); 769-P and 786-O cells were cultured in Roswell Park Memorial Institute 1640 (RPMI 1640); ACHN and HK-2 were cultured in MEM; and CAKI-1 was cultured in McCoy 5A. All cells were cultured with 10% fetal bovine serum (FBS) and 1% penicillin/streptomycin in an incubator at 37°C with 5% CO_2.

siRNAs and Antibodies

All siRNA sequences were synthesized by GenePharma (Shanghai, China). Two siRNAs of CHFR were: 5′-AGCCTT TCTGCCACCTGTATT-3′ (siCHFR_1), 5′-CCACAGCCATC AACATCGATT-3′ (siCHFR_2). RNAs were transfected at 60 nM with Lipofectamine 3000 (Thermo, L3000015). The CHFR, tubulin, and GAPDH antibodies were purchased from Proteintech (Wuhan, China).

CCK8 Cell Proliferation Assay

Cells were seeded into 96-well plates (2,000 cells/well). CCK8 (Dojindo, Japan) was used according to the manufacturer's instructions. After incubating cells for 2 h, we detected the optical density at 450 nm for each well by using a microplate reader.

Colony Formation Assay

Cells were plated into six-well plates (2,000 cells/well). Cells were cultured for 14 days and then washed three times with phosphate-buffered saline (PBS), subsequently fixed with methanol, and then stained with 0.5% crystal violet solution for 20 min. The numbers of colonies of each well were manually counted.

Transwell Migration Assay

Using Transwell chamber (8-μm pore size, Corning, United States) to perform cell migration assay. Cells were placed on the upper layer of cell-permeable membrane, in the lower chamber with 10% FBS media, incubated for 20 h, and then fixed with 4% paraformaldehyde, washed with PBS, and stained with 0.5% crystal violet; the upper chamber cells were removed. Cells that had passed through the pore and adhered to the lower membrane surface were counted.

RNA Isolation and Quantitative Real-Time PCR

RNA was isolated from cells using Trizol reagent (Sigma, United States) (Rio et al., 2010). RNA was reverse transcribed into cDNA using the mRNA RT Reagent Kit (TaKaRa). Reverse transcriptase (RT)–PCR using FastStart Universal SYBR® Green Master (ROX) (Roche, Germany) was carried out on an Applied Biosystems 7500 real-time PCR system. The gene ACTIN served as an endogenous control for normalization. The CHFR forward primer was as follows: GATGGTCACTCTGTCACCTGC, reverse primer: TTGTGGCTTCCCAGCATTGG; the ACTIN forward primer: CATCCGCAAAGACCTGTACG, reverse primer: CCTGCTTGCTGATCCACATC.

Database

The gene expression profiles and clinical data of patients with ccRCC were obtained from UCSC Xena[1] including 533 ccRCC cases in TCGA. The ccRCC cancer DNA methylation data were downloaded from the MethSurv data portal[2] (named KIRC_meth.RData, 2017), The methylation level of each probe was represented by the *b*-value, which ranges from 0 to 1, corresponding to unmethylated and fully methylated, respectively. The TIMER online tool was used to analyze the expression of the CHFR gene in different tumors.[3] The Networkanalyst software was used to analyze PPI network.

Identification of DEGs

We identified the DEGs in ccRCC from TCGA according to the following cutoff value: $p < 0.01$ and $|\log2 \text{ fold change (FC)}| > 1$.

GO and KEGG Pathway Enrichment

We used the overlapped DEGs and DEPs both in TCGA and CPTAC for gene enrichment and functional annotation analyses by "ClusterProfiler" packages in R 3.6.1.

[1]https://xenabrowser.net/datapages/

[2]https://biit.cs.ut.ee/methsurv/

[3]http://timer.comp-genomics.org

Survival Analysis

The survival R package was used to analyze the relationship between 22-hub-gene expression levels and the OS of patients from the TCGA dataset. SPSS was used to analyze the relationship between CHFR gene expression levels and PFI/DSS. We tested this relationship by Kaplan–Meier method with a log-rank test, where $p < 0.05$ was regarded as statistically significant.

Establishment of Regression Model and Construction of OS Risk Prognostic Models

Univariate and multivariate Cox models were used to investigate the correlation between *CHFR* gene expression level and certain clinical characteristics, namely, histological grade, pathological T, pathological M, pathological stage, and OS, in ccRCC patients. Time-dependent ROC analysis for OS was used to evaluate the accuracy of the prognostic model. The correlations between the aforementioned clinical characteristics were also analyzed.

Statistical Analysis

Statistical analyses were performed using SPSS Statistics software (version 23.0; IBM SPSS, Chicago, IL, United States), GraphPad Prism 8.0 (GraphPad Software, Inc., United States), and R 3.6.1. Functional and KEGG enrichment analyses were performed using the "ClusterProfiler" package. The time-dependent ROC analysis was performed using the "survivalROC" package. Kaplan–Meier analysis was performed to estimate the correlation between CHFR expression and OS, DSS, and PFI using the log-rank test. The prognostic significance of *CHFR* in ccRCC was analyzed using univariate and multivariate Cox proportional hazard regressions. To further evaluate the diagnostic value of *CHFR* mRNA expression, we generated ROC curves and calculated the AUC. All *in vitro* experiments were performed in triplicate or quintuplicate, and all data are represented as mean ± SD. Statistical significance was indicated by $p < 0.05$, and significance levels are shown as $^{*}p < 0.05$, $^{**}p < 0.01$, and $^{***}p < 0.001$.

DATA AVAILABILITY STATEMENT

The original contributions presented in the study are included in the article/**Supplementary Material**, further inquiries can be directed to the corresponding author/s.

AUTHOR CONTRIBUTIONS

XC, JL, and QC performed the experiments. XC sorted out the article ideas and wrote the manuscript. JL and QC modified the article. SL and LM participated in the data analysis. XL and TW contributed to the wound-healing assays and invasion assays. ZL conceived the project and supervised the experiments. All authors contributed to the article and approved the submitted version.

FUNDING

This research was supported by the China Postdoctoral Science Foundation (2019M663098), by the National Natural Science Foundation of China (81772736 and 81972366), the Guangdong Key Laboratory funds of Systems Biology and Synthetic Biology for Urogenital Tumors (2017B030301015).

SUPPLEMENTARY MATERIAL

The Supplementary Material for this article can be found online at: https://www.frontiersin.org/articles/10.3389/fgene.2021.720979/full#supplementary-material

Supplementary Figure 1 | Pan-cancer mRNA expression of CHFR. **(A)** Boxplots show *CHFR* expression in tumor (red) and normal (blue) tissue samples in different types of cancer. $^{*}p < 0.05$, $^{**}p < 0.01$, $^{***}p < 0.001$. **(B–D)** PRAD, LIHC, and KIRC patients with high *CHFR* expression had a worse OS rate than those with low *CHFR* expression.

Supplementary Figure 2 | Identification of CHFR overexpression in kidney tumor tissues vs. normal tissues from different Oncomine datasets.

Supplementary Figure 3 | Cox regression analysis of 23 methylation sites.

REFERENCES

Antequera, F., and Bird, A. (1993). Number of CpG islands and genes in human and mouse. *Proc. Natl. Acad. Sci. U.S.A.* 90, 11995–11999. doi: 10.1073/pnas.90.24.11995

Cao, K., Ugarenko, M., Ozark, P. A., Wang, J., Marshall, S. A., Rendleman, E. J., et al. (2020). DOT1L-controlled cell-fate determination and transcription elongation are independent of H3K79 methylation. *Proc. Natl. Acad. Sci. U.S.A.* 117, 27365–27373. doi: 10.1073/pnas.2001075117

Capitanio, U., Bensalah, K., Bex, A., Boorjian, S. A., Bray, F., Coleman, J., et al. (2019). Epidemiology of renal cell carcinoma. *Eur. Urol.* 75, 74–84.

Choueiri, T. K., and Motzer, R. J. (2017). Systemic therapy for metastatic renal-cell carcinoma. *N. Engl. J. Med.* 376, 354–366.

Craig, J. M., and Bickmore, W. A. (1994). The distribution of CpG islands in mammalian chromosomes. *Nat. Genet.* 7, 376–382. doi: 10.1038/ng0794-376

Derks, S., Cleven, A. H., Melotte, V., Smits, K. M., Brandes, J. C., Azad, N., et al. (2014). Emerging evidence for CHFR as a cancer biomarker: from tumor biology to precision medicine. *Cancer Metastasis Rev.* 33, 161–171.

Fleischer, T., Frigessi, A., Johnson, K. C., Edvardsen, H., Touleimat, N., Klajic, J., et al. (2014). Genome-wide DNA methylation profiles in progression to in situ and invasive carcinoma of the breast with impact on gene transcription and prognosis. *Genome Biol.* 15:435.

Funk, L. C., Zasadil, L. M., and Weaver, B. A. (2016). Living in CIN: mitotic infidelity and its consequences for tumor promotion and suppression. *Dev. Cell* 39, 638–652. doi: 10.1016/j.devcel.2016.10.023

Ho, T. H., Serie, D. J., Parasramka, M., Cheville, J. C., Bot, B. M., Tan, W., et al. (2017). Differential gene expression profiling of matched primary renal cell carcinoma and metastases reveals upregulation of extracellular matrix genes. *Ann. Oncol.* 28, 604–610. doi: 10.1093/annonc/mdw652

Hsieh, J. J., Purdue, M. P., Signoretti, S., Swanton, C., Albiges, L., Schmidinger, M., et al. (2017). Renal cell carcinoma. *Nat. Rev. Dis. Primers* 3:17009.

Hu, S. L., Huang, D. B., Sun, Y.-B., Wu, L., Xu, W.-P., Yin, S., et al. (2011). Pathobiologic implications of methylation and expression status of Runx3 and CHFR genes in gastric cancer. *Med. Oncol.* 28, 447–454. doi: 10.1007/s12032-010-9467-6

Jeon, T., Ko, M. J., Seo, Y.-R., Jung, S.-J., Seo, D., Park, S.-Y., et al. (2021). Silencing CDCA8 suppresses hepatocellular carcinoma growth and stemness via restoration of ATF3 tumor suppressor and inactivation of AKT/β-catenin signaling. *Cancers* 13:1055. doi: 10.3390/cancers13051055

Jin, D., Guo, J., Wu, Y., Du, J., Wang, X., An, J., et al. (2019). UBE2C, directly targeted by miR-548e-5p, increases the cellular growth and invasive abilities of cancer cells interacting with the EMT marker protein zinc finger e-box binding homeobox 1/2 in NSCLC. *Theranostics* 9, 2036–2055. doi: 10.7150/thno.32738

Kang, D., Chen, J., Wong, J., and Fang, G. (2002). The checkpoint protein Chfr is a ligase that ubiquitinates Plk1 and inhibits Cdc2 at the G2 to M transition. *J. Cell Biol.* 156, 249–259. doi: 10.1083/jcb.200108016

Kashima, L., Idogawa, M., Mita, H., Shitashige, M., Yamada, T., Ogi, K., et al. (2012). CHFR protein regulates mitotic checkpoint by targeting PARP-1 protein for ubiquitination and degradation. *J. Biol. Chem.* 287, 12975–12984. doi: 10.1074/jbc.m111.321828

Keller, J. A., and Petty, E. M. (2011). CHFR binds to and regulates MAD2 in the spindle checkpoint through its cysteine-rich domain. *Biochem. Biophys. Res. Commun.* 409, 389–393. doi: 10.1016/j.bbrc.2011.04.143

Kunath, F., Schmidt, S., Krabbe, L.-M., Miernik, A., Dahm, P., Cleves, A., et al. (2017). Partial nephrectomy versus radical nephrectomy for clinical localised renal masses. *Cochrane Database Syst. Rev.* 5:Cd012045.

Li, Z., Xie, J., Wu, J., Li, W., Nie, L., Sun, X., et al. (2014). CMTM3 inhibits human testicular cancer cell growth through inducing cell-cycle arrest and apoptosis. *PLoS One* 9:e88965. doi: 10.1371/journal.pone.0088965

Maddika, S., Sy, S. M., and Chen, J. (2009). Functional interaction between Chfr and Kif22 controls genomic stability. *J. Biol. Chem.* 284, 12998–13003. doi: 10.1074/jbc.m900333200

Miao, D., Margolis, C. A., Gao, W., Voss, M. H., Li, W., Martini, D. J., et al. (2018). Genomic correlates of response to immune checkpoint therapies in clear cell renal cell carcinoma. *Science* 359, 801–806.

Mitchell, T. J., Turajlic, S., Rowan, A., Nicol, D., Farmery, J. H. R., O'Brien, T., et al. (2018). Timing the landmark events in the evolution of clear cell renal cell cancer: tracerx renal. *Cell* 173, 611–623.

Oh, Y. M., Kwon, Y. E., Kim, J. M., Bae, S. J., Lee, B. K., Yoo, S. J., et al. (2009). Chfr is linked to tumour metastasis through the downregulation of HDAC1. *Nat. Cell. Biol.* 11, 295–302. doi: 10.1038/ncb1837

Privette, L. M., and Petty, E. M. (2008). CHFR: a novel mitotic checkpoint protein and regulator of tumorigenesis. *Transl. Oncol.* 1, 57–64. doi: 10.1593/tlo.08109

Ravindran Menon, D., Luo, Y., Arcaroli, J. J., Liu, S., KrishnanKutty, L. N., Osborne, D. G., et al. (2018). CDK1 Interacts with Sox2 and promotes tumor initiation in human melanoma. *Cancer Res.* 78, 6561–6574. doi: 10.1158/0008-5472.can-18-0330

Rio, D. C., Ares, M. Jr., Hannon, G. J., and Nilsen, T. W. (2010). Purification of RNA using TRIzol (TRI reagent). *Cold Spring Harbor. Protoc.* 2010:db.rot5439.

Sanbhnani, S., and Yeong, F. M. (2012). CHFR: a key checkpoint component implicated in a wide range of cancers. *Cell. Mol. Life Sci.* 69, 1669–1687. doi: 10.1007/s00018-011-0892-2

Shinde, S. R., Gangula, N. R., Kavela, S., Pandey, V., and Maddika, S. (2013). TOPK and PTEN participate in CHFR mediated mitotic checkpoint. *Cell Signal.* 25, 2511–2517. doi: 10.1016/j.cellsig.2013.08.013

Soutto, M., Peng, D., Razvi, M., Ruemmele, P., Hartmann, A., Roessner, A., et al. (2010). Epigenetic and genetic silencing of CHFR in esophageal adenocarcinomas. *Cancer* 116, 4033–4042. doi: 10.1002/cncr.25151

Wiechno, P., Kucharz, J., Sadowska, M., Michalski, W., Sikora-Kupis, B., Jonska-Gmyrek, J., et al. (2018). Contemporary treatment of metastatic renal cell carcinoma. *Med. Oncol.* 35:156. doi: 10.5980/jpnjurol.97.156_2

Yu, X., Minter-Dykhouse, K., Malureanu, L., Zhao, W.-M., Zhang, D., Merkle, C. J., et al. (2005). Chfr is required for tumor suppression and aurora a regulation. *Nat. Genet.* 37, 401–406. doi: 10.1038/ng1538

Zhang, D., Xu, X. L., Li, F., Sun, H.-C., Cui, Y.-Q., Liu, S., et al. (2017). Upregulation of the checkpoint protein CHFR is associated with tumor suppression in pancreatic cancers. *Oncol. Lett.* 14, 8042–8050.

Conflict of Interest: The authors declare that the research was conducted in the absence of any commercial or financial relationships that could be construed as a potential conflict of interest.

Publisher's Note: All claims expressed in this article are solely those of the authors and do not necessarily represent those of their affiliated organizations, or those of the publisher, the editors and the reviewers. Any product that may be evaluated in this article, or claim that may be made by its manufacturer, is not guaranteed or endorsed by the publisher.

frontiers in Cell and Developmental Biology

ORIGINAL RESEARCH
published: 18 October 2021
doi: 10.3389/fcell.2021.747985

Immune Signatures Combined With BRCA1-Associated Protein 1 Mutations Predict Prognosis and Immunotherapy Efficacy in Clear Cell Renal Cell Carcinoma

Ze Gao[1,2†], Junxiu Chen[1,2†], Yiran Tao[3†], Qiong Wang[1,2,4], Shirong Peng[1,2], Shunli Yu[1,2], Jianwen Zeng[5], Kaiwen Li[1,2], Zhongqiu Xie[4*] and Hai Huang[1,2,5*]*

[1] Department of Urology, Sun Yat-sen Memorial Hospital, Sun Yat-sen University, Guangzhou, China, [2] Guangdong Provincial Key Laboratory of Malignant Tumor Epigenetics and Gene Regulation, Sun Yat-sen Memorial Hospital, Sun Yat-sen University, Guangzhou, China, [3] Department of Urology, The Sixth Affiliated Hospital, Sun Yat-sen University, Guangzhou, China, [4] Department of Pathology, School of Medicine, University of Virginia, Charlottesville, VA, United States, [5] Department of Urology, Qingyuan People's Hospital, The Sixth Affiliated Hospital of Guangzhou Medical University, Qingyuan, China

OPEN ACCESS

Edited by:
Xiao Zhu,
Guangdong Medical University, China

Reviewed by:
Yanqiang Li,
Boston Children's Hospital and Harvard Medical School, United States
Heping Zheng,
Hunan University, China

***Correspondence:**
Kaiwen Li
likw6@mail.sysu.edu.cn
Zhongqiu Xie
zx8t@virginia.edu
Hai Huang
huangh9@mail.sysu.edu.cn

[†] These authors have contributed equally to this work

Specialty section:
This article was submitted to Epigenomics and Epigenetics, a section of the journal Frontiers in Cell and Developmental Biology

Received: 27 July 2021
Accepted: 20 September 2021
Published: 18 October 2021

Citation:
Gao Z, Chen J, Tao Y, Wang Q, Peng S, Yu S, Zeng J, Li K, Xie Z and Huang H (2021) Immune Signatures Combined With BRCA1-Associated Protein 1 Mutations Predict Prognosis and Immunotherapy Efficacy in Clear Cell Renal Cell Carcinoma. Front. Cell Dev. Biol. 9:747985. doi: 10.3389/fcell.2021.747985

Immunotherapy is gradually emerging in the field of tumor treatment. However, because of the complexity of the tumor microenvironment (TME), some patients cannot benefit from immunotherapy. Therefore, we comprehensively analyzed the TME and gene mutations of ccRCC to identify a comprehensive index that could more accurately guide the immunotherapy of patients with ccRCC. We divided ccRCC patients into two groups based on immune infiltration activity. Next, we investigated the differentially expressed genes (DEGs) and constructed a prognostic immune score using univariate Cox regression analysis, unsupervised cluster analysis, and principal component analysis (PCA) and validated its predictive power in both internal and total sets. Subsequently, the gene mutations in the groups were investigated, and patients suitable for immunotherapy were selected in combination with the immune score. The prognosis of the immune score-low group was significantly worse than that of the immune score-high group. The patients with BRCA1-associated protein 1 (BAP1) mutation had a poor prognosis. Thus, this study indicated that establishing an immune score model combined with BAP1 mutation can better predict the prognosis of patients, screen suitable ccRCC patients for immunotherapy, and select more appropriate drug combinations.

Keywords: immunotherapy efficacy, clear cell renal cell carcinoma, prognosis carcinoma, immune signature, BAP1 mutation

INTRODUCTION

Kidney cancer was the 16th most common cancer in 2018, with 403,262 new cases and 175,098 deaths worldwide (Bray et al., 2018). Renal cell carcinoma comprises many histological subtypes, the most common of which is clear cell renal cell carcinoma (ccRCC), which accounts for 75% of all cases (Turajlic et al., 2018). Currently, the treatment of renal cancer is mainly surgical resection.

However, approximately one-third of patients will relapse after surgery, and metastases are found in approximately 30% of patients at the time of initial diagnosis (Janzen et al., 2003). The advent of cytokine therapy, such as interleukin-2 (IL-2) and interferon alpha-2B (IFN-α), brought the earliest immunotherapy regimens (Margolin et al., 1989; Fisher et al., 2000). With the rise of targeted therapies for renal cancer, the effectiveness of vascular endothelial group factor (VEGF) and molecular target of rapamycin (mTOR) pathway inhibitors for metastatic renal cell carcinoma appears to limit the development of immunotherapy (Posadas et al., 2013). In recent years, the emergence of immune checkpoint blockade (ICB) therapy, which blocks programmed cell death protein 1 (PD-1) and programmed death-ligand 1 (PD-L1), has further advanced immunotherapy. Patients have benefited from treatment for lung cancer, Hodgkin's lymphoma, and glioblastoma (Ansell et al., 2015; Forde et al., 2018; Cloughesy et al., 2019). Therefore, exploring the relevant indicators of immunotherapy effectiveness in ccRCC is necessary.

Immune cell infiltration and the tumor mutation burden (TMB) play key roles in the efficacy of tumor immunotherapy. Neoantigens are produced by a few somatic mutations in tumors and can be recognized by the immune system (Snyder et al., 2014). These mutations can be transcribed and translated and present in the MHC complex on the surface of tumor cells (Coulie et al., 2014). However, not all mutations can produce neoantigens, and not all neopeptides present on the cell surface can be recognized by T cells (Carreno et al., 2015; Snyder and Chan, 2015). Therefore, the search for effective mutations can further enhance the efficacy of immunotherapy. Tumors are complex new organisms that contain not only malignant tumor cells but also other types of cells. Among these cells, immune infiltrating cells play a central role in the immunotherapy response (Chen and Mellman, 2017). The levels of tumor-infiltrating $CD8^+$ and $CD4^+$ T cells are correlated with the immunotherapy response (Topalian et al., 2016). Cytotoxic $CD8^+$ T cells are the main effectors of antitumor immunity and can specifically recognize and kill tumor cells carrying neoantigens (Chen and Mellman, 2013). However, not all immune cells can produce a positive immune response against tumors. In many cases, some immune cells are dysfunctional, leading to immunosuppression, supporting tumorigenesis and immune evasion, such as Treg cells (Finotello and Trajanoski, 2017). The molecules involved in Treg-mediated inhibition include IL-2, IL-10, TGF-β, IL-35, cytotoxic T lymphocyte-associated protein 4 (CTLA-4), glucocorticoid-induced TNF receptor (GITR), and cAMP (Tanaka and Sakaguchi, 2017). Therefore, quantifying the degree of immune cell infiltration in tumors, as well as the expression of immunosuppressive receptors and ligands, will help to select appropriate immunotherapeutic drugs.

In this study, to screen patients with ccRCC suitable for immune checkpoint inhibitor therapy, we assessed and quantified the level of immune infiltrating cells and screened differential genes to construct immune scores. We also explored the changes in tumor mutation burden in patients with different immune scores and combined tumor mutation burden to more accurately select immune checkpoint inhibitors (ICI) treatment patients in ccRCC.

MATERIALS AND METHODS

Samples and Data Process

The RNA-seq data (level 3) of 530 ccRCC patients were obtained from The Cancer Genome Atlas (TCGA) database[1]. The masked somatic mutation data of 336 ccRCC patients were downloaded from the TCGA database. The R packages "limma" and "maftools" were used to process the RNA-seq and calculate the total number of somatic non-synonymous point mutations within each sample, respectively.

Estimation of Immune Cell Type Fractions

To determine the cell composition in the tumor microenvironment, we used xCell and CIBERSORT to estimate immune cell types. CIBERSORT estimates immune cell subpopulations using RNA-Seq (Newman et al., 2015). It obtains aggregated high-dimensional data from tumor cell mixtures and infers cell composition based on the expression profile of purified white blood cell subpopulations. xCell uses a set of 10,808 genes to score and estimate the degree of infiltration of 64 cell types (Aran et al., 2017). It can further accurately distinguish the activation state of $CD8^+$ T cells, a function that is impossible for CIBERSORT. To ensure the accuracy of the results, a p-value less than 0.05 was used as the criterion.

Gene Set Enrichment

We used single sample gene set enrichment analysis (ssGSEA) to quantify the enrichment level of 29 immune features of each sample, including immune cell types, functions, and pathways (Barbie et al., 2009). According to the results, hierarchical cluster analysis was performed on all patients, who were divided into two groups. To identify the regulatory pathways with the largest differences between the two groups, the R package Pi containing 205,000 genes was used for gene set enrichment analysis, and 20,000 permutations were used (Fang et al., 2019). Additionally, we performed gene set variation analysis (GSVA) between the ISL group and ISH group using the GSVA package in R language.

Constructed the Immune Score

To better measure the immune infiltration pattern and immune pathways of ccRCC, we constructed an immune score model using different immune infiltration and immune function groups. The construction process of the immune score was as follows:

First, all the samples were divided into two groups according to the activity, enrichment level, and function of immune infiltration cells. The differentially expressed genes (DEGs) were identified from the immune high group and immune low group with $|\log2\text{FoldChange}| > 1$ and false discovery rate (FDR) < 0.05 using the limma package. Next, we used the univariate Cox regression model to analyze the prognosis of DEGs, with $p < 0.01$ as the standard. We then extracted the genes with significant prognostic significance for principal component analysis (PCA) and extracted principal component 1 as the signature score.

[1] https://portal.gdc.cancer.gov/

Subsequently, all the patients were randomly assigned to a training set (1/2 for all patients) and a test set (1/2 for all patients). We used a similar method to define the immune score (IS) (Sotiriou et al., 2006; Zeng et al., 2019; Zhang et al., 2020).

$$\text{Immune Score} = \Sigma \text{PC1}_i - \Sigma \text{PC1}_j$$

where i is the expression of DEGs whose Cox coefficient is positive, and j is the expression of DEGs whose Cox coefficient is negative.

Predicting the Response to Immunotherapy

The immunophenoscore (IPS) is a quantitative score for tumor immunogenicity and is divided into 0–10 points. The IPS predicts the patient's response to ICI treatment, and the IPS value is positively correlated with tumor immunogenicity (Charoentong et al., 2017). The IPS data were downloaded from The Cancer Immunome Atlas[2].

Statistical Analysis

R language software (Version 4.0.1) was used for statistical analysis. The Wilcox *T*-test was used to compare variables between groups. Univariate Cox regression analysis was used to assess the relationship between the total survival time and expression value of DEGs from the ccRCC cohort. With a p-value < 0.01 as the screening criteria, the prognostic value of this gene was considered statistically significant. The predictive accuracy of the immune score model was assessed by time-dependent receiver operating characteristic (ROC) curves using the survival ROC package. A p-value < 0.05 was considered statistically significant if no specific explanation was available.

RESULTS

Landscape of Immune Cell Infiltration in Clear Cell Renal Cell Carcinoma

The 530 ccRCC samples in the TCGA database were scored by ssGSEA to quantify the activity, enrichment level and function of immune cells in each sample, and then they were divided into two groups using hierarchical cluster analysis (**Figure 1A** and **Supplementary Figure 1A**). Next, we used ESTIMATE to evaluate the level of immune cell infiltration, tumor purity, and matrix content (stromal score) of each ccRCC sample and defined the two clusters as Immunity High (Immunity_H) and Immunity Low (Immunity_L) (**Figure 1A**). We found that the stromal score and immune cell infiltration were significantly higher in the Immunity_H group than in the Immunity_L group, and tumor purity was significantly lower in the Immunity_H group group than in the Immunity_L group. To further investigate the reasons for the differences in immune activity between the different groups, we analyzed the gene expression changes between the Immunity_H and Immunity_L cohorts. We obtained a total of 437 upregulated genes and 77 downregulated genes in the Immunity_H cohort using $|\log2FC| > 1$ and FDR < 0.05 as the criteria (**Figure 1B**). To further obtain DEGs related to prognosis, 514 DEGs were subjected to univariate Cox regression analysis. The genes were reserved for subsequent unsupervised cluster analysis with a p-value < 0.01. According to the screening criteria, 182 DEGs related to prognosis were obtained (**Supplementary File 1**), and the top 30 are shown in **Figure 1C**. To specifically investigate the role of these candidate DEGs in different immune subgroups, we divided the ccRCC samples into different subgroups according to the expression similarity of these related genes using the ConsensusClusterPlus package in R language (**Supplementary Figures 1B–F**). A k value of 2 proved to be the most suitable choice for dividing the ccRCC patient cohort into two clusters—namely, Cluster 1 and Cluster 2 (**Supplementary File 2**). Survival analysis showed that the two subtypes had obvious clinical significance, and the prognosis of Cluster 2 was significantly worse than that of Cluster 1 (**Figure 1D**). Therefore, we believed that these 182 DEGs could be used to assess the immune status of each patient with ccRCC and to predict the prognosis of the patients.

Generation of Immune-Related Gene Signatures and Functional Annotation

We performed PCA on the gene expression matrix of 530 ccRCC samples, extracted principal component 1 of 182 DEGs, and constructed the immune score (IS). Subsequently, all patients were randomly assigned to a training set (1/2 for all patients) and a testing set (1/2 for all patients). According to the IS, the samples were defined as the immune score low (ISL) group and immune score high (ISH) group in the training set, testing set, and total set. In the training set, compared with the ISH group, the overall survival of the ISL group was significantly reduced (**Figure 2A**). For overall survival (OS) prediction, the 3-, 5-, and 7-year AUCs of the ROC curve were 0.64, 0.62, and 0.67, respectively, which were higher than 0.6 and had good survival prediction ability (**Figure 2B**). The survRM2 package was used to calculate the restricted mean survival time (RMS time) of ccRCC patients during the 9-year follow-up. The RMS time is simply the overall average of the event-free survival time during the initial period of follow-up. This period can be evaluated by calculating the area under the KM curve. The RMS time in the ISH group was 6.08 years, and that in the ISL group was 5.21 years, a finding that also confirmed a better prognosis in the high group (**Figure 2C**). The predictive ability of the immune score was further verified in the testing set and total set.

According to the immune score constructed above, each patient in the test set and total dataset was divided into the ISL group and ISH group. Survival analysis showed that patients with high immune scores had longer OS in the testing set (**Figure 2F**). The 3-, 5-, and 7-year AUCs of the ROC curve were 0.6, 0.61, and 0.67, respectively (**Figure 2G**). The RMS time in the ISH group was 6.61 years, and that in the ISL group was 5.03 years (**Figure 2H**).

Additionally, the prognosis of the ISL group in the total dataset was significantly worse than that of the ISH group (**Figure 3A**). The 3-, 5-, and 7-year AUCs of the ROC curve

[2]https://tcia.at/

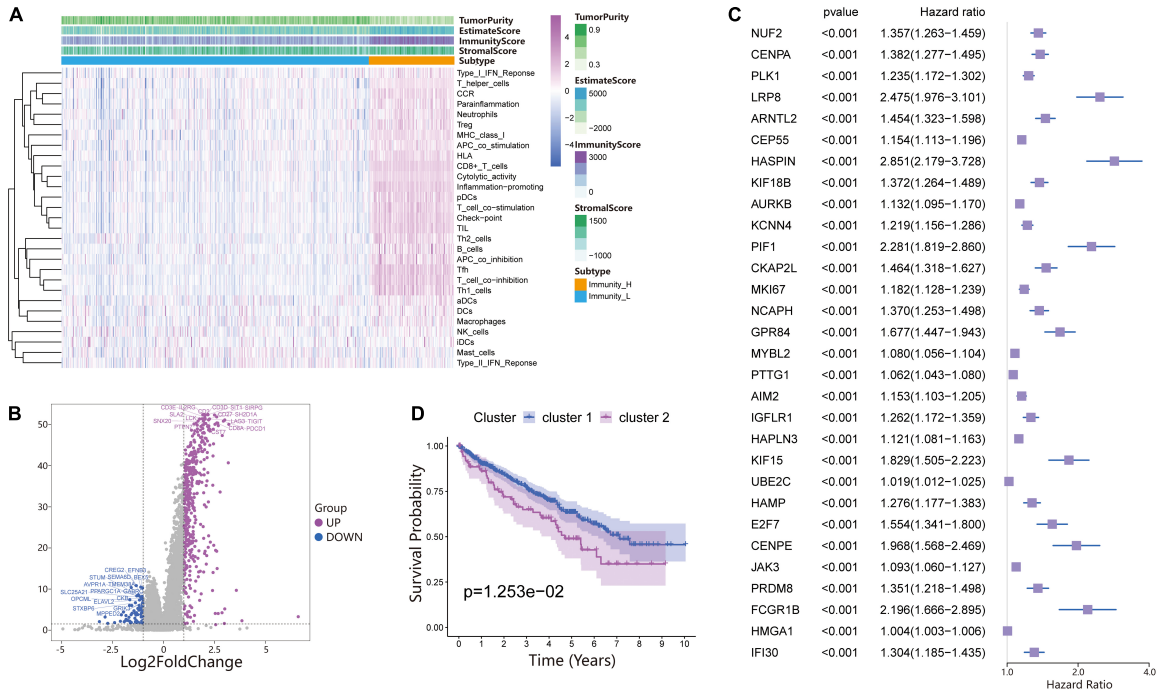

FIGURE 1 | Investigation of the immune infiltration-dependent expression change in clear cell renal cell carcinoma (ccRCC). **(A)** Twenty-nine immune-related gene sets were enriched in ccRCC. These genes comprised immune cells and immune processes. The tumor purity, estimates, immunity scores, and stromal scores are also shown in the heatmap. Immunity High: Immunity_H, Immunity Low: Immunity_L. **(B)** Volcano plot of 514 genes differentially expressed between Immunity_L and Immunity_H. Purple dots and blue dots represent upregulated and downregulated genes, respectively. The screening criteria were | log2FC| > 1.0 and *p*-value < 0.05. **(C)** Univariate Cox regression analysis was used to screen genes significantly associated with prognosis with a *p*-value < 0.01. The top 30 genes are shown in the forest map. **(D)** Survival analysis of Cluster 1 and Cluster 2. In Cluster 1 and Cluster 2, the Kaplan–Meier curve with a log-rank *p*-value of 0.013 showed significant survival differences.

were 0.62, 0.61, and 0.67, respectively (**Figure 3B**). The RMS time in the ISH group was 6.42 years and that in the ISL group was 5.42 years (**Figure 3C**).

The Immune Score and Response of Patients to ICI Treatment

Because of the lack of immunotherapy response data matching patients in the TCGA database, we used the IPS value to replace the patient's immunotherapy response. We extracted two IPS values (IPS-PD-1/PD-L1/PD-L2_pos and IPS-CTLA-4_pos) from the TCIA database to measure the response of ccRCC patients to anti-PD-1/PD-L1 and anti-CTLA4 treatment alternatives. The ISL group had a higher relative probability of responding to anti-PD-1/PD-L1 and anti-CTLA4 treatment in the training set, testing set, and total set (**Figures 2D,E,I,J**, **3D,E**). These results indicated that patients with low immune scores were more likely to benefit from immunotherapy.

Functional Annotation and Pathway Enrichment of the Immune Score

The above results proved the accuracy of the immune score model. Therefore, we used the total set for subsequent analysis. To further explore the biological behaviors among different immune groups, we performed GSVA enrichment analysis for KEGG pathway analysis in the total set. The ISL group was markedly enriched in immune-related pathways, such as natural killer cell-mediated cytotoxicity, the T-cell receptor signaling pathway, the B-cell receptor signaling pathway, and primary immunodeficiency (**Figure 3F**). The enrichment pathways in the ISH group were mainly concentrated in the TGF beta signaling pathway, PPAR signaling pathway, and WNT signaling pathway (**Figure 3F**). Similarly, we used GSEA to perform GO analysis to reveal specific biological processes related to immunity. The biological processes in the ISL group were mainly related to the T-cell receptor signaling pathway, B-cell-mediated immunity, positive regulation of the immune effector process, leukocyte-mediated immunity, and adaptive immune response (**Figure 4A**). Therefore, we believed that the constructed immune score could determine the immune status of different groups and predict the prognosis. Interestingly, we found that the immune status was active in the ISL group, but the prognosis of patients was worse in the ISL group. From the above, we hypothesized that although the immune state was active in the ISL group, its function might be inhibited.

Immune Cell Infiltration in Clear Cell Renal Cell Carcinoma

To identify the infiltration status of immune cells in different groups, CIBERSORT was used to process the data and select

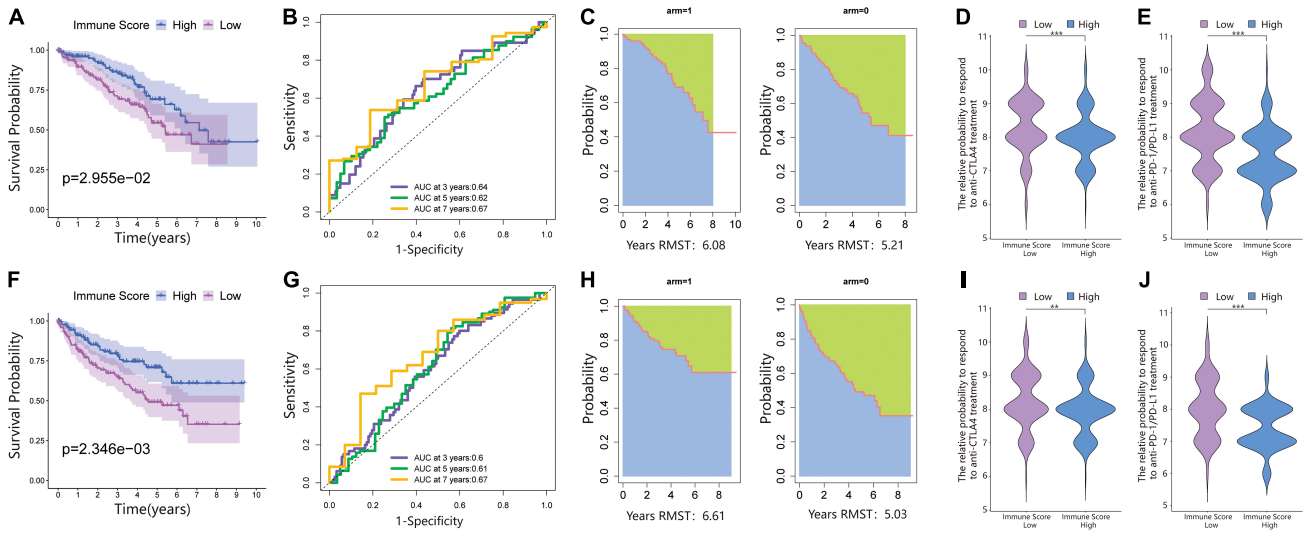

FIGURE 2 | An immune score was constructed in the training set and verified in the validation set. **(A)** Survival analysis of the ISL group and ISH group in the training set. In these two groups, the Kaplan–Meier curve with a log-rank *p*-value of 0.030 showed significant survival differences. **(B)** Time-dependent receiver operating characteristic (ROC) curve analysis of the immune score in the training set. The 3-, 5-, and 7-year area under curves (AUCs) in all samples were 0.64, 0.62, and 0.67, respectively. **(C)** The restricted mean survival (RMS) curve for the immune scores was plotted in the training set. In the ISL and ISH groups, the RSM times were 6.08 and 5.21, respectively. The blue part represents the RMS time, and the green part represents the restricted mean time lost (RMTL). **(D,E)** The relative probabilities of anti-cytotoxic T lymphocyte-associated protein 4 (CTLA4) and anti-programmed cell death protein 1 (PD-1)/programmed death-ligand 1 (PD-L1) treatment between the immune score low (ISL) and ISH groups in the training set. **(F)** Survival analysis of the ISL group and ISH group in the testing set. In these two groups, the Kaplan–Meier curve with a log-rank *p*-value of 0.002 showed significant survival differences. **(G)** Time-dependent ROC curve analysis of the immune score in the testing set. The 3-, 5-, and 7-year AUCs in all samples were 0.60, 0.61, and 0.67, respectively. **(H)** The RMS curve for immune scores was plotted in the testing set. In the ISL and ISH groups, the RSM times were 6.61 and 5.03, respectively. The blue part represents the RMS time, and the green part represents the restricted mean time lost (RMSL). **(I,J)** The relative probabilities of anti-CTLA4 and anti-PD-1/PD-L1 treatment between the ISL and ISH groups in the testing set.

samples with *p*-values less than 0.05. The immune infiltration landscapes of the ISL group (n = 253) and ISH group (n = 166) are shown in **Supplementary Figure 2A**, and the correlations of immune cells are shown in **Figure 5O** and **Supplementary File 3**. Different immune cells were weakly correlated or moderately correlated in tumor tissues in both subgroups. The interaction between immune cells was higher in the lower group than in the higher group. The highest positive correlations were found with $CD8^+$ T cells and gamma delta T cells, follicular helper T cells, and activated NK cells in the ISL group. The highest negative correlations were found with $CD8^+$ T cells and resting memory $CD4^+$ T cells, and M2 macrophages in ISL. In the ISH group, only follicular helper T cells had a higher positive correlation. Similarly, resting memory CD4 T cells and M2 macrophages had a negative correlation with $CD8^+$ T cells. In the ISL group, the degree of infiltration of $CD8^+$ T cells, gamma delta T cells, regulatory T cells (Tregs), and follicular helper T cells were significantly higher than that in the ISH group ($p < 0.05$) (**Figure 5A**). Likewise, the degree of infiltration of resting memory $CD4^+$ T cells, activated dendritic cells, M2 macrophages, and monocytes was higher in the ISH group. To accurately distinguish the status of $CD8^+$ T cells, we used xCell to specifically quantify their classification (**Supplementary File 4**; Aran et al., 2017). The infiltration degree of $CD8^+$ central memory T cells (Tcm) and $CD8^+$ effective memory T cells (Tem) in the ISL group was higher than that in the ISH group (**Figure 5B**). Tem had a rapid effector function and easily differentiated into effector T cells, which secreted a large amount of IFN and was highly cytotoxic. Tcm also differentiated into effector T cells, but the differentiation speed was slower than that of Tem. At the same time, analysis of HLA expression in the two groups also confirmed the difference in the immune infiltration status (**Supplementary Figure 2B**). Additionally, the TIME correlation scores of the two groups showed significant differences (**Figures 4F–I**). This finding was consistent with our previous results that the infiltration and activation of $CD8^+$ T cells in the ISL group were higher than those in the ISH group. Many $CD8^+$ memory T cells in the low immune group were also potential targets for immunotherapy.

Factors That Regulate the Recruitment and Activation of $CD8^+$ T Cells

The above results indicated that the degree of infiltration of $CD8^+$ T cells in the ISL group was higher than that in the ISH group, but the degree of activation was lower than that in the ISH group. By comparing the chemokines of $CD8^+$ T cells, we found that the expression levels of *CXCL9/10/11/16* in the ISL group were significantly higher than those in the ISH group ($p < 0.001$) (**Figures 4B–E**). These results indicated that other components of the tumor microenvironment in the ISL group secreted these chemokines to recruit more $CD8^+$ T

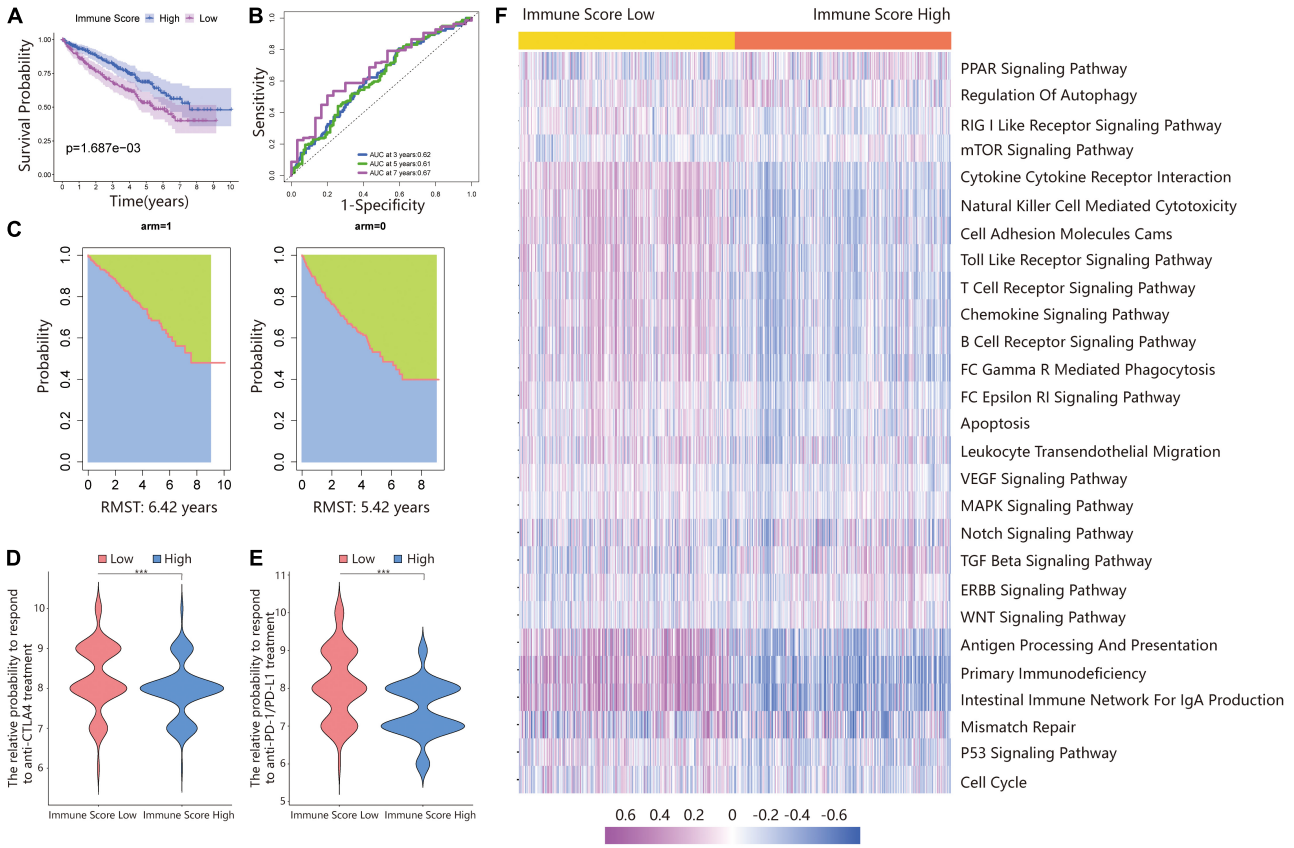

FIGURE 3 | Validating the immune score in the total dataset. **(A)** Survival analysis of the ISL group and ISH group in the total set. In these two groups, the Kaplan–Meier curve with a log-rank *p*-value of 0.002 showed significant survival differences. **(B)** Time-dependent ROC curve analysis of the immune score in all samples. The 3-, 5-, and 7-year AUCs in all samples were 0.62, 0.61, and 0.67, respectively. **(C)** The RMS curve for the immune scores was plotted for all ccRCC samples. In the ISL and ISH groups, the RSM times were 6.42 and 5.42, respectively. The blue part represents the RMS time, and the green part represents the restricted mean time lost (RMSL). **(D,E)** Relative probabilities of anti-CTLA4 and anti-PD-1/PD-L1 treatment between the ISL and ISH groups in the total set. **(F)** Gene set variation analysis (GSVA) enrichment analysis of the activation states of biological pathways in distinct immune score groups. These biological processes are shown in the heatmap. Purple represents the activated pathway, and blue represents the inhibited pathway.

cells into the tumor tissue. At the same time, we explored the expression of inhibitory receptors and ligands in $CD8^+$ T cells. In the ISL group, the inhibitory receptors of $CD8^+$ T cells, such as *CTLA4*, *PD-1*, *LAG3*, *TIM-3*, *BTLA*, and *TIGIT*, were significantly increased compared with those in the ISH group ($p < 0.001$) (**Figures 5C–H**). In addition to *NECTIN2* and *PVR*, the inhibitory ligands *PD-L1*, *PD-L2*, *TNFSF14*, and *LGALS9* of $CD8^+$ T cells were also significantly increased in the ISL group ($p < 0.01$) (**Figures 5I–N**). From the above results, although the infiltration degree of $CD8^+$ T cells increased in the ISL group, their functions were significantly inhibited. This finding might explain why the prognosis of the ISL group was worse than that of the ISH group.

Comparisons of Somatic Mutations Under Different Immune Score Groups

The waterfall map showed the highly mutated genes and their mutation classifications in the ISL (n = 162) group and ISH group (n = 170) (**Figures 6A,B**). In the ISL group, 139 patients had somatic mutations altered, accounting for 85.8%. In the ISH group, 142 patients had somatic mutations, accounting for 83.53%. In the ISL group, the top five genes with mutation frequencies were *VHL*, *PBRM1*, *SETD2*, *BAP1*, and *TTN*. In the ISH group, the top five genes with mutation frequencies were *PBRM1*, *VHL*, *TTN*, *SETD2*, and *MTOR*. The most common types of mutations were missense mutations in both the ISL and ISH groups (**Supplementary Figures 3A,B**). In the ISL and ISH groups, the median value of variants was 42 and 40, respectively, with no significant difference. Single nucleotide polymorphisms (SNPs) were the most common type of variation compared with deletions (DELs) and insertions (INSs). Additionally, C > T had the highest incidence among the six variation types in both groups. Interestingly, *VHL* and *PBRM1* both had a higher mutation frequency in ccRCC. However, no significant difference was found after comparing the mutation sites in the two cohorts (**Supplementary Figures 3C,F**). This finding indicated that they might have a lower effect on the infiltration of immune cells in tumor tissues and were more involved in tumorigenesis. At the same time, we used

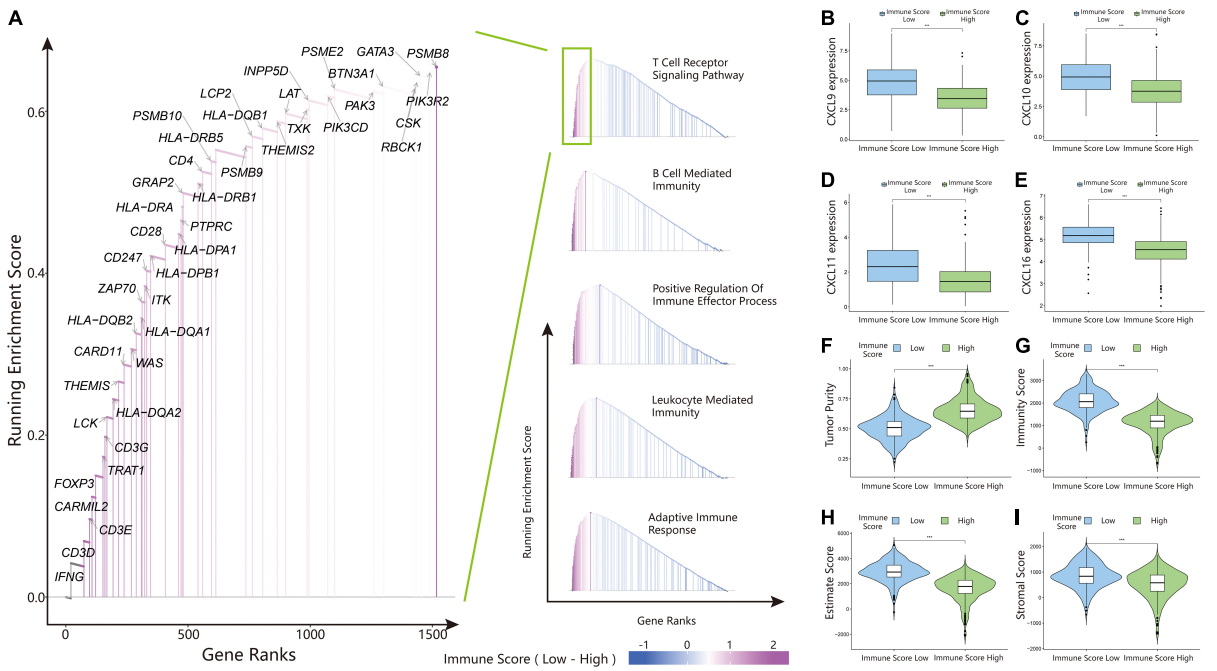

FIGURE 4 | Gene set enrichment analysis (GSEA), chemokine expression, and estimateScore results in the ISL and ISH groups. **(A)** Gene ontology (GO) enrichment analysis of the activation states of immune-related pathways in distinct immune score groups. **(B–E)** Expression of CXCL9/10/11/16 between the ISL and ISH groups. The upper and lower ends of the box indicate the interquartile range of values. The line in the box indicates the median value, and the black dot indicates the outlier. The asterisk indicates the statistical *p*-value (*** <0.001). **(F–I)** Violin plot of the estimateScore between the ISL and ISH groups, including the tumor purity **(F)**, immunity score **(G)**, estimate score **(H)** and stromal score **(I)**. The asterisk indicates the statistical *p*-value (*** <0.001).

the maftools package to obtain drug-gene interactions and druggability information. **Supplementary Figures 3D,E** show the potential gene categories for drug therapy and the top five genes involved in them. Subsequently, we investigated co-occurring and exclusive mutations in the top 20 most frequently mutated genes (**Figure 6C**). In the two cohorts, *PBRM1-SETD2* and *PBRM1-LRP2* showed significant co-occurrence. This finding indicated that they might have redundant effects in the same pathway, and they had selective advantages between them that could retain multiple mutant copies. Additionally, some of the genes had different mutation frequencies in the two groups. Fisher's test was used to detect the differentially expressed genes with a *p*-value less than 0.05 (**Figure 6D**). We further analyzed the effect of these genes with higher mutation frequency on the survival prognosis in different cohorts and all sample cohorts. Except for *BAP1*, mutations in other genes had no significant effect on the prognosis in different cohorts (**Figure 6E**) or all sample cohorts (**Figures 6F–H** and **Supplementary Figures 2C–V**).

BRCA1-Associated Protein 1 Mutation Pattern in the Immune Score Cohort of Clear Cell Renal Cell Carcinoma

BRCA1-associated protein 1 (BAP1) is a tumor suppressor that regulates multiple processes, such as cell cycle control, programmed cell death, DNA damage repair, chromatin modification, and the immune response. In the ISL group, the mutation frequency of *BAP1* was 12.96% higher than that of the ISH group (7.06%) (**Figure 7A**). Additionally, by analyzing the infiltration of immune cells in different immune score cohorts and whole sample groups, we found that *BAP1* mutation might regulate the immune response in tumor tissues by affecting Treg cells (**Figure 7B**). At the same time, we used GSEA to analyze the biological behavior difference between the *BAP1* mutant and *BAP1* wild type. The *BAP1* mutation was mainly enriched in the CTLA4 pathway, T helper cell lineage commitment, interleukin 10 signaling and regulation of lymphocyte apoptotic process, while wild-type *BAP1* was mainly enriched in ligand-activated transcription factor activity, maintenance of synapse structure, pathway regulating Hippo signaling and transforming growth factor β receptor binding (**Figure 7C**). Additionally, the expression level of *BAP1* in the ISL group was significantly lower than that in the ISH group ($p < 0.01$) (**Figure 7D**). Furthermore, the prognosis of patients with high *BAP1* expression was similar to that of patients with low expression (**Figure 7E**). These results indicated that the *BAP1* mutation could regulate the immune response in tumor tissues.

DISCUSSION

With the increased use of immunotherapy, many studies have investigated potential immunotherapy markers. Presently, the choice of immunotherapy is mainly based on the level of expression of immune checkpoints, leading to some patients

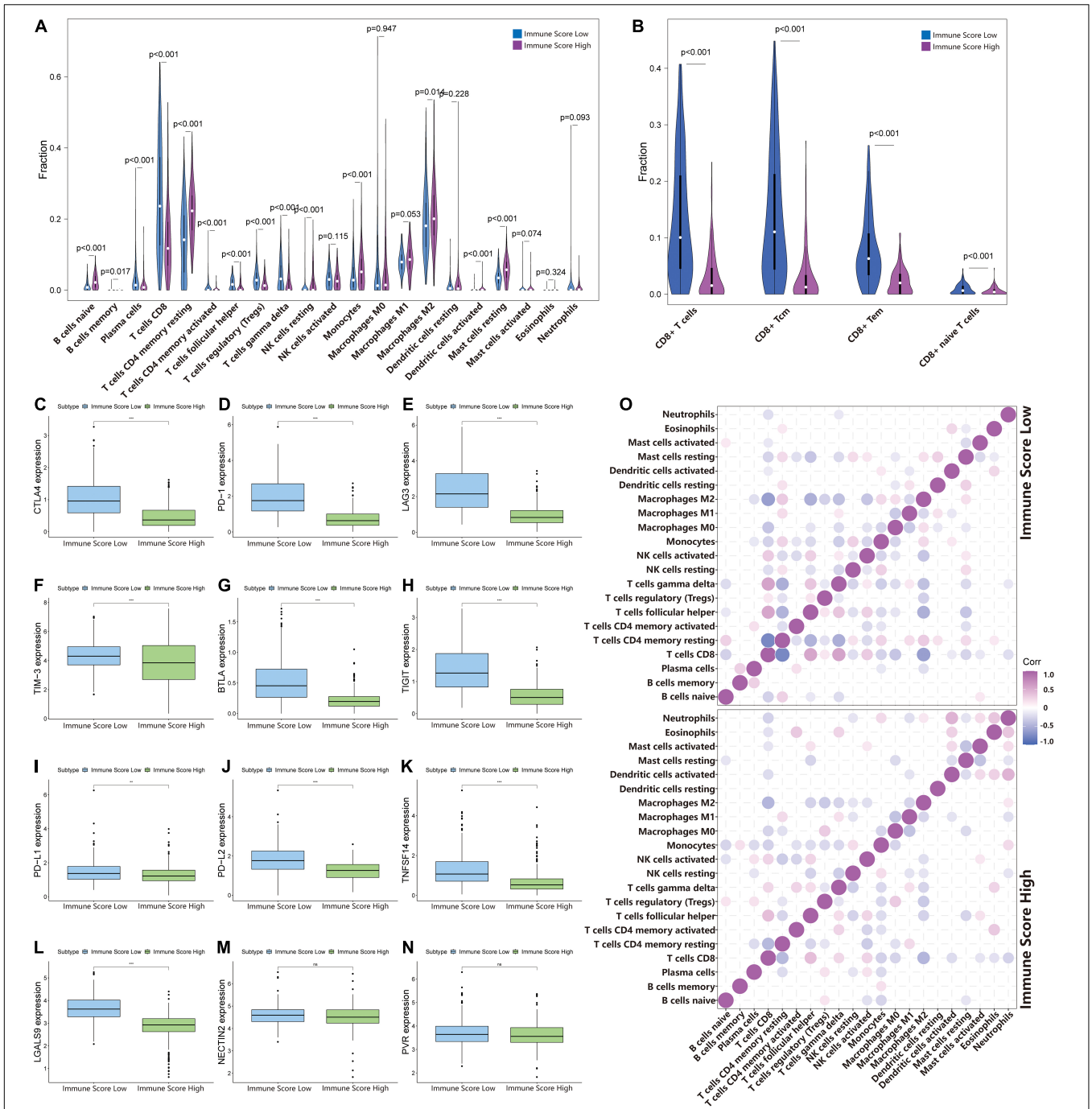

FIGURE 5 | Changes in immune cell infiltration in different immune score groups. **(A,B)** The horizontal axis and vertical axis represent tumor infiltrating immune cells and relative percentages, respectively. Blue and purple represent the ISL group and ISH group, respectively. The data were evaluated using Wilcox tests. **(C–N)** The expression of inhibitory receptors and inhibitory ligands of $CD8^+$ T cells between the ISL group and ISH group. The upper and lower ends of the box indicate the interquartile range of values. The line in the box indicates the median value, and the black dot indicates the outlier. Asterisks indicate statistical *p*-values (**<0.01, ***<0.001). **(O)** The relationship between the abundance ratios of different tumor immune infiltrating cells. The dot indicates that the *p*-value is less than 0.05, and the area is negatively correlated with the *p*-value. Purple indicates a positive correlation, and blue indicates a negative correlation.

not benefiting from immunotherapy. Thus, in a complex tumor environment, it is difficult for drugs to achieve a perfect therapeutic effect based only on the immune checkpoint. Our study aimed to screen and identify genes related to immune infiltration and tumor mutation in the tumor microenvironment and to accurately identify not only patients but also drugs suitable for immunotherapy. We propose new research ideas concerning immunotherapy for other tumors.

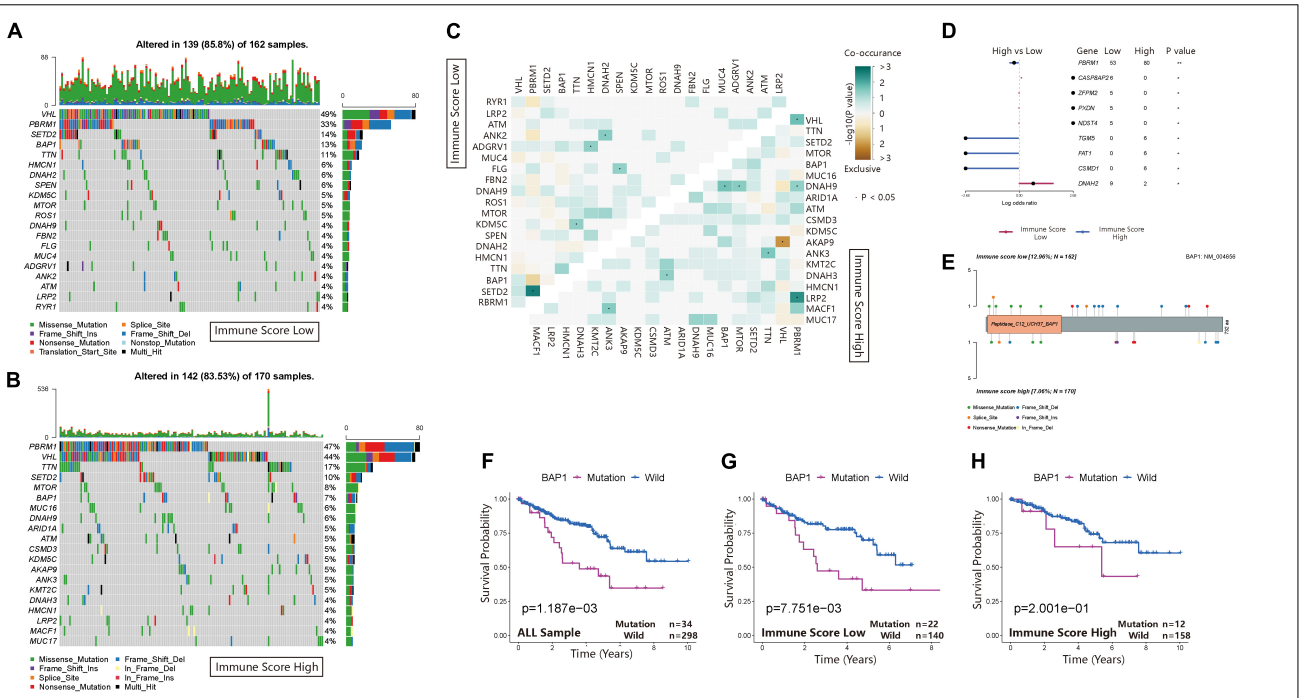

FIGURE 6 | Landscape of somatic mutations in the ISL and ISH groups. **(A,B)** Waterfall plot of tumor somatic mutations established by those with low immune scores (A) and high immune scores **(B)**. Each column represents an individual patient. The bar plot above the figure shows the tumor mutation burden (TMB), and the number on the right represents the mutation frequency of each gene. **(C)** The heat map shows the mutual co-occurring and exclusive mutations of the top 20 frequently mutated genes. The color or symbol of each cell represents the statistical significance of the exclusivity or co-occurrence of each pair of genes, respectively. Green represents mutual co-occurrence, and brown represents exclusive mutation. Asterisks indicate statistical *p*-values (* <0.05). **(D)** Forest plot of statistically significant mutant genes between the groups. Asterisks indicate statistical *p*-values (*<0.05, **<0.01) **(E)** The lollipop plot illustrates the differential distribution of variants for BRCA1-associated protein 1 (BAP1). **(F–H)** Kaplan–Meier curves show the independent relevance between the overall survival time and BAP1 mutation in the ISL group, ISH group and all cohorts.

In the present study, we first used ssGSEA to quantify the activity, enrichment level, function, and pathway of immune cells in each sample. Next, through hierarchical cluster analysis, the patients were divided into an immunity high group and an immunity low group. We identified differentially expressed genes by comparing the two groups. We believed that these DEGs were immune-related DEGs. Subsequently, univariate Cox regression analysis was used to further screen the prognosis-related DEGs. Based on these genes, the patients were divided into two groups (Cluster 1 and Cluster 2) through unsupervised cluster analysis. The prognosis of Cluster 2 was worse than that of Cluster 1. Therefore, we speculated that the prognosis-related DEGs could be used as genes to construct immune score models. After that, we used principal component analysis to extract principal component 1 and calculated the immune score according to relevant literature (Sotiriou et al., 2006; Zeng et al., 2019; Zhang et al., 2020). All the patients were randomly assigned to a training set (1/2 for all patients) and a test set (1/2 for all patients). We used the training set to construct the immune score model and verified it in the validation set and total set. The patients were divided into ISL and ISH groups according to the immune score. The 3-, 5-, and 7-year AUCs were all greater than 0.6, and the RSM time in the ISH group was longer than that in the ISL group, proving the sensitivity and predictability of the immune score model. Thus, the immune score model accurately predicted the prognosis of patients. Therefore, we used the total set for subsequent analysis. Using GSEA and GSVA, differences were found in immune-related pathways between the groups. By comparing HLA-related genes and related scores in the immune microenvironment, we also confirmed that the immune activity status of the ISL group was higher than that of the ISH group. Interestingly, the ISL group, which had a poor prognosis, had a higher level of immune activity. Hence, we speculated whether the function of immune cells was inhibited in the ISL group. We used CIBERSORT and xCell to further quantify the types of infiltrating immune cells in each sample. $CD8^+$ T cells are the main immune killer cells in tumor tissues. Therefore, we evaluated the status of $CD8^+$ T cells in different immune score groups. Because of the increased secretion of *CXCL9/10/11/16* chemokines, we believed that the infiltration of $CD8^+$ T cells in the ISL group was significantly higher than that in the ISH group. At the same time, the inhibitory ligands and inhibitory receptors of $CD8^+$ T cells in the ISL group were also significantly increased compared with those in the ISH group. Therefore, we hypothesized that despite the higher immune activity and infiltration of $CD8^+$ T cells in the ISL group, smart tumor cells would express their inhibitory ligands to prevent its function.

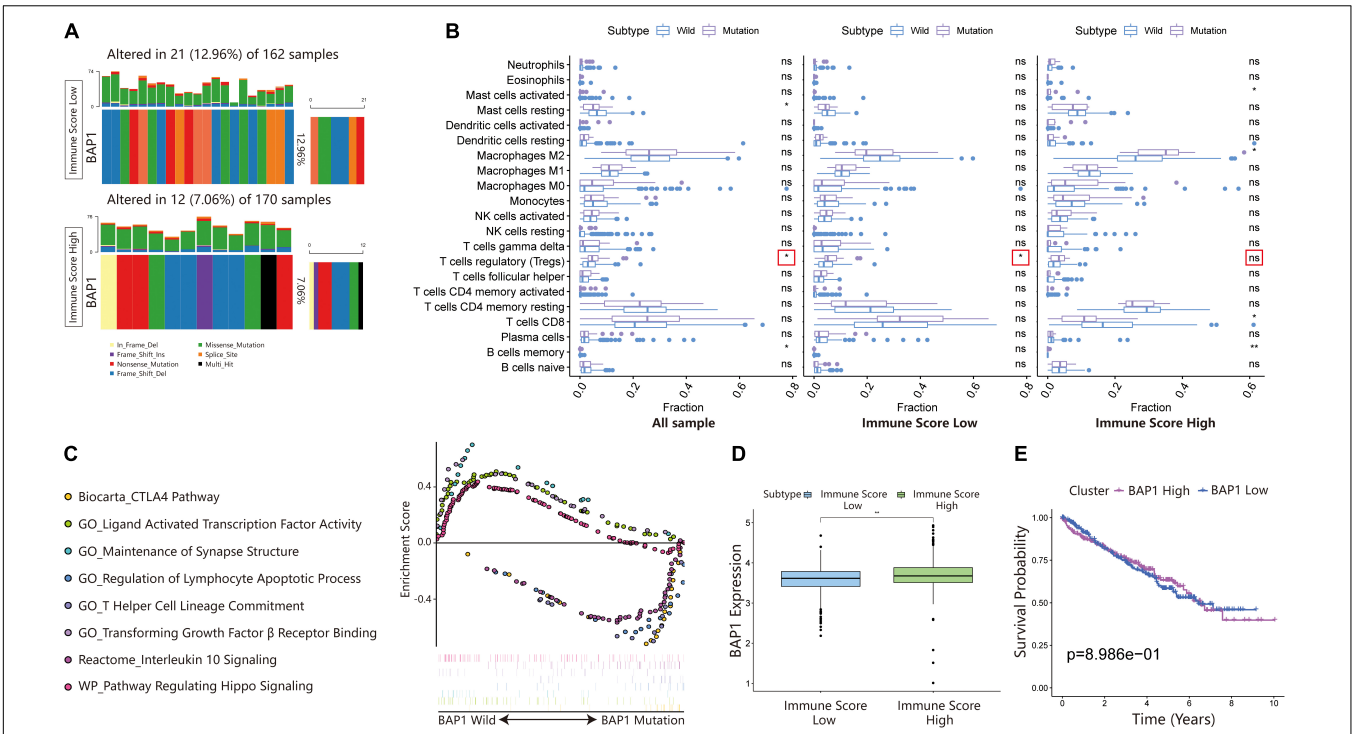

FIGURE 7 | Changes in BAP1 mutations in ISL and ISH groups. **(A)** Mutation frequency of BAP1 in the ISL group and ISH group. Each column represents an individual patient. The bar plot above the figure shows the TMB, and the number on the right represents the mutation frequency of each gene. **(B)** Effect of BAP1 mutation on tumor immune infiltrating cells in the ISL group, ISH group, and whole samples (*p*-value, * < 0.05, ** < 0.01, ns > 0.05). **(C)** Gene set enrichment analysis comparing the BAP1 phenotype between the mutation group and wild-type group with FDR < 0.25. **(D)** The expression of BAP1 between the ISL group and ISH group (*p*-value, ** < 0.01). **(E)** The survival curve shows that the expression level of BAP1 is not related to the prognosis of ccRCC patients.

This finding may also explain the poor prognosis in the ISL group. In the low group, the massive infiltration of Tem and Tcm cells also serve as potential targets for subsequent immunotherapy. Although the model has certain deficiencies in the accuracy of the prognosis and effect of immunotherapy, we recognize that the reason may be the insufficient number of modeling samples. If conditions permit continued expansion of the sample size, the accuracy of the model may be further improved. Additionally, if the sequencing data before and after immunotherapy can be further collected, further optimization of the model will be valuable.

Generally, two indicators are related to tumor immunotherapy: the degree of immune cell infiltration and tumor mutation burden. Therefore, to accurately select patients suitable for immunotherapy, both factors must be considered. By comparing the mutant landscapes of the ISL group and ISH group, we found that the mutation frequency of the two groups was not significantly different. Both *VHL* and *PBRM1* had very high mutation rates in both groups. This finding confirmed that *VHL* and *PBRM1* played a key role in the pathogenesis of ccRCC (Gu et al., 2017; Hsieh et al., 2017; Zhang J. et al., 2018; Cai et al., 2019). However, the genes with a high mutation frequency did not significantly affect the prognosis compared with all the other genes except *BAP1*, whether in the ISL group, ISH group or whole sample group. *BAP1* regulates DNA damage repair pathways (Nishikawa et al., 2009; Zhao et al., 2017), the cell cycle, and cell proliferation (Yu et al., 2010; Okino et al., 2015), chromatin (Scheuermann et al., 2010), and cell death pathways (Sime et al., 2018; Zhang Y. et al., 2018). Additionally, *BAP1* is implicated in immune regulation (Gezgin et al., 2017; Figueiredo et al., 2020). However, the mechanism of IMMUNE regulation by *BAP1* remains unclear. The mutation frequency of *BAP1* in the ISL group was higher than that in the ISH group. The effects of *BAP1* mutation on infiltrating immune cells were compared in the ISL group, ISH group, and full sample group. *BAP1* mutation increased the infiltration degree of Treg cells. The *BAP1* mutation was mainly enriched in the CTLA4 pathway, T helper cell lineage commitment, interleukin 10 signaling, and regulation of the lymphocyte apoptotic process pathway by GSEA. These results indicated that *BAP1* mutation can inhibit the activity of immune cells in tumor tissues by regulating Treg cells. Therefore, we believe that combining the immune score and *BAP1* mutation can better screen patients suitable for immunotherapy. Additionally, inhibitors of Treg cells can be combined to achieve better therapeutic effects.

CONCLUSION

Our study predicted the prognosis of renal cancer patients by constructing a new immune score combined with the

BAP1 mutation. At the same time, it provides a new way to identify patients suitable for immunotherapy and explore effective immunotherapy strategies in ccRCC patients.

DATA AVAILABILITY STATEMENT

The datasets presented in this study can be found in online repositories. The names of the repository/repositories and accession number(s) can be found in the article/ **Supplementary Material**.

AUTHOR CONTRIBUTIONS

HH and KL designed the study and analyzed the data. ZG and JC wrote the manuscript and performed the data analysis. YT and SY critically revised the draft for important intellectual content. JZ and QW participated in the picture drawing and processing. SP and JC performed the statistical analysis. ZX was mainly responsible for article modification and technical support. All authors read and approved the final manuscript.

FUNDING

This work was supported by the National Natural Science Foundation of China (Nos. 81672550, 81974395, and 82173036), Guangdong Basic and Applied Basic Research Foundation (No. 2019A1515011437), International Science and Technology Cooperation Project Plan of Guangdong Province (No. 2021A0505030085), Sun Yat-sen University Clinical Research 5010 Program (No. 2019005), Sun Yat-sen Clinical Research Cultivating Program (No. 201702), Guangdong Province Key Laboratory of Malignant Tumor Epigenetics and Gene Regulation (No. 2020B1212060018OF006), and Guangdong Provincial Clinical Research Center for Urological Diseases (2020B1111170006) to HH. KL was supported by the National Natural Science Foundation of China (No. 81702527). This work was also supported by grants from the Guangdong Science and Technology Department.

SUPPLEMENTARY MATERIAL

The Supplementary Material for this article can be found online at: https://www.frontiersin.org/articles/10.3389/fcell.2021.747985/full#supplementary-material

Supplementary Figure 1 | Unsupervised clustering grouping in ccRCC. **(A)** Unsupervised hierarchical clustering algorithm in ccRCC patients. **(B–F)** Unsupervised clustering of 182 DEGs in the ccRCC cohort and consensus matrices for $k = 2$–5.

Supplementary Figure 2 | Immune infiltration status and prognosis of different mutated genes in different immune score groups. **(A)** Immune cell abundance ratios in the two immune scoring cohorts. Each column represents a sample, and each column uses a different color and height to indicate the abundance ratio of immune cells in the sample. **(B)** The RNA expression levels of HLA genes in samples from the ISL group and ISH group (p-value, *** < 0.001). **(C–V)** K-M analysis of genes with higher mutation frequencies in ccRCC samples and different immune score cohorts.

Supplementary Figure 3 | Mutations in different immune score groups and possible drug pathways. **(A,B)** Summary of the mutation information with statistical calculations. The mutation types were classified according to different categories. Among them, missense mutations accounted for the largest proportion, SNPs appeared more frequently than insertions or deletions, and C > T was the most common mutation in SNVs. The top 10 mutated genes in the two cohorts are also displayed. **(C,F)** The lollipop plot illustrates the differential distribution of variants for VHL and PBRM1. **(D,E)** The potential gene categories for drug therapy in the two cohorts and the top five genes involved.

Supplementary File 1 | The univariate Cox regression analysis results of DEGs with the p-value < 0.01.

Supplementary File 2 | The groups of unsupervised cluster analysis.

Supplementary File 3 | The correlations of immune cells in the ISL and ISH groups.

Supplementary File 4 | The quantitative results of immune infiltrating cells in tissues of ccRCC patients used by xCell.

REFERENCES

Ansell, S. M., Lesokhin, A. M., Borrello, I., Halwani, A., Scott, E. C., Gutierrez, M., et al. (2015). PD-1 blockade with nivolumab in relapsed or refractory Hodgkin's lymphoma. *N. Engl. J. Med.* 372, 311–319. doi: 10.1056/NEJMoa1411087

Aran, D., Hu, Z., and Butte, A. J. (2017). xCell: digitally portraying the tissue cellular heterogeneity landscape. *Genome Biol.* 18:220. doi: 10.1186/s13059-017-1349-1

Barbie, D. A., Tamayo, P., Boehm, J. S., Kim, S. Y., Moody, S. E., Dunn, I. F., et al. (2009). Systematic RNA interference reveals that oncogenic KRAS-driven cancers require TBK1. *Nature* 462, 108–112. doi: 10.1038/nature08460

Bray, F., Ferlay, J., Soerjomataram, I., Siegel, R. L., Torre, L. A., and Jemal, A. (2018). Global cancer statistics 2018: GLOBOCAN estimates of incidence and mortality worldwide for 36 cancers in 185 countries. *CA Cancer J. Clin.* 68, 394–424. doi: 10.3322/caac.21492

Cai, W., Su, L., Liao, L., Liu, Z. Z., Langbein, L., Dulaimi, E., et al. (2019). PBRM1 acts as a p53 lysine-acetylation reader to suppress renal tumor growth. *Nat. Commun.* 10:5800. doi: 10.1038/s41467-019-13608-1

Carreno, B. M., Magrini, V., Becker-Hapak, M., Kaabinejadian, S., Hundal, J., Petti, A. A., et al. (2015). Cancer immunotherapy. A dendritic cell vaccine increases the breadth and diversity of melanoma neoantigen-specific T cells. *Science* 348, 803–808. doi: 10.1126/science.aaa3828

Charoentong, P., Finotello, F., Angelova, M., Mayer, C., Efremova, M., Rieder, D., et al. (2017). Pan-cancer immunogenomic analyses reveal genotype-immunophenotype relationships and predictors of response to checkpoint blockade. *Cell Rep.* 18, 248–262. doi: 10.1016/j.celrep.2016.12.019

Chen, D. S., and Mellman, I. (2013). Oncology meets immunology: the cancer-immunity cycle. *Immunity* 39, 1–10. doi: 10.1016/j.immuni.2013.07.012

Chen, D. S., and Mellman, I. (2017). Elements of cancer immunity and the cancer-immune set point. *Nature* 541, 321–330. doi: 10.1038/nature21349

Cloughesy, T. F., Mochizuki, A. Y., Orpilla, J. R., Hugo, W., Lee, A. H., Davidson, T. B., et al. (2019). Neoadjuvant anti-PD-1 immunotherapy promotes a survival benefit with intratumoral and systemic immune responses in recurrent glioblastoma. *Nat. Med.* 25, 477–486. doi: 10.1038/s41591-018-0337-7

Coulie, P. G., van den Eynde, B. J., van der Bruggen, P., and Boon, T. (2014). Tumour antigens recognized by T lymphocytes: at the core of cancer immunotherapy. *Nat. Rev. Cancer* 14, 135–146. doi: 10.1038/nrc3670

Fang, H., Consortium, U.-D., De Wolf, H., Knezevic, B., Burnham, K. L., Osgood, J., et al. (2019). A genetics-led approach defines the drug target landscape of 30 immune-related traits. *Nat. Genet.* 51, 1082–1091. doi: 10.1038/s41588-019-0456-1

Figueiredo, C. R., Kalirai, H., Sacco, J. J., Azevedo, R. A., Duckworth, A., Slupsky, J. R., et al. (2020). Loss of BAP1 expression is associated with an immunosuppressive microenvironment in uveal melanoma, with implications for immunotherapy development. *J. Pathol.* 250, 420–439. doi: 10.1002/path.5384

Finotello, F., and Trajanoski, Z. (2017). New strategies for cancer immunotherapy: targeting regulatory T cells. *Genome Med.* 9:10. doi: 10.1186/s13073-017-0402-8

Fisher, R. I., Rosenberg, S. A., and Fyfe, G. (2000). Long-term survival update for high-dose recombinant interleukin-2 in patients with renal cell carcinoma. *Cancer J. Sci. Am.* 6(Suppl. 1), S55–S57.

Forde, P. M., Chaft, J. E., Smith, K. N., Anagnostou, V., Cottrell, T. R., Hellmann, M. D., et al. (2018). Neoadjuvant PD-1 blockade in resectable lung cancer. *N. Engl. J. Med.* 378, 1976–1986. doi: 10.1056/NEJMoa1716078

Gezgin, G., Dogrusoz, M., van Essen, T. H., Kroes, W. G. M., Luyten, G. P. M., van der Velden, P. A., et al. (2017). Genetic evolution of uveal melanoma guides the development of an inflammatory microenvironment. *Cancer Immunol. Immunother.* 66, 903–912. doi: 10.1007/s00262-017-1991-1

Gu, Y. F., Cohn, S., Christie, A., McKenzie, T., Wolff, N., Do, Q. N., et al. (2017). Modeling renal cell carcinoma in mice: Bap1 and Pbrm1 inactivation drive tumor grade. *Cancer Discov.* 7, 900–917. doi: 10.1158/2159-8290.CD-17-0292

Hsieh, J. J., Purdue, M. P., Signoretti, S., Swanton, C., Albiges, L., Schmidinger, M., et al. (2017). Renal cell carcinoma. *Nat. Rev. Dis. Primers* 3:17009. doi: 10.1038/nrdp.2017.9

Janzen, N. K., Kim, H. L., Figlin, R. A., and Belldegrun, A. S. (2003). Surveillance after radical or partial nephrectomy for localized renal cell carcinoma and management of recurrent disease. *Urol. Clin. North Am.* 30, 843–852. doi: 10.1016/s0094-0143(03)00056-9

Margolin, K. A., Rayner, A. A., Hawkins, M. J., Atkins, M. B., Dutcher, J. P., Fisher, R. I., et al. (1989). Interleukin-2 and lymphokine-activated killer cell therapy of solid tumors: analysis of toxicity and management guidelines. *J. Clin. Oncol.* 7, 486–498. doi: 10.1200/JCO.1989.7.4.486

Newman, A. M., Liu, C. L., Green, M. R., Gentles, A. J., Feng, W., Xu, Y., et al. (2015). Robust enumeration of cell subsets from tissue expression profiles. *Nat. Methods* 12, 453–457. doi: 10.1038/nmeth.3337

Nishikawa, H., Wu, W., Koike, A., Kojima, R., Gomi, H., Fukuda, M., et al. (2009). BRCA1-associated protein 1 interferes with BRCA1/BARD1 RING heterodimer activity. *Cancer Res.* 69, 111–119. doi: 10.1158/0008-5472.CAN-08-3355

Okino, Y., Machida, Y., Frankland-Searby, S., and Machida, Y. J. (2015). BRCA1-associated protein 1 (BAP1) deubiquitinase antagonizes the ubiquitin-mediated activation of FoxK2 target genes. *J. Biol. Chem.* 290, 1580–1591. doi: 10.1074/jbc.M114.609834

Posadas, E. M., Limvorasak, S., Sharma, S., and Figlin, R. A. (2013). Targeting angiogenesis in renal cell carcinoma. *Expert Opin. Pharmacother.* 14, 2221–2236. doi: 10.1517/14656566.2013.832202

Scheuermann, J. C., de Ayala Alonso, A. G., Oktaba, K., Ly-Hartig, N., McGinty, R. K., Fraterman, S., et al. (2010). Histone H2A deubiquitinase activity of the Polycomb repressive complex PR-DUB. *Nature* 465, 243–247. doi: 10.1038/nature08966

Sime, W., Niu, Q., Abassi, Y., Masoumi, K. C., Zarrizi, R., Kohler, J. B., et al. (2018). BAP1 induces cell death via interaction with 14-3-3 in neuroblastoma. *Cell Death Dis.* 9:458. doi: 10.1038/s41419-018-0500-6

Snyder, A., and Chan, T. A. (2015). Immunogenic peptide discovery in cancer genomes. *Curr. Opin. Genet. Dev.* 30, 7–16. doi: 10.1016/j.gde.2014.12.003

Snyder, A., Makarov, V., Merghoub, T., Yuan, J., Zaretsky, J. M., Desrichard, A., et al. (2014). Genetic basis for clinical response to CTLA-4 blockade in melanoma. *N. Engl. J. Med.* 371, 2189–2199. doi: 10.1056/NEJMoa1406498

Sotiriou, C., Wirapati, P., Loi, S., Harris, A., Fox, S., Smeds, J., et al. (2006). Gene expression profiling in breast cancer: understanding the molecular basis of histologic grade to improve prognosis. *J. Natl. Cancer Inst.* 98, 262–272. doi: 10.1093/jnci/djj052

Tanaka, A., and Sakaguchi, S. (2017). Regulatory T cells in cancer immunotherapy. *Cell Res.* 27, 109–118. doi: 10.1038/cr.2016.151

Topalian, S. L., Taube, J. M., Anders, R. A., and Pardoll, D. M. (2016). Mechanism-driven biomarkers to guide immune checkpoint blockade in cancer therapy. *Nat. Rev. Cancer* 16, 275–287. doi: 10.1038/nrc.2016.36

Turajlic, S., Swanton, C., and Boshoff, C. (2018). Kidney cancer: the next decade. *J. Exp. Med.* 215, 2477–2479. doi: 10.1084/jem.20181617

Yu, H., Mashtalir, N., Daou, S., Hammond-Martel, I., Ross, J., Sui, G., et al. (2010). The ubiquitin carboxyl hydrolase BAP1 forms a ternary complex with YY1 and HCF-1 and is a critical regulator of gene expression. *Mol. Cell. Biol.* 30, 5071–5085. doi: 10.1128/MCB.00396-10

Zeng, D., Li, M., Zhou, R., Zhang, J., Sun, H., Shi, M., et al. (2019). Tumor microenvironment characterization in gastric cancer identifies prognostic and immunotherapeutically relevant gene signatures. *Cancer Immunol. Res.* 7, 737–750. doi: 10.1158/2326-6066.CIR-18-0436

Zhang, B., Wu, Q., Li, B., Wang, D., Wang, L., and Zhou, Y. L. (2020). m(6)A regulator-mediated methylation modification patterns and tumor microenvironment infiltration characterization in gastric cancer. *Mol. Cancer* 19:53. doi: 10.1186/s12943-020-01170-0

Zhang, J., Wu, T., Simon, J., Takada, M., Saito, R., Fan, C., et al. (2018). VHL substrate transcription factor ZHX2 as an oncogenic driver in clear cell renal cell carcinoma. *Science* 361, 290–295. doi: 10.1126/science.aap8411

Zhang, Y., Shi, J., Liu, X., Feng, L., Gong, Z., Koppula, P., et al. (2018). BAP1 links metabolic regulation of ferroptosis to tumour suppression. *Nat. Cell Biol.* 20, 1181–1192. doi: 10.1038/s41556-018-0178-0

Zhao, W., Steinfeld, J. B., Liang, F., Chen, X., Maranon, D. G., Jian Ma, C., et al. (2017). BRCA1-BARD1 promotes RAD51-mediated homologous DNA pairing. *Nature* 550, 360–365. doi: 10.1038/nature24060

Conflict of Interest: The authors declare that the research was conducted in the absence of any commercial or financial relationships that could be construed as a potential conflict of interest.

Publisher's Note: All claims expressed in this article are solely those of the authors and do not necessarily represent those of their affiliated organizations, or those of the publisher, the editors and the reviewers. Any product that may be evaluated in this article, or claim that may be made by its manufacturer, is not guaranteed or endorsed by the publisher.

frontiers in Cell and Developmental Biology

REVIEW
published: 16 November 2021
doi: 10.3389/fcell.2021.735107

Collateral Victim or Rescue Worker?—The Role of Histone Methyltransferases in DNA Damage Repair and Their Targeting for Therapeutic Opportunities in Cancer

Lishu He[1,2,3] *and Gwen Lomberk*[1,2,3,4]*

[1] Department of Pharmacology and Toxicology, Medical College of Wisconsin, Milwaukee, WI, United States, [2] Division of Research, Department of Surgery, Medical College of Wisconsin, Milwaukee, WI, United States, [3] Genomic Sciences and Precision Medicine Center, Medical College of Wisconsin, Milwaukee, WI, United States, [4] LaBahn Pancreatic Cancer Program, Medical College of Wisconsin, Milwaukee, WI, United States

OPEN ACCESS

Edited by:
Zhenhua Xu,
Children's National Hospital,
United States

Reviewed by:
Naoko Hattori,
National Cancer Center Research Institute, Japan
Mark Nicholas Cruickshank,
University of Western Australia, Australia

***Correspondence:**
Gwen Lomberk
glomberk@mcw.edu

Specialty section:
This article was submitted to Epigenomics and Epigenetics, a section of the journal Frontiers in Cell and Developmental Biology

Received: *02 July 2021*
Accepted: *01 October 2021*
Published: *16 November 2021*

Citation:
He L and Lomberk G (2021) Collateral Victim or Rescue Worker?—The Role of Histone Methyltransferases in DNA Damage Repair and Their Targeting for Therapeutic Opportunities in Cancer. Front. Cell Dev. Biol. 9:735107. doi: 10.3389/fcell.2021.735107

Disrupted DNA damage signaling greatly threatens cell integrity and plays significant roles in cancer. With recent advances in understanding the human genome and gene regulation in the context of DNA damage, chromatin biology, specifically biology of histone post-translational modifications (PTMs), has emerged as a popular field of study with great promise for cancer therapeutics. Here, we discuss how key histone methylation pathways contribute to DNA damage repair and impact tumorigenesis within this context, as well as the potential for their targeting as part of therapeutic strategies in cancer.

Keywords: cancer epigenetics, chromatin, epigenetic drugs, histone methyltransferases, DNA damage repair (DDR)

INTRODUCTION—THE ACCIDENT SCENE

Since the discovery of DNA by Swiss scientist Friedrich Miescher in 1869, numerous researchers have expanded on his work and contributed to our understanding of how genetic information was encoded, preserved, and stably transmitted across generations by DNA (Ciccia and Elledge, 2010). Now we know that DNA is liable to change, as it is subject to extensive lesion formation due to constant genomic insults from endogenous and exogenous sources such as hydrolysis, oxidation, ionizing radiation, UV radiation, and various chemical agents among others (Friedberg et al., 2006; Hakem, 2008; Chatterjee and Walker, 2017). If not repaired timely and correctly, these lesions may damage genome maintenance machinery, trigger mutagenesis, and threaten cell integrity.

The explosion of the field of DNA damage response (DDR), however, came long after Watson and Crick published their theory of the DNA double helix in the 1950s (Watson and Crick, 1953; Friedberg et al., 2006). Various mechanisms through which DNA damage is resolved on a molecular level have been identified. The most notable discoveries are those by the three pioneers in DNA repair who shared the 2015 Nobel Prize in Chemistry: Tomas Lindahl for establishing the role of DNA glycosylase enzymes in base excision repair (BER) (Krokan and Bjørås, 2013), Paul Modrich for mismatch repair (MMR) (Lahue et al., 1989), and Aziz Sancar for defining the reversal of ultraviolet damage to DNA by nucleotide excision repair (NER) (Petit and Sancar, 1999).

When DNA lesions remain unrepaired, they may accumulate and block DNA replication progression, resulting in double-stranded breaks (DSBs) that are more difficult to repair and far more toxic (Khanna and Jackson, 2001; Jackson and Bartek, 2009). So far, studies have elucidated two umbrella pathways of DSB repair, namely, homologous recombination (HR) and non-homologous end-joining (NHEJ). HR utilizes template DNA and exchanges of equivalent DNA regions between homologous chromosomes to promote high-fidelity DSB repair, preserving genomic stability (Sung and Klein, 2006; Tubbs and Nussenzweig, 2017). NHEJ, on the other hand, is more prone to deletions and insertions as it ligates broken DNA ends without a template (Lieber, 2008; Tubbs and Nussenzweig, 2017). The initial detection of DNA damage and cellular response that triggers cell cycle arrest to allow repair or undergo cell death is coordinated by various DNA damage signaling cascades, contributing to the cells' ability to defend against potential mutagenesis (Hanawalt, 2015). These damage sensing pathways are extensively reviewed in Jackson and Bartek (2009), Ciccia and Elledge (2010), Hanawalt (2015). Together, the DNA damage sensing and DDR pathways are the core molecular machinery responsible for rescuing the cell from deleterious effects of DNA damage and evading pathobiology outcomes, such as cancer.

With recent advances in understanding the human genome and gene regulation in the context of DNA damage, epigenetics has emerged as a rapidly growing field with great promise for therapeutics. Epigenetics refers to the study of reversible, heritable changes in genome function that occur without alterations to the DNA sequence (Russo et al., 1996). Different epigenetic changes, such as DNA methylation and histone post-translational modifications (PTMs) or "marks," regulate gene expression and underlie both healthy and diseased human physiology. Nucleosomes, organized modules of duplexed DNA wrapping around histones, serve as the basic units for chromatin, which is the fundamental packaging structure of all eukaryotic genomes (Li et al., 2007). It can be "closed" or "open," generally associating with transcription repression and activation, respectively (Gillette and Hill, 2015). There is dynamic regulation of chromatin to modify accessibility to DNA during processes such as replication, transcription, DDR, and more (Hanawalt, 2015). Chromatin marks impact DNA accessibility by modulating histone-DNA interactions and serving as docking sites for "reader" proteins, dedicated effectors of those PTMs to achieve their specific transcriptional outcome (Musselman et al., 2012; Gillette and Hill, 2015). In addition to the reader proteins, other proteins involved in altering chromatin status include "writer" proteins, which are enzymes that add PTMs to histones, and "erasers," which remove these marks (Musselman et al., 2012). Furthermore, epigenetic modifications can facilitate responses to DNA damage. Conceptually, during DNA damage, epigenetic marks can occur in a collateral event either as part of the chromatin disruption in the wake of DNA damage or as a flag to identify a genomic region that requires repair. Alternatively, the role of epigenetic marks during DDR processes can be a more active function that mechanistically contributes to rescue the cell from DNA damage. Because of the dynamic functions of histone PTMs and their mediators, they have been increasingly considered as therapeutic targets by the pharmaceutical industry and academic pharmacologists. Here, we discuss how chromatin modifiers and their histone modifications, specifically key histone methylation pathways, contribute to DNA damage repair and impact tumorigenesis within this context, as well as the potential for their targeting as therapeutic strategies in cancer.

LIGHTS AND SIRENS—THE CHROMATIN RESPONSE IN DNA DAMAGE REPAIR

While various players in the DDR pathways have long been studied, there is a rapidly growing understanding that higher-order chromatin also significantly impacts DDR via remodeling and post-translational modification from the moment DNA damage strikes. In other words, the chromatin landscape is not only pivotal to the regulation of epigenetic changes for healthy human physiology, but also significant to our heritable cell machinery for DNA transcription, replication, and repair. To protect against endogenous and exogenous agents from causing deleterious DNA damage, chromatin controls accessibility to the genetic material it packages as well as facilitates swift recognition and precise repair of any damage that has occurred (Kouzarides, 2007).

Among the known histone PTMs, acetylation, phosphorylation, and ubiquitylation are among some of the most widely studied participants in key DDR pathways (Gong and Miller, 2013). For example, the histone variant H2AX is phosphorylated on Ser139 upon DNA damage by the phosphatidylinositol-3 kinase (PIKK) family proteins that include key DDR pathway components, such as ataxia telangiectasia mutated (ATM), DNA-dependent protein kinase (DNA-PK), as well as ATM and RAD3-related (ATR) (Fernandez-Capetillo et al., 2002; Bonner et al., 2008; Gong and Miller, 2019). The phosphorylated H2AX is then recognized by MDC1, triggering a downstream ubiquitylation cascade via the recruitment of RNF8, a RING-domain ubiquitin ligase (Stucki et al., 2005; Ciccia and Elledge, 2010; Bekker-Jensen and Mailand, 2011). RNF168, another ubiquitin ligase, binds and amplifies the RNF8-initiated cascade and leads to recruitment of chromatin-associated genome caretakers that assist in DSB repair (Bekker-Jensen and Mailand, 2011). MDC1 also recruits NuA4 and the histone acetyltransferase TIP60, whose activity contributes to local chromatin relaxation, ATM activity, and DNA damage-induced phosphorylation (Bonner et al., 2008; Xu and Price, 2011; Gong and Miller, 2019). Here, we will focus on histone methylation as well as their modifiers in the various DDR pathways and provide an overview of applications of histone methyltransferase inhibitors within the context of DDR as novel therapeutic strategies for cancer.

First discovered in the 1960s (Murray, 1964), histone methylation has been identified as a critical modulator of DDR pathways, and studies exploring this role have been steadily increasing. Mostly known for their function in transcriptional regulation, histone methylation occurs as mono- (me), di- (me2) or tri- (me3) methyl groups on the ε-amino group of lysine

residues, as well as in a mono- (me), di-symmetrical (me2s), or di-asymmetrical (me2a) state on arginine residues (Kouzarides, 2002; Greer and Shi, 2012; Gong and Miller, 2019). These reactions are catalyzed by histone methyltransferases (HMTs) through transferring methyl groups donated by S-adenosyl methionine (SAM) to their target residues (Murray, 1964; Greer and Shi, 2012; Gong and Miller, 2019). So far, three major groups of HMTs have been identified: SET domain-containing lysine methyltransferases (KMTs), Dot1-Like KMT with no SET domain, and protein arginine methyltransferases (PRMTs) (Okada et al., 2005; Black et al., 2012; Yang and Bedford, 2013). Apart from core histone proteins, HMTs can also methylate free histones and non-histone proteins, such as p53, TAF10, VEGFR1, among others (Murray, 1964; Kouzarides, 2002; Chuikov et al., 2004; Okada et al., 2005; Bekker-Jensen and Mailand, 2011; Xu and Price, 2011; Black et al., 2012; Greer and Shi, 2012; Yang and Bedford, 2013). The diverse array of various methylation events possesses tremendous regulatory power and frequently contributes to human diseases, including cancers (Bonner et al., 2008; Greer and Shi, 2012; Yang and Bedford, 2013).

One of the first and most notable discoveries illuminating a relationship between histone methylation and DNA damage was that methylation of histone H3 Lys 79 (H3K79) promotes chromatin accumulation of p53-binding protein 1 (53BP1), a key mediator of DDR, through its Tudor domain (Huyen et al., 2004). Many HMTs, including but not limited to those for H3K4, H3K9, H3K27, H3K36, H3K79, and histone H4 lysine 20 (H4K20), have since been found to rapidly work to mark histones at sites of DNA damage and modulate DDR machinery. Following, we review our current understanding of some prominent HMTs within the context of distinct DDR pathways (**Figure 1**).

EMERGENCY DISPATCH OF FIRST RESPONDERS—THE RELATIONSHIP OF CHROMATIN AND EPIGENETIC REGULATORS IN DNA DAMAGE REPAIR

Homologous Recombination—Tending to Damage With a Stretch(er) of DNA

HR, which is the more faithful mechanism of the two for repair of DSBs, utilizes homologous DNA sequences as templates to repair damaged DNA (Sung and Klein, 2006; Tubbs and Nussenzweig, 2017). HR occurs mainly after DNA replication in the S and G2 phases of the cell cycle when homologous sister chromatids are readily available to serve as repair templates (Sung and Klein, 2006; Hustedt and Durocher, 2017). It is initiated when 3′ single-stranded DNA (ssDNA) overhangs are generated from DSB resection by helicases and nucleases. The RAD51 recombinase then assembles onto the ssDNA overhangs and recruits its template for repair DNA synthesis by invading homologous duplex DNA (Chapman et al., 2012). During the process of HR, the steps from resection to duplex DNA invasion through DNA synthesis and final resolution require transient yet extensive disruption and restoration of chromatin structure in a rapid manner.

The activities of many histone methylation marks and their respective HMTs change during the HR process. For example, tri-methylated H3 lysine 36 (H3K36me3), mediated by SETD2/HYPB methyltransferase, was established by Carvalho et al. (2014) and Pfister et al. (2014) to be required for HR repair, to promote the formation of presynaptic RAD51 filaments and subsequent loading of RAD51 to resected DNA ends. The H3K79 histone methyltransferase DOT1L (Disruptor of telomeric silencing 1-like) and some H3K9-specific KMTs, such as SETDB1, and its reader protein, HP1 (Heterochromatin Protein 1), among others, were also discovered to play pivotal roles to facilitate the recruitment of 53BP1 to DSBs and direct HR (Alagoz et al., 2015). DOT1L is structurally unique because it does not contain a SET domain that is evolutionarily conserved among KMTs (Okada et al., 2005). So far, DOT1L has been demonstrated to regulate several molecular processes, including but not limited to telomeric silencing, gene transcription, and most notably, DNA damage repair (Kari et al., 2019). Huyen et al. (2004) and Ljungman et al. (2017) suggested that DOT1L-mediated H3K79me2 marks, otherwise hidden in chromatin under normal conditions, can modify binding by the tandem tudor domain of the human 53BP1 protein after nearby DSB induction. Similar findings were found in colorectal cancer, where DOT1L-mediated H3K79me is required for chromosome structure maintenance, DNA damage checkpoint, and cell recovery via HR (Ljungman et al., 2017; Wood et al., 2018).

There are several methyltransferases that interact with and modify H3K9. The euchromatic histone-lysine *N*-methyltransferase 1/2 complex, also known as GLP/G9a, catalyzes H3K9 mono- and di-methylation and is associated with transcriptional repression (Tachibana et al., 2008). These two components can be phosphorylated by ATM, and their disruption leads to genomic instability, suggesting a role in DDR (Agarwal and Jackson, 2016; Ginjala et al., 2017). G9a is recruited to chromatin and interacts with replication protein A (RPA), a heterotrimeric protein complex that directly participates in HR by binding to the 3′ ssDNA tails and stimulating end resection (Yang et al., 2017). This interaction also modifies Rad51 foci formation, allowing for efficient HR (Gasior et al., 1998; Raderschall et al., 1999). GLP localization at DNA break sites is largely dependent on G9a (Tachibana et al., 2005, 2008). Interestingly, GLP activity on its own, for example GLP-catalyzed H4K16 methylation, was found to contribute to NHEJ (see below). SETDB1 and SUV39, two methyltransferases that tri-methylate H3K9, work with BRCA1 and HP1 to promote HR integrity by ensuring repositioning of 53BP1 to extend resection during HR in cells at G2 phase (Alagoz et al., 2015).

Compared to KMTs, PRMTs and their associated histone arginine methylation marks are not as well understood in these processes. So far, 9 PRMTs have been characterized, producing 3 categories of methylarginines: monomethylarginine, asymmetric dimethylarginine (ADMA), and symmetric dimethylarginine (SDMA) (Bedford, 2007). Type I PRMTs (PRMT1-4, 6, and 8) catalyze formation of MMA and ADMA, while type II PRMTs (PRMT5, 7, and 9) catalyze production of MMA and

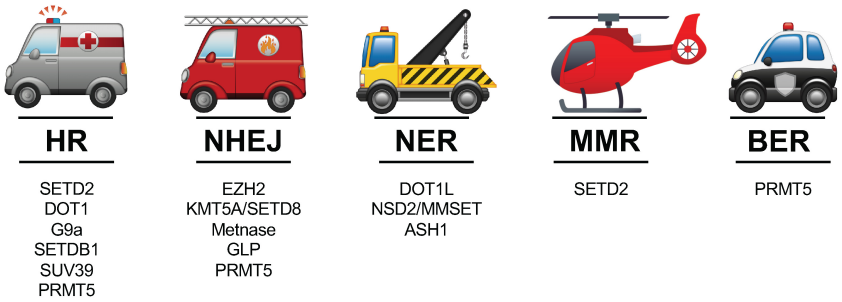

FIGURE 1 | The 5 major DDR pathways and prominent HMTs involved in the context of those distinct pathways. See text for references of studies highlighting the various roles of HMTs in these pathways.

SDMA (Bedford, 2007; Gong and Miller, 2019). Protein arginine methylation is abundant in modifying signal transduction, gene transcription, DNA repair, mRNA splicing, and more (Yang and Bedford, 2013). PRMTs have also been linked to carcinogenesis and metastasis of various cancers. PRMT5 is a type II methyltransferase that mediates MMA or SDMA of residues such as H3R8, H2AR3, H3R2, and H4R3 (Bedford, 2007). Recent studies have reported that depletion or inhibition of PRMT5 impairs HR, inducing DNA damage accumulation, cell cycle arrest, and eventually cell death. Mechanistically, PRMT5 depletion or inhibition potentially mediates this by inducing abnormal splicing of TIP/KAT5, a DNA repair factor, or disrupting methylation of KLF4, a transcriptional regulator modulating DNA end resection, HR efficiency and TIP60 expression (Hamard et al., 2018; Checa-Rodríguez et al., 2020). Overall, there are many studies that suggest an active role of HMTs in rescuing DSB via HR (**Figure 1**), although the mechanisms underlying this involvement require further elucidation.

Non-homologous End-Joining —Putting Out Destructive Fires Rapidly

NHEJ, the other main repair pathway for eukaryotic DSBs, was first named by Moore and Haber in 1996 (Moore and Haber, 1996; Lieber, 2008; Yamagishi and Uchimaru, 2017). NHEJ is referred to as "non-homologous" because in this pathway, contrary to HR, the broken ends are directly ligated without any homologous template (Lieber, 2008). Complementary to HR, NHEJ is generally favored for DDR occurring in the G1 phase of the cell cycle (Lieber, 2008; Chapman et al., 2012; Hustedt and Durocher, 2017). In this pathway, the Ku70/80 heterodimer rapidly binds to the breakage site and forms a complex with the DNA, thereby acting as a node for docking of nuclease, polymerase and ligase components (Lieber, 2008). Subsequently, the catalytic subunit of DNA-PK (DNA-PKcs), responsible for maintaining the broken DNA ends in close proximity, is recruited and activated in preparation to engage other end-processing factors and eventually re-join the broken ends (Lieber, 2008; Hustedt and Durocher, 2017). Finally, re-ligation of the broken DNA ends occurs via the DNA ligase complex. Among the many HMTs involved in NHEJ, we summarize knowledge in this context for EZH2, KMT5A, Metnase, GLP, and PRMT5 (**Figure 1**).

EZH2 (Enhancer of Zeste 2) is an H3K27 methyltransferase and essential component of polycomb repressive complex 2 (PRC2), regulating cell sensitivity to DNA damage via alteration of chromatin architecture as well as expression of many functional genes that participate in lineage specification, cell cycle regulation, and DNA repair (Yamagishi and Uchimaru, 2017). EZH2 has been demonstrated to interact directly with the NHEJ-related protein, Ku80. Ku80 bridges EZH2 to DNA-PK complexes, facilitating phosphorylation of EZH2 by DNA-PK and subsequent modulation of EZH2 methyltransferase activity as well as its target gene expression (Wang et al., 2016).

KMT5A, also known as SETD8, is a SET domain containing methyltransferase of H4K20 mono-methylation, which is required before di-methylation and tri-methylation can take place [54]. Although it is primarily known to use H4K20 as a substrate, evidence also exists to indicate that KMT5A interacts with non-histone proteins (Checa-Rodríguez et al., 2020). It has been shown to be vital during replication, transcription, and chromosome segregation (Moore and Haber, 1996). Like DOT1L, KMT5A function also affects 53BP1 recruitment to DSBs. Although depletion of SETD8 only moderately decreased HR efficiency in human osteosarcoma cells, the same experiment resulted in a severe abrogation in NHEJ (Dulev et al., 2014), suggesting that SETD8 promotes DSB repair via the NHEJ pathway.

Metnase is a DNA repair protein with a unique fusion of a SET domain, a nuclease domain, and a transposase/integrase domain (Lee et al., 2005). Fnu et al. (2011) found that Metnase enhances NHEJ following DSBs and that its SET domain is required for Metnase activities in DNA damage. Metnase at DSBs can also directly dimethylate H3K36, which then recruits and stabilizes DNA repair proteins at the breakage site, facilitating NHEJ efficiency (Lee et al., 2005; Fnu et al., 2011).

Although GLP localization to DNA break sites largely depends on G9a (Tachibana et al., 2005, 2008), which together are responsible for the H3K9me2 mark, GLP-catalyzed H4K16me1 is also part of its response to DNA damage (Lu et al., 2019). GLP-catalyzed H4K16me1 levels drastically increase during the early stages of DDR and cooperate with H4K20me2 to facilitate 53BP1 recruitment, favoring NHEJ-mediated DDR. The fact that GLP

is commonly studied in conjunction with G9a often complicates experimental interpretations. For example, previous studies have shown that pharmacological inhibition of G9a/GLP hindered HR with contentious impact on NHEJ (Fukuda et al., 2015; Ginjala et al., 2017). However, GLP knockdown alone impaired 53BP1 foci formation and NHEJ following damage induction, while G9a knockdown only had a mild effect on NHEJ but caused severe HR defects in reporter assays (Fnu et al., 2011). This suggests G9a and G9a-catalyzed H3K9 methylation may be more significant in facilitating HR, while GLP and GLP-catalyzed H4K16me1 play a greater role in NHEJ.

In terms of PRMT involvement in this DDR pathway, Hwang et al. found that PRMT5 regulates NHEJ via methylation and stabilization of 53BP1 to promote cell survival (Hwang et al., 2020). Interestingly, these investigators also discovered a regulatory mechanism in which Src kinase phosphorylates PRMT5 at residue Y324 to suppress PRMT5 activity and block NHEJ repair. Thus, along with the aforementioned studies implicating participation of PRMT5 in HR, it is likely that PRMT5 is involved in both main pathways, possibly through 53BP1 modulation. Further studies are needed to characterize its overall involvement in DDR and determine whether favoring one pathway over another depends on specific molecular contexts, such as elevated Src activity.

Nucleotide Excision Repair—Towing Away Helix-Distorting Lesions

Different DDR pathways are instigated to resolve damage in a substrate-dependent manner (Chatterjee and Walker, 2017). NER plays a significant role to remove helix-distorting DNA lesions such as bulky chemical adducts and photoproducts produced by UV light (Thoma, 1999; Gong et al., 2005). It is a "broad spectrum" DDR pathway, repairing a wide range of DNA damage. Mechanistically, NER acts via dual incisions on both sides of the target lesions by two different nucleases, one at the 3′ end followed by the other at the 5′ end (Petit and Sancar, 1999). After targets are removed, new DNA is synthesized to fill the gap using the complementary strand as a template and ligated back into the segment (Petit and Sancar, 1999; Gong et al., 2005).

The chromatin organization via histone displacement often impacts how cells detect and repair lesions as well as other DNA-dependent reactions. As NER acts primarily in the context of DNA, this chromatin organization becomes an important process during NER initiation (Fukuda et al., 2015; Hwang et al., 2020). For repair processes like NER to happen efficiently, lesion detection mechanisms need to activate both NER and chromatin remodeling. Previous studies have linked UV-induced histone acetylation prior to NER with increased accessibility to repair proteins, at least in the more condensed regions of chromatin (Teng et al., 2002; Gong et al., 2005). Evidence has also emerged to support the involvement of a few histone methylation pathways (**Figure 1**), such as DOT1L-mediated H3K79, NSD2-catalyzed H4K20, and ASH1L-mediated H3K4 methylation, in this process, which are discussed below.

Interestingly, Dot1, the yeast homolog of the methyltransferase for H3K79 methylation, also has roles in NER apart from its aforementioned involvement in HR. Dot1 promotes transcriptional restart of paused RNA polymerases following NER completion and ensures proper replication timing during the cell cycle (Chaudhuri et al., 2009; Ljungman et al., 2017). Yeast cells with H3K79R mutations and Dot1 mutations were found to be hyper-sensitive to UV light and have affected NER (Chaudhuri et al., 2009). The exact mechanisms by which Dot1 and H3K79 methylation impact NER, however, remain to be elucidated.

NSD2 and ASH1L are two additional histone methyltransferases that have been identified as players in genome-wide NER activity (Gong et al., 2005; Gillet and Schärer, 2006; Balbo Pogliano et al., 2017). NSD2 (nuclear receptor SET domain 2), also known as Multiple Myeloma SET (MMSET) or Wolf-Hirschhorn Syndrome Candidate 1 (WHSC1), is a SET domain containing KMT that primarily catalyzes di- and tri-methylation of H3K36, which regulates crucial developmental genes as well as modulates DSB repair (Nimura et al., 2009). Notably, NSD2 has also been found to catalyze H4K20 methylation and subsequent 53BP1 accumulation at DNA damage sites upon DSB induction (Pei et al., 2011). Previous studies by Chitale and Richly reported the collaboration between NSD2 and the endonuclease DICER, which facilitates heterochromatin formation and generates small non-coding RNAs that include the sequence of the damaged locus (Chitale and Richly, 2018). They later reported a mechanism by which NSD2 relocates to chromatin in a DICER-dependent manner and sets the stage for H4K20me2 to recruit XPA, a protein that binds to damaged DNA and acts as a scaffold for other repair proteins, at sites of UV lesions for genome-wide NER (Thoma, 1999; Pei et al., 2011; Chitale and Richly, 2018).

ASH1L (Absent, Small, or Homeotic discs 1-Like) is a member of the *trithorax* transcriptional regulators crucial for normal development, organ function, fertility, euchromatin formation, and ongoing transcription (Balbo Pogliano et al., 2017). It performs its regulatory functions by histone modification and chromatin remodeling via methylation of H3K4 and H3K36 (Balbo Pogliano et al., 2017). Balbo Pogliano et al. (2017) have reported a helper role of ASH1L for effective genome-wide NER. They found that DDB2, a specialized damage sensor, promotes excision of mutagenic lesions from UV damage by recruiting ASH1L, which methylates H3K4 and in turn facilitates docking of downstream NER effectors to ensure uninterrupted repair activity. Without ASH1L, the otherwise effective handoff between different NER damage recognition factors would be disrupted (Balbo Pogliano et al., 2017; Gsell et al., 2020). Thus, as with other types of DDR, histone methylation seems to have a clear role in the repair of helix-distorting DNA lesions, necessitating additional investigations to understand the full breadth of this involvement.

Mismatch Repair—Evacuating Mis-Incorporated Bases

MMR helps protect genome integrity at replication by removing mis-incorporated bases and insertion-deletion mis-pairs from newly synthesized daughter DNA strands (Li et al., 2016). In

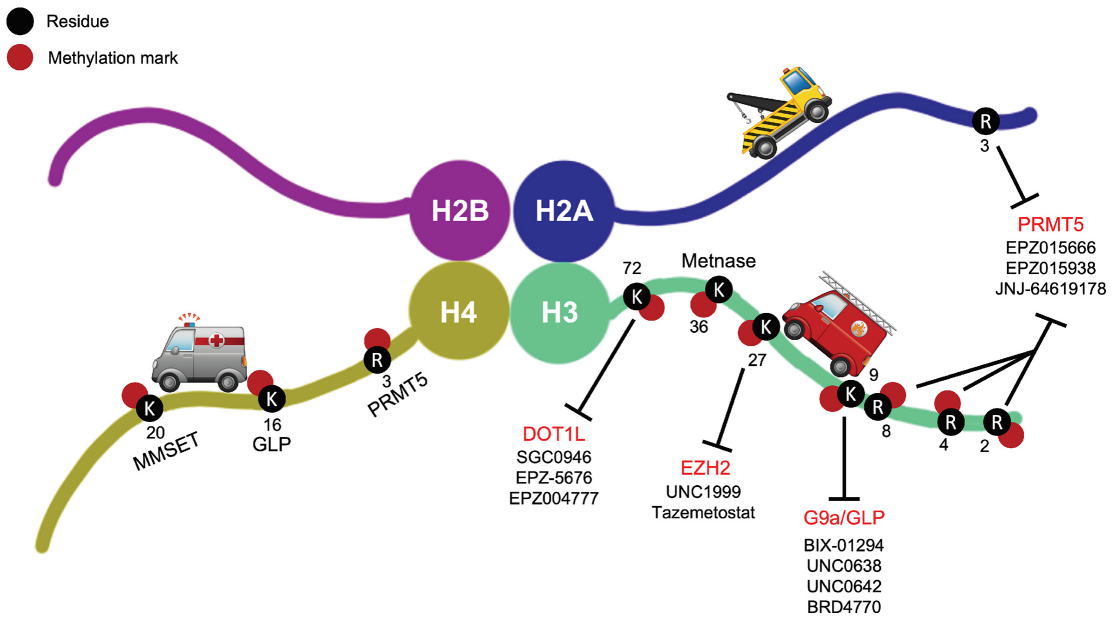

FIGURE 2 | Small molecule inhibitors of DOT1L, G9a/GLP, EZH2, and PRMT5 shown with their respective target methylation marks on the histone tails. These are examples of prominent small molecule HMT inhibitors in pre-clinical testing or early stages of clinical trials as part of promising standalone or combinatorial cancer treatments.

humans, MMR starts with mismatch recognition on newly synthesized strands by the heterodimer complexes hMutSα or hMutSβ, which lead to the excision of the mismatch by an exonuclease, EXO1 (Hombauer et al., 2011; Li et al., 2016). As a result, a single-stranded DNA gap is generated, filled, and ligated, concluding the repair (Hombauer et al., 2011; Li, 2013). The most notable HMT-MMR interaction is that of SETD2 and hMutSα (**Figure 1**). SETD2 tri-methylates H3K36, which is required *in vivo* to recruit hMutSα onto chromatin for downstream repair (Li et al., 2013). Cells depleted of SETD2 display characteristics of MMR-deficient cells, suggesting a significant role of H3K36me3 in proper MMR progression (Li, 2013; Li et al., 2013, 2016). However, much remains to be discovered in terms of how chromatin states and their modifiers modulate the coupled MMR and replication processes.

Base Excision Repair—Chasing Down Damaged Nucleotides

BER resolves endogenous DNA damage raised from deamination, oxidation and alkylation by removing damaged bases without causing excessive distortion to the DNA helix (Krokan and Bjørås, 2013). Protecting against various detrimental processes such as cancer, aging, and neurodegeneration (Jeppesen et al., 2011; Krokan and Bjørås, 2013), much of BER occurs in the nuclei, as well as mitochondria, and is a highly conserved system from bacteria to human. The process is initiated by one of at least 11 distinct DNA glycosylases, such as 8-Oxoguanine-DNA glycosylase (OGG1), that recognizes and removes a damaged base by cleaving its N-glycosyl bond to allow its subsequent release (Jeppesen et al., 2011). Following excision, an abasic, apurinic/apyrimidinic site, known as an AP site, remains in the absence of the base. AP endonuclease 1 (APE1) then recognizes the AP site and cleaves its backbone to produce an intermediate that is properly processed through BER (Jeppesen et al., 2011; Yu et al., 2012). Within BER, (short-patch) (SP-)BER only adds one nucleotide to the 3′-end of the cleaved AP site, followed by Pol β which helps produce a nick sealable by X-ray repair cross-complementing protein 1 and Ligase IIIα (XRCC1/Ligase IIIα) (Sobol et al., 1996; Demple and Sung, 2005). On the other hand, (long patch) LP-BER utilizes Pol β in a different manner, generating a short DNA flap cleaved by flap endonuclease 1 (FEN1) and sealed by DNA ligase I (Sobol et al., 1996; Jeppesen et al., 2011).

To date, there have been few studies illuminating effects of HMTs and their methylation marks in BER (**Figure 1**). The most notable HMT studied in the context of BER is PRMT5. Recent studies by Zhou et al. (2018) identified interactions between symmetrical dimethylarginine of histone H4 (H4R3me2s), catalyzed by PRMT5, and OGG1, the glycosylase initiating BER activities. OGG1 directly interacts with PRMT5, affecting its binding to histone H4 and thereby regulating H4R3me2s levels. FEN1 binds to symmetrically dimethylated H4R3, which was found to enhance its substrate binding, thereby increasing its efficiency in BER (Zhou et al., 2018). Depletion of PRMT5 decreased OGG1 activity, BER efficiency and cell survival ratio *in vitro*, suggesting that H4R3me2s can be an important downstream factor of PRMT5 function in DDR, and the PRMT5-H4R3me2s relationship bridges endogenous lesion detection by OGG1 and downstream repair. Similar to MMR, the identification of a role for PRMT5

in BER only indicates the beginning of this intriguing new area revealing the involvement of HMTs in a wide range of DDR pathways.

UTILIZING A SAFETY HARNESS—TARGETING DNA DAMAGE RESPONSE VIA HISTONE METHYLTRANSFERASES IN CANCER FOR IMPROVED TREATMENT STRATEGIES

DNA damage, as well as inadequate DDR, is one of the main causes for genomic instability and tumorigenesis. However, these very defects in DDR mechanisms serendipitously also offer therapeutic opportunities to cause lethality in cancer cells while sparing normal ones. Cancer researchers have recently popularized the term "synthetic lethality," originally described back in 1922 and later coined in 1946, for phenomena where disruption of one gene maintains cell viability, but the added disruption of a second gene kills cells (Nijman, 2011). The first example of exploiting this approach in molecularly targeted cancer therapy was the inhibition of members of the enzyme family Poly (ADP-ribose) polymerase (PARP), key players involved in DDR, in *BRCA1/2* deficient tumors (Lord and Ashworth, 2017; Huang et al., 2020). In fact, this concept has been tested in several clinical trials (ClinicalTrials.gov Identifier: NCT00494234, NCT00494442) with great success. Because of the dynamic functions of HMTs and their heavy involvement in DNA damage, among other processes, they have been increasingly considered as druggable targets for discovery and pharmacological intervention of various cancers. Just in the past decade, pharmacological targeting of HMTs in the context of DDR has become a promising avenue for novel cancer therapies. It is worth noting, however, that although evidence suggests the exciting potential of novel therapeutic targets among HMTs, the field of epigenetic therapies has only recently started making significant progress toward improved targeting. Many issues remain to be resolved. For example, synergistic combinations of pharmacological HMT inhibitors and other treatment modalities, i.e., chemotherapy and radiation, still need to be evaluated and optimized for more beneficial clinical outcomes. Here, we briefly summarize several small molecule inhibitors targeting HMTs that have emerged in pre-clinical testing or early stages of clinical trials as part of promising standalone or combinatorial cancer treatments, including pharmacological inhibitors of DOT1L, G9a, EZH2, and PRMT5, and discuss their potential in combination strategies with canonical DNA damaging agents or DDR inhibitors (**Figure 2** and **Table 1**).

DOT1L

A lot of small molecule inhibitors for DOT1L target the common cofactor-binding site for SAM within the methyltransferase structure (Yu et al., 2012). Utilizing structure-guided medicinal chemistry, EPZ004777, a SAM-competitive DOT1L inhibitor, was the first meaningful proof-of-concept for targeting any HMT (Daigle et al., 2011). Since then, SGC0946, a brominated analog of EPZ004777 that takes advantage of a hydrophobic cleft in DOT1L surrounding its adenine ring, and EPZ-5676, an aminonucleoside analog which became the first reported HMT inhibitor to enter human clinical trials, have been also developed (Daigle et al., 2013). Both molecules better occupy the SAM-binding pocket and disrupt its structural integrity via conformational rearrangement to improve inhibition of DOT1L over EPZ004777 (Yu et al., 2012).

As previously discussed, DOT1L is a key player in DSB repair via HR in several cancers. Depletion of DOT1L methyltransferase activity after SGC0946 and EPZ-5676 treatments leads to an impaired DNA damage response indicated by decreased γH2AX levels as well as defective HR-mediated DSB repair without affecting NHEJ in colorectal cancer cell lines (Kari et al., 2019). Continuous infusion of EPZ-5676 for 21 days in nude rat subcutaneous xenograft models of MLL-rearranged leukemia achieved well-tolerated, complete, and sustained tumor regression for more than 30 days post-treatment (Daigle et al., 2013). Reductions in both treatment duration and dose in the same model still sustained tumor regression, albeit with slightly lower efficacy.

EPZ-5676, also referred to as Pinometostat, has completed phase 1 trials in adult and pediatric patients with relapsed or refractory acute myeloid leukemia (AML) and acute lymphoblastic leukemia (ALL) harboring rearrangements of the MLL gene (ClinicalTrials.gov identifiers: NCT01684150, NCT02141828). These trials demonstrated only modest clinical efficacy (Stein et al., 2018). However, additional preclinical investigations have indicated that combination strategies of DOT1L inhibitors with chemotherapeutic agents or other chromatin modifying drugs may offer benefit (Klaus et al., 2014; Liu et al., 2014). Interestingly, inhibition of DOT1L sensitized MLL-rearranged leukemia cells to DNA damage-inducing chemotherapy by inhibiting their DNA damage response (Liu et al., 2014). In rectal cancer cells, the depletion of DOT1L has also recently been demonstrated to increase sensitivity to inhibition of PARP-1 (Kari et al., 2019). Pharmacological inhibition of PARP-1 delays DNA lesion repair and increases sensitivity to further damage. Taking this one step further, PARP inhibition may result in inadequate SSB repair (Dantzer et al., 2000). SSBs may then accumulate and result in DSBs, and if cells have any defects in DSB repair, they will face great, often fatal challenges to survive and proliferate. Cells with *BRCA1/2* mutations can be highly sensitive to further blockade of SSB repair via PARP inhibition due to their compromised ability to repair DSBs properly and efficiently via HR. These studies highlight the significant involvement of DOT1L in DDR and suggest great clinical potential for DOT1L inhibition in combination with DNA damaging chemotherapies. To date, the National Cancer Institute (NCI) has two clinical trials currently recruiting to examine the combination of Pinometostat and standard cancer treatment modalities (ClinicalTrials.gov identifiers: NCT03701295, NCT03724084).

TABLE 1 | Small molecule inhibitors of DOT1L, G9a/GLP, EZH2, and PRMT5 and their anticancer activities in relation to DNA damage repair.

Target protein	Compound	Mode of action	Documented effects on DNA damage	Clinical trial
DOT1L	SGC0946	SAM-competitive	In colorectal cancer *in vitro*, treatment of SGC0946 resulted in decreased γH2AX levels, defective HR-mediated DSB repair (Kari et al., 2019)	N/A
	EPZ-5676 (Pinometostat)	SAM-competitive	In colorectal cancer *in vitro*, treatment of SGC0946 resulted in decreased γH2AX levels, defective HR-mediated DSB repair (Kari et al., 2019); Rectal cancer cells were sensitized to DNA damage-inducing chemotherapy and PARP inhibition following EPZ-5676 treatment (Amé et al., 2004; Liu et al., 2014)	Phase I trial completed in adult and pediatric patients with relapsed or refractory acute myeloid leukemia (AML) and acute lymphoblastic leukemia (ALL) harboring MLL gene rearrangements (ClinicalTrials.gov identifiers: NCT01684150, NCT02141828); Clinical trials currently ongoing to examine the combination of Pinometostat and standard DNA damage-inducing cancer treatment modalities (ClinicalTrials.gov identifiers: NCT03701295, NCT03724084)
	EPZ004777	SAM-competitive	N/A	N/A
EZH2	UNC1999	SAM-competitive	UNC1999 aggravated genotoxic effects induced by treatments of olaparib, an FDA approved PARP inhibitor in cells deficient in DDR pathways, enhancing its synthetic lethal effects in BRCA-deficient cell lines and AML patient cells (Caruso et al., 2018)	N/A
	EPZ-6438 (Tazemetostat)	SAM-competitive	Treatment of Tazemetostat sensitized PARPi effect in BRCA-defective cancer cells *in vitro* and *in vivo* (Yamaguchi et al., 2018)	Approved by FDA for patients 16 years and older with metastatic or locally advanced epithelioid sarcoma ineligible for complete resection as well as relapsed/refractory follicular lymphoma
G9a/GLP	UNC0638	Substrate-competitive	Treatment of U2OS cells with UNC0638 disrupted BRCA-BARD retention at DNA damage sites (Wu et al., 2015). The use of the PARP inhibitor Olaparib in combination with UNC0638 also resulted in a synergistic reduction of clonogenic survival in breast cancer cells (Carvalho et al., 2014)	N/A
	BIX-01294	Substrate-competitive	Loss of H3K9 methylation through G9a inhibition with BIX-01294 increased radiosensitivity of a panel of glioma cells (Gursoy-Yuzugullu et al., 2017)	N/A
	UNC0642	Substrate-competitive	G9a inhibition with UNC0642 conveyed a significant reduction in both NHEJ and HR repair in ovarian carcinoma cells (Watson et al., 2019)	N/A
	BRD4770	SAM-competitive	Combined inhibition of Checkpoint kinase 1 (Chk1), a key regulator of cell cycle transition in response to DNA damage, and G9a with BRD4770 disrupted pancreatic cancer cell growth, replication fork progression, and DNA damage signaling, ultimately leading to induction of cell death (Urrutia et al., 2020)	N/A
PRMT5	EPZ015666	Peptide-competitive	Loss of PRMT5 activity via EPZ015666 resulted in impaired HR, leading to DNA-damage accumulation, p53 activation, cell-cycle arrest, and cell death (Hamard et al., 2018)	N/A
	EPZ015938	Substrate-competitive	The combination of Gemcitabine and EPZ015938 resulted in synergistic accumulation of Gem-induced DNA damage in pancreatic cells *in vitro* and *in vivo* (Wei et al., 2020)	Phase I safety and clinical activity study underway in myelodysplastic syndrome and AML (ClinicalTrials.gov Identifier: NCT03614728); Phase I dose escalating study ongoing in solid tumors and non-Hodgkin lymphoma (ClinicalTrials.gov Identifier: NCT02783300)
	JNJ-64619178	SAM-competitive and peptide-competitive (simultaneous)	N/A	Phase I clinical trial continuing as a potential treatment for B cell non-Hodgkin lymphoma, lower risk MDS and advanced solid tumors (ClinicalTrials.gov Identifier: NCT03573310)

Thus, explorations for the optimal use of DOT1L inhibitors have just started.

G9a

Various studies have identified G9a as a regulator of HR in response to DSB formation. In human cancers, the G9a complex is often recruited to chromatin and modulates efficient HR through its interaction with RPA. G9a deficiency has been shown to impair DDR and sensitize cancer cells to more DSBs by disrupting Rad51 and RPA foci formation in response to damage (Yang et al., 2017). BIX-01294, the first G9a complex inhibitor discovered through high through-put screening (Kubicek et al., 2007), is an H3 peptide substrate-mimetic molecule. While highly specific, this small molecule also shows cell toxicity not attributed to its inhibitory effects. Despite these shortcomings, however, BIX01294 offered hope to the treatment of various diseases mediated by this epigenetic pathway and provided a backbone for the design and synthesis of several subsequent G9a inhibitors, such as UNC0638, UNC0642, and more (Vedadi et al., 2011; Liu et al., 2013). In pre-clinical studies, loss of H3K9me through BIX-01294, UNC0638, and UNC0642 treatments hypersensitized tumor cells to DSB-inducing treatment modalities and resulted in inhibited DSB repair through, interestingly, both HR and NHEJ (Agarwal and Jackson, 2016; Gursoy-Yuzugullu et al., 2017; Watson et al., 2019). This may be related to the fact that most G9a inhibitors also target its complex partner, GLP, which has been implicated in NHEJ (Watson et al., 2019).

As mentioned, cells harboring *BRCA1/2* mutations are highly sensitive to defective DDR following PARP inhibition (Dantzer et al., 2000; Amé et al., 2004). BRCA1 must be recruited and retained at DNA damage sites for it to carry out its regulatory functions in HR (Scully et al., 1997). This process is dependent on the BRCT domains of BRCA1 (BRCA1-BRCT) and BRCA1 forming a complex with the BRCA1-associated RING domain (BARD1) protein (Wu et al., 1996). BARD1 has been shown to interact with H3K9me2 in response to DNA damage via direct binding of HP1, a H3K9 reader protein, to the BRCT domain of BARD-1 (Wu et al., 2015). Treatment of U2OS cells with H3K9 specific HMT inhibitor UNC0638 disrupted BRCA-BARD retention at DNA damage sites. In breast cancer, treatment with the PARP inhibitor olaparib in combination with UNC0638 also resulted in a synergistic reduction of clonogenic survival, suggesting that leveraging H3K9 methyltransferases as a target with PARP inhibitors in cancer might have therapeutic potential (Carvalho et al., 2014).

In terms of SAM-competitive small molecule G9a complex inhibitors, a notable example is BRD4770, which was discovered by Yuan et al. (2012). BRD4770 reduced cellular levels of H3K9me2 and H3K9me3, induced cell senescence, inhibited both anchorage-dependent and independent proliferation and resulted in G2/M cell cycle arrest in Panc-1, a pancreatic cancer cell line (Yuan et al., 2012). Work from our laboratory has shown that combined inhibition of Checkpoint kinase 1 (Chk1), a key regulator of cell cycle transition in response to DNA damage, with prexasertib, and G9a, using BRD4770, disrupted pancreatic cancer cell growth, replication fork progression, and DNA damage signaling, ultimately leading to induction of cell death (Urrutia et al., 2020), further supporting the strategy of DDR targeting in conjunction with G9a complex inhibition.

Although many potent G9a/GLP inhibitors have been discovered with promising results *in vitro* and progress has been made with some of these inhibitors for *in vivo* studies in recent years, no inhibitor has advanced to clinical trials so far due to challenges with pharmacodynamics and pharmacokinetics optimization (Vedadi et al., 2011; Liu et al., 2013). More studies are needed to augment pharmacodynamics and pharmacokinetics characteristics as well as toxicity profiles of current and future inhibitors. Due to the promise of this pathway as a target for anti-cancer agents, improved development and use of G9a inhibitors will continue to be in high demand.

EZH2

EZH2 regulates the expression of many genes instrumental to lineage specification, cell cycle regulation, and DNA repair (Yamagishi and Uchimaru, 2017). Most of the EZH2 inhibitors confer their highly selective and potent inhibition through SAM competition via a conserved 2-pyridone core, the most notable being UNC1999 and EPZ-6438, also known as tazemetostat (Duan et al., 2020). So far, tazemetostat has been approved by FDA for patients 16 years and older with metastatic or locally advanced epithelioid sarcoma ineligible for complete resection as well as relapsed/refractory follicular lymphoma (U.S. Food and Drug Administration, and Center for Drug Evaluation and Research, 2020).

Interestingly, targeting EZH2 may promote synthetic lethality approaches in an HR-related capacity to improve the anti-tumor efficacy of PARP1 inhibition in *BRCA1/2*-deficient cancers. PARP1 interacts with and regulates EZH2 following alkylating DNA damage (Caruso et al., 2018). PARylation of EZH2, which is the addition of negatively charged ADP-ribose polymers in an enzymatic reaction, resulted in inhibition of EZH2 HMT activity (Masutani et al., 2003; Caruso et al., 2018). Caruso et al. (2018) also demonstrated that EZH2 inhibition via pharmacological inhibitor UNC1999 aggravated genotoxic effects induced by treatments of olaparib, an FDA approved PARP inhibitor, enhancing its synthetic lethal effects in BRCA-deficient cell lines and AML patient cells. As research ensues to illuminate the potential of targeting EZH2 as a part of combinatorial therapies with DDR inhibitors for more malignancies, more patients will be able to benefit from these new therapeutic strategies.

PRMT5

Notably, PRMT5 acts as part of a multimeric complex with a variety of partner proteins that regulate its function and specificity (Antonysamy et al., 2012). One of its key interacting partners is MEP50, a WD-repeat–containing protein, which forms a $(PRMT5)_4(MEP50)_4$ octamer that has higher enzymatic activity than PRMT5 alone. Together, the PRMT5-MEP50 complex is regarded as the active "methylosome" *in vivo*, which is an important consideration for its therapeutic targeting. As described, PRMT5 is also a key player in DDR. It has been shown to cooperate with various factors to act as a wide-spectrum epigenetic regulator of DDR genes involved in HR, NHEJ, and G2 cell cycle arrest upon detection of DNA damage. In some studies,

pharmacological targeting of PRMT5 decreased expression of some DDR genes and hindered DSB repair in multiple cancers *in vitro*, resulting in genomic instability, cell cycle defects, aberrant splicing of key DDR regulators, and ultimately DNA damage accumulation (Bedford, 2007; Hamard et al., 2018; Zhou et al., 2018; Checa-Rodríguez et al., 2020; Hwang et al., 2020).

The first pharmacological inhibitor of the PRMT5-MEP50 complex, EPZ015666, was discovered by Chan-Penebre et al. (2015). It binds to the peptide binding site of PRMT5 and has anti-proliferative effects on mantle cell lymphoma cell lines and xenograft models (Penebre et al., 2014; Chan-Penebre et al., 2015). GSK3326595 (EPZ015938) a substrate-competitive, improved PRMT5-MEP50 inhibitor, is currently under two clinical trials: a phase I safety and clinical activity study in myelodysplastic syndrome (MDS) and AML (ClinicalTrials.gov Identifier: NCT03614728); and a phase I dose escalating study in solid tumors and non-Hodgkin lymphoma (ClinicalTrials.gov Identifier: NCT02783300). JNJ-64619178, which inhibits the PRMT5 complex through simultaneously binding the SAM- and protein substrate-binding pockets, is also under phase I clinical trial as a potential treatment for B cell non-Hodgkin lymphoma, lower risk MDS and advanced solid tumors (ClinicalTrials.gov Identifier: NCT03573310). In 2019, PF-06939999 and PRT543, two of the latest PRMT5 complex inhibitors, also entered early phase clinical trials (ClinicalTrials.gov Identifier: NCT03854227, NCT03886831). Interestingly, the DOT1L inhibitor EPZ004777 also inhibits PRMT5, albeit at >1000-fold lower selectivity with an IC_{50} of ∼500nM against isolated PRMT5 (Daigle et al., 2011). However, this compound was later found inactive against PRMT5 in complex with MEP50 (Yu et al., 2012), suggesting that EPZ004777 is not effective to target the active PRMT5 complex *in vivo*.

Expression of *PRMT5* correlates with multiple gene players in the DDR pathway across various clinical cancer datasets and its depletion leads to accumulated DNA damage in cancers (Hamard et al., 2018; Hwang et al., 2020). Furthermore, targeting PRMT5 in the context of some of its non-histone substrates may also impact DDR integrity to offer additional therapeutic vulnerabilities. For instance, when DNA damage occurs, PRMT5 methylates p53 at residues R333, R335, and R337, which promotes p53 oligomerization and targeting to the nucleus (Jansson et al., 2008). Moreover, PRMT5 stimulates p53-mediated cell cycle arrest, while its depletion triggers p53-dependent apoptosis, suggesting that p53 methylation via PRMT5 plays a central role in determining the type of response to DNA damage. PRMT5 also methylates E2F-1, which is often phosphorylated by ATM/ATR and Chk1/Chk2 to augment apoptosis upon DNA damage (Cho et al., 2012). PRMT5-mediated methylation of E2F-1 negatively regulates its function and impacts protein stability. Depleting PRMT5 by siRNA resulted in stabilization of E2F-1 protein levels, an increase in E2F target gene expression, reduced growth rate and restored apoptosis. RAD9, a protein heavily involved in cell cycle checkpoint in response to DNA damage, was also reported to interact with and be methylated by PRMT5 (He et al., 2011). He et al. (2011) showed that PRMT5-mediated methylation of RAD9 at R172, R174, and R175 is required for cellular resistance to DNA damage, and loss of this methylation by alanine mutagenesis caused S/M and G2/M checkpoint defects in mouse embryonic stem cells. Thus, the concept of targeting PRMT5 in combination with DNA damage-inducing therapies, such as radiation or chemotherapy, or other DDR deficiencies is an exciting avenue for investigation.

In support of utilizing PRMT5 inhibitors within the context of DDR, pharmacological inhibition of PRMT5 sensitizes tumors to treatments inducing DDR that are otherwise prone to resistance (Hamard et al., 2018; Secker et al., 2019; Hwang et al., 2020). For example, treatment of osteosarcoma cells with PRMT5 inhibitors reduces 53BP1 protein levels upon DNA damage as well as enhances cell senescence mediated by chemotherapy such as cisplatin (Hwang et al., 2020; Li et al., 2020). An *in vivo* CRISPR screen using a pancreatic cancer orthotopic patient-derived xenograft model identified PRMT5 as a target to synergistically enhancing cytotoxicity of gemcitabine, a first- or second-line chemotherapy for pancreatic cancer (Wei et al., 2020). This is likely due to the accumulation of excessive DNA damage from impaired HR activities (Wei et al., 2020). Congruent with the demonstrated role for PRMT5 in HR and the sensitization of HR deficient cells to PARP inhibition, combined inhibition of PRMT5 and PARP has synergistic cytotoxic effects on AML cells while sparing normal hematopoietic cells (Hamard et al., 2018). These studies represent a promising new therapeutic approach to harness targeting DDR via an HMT such as PRMT5 for AML and likely offers the opportunity to serve as an effective approach in other cancers as well.

PERSPECTIVES AND CONCLUSION—RISK ASSESSMENT AND PREPAREDNESS PLAN

Histone methyltransferases have long been established as critical players in gene transcription, expression regulation, DNA damage repair, and many more processes instrumental to cell integrity and normal physiology. Many of the HMTs have also been validated and implicated as viable drug targets in emerging epigenetic cancer therapies. We reviewed prominent histone methylation marks involved in DDR pathways and the potential of their respective small molecule inhibitors as not just therapeutic targets, but also probes for further elucidating HMT functions in cancer epigenetic regulation. It is truly exciting that there has been a notable array of potent and selective inhibitors of HMTs, many of which have undergone rigorous pre-clinical studies and demonstrated clinical usefulness in the context of DNA damage.

Challenges remain, however, for targeting HMTs in DDR pathways effectively as cancer therapies. As histone methylation is fundamental in normal human physiology, inhibition of HMTs may lead to toxicities in patients. Therefore, toxicology studies are warranted to ensure safe clinical success. Finding potent small molecule inhibitors with low off-target effects is also a major challenge, as many HMTs share structural similarities as well as evolutionarily conserved domains and co-factors (Huang et al., 2020). Researchers in the field will need to complete rigorous examinations of pharmacokinetics,

toxicities, functional validation, and medicinal chemistry profiles to confirm the roles of such inhibition in cancers and the validity of candidate compounds.

As drug resistance and heavy side effects from high drug doses become more persistent among cancer patients due to the overwhelming complexity of DDR pathways, combination therapy has become a promising approach to combat the issue, improve patients' quality of life via more sparing treatment regimens, and increase efficacy of currently in-use treatment modalities. As reviewed here, we have seen tremendous progress in the discovery of novel, synergistic therapeutic combinations with inhibitors of HMTs and DDR pathway protein members.

While there remain gaps in knowledge regarding the complete "accident scene" as to whether some histone methylation events succumb to the fate of a collateral victim in the wake of DNA damage, there is evidence to support that certain HMTs play a more active role in the DDR process as part of the critical rescue team. Targeting HMTs in the context of DNA damage is a promising strategy for cancer therapeutics, although its promise lies in the ability for us to mechanistically study oncogenesis, as well as overcome drug resistance and high toxicity profiles by discovering and designing optimized, synergistic combination therapies. Ultimately, a multi-pronged approach to harness chromatin-related DDR effectors along with induction of DNA damage or inhibition of other key nodes in DDR pathways could offer a full arsenal of valuable strategies to destroy cancer cells.

AUTHOR CONTRIBUTIONS

LH searched the related published articles and wrote the original draft. GL designed and supervised the study, as well as revised the manuscript. Both authors contributed to the article and approved the submitted version.

FUNDING

This work was financially supported by the NIH Grants R01CA247898 (GL) and R01DK52913 (GL), Advancing a Healthier Wisconsin Endowment (GL), and the We Care Fund for Medical Innovation and Research (GL).

REFERENCES

Agarwal, P., and Jackson, S. P. (2016). G9a inhibition potentiates the anti-tumour activity of DNA double-strand break inducing agents by impairing DNA repair independent of p53 status. *Cancer Lett.* 380, 467–475. doi: 10.1016/j.canlet.2016.07.009

Alagoz, M., Katsuki, Y., Ogiwara, H., Alagoz, M., Katsuki, Y., Ogiwara, H., et al. (2015). SETDB1, HP1 and SUV39 promote repositioning of 53BP1 to extend resection during homologous recombination in G2 cells. *Nucleic Acids Res.* 43, 7931–7944. doi: 10.1093/nar/gkv722

Amé, J. C., Spenlehauer, C., and De Murcia, G. (2004). The PARP superfamily. *BioEssays* 26, 882–893. doi: 10.1002/bies.20085

Antonysamy, S., Bonday, Z., Campbell, R. M., Doyle, B., Druzina, Z., Gheyi, T., et al. (2012). Crystal structure of the human PRMT5:MEP50 complex. *Proc. Natl. Acad. Sci. U.S.A.* 109, 17960–17965. doi: 10.1073/pnas.1209814109

Balbo Pogliano, C., Gatti, M., Rüthemann, P., Garajovà, Z., Penengo, L., and Naegeli, H. (2017). ASH1L histone methyltransferase regulates the handoff between damage recognition factors in global-genome nucleotide excision repair. *Nat. Commun.* 8:1333. doi: 10.1038/s41467-017-01080-8

Bedford, M. T. (2007). Arginine methylation at a glance. *J. Cell Sci.* 120, 4243–4246. doi: 10.1242/jcs.019885

Bekker-Jensen, S., and Mailand, N. (2011). The ubiquitin- and SUMO-dependent signaling response to DNA double-strand breaks. *FEBS Lett.* 585, 2914–2919. doi: 10.1016/j.febslet.2011.05.056

Black, J. C., Van Rechem, C., and Whetstine, J. R. (2012). Histone lysine methylation dynamics: establishment, regulation, and biological impact. *Mol. Cell* 48, 491–507. doi: 10.1016/j.molcel.2012.11.006

Bonner, W. M., Redon, C. E., Dickey, J. S., Nakamura, A. J., Sedelnikova, O. A., Solier, S., et al. (2008). GammaH2AX and cancer. *Nat. Rev. Cancer* 8, 957–967. doi: 10.1038/nrc2523

Caruso, L. B., Martin, K. A., Lauretti, E., Hulse, M., Siciliano, M., Lupey-Green, L. N., et al. (2018). Poly(ADP-ribose) Polymerase 1, PARP1, modifies EZH2 and inhibits EZH2 histone methyltransferase activity after DNA damage. *Oncotarget* 9, 10585–10605. doi: 10.18632/oncotarget.24291

Carvalho, S., Vítor, A. C., Sridhara, S. C., Martins, F. B., Raposo, A. C., Desterro, J. M., et al. (2014). SETD2 is required for DNA double-strand break repair and activation of the p53-mediated checkpoint. *Elife* 3:e02482. doi: 10.7554/eLife.02482

Chan-Penebre, E., Kuplast, K. G., Majer, C. R., Boriack-Sjodin, P. A., Wigle, T. J., Johnston, L. D., et al. (2015). A selective inhibitor of PRMT5 with in vivo and in vitro potency in MCL models. *Nat. Chem. Biol.* 11, 432–437. doi: 10.1038/nchembio.1810

Chapman, J. R., Taylor, M. R. G., and Boulton, S. J. (2012). Playing the end game: DNA double-strand break repair pathway choice. *Mol. Cell* 47, 497–510. doi: 10.1016/j.molcel.2012.07.029

Chatterjee, N., and Walker, G. C. (2017). Mechanisms of DNA damage, repair, and mutagenesis. *Environ. Mol. Mutagen.* 58, 235–263. doi: 10.1002/em.22087

Chaudhuri, S., Wyrick, J. J., and Smerdon, M. J. (2009). Histone H3 Lys79 methylation is required for efficient nucleotide excision repair in a silenced locus of Saccharomyces cerevisiae. *Nucleic Acids Res.* 37, 1690–1700. doi: 10.1093/nar/gkp003

Checa-Rodríguez, C., Cepeda-García, C., Ramón, J., López-Saavedra, A., Balestra, F. R., Domínguez-Sánchez, M. S., et al. (2020). Methylation of the central transcriptional regulator KLF4 by PRMT5 is required for DNA end resection and recombination. *DNA Repair (Amst)* 94:102902. doi: 10.1016/j.dnarep.2020.102902

Chitale, S., and Richly, H. (2018). DICER- and MMSET-catalyzed H4K20me2 recruits the nucleotide excision repair factor XPA to DNA damage sites. *J. Cell Biol.* 217, 527–540. doi: 10.1083/jcb.201704028

Cho, E. C., Zheng, S., Munro, S., Liu, G., Carr, S. M., Moehlenbrink, J., et al. (2012). Arginine methylation controls growth regulation by E2F-1. *EMBO J.* 31, 1785–1797. doi: 10.1038/emboj.2012.17

Chuikov, S., Kurash, J. K., Wilson, J. R., Xiao, B., Justin, N., Ivanov, G. S., et al. (2004). Regulation of p53 activity through lysine methylation. *Nature* 432, 353–360. doi: 10.1038/nature03117

Ciccia, A., and Elledge, S. J. (2010). The DNA damage response: making it safe to play with knives. *Mol. Cell* 40, 179–204. doi: 10.1016/j.molcel.2010.09.019

Daigle, S. R., Olhava, E. J., Therkelsen, C. A., Basavapathruni, A., Jin, L., Boriack-Sjodin, P. A., et al. (2013). Potent inhibition of DOT1L as treatment of MLL fusion leukemia. *Blood* 122, 1017–1025. doi: 10.1182/blood-2013-04-497644

Daigle, S. R., Olhava, E. J., Therkelsen, C. A., Majer, C. R., Sneeringer, C. J., Song, J., et al. (2011). Selective killing of mixed lineage leukemia cells by a potent small-molecule DOT1L inhibitor. *Cancer Cell* 20, 53–65. doi: 10.1016/j.ccr.2011.06.009

Dantzer, F., De La Rubia, G., Ménissier-De Murcia, J., Hostomsky, Z., De Murcia, G., and Schreiber, V. (2000). Base excision repair is impaired in mammalian cells lacking poly(ADP- ribose) polymerase-1. *Biochemistry* 39, 7559–7569. doi: 10.1021/bi0003442

Demple, B., and Sung, J. S. (2005). Molecular and biological roles of Ape1 protein in mammalian base excision repair. *DNA Repair (Amst)* 4, 1442–1449. doi: 10.1016/j.dnarep.2005.09.004

Duan, R., Du, W., and Guo, W. (2020). EZH2: a novel target for cancer treatment. *J. Hematol. Oncol.* 13:104. doi: 10.1186/s13045-020-00937-8

Dulev, S., Tkach, J., Lin, S., and Batada, N. N. (2014). SET 8 methyltransferase activity during the DNA double-strand break response is required for recruitment of 53BP1. *EMBO Rep.* 15, 1163–1174. doi: 10.15252/embr.201439434

Fernandez-Capetillo, O., Chen, H. T., Celeste, A., Ward, I., Romanienko, P. J., Morales, J. C., et al. (2002). DNA damage-induced G2-M checkpoint activation by histone H2AX and 53BP1. *Nat. Cell Biol.* 4, 993–997. doi: 10.1038/ncb884

Fnu, S., Williamson, E. A., De Haro, L. P., Brenneman, M., Wray, J., Shaheen, M., et al. (2011). Methylation of histone H3 lysine 36 enhances DNA repair by nonhomologous end-joining. *Proc. Natl. Acad. Sci. U.S.A.* 108, 540–545. doi: 10.1073/pnas.1013571108

Friedberg, E. C., Walker, G. C., Siede, W., Wood, R. D., Schultz, R. A., and Ellenberger, T. (2006). *DNA Repair and Mutagenesis*, 2nd Edn. Hoboken, NJ: Wiley, doi: 10.1128/9781555816704

Fukuda, T., Wu, W., Okada, M., Maeda, I., Kojima, Y., Hayami, R., et al. (2015). Class I histone deacetylase inhibitors inhibit the retention of BRCA1 and 53BP1 at the site of DNA damage. *Cancer Sci.* 106, 1050–1056. doi: 10.1111/cas.12717

Gasior, S. L., Wong, A. K., Kora, Y., Shinohara, A., and Bishop, D. K. (1998). Rad52 associates with RPA and functions with rad55 and rad57 to assemble meiotic recombination complexes. *Genes Dev.* 12, 2208–2221. doi: 10.1101/gad.12.14.2208

Gillet, L. C. J., and Schärer, O. D. (2006). Molecular mechanisms of mammalian global genome nucleotide excision repair. *Chem. Rev.* 106, 253–276. doi: 10.1021/cr040483f

Gillette, T. G., and Hill, J. A. (2015). Readers, writers, and erasers: chromatin as the whiteboard of heart disease. *Circ. Res.* 116, 1245–1253. doi: 10.1161/CIRCRESAHA.116.303630

Ginjala, V., Rodriguez-Colon, L., Ganguly, B., Gangidi, P., Gallina, P., Al-Hraishawi, H., et al. (2017). Protein-lysine methyltransferases G9a and GLP1 promote responses to DNA damage. *Sci. Rep.* 7:16613. doi: 10.1038/s41598-017-16480-5

Gong, F., Kwon, Y., and Smerdon, M. J. (2005). Nucleotide excision repair in chromatin and the right of entry. *DNA Repair (Amst)* 4, 884–896. doi: 10.1016/j.dnarep.2005.04.007

Gong, F., and Miller, K. M. (2013). Mammalian DNA repair: HATs and HDACs make their mark through histone acetylation. *Mutat. Res. Fundam Mol. Mech. Mutagen.* 750, 23–30. doi: 10.1016/j.mrfmmm.2013.07.002

Gong, F., and Miller, K. M. (2019). Histone methylation and the DNA damage response. *Mutat. Res. Rev. Mutat. Res.* 780, 37–47. doi: 10.1016/j.mrrev.2017.09.003

Greer, E. L., and Shi, Y. (2012). Histone methylation: a dynamic mark in health, disease and inheritance. *Nat. Rev. Genet.* 13, 343–357. doi: 10.1038/nrg3173

Gsell, C., Richly, H., Coin, F., and Naegeli, H. (2020). A chromatin scaffold for DNA damage recognition: how histone methyltransferases prime nucleosomes for repair of ultraviolet light-induced lesions. *Nucleic Acids Res.* 48, 1652–1668. doi: 10.1093/nar/gkz1229

Gursoy-Yuzugullu, O., Carman, C., Serafim, R. B., Myronakis, M., Valente, V., and Price, B. D. (2017). Epigenetic therapy with inhibitors of histone methylation suppresses DNA damage signaling and increases glioma cell radiosensitivity. *Oncotarget* 8, 24518–24532. doi: 10.18632/oncotarget.15543

Hakem, R. (2008). DNA-damage repair; the good, the bad, and the ugly. *EMBO J.* 27, 589–605. doi: 10.1038/emboj.2008.15

Hamard, P. J., Santiago, G. E., Liu, F., Karl, D. L., Martinez, C., Man, N., et al. (2018). PRMT5 regulates DNA repair by controlling the alternative splicing of histone-modifying enzymes. *Cell Rep.* 24, 2643–2657. doi: 10.1016/j.celrep.2018.08.002

Hanawalt, P. C. (2015). Historical perspective on the DNA damage response. *DNA Repair (Amst)* 36, 2–7. doi: 10.1016/j.dnarep.2015.10.001

He, W., Ma, X., Yang, X., Zhao, Y., Qiu, J., and Hang, H. (2011). A role for the arginine methylation of Rad9 in checkpoint control and cellular sensitivity to DNA damage. *Nucleic Acids Res.* 39, 4719–4727. doi: 10.1093/nar/gkq1264

Hombauer, H., Campbell, C. S., Smith, C. E., Desai, A., and Kolodner, R. D. (2011). Visualization of eukaryotic DNA mismatch repair reveals distinct recognition and repair intermediates. *Cell* 147, 1040–1053. doi: 10.1016/j.cell.2011.10.025

Huang, A., Garraway, L. A., Ashworth, A., and Weber, B. (2020). Synthetic lethality as an engine for cancer drug target discovery. *Nat. Rev. Drug Discov.* 19, 23–38. doi: 10.1038/s41573-019-0046-z

Hustedt, N., and Durocher, D. (2017). The control of DNA repair by the cell cycle. *Nat. Cell Biol.* 19, 1–9. doi: 10.1038/ncb3452

Huyen, Y., Zgheib, O., DiTullio, R. A., Gorgoulis, V. G., Zacharatos, P., Petty, T. J., et al. (2004). Methylated lysine 79 of histone H3 targets 53BP1 to DNA double-strand breaks. *Nature* 432, 406–411. doi: 10.1038/nature03114

Hwang, J. W., Kim, S. N., Myung, N., Song, D., Han, G., Bae, G., et al. (2020). PRMT5 promotes DNA repair through methylation of 53BP1 and is regulated by Src-mediated phosphorylation. *Commun. Biol.* 3:428. doi: 10.1038/s42003-020-01157-z

Jackson, S. P., and Bartek, J. (2009). The DNA-damage response in human biology and disease. *Nature* 461, 1071–1078. doi: 10.1038/nature08467

Jansson, M., Durant, S. T., Cho, E. C., Seahan, S., Edelmann, M., Kessler, B., et al. (2008). Arginine methylation regulates the p53 response. *Nat. Cell Biol.* 10, 1431–1439. doi: 10.1038/ncb1802

Jeppesen, D. K., Bohr, V. A., and Stevnsner, T. (2011). DNA repair deficiency in neurodegeneration. *Prog. Neurobiol.* 94, 166–200. doi: 10.1016/j.pneurobio.2011.04.013

Kari, V., Raul, S. K., Henck, J. M., Kitz, J., Kramer, F., Kosinsky, R. L., et al. (2019). The histone methyltransferase DOT1L is required for proper DNA damage response, DNA repair, and modulates chemotherapy responsiveness. *Clin. Epigenet.* 11:4. doi: 10.1186/s13148-018-0601-1

Khanna, K. K., and Jackson, S. P. (2001). DNA double-strand breaks: signaling, repair and the cancer connection. *Nat. Genet.* 27, 247–254. doi: 10.1038/85798

Klaus, C. R., Iwanowicz, D., Johnston, D., Campbell, C. A., Smith, J. J., Moyer, M. P., et al. (2014). DOT1L inhibitor EPZ-5676 displays synergistic antiproliferative activity in combination with standard of care drugs and hypomethylating agents in MLL-rearranged leukemia cells. *J. Pharmacol. Exp. Ther.* 350, 646–656. doi: 10.1124/jpet.114.214577

Kouzarides, T. (2002). Histone methylation in transcriptional control. *Curr. Opin. Genet. Dev.* 12, 198–209. doi: 10.1016/S0959-437X(02)00287-3

Kouzarides, T. (2007). Chromatin modifications and their function. *Cell* 128, 693–705. doi: 10.1016/j.cell.2007.02.005

Krokan, H. E., and Bjørås, M. (2013). Base excision repair. *Cold Spring Harb. Perspect. Biol.* 5:a012583. doi: 10.1101/cshperspect.a012583

Kubicek, S., O'Sullivan, R. J., August, E. M., Hickey, E. R., Zhang, Q., Teodoro, M. L., et al. (2007). Reversal of H3K9me2 by a small-molecule inhibitor for the G9a histone methyltransferase. *Mol. Cell* 25, 473–481. doi: 10.1016/j.molcel.2007.01.017

Lahue, R. S., Au, K. G., and Modrich, P. (1989). DNA mismatch correction in a defined system. *Science* 245, 160–164. doi: 10.1126/science.2665076

Lee, S. H., Oshige, M., Durant, S. T., Rasila, K. K., Williamson, W. A., Ramsey, H., et al. (2005). The SET domain protein Metnase mediates foreign DNA integration and links integration to nonhomologous end-joining repair. *Proc. Natl. Acad. Sci. U.S.A.* 102, 18075–18080. doi: 10.1073/pnas.0503676102

Li, B., Carey, M., and Workman, J. L. (2007). The Role of Chromatin during Transcription. *Cell.* 128, 707–719. doi: 10.1016/j.cell.2007.01.015

Li, F., Mao, G., Tong, D., Huang, J., Gu, L., Yang, W., et al. (2013). The histone mark H3K36me3 regulates human DNA mismatch repair through its interaction with MutSα. *Cell* 153, 590–600. doi: 10.1016/j.cell.2013.03.025

Li, F., Ortega, J., Gu, L., and Li, G. M. (2016). Regulation of mismatch repair by histone code and posttranslational modifications in eukaryotic cells [published correction appears in DNA Repair (Amst). 2019 Aug;80:96-99]. *DNA Repair (Amst)* 38, 68–74. doi: 10.1016/j.dnarep.2015.11.021

Li, G. M. (2013). Decoding the histone code: role of H3K36me3 in mismatch repair and implications for cancer susceptibility and therapy. *Cancer Res.* 73, 6379–6383. doi: 10.1158/0008-5472.CAN-13-1870

Li, Y. H., Tong, K. L., Lu, J. L., Lin, J. B., Li, Z. Y., Sang, Y., et al. (2020). PRMT5-TRIM21 interaction regulates the senescence of osteosarcoma cells by targeting the TXNIP/p21 axis. *Aging (Albany NY)* 12, 2507–2529. doi: 10.18632/aging.102760

Lieber, M. R. (2008). The mechanism of human nonhomologous DNA End joining. *J. Biol. Chem.* 283, 1–5. doi: 10.1074/jbc.R700039200

Liu, F., Barsyte-Lovejoy, D., Li, F., Xiong, Y., Korboukh, V., Huang, X. P., et al. (2013). Discovery of an in vivo chemical probe of the lysine methyltransferases

G9a and GLP. *J. Med. Chem.* 56, 8931–8942. doi: 10.1021/jm401480r

Liu, W., Deng, L., Song, Y., and Redell, M. (2014). DOT1L inhibition sensitizes MLL-rearranged AML to chemotherapy. *PLoS One* 9:e98270. doi: 10.1371/journal.pone.0098270

Ljungman, M., Parks, L., Hulbatte, R., and Bedi, K. (2017). The role of H3K79 methylation in transcription and the DNA damage response. *Mutat. Res. Rev. Mutat. Res.* 780, 48–54. doi: 10.1016/j.mrrev.2017.11.001

Lord, C. J., and Ashworth, A. (2017). PARP inhibitors: synthetic lethality in the clinic. *Science* 355, 1152–1158. doi: 10.1126/science.aam7344

Lu, X., Tang, M., Zhu, Q., Yang, Q., Li, Z., Bao, Y., et al. (2019). GLP-catalyzed H4K16me1 promotes 53BP1 recruitment to permit DNA damage repair and cell survival. *Nucleic Acids Res.* 47, 10977–10993. doi: 10.1093/nar/gkz897

Masutani, M., Nakagama, H., and Sugimura, T. (2003). Poly(ADP-ribose) and carcinogenesis. *Genes Chromosom. Cancer* 38, 339–348. doi: 10.1002/gcc.10250

Moore, J. K., and Haber, J. E. (1996). Cell cycle and genetic requirements of two pathways of nonhomologous end-joining repair of double-strand breaks in *Saccharomyces cerevisiae*. *Mol Cell Biol.* 16, 2164–2173. doi: 10.1128/MCB.16.5.2164

Murray, K. (1964). The occurrence of ϵ-N-methyl lysine in histones. *Biochemistry* 3, 10–15. doi: 10.1021/bi00889a003

Musselman, C. A., Lalonde, M. E., Côté, J., and Kutateladze, T. G. (2012). Perceiving the epigenetic landscape through histone readers. *Nat. Struct. Mol. Biol.* 19, 1218–1227. doi: 10.1038/nsmb.2436

Nijman, S. M. (2011). Synthetic lethality: general principles, utility and detection using genetic screens in human cells. *FEBS Lett.* 585, 1–6. doi: 10.1016/j.febslet.2010.11.024

Nimura, K., Ura, K., Shiratori, H., Ikawa, M., Okabe, M., Schwartz, R. J., et al. (2009). A histone H3 lysine 36 trimethyltransferase links Nkx2-5 to Wolf-Hirschhorn syndrome. *Nature* 46, 287–291. doi: 10.1038/nature08086

Okada, Y., Feng, Q., Lin, Y., Jiang, Q., Li, Y., Coffield, V. M., et al. (2005). hDOT1L links histone methylation to leukemogenesis. *Cell* 121, 167–178. doi: 10.1016/j.cell.2005.02.020

Pei, H., Zhang, L., Luo, K., Qin, Y., Chesi, M., Fei, F., et al. (2011). MMSET regulates histone H4K20 methylation and 53BP1 accumulation at DNA damage sites. *Nature* 470, 124–128. doi: 10.1038/nature09658

Penebre, E., Kuplast, K. G., Majer, C. R., Johnston, L. D., Rioux, N., Munchhof, M., et al. (2014). Identification of a first-in-class PRMT5 inhibitor with potent in vitro and in vivo activity in preclinical models of mantle cell lymphoma. *Blood* 124:438. doi: 10.1182/blood.V124.21.438.438

Petit, C., and Sancar, A. (1999). Nucleotide excision repair: from *E. coli* to man. *Biochimie* 81, 15–25. doi: 10.1016/S0300-9084(99)80034-0

Pfister, S. X., Ahrabi, S., Zalmas, L. P., Sarkar, S., Aymard, F., Bachrati, C. Z., et al. (2014). SETD2-dependent histone H3K36 trimethylation is required for homologous recombination repair and genome stability. *Cell Rep.* 7, 2006–2018. doi: 10.1016/j.celrep.2014.05.026

Raderschall, E., Golub, E. I., and Haaf, T. (1999). Nuclear foci of mammalian recombination proteins are located at single-stranded DNA regions formed after DNA damage. *Proc. Natl. Acad. Sci. U.S.A.* 96, 1921–1926. doi: 10.1073/pnas.96.5.1921

Russo, V. E. A., Martienssen, R. A., and Riggs, AD, eds (1996). *Epigenetic Mechanisms of Gene Regulation*. Cold Spring Harbor, NY: Cold Spring Harbor Laboratory Press.

Scully, R., Chen, J., Ochs, R. L., Keegan, K., Hoekstra, M., Feunteun, J., et al. (1997). Dynamic changes of BRCA1 subnuclear location and phosphorylation state are initiated by DNA damage. *Cell* 90, 425–435. doi: 10.1016/S0092-8674(00)80503-6

Secker, K. A., Keppeler, H., Duerr-Stoerzer, S., Schmid, H., Schneidawind, D., Hentrich, T., et al. (2019). Inhibition of DOT1L and PRMT5 promote synergistic anti-tumor activity in a human MLL leukemia model induced by CRISPR/Cas9. *Oncogene* 38, 7181–7195. doi: 10.1038/s41388-019-0937-9

Sobol, R. W., Horton, J. K., Kühn, R., Gu, H., Singhal, R. K., Prasad, R., et al. (1996). Requirement of mammalian DNA polymerase-β in base-excision repair. *Nature* 379, 183–196. doi: 10.1038/379183a0

Stein, E. M., Garcia-Manero, G., Rizzieri, D. A., Tibes, R., Berdeja, J. G., Savona, M. R., et al. (2018). The DOT1L inhibitor pinometostat reduces H3K79 methylation and has modest clinical activity in adult acute leukemia. *Blood* 131, 2661–2669. doi: 10.1182/blood-2017-12-818948

Stucki, M., Clapperton, J. A., Mohammad, D., Yaffe, M. B., Smerdon, S. J., and Jackson, S. P. (2005). MDC1 directly binds phosphorylated histone H2AX to regulate cellular responses to DNA double-strand breaks. *Cell* 123, 1213–1226. doi: 10.1016/j.cell.2005.09.038

Sung, P., and Klein, H. (2006). Mechanism of homologous recombination: mediators and helicases take on regulatory functions. *Nat. Rev. Mol. Cell Biol.* 7, 739–750. doi: 10.1038/nrm2008

Tachibana, M., Matsumura, Y., Fukuda, M., Kimura, H., and Shinkai, Y. (2008). G9a/GLP complexes independently mediate H3K9 and DNA methylation to silence transcription. *EMBO J.* 27, 2681–2690. doi: 10.1038/emboj.2008.192

Tachibana, M., Ueda, J., Fukuda, M., Takeda, N., Ohta, T., Iwanari, H., et al. (2005). Histone methyltransferases G9a and GLP form heteromeric complexes and are both crucial for methylation of euchromatin at H3-K9. *Genes Dev.* 19, 815–826. doi: 10.1101/gad.1284005

Teng, Y., Yu, Y., and Waters, R. (2002). The *Saccharomyces cerevisiae* histone acetyltransferase Gcn5 has a role in the photoreactivation and nucleotide excision repair of UV-induced cyclobutane pyrimidine dimers in the MFA2 gene. *J. Mol. Biol.* 316, 489–499. doi: 10.1006/jmbi.2001.5383

Thoma, F. (1999). Light and dark in chromatin repair: repair of UV-induced DNA lesions by photolyase and nucleotide excision repair. *EMBO J.* 18, 6585–6598. doi: 10.1093/emboj/18.23.6585

Tubbs, A., and Nussenzweig, A. (2017). Endogenous DNA damage as a source of genomic instability in cancer. *Cell* 168, 644–656. doi: 10.1016/j.cell.2017.01.002

U.S. Food and Drug Administration, and Center for Drug Evaluation and Research (2020). *Tazverik (Tazemetostat) NDA 211723/213400 Approval Letters, Jan 23 and June 18, 2020*. Silver Spring, MD: U.S. Food and Drug Administration.

Urrutia, G., Salmonson, A., Toro-Zapata, J., de Assuncao, T. M., Mathison, A., Dusetti, N., et al. (2020). Combined targeting of G9a and checkpoint kinase 1 synergistically inhibits pancreatic cancer cell growth by replication fork collapse. *Mol. Cancer Res.* 18, 448–462. doi: 10.1158/1541-7786.MCR-19-0490

Vedadi, M., Barsyte-Lovejoy, D., Liu, F., Rival-Gervier, S., Allali-Hassani, A., Labrie, V., et al. (2011). A chemical probe selectively inhibits G9a and GLP methyltransferase activity in cells. *Nat. Chem. Biol.* 7, 566–574. doi: 10.1038/nchembio.599

Wang, Y., Sun, H., Wang, J., Wang, H., Meng, L., Xu, C., et al. (2016). DNA-PK-mediated phosphorylation of EZH2 regulates the DNA damage-induced apoptosis to maintain T-cell genomic integrity. *Cell Death Dis.* 7:e2316. doi: 10.1038/cddis.2016.198

Watson, J. D., and Crick, F. H. C. (1953). Molecular structure of nucleic acids: a structure for deoxyribose nucleic acid. *Nature* 171, 737–738. doi: 10.1038/171737a0

Watson, Z. L., Yamamoto, T. M., McMellen, A., Kim, H., Hughes, C. J., Wheeler, L. J., et al. (2019). Histone methyltransferases EHMT1 and EHMT2 (GLP/G9A) maintain PARP inhibitor resistance in high-grade serous ovarian carcinoma. *Clin. Epigenet.* 11:165. doi: 10.1186/s13148-019-0758-2

Wei, X., Yang, J., Adair, S. J., Ozturk, H., Kuscu, C., Lee, K. Y., et al. (2020). Targeted CRISPR screening identifies PRMT5 as synthetic lethality combinatorial target with gemcitabine in pancreatic cancer cells. *Proc. Natl. Acad. Sci. U.S.A.* 117, 28068–28079. doi: 10.1073/pnas.2009899117

Wood, K., Tellier, M., and Murphy, S. (2018). DOT1L and H3K79 methylation in transcription and genomic stability. *Biomolecules* 8:11. doi: 10.3390/biom8010011

Wu, L. C., Wang, Z. W., Tsan, J. T., Spillman, M. A., Phung, A., Xu, X. L., et al. (1996). Identification of a RING protein that can interact in vivo with the BRCA1 gene product. *Nat. Genet.* 14, 430–440. doi: 10.1038/ng1296-430

Wu, W., Nishikawa, H., Fukuda, T., Vittal, V., Asano, M., Miyoshi, Y., et al. (2015). Interaction of BARD1 and HP1 Is Required for BRCA1 Retention at Sites of DNA Damage. *Cancer Res.* 75, 1311–1321. doi: 10.1158/0008-5472.CAN-14-2796

Xu, Y., and Price, B. D. (2011). Chromatin dynamics and the repair of DNA double strand breaks. *Cell Cycle* 10, 261–267. doi: 10.4161/cc.10.2.14543

Yamagishi, M., and Uchimaru, K. (2017). Targeting EZH2 in cancer therapy. *Curr. Opin. Oncol.* 29, 375–381. doi: 10.1097/CCO.0000000000000390

Yamaguchi, H., Du, Y., Nakai, K., Ding, M., Chang, S. S., Hsu, J. L., et al. (2018). EZH2 contributes to the response to PARP inhibitors through its PARP-mediated poly-ADP ribosylation in breast cancer. *Oncogene* 37, 208–217. doi: 10.1038/onc.2017.311

Yang, Q., Zhu, Q., Lu, X., Du, Y., Cao, L., Shen, C., et al. (2017). G9a coordinates with the RPA complex to promote DNA damage repair and cell survival. *Proc. Natl. Acad. Sci. U.S.A.* 114, E6054–E6063. doi: 10.1073/pnas.1700694114

Yang, Y., and Bedford, M. T. (2013). Protein arginine methyltransferases and cancer. *Nat. Rev. Cancer* 13, 37–50. doi: 10.1038/nrc3409

Yu, W., Chory, E. J., Wernimont, A. K., Tempel, W., Scopton, A., Federation, A., et al. (2012). Catalytic site remodelling of the DOT1L methyltransferase by selective inhibitors. *Nat. Commun.* 3:1288. doi: 10.1038/ncomms2304

Yuan, Y., Wang, Q., Paulk, J., Kubicek, S., Kemp, M. M., Adams, D. J., et al. (2012). A small-molecule probe of the histone methyltransferase G9a induces cellular senescence in pancreatic adenocarcinoma. *ACS Chem. Biol.* 7, 1152–1157. doi: 10.1021/cb300139y

Zhou, X., Wang, W., Du, C., Yan, F., Yang, S., He, K., et al. (2018). OGG1 regulates the level of symmetric dimethylation of histone H4 arginine-3 by interacting with PRMT5. *Mol. Cell Probes.* 38, 19–24. doi: 10.1016/j.mcp.2018.01.002

Conflict of Interest: The authors declare that the research was conducted in the absence of any commercial or financial relationships that could be construed as a potential conflict of interest.

Publisher's Note: All claims expressed in this article are solely those of the authors and do not necessarily represent those of their affiliated organizations, or those of the publisher, the editors and the reviewers. Any product that may be evaluated in this article, or claim that may be made by its manufacturer, is not guaranteed or endorsed by the publisher.

Advantages of publishing in Frontiers

OPEN ACCESS
Articles are free to read for greatest visibility and readership

FAST PUBLICATION
Around 90 days from submission to decision

HIGH QUALITY PEER-REVIEW
Rigorous, collaborative, and constructive peer-review

TRANSPARENT PEER-REVIEW
Editors and reviewers acknowledged by name on published articles

Frontiers
Avenue du Tribunal-Fédéral 34
1005 Lausanne | Switzerland

Visit us: www.frontiersin.org
Contact us: frontiersin.org/about/contact

REPRODUCIBILITY OF RESEARCH
Support open data and methods to enhance research reproducibility

DIGITAL PUBLISHING
Articles designed for optimal readership across devices

FOLLOW US
@frontiersin

IMPACT METRICS
Advanced article metrics track visibility across digital media

EXTENSIVE PROMOTION
Marketing and promotion of impactful research

LOOP RESEARCH NETWORK
Our network increases your article's readership